Field Trip Guidebook:

REGIONAL METAMORPHISM AND METAMORPHIC PHASE RELATIONS IN NORTHWESTERN AND CENTRAL NEW ENGLAND

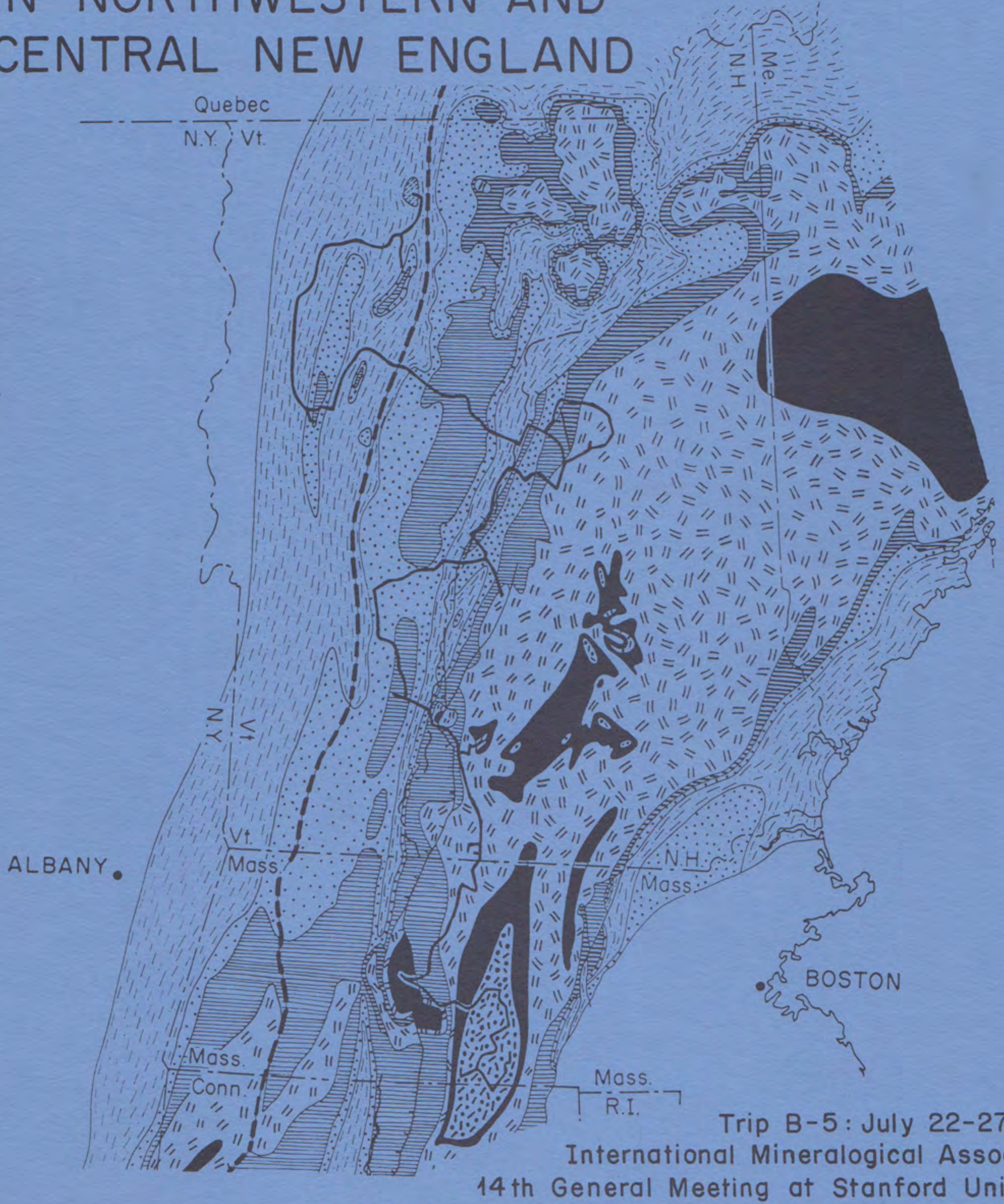
Quebec
N.Y.
Vt.
N.H.
Me.
N.Y.
Vt.
Vt.
Mass.
ALBANY
N.H.
Mass.
BOSTON
Mass.
Conn.
Mass.
R.I.

Trip B-5: July 22-27, 1986
International Mineralogical Association
14th General Meeting at Stanford University
Contribution No. 59, Department of Geology and Geography
University of Massachusetts, Amherst, Massachusetts

FIELD TRIP GUIDEBOOK :

REGIONAL METAMORPHISM AND METAMORPHIC PHASE RELATIONS IN NORTHWESTERN AND CENTRAL NEW ENGLAND

by

Peter Robinson[1], Jo Laird[2], Wallace A. Bothner[2], Douglas Rumble III[3,8], Mel P. Dickenson[4], Frank S. Spear[5], James B. Thompson, Jr.[6], John T. Cheney[7], C. Page Chamberlain[8], John C. Schumacher[10], Kurt T. Hollocher[9], Robert J. Tracy[4], and Henry N. Berry IV[1]

Peter Robinson[1], Editor
David C. Elbert[1], Associate Editor

[1] Department of Geology and Geography, University of Massachusetts, Amherst, MA 01003
[2] Department of Geology, University of New Hampshire, Durham, NH 03824
[3] Earth Science Division, National Science Foundation, Washington, D.C. 20550
[4] Department of Geological Sciences, Virginia Polytechnic Institute and State University, Blacksburg, VA 24061
[5] Department of Geology, Rensselaer Polytechnic Institute, Troy, NY 12181
[6] Department of Geological Sciences, Harvard University, Cambridge, MA 02138
[7] Department of Geology, Amherst College, Amherst, MA 01002
[8] Geophysical Laboratory, Carnegie Institution, 2801 Upton Street, N.W., Washington, D.C. 20008
[9] Department of Geology, Union College, Schenectady, NY 12308
[10] Mineralogisch-Petrographisches Institut and Museum der Universitat Kiel, Olshausenstrasse 40, D-2300, Kiel, Federal Republic of Germany

Trip B-5: July 22-27, 1986
14th General Meeting, International Mineralogical Association at Stanford University

Contribution No. 59, Department of Geology and Geography
University of Massachusetts, Amherst, Massachusetts

CONTENTS

Page

A. INTRODUCTION

by Peter Robinson 1

Purpose of Trip 1
Very Brief History of Metamorphic Petrology in New England 1
Regional Stratigraphic and Structural Setting 3
Regional Distribution of Metamorphic Zones 7
Taconian Metamorphism in the Context of Plate Tectonics 9
Acadian Metamorphism in the Context of Plate Tectonics 10
Editor's Acknowledgements 10

B. METAMORPHISM IN THE NORTHERN GREEN MOUNTAINS OF VERMONT

by Jo Laird and Wallace A. Bothner 11

INTRODUCTION AND OBJECTIVES FOR THE DAY 11
STRATIGRAPHIC AND STRUCTURAL SETTING 11
DISTRIBUTION AND AGE OF METAMORPHIC ZONES 13
METAMORPHISM OF MAFIC ROCKS 15
METAMORPHISM OF PELITIC SCHIST 16
FIELD TRIP ITINERARY 26
  A Hike to Tillotson Camp, Locality 1 26
  A Hike to Arden Albee's Pelitic Schist Locality, Lincoln Mountain Quadrangle, Vermont (Locality 2) 32

C. A FIELD TRIP GUIDE TO BLACK MOUNTAIN, WILDWOOD ROADCUT AND BEAVER BROOK, MT. MOOSILAUKE AREA, NEW HAMPSHIRE

by Douglas Rumble, III and M.P. Dickenson 37

INTRODUCTION 37
MAPS AND LITERATURE 37
STRATIGRAPHY AND GEOLOGIC HISTORY 37
BLACK MOUNTAIN 39
  Access 39
  Hiking Route 39
WILDWOOD ROADCUT 45
  Access 45
  Location of Rock Types 45
  Introduction 46
  Geologic Setting 46
  Analytical Methods 46
  Petrography and Mineral Chemistry 46
  Mineralogy 47
  Geothermometry and Geobarometry 48
  Phase Equilibria 48
BEAVER BROOK FOSSIL LOCALITY 51
  Access 51
  Hiking Route 51

D. MINERALOGY, PETROLOGY AND P-T EVOLUTION OF THE ORFORDVILLE AREA, WEST-CENTRAL NEW HAMPSHIRE AND EAST-CENTRAL VERMONT
by Frank S. Spear and Douglas Rumble, III........ 57

INTRODUCTION........ 57
GEOLOGIC SETTING........ 57
Stratigraphy........ 57
Structure........ 61
METAMORPHISM AND P-T EVOLUTION........ 63
P-T Paths from Zoned Garnets........ 63
P-T Paths from Amphibolite Parageneses........ 68
MULTIPLE AMPHIBOLE ASSEMBLAGES IN THE AMMONOOSUC VOLCANICS........ 70
Orthoamphiboles........ 70
Four-Amphibole Assemblages........ 72
Coexisting Plagioclase........ 72
PHASE RELATIONS OF THE AMMONOOSUC VOLCANICS........ 78
DISCOVERY AND CHARACTERIZATION OF WONESITE........ 82
BEHAVIOR OF METAMORPHIC FLUIDS BASED ON OXYGEN ISOTOPES........ 87
ACKNOWLEDGEMENTS........ 90
ITINERARY........ 90
Stop 1: Lower Baker Pond........ 90
Stop 2: U.S. Route 5 Locality........ 91
Stop 3A, Upper Quarry........ 92
Stop 3B, Wonesite Locality........ 92
Stop 3C, Oxygen Isotope Sample Traverse........ 93

E. METAMORPHISM ON THE EAST FLANK OF THE GREEN MOUNTAIN MASSIF AND CHESTER DOME
by James B. Thompson, Jr., John T. Cheney, and Peter Robinson........ 95

PURPOSE........ 95
STRATIGRAPHIC AND STRUCTURAL SETTING........ 96
Massif-Cover Relationships........ 96
The Chester Dome Area........ 96
DISTRIBUTION OF METAMORPHIC ZONES AND POLYMETAMORPHISM........ 97
ITINERARY........ 98
STOP 1. SILLIMANITE ZONE CLOUGH QUARTZITE WITH FOSSILS, NEAR ANTICLINAL HINGE OF SKITCHEWAUG NAPPE........ 99
STOP 2. STAUROLITE ZONE LITTLETON FORMATION........ 102
STOP 3. WEAVER HILL: COARSE CHLORITOID PHYLLITE........ 103
STOP 4. THE WILLIAMS QUARRY AT GASSETTS, VERMONT: CALC-SILICATE REACTION ZONES........ 105
STOP 5. THE GASSETTS SCHIST........ 107
Mineral Assemblages........ 107
AFM Phase Relations........ 108
Compositional Zoning and Mineral Inclusions in Garnet........ 112
STOP 6. THE CHESTER SOAPSTONE QUARRY........ 117
Geologic Setting of New England Ultramafic Bodies........ 118
Metasomatic Reaction Zones........ 118
Triple-Chain Silicates........ 119

F. METAMORPHIC AND TECTONIC EVOLUTION OF THE FALL MOUNTAIN NAPPE COMPLEX AND ADJACENT MERRIMACK SYNCLINORIUM
by Frank S. Spear and C. Page Chamberlain........121

INTRODUCTION: OBJECTIVES FOR THE MORNING........121
GENERAL GEOLOGIC SETTING........121
Stratigraphy........121
Structural Geology........122
Plutonic Rocks........123
METAMORPHISM........123
General........124
Fall Mountain Nappe: Upper Plate........125
Fall Mountain Nappe: Lower Plate........131
Interpretation of P-T Paths for the Upper and Lower Plates........133
MERRIMACK SYNCLINORIUM........134
Isograds........134
Geothermobarometry........134
P-T Paths........136
Interpretation of P-T Paths........138
METAMORPHIC-TECTONIC MODEL........138
Tectonic and Thermal Setting before the Nappe Stage........138
Nappe-Stage Deformation and Thermal Perturbations........140
Thermal Relaxation - Cross Folding........140
PART F. ITINERARY........140
Stop 1: Lower Plate of Fall Mountain Nappe........141
Stop 2: Upper Plate of Fall Mountain Nappe........141
Stop 3: Lower Plate of the Fall Mountain Nappe........142
Stop 4: Root Zone of the Fall Mountain Nappe - AA Intersection........143
Stop 5: Root Zone of the Fall Mountain Nappe - SS Intersection........143

G. GEDRITE-CORDIERITE GNEISSES AND RELATED METAMORPHOSED VOLCANIC ROCKS, KEENE DOME, SOUTHWESTERN NEW HAMPSHIRE
by John C. Schumacher and Peter Robinson........145

PURPOSE OF TRIP........145
LOCAL GEOLOGY........145
INTRODUCTION TO AMPHIBOLE PHASE RELATIONS........146
FEATURES OF CRYSTALLOGRAPHIC INTEREST........153
GEOCHEMISTRY OF AMMONOOSUC VOLCANICS........156
Summary of Ammonoosuc Stratigraphy........156
Chemical Distinction between the Lower and Upper Members........156
Original Versus Modified Igneous Compositions........156
ITINERARY........164
STOP 1: "IOLITE HILL"........165
Historical Note........165
Description of Outcrops........166
Petrology of Aluminous Enclaves........167
STOP 2: "AMPHIBOLE HILL"........183
Outcrop 6A9........184
Outcrop 7A0........184
Outcrop I38........184
Outcrop 7A8........186
STOP 3: STAUROLITE-SILLIMANITE SCHIST NEAR SHEOMET LAKE........193

H. THE CENTRAL MASSACHUSETTS METAMORPHIC HIGH
by Peter Robinson, Robert J. Tracy, Kurt T. Hollocher, John C. Schumacher, and Henry N. Berry IV.......195

PURPOSE OF TRIP.......195
PETROLOGICAL BACKGROUND.......195
REGIONAL SETTING.......195
STRATIGRAPHY.......196
STRUCTURAL GEOLOGY.......197
METAMORPHISM.......208
    Characterization of Metamorphic Zones.......209
    Sequence of Reactions in Pelitic Schists.......209
    Geothermometry and Geobarometry.......212
    Effects of Sulfides on the Assemblages of Silicates and Oxides in Pelitic Schists.......215
    Relation between Ti Content and Fe-Mg Ratio in Biotites.......223
    General Description of Metamorphosed Mafic Rocks in Zones IV-VI.......224
    Summary of Amphibole Dehydration Reactions.......224
    Constraints on Fe-Mg vs. Temperature Reaction Loops.......229
    Hornblende Dehydration and Plagioclase Composition.......229
    K-Feldspar - Orthopyroxene Assemblages.......232
    Partial Melting in Mafic Rocks.......234
RELATIONS BETWEEN METAMORPHISM AND STRUCTURAL DEVELOPMENT.......235
REGIONAL TECTONICS AND METAMORPHISM.......239
ITINERARY.......240
STOP 1. ZONED GEDRITE WITH EXTREME Na AND Al COMPOSITIONS.......246
STOP 2. BRIMSTONE HILL.......250
STOP 3. AMPHIBOLITE IN THE MONSON GNEISS.......251
STOP 4. LITTLETON FORMATION IN THE BIG GARNET SYNCLINE.......256
STOP 5. WHITE SCHIST MEMBER OF THE PAXTON FORMATION.......257
STOP 6. PYRRHOTITE-GARNET-BEARING SCHIST IN THE PLEASANT BROOK ANTICLINE.......258
STOP 7. SULFIDIC SCHIST AND MYLONITE IN THE WICKABOAG POND ANTICLINE.......259
STOP 8. WELL BEDDED COARSE GRAY SCHIST OF THE RANGELEY (?) FORMATION NEAR MT. PISGAH.......260
STOP 9. MASHAPAUG RD.......262
STOP 10. FOLDED GRANULITES OF PAXTON FORMATION.......265
STOP 11. COARSE CORDIERITE-GARNET-SILLIMANITE GNEISS AND SILLIMANITE PEGMATITE.......265

I. REFERENCES CITED.......267

J. APPENDIX. FURTHER NOTES TO ACCOMPANY PART D.......285

U.S. ROUTE 5 LOCALITY: WALKING LOG.......285
WONESITE LOCALITY: TRAIL LOG.......287

A. INTRODUCTION

Peter Robinson

Purpose of Trip

The purpose of this trip is to give visitors, particularly those from overseas, an opportunity to observe and collect samples of a series of exposures of metamorphic rocks in the New England Appalachians that have been studied in some detail in the last thirty years. Some of these exposures have been important in the development of metamorphic theory or discoveries concerning crystallography or crystal chemistry of rock-forming minerals. Others have been important in understanding the metamorphic evolution of the Taconian and Acadian orogens.

The route of the field trip has been designed with geographic convenience and a prograde metamorphic sequence in mind, but there was no possibility of a comprehensive coverage of metamorphic petrology in all portions of New England. Thus, a host of relevant studies from Maine, western and eastern Massachusetts, Connecticut, and Rhode Island are not even touched. Nearly all of the leaders trace their background in one way or another to a very fruitful period of research on the New England Appalachians centered at Harvard University. This was begun by Marland P. Billings in the early 1930's. It was joined in the 1950's by James B. Thompson, Jr. (already a field veteran in the 1940's) and led by him into the 1980's. Trip leaders (and assisting drivers) who are direct products of this program include Robinson, Rumble, and Chamberlain, whereas Laird, Spear, Tracy, Cheney, Schumacher, Hollocher, and Elbert studied elsewhere under the tutelage of products of this program.

Another purpose of this trip for overseas visitors is to dispell possible false impressions; for example, that the northeastern United States is mainly an urban area (although it is growing) or that outcrops are very poor and far between. The fact is that the New England Appalachians represent the results of continental collisional processes similar to, but on a grander scale, than the European Alps, and only seem less impressive on the basis of modern topography. Further, there are few places in the world where fossil-controlled stratigraphy has been so successfully traced into regions of high grade metamorphism.

Very Brief History of Metamorphic Petrology in New England

Some of the earliest studies of metamorphic rocks in New England were carried out by medical doctors and school teachers in the early 1800's. George T. Bowen (1824a, 1824b) analyzed and described sillimanite from samples collected by a Dr. McClellan in Saybrook, Connecticut. Bowen named the mineral in honor of Professor Silliman of Yale College, in whose laboratory he had been engaged in 1817. Cummingtonite was named and described by Chester Dewey in 1824 from samples collected by Dr. J. Porter in Cummington, Massachusetts. A cordierite locality studied by Dr. C.T. Jackson in 1844 will be visited on the fourth day of this fieldtrip. Early comprehensive studies included Edward Hitchcock's "Geology of Massachusetts" in 1841, and the much more sophisticated three volume work *The Geology of New Hampshire* by his son Charles Hitchcock (Hitchcock and Huntington, 1874; Hitchcock et al., 1877, 1878). Notable is a report in Volume III (1878) by George W. Hawes which gives mineral descriptions, localities, and several chemical analyses, including analyses of coexisting pyroxene and hornblende. Another Hitchcock protege, B.K. Emerson, studied petrology in Germany in the late 1800's, and many of his study thin sections from that time are still available with his hand written notes at Amherst College and the University of Massachusetts. Emerson developed the firm opinion that most of the rocks in central Massachusetts were metamorphosed in Paleozoic time.

He was also involved in cooperative research with some of the outstanding rock and mineral analysts of his time, including H.S. Washington, W.F. Hillebrand, F.W. Clarke, and others, and his analyzed sample of gedrite (1895, see section G) was listed by Rabbitt (1948) as one of the then few superior analyses of orthorhombic amphibole.

In the first thirty years of the present century, petrology benefitted from an increasing level of sophistication in optical mineralogy, crystallography, and eventually X-ray crystallography. Nevertheless in the 1932 Geologic Map of the United States, with the apparent agreement of local geologists, most of the metamorphic rocks in New England were shown as Precambrian. This state of affairs was rather abruptly terminated by M.P. Billings' work in the Littleton-Moosilauke area, New Hampshire (1937, see section C) where he mapped outward from fossil localities and showed that the same units could be traced into high grade zones and that mineralogic indicators of metamorphic grade made a sensible regional pattern. From this came a host of related studies too numerous to mention spreading southward in New Hampshire, westward into Vermont, north - eastward into Maine, and eventually to Massachusetts and Connecticut. The keynote of all this work was that, if enough attention is paid to stratigraphic detail and the petrographic description of rock types, then a firm foundation is laid for interpretation of the structural and eventually the metamorphic evolution of the region. It is as true today as it was in the days of Billings' early work, that new stratigraphic studies provide the most important information for new structural and metamorphic interpretations. Hence it may not be surprising that some workers vitally concerned with metamorphic petrology have also made major contributions in the area of stratigraphy.

As the regional studies continued, a lively and broad interest in metamorphic phase relations, experiment, and theory developed (see especially Heald, 1950; Osberg, 1952; Lyons, 1955; Chidester, 1953, 1962, 1968; Chidester et al., 1951). Intense thinking about the mineralogy of outcrops in eastern Vermont and western New Hampshire led J.B. Thompson, Jr. to his theoretical papers (1955, 1957, 1959, 1962, 1970, 1972, 1978, 1979, 1981, 1982a, 1982b; Thompson and Thompson, 1976; Thompson et al., 1982) as well as his much more voluminous class lectures. John L. Rosenfeld, a friend and contemporary of Thompson's, used the eastern Vermont setting for his painstaking pioneering studies of the relations between metamorphism and deformation using rotated garnets and other minerals (Rosenfeld, 1968, 1970; see also Karabinos, 1984), as well as for his unique work on the use of piezobirefringence in isotropic minerals as a key to P-T histories (Rosenfeld, 1969). Some students learned from Jim Thompson how to interpret mineral chemistry and mineral zoning at a time before such information was made generally available by the electron probe, others were involved in the early stages of the probe era, and still others came into petrology during its full flowering. E-an Zen carried detailed petrologic studies to the western fringes of New England Taconian metamorphism, first in very low-grade rocks in Vermont, where heavy reliance had to be placed on X-ray diffraction (Zen, 1960; Zen and Albee, 1964), and subsequently in western Massachusetts using electron probe data (Doolan et al., 1978; Zen, 1981). John Green carried out one of the earliest semiquantitative studies of metamorphic phase relations in northernmost New Hampshire (Green, 1963). Notable among the pre-probe studies was that of Arden L. Albee, in the Lincoln Mountain quadrangle, Vermont (1965a) to be visited on the first day of the trip. This was probably one of the most complete pre-probe studies ever done, backed up by oxygen isotope studies (Taylor et al., 1963), and subsequently confirmed by probe analyses (1968) corrected by the "Bence-Albee method" (1968) familiar to all in the business. Robinson and Jaffe (1969a, 1969b; Robinson et al., 1971) attacked the intriguing anthophyllite-gedrite and cummingtonite amphibolites of the Ammonoosuc Volcanics using similar techniques, supported by early probe work by Klein (1968, see this guidebook part G) and X-ray single crystal studies by Papike and Ross (1970; Ross, Papike and Shaw, 1969). This has been followed by an explosion of probe related studies on similar rocks (Stout, 1970; Brady, 1974; Spear, 1977, 1978b, 1980a; Schumacher, 1980, 1981b, 1983; and Hollocher, 1985; this trip parts D, G, and H).

An important part of probe studies has been the ability to study chemical zoning and to relate that zoning to metamorphic reactions and conditions. Examples to be visited on this trip include zoned garnets (Hess, 1969, 1971, part H; Tracy, Robinson, and Thompson, 1976, part H; Spear and Selverstone, 1983, part D; Thompson, Tracy, Lyttle and Thompson, 1977, part E; Chamberlain, 1985, part F; and Roll, 1986, part G) and zoned amphiboles (Laird, 1980, part A; Schumacher, 1983, part H). Quantitative studies were extended by Guidotti (Evans and Guidotti, 1966; Guidotti, 1970, 1974, 1978; Guidotti et al., 1983) and Cheney (Cheney and Guidotti, 1979) into western Maine and by Osberg (1971), Ferry (1976a, 1976b), and Holdaway (Holdaway et al., 1982) in central Maine.

The early oxygen isotopic studies by Albee were used to try to understand the effects and behavior of metamorphic fluids (Taylor et al., 1963). This approach has been expanded in the work of Rumble (1978; Rumble and Spear, 1983, this trip, parts C and D) and Ferry (1979; Ferry and Burt, 1982) to answer important questions concerning the nature and extent of communication between volumes of rock and volumes of metamorphic fluid. Although the results of these studies have not always agreed with Thompson's predictions, the theoretical tools he provided and is providing have proved adequate to each new situation.

Regional Stratigraphic and Structural Setting

The bedrock geology of western and central New England is exposed in three synclinorial belts separated by two major anticlinoria (Figure A-1). From west to east these are the Middlebury synclinorium, the Berkshire-Green Mountain anticlinorium, the Connecticut Valley synclinorium, the Bronson Hill anticlinorium, and the Merrimack synclinorium. In Massachusetts the east margin of the Connecticut Valley synclinorium and the west margin of the Bronson Hill anticlinorium are unconformably overlain by Upper Triassic-Lower Jurassic continental sedimentary rocks and basaltic volcanics localized along a major west-dipping listric normal fault. In Vermont the Green Mountain anticlinorium is cut by the 100 m.y. old Cuttingsville Syenite Complex and the Connecticut Valley synclinorium is cut the 120 m.y. old Ascutney Complex.

The final forms of the synclinoria and anticlinoria were produced by Acadian (Devonian) folding, but the detailed configuration of rock types is a product of both Taconian and Acadian deformations and facies relationships of rocks ranging in age from Upper Precambrian to Lower or Middle Devonian.

The Middlebury synclinorium is entirely underlain by North American Genvillian basement. This is unconformably overlain locally by Eocambrian clastic and carbonate rocks of the Dalton Formation and then by the continuous clean quartz sandstone of the Lower Cambrian Cheshire Quartzite. The Cheshire is the substrate upon which was deposited the extensive North American carbonate bank sequence of dolomites and limestones with subordinate sandstones and shales that ranges in age from Lower Cambrian through uppermost Lower Ordovician, and which was deposited on the then south coast of North America (Laurentia) for a strike length of thousands of kilometers. The carbonate bank sequence was block-faulted and locally eroded even down to basement before being overlain unconformably by a Middle Ordovician carbonaceous flysch sequence with local calcitic limestone at the base. The Middle Ordovician flysch was then tectonically overridden by the lowest and westernmost of the Taconic allochthons, consisting of a starved shale facies of strata from Eocambrian through Middle Ordovician age. We know that the Taconic facies represents a continental slope rise sequence deposited oceanward of the carbonate bank, because it contains local limestone conglomerates and carbonate-cemented clean quartz sands that had their source in the carbonate bank environment or shoreward of it. We also know that the earliest emplacement of the allochthon was during Ordovician graptolite zones 12 and 13, because fossils of these ages can be found in the matrix of a "blocks-in-shale" unit at the top of the Middle Ordovician flysch, containing lithified blocks of nearly all units of the Taconic facies. Unfor-

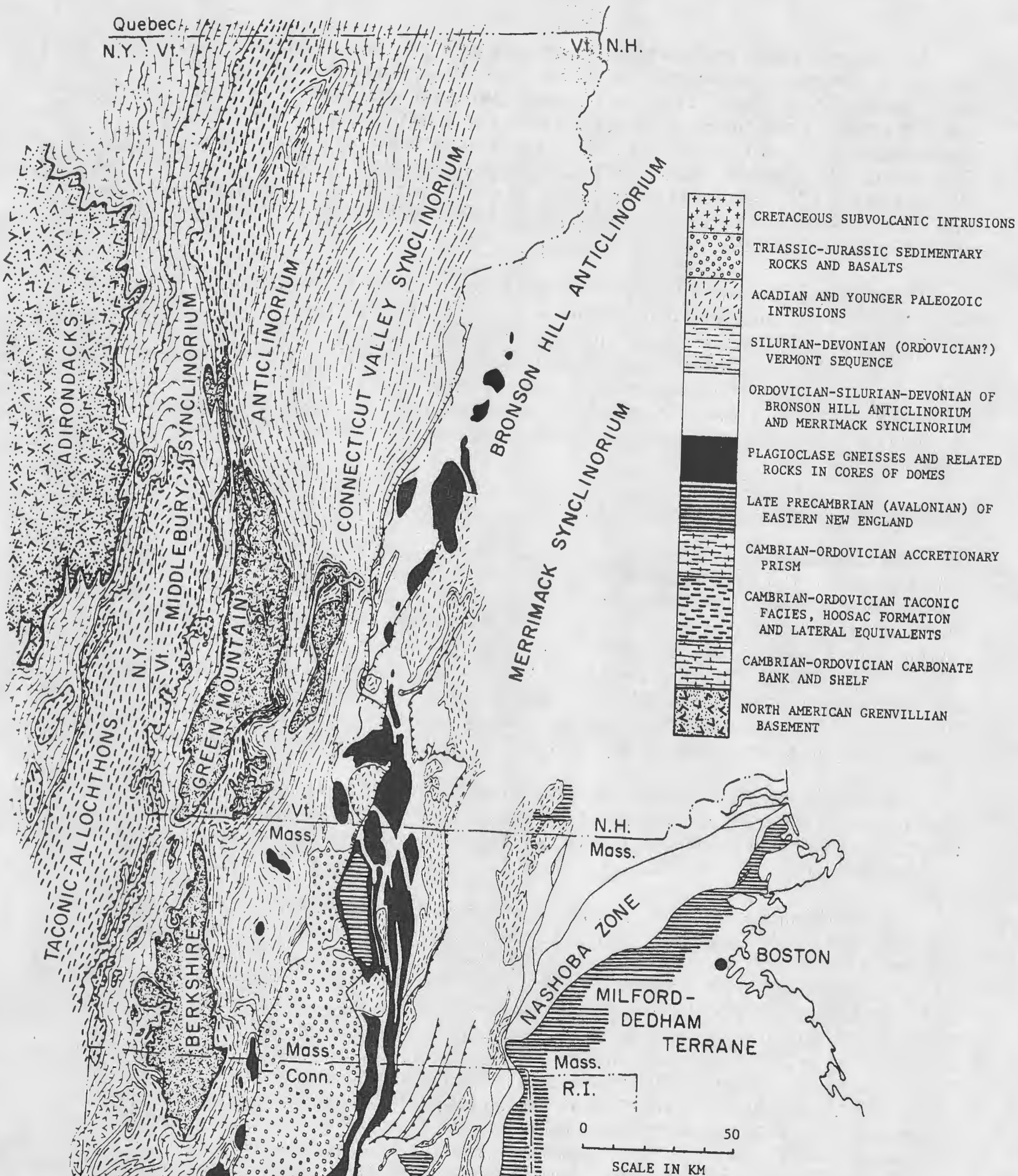
Quebec
N.Y.
Vt.
Vt.
N.H.
CRETACEOUS SUBVOLCANIC INTRUSIONS
TRIASSIC-JURASSIC SEDIMENTARY ROCKS AND BASALTS
ACADIAN AND YOUNGER PALEOZOIC INTRUSIONS
SILURIAN-DEVONIAN (ORDOVICIAN?) VERMONT SEQUENCE
ORDOVICIAN-SILURIAN-DEVONIAN OF BRONSON HILL ANTICLINORIUM AND MERRIMACK SYNCLINORIUM
PLAGIOCLASE GNEISSES AND RELATED ROCKS IN CORES OF DOMES
LATE PRECAMBRIAN (AVALONIAN) OF EASTERN NEW ENGLAND
CAMBRIAN-ORDOVICIAN ACCRETIONARY PRISM
CAMBRIAN-ORDOVICIAN TACONIC FACIES, HOOSAC FORMATION AND LATERAL EQUIVALENTS
CAMBRIAN-ORDOVICIAN CARBONATE BANK AND SHELF
NORTH AMERICAN GRENVILLIAN BASEMENT
ADIRONDACKS
MIDDLEBURY SYNCLINORIUM
N.Y.
Vt.
GREEN MOUNTAIN ANTICLINORIUM
CONNECTICUT VALLEY SYNCLINORIUM
BRONSON HILL ANTICLINORIUM
MERRIMACK SYNCLINORIUM
TACONIC ALLOCHTHONS
BERKSHIRE
Vt.
Mass.
N.H.
Mass.
NASHOBA ZONE
BOSTON
MILFORD-DEDHAM TERRANE
Mass.
Conn.
Mass.
R.I.
0
50
SCALE IN KM

Fig. A-1. Generalized geologic map of northwestern and central New England showing major stratigraphic and structural features.

tunately this "simple" picture is greatly complicated by imbricate thrusting after rocks of the Taconic facies and flysch had been metamorphosed to slate, and by the consequent production of younger tectonic mélanges.

We know that the Taconic facies was deposited east of the west margins of the Grenvillian basement in the Green Mountain and Berkshire anticlinoria, because the base of the Middlebury synclinorium sequence rests unconformably on the Grenvillian in these locations. However, the exact source of the Taconic facies east of this point is much debated. In Vermont, Karabinos (1986), Thompson et al. (1986) and Downie et al. (1986) have described a major shear zone within the Green Mountains between two basement types along which are located fault slivers and tight infolds of Eocambrian to Cambrian rocks of Taconic affinities. They suggest that this synclinal infold may pass entirely beneath the Grenvillian rocks of the eastern part of the Green Mountains and reappear as tectonic windows within the deepest exposed part of the Chester gneiss dome still farther east. In this model the Eocambrian-Cambrian strata deposited unconformably on the Grenvillian basement along the east flank of the Green Mountain anticlinorium and in the outer part of the Chester dome were deposited farther from North America than the Taconic facies. In Massachusetts, Stanley and Ratcliffe (1985) have identified the Hoosac Formation that rests on the Grenvillian basement on the east side of the Berkshires as having been deposited west of the Taconic facies. The Hoosac is in fault contact with still more easterly facies along the Whitcomb summit thrust, which is regarded in Massachusetts as the source region of the Taconic allochthons. Stanley and Ratcliffe suggest that the Whitcomb summit thrust traces along the east margin of the Hoosac Formation in Vermont and is the source region of the Taconic rocks there also, in contradiction to the opinions of Karabinos, Thompson, and Downie.

Most workers throughout the region are in agreement that the Cambrian-Lower Ordovician strata east of the Hoosac Formation in Vermont and Massachusetts belong to a complex accretionary wedge of continental slope and oceanic strata that was caught in an east-dipping subduction zone between North America and an eastern plate during Taconian closing of Iapetus (Stanley and Ratcliffe, 1985). Evidence , best exposed in adjacent Quebec, suggests that one of the earliest events in this closing was the obduction of a then young ophiolite sequence onto the North American continental margin, probably in earliest Ordovician time. One of the distinct problems related to the first day of this field trip is how metamorphosed volcanics in tectonic contact with fragments of this ophiolite were subsequently brought into conditions appropriate for blueschist facies metamorphism and then brought rapidly back near the surface to cool within the Middle Ordovician.

The pre-Silurian rocks of the Bronson Hill anticlinorium, consisting of five major lithic associations, are considered to represent the eastern plate that was overriding the accretionary wedge (Robinson and Hall, 1980; Hall and Robinson, 1982; Zen et al., 1983). The oldest exposed rocks are microcline gneisses, quartzites and related rocks in the interior of the Pelham gneiss dome (Figure A-1) that are interpreted to be a series of metamorphosed rhyolitic volcanics and interbedded sediments of late Precambrian age and show lithic affinities to rocks in southeastern Connecticut interpreted to be part of the Avalon plate. These are overlain by a complicated series of calc-alkaline plagioclase gneisses and amphibolites that may include layered mafic and felsic volcanics, mafic dikes, and gabbroic, tonalitic, and granitic intrusions. These rocks may be as old as late Precambrian, although a popular view is that they represent the Ordovician roots of an island arc. Several of the gneiss domes expose massive granitoid intrusive rocks of the Oliverian series that give apparently reliable Middle Ordovician ages, although discordant intrusive contact relations with the overlying Ammonoosuc Volcanics can rarely be demonstrated. Furthermore, local basal conglomerate and quartzite in Ammonoosuc Volcanics overlying plagioclase gneisses hint of an unconformity at this position. The Ammonoosuc Volcanics have been well characterized as arc volcanics ranging in composition from tholeiitic basalt through andesite and dacite to K-rich rhyolite that give evidence of derivation from melting of mantle or basalt protoliths without significant contributions from continental crust (Aleinikoff, 1977; Schumacher, 1981a, 1983; Leo, 1985). The underlying Oliverian granitic rocks, in contrast, show evidence of a continental heritage (Zartman and Leo, 1984) which has recently been identified as probably of Grenvillian age (Barbara Barreiro, personal communication 1986), supporting earlier suggestions (see Zen et al., 1983) that North American basement may underlie the Bronson Hill belt at depth. Above the Ammonoosuc Volcanics is the Middle Ordovician Partridge Formation dominated by metamorphosed sulfidic black shale with subordinate arc-type volcanics very like those of the Ammonoosuc (Hollocher, 1985). The Partridge has been traced discontinuously northward into northwestern Maine where it contains Middle Ordovician graptolites.

The plagioclase gneisses of the "eastern basement" extend considerably west of the present position of the Bronson Hill anticlinorium and appear from beneath younger cover in a series of gneiss domes in western Massachusetts and Connecticut. In the Bristol dome of Connecticut, Stanley (Hatch et al., 1984)has recognized a tectonic contact where the plagioclase gneisses of the "eastern basement" appear to be thrust above probable uppermost Lower Ordovician strata of the accretionary wedge in his proposed "Bristol thrust". In the Chester dome of Vermont it is possible that the plagioclase gneisses of the Barnard Volcanics also represent "eastern basement" that is thrust over the Moretown Formation of the accretionary wedge in a thrust like the Bristol thrust (see Fig. E-1). If so, then the entire thickness of the Taconian accretionary wedge may be exposed in tectonically thinned fashion on the flanks of the Chester dome (see section E).

The status of the Ammonoosuc Volcanics and Partridge Formation with respect to the proposed Bristol thrust is somewhat equivocal. These units or equivalents form a clear upper part of the sequence on the eastern side, but there is some evidence to suggest that they may also have been deposited on the west side, thus healing over the suture. It is curious in this light to note that the fossil age of the Partridge Formation is virtually identical to the youngest fossil age obtained in the matrix of the "blocks-in-shale" unit beneath the Taconic allochthons.

The Silurian-Devonian cover sequence in the western and central parts of the Connecticut Valley synclinorium has been and continue to be plagued with uncertainties. On the west, a thin sequence of conglomerate and calcareous rocks is traceable into Quebec where there are Silurian fossils, implying a Lower Devonian age for most of the overlying shales, siltstones and calcareous granulites of the Goshen, Northfield, Gile Mountain and Waits River Formations. On the east limb of the synclinorium fossil control is excellent, showing that the basal Clough Quartzite is Lower Silurian (late Llandovery), the calcareous Fitch Formation ranges up into the uppermost Silurian (Pridoli) and that the black shales and sandstones of the Littleton Formation range into the uppermost Lower Devonian (late Emsian). A structural solution to a stratigraphic dilemma in western Massachusetts implies that the lower part of the Littleton Formation is thrust westward for many 10's of kilometers on the proposed Whately thrust over the Gile Mountain and Waits River Formations and implies that these units are at least as young as Lower Devonian (Robinson et al., 1984). In apparent contradiction to this, two graptolite localities found in the last two years, one in Vermont, one in Quebec, indicate a Middle Ordovician age for some of the carbonate-bearing strata (Bothner and Finney, 1986). To further confuse the issue, newly collected plant fossils from an older locality in Quebec about twenty miles along strike from the graptolites indicate a late Lower Devonian age.

Eastward from the Bronson Hill anticlinorium into the Merrimack synclinorium, the thin Silurian section thickens rather abruptly across a "tectonic hinge" into the thick shale and clastic sequence of the Merrimack trough, the post-Taconian sedimentary basin that closed during the initial stages of the Acadian orogeny. Although fossil control in western Maine, New Hampshire and central Massachusetts is poor, lithic correlations with central Maine and thence to relatively fossil-rich Aroostook County are good and lead to a fairly clear picture of sedimentary history. The early and middle Silurian history involved clastic sedimentation with a source in the eroding Taconian orogen to the west. The upper Silurian is dominated by calcareous clastic rocks with a possible contribution from Upper Silurian volcanoes known to have existed to the east. The

Lower Devonian saw a sedimentary source reversal with clastics being shed westward from tectonic lands to the east (Hall et al., 1976), forming deltaic complexes and a marine clastic wedge that prograded westward across the site of the Bronson Hill anticlinorium and beyond.

Eastward from the line of the proposed Bristol thrust there is little or no evidence for severe Taconian deformation or metamorphism, and all major structural features are Acadian or younger. The tightly controlled Silurian-Devonian stratigraphic sequence of the Bronson Hill anticlinorium has allowed delineation of a series of early west-directed fold nappes. More recent delineation of the sequence in the Merrimack synclinorium has made it possible to show that the fold nappes are truncated by slightly younger thrust nappes (P.J. Thompson, 1985; Elbert, 1986) which locally have carried rocks of the synclinorium sequence over the top of the anticlinorium onto its present west limb. The early recumbent folds and thrusts, including both those of the Acadian and those of the Taconian west of the Bristol thrust have been further folded in the later phases of the Acadian orogeny, including the gravitationally induced formation of a series of complex gneiss domes. These domes dominate the Bronson Hill anticlinorium, but are also abundant in the adjacent Connecticut Valley synclinorium and contain a variety of buoyant core rocks ranging from Grenvillian granitic rocks to Ordovician plutons.

Regional Distribution of Metamorphic Zones

Metamorphic zones in the field trip area (Figure A-2) were produced during at least two complex metamorphic cycles, the Taconian and the Acadian. The abundance of pelitic schists throughout the region has made it possible to use the Barrovian sequence of isograd minerals with some modification over a wide area. However, the detailed meaning of these isograds can vary from place to place. For example, the kyanite zone areas in northwestern Vermont (as at Mount Grant, see part B of this guidebook) mainly contain kyanite in pelites of high Al content, commonly associated with chlorite and chloritoid. This is indicative of a much lower metamorphic intensity than the appearance of kyanite in pelites of low Al content, as, for example, in the Littleton Formation of western New Hampshire and central Massachusetts (this guidebook, parts C, D, E, F, and H) where kyanite appears only upon breakdown of the assemblage staurolite + chlorite + muscovite to produce biotite + kyanite. The metamorphic zones shown on Figure A-2 are based on the most intense metamorphism known in Phanerozoic rocks in these areas. The heavy dashed line separates areas where the most intense metamorphism was Taconian to the west from those where it was Acadian to the east (see also Figure B-2). This boundary has been very difficult to delineate and is based mainly on detailed K/Ar studies of metamorphic minerals (Lanphere and Albee, 1974; Sutter, Ratcliffe, and Mukasa, 1985; Lanphere, Laird, and Albee, 1983; Laird, Lanphere, and Albee, 1984) across areas where petrologic distinctions may be difficult or impossible to detect. West of the line there are some examples of what appear to have been Acadian retrograding of higher grade Taconian assemblages (see this guidebook, part B). East of the line, for a short distance, there are local examples of low grade relect assemblages from the Taconian overprinted by higher grade Acadian assemblages (see for example Rosenfeld, 1968; Karabinos, 1984) though this seems to be limited to rocks that belonged to the Taconian accretionary prism. The difficulty and uncertainty of this line are pointed out by the very latest K/Ar work on the peak metamorphic kyanite zone minerals at Mt. Grant (this volume, part B, locality 2) which seems to suggest an Acadian age for this zone, in contradiction both to Figure A-2 and Figure B-2. Detailed studies indicate the Taconian metamorphism was itself polyfacial, particularly as shown by detailed amphibole zoning in northern Vermont (see this guidebook, part B) and also by relict eclogites in southwestern Massachusetts (Harwood, 1979; Maggs, Cheney, and Spear, 1986).

The Acadian metamorphism is divided into distinct western and eastern highs separated by the Connecticut Valley low grade belt that is mainly in the chlorite zone. In northeastern Vermont the western high is of low-pressure facies series with andalusite and local sillimanite zones surrounding a series of cross-cutting Acadian granites. In central and southern Vermont, and western

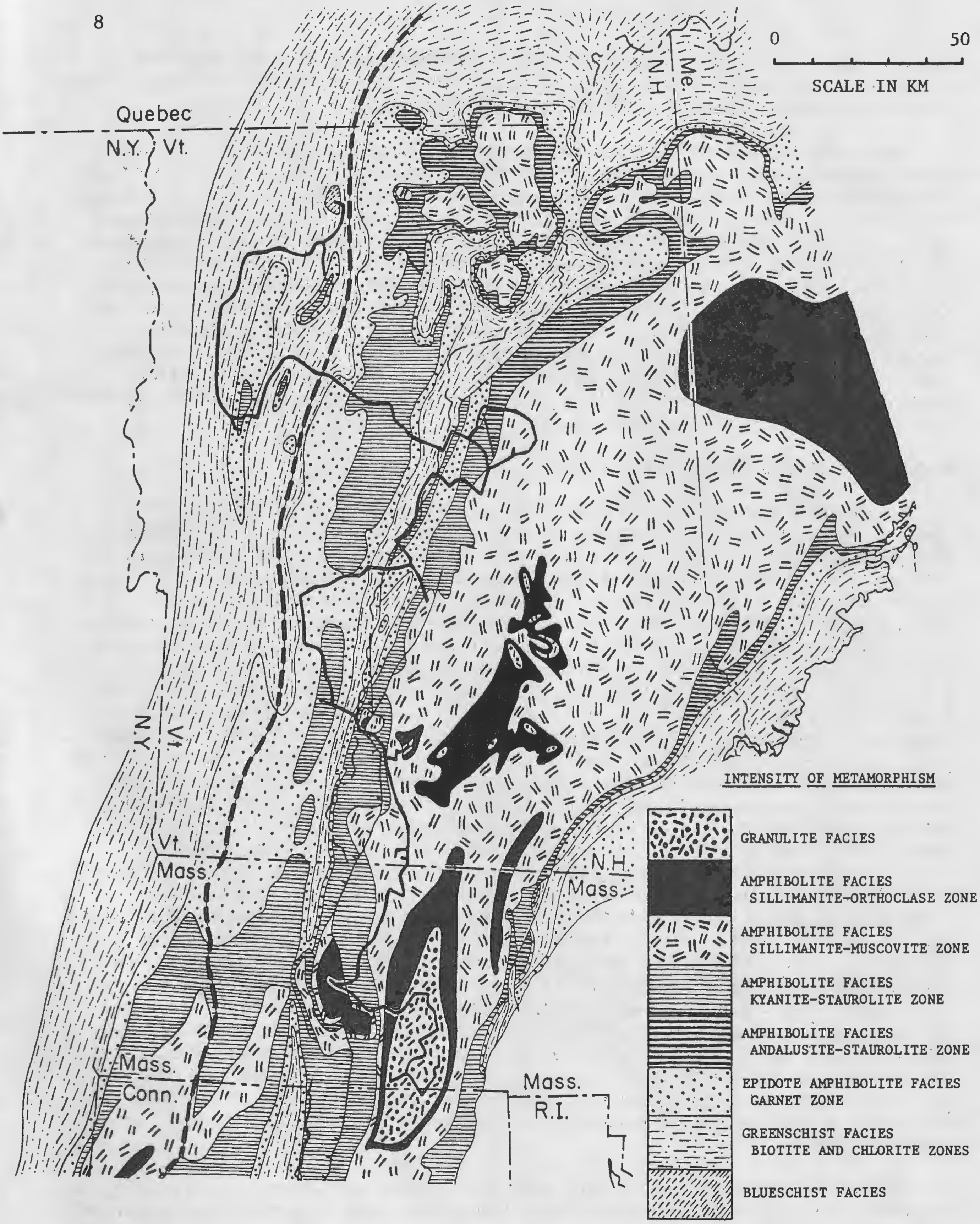
0
50
SCALE IN KM
Quebec
N.Y.
Vt.
N.H.
Me.
N.Y.
Vt.
Vt.
Mass.
N.H.
Mass.
Mass.
Conn.
Mass.
R.I.
INTENSITY OF METAMORPHISM
GRANULITE FACIES
AMPHIBOLITE FACIES SILLIMANITE-ORTHOCLASE ZONE
AMPHIBOLITE FACIES SILLIMANITE-MUSCOVITE ZONE
AMPHIBOLITE FACIES KYANITE-STAUROLITE ZONE
AMPHIBOLITE FACIES ANDALUSITE-STAUROLITE ZONE
EPIDOTE AMPHIBOLITE FACIES GARNET ZONE
GREENSCHIST FACIES BIOTITE AND CHLORITE ZONES
BLUESCHIST FACIES

Fig. A-2. Generalized metamorphic map of northwestern and central New England showing distribution of peak metamorphic assemblages of Acadian and Taconian age. Heavy dashed line separates areas to the east where peak assemblages are Acadian from areas to the west where they are mainly Taconian.

Massachusetts the western high is of intermediate-pressure facies series with kyanite at the highest grade except where there is sillimanite in western Massachusetts and adjacent Connecticut. This metamorphic high is associated with a series of Acadian gneiss domes, and local isograds are subparallel to foliation in the domes as most typically illustrated in the Chester-Athens dome (this guidebook, part E). By contrast, Acadian isograds bear no apparent relationship to exposures of Grenville basement along the Green Mountain Berkshire anticlinorium.

The eastern metamorphic high in New Hampshire, western Maine, and central Massachusetts is dominated by a broad area of sillimanite-muscovite zone rocks locally punctuated by areas with sillimanite-orthoclase assemblages. Recent work (Lux and Guidotti, 1985; Thomson and Guidotti, 1986) indicates that the sillimanite-orthoclase zone in western Maine may be related to contact effects of the late Paleozoic Sebago Pluton. In southwestern New Hampshire and south-central Massachusetts there are nine small areas and one large area characterized by sillimanite-orthoclase-garnet-cordierite assemblages. Although the characterizing pelitic assemblage is the same in all these areas, the peak metamorphic minerals appear to be late tectonic in southwestern New Hampshire (this guidebook part F) but heavily overprinted by later deformations in southern Massachusetts (this guidebook part H).

The western margin of the eastern high is complex and will be the focus of considerable attention on this fieldtrip. In northern New Hampshire this high is bordered by andalusite-bearing rocks. Further south conditions were close to those of the Al-silicate triple point (this guidebook, part C, especially Figure C-1). At the latitude of Bellows Falls (this guidebook, part F) pelitic rocks at high structural levels contain evidence of early andalusite with subsequent kyanite and sillimanite, and rocks containing sillimanite pseudomorphs after andalusite are rather widespread (Figure F-3) east of the gneiss domes, even in the sillimanite-orthoclase-garnet-cordierite zones. By contrast, pelitic rocks close to the interior of the gneiss domes were in a kyanite-sillimanite facies series on the east side of the domes (this guidebook, parts E and G), or remained in the kyanite zone on the west side. It is apparent from a wide range of studies completed or in progress (this guidebook parts C, D, E, F, G, and H) that the pattern and history of metamorphism along the west margin of the eastern Acadian metamorphic high, including several preserved metamorphic overhangs, was related to a complex thermal evolution involving early fold nappes, widespread syntectonic plutonic sheets, later thrust nappes, and still later gneiss domes. The pattern in central Massachusetts is further complicated by the thermal anomaly of the late Acadian (380 my.) Belchertown Intrusive Complex, which heated local strata above ambient kyanite zone conditions during Acadian dome-stage deformation.

Taconian Metamorphism in the Context of Plate Tectonics

Taconian metamorphism in western New England appears to have been limited to the region where the eastern North American continental margin, its cover, and the related accretionary wedge were subducted beneath the eastern plate (Stanley and Ratcliffe, 1985). The metamorphism was obviously polyfacial with the earliest high-P, low-T phase extremely difficult to study, but the details have been and will continue to be difficult to decipher, particularly because the highest grade rocks were heavily overprinted during the Acadian. In the uppermost (i.e. Middle Ordovician) strata overlying the eastern part of the accretionary wedge and in the Middle Ordovician rocks of the eastern plate, there is little or no evidence of any Ordovician metamorphism more intense than the Acadian metamorphism in immediately overlying Silurian-Devonian strata, which are locally at chlorite grade. However, in some pre-Middle Ordovician strata there is evidence of older metamorphism. This is particularly true in the Late Precambrian rocks of the Pelham Dome (Robinson et al., 1975; Roll, 1986,) where there is evidence of a pre-Acadian metamorphism of medium-pressure granulite facies, the age of which is presently unknown.

Acadian Metamorphism in the Context of Plate Tectonics

Interpretation of Acadian metamorphism in the context of plate tectonics is made difficult by the lack of evidence for a pre-existing oceanic tract near the locus of most intense deformation and metamorphism between the Bronson Hill anticlinorium and the region around Boston where late Precambrian and Cambrian strata remain little metamorphosed. There is, however, abundant evidence for the development of a Silurian marine basin, the Merrimack trough, filled with a thick clastic sequence that was covered over by Lower Devonian flysch at the beginning of the Acadian orogeny (Hall et al., 1976). A model favored by some (Chamberlain, 1986; Spear, 1986; Robinson et al., 1986) is that the Merrimack trough was formed by late Ordovician-Silurian crustal extension parallel to the west margin of a single eastern (Avalon) plate in the back-arc region of the previous Middle Ordovician volcanic arc system. Crustal thinning provided a region for high heat flow into the bottom of the sedimentary pile, a favorable environment for the emplacement of a variety of mafic to felsic plutons, and an appropriate setting for early low pressure (Buchan) phases of metamorphism and partial melting. It is suggested that this earlier phase was overprinted by higher pressure assemblages caused by tectonic burial by thrust sheets from the east and, at least in central Massachusetts, that the rocks with those peak metamorphic assemblages were subsequently involved in imbricate thrusting with development of mylonites, that carried part of the tectonic assemblage westward over the present site of the gneiss domes. Indeed, the Bronson Hill domes may have been localized near the east edge of thick Bronson Hill basement, itself possibly overlying Grenvillian basement, where the basement has been most heavily loaded by thrust sheets from the east. In such a model the Connecticut Valley metamorphic low may represent an H_2O-rich thermal blanket or wedge separating the effects of tectonically superimposed hot rocks from the east, from the effects of isotherms moving upward perpendicular to foliation planes, as shown by isograd patterns surrounding the Vermont line of gneiss domes (compare Figs. A-1 and A-2).

Editor's Acknowledgements

This volume would not have been possible without the vision and dedication of various leaders and authors over a period of eighteen months. A special indebtedness is owed to Associate Editor David C. Elbert whose computer expertise, ability to handle files from diverse sources, and sound geologic understanding, made possible most of the final editing and conversion to a distinctive and compact type format. Use of a laser printer at Smith College was made possible through the cooperation of Professors John Brady and Robert Newton. Several figures were drafted with the usual capable assistance and expertise of Marie Litterer. Several graduate and undergraduate students, in particular Margie Roll, Peter Panish, Dave Finkelstein, George Springston, and Henry Berry, IV donated their typing skills or other talents at a time when permanent secretarial staff was at a very low ebb. Particular thanks are also due to Professor John T. Cheney, who followed the concept of this field trip from the beginning, and pitched in at the last minute in the logistical and editorial aspects of part E. The work of the editor and students over the years as well as that of many of the other trip leaders was greatly assisted by grants from the National Science Foundation, Programs for Crustal Structure and Tectonics, and for Petrogenesis.

B. METAMORPHISM IN THE NORTHERN GREEN MOUNTAINS OF VERMONT

Jo Laird and Wallace A. Bothner

INTRODUCTION AND OBJECTIVES FOR THE DAY

During this field trip we shall visit two localities in the State of Vermont where combined field, structural, petrologic, and isotopic studies have been made (Loc. 1 and 2, Fig. B-1). The first locality is one of the few places in the Northern Appalachian Mountains where high-pressure facies series metamorphism is preserved (Laird and Albee, 1981a). Glaucophane occurs in both mafic and pelitic rocks; omphacite + garnet occur in the mafic rocks. The rocks were metamorphosed during the Taconian Orogeny (Middle Ordovician) and presumably record the closing of the Iapetus Ocean.

The second stop is the kyanite-chloritoid locality where Albee (1965a) documented different pelitic assemblages in rocks of different bulk composition. Albee (1965b) used this ensemble of mineral assemblages as a starting point for a petrogenetic grid for pelitic schist. Nearby mafic schists indicate medium-pressure facies series metamorphism. These rocks may have been metamorphosed during the Acadian Orogeny (Middle Devonian).

We hope to spend sufficient time at each locality so that the different mineral assemblages and structural relationships can be seen. At the first stop we will traverse along a stream and a trail that is often wet. Therefore, sturdy rubber boots or shoepacs are better than vibram sole boots. Either vibram sole boots or shoepacs will be good for the second locality which involves a hike through the woods to ledge-forming outcrops. The change in elevation is about 1400 feet at Locality 1 and 600 feet at Locality 2.

Unfortunately, the two localities are about 80 miles apart. If enthusiasm wanes or time is short, there are two alternative stops that can be made. A) At Elmore Mountain (EM, Fig. B-1) pelitic rocks contain kyanite pseudomorphed by white mica ± chloritoid and garnet pseudomorphed by chlorite + magnetite. Hornblende is overgrown by actinolite in mafic rocks. The high grade metamorphism is Ordovician, and the low grade metamorphism is Devonian. Medium-pressure facies series metamorphism is preserved here in distinction to the high-pressure facies series metamorphism at Locality 1 and the medium-high-pressure facies series metamorphism to the south and west (Fig. B-2). B) Another locality of mineralogic and petrologic interest in northeastern Vermont is a roof pendant in the Lake Willoughby pluton (LW, Fig. B-1) where Thompson (1975) describes calc-silicate diffusion zones between marble and pelitic schist.

STRATIGRAPHIC AND STRUCTURAL SETTING

Billion year old gneisses, referred to as North American or Grenville basement, underlie much of the State of Vermont. Felsic and mafic gneisses crop out in the core of the Green Mountain Anticlinorium (GMA) in south-central Vermont and in gneiss domes in southeastern Vermont (Fig. B-1). Overlying the basement, both unconformably and in fault contact, are metamorphosed felsic, pelitic, and mafic rocks of the GMA, some of which we will see on this field trip, which represent eugeoclinal deposits of the Iapetus Ocean. Ultramafic rocks occur on the east limb of the GMA. South of locality 1 ultramafic rocks have mantle affinities based on Nd-Sm isotopic studies (Shaw and Wasserburg, 1984).

West of the eugeoclinal rocks which compose the GMA are weakly metamorphosed carbonates and quartzite which define the edge of the Ordovician (Taconian) continental margin. East of the GMA, and within the Connecticut Valley-Gaspé Synclinorium (CVGS) are metamorphosed calcareous, mafic, and pelitic rocks intruded by peraluminous granite (Fig. B-1).

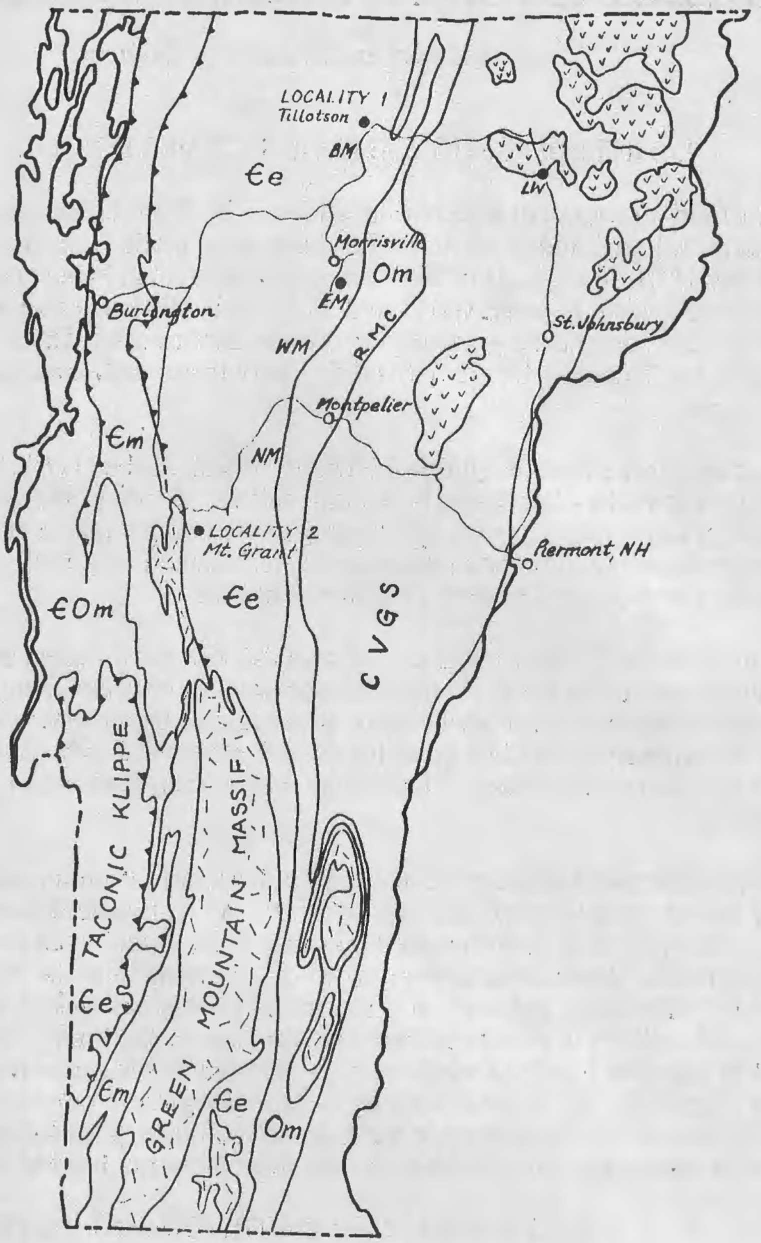
LOCALITY 1
Tillotson
BM
€e
LW
Morrisville
Om
EM
Burlington
St. Johnsbury
WM
RMC
Montpelier
€m
NM
LOCALITY 2
Mt. Grant
Piermont, NH
€Om
€e
CVGS
TACONIC KLIPPE
GREEN MOUNTAIN MASSIF
€e
€m
€e
Om

Figure B-1. Generalized geologic map of Vermont (Doll et al., 1961) showing route from Burlington to Localities 1 and 2, and to alternative stops at Elmore Mountain (EM) and Lake Willoughby (LW). WM, Worcester Mountains; NM, Northfield Mountains; BM, ultramafic body at Belvidere Mountain; randon dashes, Precambrian basement; checks, Devonian granites; €e, Cambrian eugeoclinal rocks; €m, Cambrian miogeoclinal rocks; €Om, Cambro-Ordovician miogeoclinal rocks; Om, Ordovician Moretown Formation; CVGS, Ordovician and Silurian rocks of the Connecticut Valley-Gaspe synclinorium; RMC, zone between the Taconian Orogen and the CVGS.

Fossil control on protolith ages of the eugeoclinal section in north-central Vermont is meager. Cady (1968 and references therein) bases the stratigraphic age assignments on correlations of fossiliferous Cambrian and Ordovician slates in southern Quebec and northwestern Vermont with similar but more intensely deformed and metamorphosed rocks in central Vermont. Until recently it was interpreted that these rocks dictated the stratigraphic ages of the next "underlying and overlying" units. If, however, these units are allochthonous (see below), this interpretation may not be correct. In fact, the only control we have on the protolith ages of the eugeoclinal rocks is that they are younger than the basement (1 Ga) and older than Taconian metamorphism (~470 Ma). Fossiliferous Silurian strata mark the boundary between the eugeoclinal section and the rocks of the CVGS. However, a simple stratigraphic succession above the Silurian seems no longer tenable because of recent reconfirmation of earlier recognized Ordovician graptolites in the basal unit of the CVGS (Bothner and Finney, 1986).

Except for the Taconic klippe in southwestern Vermont, contacts between units in the GMA were generally interpreted until the last decade to be stratigraphic and rocks folded into anticlinoria and synclinoria. Stanley and Ratcliffe (1985) have reinterpreted the eugeoclinal rocks to have been emplaced in an accretionary prism by east over west thrust faults between lithotectonic packages. They recognize stratigraphic continuity within individual lithotectonic packages. Interpretation of deep seismic reflection profiles in Vermont and Quebec suggest that some of the Grenville basement is also allochthonous (Ando et al., 1983; St. Julien et al., 1983) Mineral assemblages, lithologies, and structural relationships seen at and in the vicinity of Locality 1 support the presence of a Taconian subduction zone with east over west thrusting and, locally, with simultaneous or later rotation by folding about approximately east-west axes.

DISTRIBUTION AND AGE OF METAMORPHIC ZONES

Metamorphism in north-central Vermont ranges from biotite to kyanite grade with the highest grade in the cores of anticlinoria (Fig. B-2a). High- pressure facies series metamorphism is preserved at Locality 1. Medium-high- pressure facies series metamorphism is preserved over a much larger area based on the presence of NaM_4-rich amphibole in mafic schist. Elsewhere in north-central Vermont medium-pressure facies series metamorphism is recognized. In northeastern Vermont low-pressure facies series metamorphism ranges from biotite to sillimanite grade, increasing in grade toward peraluminous granites of the New Hampshire plutonic series (Fig. B-2b). $^{40/39}$Ar total fusion and stepwise heating ages on amphibole presented by Laird et al. (1984) show that high, medium-high, and medium-pressure facies series metamorphism in north-central Vermont is Ordovician, about 470 Ma. A 500 Ma $^{40/39}$Ar stepwise heating age on amphibole from mafic schist associated with the large Belvidere Mountain ultramafic body south of Locality 1 (BM, Fig. B-1) suggests that these mafic rocks were metamorphosed before being thrust along with the ultramafic rocks into their present position.

Rb/Sr whole rock ages on peraluminous granite associated with low- pressure facies series metamorphism in northeastern Vermont are Devonian (380 Ma, Naylor, 1971). The Acadian Orogeny responsible for this low-pressure facies series metamorphism caused retrogradation of Taconian assemblages farther west. Lanphere and Albee (1974) reported a 363 Ma plateau $^{40/39}$Ar age on muscovite pseudomorphous after kyanite and a 444 Ma plateau age on muscovite preserved in a quartz vein from the same locality (WM, Fig. B-1). A $^{40/39}$Ar total fusion age on magnesio-hornblende is 463 Ma, and a discordant $^{40/39}$Ar age spectrum on zoned amphibole (magnesio-hornblende overgrown by actinolite) north along the same (apparently) anticlinorial structure (EM, Fig.1) gives a plateau age of 470 Ma and an apparent age of 376 Ma for the first 36% of the ^{39}Ar released at 750°C. (The IMA amphibole nomenclature of Leake, 1978 is used throughout this field guide.)

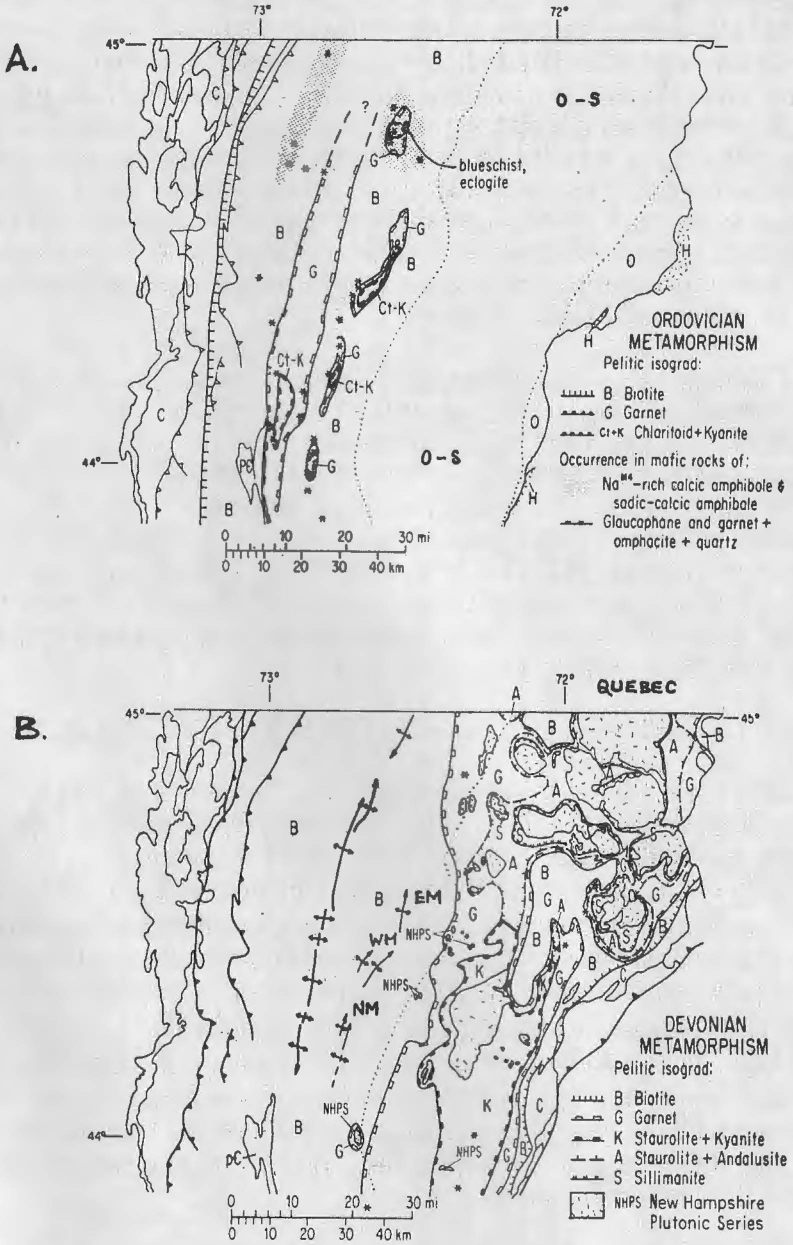
A.
73°
72°
45°
44°
B
O-S
blueschist, eclogite
G
Ct-K
C
H
O
pC
0 10 20 30 mi
0 10 20 30 40 km
ORDOVICIAN METAMORPHISM
Pelitic isograd:
B Biotite
G Garnet
Ct+K Chloritoid+Kyanite
Occurrence in mafic rocks of:
Na^{M4}-rich calcic amphibole & sodic-calcic amphibole
Glaucophane and garnet + omphacite + quartz
B.
QUEBEC
A
K
S
EM
WM
NM
NHPS
DEVONIAN METAMORPHISM
Pelitic isograd:
B Biotite
G Garnet
K Staurolite + Kyanite
A Staurolite + Andalusite
S Sillimanite
NHPS New Hampshire Plutonic Series

Figure B-2. Isograd and facies series maps for Ordovician (Taconian) and Devonian (Acadian) metamorphism in northern Vermont after Doll et al. (1961) and Laird et al. (1984). Symbols are on the high-grade side of isograds. In (A) stipple pattern delimits areas metamorphosed at medium-high-P; blueschist and eclogite at Locality 1 indicate high-P metamorphism. Dotted line – RMC (Taconian Line); C – chlorite zone; H – Ordovician felsic plutonic rocks; EM, Elmore Mountain; WM, Worcester Mountains; NM, Northfield Mountains.

How far west Devonian metamorphism occurs in northern Vermont is a matter of current debate that is being addressed by ongoing isotopic studies. M. A. Lanphere (U.S.G.S. pers. comm. 1986) obtained a 381 Ma total fusion age on actinolite south of Locality 1 and a 390 Ma incremental heating age (flat spectrum) on muscovite from Locality 2. Laird et al. (1984) reported 385 Ma $^{40/39}$Ar total fusion ages on biotite and muscovite from Locality 2, and Lanphere et al. (1983) reported similar $^{40/39}$Ar total fusion ages on biotite (387 Ma) and hornblende (382 Ma) from mafic schist 2 miles to the north. Unlike the kyanite grade rocks farther east (EM, WM, NM, Fig. B-1), kyanite is not retrograded at Locality 2. Therefore, the high grade metamorphism here may be Devonian and not Ordovician (as indicated on Fig. B-2a).

METAMORPHISM OF MAFIC ROCKS

Metamorphosed mafic rocks in Vermont are greenschist when associated with biotite grade pelitic schist and epidote amphibolite to amphibolite when associated with garnet and higher grade pelitic schist. In general the protolith appears to be pyroclastic or epiclastic. Pillow structures are seen locally both within the eugeoclinal rocks of the Taconic orogen and in the Connecticut Valley - Gaspe Synclinorium. Dikes are recognized in the unit labeled Om on Figure B-1 and are also thought to occur at Locality 1.

The mafic rocks are composed primarily of amphibole, chlorite, epidote, plagioclase, and quartz. An Fe-oxide and Ti-phase are usually present, generally magnetite and titanite in greenschist and hematite/ilmenite ± rutile in amphibolite. A carbonate, calcite and/or ankerite, and a K-mica (white mica or biotite) are commonly present. In Fe-rich rocks stilpnomelane occurs in greenschist and garnet occurs in amphibolite. Omphacite occurs in the high-pressure facies series mafic rocks at Locality 1. In greenschist the amphibole is actinolite; some grains have barroisite cores. At higher grade, hornblende, some with actinolite cores and some with actinolite rims, occurs. Barroisite, glaucophane, actinolite, and hornblende are all seen at Locality 1.

Within the assemblage amphibole + chlorite + epidote + plagioclase + quartz, minerals vary systematically in composition with the metamorphic grade of intercalated pelitic schist and with metamorphic facies series (Laird and Albee, 1981b). As in many worldwide occurrences of mafic schist, increasing metamorphic grade results in increasing $NaAlSi_{-1}$ in amphibole and $Al_2Mg_{-1}Si_{-1}$ in amphibole and chlorite. $NaSiCa_{-1}Al_{-1}$ increases in amphibole but decreases in plagioclase (see Thompson, 1981 for a discussion of exchange vector notation). Amphibole increases in mode while modal epidote and chlorite decrease.

Of the three independent net-transfer reactions necessary to explain these variations in mineral composition and mode, the following two proceed from left to right (as written, CaO - MgO - Al_2O_3 - SiO_2 - H_2O system) with progressive metamorphism:

$$\text{Albite} = 4\ \text{Quartz} + NaAlSi_{-1} \tag{1}$$

and

$$7\ \text{Clinochlore} + 12\ \text{Clinozoisite} + 14\ \text{Quartz} = 12\text{Tremolite} + 25\ AlAlMg_{-1}Si_{-1} + 22\ H_2O \tag{3}$$

The third independent net transfer reaction,

$$\begin{aligned}22\ \text{Albite} + 2\ \text{Clinochlore} = 5\ \text{Tremolite} + 15\ AlAlMg_{-1}Si_{-1} + 22\ NaSiCa_{-1}Al_{-1}\\ + 6\ \text{Clinozoisite} + 7\ \text{Quartz}\end{aligned} \tag{2}$$

proceeded from left to right (as written) to explain the high-pressure glaucophane schist assemblages at Locality 1 (Fig. B-3). However, reaction (2) proceeded from right to left (as written) during low-pressure facies series metamorphism in northeastern and east-central Vermont (units labeled Om, Fig. B-1; O-S, Fig. B-2) because the increase in anorthite content "dominated" the reaction. (Thompson et al.,1982, present a discussion of the theory involved in writing these reactions and in constructing the reaction space of Fig. B-3).

In the reaction space of Figure B-3 mafic schists from southeastern Vermont which have been metamorphosed at medium-pressure facies series (biotite to staurolite - kyanite zone) lie along the horizontal axis (reaction 3 above). Samples from north-central Vermont, that lie in between the high- and the medium-pressure facies series samples, have amphibole with cores of barroisite or NaM_4-rich actinolite. The locations of these samples are shown on Figure B-2a. Elsewhere in north-central Vermont (e.g. north of Locality 2 and at EM, Fig. B-1), medium-pressure facies series metamorphism occurred.

Amphibole grains are commonly optically and chemically zoned, complicating the interpretation of the petrology and regional geology, but making it interesting. Hornblende overgrown by actinolite at Elmore Mountain (EM, Fig. B-1) is interpreted to represent Ordovician metamorphism overprinted by Devonian metamorphism (see the previous section). A similar metamorphic history may also explain barroisite overgrown by actinolite; however, detailed structural studies by Stanley et al. (1984) and Stanley and Ratcliffe (1985) indicate that growth of both core and rim compositions occurred during the Taconic Orogeny. Amphibole from mafic schist north of Locality 2 is zoned from ferro-hornblende to ferro-tschermakitic hornblende and to ferro-tschermakite, probably recording progressive metamorphism during one "event".

At Locality 1 (Stop 1) barroisite cores are discontinuously overgrown by rims which vary continuously in composition from actinolite to actinolitic hornblende (Figs. B-4 and B-5, Table B-3, sample ABM100). Barroisite also occurs as inclusions in garnet and as cores within glaucophane rims. Glaucophane also occurs as separate grains and as cores with acinolite rims. Figure B-6 shows the compositions of the various amphibole pairs at their mutual contacts. It is suggested that the glaucophane - barroisite and glaucophane - actinolite pairs represent miscibility gaps and that the barroisite - glaucophane pair formed at an earlier time (how much earlier is not known) and higher temperature. It is unclear if the barroisite - actinolite compositions define a miscibility gap, and the relative effects of kinectics and polymetamorphism are not yet understood. Rims are zoned outward to compositions in between the gaps (Figs. B-4 and B-5, Table B-3), and the compositions across the core - rim contacts are quite different for different grains and for different areas within the same grain (Fig. B-6).

METAMORPHISM OF PELITIC SCHIST

Albee (1968) summarized the progressive metamorphism of pelitic schist in northern Vermont based on the data compiled by Doll et al. (1961) and on his own work. Table 1 lists and Figure B-7 illustrates the pelitic assemblages reported from northern Vermont in rocks of the Taconic Orogen and in rocks of the CVGS, west and east, respectively, of a zone historically referred to as the RMC (the Taconian Line of Hatch, 1982). Figure B-2 is a compilation of metamorphic isograds, believed to represent Ordovician and Devonian metamorphism (except for the possible exception of Locality 2, see section 3). In north-central Vermont Taconian garnet grade metamorphism is inferred to have extended farther north than is indicated by the presence of garnet porphyroblasts or matrix grains because almandine-rich garnet is present as inclusions in plagioclase porphyroblasts.

Kyanite zone metamorphism along the Green Mountain anticlinorium (Mt. Grant, Locality 2) probably occurred at a lower temperature than kyanite zone metamorphism along the Northfield/Worcester/Elmore Mountains (NM, WM, EM, Figs. 1 and 2) because garnet + chlorite is stable at locality 2 and kyanite + biotite and locally staurolite + biotite occur in the latter area

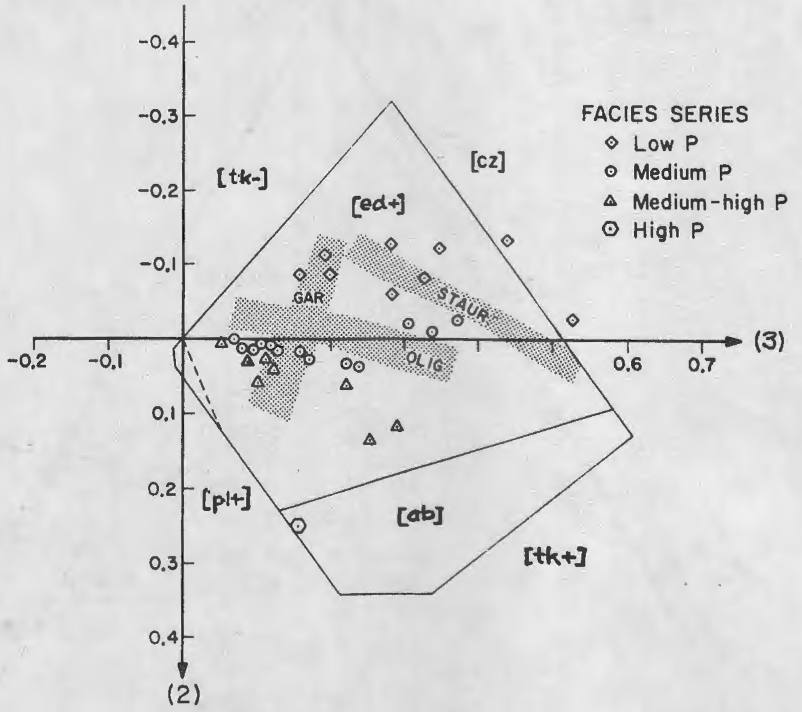

Figure B-3. Reaction polyhedron for mafic schist in Vermont showing advancement along reactions (2) and (3) in the text (after Thompson et al., 1982; Laird et al., 1984). GAR and STAUR bands separate mafic samples intercalated with biotite (closest to the origin), garnet, and staurolite grade pelitic rocks. Plagioclase in the mafic schist is albite below the OLIG band and oligoclase to anorthite above the band. Faces bounding the polyhedron are epidote out [cz]; plagioclase out [ab]; minimum and maximum $Al_2Mg_{-1}Si_{-1}$ in amphibole and chlorite [tk-] and [tk+], respectively; maximum $NaSiCa_{-1}Al_{-1}$ in amphibole and plagioclase [pl+], maximum and minimum $NaAlSi_{-1}$ in amphibole [ed+] and base of polyhedron, respectively.

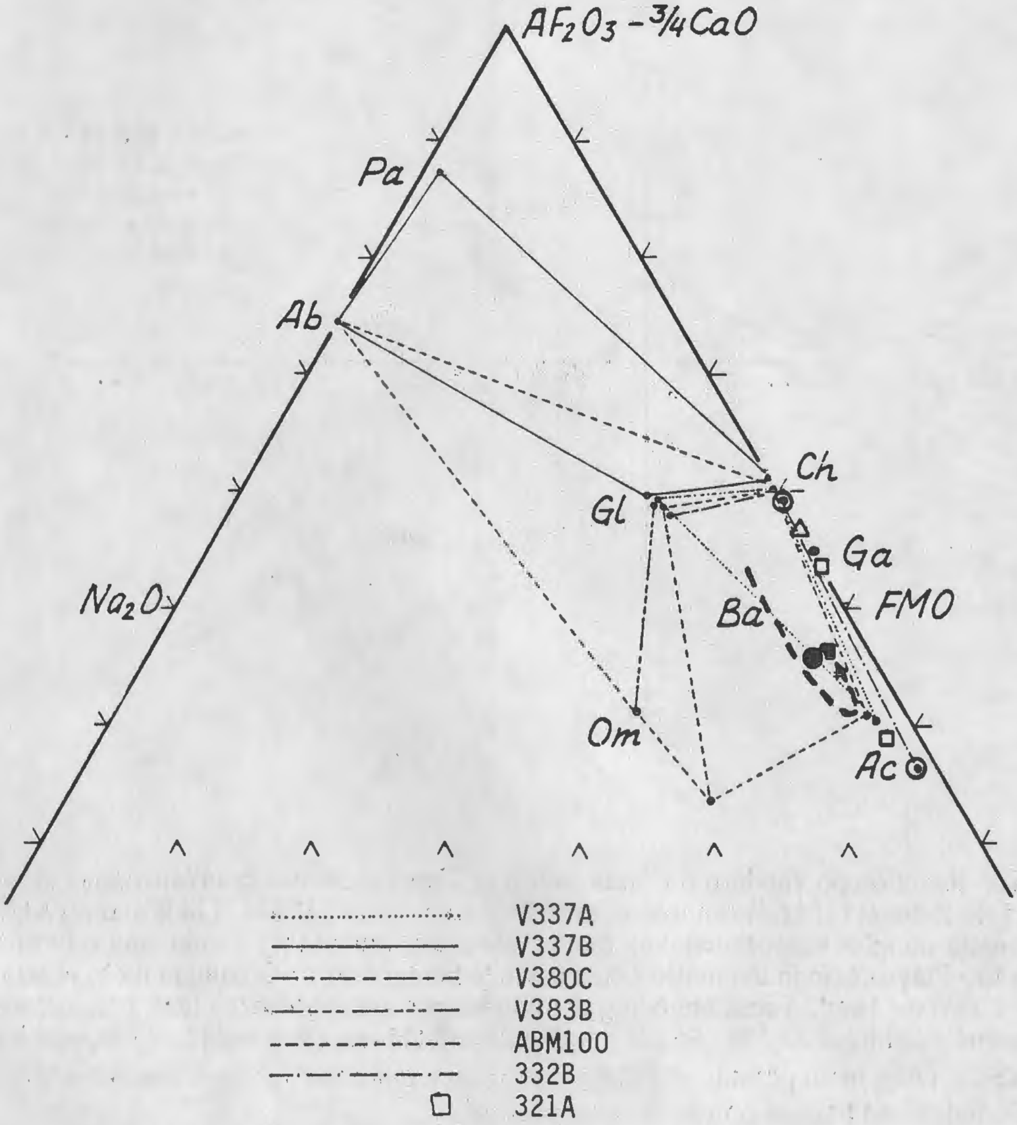

Figure B-4. Mineral assemblages from the Tillotson area, Vermont (locality 1) shown on a quartz + epidote projection onto Al_2O_3+Fe_2O_3, Na_2O, and FeO+MgO+MnO (mol units). Tie lines to garnet eliminated for clarity. Points are reprsentative electron microprobe analyses and for clarity are not distinguished by sample, except for samples 332B (circle), 321A (square), and other garnet analyses (ABM100 and 380C, triangle; V337A, solid dot). Filled symbols represent core compositions of amphibole in 332B and 321A. Dashed arrow shows zoning of sodic-calcic/calcic amphibole in ABM100. Sample locations on Figure B-8: V337 (Tillotson Peak), V380 (north of trail between Stops 2A and 3), V383 (Tilltson Pond), ABM100 (Stop 1), 332 (Stop 3), 321 (Stop 2A). Ab (albite), Ac (actinolite), Ba (barroisite), Ch (chlorite), Ga (garnet), Gl (glaucophane), Om (omphacite), Pa (paragonite).

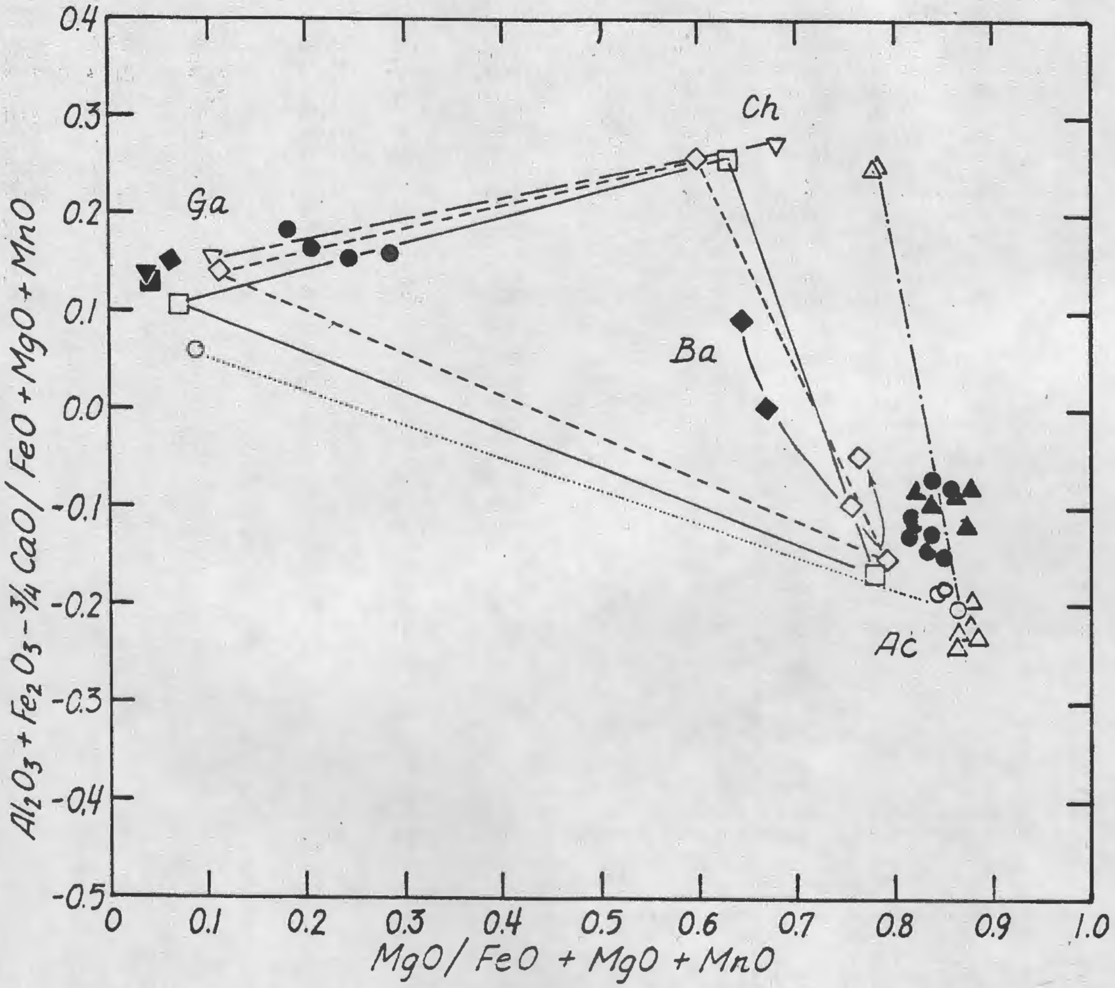

Figure B-5. Representative chlorite (Ch), garnet (Ga), and amphibole (Ba, barroisite; Ac, actinolite) compositions (mol units) from the Tillotson area, Vermon (Locality 1). Glaucophane compositions project on top of chlorite compositions. Circles (321A), squares (V337A), diamonds (ABM100), triangles (332), inverted triangles (V380C). Arrows shows zoning in sodic-calcic/calcic amphibole from ABM100. Sample locations as in Figure B-4.

Table B-3A. Representative electron microprobe analyses from mafic schist, Lockwod Brook, Tillotson ARea, Vermont (Locality 1, Stop 1, ABM 100)*

	Na/Ca-Am		Ca-Am			Na-Am			Ch	EP	
	core	core	rim	rim	rim	core	core			core	
SiO_2	48.00	50.96	53.51	54.97	52.43	57.46	56.82	57.59	26.43	37.84	38.82
Al_2O_3	12.55	9.26	5.78	3.74	6.83	10.78	10.66	11.15	19.35	24.05	26.95
Cr_2O_3	0.09	0.04	0.02	0.01	0.11	0.11	0.02	0.0	0.0	nd	nd
TiO_2	0.37	0.21	0.08	0.06	0.11	0.0	0.04	0.01	0.04	0.06	0.11
MgO	10.70	12.04	14.75	16.32	14.18	9.92	10.35	10.33	18.30	0.0	0.02
FeO_{Total}	14.02	13.43	11.98	11.41	12.86	11.12	11.84	10.82	22.24	10.84	8.26
MnO	0.07	0.07	0.04	0.08	0.11	0.02	0.02	0.07	0.30	0.04	0.03
CaO	8.29	8.42	9.64	10.65	9.37	0.90	2.55	1.20	0.03	23.66	23.93
Na_2O	3.67	3.36	2.27	1.52	2.40	6.93	6.05	6.70	0.01	nd	nd
K_2O	0.39	0.17	0.18	0.12	0.21	0.02	0.02	0.0	nd	nd	nd
F	0.0	0.13	0.0	0.08	0.34	0.07	0.0	0.01	0.0	0.0	0.0
Cl	0.0	0.0	0.0	0.0	0.0	0.0	0.0	0.0	0.02	nd	nd
Total	98.16	98.04	98.27	98.94	98.82	97.30	98.37	97.89	86.72	96.57	98.22

	Pl	Ga	Ga	Px	Cc	Wm	Tt	Mt
SiO_2	68.16	38.12	38.44	55.65	nd	50.67	30.57	0.06
Al_2O_3	19.28	20.39	21.30	8.93	nd	25.96	0.99	0.0
Cr_2O_3	nd	0.0	0.01	0.07	nd	nd	nd	0.03
TiO_2	0.0	0.17	0.06	0.03	nd	0.20	39.13	0.05
MgO	0.02	1.11	1.97	8.19	0.53	3.56	0.0	0.0
FeO_{Total}	0.12	22.08	28.11	6.69	0.89	2.77	0.46	93.37
MnO	nd	8.31	0.84	0.03	0.77	0.05	0.13	0.0
CaO	0.17	10.66	11.39	14.44	52.68	0.0	29.09	nd
Na_2O	11.49	nd	nd	6.25	nd	0.34	nd	nd
K_2O	0.03	nd	nd	nd	nd	10.58	nd	nd
F	nd	nd	nd	nd	nd	0.0	0.07	nd
Cl	nd	nd	nd	nd	nd	0.0	nd	nd
Total	99.27	100.85	102.13	100.28	54.87	94.16	100.41	93.52

Table B-3B. Representative electron microprobe analyses from mafic schist, Frank Post Trail, Tillotson Area, Vermont (Locality 1, Stop 3, 332B)*

	Ca-Am		Ch	EP	
	core	rim		core	rim
SiO_2	50.96	56.41	27.66	39.65	39.53
Al_2O_3	9.05	2.29	19.87	32.49	31.55
Cr_2O_3	0.06	0.0	0.26	nd	nd
TiO_2	0.25	0.03	0.03	0.05	0.04
MgO	17.32	19.52	24.93	0.07	0.08
FeO_{Total}	6.38	6.27	12.26	1.07	2.10
MnO	0.09	0.20	0.14	0.04	0.0
CaO	10.76	11.68	nd	24.88	24.19
Na_2O	2.71	0.99	nd	nd	nd
K_2O	0.06	0.05	nd	nd	nd
Total	97.64	97.45	85.15	98.25	97.49

*For zoned minerals analyses are ordered left to right from grain interiors to grain exteriors. Grains are optically discontinuous if analyses are annotated as core or rim.

Am (amphibole), Cc (calcite), Ch (chlorite), Ep (Epidote), Ga (Garnet), Mt (Magnetite), Pl (Plagioclase), Px (Pyroxene), Tt (Titanite), WM (White Mica).

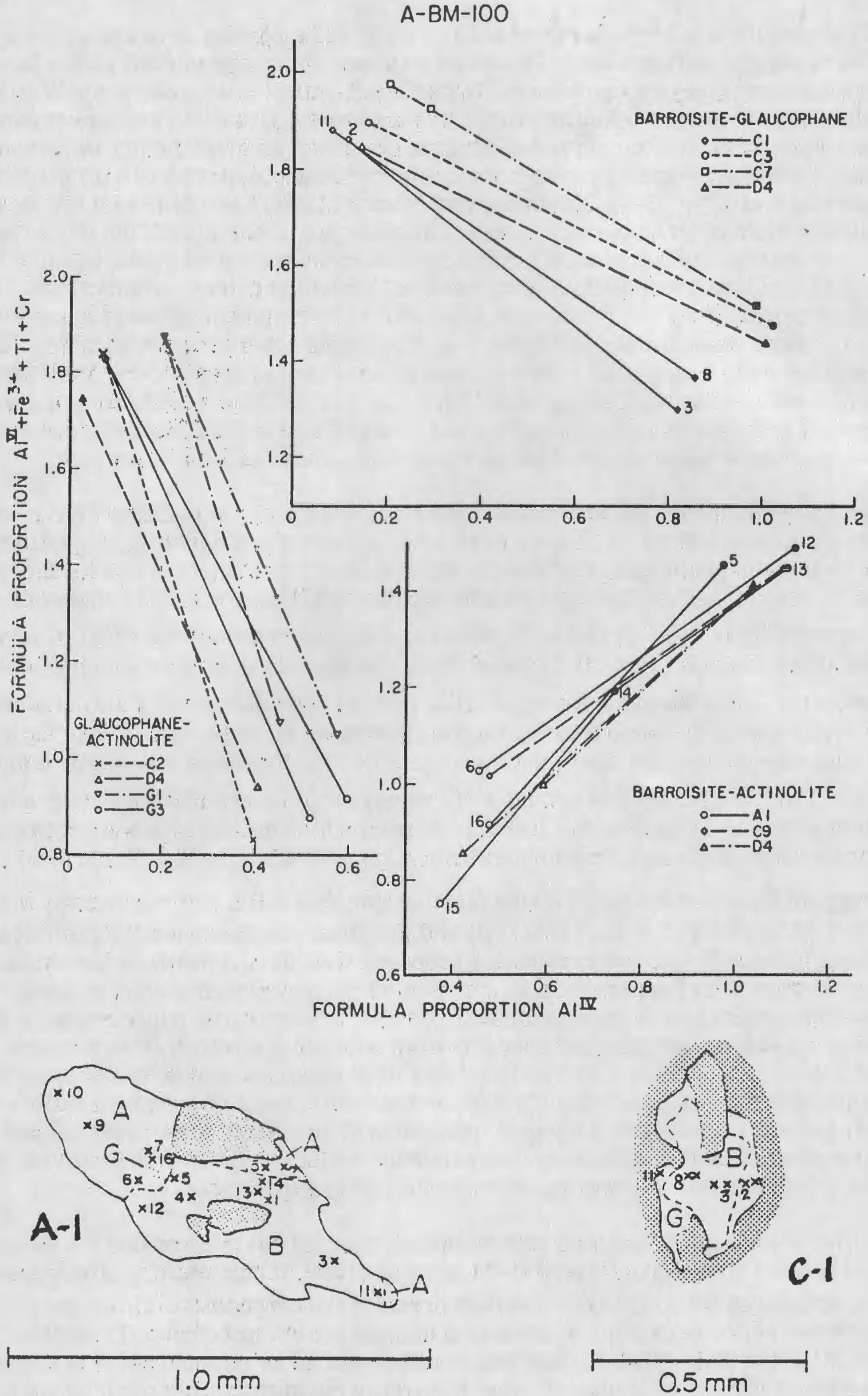

Figure B-6. Composition of barroisite, glaucophane, and actinolite at their mutual contacts in sample ABM100 (Stop 1). Numbered points keyed to the line drawings for grains A-1 and C-1. Stipple – epidote, A – actinolite, B – barroisite, G – glaucophane. Representative analyses in Table 3.

(Fig. B-7). Staurolite has been identified at Locality 2, but it appears to be stabilized by ZnO (nearly 2% by weight, Albee, 1968). These two areas are also distinguished by the fact that the kyanite grade assemblages appear to be fairly stable at Locality 2, whereas in the Worcester and Elmore Mountains kyanite is pseudomorphed by muscovite ± chloritoid and garnet is retrograded to chlorite + magnetite. Andalusite and sillimanite occur in high grade pelitic assemblages from northeastern Vermont, whereas kyanite is the aluminosilicate polymorph in high grade pelitic schist to the south and west (Fig. B-2). Thompson and Norton (1968) have delimited the location of the aluminosilicate triple point isobar in this area. The rocks are also distinct from those farther west in that they show metamorphism after deformation. The rocks are not so pelitic as some farther west (Albee, 1968), and bulk compositions are generally "below the garnet - chlorite join". The mineral assemblages reported from NE Vermont indicate that metamorphism occurred at pressures below the [Ct,C] invariant point shown on Figure B-7. Chloritoid + biotite are not stable. Therefore, pressure was not so low as is seen in low-pressure facies series rocks in New York and adjacent Vermont, Massachusetts, and Connecticut (Fig. B-7). It is not clear whether or not the assemblages reported at the present erosion surface at Locality 2 and in the Elmore/Worcester/Northfield Mountains represent a metamorphic path above or below the [Ct,C] invariant point.

Mineral assemblages in metamorphosed pelitic to felsic rocks at Locality 2 have been studied extensively by Albee (1965a) and Taylor et al. (1963). During geologic mapping of the Lincoln Mountain 15-minute quadrangle (Cady et al., 1962) Arden Albee discovered a locality where several pelitic assemblages compatible with respect to the Thompson (1957) projection occurred in different layers (Fig. B-7, Table B-1). Taylor et al. (1963) determined the $\delta^{18}O$ of several minerals within these samples (Table B-2) and showed that regardless of the mineral assemblage, the $\delta^{18}O$ values were nearly the same for a particular mineral and consequently the delta(mineral A - mineral B) values were the same for mineral pairs. Because the delta values were the same, they concluded that oxygen isotopic equilibration occurred within the rocks at the same temperature. Taylor et al. (1963) suggested that similar $\delta^{18}O$ values could be explained by oxygen exchange and equilibration across layering over the 200 m zone from which the samples were collected, perhaps by exchange with an H_2O-rich fluid in communication with all the rocks. Some local control on $\delta^{18}O$ of the pore fluid was indicated by the fact that sample LA10k had consistently higher $\delta^{18}O$ values than LA10q (0.1 to 0.3 ‰, Table B-2) and that these samples were the farthest apart (in the field) of those collected. Another explanation proposed was that the minerals may have continued to exchange oxygen with the pore fluid as temperature decreased so that each mineral, regardless of mineral assemblage, had its 18-oxygen ratio "frozen in" at a particular temperature. Albee (1965a) reported major and trace element compositions from coexisting minerals from the same samples studied by Taylor et al. (1963). Chemical analyses were obtained on minerals separated by the Frantz magnetic separator, heavy liquids, and, as necessary, hand picking by a variety of techniques: gravimetric analysis, emission spectroscopy, and X-ray fluorescence. Later Albee (1968) reported electron microprobe analyses (nonautomated instrument) that provide more data on Fe-Mg-Mn values and allow one to examine mineral zoning in garnet.

From the isotopic, chemical, and textural data Albee (1965a) inferred that the mineral assemblages at Locality 2 could have formed at the same pressure, temperature, and aH_2O and that the different assemblages are a manifestation of different rock composition. However, crossing tie lines occur when all the coexisting mineral assemblages are illustrated on a Thompson projection. Albee (1965a) noted that analytical error and error introduced by not being able to completely remove and/or correct for inclusions of other minerals were probably not sufficient to completely explain the crossing tie lines. Albee (1965a showed that in both garnet zone and kyanite zone assemblages the more Mn present in the rock the greater Mg/(Mg+Fe) is for coexisting garnet + chlorite and garnet + biotite. Therefore, crossing tie lines on the Thompson projection may be due in part to the fact that Mn is not considered.

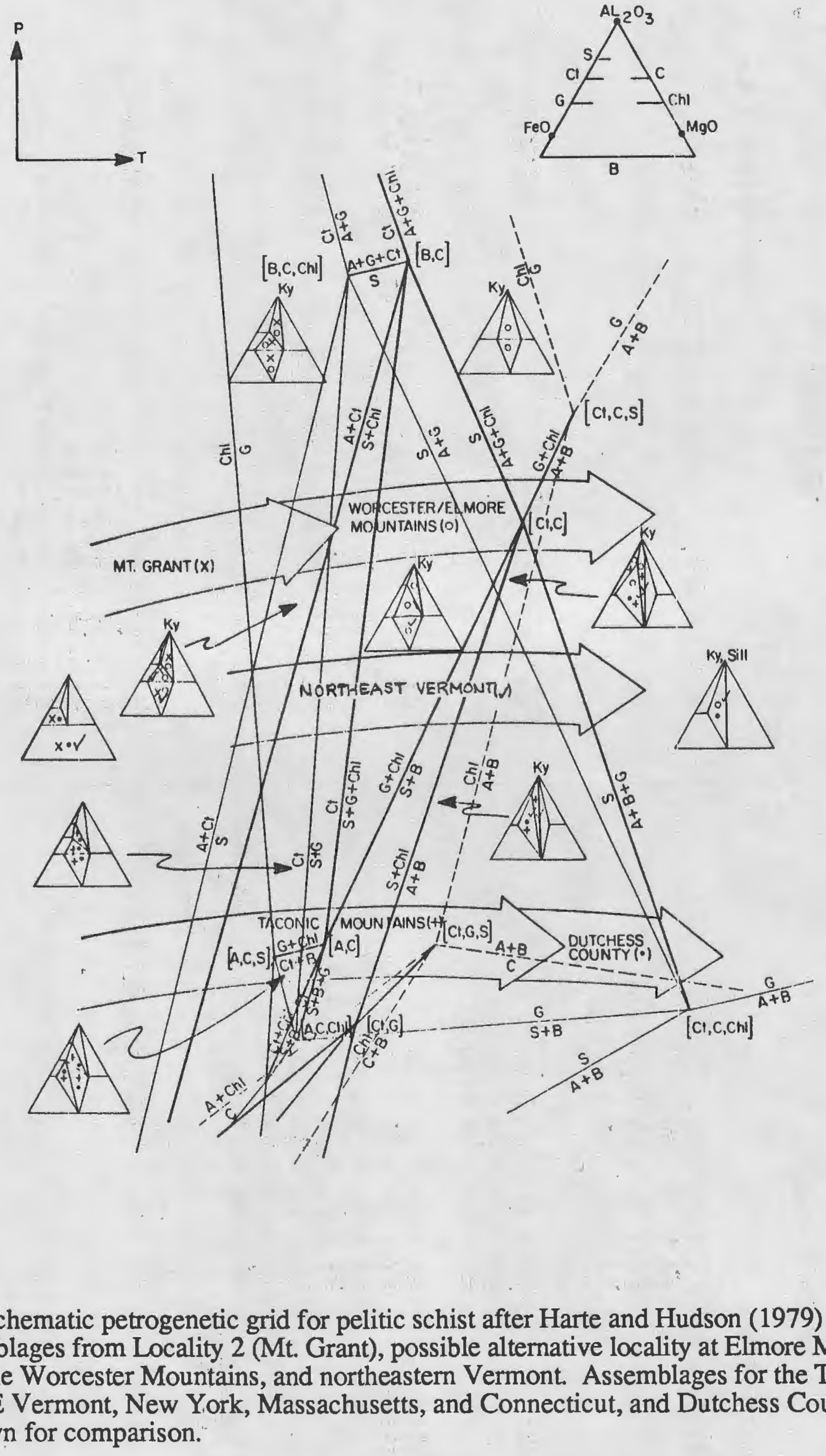
P
T
AL2O3
S
Ct
G
C
Chl
FeO
MgO
B
[B,C,Chl]
Ky
Ct A+G
Ct A+G+Chl
A+G+Ct S
[B,C]
Chl G
Ky
G A+B
[Ct,C,S]
Chl G
A+Ct S+Chl
S A+G
S A+G+Chl
G+Chl A+B
WORCESTER/ELMORE MOUNTAINS (o)
[Ct,C]
MT. GRANT (X)
Ky
Ky
Ky
Ky, Sill
NORTHEAST VERMONT (√)
x•√
Chl A+B
Ky
Ct S+G+Chl
G+Chl S+B
A+Ct S
Ct S+G
S+Chl A+B
S A+B+G
TACONIC MOUNTAINS (+)
[Ct,G,S]
A+B C
DUTCHESS COUNTY (•)
[A,C,S]
G+Chl Ct+B
[A,C]
S+B+G
[A,C,Chl]
[Ct,G]
G S+B
G A+B
[Ct,C,Chl]
S A+B
Chl C+B
A+Chl C

Figure B-7. Schematic petrogenetic grid for pelitic schist after Harte and Hudson (1979) showing mineral assemblages from Locality 2 (Mt. Grant), possible alternative locality at Elmore Mountain and south in the Worcester Mountains, and northeastern Vermont. Assemblages for the Taconic Mountains, SE Vermont, New York, Massachusetts, and Connecticut, and Dutchess County, New York are shown for comparison.

TableB-1. Mineral Assemblages (all with muscovite and quartz) in pelitic schist from Northern Vermont based on the data of Albee (1968) and Woodland (1965)*

Taconic Orogen

Metamorphic Grade		
Biotite	Ct + Ch + Pa	
	Ch + Pa + Ab	
	Ch + Ab ± Ga (w/in Ab)	
	Bi + Ch + Ab ± Ks	
Garnet	Ga + Ct + Ch + Pa	
	Ga + Ch + Pa + Ab	
	Ga + Bi + Ch + Ab	
Chloritoid-Kyanite	Ga + Bi + Ch + Ab	loc. 2
	Ky + Ct + Ch + Pa	
	Ga + Ct + Ct + Pa	
	Ky + Ct + Ch	EM, WM, NM prograde
	Ky + Ct + Ga + Ch	
	Ky + Ct + Ga + Ch	
	Ky + Ga + Ch	
$\frac{\text{Ga + Ch}}{\text{St + B, Ky + B}}$		
	Ky + Ga + Bi	
	Ky + St + Ga + Bi + Ch	

NE Vermont

		Metamorphic Grade
Bi + Ch + Pl		Biotite
Ga + Bi + Ch + Pl		Garnet
Ga + Bi + Ch		Staurolite - Andalusite/Kyanite
	$\frac{\text{Ga + Ch}}{\text{St + Bi}}$	
Ga + St + Bi		
St + Bi + Ch		
	$\frac{\text{St + Ch}}{\text{An/Ky + Bi}}$	
An/Ky + St + Bi		
An/Ky + Ga + St + Bi		
Bi + An		Sillimanite
Bi + St + An + Si + Pl		
Bi + St + Ga + Si + Pl	? $\frac{\text{St}}{\text{An/Si + Bi + G}}$	
Bi + An + Si ± Ga + Pl		
Bi + Ga + Si + Pl		

*Ab (Albite), An (Andalusite), Bi (Biotite), Ch (Chlorite), Ct (Chloritoid), Ga (Garnet), Ks (K feldspar), Ky (Kyanite), Pa (Paragonite), Pl (Plagioclase), Si (Sillimanite), St (Staurolite).

EM, WM, NM (Elmore, Worcester, Northfield Mountains. Probable prograde assemblages)

Table B-2. $^{18}O/^{16}O$ valves ($^{0}/00$) for minerals from pelitic schist, near Mt. Grant Vermont (loc. 2) from Taylor et al. (1963)

Mineral/Sample*	LA10q	LA10p	LA10k	LA10t
Quartz	16.0	15.9	15.7	15.8
Albite	13.9			
White Mica†	12.0	11.9	11.9	
Chlorite	9.2	8.9	9.0	
Biotite	8.9			
Ilmenite	6.8	6.6		

*Sample AL10q is from the Underhill Fm., LA10p from the base of the Mt. Abraham Schist, and LA10k from a glaciated outcrop of the Mt. Abraham Schist (see Table 4 for estimated modes).

† Muscovite for LA10p and LA10k; muscovite and paragonite for LA10p.

Albee (1965a) inferred that the conditions of metamorphism at Locality 2 were about 550°C and 11 kbar based on the muscovite - paragonite solvus geothermometer of Zen and Albee (1964) and the presence of kyanite and of muscovite + quartz. The muscovite - paragonite geothermometer of Eugster et al. (1972) gives a temperature of 480°C, and the oxygen isotope data of Garlick and Epstein (1967) give a temperature of 440°C using the calibrations of Friedman and O'Neil (1977). This temperature is nearly the same as that reported by Laird and Albee (1981b) for a garnet zone mafic rock north of Locality 2 (475 to 520°C, calcite - dolomite geothermometry). More recent experimental data on the aluminosilicate phase diagram by Holdaway (1971) allows a much lower pressure (minimum of about 5 kbar at 550°C and 3.5 kbar at 450 °C). This pressure is consistent with medium-pressure facies series metamorphism as indicated by mafic schist to the northeast (see previous section).

FIELD TRIP ITINERARY

Cumulative mileage from the Sunset Motel/Charlemont Restaurant, Morrisville, Vermont

0.0	Sunset Motel, turn west (right) on Rts. 100/15
1.8	Junction Rts. 100/15, turn north on Rt. 100. New road cuts are rusty weathering, carbonaceous and sulfidic schists of the Ottauquechee Formation.
7.0	Junction Rts. 100 and 100C to Johnson. Stay on Rt. 100 to the north through North Hyde Park.
11.4	Intersection of Rts. 100 and 118, Eden, Vt., continue N on 100 to Eden Mills.
12.7	Intersection of Rt. 100 and North Road, Eden Mills. Turn left (N) onto North Road.
14.4	View of Belvidere Mountain, Eden and Belvidere asbestos dumps to the west. Chidester et al. (1978) present detailed maps and discussion of this ultramafic body.
16.4	Entrance to the Belvidere Mountain asbestos mine (Vermont Asbestos Group, VAG). Dump and open pit are obvious. Belvidere Mountain amphibolite is exposed beneath the fire tower at the top of the mountain (500 Ma, Laird et al., 1984).
17.9	Dirt road (driveway) to the left (west) to the base of the Frank Post Trail.
18.4	Park beyond Jack Stark's house on the old logging road heading north. The trail heads west initially parallel to Lockwood Brook. Follow the hike to Tillotson Camp.

A Hike to Tillotson Camp, Locality 1

This area was mapped in reconnaissance by Cady et al. (1963). Because of the regional implications of the discovery of glaucophane and omphacite here (Laird and Albee, 1981a), we have undertaken a detailed field mapping project at Locality 1 and are continuing petrologic and isotopic studies. Figure B-8 shows a synthesis of our mapping and the traverse we will make. This traverse affords a good opportunity to see both mafic and intercalated pelitic rocks and to sample several mineral assemblages illustrated in Figures B-4 and B-5.

Follow the road log to the base of the Frank Post Trail (elev. ~1370') and park. (If you are following this field trip guide at a later time, permission may be obtained from Mr. Jack Stark, who lives in the house at the base of the trail to park your vehicle.) Proceed NW along an overgrown, old logging road that follows Lockwood Brook. There is another road that is much less overgrown and is a continuation of the gravel road taken to the house. This is NOT the trail.

Initially the trail is over sometimes muddy glacial till, and it is necessary to hike up hill for about an hour (slow, steady pace) to get to the first outcrop. Above about 2000 feet in elevation outcrop is very good. The pace and compass geologic map in Figure B-8 will help you find the outcrops. We have marked several stops which include several outcrops. The group is large and we hope that the group will be spread out enough to avoid "stepping on each other."

Approximate distance from base and elevation (in feet):

500 (~1410) Fork in trail. Keep right, away from the brook; following the trail marked by a blue blaze.

2950 (~1650) Trail intersects and crosses a small brook.

6235 (~2000) Large tree across trail.

Continue uphill on Frank Post Trail (blue blaze) and take either route A or route B to Lockwood Brook. The routes will be marked for this trip. The following directions should help people using this guide later.

6780 (~2100) Route A. The trail reaches a fairly open, flat area at the base of a steep section of trail. There is a small drainage coming in from the north. Two down trees may still be apparent. A rock in the trail is marked with two arrows pointing SW. Proceed into the woods ~S20W 330 feet to Lockwood Brook at the base of Stop 1.

7030 (~2150) Route B. A rock with a blue blaze in the trail is marked with an arrow pointing SW and labeled 84-10. (This is not the blue blaze on the vertical face of a rock just above A.) Proceed into the woods about 100 feet ~S40W to Lockwood Brook near the top of Stop 1.

Stop 1 (~2030 to 2150) [Sample ABM100] Continuous outcrop in stream for about 300 feet. PLEASE be careful. There is plenty of outcrop, but the rock is SLIPPERY, ESPECIALLY when wet and covered with moss.

The rock is primarily gray-brown weathered, bluish gray-green, well layered (<1cm to ~10 cm), massive to foliated, fine- to medium-grained amphibolite composed of amphibole + carbonate + chlorite + epidote + garnet + plagioclase + titanite + phengite + magnetite + apatite ± omphacite ± pyrite ± chalcopyrite. Table 3 gives representative mineral analyses. Glaucophane occurs in most samples and is commonly pseudomorphed by a fine- grained symplectite composed of chlorite + plagioclase + white mica ± calcic amphibole. Omphacite occurs locally (e.g., 25 feet up from the base of the exposure and at the top of the falls) and is also pseudomorphed by a fine-grained symplectite.

Also present at this outcrop are minor pelitic layers. A 35 cm thick layer near the bottom of this outcrop contains garnet porphyroblasts up to a cm across. Above this layer is about a 40 cm thick layer of phengite + quartz + garnet + chlorite + titanite + magnetite + apatite ± glaucophane schist with black, pod-like masses flattened within the plane of the foliation. These pods (clasts?) are composed primarily of magnetite + quartz + plagioclase and may represent iron-rich concretions. Epidote grains are locally Mn^{3+}-rich judging from the pink pleochroism.

Figure B-8. Preliminary geologic map of the Tillotson Peak and Haystack Mountain area, north-central Vermont, and pace and compass map of the Lockwood Brook area along the Frank Post and Long Trails. Numbers refer to stops described in text.

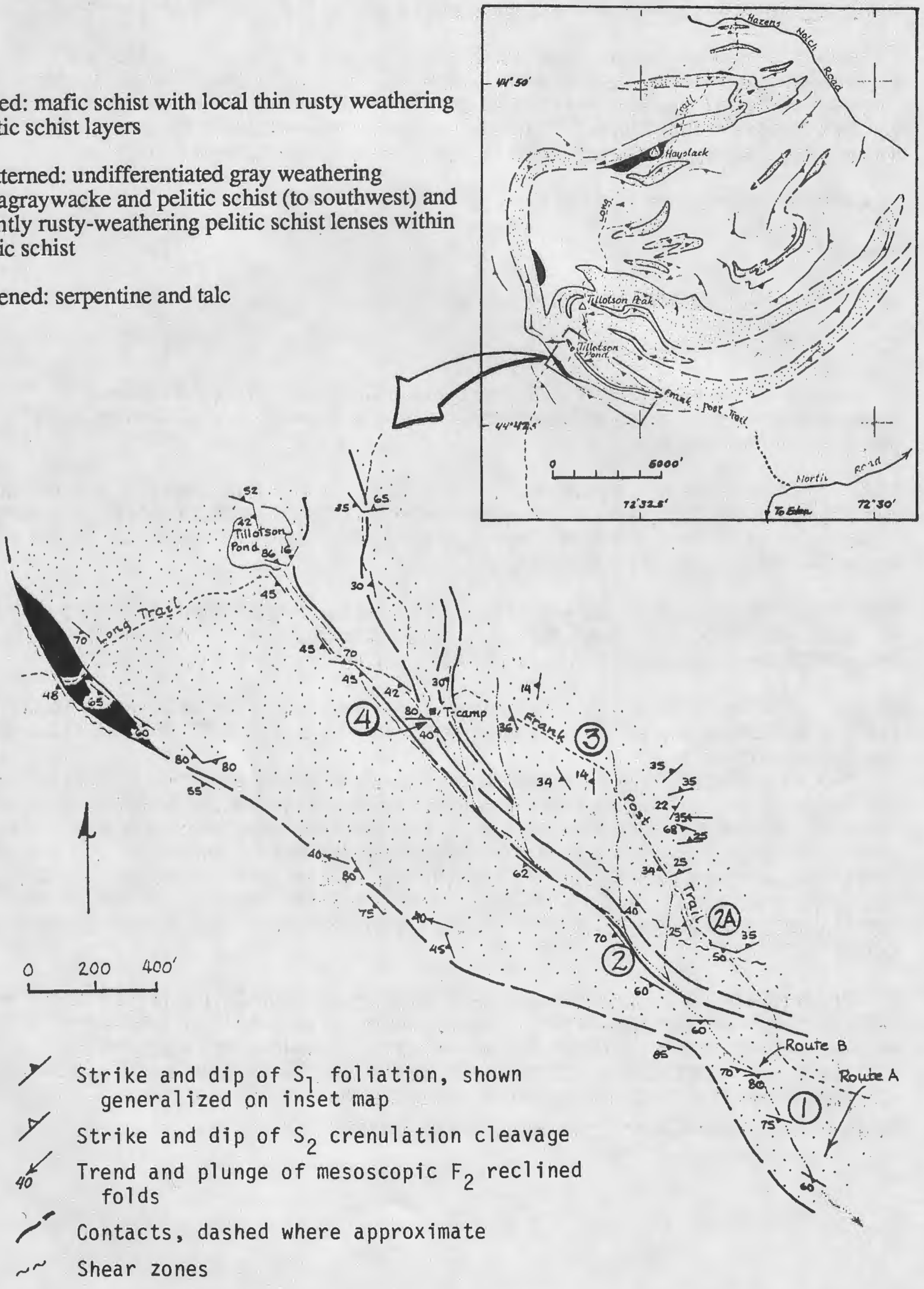
Hazens Notch Road
Trail
Haystack
Long Trail
Tillotson Peak
Tillotson Pond
Frank Post Trail
44°50'
44°47.5'
0
5000'
North Road
To Eden
72°32.5'
72°30'
52
42
Tillotson Pond
86
16
45
35
65
30
70
Long Trail
45
70
45
42
30
14
48
65
60
80
T-camp
40
36
Frank
4
3
80
80
55
34
14
35
35
Post
22
35
68
25
40
80
62
34
25
Trail
75
40
45
40
70
25
2A
35
50
2
60
60
85
Route B
70
80
Route A
1
75
60
0
200
400'
40

Stippled: mafic schist with local thin rusty weathering pelitic schist layers

Unpatterned: undifferentiated gray weathering metagraywacke and pelitic schist (to southwest) and slightly rusty-weathering pelitic schist lenses within mafic schist

Blackened: serpentine and talc

Strike and dip of S_1 foliation, shown generalized on inset map

Strike and dip of S_2 crenulation cleavage

Trend and plunge of mesoscopic F_2 reclined folds

Contacts, dashed where approximate

Shear zones

Multiple periods of mineral growth and of deformation are nicely shown in this outcrop. Zoned amphibole with barroisite cores overgrown by rims zoned outward from actinolite to actinolitic hornblende (Table B-3, Figs. B-4 and B-5, Sample ABM100) may record a decrease in temperature followed by an increase in temperature of metamorphism. If omphacite formed at the same time as barroisite, the first period of metamorphism is estimated to have occurred at 500 °C and 11 kbar based on garnet - pyroxene geothermometry and isopleths on the reaction albite = jadeite + quartz. As discussed under "Metamorphism of Mafic Rocks" compositions of barroisite and glaucophane and of actinolite or actinolitic hornblende and glaucophane may define miscibility gaps.

One sample of pelitic schist contains inclusions of glaucophane within garnet. Fine-grained pseudomorphs may thus be after glaucophane. Alternatively, these pseudomorphs may have replaced barroisite, perhaps explaining why discontinuously zoned garnets in this sample have Ca-richer rims than cores.

Over this nearly continuous outcrop, layering attitudes remain fairly constant. Early F1 isoclinal folds occur locally on surfaces normal to layering. Warps in main foliation are related to mesoscopic F2 reclined folds. At the top of Stop 1 layering in mafic schist is locally discordant, a feature that may be interpreted as a premetamorphic fault or an originally cross-cutting relationship.

Continue upstream toward Stop 2 which is at about 2400' in elevation and about 800 feet from the top of the falls (about where one hits the brook following path B). Here you can see the contact relationships between the mafic and pelitic rocks VERY well. Alternatively, if you prefer to go back to the Frank Post Trail rather than walk up the brook, you can collect pelitic rocks with glaucophane either in the drainage below Tillotson Camp or from several outcrops between Tillotson Camp and Tillotson Pond (Fig. B-8).

Option: Brook traverse. 2230 feet in elevation, about 200 feet from the top of the falls at Stop 1 is an outcrop, in the woods about 100 feet SW of the brook, of layered, schistose metagraywacke composed of albite + quartz + chlorite + epidote + white mica + magnetite + biotite. Darker-colored layers are more chlorite rich, commonly with better developed crenulation cleavage than the more felsic layers. Farther NW this contact with mafic schist and metagraywacke is marked by ultramafic slivers that suggest a fault (Fig. B-8).

Stop 2 (~2400') Series of outcrops in brook of infolded steel blue-gray, massive, fine-grained amphibolite and orange-brown weathered, dark gray pelitic schist. Mafic layers include the assemblages: glaucophane + carbonate + chlorite + epidote + garnet + quartz and actinolite + glaucophane + epidote + garnet + quartz + titanite ± chlorite ±carbonate ± gold sulfides. Pelitic layers contain white mica + garnet + quartz + glaucophane + titanite ± chlorite, carbonate, tourmaline and epidote. Mafic and pelitic layers both contain microscopic glaucophane (often altered to a fine-grained symplectite). The contact between mafic and pelitic schist from here upstream is everywhere parallel and assumed conformable. Both rock types are folded about F2 (~EW) whose reclined character is apparent at this stop.

Return to the Frank Post Trail via a side drainage (about 170 feet, ~N20E).

In the drainage brown-weathered, blue-gray, fairly massive amphibolite with calcic amphibole + glaucophane + epidote + garnet + titanite + gold sulfide crops out. It is sheared and blocks of amphibolite lie in a matrix of actinolite + chlorite + white mica + titanite + quartz. Amphibole grains are coarse enough to be seen without a hand lens and range in composition from magnesiohornblende in the cores to actinolite in the rims and along fractures. This shear zone is mapped along the Frank Post Trail at Alternate Stop 2 (Fig. B-8).

If you return to the trail after Stop 1 follow the trail uphill about 500 feet to about 2250 feet in elevation.

Alternate Stop 2 (~2250') [Sample 321A] Outcrop on NE side of trail. Sheared green-brown weathered, light gray-green, massive to schistose amphibolite with fractures filled by green amphibole + chlorite. The amphibolite is composed of amphibole + epidote + garnet + chlorite + titanite ± white mica. Coarse amphibole grains are zoned with magnesio-hornblende and actinolitic hornblende cores and actinolite rims (Figs. B-4 and B-5, Sample 321A). Some grains are pseudo - morphed by a fine-grained symplectite. Dismembered layers of epidote + amphibole + titanite (or are these clasts?) occur locally. Zoned amphibole with darker colored cores that rims occurs in the epidote-rich zones and are petrographically similar to the zoned amphibole in the amphibolite. Glaucophane is best seen in the outcrops of amphibolite about 50 feet above the trail.

Stop 3 (7530' from base of the Frank Post Trail, elevation ~2250' to 8200', elevation ~2480') [Sample 332A]. Along the trail between Alternate Stop 2 and Stops 4 are several outcrops (Fig. B-8) of brown-weathered, gray-green, medium- to coarse-grained, massive to schistose amphibolite composed of amphibole, garnet, epidote, titanite, quartz, chlorite, and, locally, glaucophane. Selected mineral compositions are given in Table B-3 (Sample 332B). Amphibole is distinctly coarser grained than that seen at stops 1 and 2. It is generally zoned with magnesio- hornblende cores and actinolite rims. Compositions are similar to zoned amphibole seen at Alternate Stop 2 and in the tributary above Stop 2. Amphibole and chlorite compositions suggest that these rocks are more Mg-rich than those at Stops 1 and 2 (Fig. B-5). Glaucophane, white mica, and magnetite are also less abundant in these rocks than the mafic schist at Stops 1 and 2.

Mafic schist exposed here strikes NW, parallel to outcrops in the brook, and dips moderately to the southwest, generally shallower than in the brook. In addition, several mesoscopic F2 folds are exposed in ledges 100-200 feet northeast of the trail that support the presence of a macro-scopic WNW- plunging, approximately reclined fold. Crops here occur on the "upper" limb. (Sample V380C, Figs. B-4 and B-5).

Continue along the Frank Post Trail to Stops 4 and toward Tillotson Camp, which is on the Long Trail at the intersection with the Frank Post Trail.

Stop 4 TO TILLOTSON CAMP (8400' from trail base)
A) About 300 feet (elev. ~2510) from and east of Tillotson Camp.

An outcrop in the trail of gray-brown weathered, bluish-gray, fine- grained, massive amphibolite with garnet porphyroblasts 1 mm across is exposed. This rock contains garnet + epidote + calcic amphibole + glaucophane + quartz + carbonate + chlorite + titanite + apatite and is more like the amphibolite at Stops 1 and 2 than the coarser grained amphibolite seen along the trail from alternate Stop 2 to here. On the joint surface over which we must climb are exposed early F1 isoclinal folds that are clearly refolded by mesoscopic F2. PLEASE do not try to sample here so that the structural relations may be preserved; besides, the rock is quite weathered.

B) About 150 feet west, the trail crosses a small drainage between A and Tillotson Camp.

Here brown weathered, silvery-gray, medium-grained pelitic schist is infolded with gray-green, fine-grained calcareous garnet amphibolite. Green, coarse-grained crenulated chlorite schist occurs at the contact. This "unit" can be readily sampled, although somewhat precariously, down this drainage where the mafic layers are composed of calcic/sodic-calcic amphibole + glaucophane + omphacite + epidote + garnet + carbonate + quartz + white mica + magnetite + titanite and pelitic layers are composed of white mica + quartz + glaucophane (altered to a fine-grained symplectite) + epidote + titanite + apatite.

C) TILLOTSON CAMP (8700' from trail base, elevation 2560').

Outcrops at Tillotson Camp are gray weathered, medium-grained glaucophane + calcic/sodic-calcic amphibole + epidote + garnet + white mica + titanite + quartz + apatite ± carbonate ± plagioclase mafic schist. The rock is well foliated and contains well developed crenulation cleavage. Early F1 isoclines are exposed on the east-facing joint surface below the camp. Because this outcrop is right on a camp site, PLEASE do not sample it. The same mineral assemblages occur at Stops 1 and 2 and in other outcrops of amphibolite in the immediate vicinity.

On a nice day Tillotson Camp is a great place for lunch. Besides good rocks there is a fine view of the Missisquoi valley and Lowell Mountains.

If there were more time we could hike the Long Trail north to Tillotson Peak (Fig. B-8, inset) where amphibolite with epidote + glaucophane + chlorite +albite + paragonite + phengite + titanite + quartz + apatite has been sampled (V337B, Fig. B-4) along with epidote + calcite + chlorite + calcic amphibole + glaucophane + quartz + titanite + magnetite + chalcopyrite + pyrite + pyrrhotite + millerite amphibolite (V337A, Figs. B-4 and B-5). There are many outcrops along the way including one east of Tillotson Pond (Fig. B-8) with epidote + glaucophane + omphacite + quartz + dolomite + calcite + titanite + magnetite + apatite + chalcopyrite (V383B, Fig. B-4). Pelitic schist contains pale pink layers with fine-grained garnet that may represent metamorphosed Mn-chert.

Alternatively, we could take the Long Trail to the southwest toward Belvidere Mountain across mafic and pelitic schists, some intercalated at a 1-2 cm scale, which crop out until a lens of serpentinized ultramafic rock is reached (Fig. B-8). Northeast of this contact with serpentinized ultramafic, gray brown weathered, bluish gray, medium grained amphibolite with calcic amphibole + epidote + plagioclase + garnet + chlorite + glaucophane + carbonate + titanite + magnetite + apatite ± omphacite occurs along with garnet (with glaucophane inclusions) + white mica + plagioclase + quartz + chlorite + stilpnomelane(?) + titanite schist with garnets up to a cm across. Southeast of the ultramafic, light greenish gray metagraywacke with quartz + plagioclase + white mica + chlorite + epidote + biotite + magnetite + apatite crops out. On the side of this outcrop and along fracture surfaces actinolite knots up to 25 cm across and crinkled actinolite + chlorite-rich layers occur. This zone is interpreted as a probable fault.

... Return to the vehicles via the Frank Post Trail

18.9	Stark driveway and North Road, turn right (S).
24.1	Intersection North Road and Rt. 100, Eden Mills. Go south on Rt. 100.
29.8	Junction Rts. 100/100C, North Hyde Park. Turn west on Rt. 100C to Johnson.
34.5	Johnson, VT, Junction Rt. 100C and Rt. 15, turn west on 15 to Jeffersonville. Outcrops along our route are predominantly graphitic schist and quartzite with sulfidic weathering (Hazens Notch Formation).
43.7	Junction Rt. 15 and Rt. 108. Stay on Rt. 15W to Cambridge.
46.1	Cross the Lamoille River.
47.1	"Y" Stay left (S) on Rt. 15 to Underhill Flats at the intersection with Rt. 104 . Our route south takes us through lovely scenery. Rocks are mapped as Underhill Formation (silvery, gray-green, qtz+white mica+plg+chl+bio schist with abundant quartz segregations).
56.0	Underhill Flats, stay on Rt. 15.
58.0	Turn left on paved, but unnamed, road to Jericho Center.
60.4	Stay straight at yield sign

61.5	Bear left just south of Jericho Center. Continue south until you pass beneath I-89. Turn left at "T"
66.4	Intersection with Rt. 2W at Richmond. Drive straight through towards Huntington.
67.7	Turn left on paved road to Huntington
73.5	Huntington
74.4	Bear left
76.1	Huntington Center
76.9	Bear left, paved road to Hanksville
80.1	Road changes to dirt for about 0.6 miles then back to hardtop.
82.4	Junction with Rt. 17, turn right (west) toward Bristol.
85.6	Turn left on gravel road toward Jerusalem, continue east into the town of Jerusalem then south on the same road.
89.5	Downingville, hardtop road.
90.9	"T" intersection, turn left (S) towards Lincoln.
91.0	Left across creek
91.8	Lincoln. Turn left through town.
92.9	"Crash Bridge", turn right (S) onto road to South Lincoln along the east bank of the New Haven River. Outcrops in the river are gneisses of the Grenville basement.
94.0	Straight ahead on gravel road
94.8	Straight ahead again (do not take Grimes Road across the New Haven River). At "Y" turn right into South Lincoln.
96.6	Turn left onto a narrow dirt driveway .
97.0	Park behind the house and we will proceed by foot up the drainage.

A Hike to Arden Albee's pelitic schist locality, Lincoln Mountain quadrangle, Vermont (Locality 2)

Because we have not worked here our main role at this locality is to help you find the outcrops and benefit from inevitable discussions. The petrologic studies done by Arden are presented in Albee (1965a), Albee (1968), and Taylor et al. (1963) and were summarized under "Metamorphism of Pelitic Schist". Recent field and structural studies in this area have been done by Lapp and O'Loughlin (1986). Follow the Road Log and park in the open area by the house. If you come at a later time, permission to park may be requested from Mrs. Barbara B. Austin, 14 Victory St., Vergennes, VT 05491 to park here.

Follow the path and drainage into the woods and uphill to the east for about 2000 feet (Fig. B-9). At about 2200 feet in elevation there is an abrupt increase in slope. Here, rusty-weathered, dark gray (due to graphite) quartz + chlorite + albite + muscovite + biotite + ilmenite + garnet schist crops out. This is mapped as the Underhill Formation. Walk north and uphill until you reach a layer of rusty-weathering pelitic schist with garnet porphyroblasts 1 to 1.5 cm across. This layer is considered to be the base of the Mt. Abraham schist by Albee and is composed of muscovite + paragonite + quartz + chloritoid + garnet + chlorite + ilmenite.

Above the layer with large garnet porphyroblasts are glaciated ledges of tightly folded, light gray quartz + muscovite + paragonite + chlorite + chloritoid + rutile ± kyanite schist with abundant quartz veinlets and pods. Kyanite is abundant in some layers on these ledges, but finding it is definitely a hand lens/hands and knees "operation." (We will have samples to minimize frustration and damage to the outcrop). Garnet is sparse on these ledges and is locally very Mn-rich. Discontinous bull quartz layers and pods commonly define the gently south-plunging folds far better than the rather vague lithologic layering. Taylor et al. (1963) suggested that quartz pods present at Locality 2 may have crystallized under lower temperature than the schists because delta (quartz - ilmenite) was higher in the pods. However, Albee (1965a, p. 252) reported that the "ilmenite" is hematite, so delta (quartz - ilmenite) values cannot be compared between schists and quartz pods.

Figure B-9 shows the locations sampled and discussed in Albee's papers. Table B-4 gives the estimated modes reported. This Figure and Table should be helpful in locating the different assemblages. The outcrops in the woods allow one to examine and sample the lower Al assemblages reported by Albee. The glaciated outcrops provide an opportunity to examine more Al-rich assemblages and, hopefully, to get a good view of the setting sun.

Return to the vehicles and follow the Road Log to our home for the night.

Retrace route to "Crash Bridge"

101.1 Turn right (east) to Lincoln Mountain Road - the vans should make it!

103.4 Outcrop in the woods to the north of garnet-grade, medium-pressure facies series mafic schist dated by M.A.Lanphere at about 385 Ma (hornblende and biotite $^{40/39}$Ar total fusion).

104.9 Lincoln Gap, elevation 2424', outcrops of the Underhill Formation.

108.8 Outcrop of mafic schist on left has barroisite cores and actinolite rims (Hazens Notch Fm.)

109.0 Intersection of Lincoln Mountain Road and Rt.100 at Warren. Crops of sheared qtz+plg+chl+bio schist with abundant plg porphyroblasts (Pinney Hollow Fm.) occur on the east side of the intersection. Turn left (N) to Waitsfield. Outcrops of biotite grade pelitic schist and greenschist (Pinney Hollow Fm) on both sides of the road as we proceed N along the Mad River.

114.7 Junction Rts. 100 and 17. Stay on Rt. 100 to Moretown.

120.2 Junction Rts. 100 and 100B. Stay right (NE) on Rt. 100B.

121.2 Moretown, VT, underlain by the Stowe Formation (intercalated pelitic schist and greenschist here).

Figure B-9. Sketch map of the Mt. Grant pelitic schist locality (Albee, 1965b). Outcrop localities transferred approximately to an enlarged Lincoln Mountain topographic base. Contact between the Underhill Formation (ЄZu) and the Mt. Abraham Schist (ЄZa) occurs at approximately 2200' (Lapp and O'Loughlin, 1986). Assemblages all with quartz and mica (see Table B-4 for estimated modes).

▲ kyanite - chloritoid - chlorite
△ garnet - chloritoid - chlorite - paragonite
▽ kyanite - garnet - chlorite
□ chloritoid - chlorite
● kyanite - chlorite
⊠ chloritoid

▼ garnet - biotite - chlorite
○ garnet - chlorite
■ biotite - chlorite - albite
◪ chlorite - albite

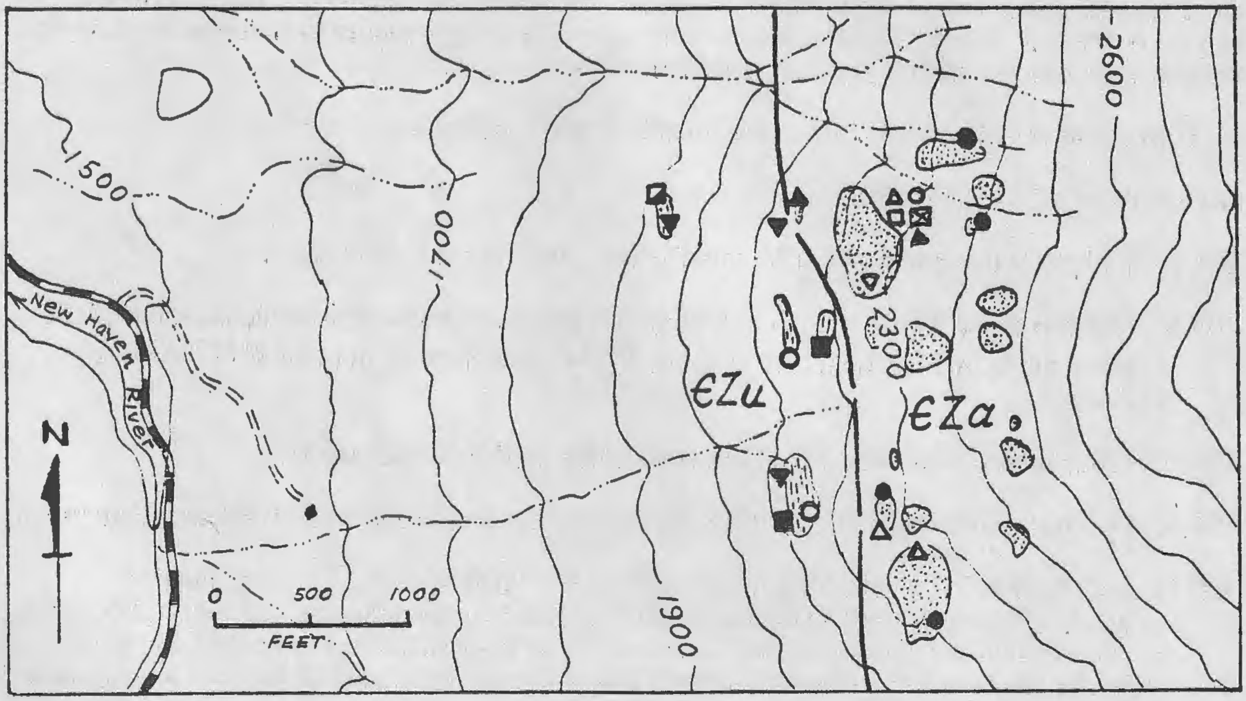

Table B-4. Estimated modes of samples analyzed by Albee (1965a) in the area covered by fig. 9*

Underhill Fm.

Assemblage	Ky	Ct	Ga	Ch	Bi	Qz	Mu	Pa	Ab	Accessories
▼ G† (La10q)			5	10	3	55	20		5	Ap, Tr, Gp, Py, Il
G			2	10	5	40			10	Ap, Tr, Gp, Cz, Py, Il
G			1	14	4	50			5	Ap, Gp, Il

Mt. Abraham schist

Assemblage	Ky	Ct	Ga	Ch	Bi	Qz	Mu	Pa	Ab	Accessories
△ B† (La10p)		15	12	10		20	-40-			Ap, Tr, Il
B		17	1	15		20	-55-			Tr, Cz, Il/Rt
B		10	10	10		15	-55-			Ap, Cz, Il/Rt
B		15	1	15		20	-50-			Ap, Tr, Il/Rt
A† (LA10k)	5	23		9		25	40			Ap, Cz, Rt
C	15		2	3		15	-60-			Ap, Tr, Cz, Hm(5)

*Abbreviations: Albite (Ab), Apatite (Ap), Biotite (Bi), Chlorite (Chl), Chloritoid (Ct), Clinozoisite (Cz), Garnet (Ga), Graphite (Gp), Hematite (Hm), Ilmenite (Il), Kyanite, (Ky), Muscovite (Mu), Pargonite (Pa), Pyrite (Py), Quartz (Qz), Rutile (Rt), Tourmaline (Tr). Muscovite and paragonite present in assemblage -xx-.

†Sample also studied by Taylor et al. (1963).

127.2 Middlesex, intersection with Rt. 2. Turn left (NW) to join I-89

127.8 Turn right to enter I-89 South

132.8 Pass Exit 8 to Montpelier. Outcrops on the east side contain the contact between the Cambro-Ordovician eugeoclinal rocks of central Vermont and those of the CVGS (the "RMC"). If there is still sufficient light, the dark brown weathering rocks are metalimestones intercalated with gray pelitic phyllites of the Waits River Formation, that have recently yielded Ordovician graptolites.

136.0 Take Exit 7 east to Barre via Rt. 62 to join Rt. 302.

139.0 Barre, junction with Rt. 302. Follow Rt. 302 through town.

143.0 Websterville, stay on 302.

150.0 Intersection of Rts. 302 and 25. Turn right (S) on 25.

166.0 Intersection of Rt. 25 and I-91 at Bradford. Stay on 25 to Piermont.

167.0 Cross the Connecticut River, leaving the CVGS for today. Enter Piermont, New Hampshire and follow a Dartmouth alum to the Ravine Lodge.

C. A FIELD TRIP GUIDE TO BLACK MOUNTAIN, WILDWOOD ROADCUT AND BEAVER BROOK, MT. MOOSILAUKE AREA, NEW HAMPSHIRE

Douglas Rumble, III and M.P Dickenson

INTRODUCTION

The purpose of the field trip to Black Mountain, Wildwood Roadcut and Beaver Brook is to study three localities that show well exposed evidence of different types of fluid-rock interactions. The rocks of Black Mountain and Wildwood roadcut show examples of the bed-by-bed control of fluid compositions by mineral assemblage buffering. Infiltration, in contrast, is the prevalent mode of fluid-rock behavior at Beaver Brook. An important question to keep in mind throughout the field trip is "Why did Beaver Brook experience infiltration during metamorphism while Black Mountain and Wildwood did not?"

MAPS AND LITERATURE

The area of the field trip is covered by two 7-1/2', 1/24,000, topographic maps: East Haverhill, N.H. and Mt. Moosilauke, N.H. (Fig. C-1). A key reference on the geology and petrology of the area is the seminal work of Marland P. Billings "Regional metamorphism of the Littleton-Moosilauke area, N.H." (1937). The distribution of Al_2SiO_5 minerals in the region is described by Rumble (1973). Pressure-temperature (P-T) estimates are given by K.V. Hodges and F.S. Spear (1982). The Black Mtn. and Beaver Brook localities are discussed, respectively, by Rumble (1978) and by Rumble, Ferry, Hoering, and Boucot (1982). The Wildwood roadcut is presented in this guidebook by M.P. Dickenson.

STRATIGRAPHY AND GEOLOGIC HISTORY

The oldest stratified rocks in the Mt. Moosilauke region are the Ammonoosuc Volcanics of Ordovician age. There are at least several kilometers of felsic and mafic volcanics in the Ammonoosuc. A more accurate estimate of thickness cannot be made because the bottom of the unit is cut out by magnetite-bearing granitoids of the Ordovician Oliverian magma series. Intrusive rocks of the Oliverian series occupy the cores of domal uplifts and are mantled by Ammonoosuc volcanics and younger rocks. An Ordovician magmatic arc composed of Ammonoosuc Volcanics and Oliverian plutons is known to extend parallel to regional strike trends from Connecticut, across Massachusetts, along the western edge of New Hampshire, and finally curving eastward into Maine. The arc is now exposed within a Devonian structure, the Bronson Hill anticlinorium.

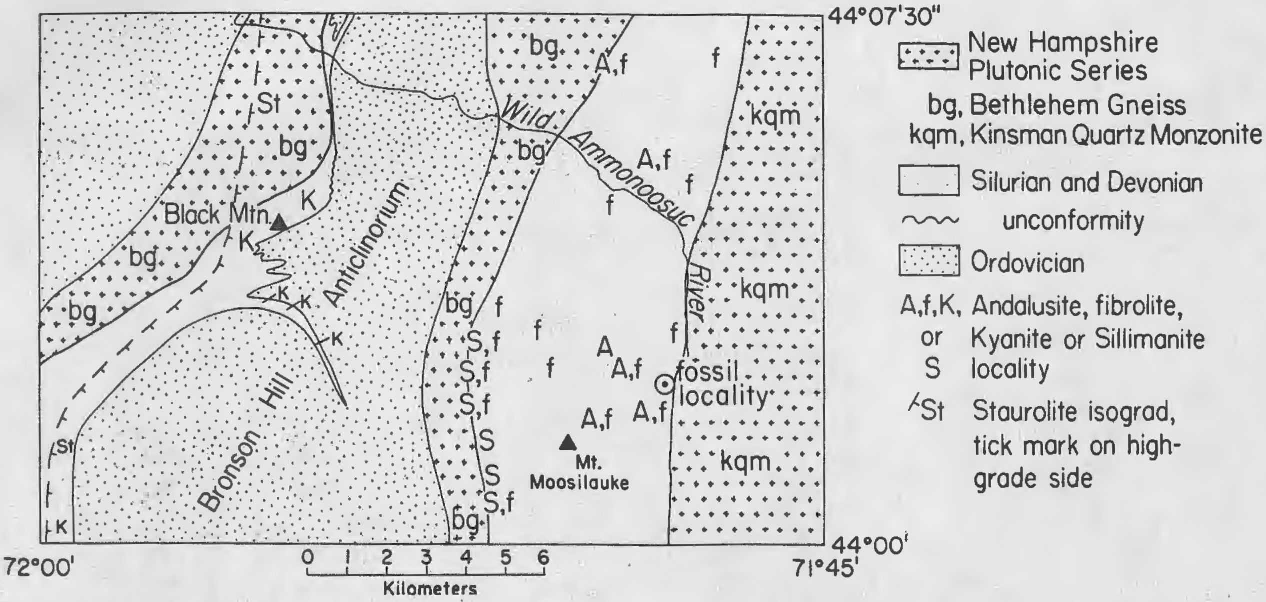
44°07'30"
New Hampshire Plutonic Series
bg, Bethlehem Gneiss
kqm, Kinsman Quartz Monzonite
Silurian and Devonian
unconformity
Ordovician
A,f,K, or S Andalusite, fibrolite, Kyanite or Sillimanite locality
St Staurolite isograd, tick mark on high-grade side
Black Mtn.
Bronson Hill
Anticlinorium
Wild Ammonoosuc River
fossil locality
Mt. Moosilauke
bg
kqm
A,f
S,f
St
K
0 1 2 3 4 5 6
Kilometers
72°00'
71°45'
44°00'

Fig. C-1. Location of Black Mountain , Beaver Brook fossil locality, and distribution of Al_2SiO_5 polymorphs in southern half of Mt. Moosilauke 15' quadrangle. Wildwood roadcut is near the first "o" in the label "Wild Ammonoosuc River".

Rocks of the Ordovician magmatic arc are overlain unconformably by (1) Silurian conglomerates and quartzites of the Clough Quartzite; (2) marbles and calc-silicates of the Silurian Fitch Formation; and (3) pelitic mica schists and micaceous quartzites of the Lower Devonian Littleton Formation. The thicknesses of the Clough and Fitch are highly variable: in some areas the units are absent because of lack of deposition or boudinage; in other areas, as at Black Mountain, the exposed outcrop breadth of the Clough is hundreds of meters, however, some of this apparent thickness may be due to repetition by isoclinal folding. The Littleton Formation may be several kilomters thick but its top is not exposed owing to uplift and erosion. Sections of the Littleton show well developed graded beds, 10-20 cm thick; in other outcrops only massive mica schists are seen. The Littleton is intruded by foliated sill-like plutons of ilmenite-bearing granitoids, the Bethlehem Gneiss and Kinsman Quartz Monzonite of the New Hampshire series. The plutons show neither a contact metamorphic aureole nor chill zones. These features, combined with the presence of primary igneous muscovite, suggest emplacement during active regional metamorphism at depths of 10 km, or more.

The age of regional metamorphism and deformation is constrained by the presence of unaffected Mesozoic intrusives and volcanics of the White Mountain magma series in nearby Franconia Notch. Metamorphism and deformation were traditionally assigned to the Devonian, an age confirmed by the Rb-Sr dating of the syn-metamorphic Bethlehem and Kinsman at 405-415 m.y. Deformation and metamorphism were synchronous during early stages of tectonism: porphyroblasts grew and the preferred orientation of schistosity was established during emplacement of large nappes. Later, metamorphic intensity waned but folding continued as the Bronson Hill anticlinorium and its component domes were built. The sense of transport during the nappe episode was from E to W; in consequence, hotter rocks were stacked on top of cooler rocks. The domes of the Bronson Hill not only refold the nappes but also deform isograds.

BLACK MOUNTAIN

Access

Black Mtn. may be reached by following New Hampshire route 25 to the village of East Haverhill (about 5 miles E. of the intersection of route 10 and route 25). A short detour, a few hundred meters E. of the village on rt. 25, reveals an impressive view of Black Mtn., Sugarloaf Mtn., and the Hogsback, all composed of white Clough quartzite. The arcuate quartzite cliffs of the Hogsback delineate the northerly plunge of the Owls Head dome. The thick accumulations of quartzite at the Sugarloaf and Black Mtn. illustrate the effects of isoclinal folding in the nappes. Returning to East Haverhill village, turn N. and follow Lime Kiln Road to Lime Kiln Camps. The IMA trip will follow Chippewa Trail to the top of Black Mtn. Those visiting at another time can ask for directions in the camp office.

Hiking Route

The IMA group will proceed directly to the summit of Black Mtn. We will begin detailed study of outcrops at the summit and then retrace our steps slowly downward so that we can stay together for good discussions. The rock types that will be seen are conglomerates, quartzites, and quartz-mica schists of the Clough Quartzite.

The summit was formerly marked by an observation tower (Fig. C-2). One can still find the location of its concrete foundation. Facing S. from the site of the tower, the back sides of Hogsback and Sugarloaf are visible. The northerly plunge of the Owls Head Dome beneath Black Mtn. can be easily visualized. The structure to the N. is not well displayed but mapping shows a southerly plunging dome. Thus, Black Mtn. lies in a structural saddle formed by a plunge depression between two domes. Other summits underlain by Clough Quartzite stand to the S. including Piermont Mtn., Mt. Cube, and Croydon Peak. They trace the continuation of the Bronson Hill anticlinorium.

Oxygen isotope geothermometry of Black Mtn. rocks (quartz-magnetite) gives a temperature estimate of $495^{\circ}C$ ($\pm 10^{\circ}C$). Pressure is estimated to lie within 0.5 kbars of the Al_2SIO_5 triple point, i.e. 3.8 kbars according to Holdaway.

In ledges a few meters S. of the tower, there is abundant kyanite occurring as felted layers defining schistosity. Note how kyanite has been folded. The minor folds that fold kyanite are parasitic to the domes.

Turn back N. and look down at the tower foundations. Here you will find chloritoid-staurolite-chlorite assemblages of 71-60E and extremely Fe-rich assemblages with garnet (71-60F, 71-60R). The Fe-rich, garnet-bearing assemblages have reduced oxides with $FeTiO_3$ in ilmenite of 95%, or more. (Data on mineral assemblages summarized in figures C-3 through C-10.)

Walk just to the E., beyond the tower site and you will find tourmaline-filled joints. Careful searching may find beds of staurolite-chloritoid-garnet assemblages that have been almost completely replaced by tourmaline, within a few cm of the joints.

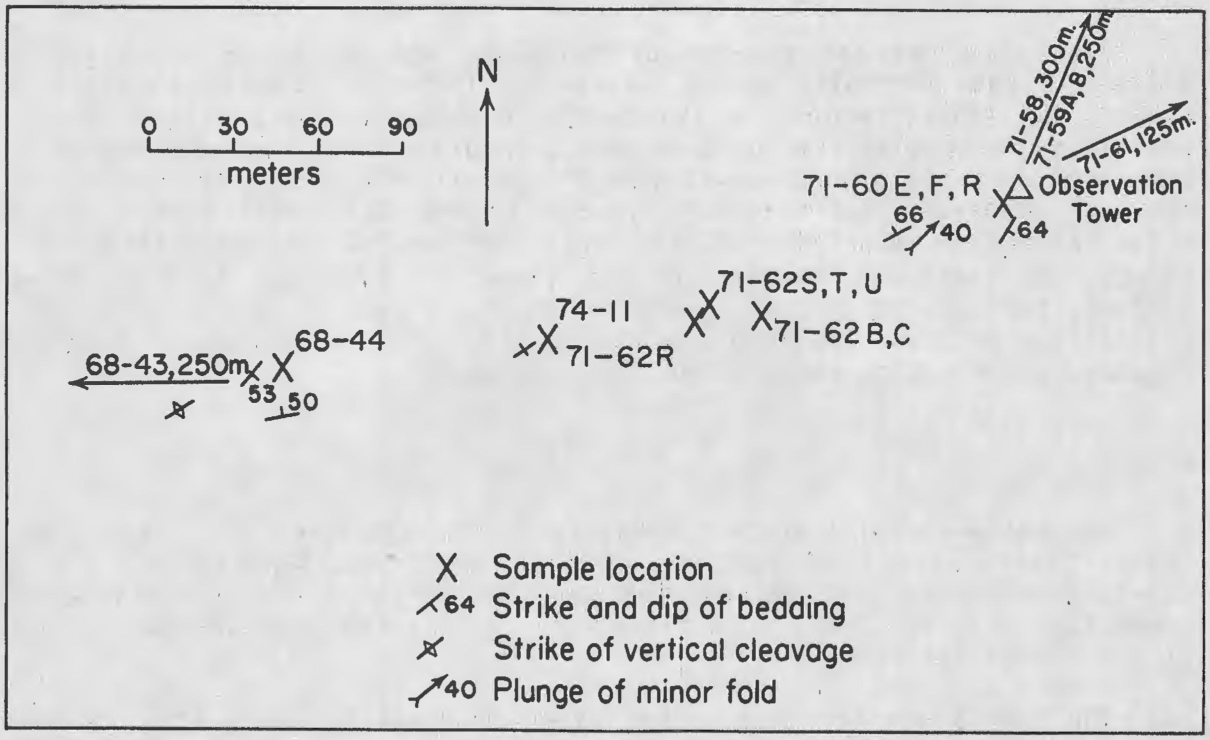
N
0 30 60 90
meters
71-58, 300m.
71-59A,B, 250m.
71-61, 125m.
71-60 E, F, R
Observation Tower
66
40
64
71-62S, T, U
74-11
71-62 B, C
71-62R
68-43, 250m.
68-44
53
50
X Sample location
64 Strike and dip of bedding
Strike of vertical cleavage
40 Plunge of minor fold

Fig. C-2. Location of samples collected along summit ridge of Black Mtn. Field trip route begins at site of observation tower and proceeds SW, towards 68-44.

Before beginning the descent, look SE. Mt. Moosilauke dominates the skyline. Beaver Brook, the third stop of today's trip, lies on the E. slopes of Mt. Moosilauke, and Wildwood roadcut at the N. end of the mountain. Mica schists on the slopes of the mountain contain abundant andalusite and sillimanite. The site of the Al_2SiO_5 triple point is between where we are standing on Black Mtn. and Mt. Moosilauke.

Turn towards the SW and begin to descend towards the cars. Remember to keep along the rocky spine of the ridge in order to see the best outcrops. The first steep scramble downward, just a few 10's of meters from the tower site, leads past abundant dome-stage minor folds and kyanite schists. The kyanite schists typically have the assemblage quartz-muscovite-kyanite-ilmenohematite-magnetite: they are highly oxidized.

Beyond the steep scramble one reaches a knob on the ridge. Just S. of the knob is a gently-dipping, tourmaline-coated joint. The knob is the site of a chlorite schist with staurolite-chloritoid-chlorite-magnetite-ilmenite (FeTiO3 = 98%). Adjacent to the chlorite schist are outcrops of kyanite-staurolite-chloritoid-chlorite-magnetite-ilmenohematite ($FeTiO_3$ = 28%) schist (71-62B, 71-62S, 71-62T, 71-62U). Here, separated by a meter or so, are rocks whose fluids differed by 20-30% in X_{H2O} and by the same amount (antipathetically) in

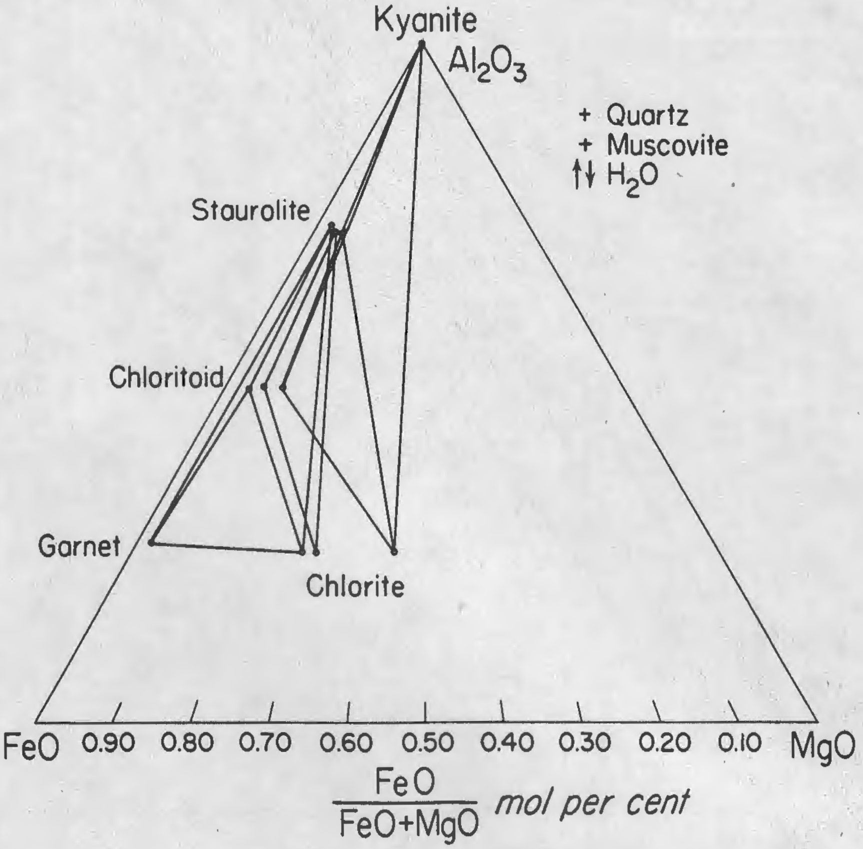
Kyanite
Al_2O_3
+ Quartz
+ Muscovite
↑↓ H_2O
Staurolite
Chloritoid
Garnet
Chlorite
FeO
0.90
0.80
0.70
0.60
0.50
0.40
0.30
0.20
0.10
MgO
$\frac{FeO}{FeO+MgO}$ mol per cent

Fig. C-3. Thompson projection of kyanite, staurolite, chloritoid, garnet, and chlorite compositions (ubiquitous minerals quartz and muscovite; also, projection through H_2O).

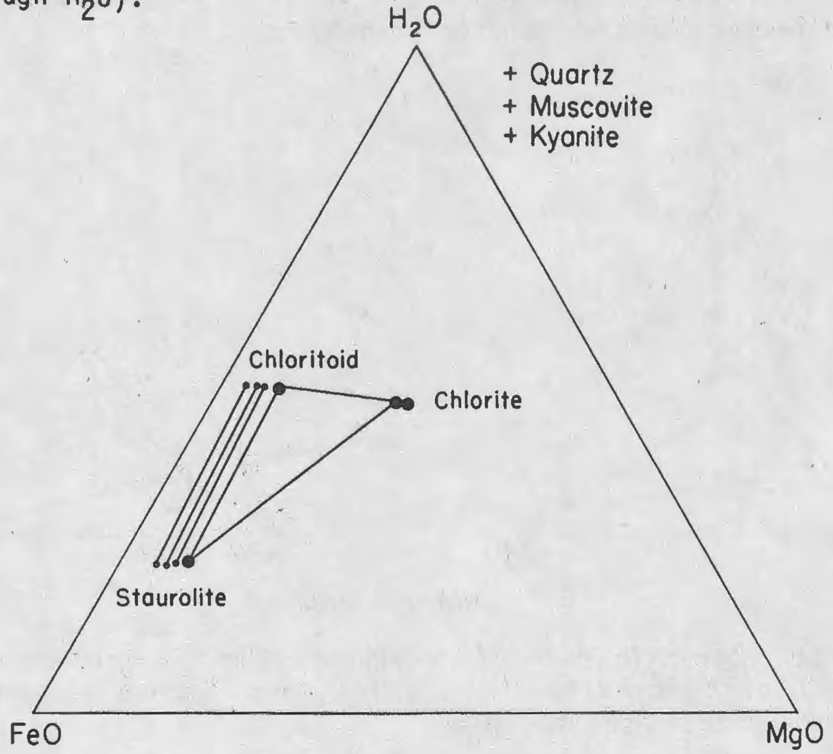
H_2O
+ Quartz
+ Muscovite
+ Kyanite
Chloritoid
Chlorite
Staurolite
FeO
MgO

Fig. C-4. Projection of chloritoid-chlorite-staurolite compositions from the ubiquitous minerals quartz-muscovite-kyanite.

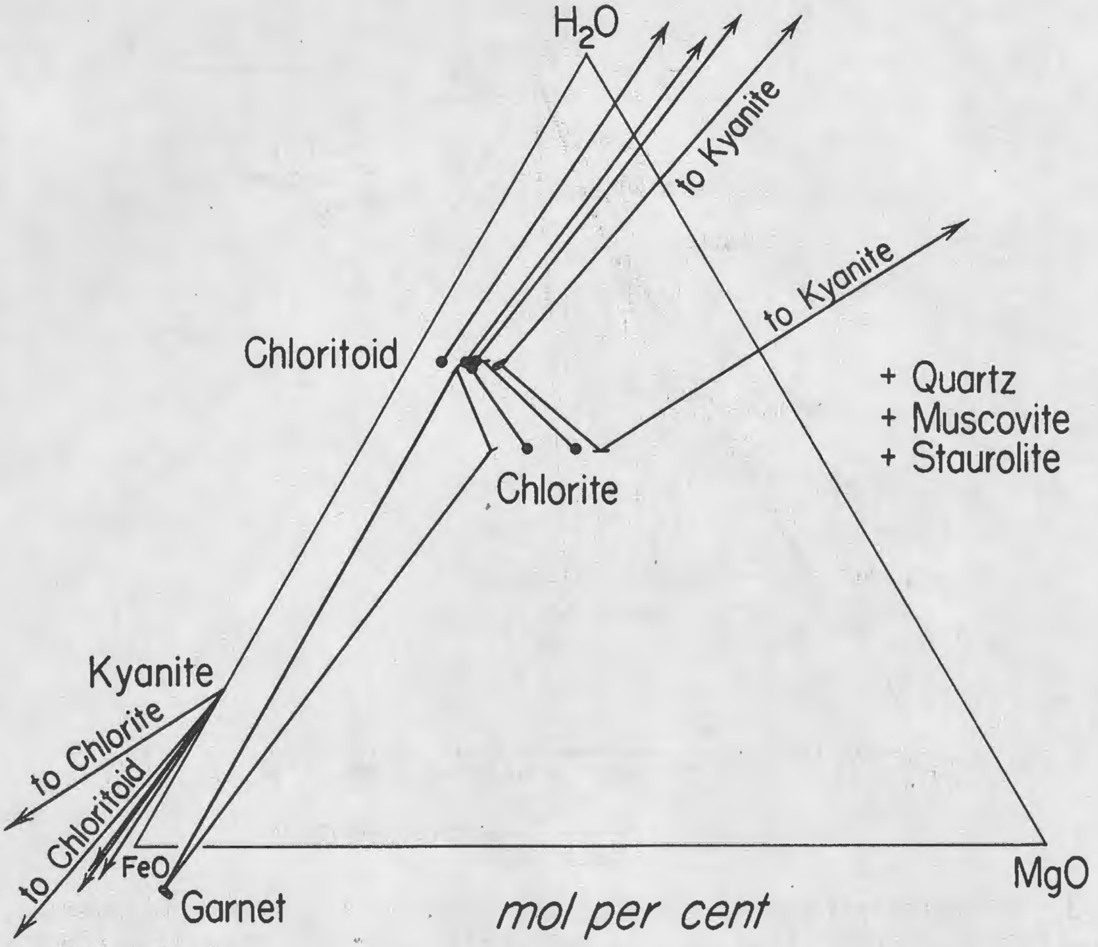
H₂O
to Kyanite
to Kyanite
Chloritoid
Chlorite
+ Quartz
+ Muscovite
+ Staurolite
Kyanite
to Chlorite
to Chloritoid
FeO
Garnet
MgO
mol per cent

Fig. C-5. Projection of chloritoid-chlorite-garnet-kyanite from the ubiquitous minerals quartz-muscovite-staurolite.

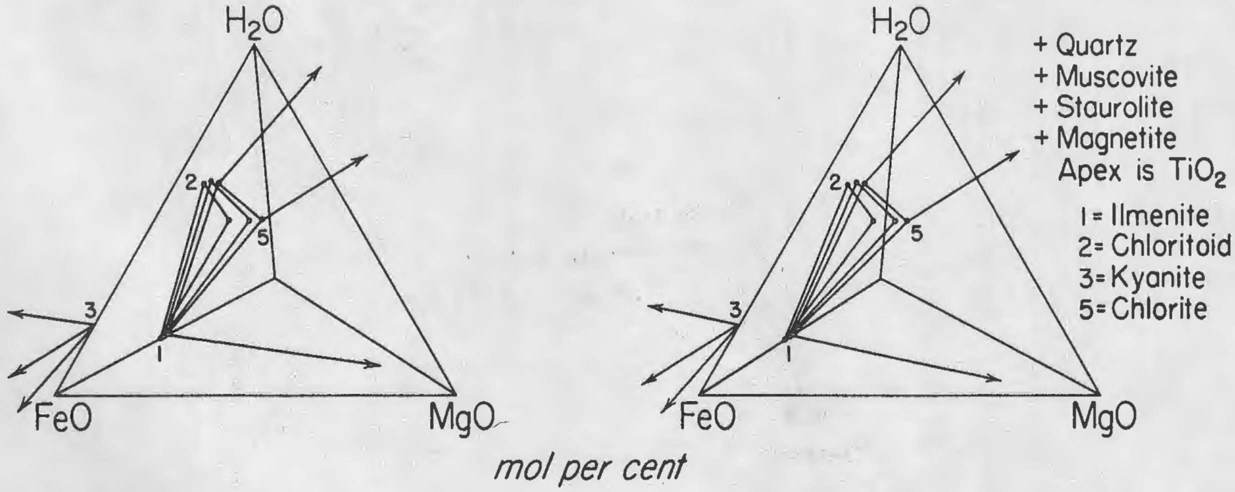
H₂O
2
5
3
1
FeO
MgO
H₂O
2
5
3
1
FeO
MgO
+ Quartz
+ Muscovite
+ Staurolite
+ Magnetite
Apex is TiO₂
1 = Ilmenite
2 = Chloritoid
3 = Kyanite
5 = Chlorite
mol per cent

Fig. C-6. Stereographic pair of tetrahedra showing projection of ilmenite-chloritoid-chlorite-kyanite from ubiquitous minerals quartz-muscovite-staurolite-magnetite. Apex is TiO_2.

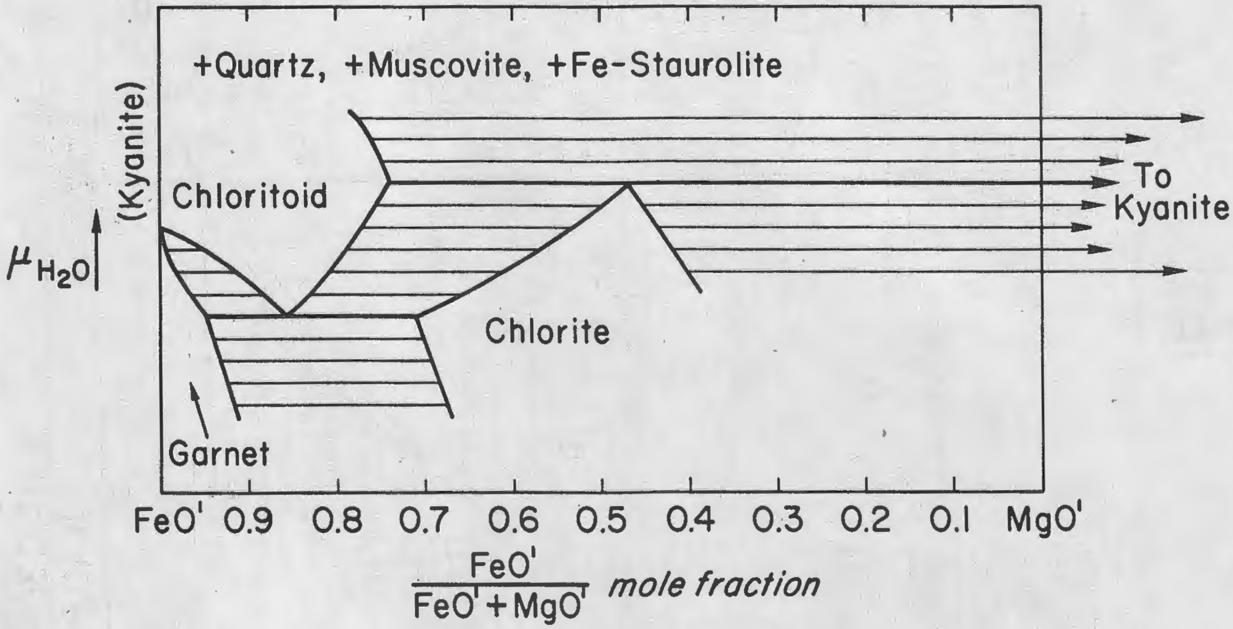
+Quartz, +Muscovite, +Fe-Staurolite
(Kyanite)
μ_{H_2O}
Chloritoid
To Kyanite
Chlorite
Garnet
FeO' 0.9 0.8 0.7 0.6 0.5 0.4 0.3 0.2 0.1 MgO'
$\frac{FeO'}{FeO'+MgO'}$ mole fraction

Fig. C-7. Isothermal, isobaric variation of μH_2O with mineral assemblage and mineral composition (cf. Fig. C-5).

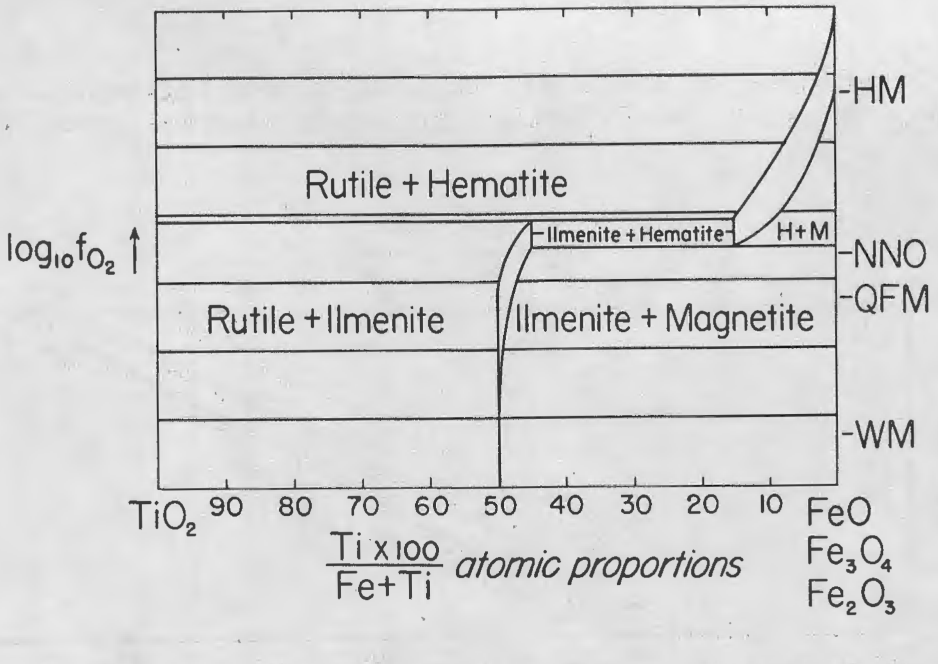
-HM
Rutile + Hematite
Ilmenite + Hematite
H+M
-NNO
-QFM
$\log_{10} f_{O_2}$
Rutile + Ilmenite
Ilmenite + Magnetite
-WM
TiO_2 90 80 70 60 50 40 30 20 10 FeO
Fe_3O_4
Fe_2O_3
$\frac{Ti \times 100}{Fe+Ti}$ atomic proportions

Fig. C-8. Isothermal, isobaric variation of fO_2 with mineral assemblage and mineral composition.

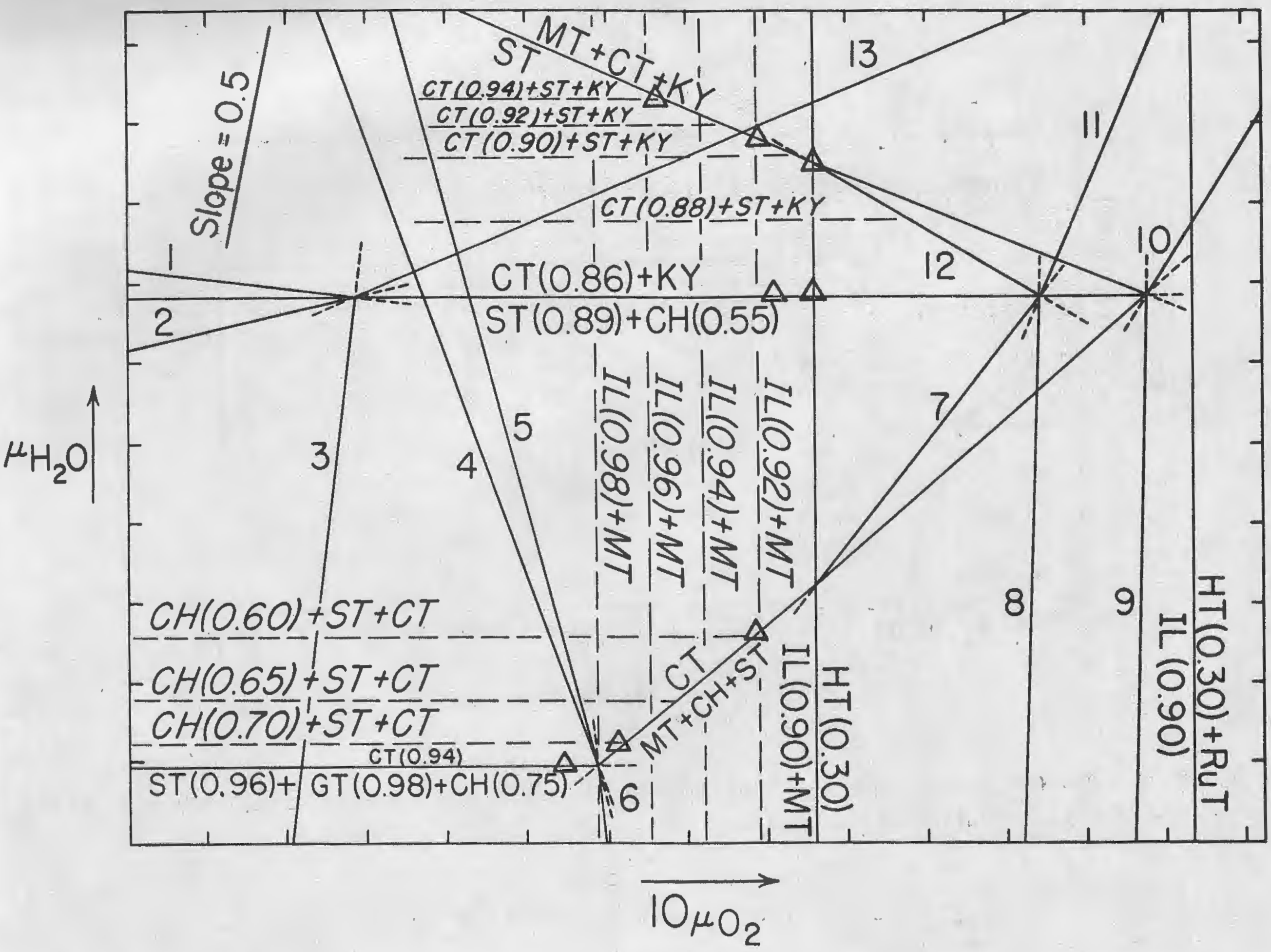
Slope = 0.5
MT+CT+KY
ST
CT(0.94)+ST+KY
CT(0.92)+ST+KY
CT(0.90)+ST+KY
CT(0.88)+ST+KY
13
11
10
12
1
2
CT(0.86)+KY
ST(0.89)+CH(0.55)
3
4
5
7
IL(0.98)+MT
IL(0.96)+MT
IL(0.94)+MT
IL(0.92)+MT
8
9
HT(0.30)+RuT
IL (0.90)
CH(0.60)+ST+CT
CH(0.65)+ST+CT
CH(0.70)+ST+CT
CT(0.94)
ST(0.96)+ GT(0.98)+CH(0.75)
6
CT
MT+CH+ST
IL(0.90)+MT
HT(0.30)
μH2O
10μO2

Fig. C-9. Variation of μH_2O and μO_2 with mineral assemblage and mineral composition. Triangles show relative positions of observed assemblages.

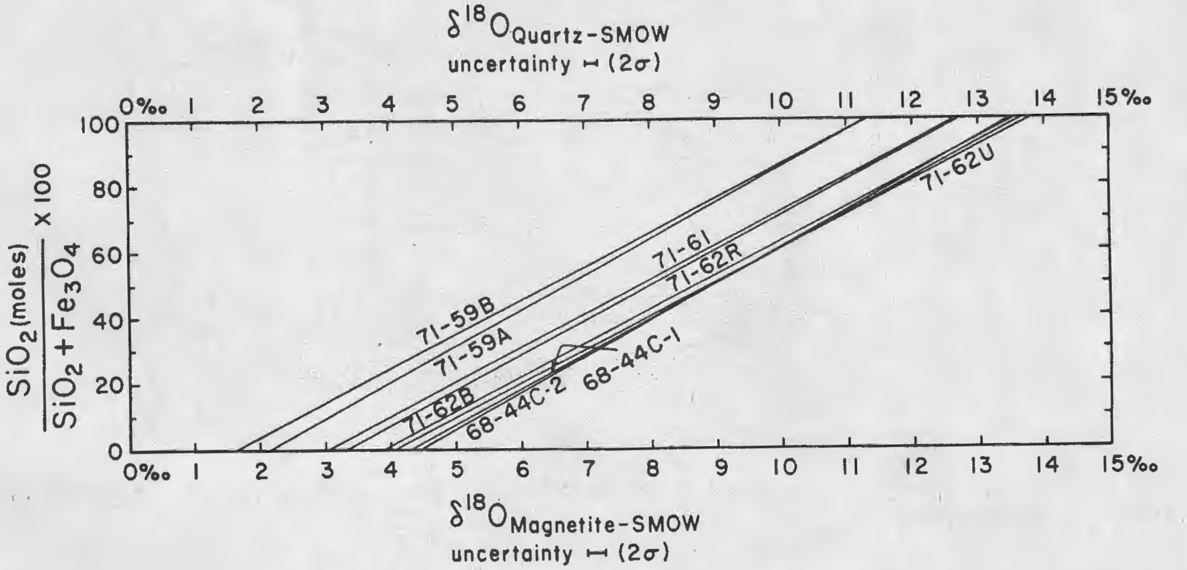

Fig. C-10. Oxygen isotope exchange equilibrium diagram for coexisting quartz and magnetite.

X_{H2}. Oxygen isotope analyses of co-existing quartz and magnetite show the minerals to have the same partitioning of $^{18}O/^{16}O$ but the quartz and magnetite of 71-62U and 71-62B are $1^{o}/oo$ enriched in $\delta\, ^{18}O$ relative to 71-62R. Thus, inferences of fluid inhomogeneity based on mineral assemblages are supported by oxygen isotope analyses.

Turn SW from the knob and continue to descend, following blazed trail through the scrub to avoid a steep place on the ridge. Shortly, the trail emerges on broad, open, bare-rock ledges. The kyanite-chloritoid-staurolite-paragonite quartzite of 68-44 is located in low ledges N. of the trail. In thin sections it may be seen that kyanite chloritoid, and staurolite are intergrown epitaxially, presumably along the chains of aluminum octahedra they all share.

Turn SW and continue to follow the blazed trail through the ledges of quartzite. Be on the lookout for current bedding, tourmaline-covered joints, and quartz-mica schist with very Fe^{2+}-rich garnets. The garnets may be readily recognized because of their tendency towards rusty weathering.

Return to cars for the drive to Wildwood roadcut.

WILDWOOD ROADCUT

Access

Wildwood roadcut is located on New Hampshire route 112, 1.2 km E. of its intersection with route 116. The roadcut is near the first "o" in the label "Wild Ammonoosuc River" on Fig. C-1.

Location of Rock Types

The phase petrology of rocks in the roadcut is discussed by M.P. Dickenson in the following sections. The andalusitechlorite-biotite-staurolite assemblages are located at the E. end of the roadcut on both sides of the road. Andalusite occurs as dark, non-descript porphyroblasts. An excellent example of reaction textures may be reached by proceeding to the W. end of the roadcut and climbing up the N. wall of the roadcut. Here, on westward dipping schistosity surfaces, may be seen pseudomorphs after cigar-size, cigar-shape aluminosilicate porphyroblasts (prismatic sillimanite? staurolite?) The pseudomorphs now consist of quartz, a mesh of muscovite, small garnets, and clusters of mm-sized euhedra of staurolite. M.P. Billings first described these textures in 1937. The pseudomorphs are found scattered on the W. slopes of Mt. Moosilauke. At Hurricane Mtn. (about 4km S. of Mt. Moosilauke) the pseudomorphs contain andalusite euhedra rather than staurolite.

Elsewhere in the roadcut "coticules" (i.e. spessartine garnet rocks) may be found.

Introduction

The classical model of metamorphism assumes that mineral assemblages on an outcrop are in equilibrium with a reservoir of external fluid of fixed composition. Thus all mineral assemblages are assumed to have equilibrated with a common volatile or fluid phase. Recent studies, however, have shown that along a single outcrop the composition of the volatile phase, as deduced from petrologic/mineralogic data, varies with changes in the mineral assemblage (Ferry, 1979; Rumble, 1974, 1978; others). Furthermore, at fixed temperature and pressure within a given mineral assemblage, the change in mineral composition for various solid solution minerals is also related to changes in the composition of the volatile phase (Rumble, 1976a, 1978; Dickenson, 1984). The studies clearly demonstrate that the classical model for metamorphism is not always valid.

This study presents mineralogical and petrological data from a single outcrop of amphibolite grade metamorphosed pelite schist. The results indicate several important concepts related to pelite metamorphism: (1) Differences in the chemical potential of H_2O are recorded in bed-to-bed relationships; (2) these differences are probably related to initial compositional parameters and the buffer capacity of the mineral assemblage; and (3) the magnitude of chemical potential differences is small, suggesting little or no infiltration of externally derived fluid.

Geologic Setting

Samples were collected along a single outcrop of amphibolite grade pelitic schist on Route 112 in the Moosilauke Quandrangle, N.H. The rock unit was originally mapped as Littleton Formation, an early Devonian stratigraphic unit (Billings, 1937).

The outcrop lies within a N-S band of pelitic rocks called the Moosilauke septum. This band is typically of medium amphibolite grade, commonly including staurolite-andalusite and/or sillimanite pelitic assemblages. Mineral textures reveal a complex reaction history that is most likely a function of a complicated history of changes in intensive parameters (pressure, temperature, and fluid composition) in response to tectonic evolution. This study examines only the latest texturally equilibrated mineral assemblages and does not address the complicated reaction history.

Analytical Methods

Mineral analyses were carried out on a CAMECA automated electron microprobe located at Harvard University. All analyses were collected using 15 kV accelerating potential with a beam current of approximately 15 nA, measured by a retractable Faraday Cup. X-ray intensities were converted to oxide weight percents using the methods of Albee and Ray (1970), and simple silicates and oxides were used as standards. Reported mineral compositions represent the average of several separate grains with two to four analyses collected on each grain.

Petrography and Mineral Chemistry

The mineral assemblages described in this study occur in amphibolite grade pelitic schists. The critical assemblages addressed include three varieties (all with quartz, muscovite, garnet, ilmenite and graphite):

(1) chlorite + biotite + staurolite
(2) chlorite + biotite + staurolite + andalusite
(3) chlorite + biotite + andalusite.

Although the assemblages record a history of crystallization, mineral textures indicate that the above assemblages are the last texturally equilibrated assemblages. For example, andalusite in assemblage (3) contains inclusions of staurolite but no staurolite in the matrix. Likewise, chlorite in all assemblages appears as late porphyroblasts, crosscutting the latest foliation.

Mineralogy

Chlorites analyzed in this study are solid solutions of $F_{4.5}Al_3Si_{2.5}O_{10}(OH)_8$-$Mg_{4.5}Al_3Si_{2.5}O_{10}(OH)_8$. Biotites are solid solutions of the components $KFe_{2.5}Al_2Si_{2.5}O_{10}(OH)_2$-$KMg_{2.5}Al_2Si_{2.5}O_{10}(OH)_2$ and contain up to 1.75 wt % TiO_2. Muscovites are solid solutions of $K\,Al_3Si_3O_{10}(OH)_2$ - $NaAl_3Si_3O_{10}\,(OH)_2$ - $KFeAlSi_4O_{10}(OH)_2$ - $KMgAlSi_4O_{10}(OH)_2$ with relatively constant Na/K, constant (Fe + Mg)/Si and containing up to 1.1 wt % FeO + MgO and 0.40 wt % TiO_2. Both biotite and muscovite contain deficiencies of alkalies (Guidotti, 1974; Rumble, 1978).

Staurolites display a limited amount of solid solution of the components $Fe_2Al_9Si_4O_{24}H_2$-$Mg_2Al_9Si_4O_{24}H_2$-$Fe_{1.625}Al_{9.25}Si_4O_{24}H_2$, with the Al_2O_3 content decreasing with increasing MgO/FeO in assemblage (1) (Fig. C-11). The mineral contains up to 0.15 wt % MnO with little ZnO (0.25 wt %) and TiO_2 (0.50 wt %).

Andalusites contain approximately 0.25 wt % Fe_2O_3 (measured as FeO) with minor TiO_2. Ilmenites are nearly pure $FeTiO_3$ with minor amounts of SiO_2, Al_2O_3, MgO and MnO. No measurable amounts of hematite components are present. The negligible amounts of observed Fe_2O_3 component are consistent with the ubiquitous presence of graphite in all samples. The ilmenite-graphite oxide assemblage is indicative of reducing conditions and suggests that all Fe-Mg silicates have low to negligible amounts of Fe_2O_3 (Rumble, 1973; 1976b).

Garnets are the only mineral with appreciable amounts of CaO (1.2 wt %) and MnO (2 wt %) but are composed predominantly of almandine component (∿83-85 mol %).

Geothermometry and Geobarometry

Temperatures calculated for the sample area are calibrated using the Ferry and Spear (1978) Gt-Bt geothermometer. Pressures are estimated using the Ghent (1976) Plag-Als-Gt-Qtz geobarometer, as several assemblages do contain plagioclase (these are not considered for the analysis of phase equilibria). Results indicate that a temperature of $\sim 520^{\circ}C$ and pressures of 3.5-4 kbar are associated with the last texturally equilibrated assemblages. These results are in good agreement with data from Hodges and Spear (1982) compiled from pelitic rocks in the general area of the Moosilauke septum.

Phase Equilibria

Geometric relationships. As discussed above, the classical model of metamorphism assumes that all mineral assemblages in a single outcrop attained equilibrium with a single externally derived fluid of fixed composition (i.e., the chemical potential of water, μH_2O, is constant). This assumption is also implicit in the Thompson AFM projection (Fig. C-11) displaying the various mineral assemblages. Tie-lines for the three mineral assemblages are displayed in Figure C-11 which is a projection from the minerals quartz, muscovite and ilmenite, and assumes a constant value of μH_2O for all assemblages. Garnet is not displayed in the phase diagram in Figure C-11 and will not be considered further due to the solubility of significant amounts of CaO and MnO, which effectively remove Gt off the AFM plane, relegating it as an extra phase in the model KFMASH system. In the model KFMASH system assemblages (1) and (3) are trivariant, while assemblage (2) is divariant. Thus, at constant values of pressure and temperature, assemblage (2) is invariant to changes in intensive variables, while assemblages (1) and (3) are univariant.

As viewed in the AFM projection, various examples of crossing tie-lines are observed. The presence of crossing tie-lines can be caused by several relationships: (1) the mineral assemblages crystallized at different pressure and/or temperature; (2) chemical components other than those considered occur in one or more minerals; (3) the chemical potential of water (μH_2O) is not constant for all mineral assemblages. Since all assemblages have crystallized in one outcrop (suggesting constant P and T) and reside mainly in the system KFMASH (minimizing the effects of extra chemical components), only a variable μH_2O appears likely as the cause for crossing tie-lines. The effects of variable μH_2O can be rigorously evaluated by allowing H_2O to be a component of the phase diagram (Fig. C-12). This four-component phase diagram (AFM-H_2O) effectively allows mineral assemblages to be associated with variable values of μH_2O. Inspection of Figure C-12 demonstrates that the problem of crossing tie-lines is resolved by considering H_2O as a component of the phase diagram. Planes of the St-Bt-Chl assemblages lie to the Fe-side of the four-phase volume, St-Bt-Chl-And, while planes of And-Chl-Bt lie to the Mg-side of the four-phase volume (Fig. C-12.) This arrangement of three-phase planes and four-phase volume demonstrates that the trivariant, three-phase assemblages [(1) and (3)] may equilibrate with variable values of μH_2O (each separate three-phase plane is associated with a unique value for μH_2O), while the divariant, four-phase assemblages (2) occurs at a unique and fixed value of μH_2O.

The compositonal relationships between the three mineral assemblages in

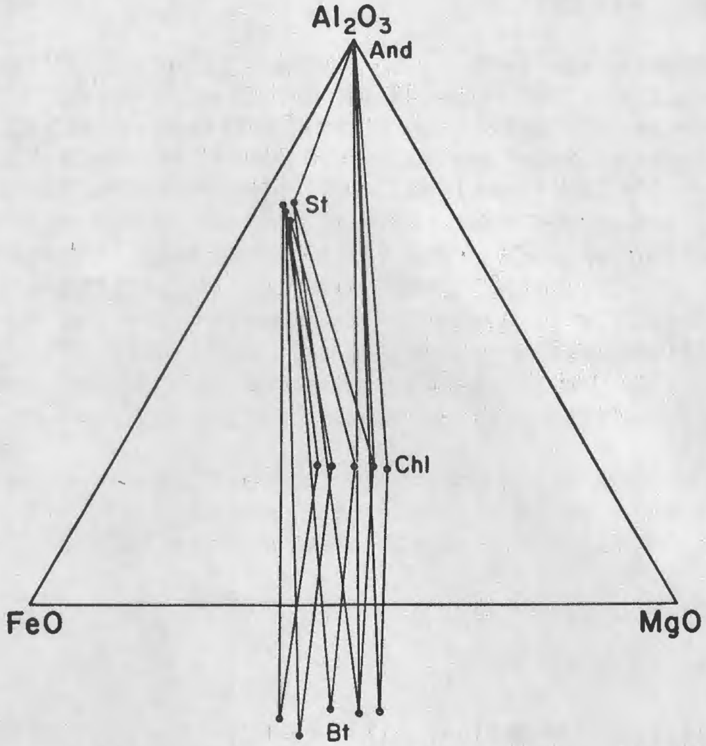
Al_2O_3
And
St
Chl
FeO
MgO
Bt

Fig. C-11. AFM projection of Wildwood mineral assemblages (And = andalusite, St = staurolite, Chl = chlorite, Bt = biotite, plus quartz and muscovite).

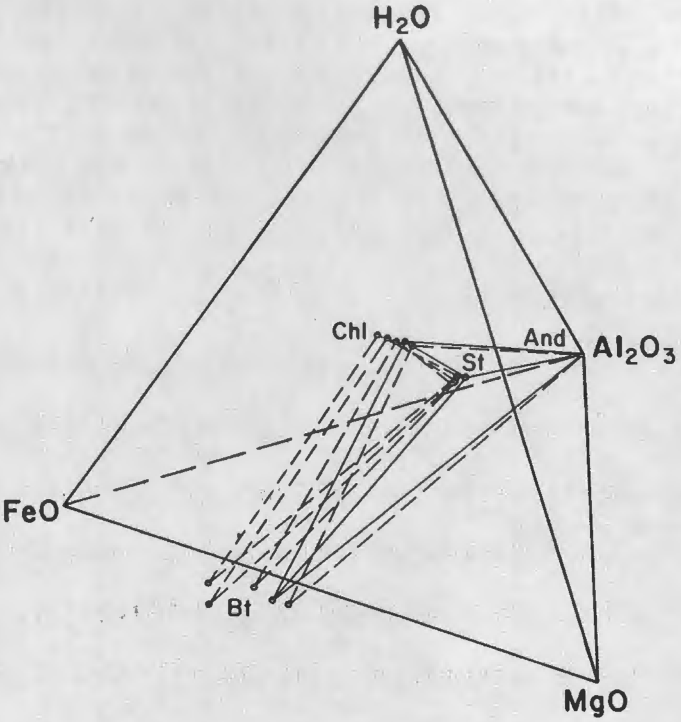
H_2O
Chl
And
Al_2O_3
St
FeO
Bt
MgO

Fig. C-12. AFM - H_2O phase diagram of Wildwood assemblages. Three-phase assemblages define planes (Chl-Bt-St and Chl-And-Bt); while the four-phase assemblage (And-St-Chl-Bt) forms a sub-volume within the AFM-H_2O tetrahedron.

Figure C-12 demonstrate that μH_2O varies from assemblage to assemblage. The diagram can also provide information constraining the relative change in μH_2O for these three assemblages. In a phase diagram like Figure C-12 any ray drawn from one of the component apices describes a decrease in that component as one proceeds along the arbitrary ray away from that component (Korzhinskii, 1959). For example, a ray drawn from the H_2O apex describes decreasing μH_2O along the ray. Construction of such a ray illustrates that the ray would first intersect the most Fe-rich St-Chl-Bt plane and would successively pierce more Mg-rich St-Chl-Bt planes. This geometric relationship is due to the fact that Chl is always the most magnesian phase and acts to "lean" the planes over towards the Mg-side. Thus, in the St-Ch-Bt assemblage decreasing μH_2O is associated with increasing X_{Mg} in the three phases. Similar arguments can be made for assemblages (2) and (3) such that the four-phase volume (assemblage 2)) is associated with a value for μH_2O intermediate to that for assemblages (1) and (3), and that in assemblage (3) decreasing μH_2O is also associated with increasing X_{Mg}.

Analytical representation. The change in both mineral composition and chemical potential of water illustrated in the phase diagram in Figure C-12 can be viewed in a more quantitative fashion. The phase equilibria can be analytically formulated using the Gibbs Technique (Spear et al., 1982). This approach quantitatively relates changes in mineral composition to changes in various intensive parameters. In Figure C-13 the change in mineral composition in assemblages (1) and (3) is plotted versus $\Delta\mu H_2O$. Differences in μH_2O are calculated relative to assemblage (2) that has arbitrarily been fixed to a value of 0. The calculations are performed for mineral compositions in the model KFMASH systems. Components such as Na_2O and TiO_2 have been omitted due to the fact that the Na/K ratios in both biotite and muscovite remain constant, and TiO_2 contents are both small and constant in all mineral phases. Ferry (1979) has also shown that small amounts of Na_2O and TiO_2 in biotite and muscovite do not signicantly effect calculations of this type.

The diagram in Figure C-13 was calculated by solving for the variable $(\partial\mu H_2O/\partial X_{Fe}^{Bt})$ at constant P and T. This variable was then integrated over values of ΔX_{Fe} of 0.01 and resolved iteratively over the given range of X_{Fe}. Initial mineral compositions for assemblages (2) are the starting points for the calculations in both assemblages (1) and (3). Mineral K_D's are assumed to be constant and equal to those measured in assemblage (2). The data collected from various examples of assemblages (1) and (3) are also plotted in Figure C-13. These data points were calculated by solving for the variable $(\partial\mu H_2O/\partial X_{Fe}^{Chl})_{P,T}$ and multiplying by the observed ΔX_{Fe}^{Chl} relative to that in assemblage (2). Chlorite was used to independently evaluate the accuracy of the phase diagram which was calculated using $(\partial\mu_{H_2O}/\partial X^{Bt}_{Fe})_{P,T}$. The agreement between calculated and measured values is very good and confirms the conclusions concerning mineral composition and chemical potential of water.

Discussion and conclusions. The data illustrated in Figures C-12 and C-13 clearly demonstrate that interbedded amphibolite grade pelitic metasediments preserve differences in the chemical potential of water. Furthermore, the algebraic analysis presented in Figure C-13 suggests that the magnitude of the differences is on the order of 100 cal. These observations have implications concerning both the behavior of a volatile phase during the amphibolite grade metamorphism and the ultimate processes that led to the formation of these differences.

The first and most obvious conclusion is that these interbedded pelites have not equilibrated with an external reservoir of fluid of fixed composition. In contrast, the data suggest that various beds have equilibrated with fluids of variable composition. This is inconsistent with massive infiltration of externally derived fluid. Such an infiltration process would most certainly eliminate such small preserved differences. This is due to the fact that the buffer capacity of trivariant assemblages is relatively small. These types of assemblages **respond** to changes in intensive variables; they do not effectively **resist** changes as do divariant assemblages.

Several other processes, however, could be responsible for the observed differences in μH_2O. These include (1) initial compositional variations, (2) small amounts of infiltration varying from bed to bed, and (3) small amounts of infiltration of differing fluid composition. The third possibility can probably be ruled out because it is geologically unrealistic to have several different fluid compositions selectively moving through various beds. The criteria for differentiating between the first two possibilities are not straightforward, as the data are consistent with both processes. Thus, either small amounts of differing infiltration of externally derived fluids or initial differences in bulk composition are most likely responsible for the observed differences in the chemical potential of water on this single outcrop.

BEAVER BROOK FOSSIL LOCALITY

Access

Drive along New Hampshire rt. 112 to a point approximately 0.75 km W. of Lost River. Here there are signs marking the Appalachian Trail. Park cars under the trees, on the S. side of the road, near Appalachian Trail signs. The Beaver Brook fossil locality may be reached by following the white-blazed, Appalachian trail S., across the floor of Kinsman Notch, and climbing about 0.5 km up the lower slopes of Mt. Moosilauke.

Hiking Route

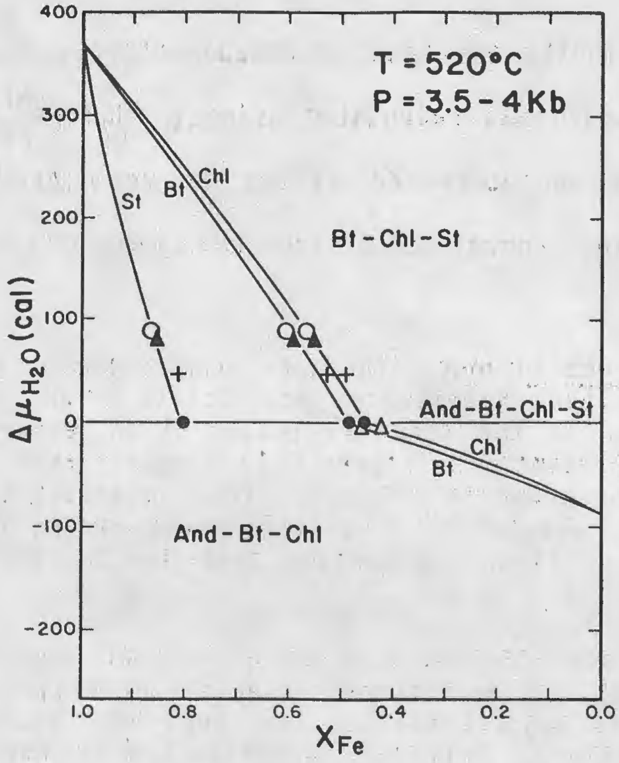

Fig. C-13. Calculated μ H_2O vs. X_{Fe} diagram for Wildwood assemblages. Pairs and triples of identical symbols depict co-existing minerals.

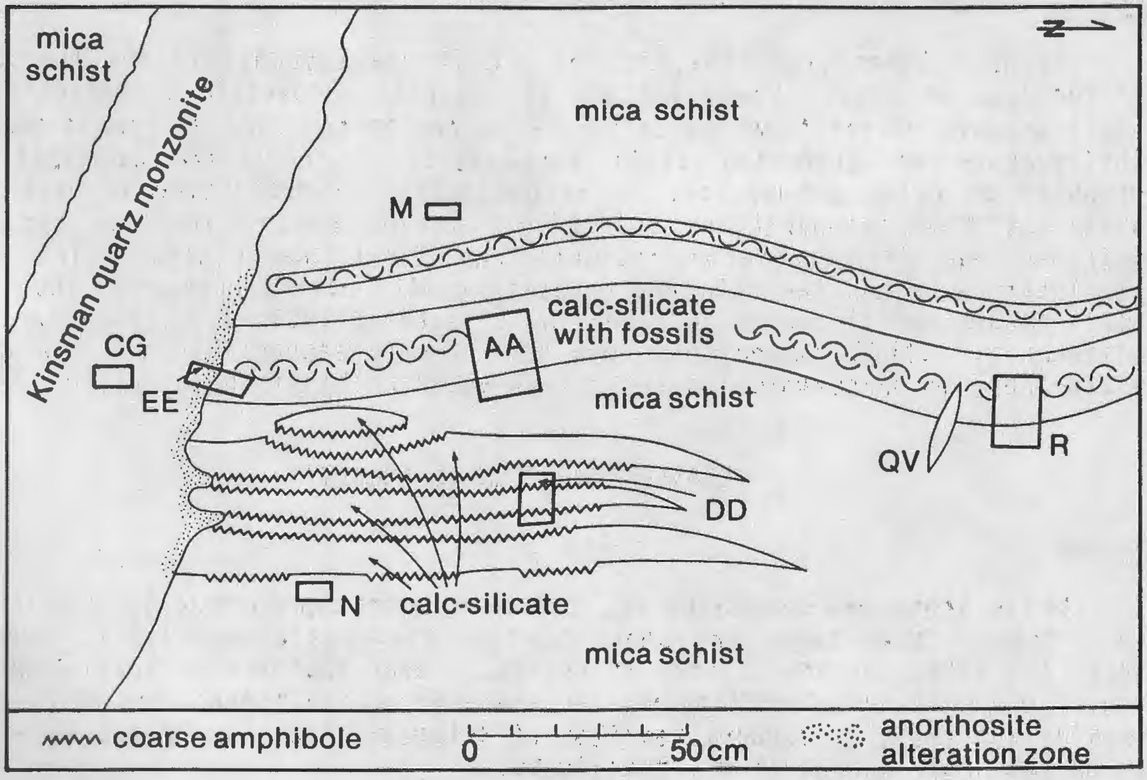
N
mica schist
mica schist
Kinsman quartz monzonite
M
calc-silicate with fossils
AA
CG
EE
mica schist
QV
R
DD
N
calc-silicate
mica schist
coarse amphibole
0
50 cm
anorthosite alteration zone

Fig. C-14. Outcrop map of Beaver Bk. fossil locality. Sample locations given by letter symbols.

WARNING: CASCADES OF BEAVER BROOK ARE VERY SLIPPERY. EXERCISE EXTREME CAUTION.

Hike S. on the trail (white blazes) for about 0.5 km to the first cascades of Beaver brook. At your feet are large feldspar phenocrysts (up to 10 cm) in the Kinsman Quartz Monzonite. Visible in the cascades are mica schists of the Littleton Formation cross-cut by aplite dikes. A knife-sharp contact between Kinsman and Littleton may be found at the base of the ledge, down in the Brook (CAUTION: SLIPPERY WHEN WET!).

Continue following the white-blazed trail climbing alongside the cascades. Do not attempt to climb straight up the cascades because the rocks are very slippery. Over the course of the next 0.5 km you will notice that the Littleton mica schists are not nearly so aluminous as those at Wildwood roadcut. There are some muscovite-garnet schists but most rocks lack muscovite, have biotite with intermediate Fe/(Fe + Mg), and contain calcic-plagioclase. In at least one case (sample 70-184-N) there are two coexisting plagioclases: An 83 and An 67. The fossiliferous calc-silicate is usually interbedded with calcic mica schists rather than with aluminous pelites such as those at Wildwood roadcut.

There are no obvious landmarks to help locate the fossil locality. It will be marked for the IMA trip so you can't miss it. We will have to cross the Brook, then climb a gently sloping ledge to the base of a cascade. USE EXTREME CAUTION: ROCKS ARE VERY SLIPPERY.

Fluid-rock behavior at Beaver Brook was dramatically different from that at Black Mountain or Wildwood roadcut. You will be able to see two different types of evidence for fluid infiltration with your own naked eyes. Still other evidence for infiltration is given in the accompanying figures and will be discussed on the outcrop. Take a moment for orientation and note the color contrasts between pink-orange and green banded calc-silicates, dark gray mica schists, and pale gray-dirty white dikes of aplite and quartz monzonite. Thermobarometry for these rocks gives metamorphic conditions of 3.5 kbars and 600°C (Fig. C-14).

There are two pieces of evidence for infiltration that may be seen in the ledge before you. These are (1) a sharp, infiltration metasomatic front of anorthite in the margin of the quartz monzonite dike, on the left side of the ledge; and (2) fossil brachiopods replaced by wollastonite, on the right side.

A close inspection of the quartz monzonite dike shows a creamy, translucent zone (2-4 cm thick) in the dike margin where it truncates calc-silicate beds. The zone is absent where the dike crosscuts mica schist. Microscopy shows that the marginal zone consists of myrmekitic anorthite (An 95-98) - quartz pseudomorphs after the quartz monzonites's primary oligoclase and microline. A microprobe traverse across the replacement front reveals a change in plagioclase composition from An 95 to An 19 over a distance of 1-2 mm. The anorthite zone has features diagnostic of infiltration metasomatism (as discussed by Korzhinskii and Hofmann) including (1) one-way mass transfer (i.e. Ca from calc-silicate to dike rock) and (2) a sharp replacement front separating mineral assemblages that are not in chemical equilibrium. The anorthite zone documents a component of the direction of

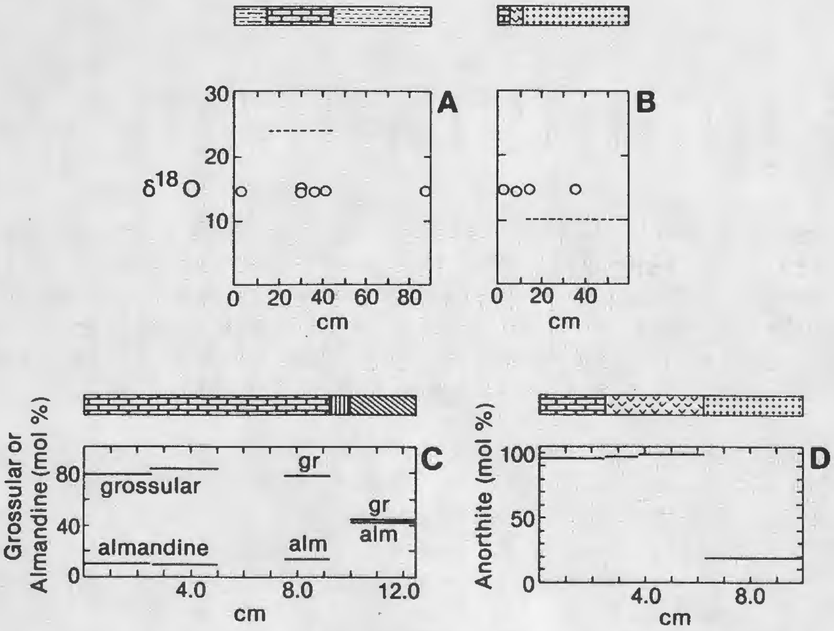

Fig. C-15. (A) shows $\delta^{18}O$ values vs. distance perpendicular to bedding for traverses AA and R, combined, and samples M and N. Circles show measured data. Dashed line gives inferred pre-metamorphic isotopic composition. Dashed pattern denotes mica schist, brick work is calc-silicate. (B) is a plot of ^{18}O vs. distance perpendicular to dike/country rock contact for traverse EE and CG. The "V" pattern is anorthite replacement zone, the "+" pattern is Kinsman Quartz Monzonite. (C) shows garnet composition vs. distance perpendicular to bedding for traverse AA. Vertical ruled pattern is non-garnetiferous calc-silicate, diagonal ruled pattern is amphibolite. (D) is a plot of plagioclase composition vs. distance perpendicular to the dike/country rock contact for traverse EE and CG.

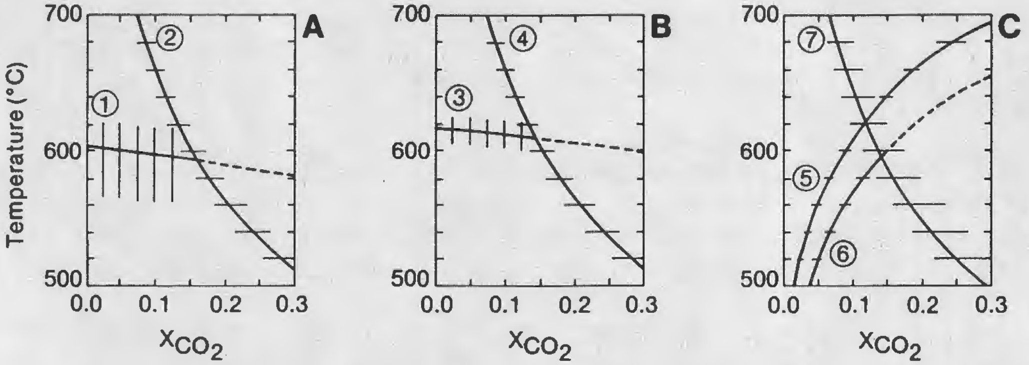

Fig. C-16. Thermobarometry on T- XCO_2 diagrams at 3.5 kbars. Short horizontal and vertical bars give uncertainties in location of equilibrium curves for a range of 2 about average values of equilibrium constants. In (A) equilibrium 1 is Amp + Czo + 2Q = 5 Cpx + 9 Pl + $4H_2O$, (samples AA, R, DD, and EE) and 2 is Czo + CO_2 = 3 Pl + Cc + H_2O. (B) shows equilibrium 3, 4 Czo + Q = 5 Pl + Gt + 2 H_2O (sample AA) and equilibrium 4, Czo + CO_2 = 3 Pl + Cc + H_2O. In (C) equilibrium 5 is Cc + Q = Wo + CO_2 (sample R) equilibrium 6 is 2 Czo + 5 Cc + 3Q = 3Gt + 5 CO_2 + H_2O. Dashed lines are metastable extensions. (Amp = amphibole, Czo = clinozoisite, Q = quartz, Cpx = clinopyroxene, Pl = plagioclase, Cc = calcite, Gt = garnet, Wo = wollastonite).

fluid flow. Calcic aqueous solutions flowed from calc-silicate wall rocks into the quartz monzonite dike.

Fossil brachiopods replaced by wollastonite are located on the right side of the ledge. The original discovery of fossils (by C.V. Guidotti) was made on an exposed portion of the ledge where weathering had etched out their distinctive forms. Weathered material has since been quarried away for examination by A.J. Boucot who identified four genera of Early Devonian brachiopods including Acrospirifer, Leptocoelia, Atrypa, and either Leptostrophia or Protoleptostrophia. The present outcrop surface has not as yet weathered very deeply. You should be able to see, however, the characteristic cross-section of brachiopod shells, e.g. a shape like a flattened parenthesis.

The presence of the assemblage wollastonite-quartz-calcite in the fossil shells is evidence of fluid infiltration during metamorphism. Fluid/rock ratios may be calculated with the model of J.M. Ferry. Consider the decarbonation reaction Quartz + Calcite = Wollastonite + CO_2. At the conditions of metamorphism at Beaver Brook, 3.5 kbars and $600^{\circ}C$, the equilibrium XCO_2 for this reaction is 0.09. But, the reaction produces pure CO_2. The decarbonation reaction would saturate a rock of normal porosity with CO_2 after only a miniscule amount of reaction. Thus, reaction would cease after formation of an undetectable amount of wollastonite. We are faced with a problem: How does one make wollastonite in detectable amounts at temperatures well below its stability limit in pure CO_2? The answer is to infiltrate the rock with a fluid whose XCO_2 is less than the equilibrium value. The infiltrating fluid sweeps away product CO_2 and makes it possible for decarbonation reactions to operate until reactants are exhausted. Calculated fluid/rock ratios at Beaver Brook range from 1.5 to 5.0, with a value of 4.0 (by volume) in the wollastonite bed.

Additional evidence of infiltration include possible hydrothermal graphite in the quartz monzonite dike and changes in $\delta^{18}O$ inferred to have occurred during metamorphism. These features cannot be seen in outcrop but will be discussed with the aid of the accompanying figures (Figs. C-15 through C-18).

Why did Beaver Brook experience infiltration during metamorphism while Black Mountain and Wildwood did not?

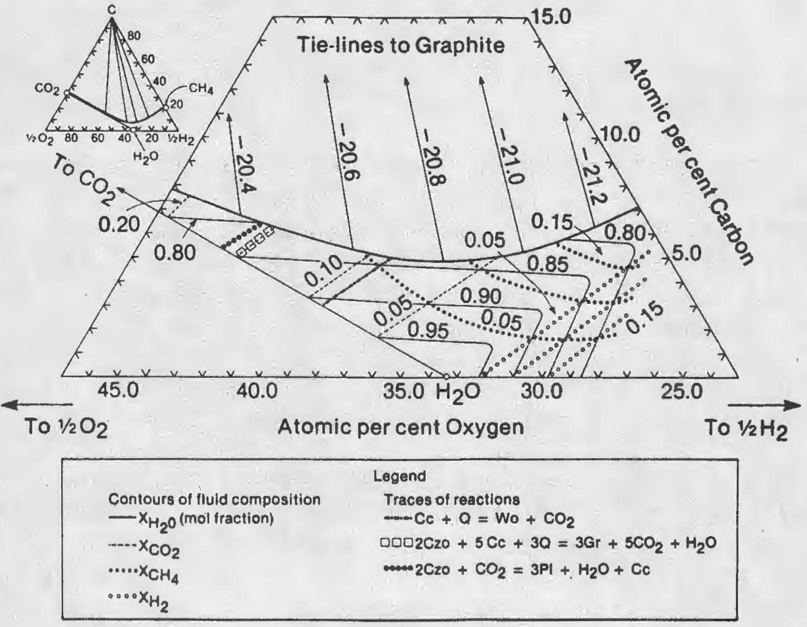
C
80
60
40
20
CO_2
CH_4
½O_2 80 60 40 20 ½H_2
H_2O
Tie-lines to Graphite
15.0
10.0
5.0
Atomic per cent Carbon
-20.4
-20.6
-20.8
-21.0
-21.2
To CO_2
0.20
0.80
0.10
0.05
0.15
0.80
0.85
0.90
0.05
0.95
0.05
0.15
45.0
40.0
35.0 H_2O
30.0
25.0
To ½O_2
Atomic per cent Oxygen
To ½H_2
Legend
Contours of fluid composition
—— X_{H_2O} (mol fraction)
----- X_{CO_2}
••••• X_{CH_4}
∘∘∘∘ X_{H_2}
Traces of reactions
Cc + Q = Wo + CO_2
□□□ 2Czo + 5 Cc + 3Q = 3Gr + 5CO_2 + H_2O
••••• 2Czo + CO_2 = 3Pl + H_2O + Cc

Fig. C-17. Phase diagram of system C-O-H at 600°C, 3.5 kbars. Small triangle shows entire C-O-H diagram. Heavy line is graphite saturation curve and straight lines from it to graphite corner are two-phase lines. Large trapezoidal diagram is enlargement of H_2O-rich region. Contours of fluid composition drawn in one-phase fluid field. Tie-lines labeled with log fo_2 shown in two-phase, graphite-fluid region. Traces of three decarbonation or combined decarbonation-dehydration reactions are given. Dehydration reactions lie parallel to contours of XH_2O.

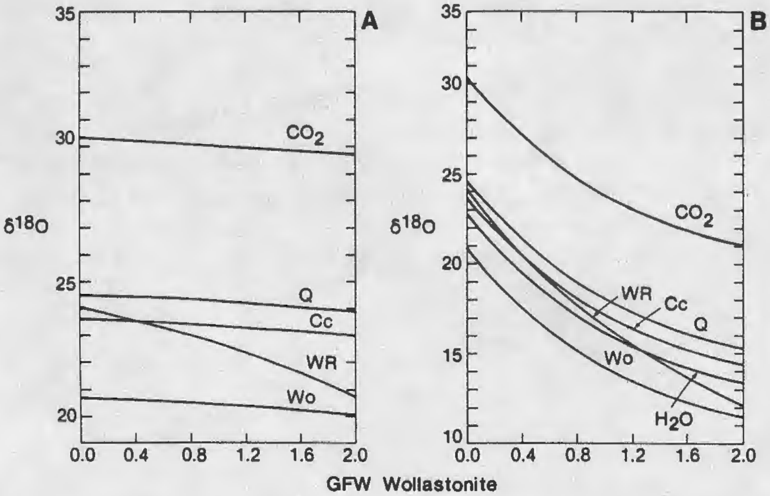

Fig. C-18. Plots of $\delta^{18}O$ vs. number of gram formula weight (gfw) units of wollastonite formed in the reaction Cc + Q = Wo + CO_2. (A) shows expected changes in $\delta^{18}O$ as function of reaction progress when Rayleigh distillation is operative. Fluid evolved is pure CO_2. (B) gives expected changes in $\delta^{18}O$ in a rock infiltrated by H_2O with a $\delta^{18}O$ value of 12.5°/oo. Initial whole rock $\delta^{18}O$ = 24°/oo.

D. MINERALOGY, PETROLOGY AND P-T EVOLUTION OF THE ORFORDVILLE AREA, WEST-CENTRAL NEW HAMPSHIRE AND EAST-CENTRAL VERMONT

Frank S. Spear and Douglas Rumble, III

INTRODUCTION

In the vicinity of Orfordville, New Hampshire, a wide variety of different rock types crop out, offering the opportunity to examine the metamorphism of different bulk compositions within a restricted geographical area. These different rock types include pelitic schists, amphibolites, calc-silicates, iron formations, ultramafics, and granitic gneisses. Within these units there are a variety of interesting and well characterized mineral assemblages including multiple amphibole assemblages, coexisting plagioclase feldspars, and the type locality of wonesite. The relationship between fluid flow and metamorphic evolution has been investigated in certain localities and recently, the relationship between the structural and pressure-temperature evolution of the belt has been examined.

The purpose of this trip is to examine various aspects of the mineralogy, petrology, P-T and fluid evolution of rocks from the vicinity of Orfordville, N.H.. The objectives of the trip are: (1) to examine the geologic setting and phase relations of multiple amphibole-bearing assemblages; (2) to discuss the phase relations in multiple plagioclase-bearing assemblages; (3) to examine the type locality of the Na-mica, wonesite; (4) to discuss the detailed behavior of the fluid phase during metamorphism; (5) to examine the regional structural setting, and finally; (6)to discuss the P-T evolution of the Orfordville anticlinorium and the evidence for this evolution.

GEOLOGIC SETTING

The general geologic setting of the Orfordville Area is shown in Figure D-1. Figure D-2 shows an enlargement of the S.W. corner of the Mt. Cube quadrangle, which contains most of the stops for this excursion. The area consists of a sequence of metamorphosed Ordovician igneous and sedimentary rocks separated by an unconformity from a sequence of metamorphosed Silurian and Devonian strata. The general structural setting is one of two, NNE trending anticlinoria, the Bronson Hill anticlinorium and the Orfordville anticlinorium. The area of investigation includes portions of the Strafford, Mt. Cube, Rumney, Hanover, Mascoma, Cardigan, Claremont and Sunapee 15' quadrangles, in west-central New Hampshire and east-central Vermont (Figs. D-1 and D-2). General references to the geology of the area include Hadley (1942), Lyons (1955), Chapman (1939).

Stratigraphy (Stratigraphic relations are shown in the legend of Figure D-1)

Oliverian Magma Series. The basement is comprised of felsic gneisses and magnetite-bearing granitoids belonging to the Oliverian Magma series of Billings (1956), which crop out in a sequence of gneiss domes along the Bronson Hill anticlinorium (the Croydon dome, the Mascoma dome, the Smarts Mountain dome and the Owls Head dome) and within the Lebanon dome in the Orfordville anticlinorium. Whole-rock Rb-/Sr isochron ages (Naylor, 1969) for the Lebanon and Mascoma domes are 440 ±20 and 440 ±45 Ma respectively, with initial Sr^{87}/Sr^{86} ratios of 0.706 and 0.705. Pb^{207}/Pb^{206} ages on zircon separates from the gneisses of the Mascoma dome are 450 ±25 (Naylor, 1969). The Oliverian rocks in the cores of the Bronson Hill gneiss domes are generally believed to represent arc-derived volcanics from a Taconian island arc complex (the Bronson Hill plate of Robinson and Hall, 1980).

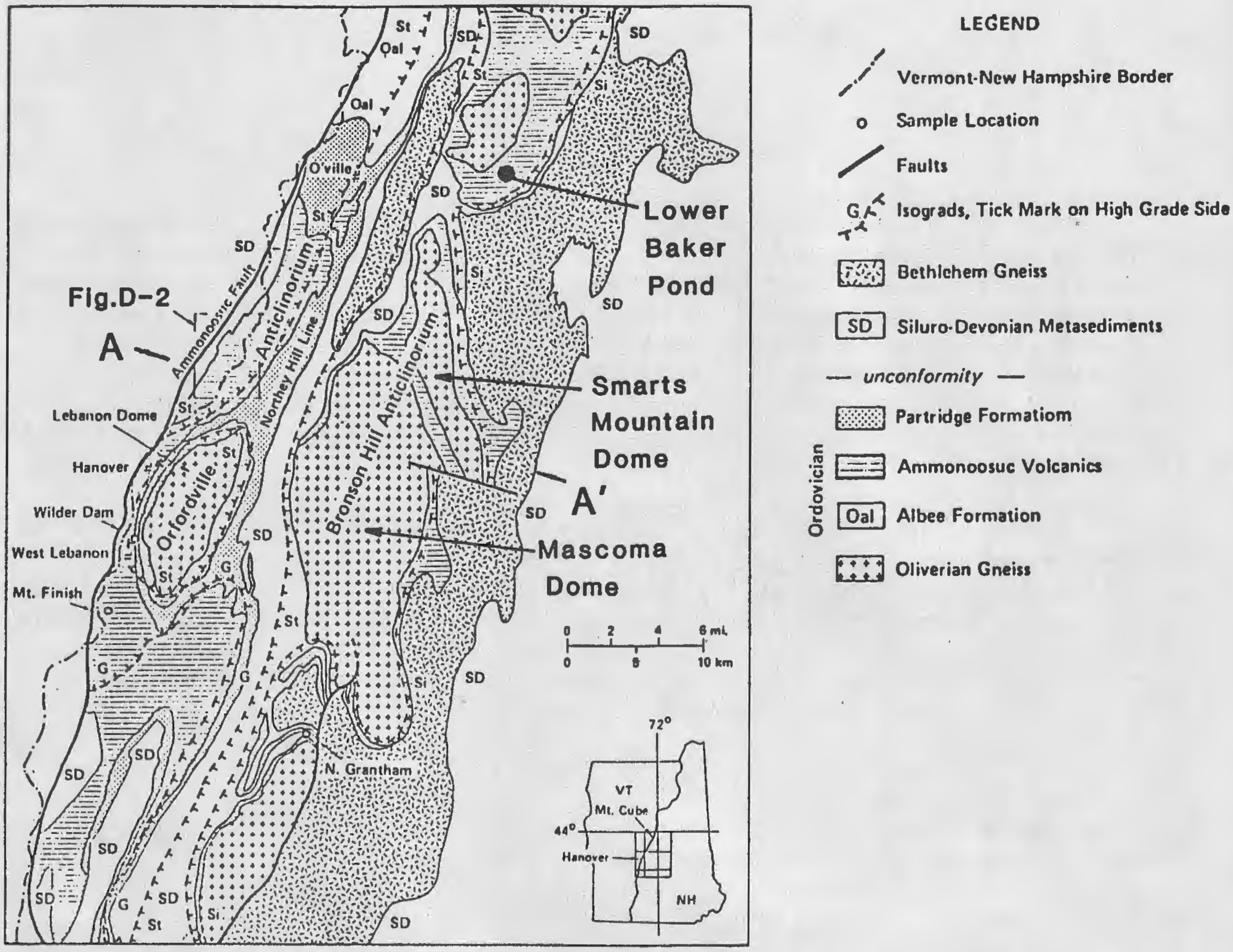
LEGEND
Vermont-New Hampshire Border
Sample Location
Faults
Isograds, Tick Mark on High Grade Side
Bethlchem Gneiss
SD
Siluro-Devonian Metasediments
— unconformity —
Partridge Formatiom
Ammonoosuc Volcanics
Oal
Albee Formation
Oliverian Gneiss
Ordovician
Lower Baker Pond
Smarts Mountain Dome
Mascoma Dome
Fig.D-2
A
A'
Ammonoosuc Fault
Orfordville Anticlinorium
Northey Hill Line
Bronson Hill Anticlinorium
Lebanon Dome
Hanover
Wilder Dam
West Lebanon
Mt. Finish
O'ville
N. Grantham
SD
St
Si
G
Oal
0 2 4 6 mi.
0 5 10 km
72°
44°
VT
Mt. Cube
Hanover
NH

Figure D-1. Geologic map of west-central New Hampshire and adjacent Vermont depicting the general geology of the Orfordville and Bronson Hill anticlinoria. Isograds shown are G=garnet, St=staurolite, and Si=sillimanite. Towns are shown with # symbols and sample locations with circles. The location of Figure D-2 is shown by the box. Line A-A' shows position of cross section in Figure D-3. Geology is after Hadley (1942), Billings (1956), Lyons (1955), Rumble (1969), Thompson et al. (1968), Thompson and Norton (1968), and the authors' mapping.

Albee Formation. The Albee Formation is the oldest of the metamorphosed sedimentary units exposed in the area and is comprised of a sequence of pin-striped quartzites and semi-schists. It is restricted in outcrop area to regions west of the Bronson Hill anticlinorium. In Figure D-2 it can be seen to the NE of the village of Orfordville.

Ammonoosuc Volcanics (and Post Pond Volcanics). The Ordovician (?) Ammonoosuc Volcanics crop out in two distinct belts in the study area. Along the Bronson Hill anticlinorium, the Ammonoosuc overlies the Oliverian gneisses. In the Orfordville anticlinorium, the Ammonoosuc overlies the gneisses of the Lebanon dome and also crops out in extensive areas to the south and north of the dome. Along the Orfordville anticlinorium, the Ammonoosuc structurally underlies the Albee formation, as can be seen in the north-central part of Figure D-1. This observation led Hadley (1942) to map these volcanic units and associated black schists as a separate formation, older than the Albee, which he termed the Orfordville Formation. The Orfordville Formation was made up of a Post Pond Volcanics member, a black schist member, and the Brick Hill schist member. Reinterpretation of the stratigraphy and structure by Thompson et al. (1968) and Rumble (1969) led to the correlation of these units with the Ammonoosuc Volcanics, Partridge Formation and Littleton Formations, respectively. As will be discussed below, reinterpretation of the stratigraphic correlations has important implications for the interpretation of the structure of the area. The stratigraphic correlations are given here because much of the cited literature uses the nomenclature of Hadley (1942).

The Ammonoosuc Volcanics are comprised of metamorphosed mafic to felsic volcanic rocks and volcanogenic sediments with generally more mafic compositions in the lower part of the section and felsic compositions in the upper part. In places, relic igneous features such as pillows, crosscutting dikes and chill margins can be observed. Some of the volcanic units are interpreted to have been hydrothermally altered, presumably by sub-sea floor hydrothermal processes, giving rise to bulk compositions low in Ca and with a low Fe/(Fe+Mg). It is these bulk compositions that give rise to the cordierite-orthoamphibole gneisses. Other sequences are interpreted to have had an admixture of sedimentary material such as clays, giving rise to aluminous staurolite-hornblende bearing assemblages. Most of the localities to be visited in this area are in the Ammonoosuc Volcanics. The Ammonoosuc is believed to represent island-arc related volcanics generated during the Taconian Orogeny.

Partridge Formation. The Ordovician Partridge Formation is a sequence of rusty-weathering graphitic schists with minor volcanics and turbidite. In this area, only minor outcrops of Partridge are observed along the Bronson Hill anticlinorium, but extensive exposures are found in the Orfordville anticlinorium.

Silurian-Devonian Sequence. The Taconian unconformity separates the pre-Silurian Albee, Ammonoosuc, Partridge sequence from the overlying Silurian-Devonian Sequence. Locally along the unconformity is the basal Silurian Clough Quartzite, which is locally overlain by the Silurian Fitch Formation. The Fitch is comprised dominantly of calc-silicates and calcareous schists.

Overlying the Fitch is the Devonian Littleton Formation, which, in this area, is comprised dominantly of pelitic schist. The Littleton crops out along the west side of the Orfordville anticlinorium and in the synclinorium that separates the Bronson Hill and Orfordville anticlinoria.

New Hampshire Magma Series. Pre- to syntectonic ilmenite-bearing granitoid sheets, collectively known as the New Hampshire Magma series, crop out along, and to the east of, the Bronson Hill anticlinorium. The only representative of the New Hampshire Magma Series in the area of Figure D-2 is the Bethlehem Gneiss. The Bethlehem Gneiss has yielded an Rb/Sr isochron age of 405 ±78 Ma (Lyons and Livingston, 1977) and a recent zircon age of approximately 400 Ma (J. Aleinekoff, personal communication, 1986).

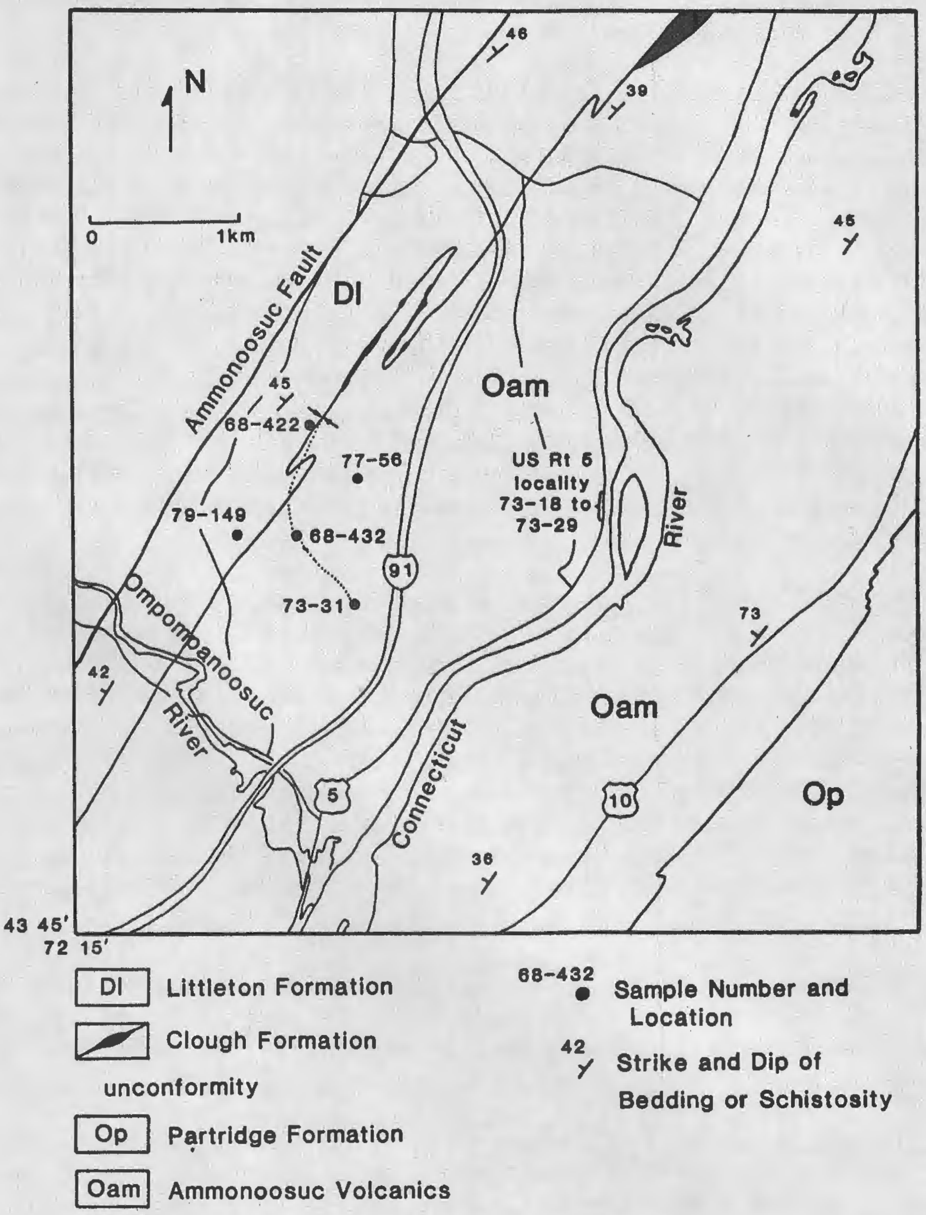
N
0
1km
46
39
45
Ammonoosuc Fault
Dl
Oam
45
68-422
77-56
US Rt 5
locality
73-18 to
73-29
River
79-149
68-432
91
73-31
Ompompanoosuc
River
42
73
Connecticut
Oam
5
10
Op
36
43 45'
72 15'
Dl
Littleton Formation
Clough Formation
unconformity
Op
Partridge Formation
Oam
Ammonoosuc Volcanics
68-432
Sample Number and Location
42
Strike and Dip of Bedding or Schistosity

Figure D-2. Geologic map of the south-west corner of the Mt. Cube quadrangle showing sample localities and structural information.

Structure

The structural grain in the field area is dominated by the two NNW-trending anticlinoria: the Bronson Hill and Orfordville anticlinoria. The Bronson Hill extends from Connecticut to Maine and is characterized by a series of gneiss domes mantled by Ordovician and Silurian-Devonian Strata. The Orfordville anticlinorium crops out for approximately 100 km along strike and contains symmetrical flanking belts of Silurian-Devonian and a core of axially asymmetric pre-Silurian rocks. Two domal structures are present in the Orfordville anticlinorium in the area of Figure D-1: the Lebanon dome, which has a core of Oliverian gneisses, and an unnamed dome centered near the village of Orfordville.

The second dominant structural element, which is not so apparent in the map pattern of Figure D-1, is a set of large scale, westward-verging recumbent nappes. Recumbent folds associated with the Skitchewaug nappe are found along the Bronson Hill anticlinorium. The pattern of refolded folds in the vicinity of N. Grantham (Fig D-1) is the result of refolding of the Skitchewaug nappe. The map pattern in the Orfordville anticlinorium is also interpreted as a large scale recumbent fold: the Cornish nappe (Thompson et al., 1968).

An interpretative cross section through the study area is shown in Figure D-3. The figure depicts the two anticlinorial structures, and the two recumbent folds. It should be noted that there is some debate as to whether or not the Cornish nappe exists. If it does exist, however, it is clearly the largest fold nappe in the region. The Skitchewaug nappe, which has a considerable aerial extent in southern New Hampshire, is dying out at this latitude.

In addition to the Skitchewaug and Cornish nappes, there is also metamorphic evidence for additional, higher structural level nappes that are now completely removed by erosion in the map area. In the vicinity of Bellows Falls, Vermont, the Fall Mountain nappe is exposed immediately above the Bellows Falls Pluton of the Bethlehem Gneiss and the Skitchewaug nappe (see Spear and Chamberlain, this guidebook, part F). In the area of Figure D-1 (see cross section in D-3 also), an outlier of Bethlehem gneiss crops out just to the north of the Mascoma dome in the synclinorium between the Bronson Hill and Orfordville anticlinoria, in the same structural position as the Bellows Falls Pluton to the south. Metamorphic P-T paths from the area (to be discussed below) are consistent with the emplacement of thrust sheets at structural levels above the present erosion level. It is tempting to speculate that these include a northern extension of the Fall Mountain nappe.

Two other tectonic elements shown in Figure D-1 and D-3 are worthy of note. The Northey Hill line defines the eastern border of the Orfordville anticlinorium. Originally mapped as a thrust fault (Hadley, 1942), the Northey Hill Line is now believed to represent a folded unconformity offset by numerous faults. The Northey Hill line is also the locus of a vertical cleavage belt that apparently accommodated much of the strain associated with the development of the Bronson Hill and Orfordville anticlinoria. The other feature is the Ammonoosuc Fault, which bounds the west side of the map area of Figure D-2. The Ammonoosuc Fault is a late stage, low angle normal fault, which dips approximately 40^{o} to the west and juxtaposes garnet to kyanite grade rocks on the east against chlorite grade rocks on the west. Movement along the fault probably occurred during the Mesozoic and is associated with the rifting along the Connecticut Valley.

In summary, the structural evolution during the Acadian Orogeny consisted of early, west-verging recumbent folds and thrust nappes (the Cornish, Skitchewaug and possibly Fall Mountain nappes) followed by intense folding and uprising of the gneiss domes that created the Bronson Hill and Orfordville anticlinoria and intervening synclinorium.

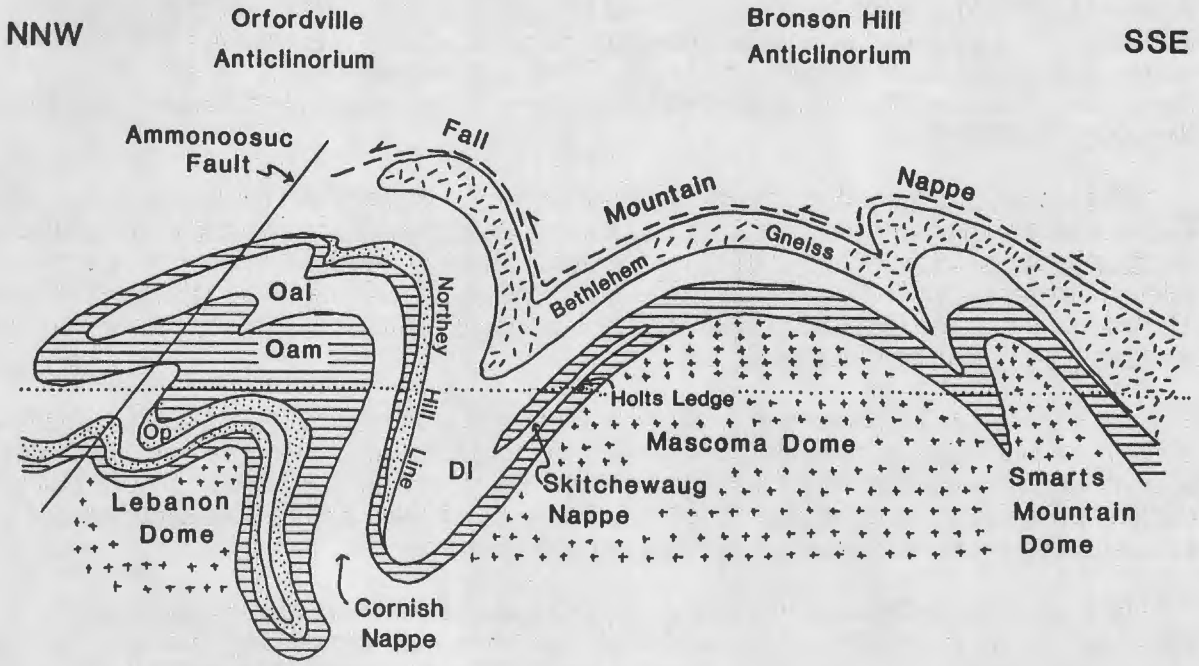
NNW
Orfordville Anticlinorium
Bronson Hill Anticlinorium
SSE
Ammonoosuc Fault
Fall Mountain Nappe
Bethlehem Gneiss
Oal
Oam
Op
Northey Hill Line
Dl
Holts Ledge
Mascoma Dome
Skitchewaug Nappe
Lebanon Dome
Cornish Nappe
Smarts Mountain Dome

Figure D-3. Schematic cross section across the Orfordville and Bronson Hill anticlinoria. Movement along the Ammonoosuc Fault has been restored. The Fall Mountain Nappe does not crop out in this area, but is inferred from the P-T paths of metamorphic rocks from the region.

METAMORPHISM AND P-T EVOLUTION

The metamorphic grade in the area of investigation ranges from biotite grade in the SW part of the Orfordville anticlinorium up to staurolite-kyanite grade along strike to the NW and up to sillimanite grade across strike to the east (see Fig. D-1). Note, however, that the Northey Hill line is the locus of a belt of low-grade metamorphism suggesting that the synclinorium separating the Bronson Hill from the Orfordville anticlinoria contains downfolded high-level, low grade rocks.

The metamorphic field gradient is of Barrovian kyanite-sillimanite type. P-T conditions from geothermobarometry are 450-500 °C for the biotite to garnet zone up to 560-570 °C for the staurolite-kyanite zone with computed pressures of 4-5.5 kbar (see Fig. D-4). The metamorphic field gradients in the area, shown by the lines in Figure D-4, are approximately 125 °C/kbar (35 °C/km) in a SSW-NNE direction along the strike of the Orfordville anticlinorium and approximately isobaric across strike of the two anticlinoria in a W-E direction. As will be discussed below, these P-T conditions represent only single points on what are complex and diverse P-T paths.

Metamorphic P-T trajectories have been described for several samples from the area by Spear and Rumble (1986) and Orange(1985). By combining detailed petrographic analysis, geothermobarometry on matrix and inclusion minerals, quantitative modelling of zoned minerals such as garnet, and Schreinemakers' analysis of amphibolite assemblages, it was possible to deduce a portion of the prograde P-T path of these rocks.

P-T Paths From Zoned Garnets

Chemical zoning profiles in metamorphic garnets have been used to model quantitatively the metamorphic reactions responsible for the generation of the zoning profile and from this infer the P-T trajectory of metamorphism. The method is that described by Spear and Selverstone (1983) and involves solution of a system of simultaneous linear differential equations for the slopes of T-X and P-X isopleths. The change in T and P can then be computed from the total differential of T and P:

$$dT = \left(\frac{\partial T}{\partial X_1}\right)_{X_{j\neq 1}} dX_1 + \left(\frac{\partial T}{\partial X_2}\right)_{X_{j\neq 2}} dX_2 + \ldots \left(\frac{\partial T}{\partial X_n}\right)_{X_{j\neq n}} dX_n,$$

and

$$dP = \left(\frac{\partial P}{\partial X_1}\right)_{X_{j\neq 1}} dX_1 + \left(\frac{\partial P}{\partial X_2}\right)_{X_{j\neq 2}} dX_2 + \ldots \left(\frac{\partial P}{\partial X_n}\right)_{X_{j\neq n}} dX_n,$$

where dX_i is the change in garnet composition along the zoning profile.

Figure D-5 shows an example of the zoning observed in a typical garnet from a pelitic schist in the staurolite-kyanite zone (sample 79-149D; see Fig. D-2). Spessartine displays a bell-shaped zoning profile, decreasing systematically to a small valley near the top of the garnet (Fig. D-5D); grossular zoning is similar (Fig. D-5C). Almandine zoning is antithetical to spessartine and Fe/(Fe+Mg) is irregular. Zoning is asymmetrical, indicating that the garnet grew preferentially in a direction parallel to foliation that is N-S in Figure D-5.

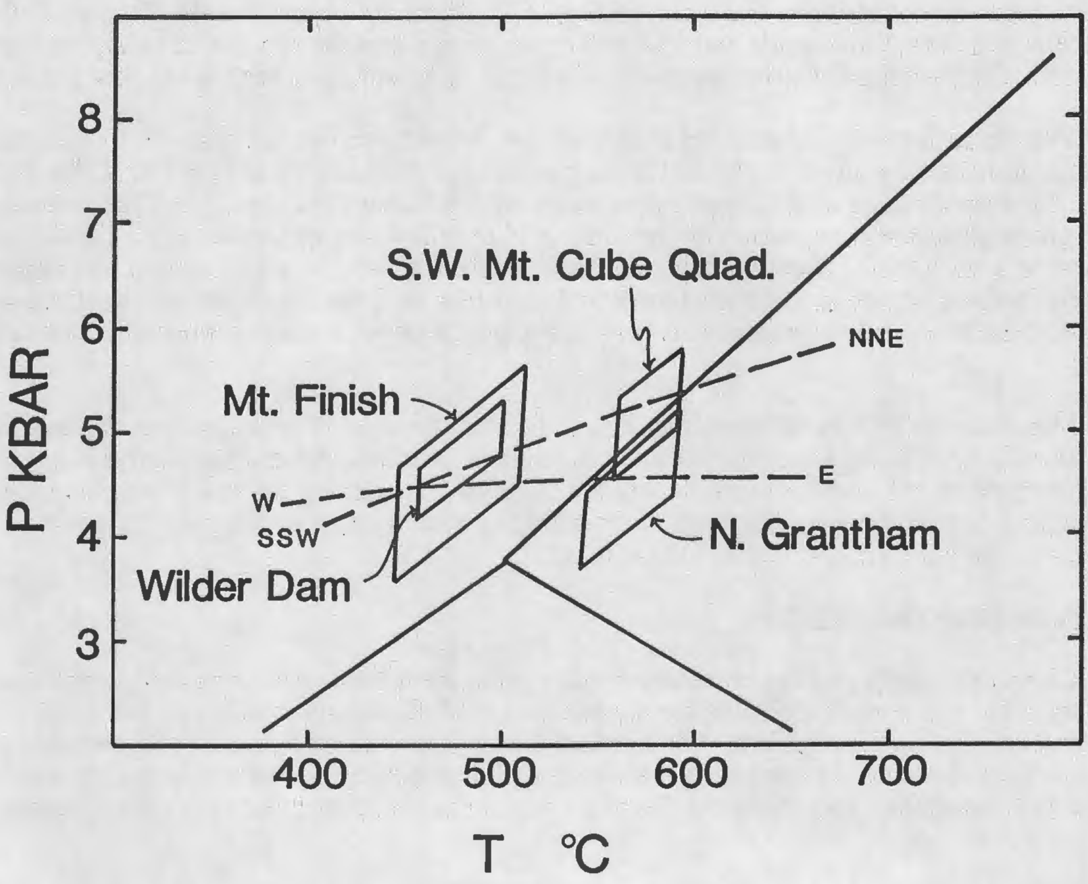

Figure D-4. P-T diagram showing conditions of peak metamorphism for four localities. The metamorphic field gradient is shown by dashed lines in a SSW-NNE direction along the Orfordville anticlinorium and in a W-E direction across the Orfordville and Bronson Hill anticlinoria. From Spear and Rumble (1986).

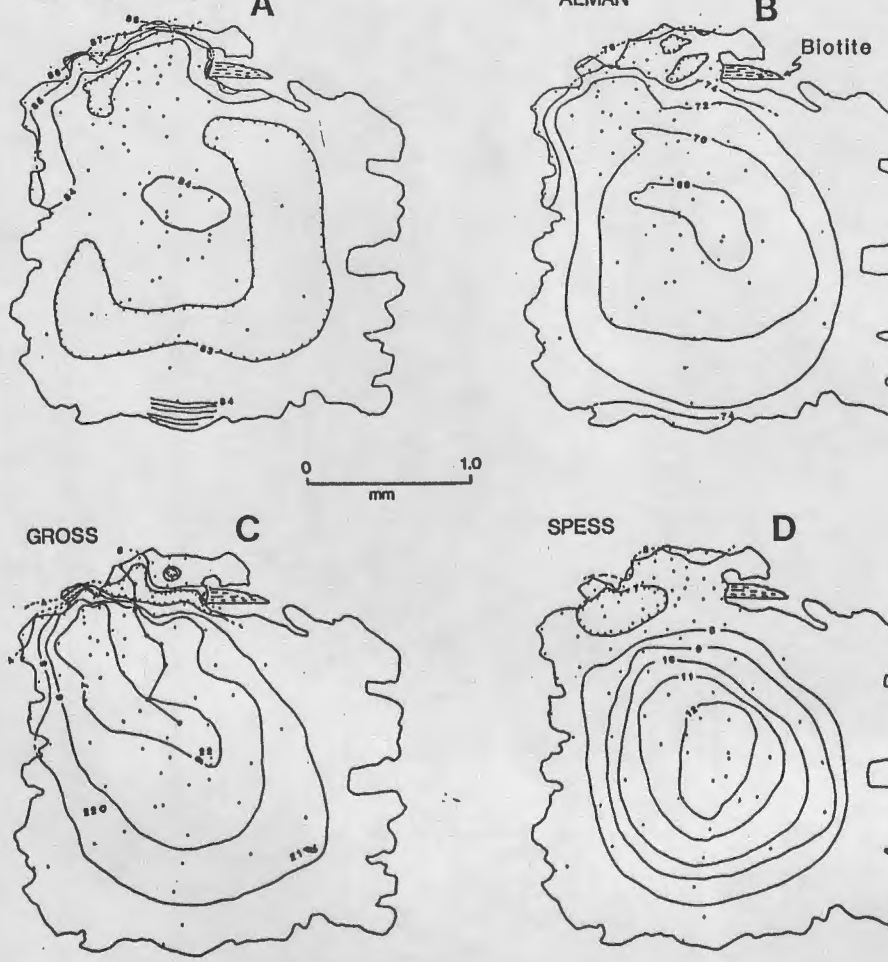
Fe/(Fe+Mg)
A
ALMAN
B
Biotite
0
1.0
mm
GROSS
C
SPESS
D

Figure D-5. Chemical zoning map for a typical garnet from a pelitic schist from the SW corner of the Mt Cube quadrangle (sample 79-149D). (A) Fe/(Fe+Mg); (B) almandine; (C) grossular; (D) spessartine. The compositions and locations of three plagioclase inclusions are shown in (C). From Spear and Rumble (1986).

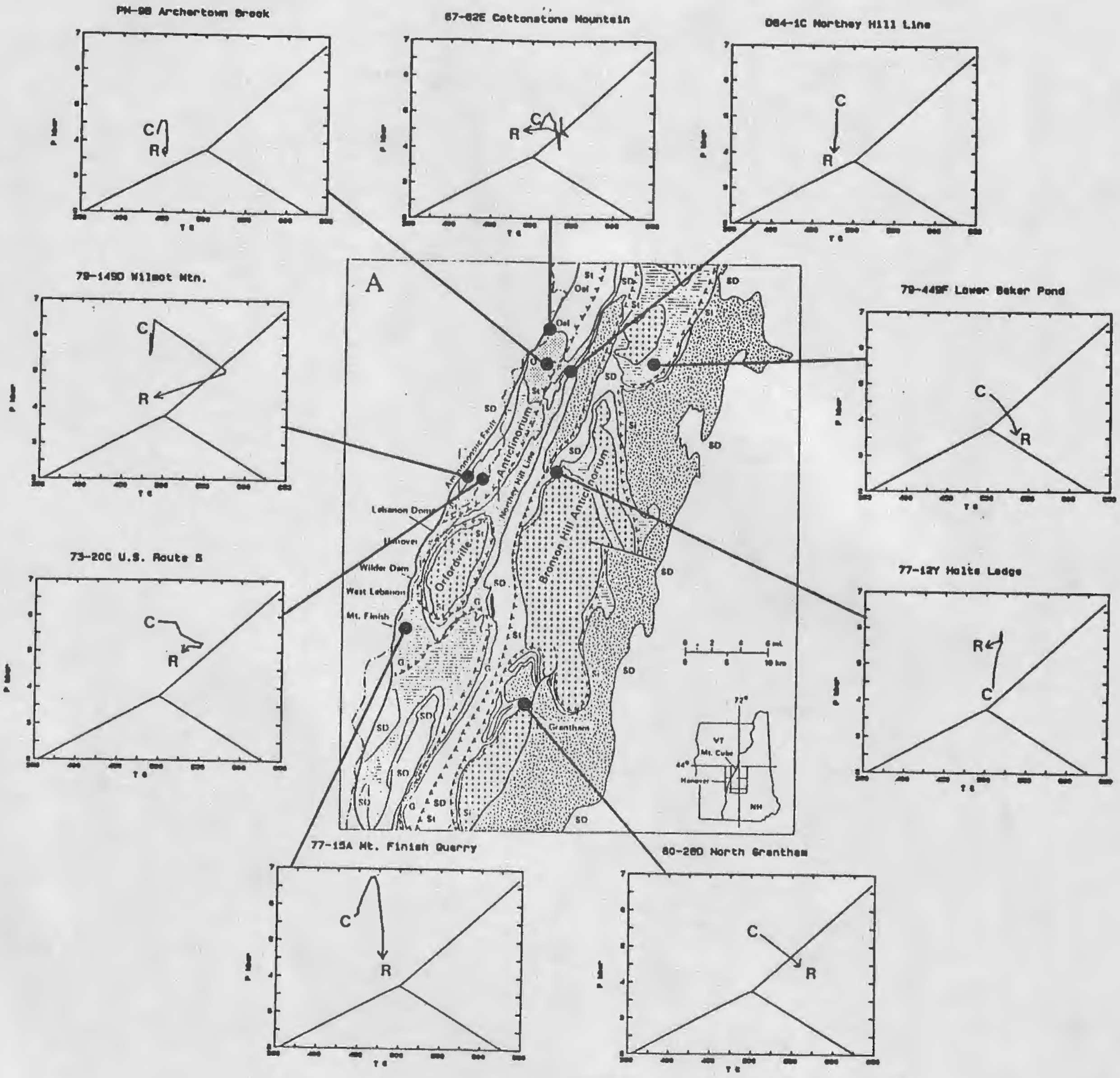
PN-98 Archertown Brook
C
R
67-62E Cottonstone Mountain
C
R
D84-1C Northey Hill Line
C
R
79-149D Wilmot Mtn.
C
R
79-449F Lower Baker Pond
C
R
73-20C U.S. Route 5
C
R
77-12Y Holts Ledge
R
C
77-15A Mt. Finish Quarry
C
R
80-28D North Grantham
C
R
A
St
Osl
SD
G
Ammonoosuc Fault
Anticlinorium
Northey Hill Line
Bronson Hill Anticlinorium
Orfordville
Lebanon Dome
Hanover
Wilder Dam
West Lebanon
Mt. Finish
Grantham
0 2 4 6 mi.
0 5 10 km
72°
44°
VT
Mt. Cube
Hanover
NH
T C
P kbar

Figure D-6. P-T paths for various units in the area plotted on the geologic map (A) and on the cross section (B). Paths were computed after the method of Spear and Selverstone (1983). Data are from Spear and Rumble (1986), Orange (1985) and unpublished data.

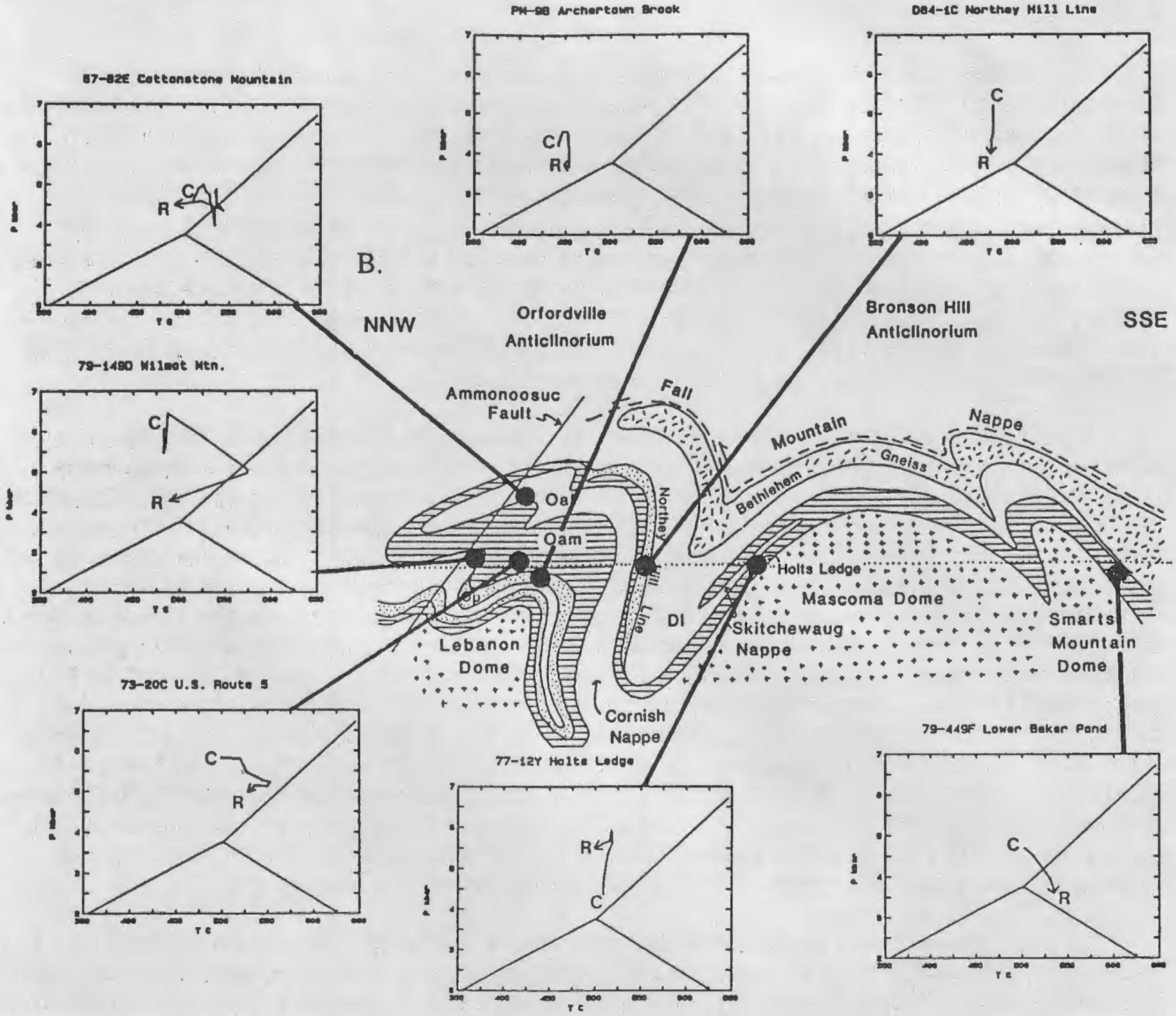
B.
NNW
SSE
Orfordville
Anticlinorium
Bronson Hill
Anticlinorium
Ammonoosuc
Fault
Fall
Mountain
Nappe
Bethlehem
Gneiss
Oa
Oam
Op
Northey
Hill
Line
Dl
Holts Ledge
Mascoma Dome
Skitchewaug
Nappe
Lebanon
Dome
Cornish
Nappe
Smarts
Mountain
Dome
87-82E Cottonstone Mountain
PM-98 Archertown Brook
D84-1C Northey Hill Line
79-149D Wilmot Mtn.
73-20C U.S. Route 5
77-12Y Holts Ledge
79-449F Lower Baker Pond
C
R
7
T C

The matrix assemblage in sample 79-149D is garnet + biotite + staurolite + kyanite + plagioclase + muscovite + quartz + ilmenite. Extensive analysis of mineral inclusions within garnet, kyanite and staurolite indicate that this assemblage was not present over the entire growth history of the garnet, but evolved from an early assemblage of garnet + chlorite + biotite (+ quartz + plagioclase + muscovite) to garnet + chlorite + biotite + staurolite to garnet + staurolite + biotite + kyanite. Calculations of the P-T trajectory from the zoning profile have incorporated this change in assemblage into the model.

The results of the P-T path calculations for this and other assemblages from the area are shown in Figures D-6A and B. Along the western portion of the study area (along the Orfordville anticlinorium), P-T paths are dominantly clockwise with the maximum pressure having been attained early in the history of the rocks, and the maximum temperature being attained later than the maximum pressure and at somewhat lower pressure than P_{max}. Similar types of paths are observed along the axis of the Bronson Hill anticlinorium (e.g. Lower Baker Pond and North Grantham), although the maximum pressures attained appear to have been slightly less than along the Orfordville anticlinorium. The noteworthy exception is the P-T path from Holt's Ledge, which shows nearly isothermal compression for approximately 1.5 kbar followed by cooling with decompression. P-T paths in the synclinorium separating the two anticlinoria (along the Northey Hill line) show nearly isothermal decompression for 1-2 kbar.

A generalized P-T path for the Orfordville anticlinorium is shown in Figure D-7. Correlation of mineral growth with fabric evolution permits a rough correlation of the P-T path with the two major deformation events experienced by the area; the nappe stage and the dome stage. The cores of the garnets in the core of the Orfordville anticlinorium grew following, and in part during, the formation of an early foliation. The cores of these rotated garnets record the highest pressures (up to 7 kbar or approximately 25 km depth), as well as reversals in the P-T paths where a nearly isothermal increase in pressure follows a stage of heating with decompression (for example, B to D in Fig D-7). The high pressures and reversals in the P-T paths are interpreted to have developed in response to the nappe stage of deformation (D1). The dominantly clockwise portions of the P-T paths from D to F in Figure D-7 is interpreted to have resulted from relaxation of perturbed isotherms, accompanied by domal uplift and erosion. P-T paths along the Northey Hill line are somewhat more difficult to explain, because the structural setting is not so clear-cut. The Northey Hill line is the locus of a late-stage NNE trending vertical cleavage belt (the Sunday Mountain Cleavage Belt of Rumble, 1969). Rotational axes in garnets indicate that the garnets grew, at least in part, during the formation of this cleavage belt. This in turn suggests that the Northey Hill line was undergoing isothermal decompression during the formation of the cleavage belt.

It should be noted with reference to the cross section in Figure D-3, that the shapes of the P-T paths along the west flank of the Bronson Hill anticlinorium (e.g. Holt's Ledge) suggest the existence of higher level nappes, which are now removed by erosion. Specifically, the path from Holt's Ledge suggests overthrusting of at least 5-6 km of crust. As will be discussed by Spear and Chamberlain (this guidebook, section F) there is ample evidence to the south for the existence of a higher level nappe,the Fall Mountain nappe, which carries hot rocks from central New Hampshire over cooler rocks of the Bronson Hill anticlinorium. The P-T paths from the latitude of Figure 1 are consistent with this thrust sheet having extended at least this far north.

P-T Paths From Amphibolite Parageneses

Amphibolites from along the Orfordville anticlinorium display a large variety of textures and mineral reactions that can be used to place constraints on the P-T evolution. For this purpose, a petrogenetic grid has been constructed for orthoamphibole-bearing amphibolites (Fig. D-8). The grid was constructed from Schreinemakers rules using natural assemblages to constrain the P-T

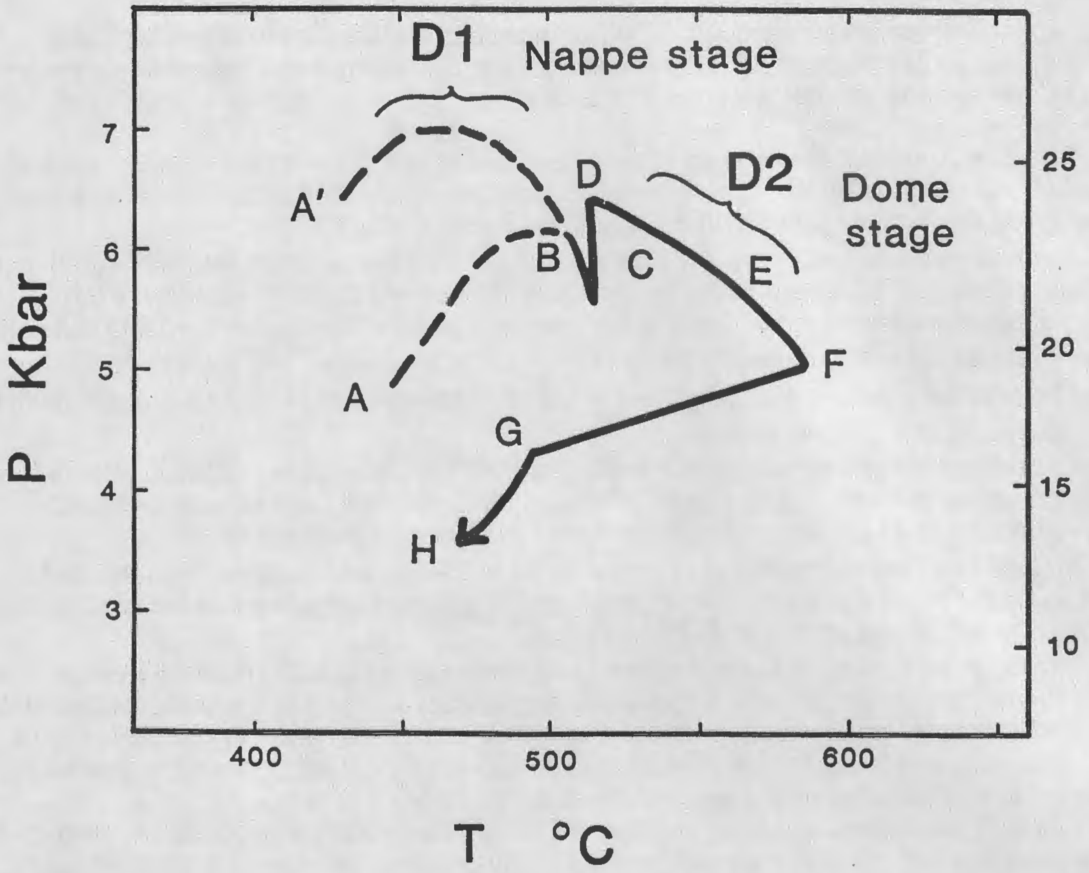

Figure D-7. Generalized P-T path for rocks from the south-west corner of the Mt Cube quadrangle. D1 is the portion of the path inferred to have been followed by the rocks during the nappe stage of deformation and D2 is the path followed during the dome stage. Letters events discussed in the text. From Spear and Rumble (1986).

location of the grid and tabulated values of entropy and volume to constrain the slopes (see Spear and Rumble, 1986, for further details).

The textural observations from amphibolites located in the SW corner of the Mt Cube quadrangle (Fig. D-2) are described below; numbers corresponding to the reactions suggested by the textural observation are indicated on the grid in Figure D-8.

1) Pseudomorphs that now consist of kyanite + quartz in a volume ratio of approximately 2:3 are found in one sample (79-38). These pseudomorphs are interpreted as having formed after pyrophyllite by the reaction pyrophyllite = kyanite + 3quartz + H_2O.

2) Textures in the orthoamphiboles indicate that gedrite always forms first and anthophyllite always overgrows gedrite. Presumably the reactions responsible for the formation of the orthoamphiboles are garnet + chlorite + cummingtonite = gedrite ± hornblende + H_2O and chlorite + gedrite + cummingtonite = anthophyllite + H_2O.

3) The reaction gedrite + cummingtonite = garnet + anthophyllite + H_2O has occurred in the prograde sequence of these amphibolites.

4) Staurolite + gedrite coexist stably in the matrix of several samples and staurolite inclusions are common within gedrite. This texture is consistent with the reaction staurolite + chlorite = kyanite + gedrite + H_2O having occurred during the evolution of these rocks.

5) Inclusions of kyanite within gedrite are found within several samples from the area, although kyanite and gedrite do not coexist stably in the matrix, suggesting that the reaction kyanite + chlorite = cordierite + gedrite + H_2O has occurred.

6) Similarly, inclusions of kyanite within cordierite suggests that the reaction kyanite + gedrite = staurolite + cordierite, which terminates the stability of kyanite + gedrite, has occurred.

7) Retrograde chlorite is common around staurolite and garnet, often in association with gedrite. Reactions that could have produced this retrograde chlorite are cordierite + gedrite = staurolite + chlorite and staurolite + gedrite = garnet + chlorite.

8) Fibrolitic sillimanite ± chlorite is observed locally along cordierite-cordierite, cordierite-gedrite and plagioclase-plagioclase grain boundaries, suggesting that the P-T path must have passed through the sillimanite field during cooling.

Collectively, these observations support the clockwise P-T path shown in Figures D-7 and D-8. It is interesting to note that while the amphibolites record essentially the same P-T history as the pelitic rocks, the form in which this information is stored in the rock is considerably different owing to the different reactions encountered by the different bulk compositions.

MULTIPLE AMPHIBOLE ASSEMBLAGES IN THE AMMONOOSUC VOLCANICS

Multiple amphibole assemblages are common in the Ammonoosuc Volcanics. These assemblages consist of various combinations of the orthorhombic amphiboles anthophyllite and gedrite as well as the monoclinic amphiboles hornblende, cummingtonite and actinolite. No sodic amphiboles have been reported from the Ammonoosuc Volcanics.

Orthoamphiboles

Coexisting subsolvus orthoamphiboles from the area have been described by Spear (1980A). High Al-Na gedrites and low Al-Na anthophyllites coexist in a variety of textures that have been interpreted as equilibrium textures, including (1) discrete grains, (2) bladed intergrowths, (3) patchy intergrowths, (4) overgrowths and (5) lamellar intergrowths with lamellae parallel to (120). Coexisting orthoamphiboles also display exsolution lamellae parallel to (010) with the size of the exsolution lamellae much larger in gedrite than in anthophyllite suggesting that the solvus between these two phases is steeper on the anthophyllite limb than on the gedrite limb.

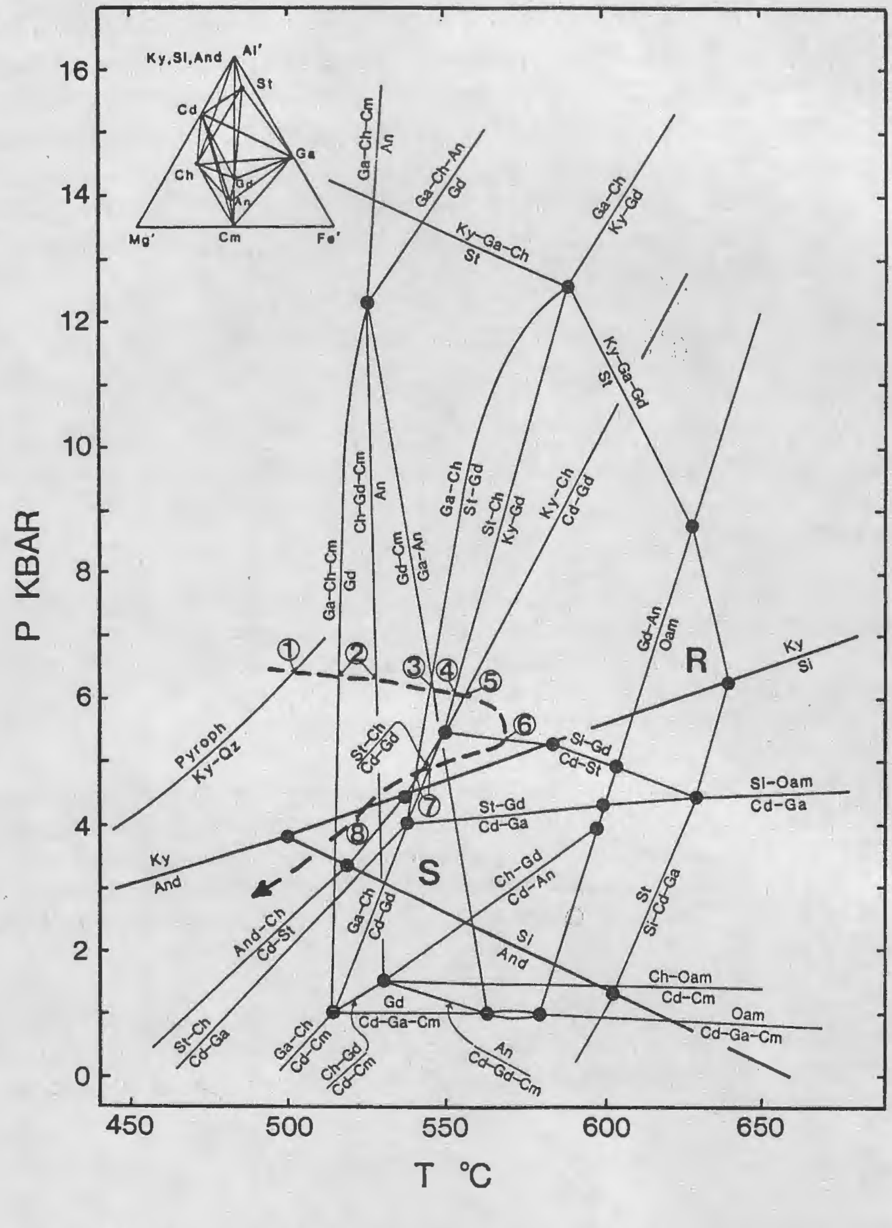

Figure D-8. Petrogenetic grid for amphibolites constructed from tabulated entropy and volume data and Schreinemakers' rules. The P-T location of the grid has been constrained by mineral assemblages reported by Robinson and Jaffe (1969b; labeled R), Stout (1972; labeled S), Spear (1978A, 1978B, 1980A, 1982) and Crowley and Spear (1981). Al_2SiO_5 triple point after Holdaway (1971). The P-T locations of invariant points at high and low pressures are uncertain; some reaction boundaries emanating from these invariant points have been distorted for clarity. Inset shows phase compatibilities in a projection from hornblende, plagioclase (An_{30}), quartz and H_2O. Abbreviations are Ga=garnet, Cm=cummingtonite, An=anthophyllite, Gd=gedrite, Oam=orthoamphibole (supersolvus), Ch=chlorite, Cd=cordierite, St=staurolite, Ky=kyanite, Pyroph=pyrophyllite. The circled numbers refer to reactions encountered by the amphibolites as discussed in the text. From Spear and Rumble (1986).

The compositions of coexisting orthoamphiboles define a solvus, which can be described as miscibility gaps in the edenite ($NaAl^{IV}$ = oSi) and tschermakite ($Al^{VI}Al^{IV}$ = MgSi) substitutions. The width of the solvus is a function of Fe/(Fe+Mg) with Fe-rich samples showing the widest gap. These results are displayed in a series of diagrams with Fe/(Fe+Mg) plotted against A-site occupancy, Al^{IV} and Al^{VI} in Figure D-9. Collectively, the suite of samples span a large range of Fe/(Fe+Mg). An interesting feature of the compositions of the coexisting orthoamphiboles is that along the tschermak exchange vector ($Al^{VI}Al^{IV}$ = (Fe,Mg)Si), the Fe content of the amphibole changes little, whereas the Mg content is inversely proportional to the Al^{VI} content (see Fig. D-10). This confirms crystallographic studies (Papike and Ross, 1970) showing that the M2 site of the orthoamphibole is preferentially enriched in Mg relative to Fe so that substitution of Al^{VI} into the M2 site results in removal of Mg but not Fe.

The compositions of coexisting orthoamphiboles from the Ammonoosuc Volcanics are plotted against temperature in Figure D-11, along with published data from Stout (1971,1972), James et al. (1978) and Robinson et al. (1971). Based on the size of the solvus from this locality, and the existence of supersolvus orthoamphiboles from the Amphibole Hill Area described by Robinson et al. (1971), the crest of the orthoamphibole solvus can be located at approximately 600 ±25 °C.

Four-Amphibole Assemblages

A variety of two and three-amphibole assemblages occur in the area. In garnet-oligoclase grade rocks, various combinations of actinolite - hornblende - cummingtonite assemblages are found. In the SW corner of the Mt Cube quadrangle, which will be visited in this trip, actinolite is rare and is restricted to Mg- and Ca-rich bulk compositions. The typical four-amphibole assemblage consists of hornblende + cummingtonite + anthophyllite + gedrite.

Multiple amphibole assemblages are important because they provide information on the solubility limits of the various amphibole solid solutions. Four-amphibole assemblages containing hornblende + cummingtonite + anthophyllite + gedrite have been found that span a large range of Fe-Mg composition space. The most Fe-rich varieties coexist with garnet and the most Mg-rich varieties coexist with chlorite. Four amphibole assemblages with intermediate Fe/(Fe+Mg) contain neither garnet or chlorite.

The compositions of coexisting amphiboles in several 4-amphibole assemblages are shown in Figure D-12 on an Fe-Mg-Al plot. Hornblende is the most aluminous amphibole followed by gedrite, anthophyllite and cummingtonite. The relative Fe/Mg enrichment is gedrite > anthophyllite = cummingtonite = hornblende.

Coexisting Plagioclase

Several samples containing coexisting plagioclase have been found in the area (Spear, 1980B, 1981). In garnet-grade samples, in the vicinity of Mt Finish (see Fig D-2), coexisting albite + oligoclase are found. In the staurolite-kyanite grade, in the SW corner of the Mt Cube quadrangle, coexisting andesine (An_{40}) and anorthite-bytownite (An_{87-92}) are found. Also note that coexisting An_{67} and An_{83} are found at Beaver Brook, Moosilauke quadrangle. The compositions of these feldspars are presented on the subsolidus plagioclase phase diagram of Smith (1974) in Figure D-13.

A test as to whether or not these multiple plagioclase assemblages represent chemical equilibrium can be made by examining the partitioning of Na and Ca between plagioclase and amphibole. There are two independent equilibria involving plagioclase and amphibole:

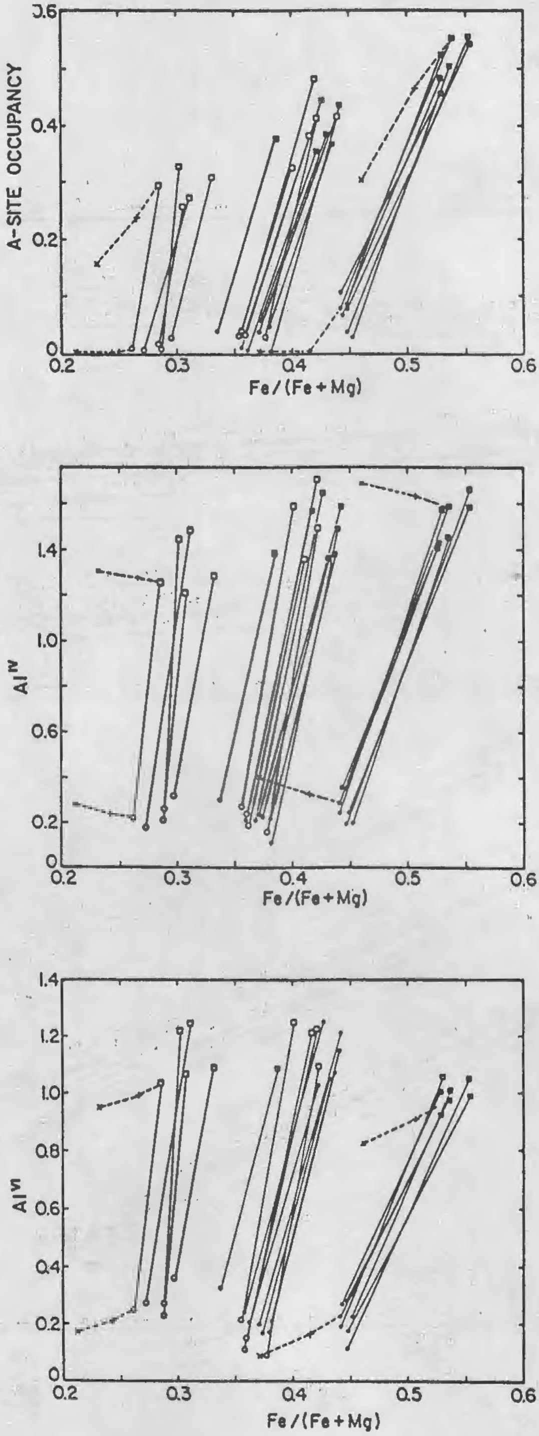

Figure D-9. Plots of Al^{IV}, Al^{VI} and A-site occupancy vs Fe/(Fe+Mg) for coexisting anthophyllite (circles) and gedrite (squares) from the south-west corner of the Mt Cube quadrangle. Tie-lines connect coexisting phases. Filled symbols are for samples containing hornblende; open symbols are for samples without hornblende. The "+" and "X" indicate plotting positions of gedrite and anthophyllite (connected by dashed line) with $Fe^{3+}/(Fe^{3+} + Fe^{2+})$ calculated at 10% and 25%, respectively. Note that the Fe-rich samples contain hornblende whereas the Mg-rich samples do not. From Spear (1980A).

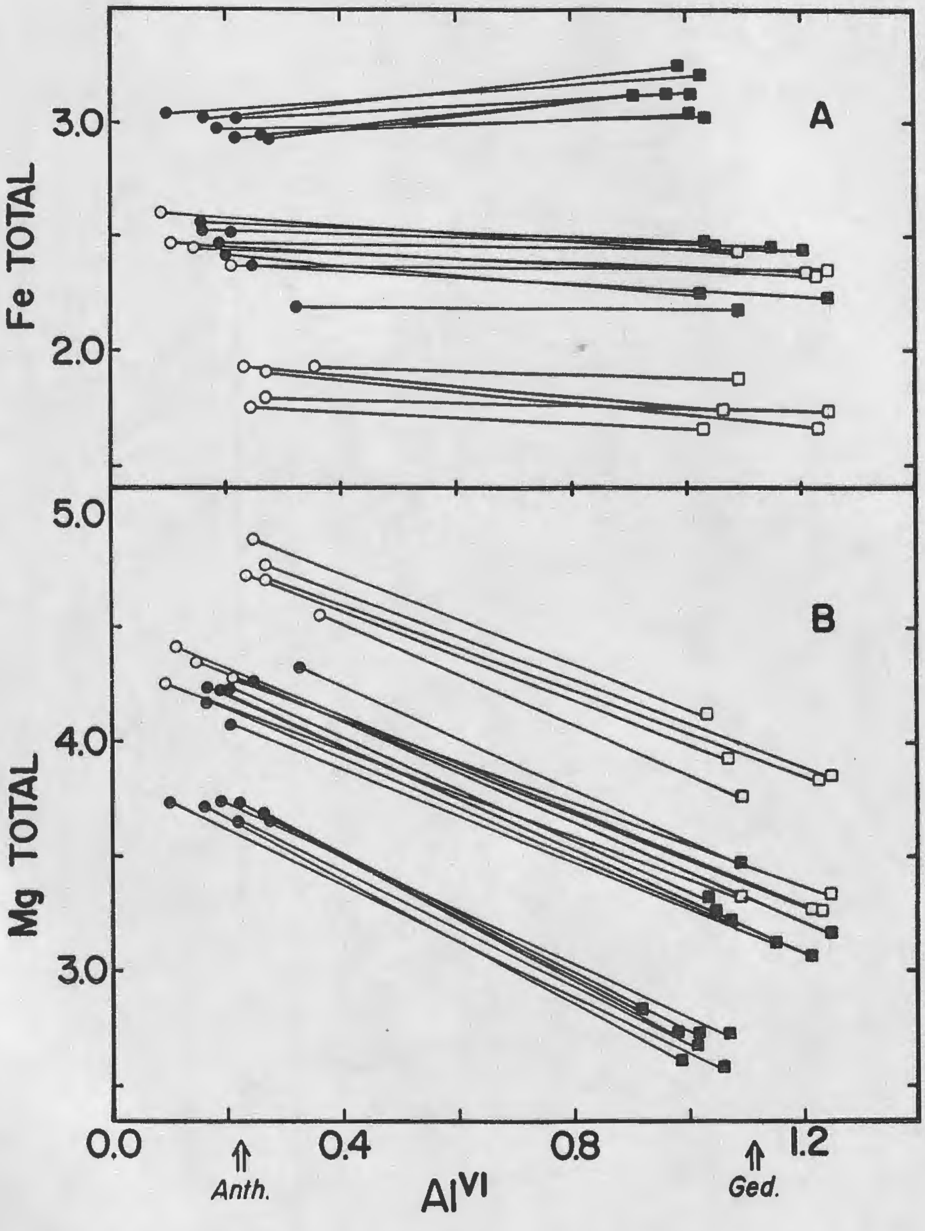

Figure D-10. Plots of (A) total Fe vs Al^{VI} and (B) total Mg vs Al^{VI} for coexisting anthophyllite (circles) and gedrite (squares). From Spear (1980A).

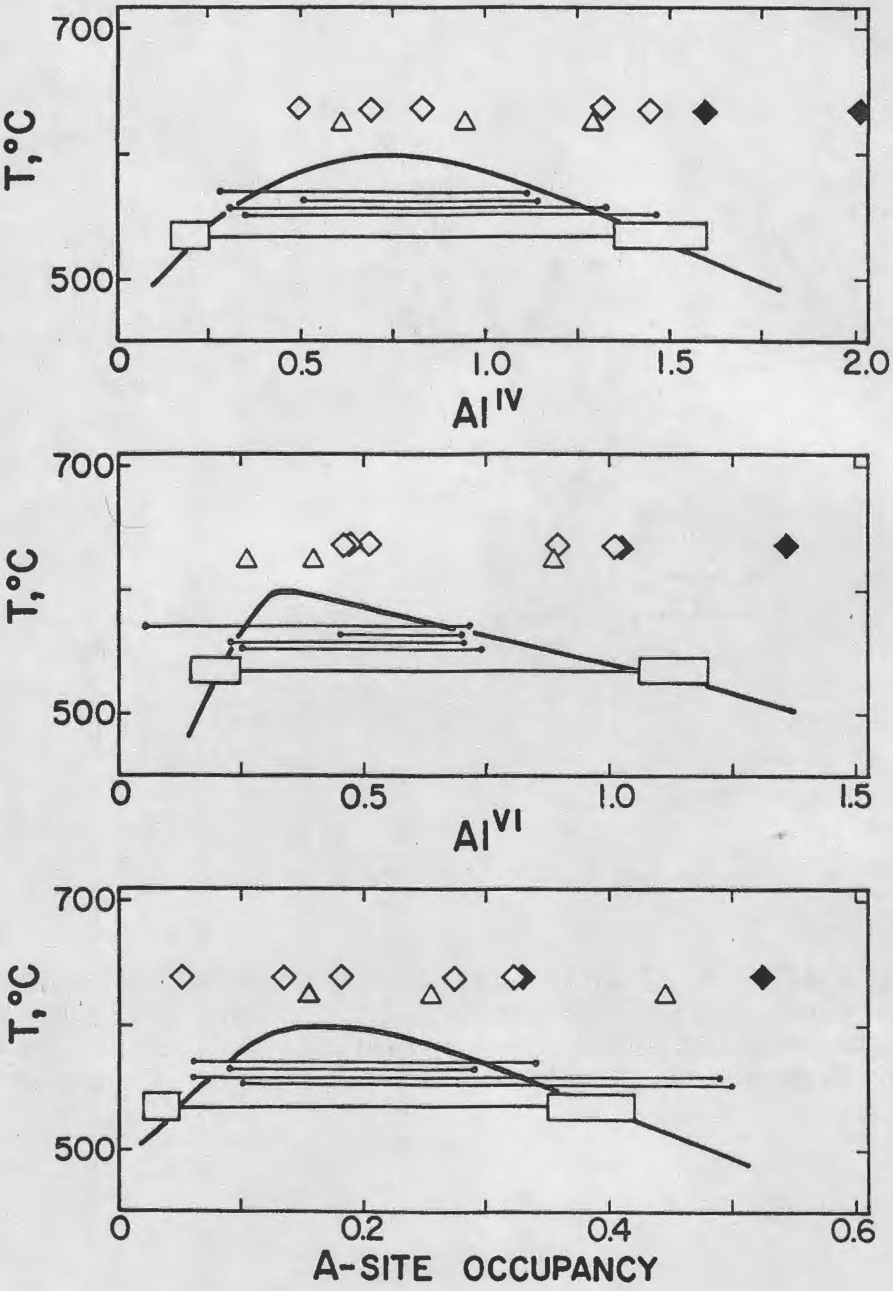

Figure D-11. Hypothetical T-X solvus for orthoamphiboles drawn at $Fe^{2+}/(Fe^{2+} + Mg) = 0.4$, based on data from Spear (1980A) (large boxes), Stout (1971, 1972; circles), James et al. (1978; triangles) and Robinson et al. (1971; diamonds). Filled diamonds are orthoamphiboles from Robinson et al. showing no exsolution whereas open diamonds are amphiboles that display exsolution. From Spear (1980A).

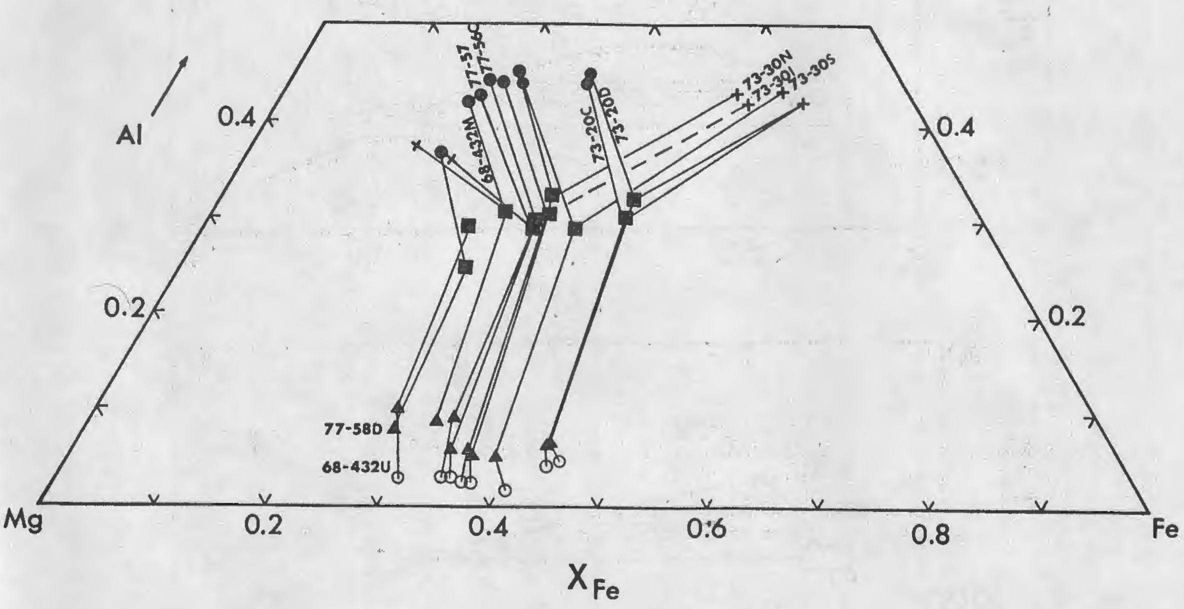

Figure D-12. Portion of the Al-Fe-Mg triangle showing compositions of 3 and 4-amphibole assemblages. Filled circles are hornblende, open circles are cummingtonite, filled squares are gedrite, triangles are anthophyllite, + symbol is garnet and x is chlorite. Tie-lines connect all phases from a single rock, but not all tie-lines are shown for clarity. From Spear (1982).

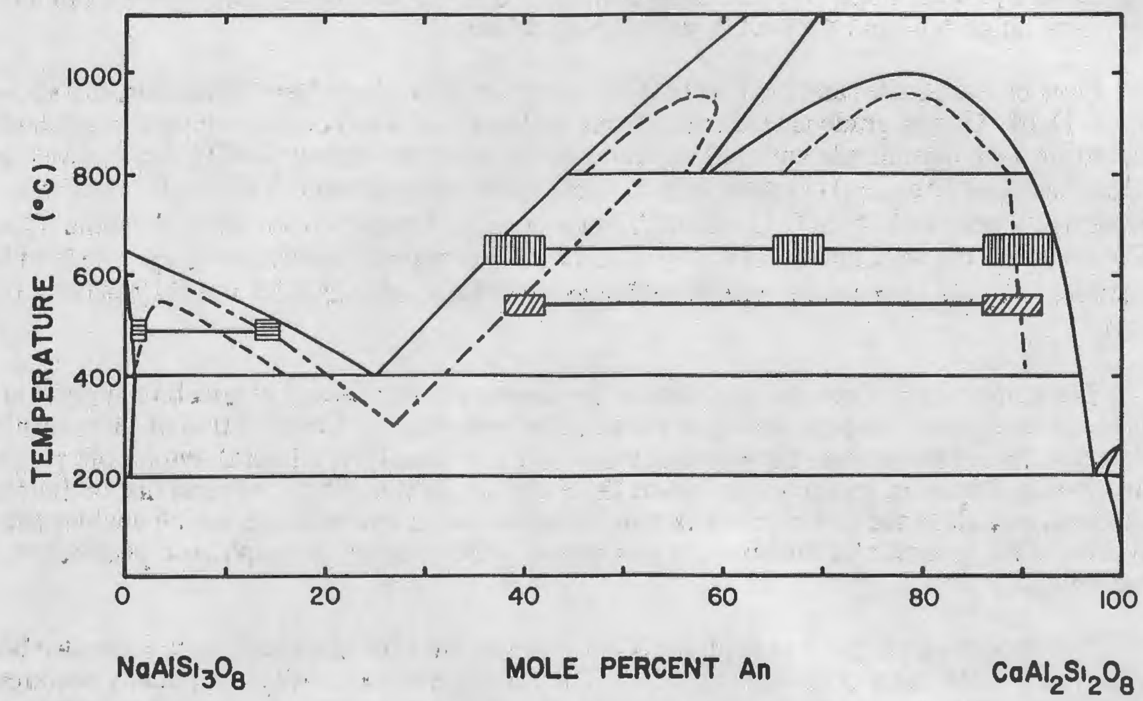
1000
800
600
400
200
TEMPERATURE (°C)
0
20
40
60
80
100
NaAlSi3O8
MOLE PERCENT An
CaAl2Si2O8

Figure D-13. Hypothetical subsolidus phase diagram for plagioclase after Smith (1974) with additional data on coexisting plagioclase added. Horizontal ruled boxes are coexisting albite and oligoclase from the Mt Finish quarry; diagonal ruled boxes are coexisting andesine and bytownite/anorthite from the U.S.Route 5 locality; vertical ruled boxes are coexisting andesine, labradorite and bytownite/anorthite from Wenk and Wenk (1977). Note that coexisting labradorite and bytownite/anorthite is also found at the Beaver Brook locality (see Rumble and Dickenson, this guidebook). Dot-dash lines are solvus limbs, inferred from coexisting metamorphic plagioclase. From Spear (1980B).

Albite + Tremolite = Edenite + 4 Quartz

and

2 (Albite - Anorthite) = Glaucophane - Tschermakite

These two equilibria imply a relationship between the A-site occupancy and the Na/Ca in the M4 site of the amphibole and the Na/Ca ratio of plagioclase.

Plots of Na (A-site) and Na/Ca (M4) for localities in northern New Hampshire are shown in Figure D-14. Garnet-grade amphibolites from Mt Finish (D-14A) contain albite + oligoclase coexisting with hornblende with A-site occupancies of approximately 0.4-0.5 and Na(M4) of 0.20-0.25. Andesine (An_{20-35}) coexists with actinolite + hornblende with Na(A) = 0.1 and 0.3, respectively and Na(M4) of 0.15 and 0.20, respectively. Samples from the U.S. Route 5 locality (SW corner of the Mt Cube quadrangle) (Fig. D-14C) contain andesine (An_{38-42}) + bytownite-anorthite (An_{87-92}) coexisting with hornblende with Na(A) of 0.25-0.38 and Na(M4) of 0.05-0.10.

The systematics of the compositions of coexisting amphibole and plagioclase suggest an approach to equilibrium partitioning between these two phases. Combination of these results with other data from the literature permits construction of a series of hypothetical amphibole-plagioclase partitioning diagrams, as shown in Figure D-15 (Spear, 1980b,1981). Several discontinuous reactions, as well as the continuous reactions cited above are encountered, which enables sub - division of the greenschist, amphibolite and granulite facies based on amphibole-plagioclase assemblages.

The coexisting plagioclase from the SW Corner of the Mt Cube quadrangle have also been the subject of a TEM study (Grove, et al., 1983, Thetford, Vermont locality). Optically homogeneous bytownite-anorthite contains domains with both P1 and I1 symmetry. Huttenlocher intergrowths with lamellae spanning the composition range An_{66}-An_{87} are also present, as are grains of andesine (An_{40}) surrounded by Huttenlocher intergrowths. Whether these intergrowths are a product of phase separation on slow cooling or represent a complication to the amphibole-plagioclase equilibrium phase relations discussed above is uncertain.

PHASE RELATIONS OF THE AMMONOOSUC VOLCANICS

Mineral assemblages that span a large portion of the composition space defined by the components SiO_2-Al_2O_3-TiO_2- MgO-FeO-CaO-Na_2O-H_2O are found in the Ammonoosuc (Post Pond) Volcanics in the SW corner of the Mt Cube quadrangle, as discussed by Spear (1982). Representative assemblages are presented in Table D-1. Representation of a large number of these assemblages can be accomplished on a projection from quartz, H_2O, plagioclase (An_{35}) and hornblende onto the plane FeO-MgO-Al_2O_3. The projection is not strictly rigorous because the compositions of the projection phases change over the diagram. Nevertheless, the projection works fairly well because the phases that are to be represented on the diagram contain little or no CaO or Na_2O. The compositions of selected low-variance assemblages are shown in this projection in Figure D-16. Assemblages represented include (all with quartz + plagioclase (An_{30-40}) + hornblende + H_2O),

garnet + chlorite + staurolite + anorthite,
garnet + chlorite + staurolite + gedrite,
garnet + gedrite + anthophyllite + cummingtonite,
gedrite + anthophyllite + cummingtonite,

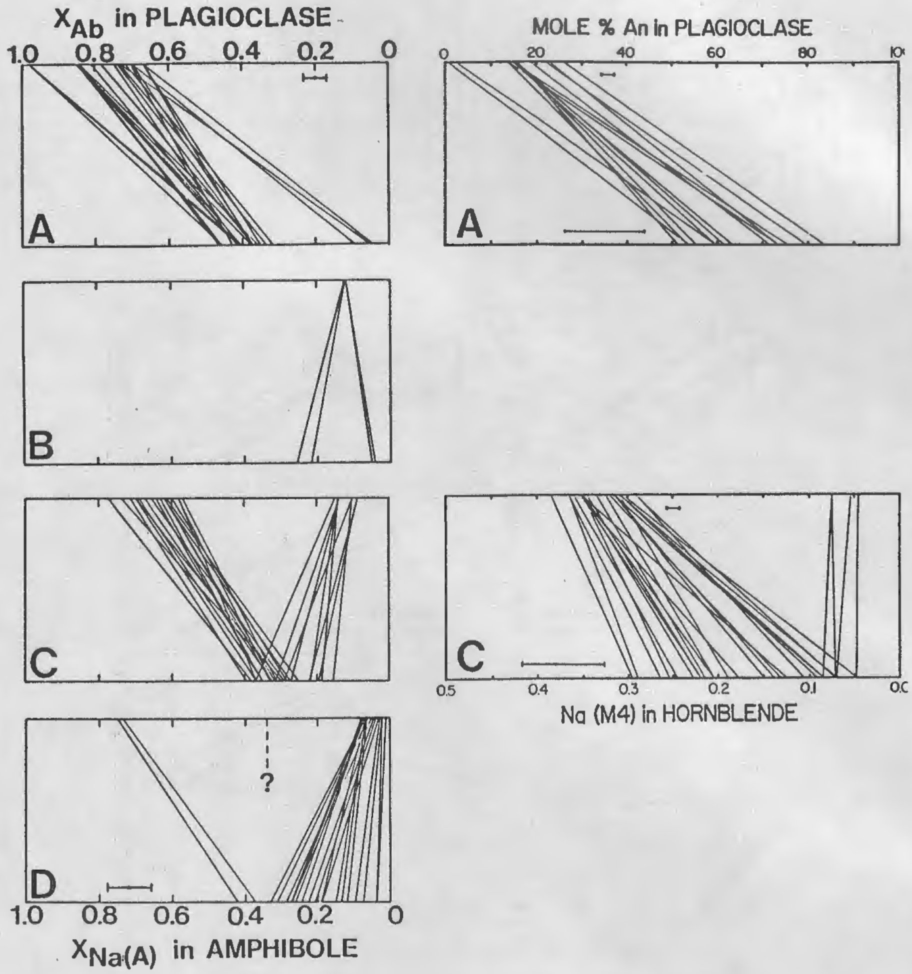

Figure D-14. Plots of X_{Ab} in plagioclase vs $X_{Na,A\text{-}site}$ in amphibole (left side) and Na(M4) in amphibole (right side) from various New England localities. (A) samples from middle garnet-oligoclase zone at the Mt Finish quarry up to the staurolite isograd; (B) Samples from Reel Brook, Moosilauke quadrangle, sillimanite-staurolite grade; (C) samples from the middle staurolite-kyanite zone, U.S. Route 5 locality, south-west corner of the Mt Cube quadrangle; (D) sillimanite zone, Beaver Brook locality, Moosilauke quadrangle. Note that the scale for Na(M4) in amphibole has been expanded relative to that for plagioclase. Compiled from Spear (1980B, 1981).

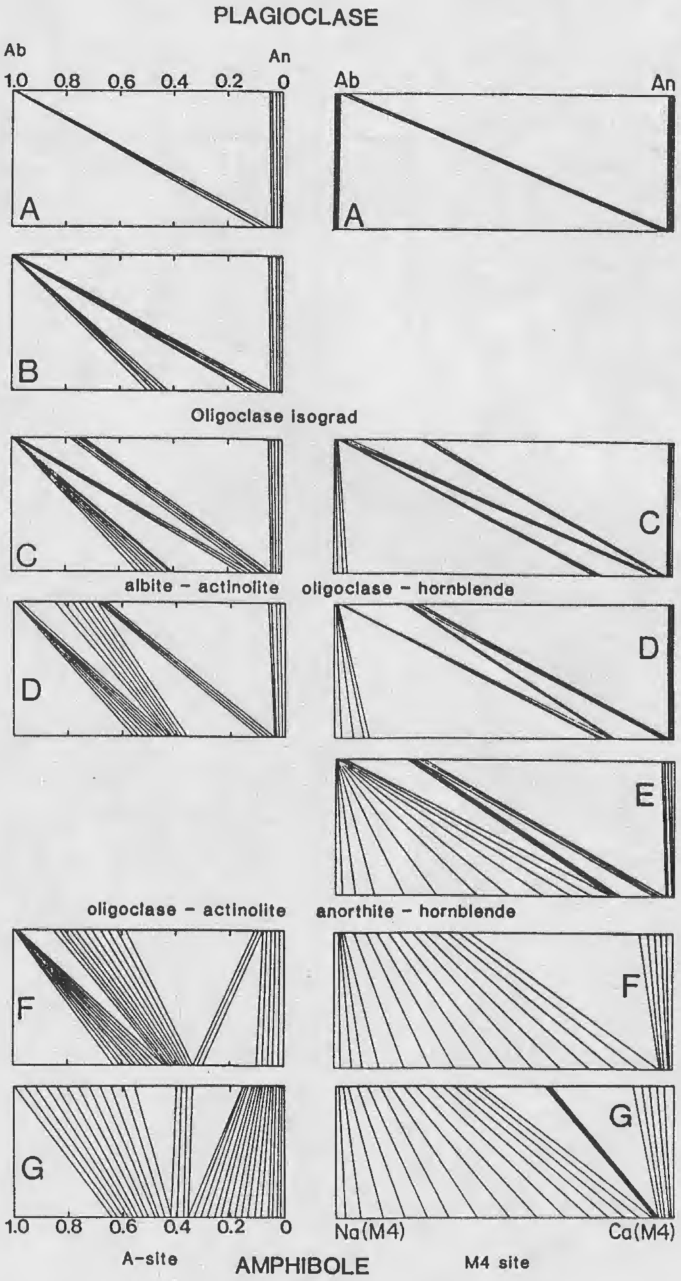
PLAGIOCLASE
Ab
An
1.0 0.8 0.6 0.4 0.2 0
Ab
An
A
A
B
Oligoclase isograd
C
C
albite – actinolite
oligoclase – hornblende
D
D
E
oligoclase – actinolite
anorthite – hornblende
F
F
G
G
1.0 0.8 0.6 0.4 0.2 0
Na(M4)
Ca(M4)
A-site
AMPHIBOLE
M4 site

Figure D-15. Plots of X_{Ab} in plagioclase vs $X_{A\text{-site}}$ (left side) and Na(M4) (right side) in amphibole depicting schematic topologies for the progressive metamorphism of hornblende + plagioclase ± quartz assemblages. (A) Chlorite zone (lower greenschist facies). (B) Chlorite-biotite zone (middle greenschist facies). Between (B) and (C) is the oligoclase isograd. (C) oligoclase zone (middle to upper greenschist facies). Between (C) and (D) is the reaction albite + actinolite = oligoclase + hornblende. (D) Garnet- oligoclase zone (greenschist to amphibolite facies). Between (D) and (E) is the closing of the hornblende-glaucophane solvus (amphibolite facies?). Between (D) and (F) is the reaction oligoclase + actinolite = anorthite + hornblende. (F) Staurolite - kyanite grade (middle amphibolite facies). (G) Upper amphibolite to granulite facies. Compiled from Spear (1980B, 1981).

Table D-1. Mineral assemblages from the Ammonoosuc Volcanics, SW corner of the Mt. Cube quadrangle, NH and VT.

Assemblage data for amphibolites from the Post Pond Volcanics

	Quartz	*Plag-1*	*Plag-2*	*Hornblende*	*Actinolite*	*Cummingtonite*	*Gedrite*	*Anthophyllite*	*Garnet*	*Staurolite*	*Cordierite*	*Chlorite*	*Biotite*	*Wonesite*	*Talc*	*Epidote*	*Scapolite*	*Calcite*	*Dolomite*	*Apatite*	*Sphene*	*Ilmenite*	*Rutile*	*Magnetite*	*Hematite*	*Pyrite*	*Pyrrhotite*
Carbonate-bearing assemblages																											
73–18B	+	28–60[1]		+								+				+	+	+	0·19[3]			+		+	+		
73–19A	+	38–41		+												+	+	+	0·19	+	+						
73–19B	+	25–33		+	+	+						+	+					+	0·25		+	+		+			
73–19D	+	36–38		+		+						+	+					+	0·14				+				
73–25A	+	38–42	86–88	+												+		+	0·45			+					
73–25C	+	32–35		+		+						+							0·31			+		+		+	+
73–28E	+	38–40	86–90	+					+				+			+		+	0·30			+					
73–30A	+	38–40	85–90	+					+				+						0·30			+					+
Carbonate-absent assemblages																											
73–20A	+	40–42	85–86	+					+							+						+					
73–20C	+	28–31		+		+	+	+	+													+		+			
73–28A	+	36–43	87–93	+					+	+		+										+					
73–29D	+	26–35		+			+		+	+		+	+									+				+	
73–30I	?[2]	32–38		+		+	+	+					+									+					
73–30N	+	30–35		+		+	+	+	+				+									+				+	+
73–30S	+	25–29		+		+	+	+	+				+									+					
77–56C	?	30–33		+		+	+	+														+					
77–57	+	30–33		+		+	+	+				+	+									+	+				
77–58D	?	35–38		+			+	+															+			+	+
68–432M	+	30–37		+			+	+				+	+										+				
Hornblende-absent assemblages																											
77–37N	+	23–40				+	+	+	+				+							+			+				
79–146C	+	17–18					+			+	+	+											+				
68–432A	+	19–32					+			+	+												+				
68–432D	+	15–29					+				+	+	+	+									+				
68–432G	+							+			+	+	+	+	+								+				
68–432J	+	18–20					+	+				+	+		+					+			+				

[1] An per cent of plagioclase feldspar.

[2] ? = Quartz was detected by electron microprobe, but only along grain boundaries.

[3] Fe/(Fe + Mg) of dolomite.

gedrite + anthophyllite + cummingtonite + chlorite, and
gedrite + anthophyllite + chlorite.

Note that anorthite (An_{87-92}), which coexists with andesine (An_{40}), plots negatively in this projection.

As can be seen in Figure D-16, the phase volumes defined by the assemblages from this area overlap considerably in composition space. Element partitioning between phases is systematic, and this overlap has been interpreted as the result of different assemblages having crystallized at different values of the chemical potential of H_2O (μH_2O) (Spear, 1982). By consideration of the various hydration states of the different assemblages, and the change in Fe/Mg partitioning with μH_2O, it is possible to construct two different phase diagrams, representative of the phase relations at high and low values of μH_2O (Fig D-17) so that there is no overlap in phase volumes. This result is consistent with the existence of gradients in the chemical potential of H_2O between assemblages. It is suggested that these gradients reflect initial differences in H_2O content between different compositional layers. How these gradients are preserved during the metamorphic episode is uncertain, but it is possible that fluid flow was channelized along layers and was restricted between adjacent layers. In this case, gradients could be maintained with only limited flow across layers because of the buffer capacity of different mineral assemblages.

DISCOVERY AND CHARACTERIZATION OF WONESITE

A sodium-rich trioctahedral mica with a composition intermediate between Na-phlogopite ($NaMg_3AlSi_3O_{10}(OH)_2$) and talc ($Mg_3Si_4O_{10}(OH)_2$) was discovered in the Ammonoosuc (Post Pond) Volcanics in the SW corner of the Mt Cube quadrangle in 1979 and described by Spear, et al. (1981). The mineral was named wonesite in honor of David R. Wones.

Wonesite occurs in rocks that have been interpreted as altered volcanics and is associated with the minerals phlogopite, talc, chlorite, cordierite, anthophyllite and quartz. Wonesite is typically intergrown with K-phlogopite and talc. The mineral displays extinction behavior characteristic of the non-brittle micas, and pleochroism similar to, although slightly paler than, coexisting phlogopite. Individual grains of wonesite are practically impossible to identify without the aid of the electron microprobe, but wonesite intergrown with phlogopite can be recognized by the slightly paler color and pleochroism.

The composition of wonesite and coexisting phlogopite and talc are presented in Table D-2 and plotted in Figure D-18. Wonesite has an Na/(Na+K) of approximately 0.9, in contrast to coexisting phlogopite with a ratio of approximately 0.2. Wonesite also displays considerable alkali deficiency, with more than half of the alkali site vacant (Fig. D-18A). Wonesite also displays considerable tschermak exchange with up to 0.7 Al^{VI}/22 oxygen formula unit.

A TEM study of wonesite from the type locality by Veblen (1983) showed that wonesite actually contains lamellae of talc and a more Na-rich phlogopite, with lamellae ranging in size from a few hundred angstroms to about 0.5 µm. The orientation of the talc lamellae is irrational and lies approximately 37° from (001). Structural mismatch between the alkali-deficient talc lamellae and alkali-rich wonesite lamellae is minimized by the formation of lenticular voids in the talc lamellae parallel to (001). It is suggested by Veblen (1983) that the orientation of the lamellae is in part kinetically controlled and is possible because it requires diffusion only along (001) layers, rather than across layers. Natural wonesite does not expand in either water or ethylene glycol, presumably because the talc layers hold the structure physically together.

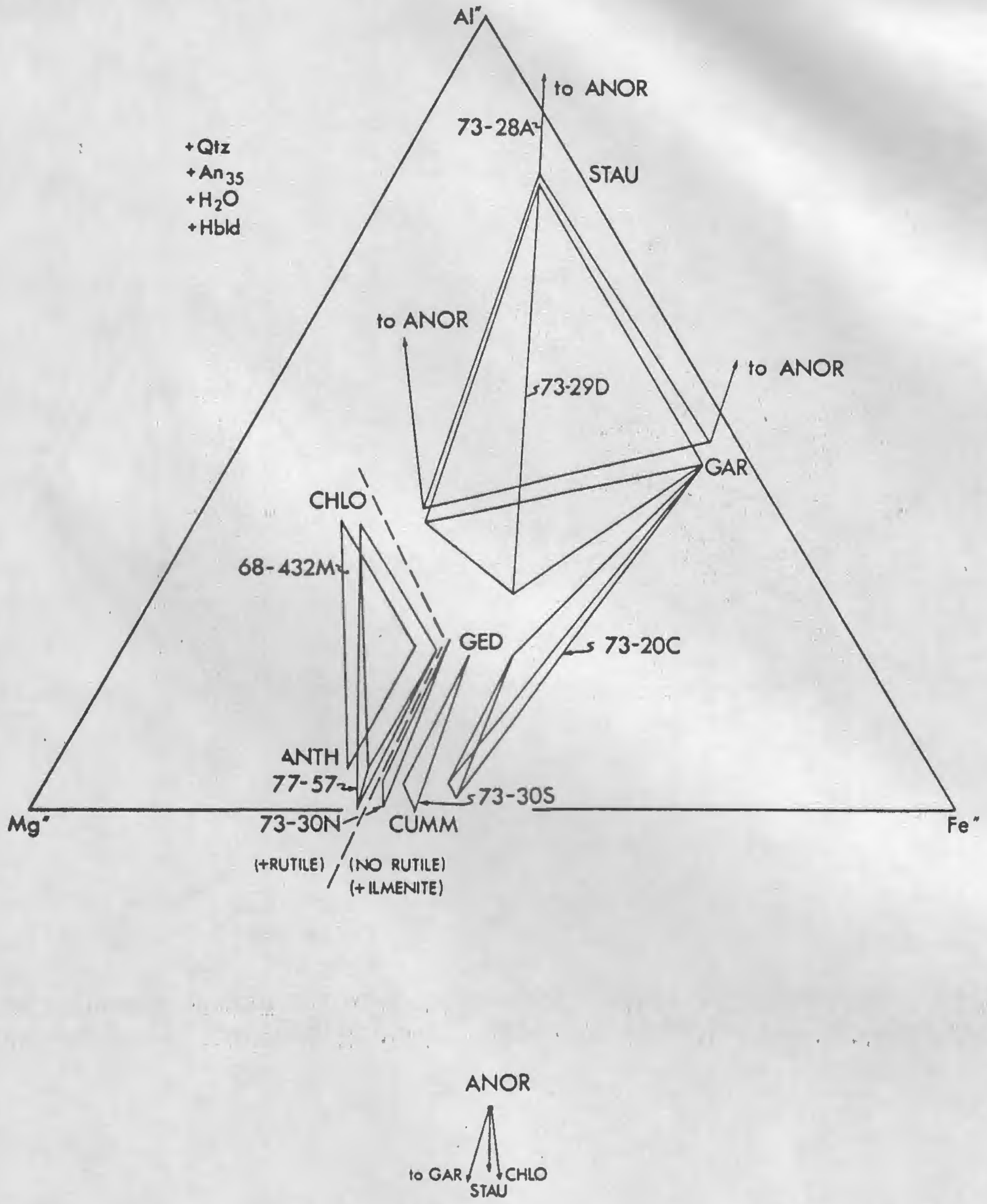
Al"
to ANOR
73-28A
STAU
+Qtz
+An35
+H2O
+Hbld
to ANOR
73-29D
to ANOR
GAR
CHLO
68-432M
GED
73-20C
ANTH
77-57
73-30S
Mg"
73-30N
CUMM
Fe"
(+RUTILE)
(NO RUTILE)
(+ILMENITE)
ANOR
to GAR
CHLO
STAU

Figure D-16. Projection of amphibolite assemblages from the south-west corner of the Mt Cube quadrangle from quartz, H_2O, plagioclase (An_{35}) and hornblende onto the plane Al-Fe-Mg. Note that anorthite projects through infinity, thus tie-lines between anorthite and chlorite, staurolite and garnet must project through infinity. Abbreviations include ANOR=anorthite, STAU= staurolite, GAR=garnet, CHLO=chlorite, GED=gedrite, ANTH=anthophyllite, CUMM=cummingtonite. The dashed line separates assemblages that contain rutile (the Mg-rich assemblages) from those that contain ilmenite (the Fe-rich assemblages). From Spear (1982).

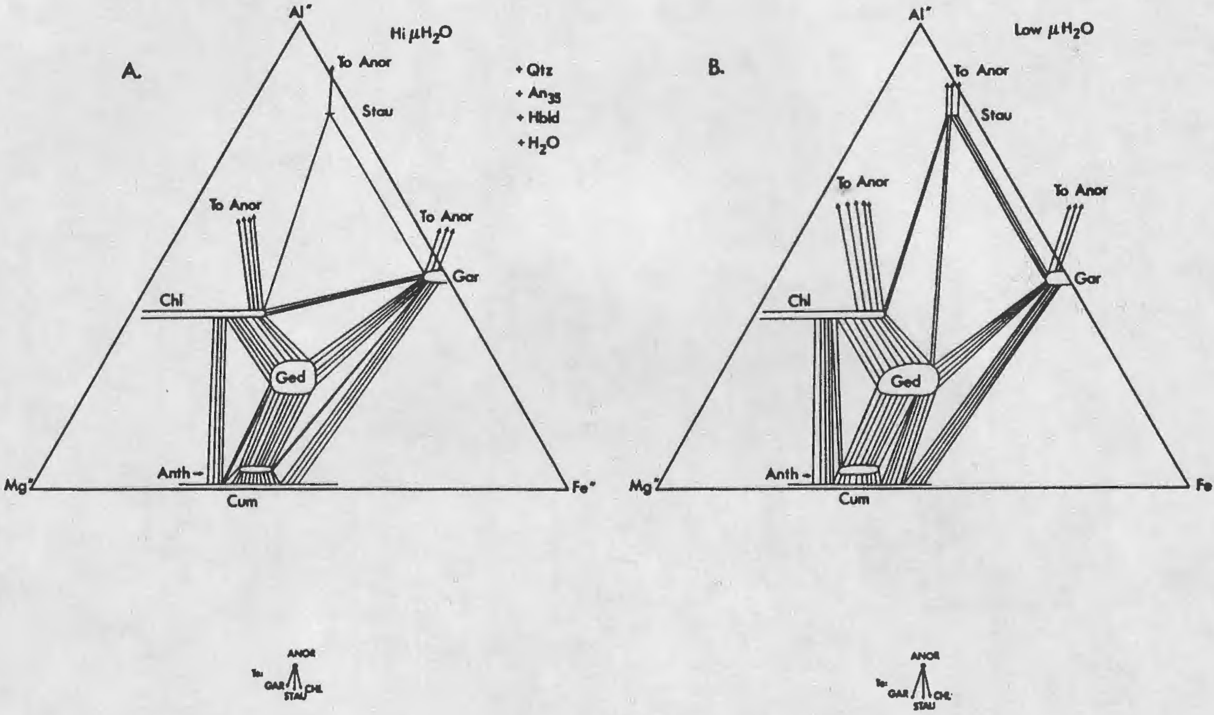
A.
Al″
Hi μH₂O
To Anor
Stau
+ Qtz
+ An₃₅
+ Hbld
+ H₂O
To Anor
To Anor
Gar
Chl
Ged
Anth
Mg″
Cum
Fe″
B.
Al″
Low μH₂O
To Anor
Stau
To Anor
To Anor
Gar
Chl
Ged
Anth
Mg″
Cum
Fe″
ANOR
To:
GAR
STAU
CHL
ANOR
To:
GAR
STAU
CHL

Figure D-17. Schematic phase relations for hornblende-bearing assemblages at high values of μH_2O (A) and low values of μH_2O (B). Abbreviations as in Figure D-16. From Spear (1982).

Table D-2. Representative electron microprobe analyses of coexisting wonesite, phlogopite and talc.

	Weight % Oxides					
	Wonesite		Phlogopite		Talc	
SiO_2	48.53		40.28		60.76	
Al_2O_3	13.73		17.70		2.87	
TiO_2	0.77		0.77		0.06	
Cr_2O_3	0.08		0.07		0.0	
MgO	22.11		19.61		27.34	
FeO*	7.02		8.87		4.25	
MnO	0.04		0.04		0.03	
CaO	0.04		0.0		0.01	
Na_2O	3.07		0.50		0.32	
K_2O	0.85		7.84		0.17**	
F†	0.15		0.26		0.11	
Total††	96.39		95.94		95.92	
	Cations based on 22 oxygens					
Si	6.466	8.000	5.704	8.000	7.795	8.000
Al^{IV}	1.534		2.296		0.205	
Al^{VI}	0.620	5.874	0.660	5.934	0.228	5.914
Ti	0.074		0.079		0.003	
Cr	0.008		0.004		0.0	
Mg	4.390		4.140		5.227	
Fe	0.778		1.047		0.456	
Mn	0.004		0.004		0.0	
Ca	0.004	0.939	0.0	1.550	0.0	0.101
Na	0.790		0.137		0.075	
K	0.145		1.413		0.026	
Fe/(Fe + Mg)	0.151		0.202		0.080	

*All Fe computed as FeO.

**K_2O content of this talc is anomalously high and may represent contamination with phlogopite. Most talc analyses show 0.02-0.05 wt % K_2O.

†Fluorine analysis by R. Jones.

††Ideal H_2O content for phlogopite is 4.31 wt %, which would bring totals up to approximately 100 wt %.

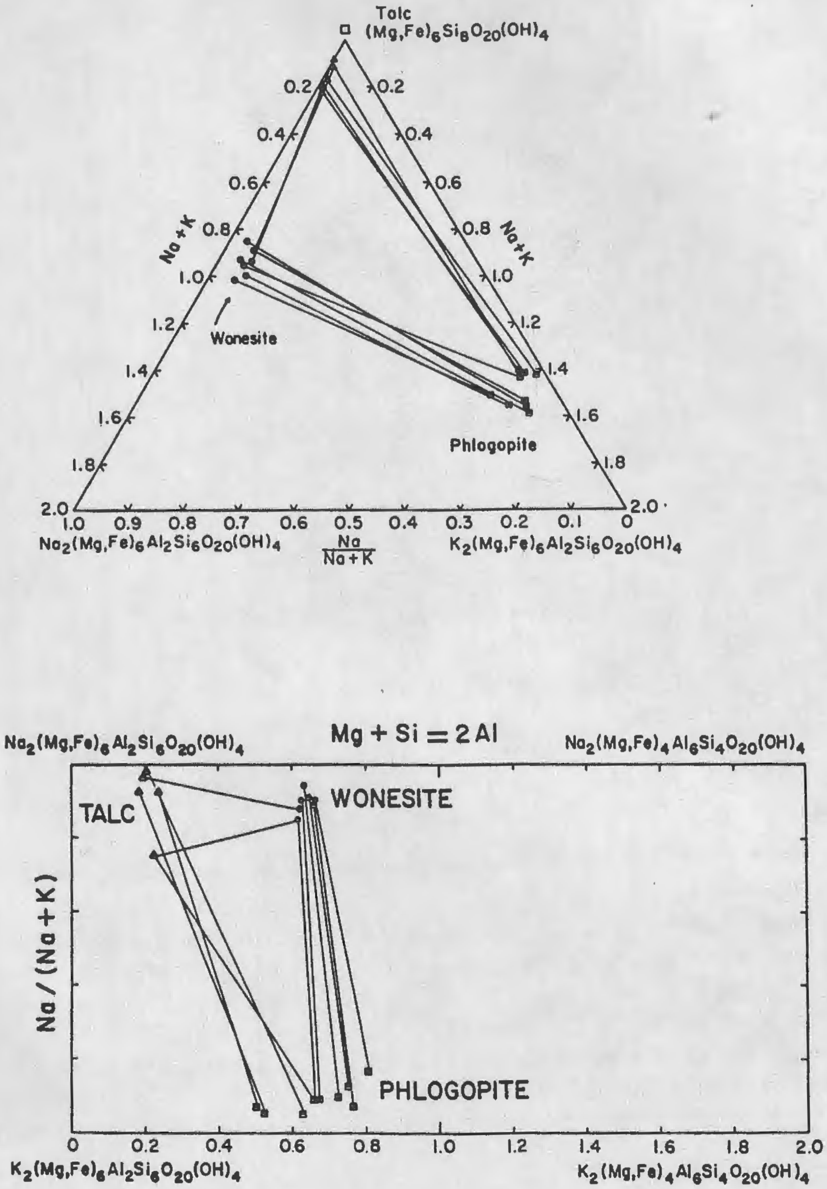

Figure D-18. Compositions of coexisting wonesite (circles), phlogopite (squares) and talc (triangles) plotted in (A) as a function of Na/(Na+K) and number of alkali vacancies and in (B) as a function of Na/(Na+K) and Tschermak substitution. Tie lines connect coexisting phases. From Spear et al. (1981).

The lamellar intergrowths of wonesite and talc are interpreted as having originated by exsolution from an initially homogeneous wonesite. Microprobe analyses of wonesite plotted in Figure D-18 likely represent the pre-exsolution bulk composition, inasmuch as the size of the lamellae is smaller than the electron beam size. Veblen (1983) used this constraint to compute the composition of the talc and wonesite exsolution lamellae, by assuming molar volume relations. The results are shown in Figure D-19, where it can be seen that wonesite has shifted composition to a greater extent than the coexisting talc. This suggests that the solvus between wonesite and talc is asymmetric, with the steeper limb on the talc side (Fig. D-19B), similar to the solvus relation between anthophyllite and gedrite, which also involves similar substitution mechanisms.

BEHAVIOR OF METAMORPHIC FLUIDS BASED ON OXYGEN ISOTOPES

Rumble and Spear (1983) presented the results of an oxygen isotope study that was designed to test the relative efficacy of diffusion vs infiltration mechanisms for the movement of fluids during regional metamorphism. Oxygen isotopes were used as tracers of fluid migration along two detailed profiles: one from blueschist facies rocks from the Franciscan Formation of California, and the other in kyanite-staurolite grade rocks from west-central New Hampshire. This later profile is located in the SW corner of the Mt Cube quadrangle (see Fig. D-2). Samples were collected at intervals of a few centimeters in a direction perpendicular to bedding across heterogeneous outcrops that could be inferred to have possessed strongly dissimilar oxygen-isotope compositions prior to metamorphism. In addition, chemical analyses of Fe-Ti oxide minerals were made to test the extent of chemical homogenization.

For the Vermont profile, the rock types across the sampling profile consisted of (1) muscovite schist of the Littleton Formation with the assemblage quartz + muscovite + kyanite + staurolite + garnet + biotite + ilmenite, which locally encloses 5 cm-thick calc-silicate lenses with the assemblage quartz + plagioclase + amphibole + garnet + clinozoisite + sphene + ilmenite; (2) biotite schist with the assemblage quartz + plagioclase + biotite + garnet + ilmenite; (3) fine-grained manganiferous garnet + biotite + quartz + magnetite + ilmenite rock (termed coticule); and (4) hornblende amphibolite of the Ammonoosuc Volcanics with the assemblage hornblende + plagioclase + quartz + sphene + magnetite + ilmenite. The Taconian unconformity lies in the interval between types (1) (Littleton) and (4) (Ammonoosuc) and it is not certain as to which formations units 2 and 3 belong. All rocks were metamorphosed during the Acadian Orogeny.

The results of the Vermont sampling profile are shown in Figure D-20 where $FeTiO_3$ and $MnTiO_3$ compositions of ilmenite, along with $\delta^{18}O$ compositions of quartz are plotted against distance. As can be seen from the figure, plots of $\delta^{18}O$ vs distance show sharp irregularities and reversals between the mica schist and amphibolite, as well as significant differences (as much as 1 ‰) between layers only 1-2 cm apart. These results indicate that oxygen-isotope exchange was not effective over distances as great as bedding thickness in these samples. Similarly, chemical equilibration between beds was also not achieved as shown by the variability in Mn content of ilmenites from adjacent beds. There is also a variation in Fe_2O_3 content of the ilmenites suggesting that there may have been differences in oxygen fugacity between adjacent beds as well.

In contrast, data presented by Rumble and Spear (1983) indicates that there has been considerable oxygen-isotope exchange between metachert and metabasalt during blueschist-grade metamorphism of the Franciscan Formation.

The interpretation of the above results is that the Vermont samples have not experienced significant amounts of fluid flow so that the isotopic composition of the rocks were little changed from their pre-metamorphic values, whereas the Franciscan rocks experienced considerable fluid flow. The reason for the difference is attributed to the relative permeabilities of the two sections.

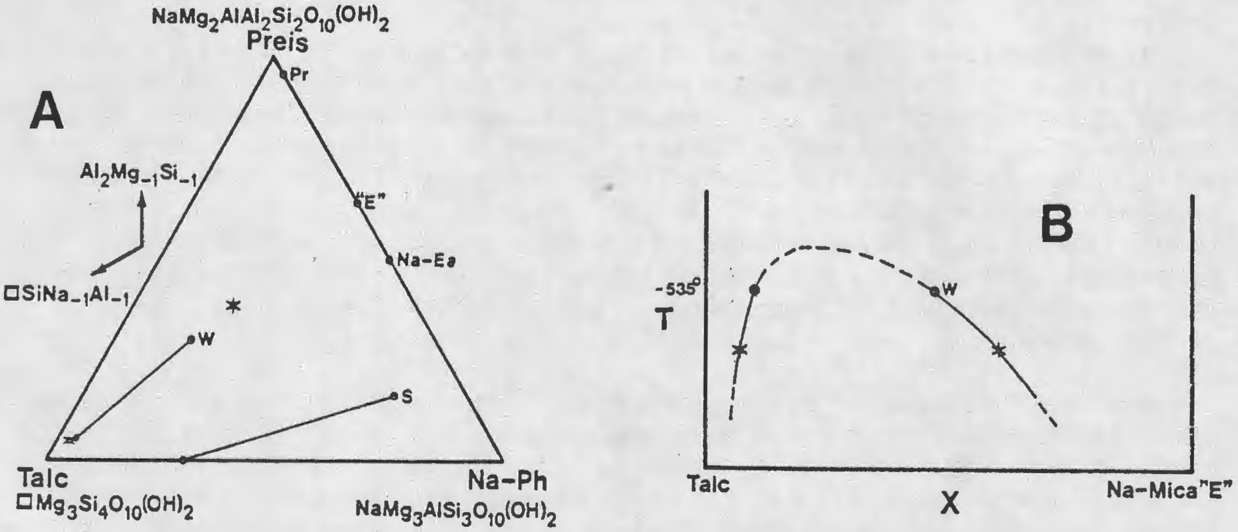
$NaMg_2AlAl_2Si_2O_{10}(OH)_2$
Preis
Pr
A
$Al_2Mg_{-1}Si_{-1}$
$\square SiNa_{-1}Al_{-1}$
"E"
Na-Ea
*
W
S
Talc
$\square Mg_3Si_4O_{10}(OH)_2$
Na-Ph
$NaMg_3AlSi_3O_{10}(OH)_2$
B
-535°
T
W
Talc
X
Na-Mica"E"

Figure D-19. (A) The composition diagram talc - Na-phlogopite - preiswerkite, showing compositions of selected sodium micas. "W" indicates wonesite from the Mt Cube quadrangle (Spear et al., 1981), "S" indicates the Na-phlogopite of Schreyer et al. (1980). Both of these micas coexist with talc as indicated by the tie-lines. "Pr" is the preiswerkite of Keusen and Peters (1980). The compositions marked "*" were derived for the exsolution lamellae in wonesite by X-ray analysis. (B) Schematic T-X diagram showing the talc-wonesite miscibility gap. Compositions marked by dots are microprobe analyses of bulk wonesite and talc from the Mt Cube quadrangle (Spear et al., 1981). The compositions marked by "*" are computed from X-ray analysis of exsolution lamellae. The analyses suggest a solvus that is asymmetric towards talc. From Velben (1983).

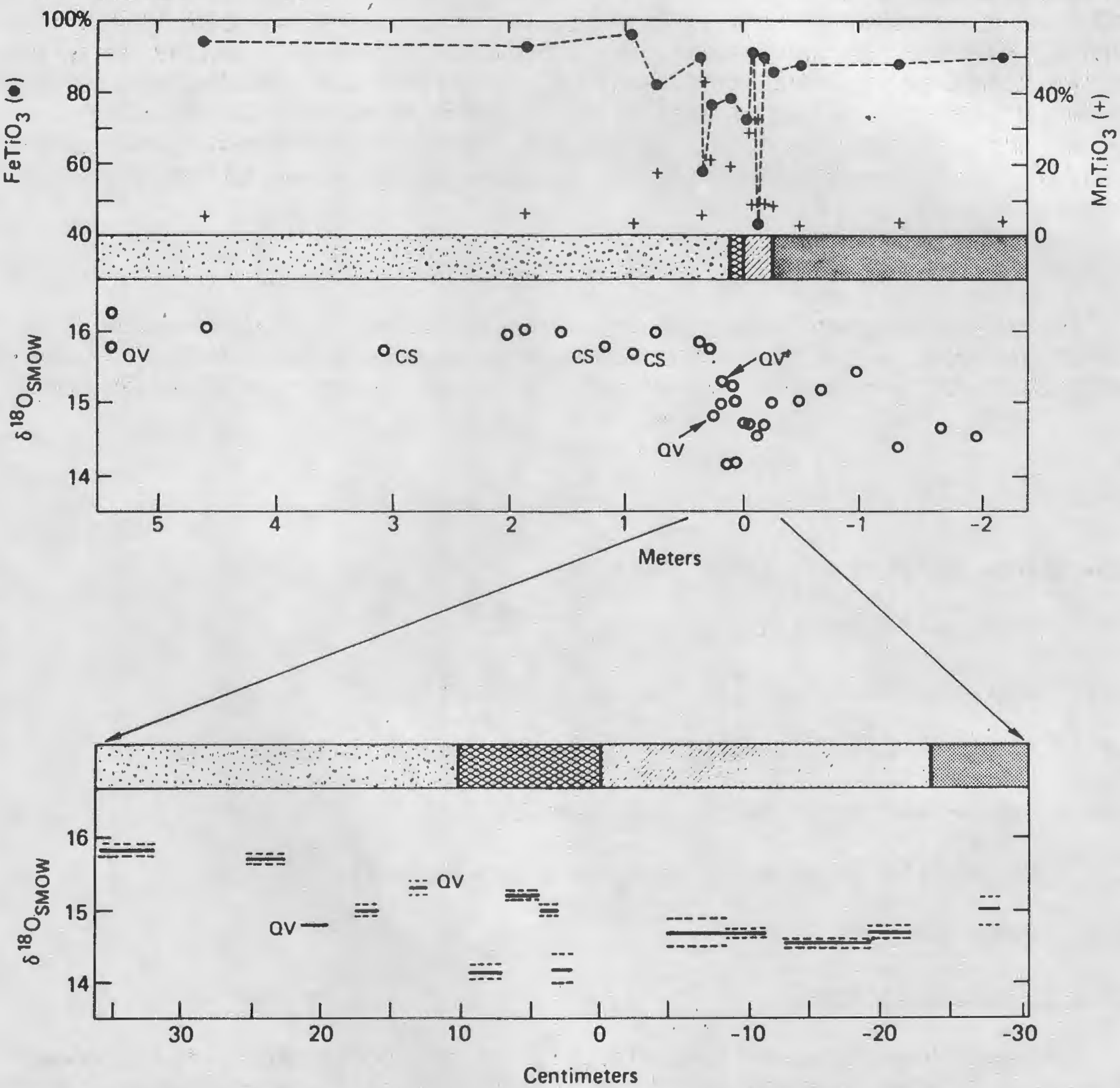

Figure D-20. Plots of $\delta^{18}O_{SMOW}$ of quartz, and $FeTiO_3$ and $MnTiO_3$ contents of ilmenite (mol %) vs distance perpendicular to bedding for traverse in the south-west corner of the Mt Cube quadrangle. Rock types are given by the bar graph: irregularly stippled pattern is muscovite schist (Littleton Formation); cross-hatched pattern is biotite schist; diagonal shading is garnet-quartz rock (coticule); and densely stippled pattern is hornblende amphibolite (Ammonoosuc Volcanics). The symbol "CS" identifies calc-silicate lenses and "QV" is quartz segregations. In the lower graph, the spacing of dashed lines gives two times standard deviation of duplicate or triplicate analyses. From Rumble and Spear (1983).

The Franciscan rocks contain an abundance of veins and healed fractures, which may be interpreted as representing fluid channelways during metamorphism. The Vermont samples contain few veins or healed fractures. The reason for the differences in permeabilities of the two sections is speculative, and two possibilities can readily be imagined. (1) The two sections may have been in two different crustal rheological regimes (brittle vs ductile), thus permitting brittle failure in the Franciscan rocks under differential stress whereas the Vermont rocks responded by plastic deformation. (2) Different bulk compositions give rise to different metamorphic reactions during progressive metamorphism. Metamorphic reactions have the potential of enhancing permeability in two ways: by porosity increase resulting from a decrease in the volume of solids and by hydrofracturing resulting from fluid overpressure as a consequence of devolatilization reactions. Both of these mechanisms probably influence the relative amount of fluid flow experienced by the two suites of rocks.

ACKNOWLEDGMENTS

This work was supported in part by a grant from the National Science Foundation, EAR-8514659 (to Spear). The authors wish to acknowledge the constructive reviews of P. Robinson and D. Elbert and the willing and able assistance of M. Kohn in preparation of this field guide.

ITINERARY

Leave Ravine Lodge, drive to Lower Baker Pond.

0.0	Moosilauke Ravine Lodge
1.5	Intersection with Route 118. Turn right (west).
7.4	Junction of Route 118 and Route 25. Bear left (south) on Routes 25 and 118.
8.0	Junction with Route 25C. Stay on Route 25.
12.2	Junction with Route 25A. Turn right (west) on Route 25A.
15.2	Pull off on right.

STOP 1: Lower Baker Pond

The small spillway at Lower Baker Pond provides some good exposures of Ammonoosuc Volcanics with highly aluminous assemblages. The composition of these amphibolites is unusual for metavolcanic rocks. It has been suggested that these bulk compositions have been derived from hydrothermal alteration (possibly by seawater) of basaltic rocks. Several kilometers to the north east in the same outcrop belt similar rocks are exposed in the hanging wall of a massive sulfide deposit suggesting a genetic relationship between the hydrothermal alteration and the deposition of the sulfide mineralization. Similar rocks, again with associated massive sulfides will be examined later in the day at the wonesite locality.

The principal assemblage that has been observed here is garnet + cordierite + sillimanite + biotite + quartz ± staurolite ± rutile.

The best exposures of this assemblage are the large boulders near the road that have been blasted to form the spillway and in the outcrops under the trees on the far side of the spillway. Staurolite and kyanite inclusions are found within cordierite. Locally sillimanite is observed to overgrow kyanite, suggesting a P-T path that involves heating with decompression. The P-T path computed for these rocks from garnet zoning also indicates heating with decompression (see Figure D-6).

15.2 Continue west on Route 25A. Along the route, pass outcrops of Bethlehem Gneiss

23.0 Cross Northey Hill line at bridge. Rocks in the vicinity of Orfordville are Ordovician Partridge Formation.

26.9 Junction with Route 10 in Orford. Turn right (north) on Routes 25A and 10.

27.2 Turn left (west) across Connecticut River toward Fairlee, Vermont. River bed here is location of the Ammonoosuc fault.

27.5 Junction with Route 5. Turn left (south) on Route 5.

38.4 Road cuts on right (west) side of Route 5.

Stop 2: U.S.Route 5 Locality

WARNING: There is abundant POISON IVY along this roadcut.

The rocks at this locality consist of well bedded amphibolites and volcanogenic sediments of the Ammonoosuc (=Post Pond) Volcanics. Locally the foliation is folded in open folds of the dome stage.

Numerous assemblages are found at this outcrop, as listed in Table D-1 (sample numbers 73-18 to 73-29). Some of the more interesting assemblages include four coexisting amphiboles (anthophyllite + gedrite + cummingtonite + hornblende) ± garnet + plagioclase + quartz + ilmenite and staurolite + hornblende ± gedrite ± garnet + quartz + plagioclase + ilmenite (see Figures D-12, D-16 and D-17). Two coexisting plagioclase feldspars (An_{40} + An_{87-92}) have also been found in several samples as has scapolite (see Figures D-13, D-14 and D-15) . The staurolite-bearing assemblages occur at the extreme south end of the outcrop, the four-amphibole assemblages in the middle and the scapolite-bearing assemblages at the extreme north end.

Collectively, these assemblages define a large portion of the composition space SiO_2-Al_2O_3-MgO-FeO-CaO-Na_2O-H_2O. However, crossing tie-line relations are observed between assemblages which can be resolved by consideration of variations in μH_2O between beds (see Figures D-16 and D-17). Gradients of 0.2 to 2.0 Kcal have been estimated between beds.

A P-T path has been computed for a garnet from this locality (sample 73-20C) that shows a general clockwise path (see Figure D-6). Numerous textural observations, discussed in the text, have also been used to constrain the general clockwise shape of the P-T path with the aid of a petrogenetic grid (see Figure D-8).

38.4 Continue south on Route 5.

40.2 Pompanoosuc. Turn right (west) on Route 132.

40.6 Hogback Road. Turn right (north) up hill.

40.8 Drew Farm. Permission is needed here to enter private property and drive to upper quarry.

41.5 Unload near upper quarry. Drivers proceed to pick-up point beyond Stop 3C.

Stop 3A. Upper Quarry

This stop begins a traverse through the woods to the wonesite locality and the oxygen isotope sampling profile. Approximate time for traverse is 2 hours. Vans will drive around and pick up party along road to the north east.

The rocks in the upper quarry (sample locality 73-30) are amphibolites of the Ammonoosuc Volcanics. There are cross cutting dikes, agglomerate textures and other evidence for the original volcanic character of these rocks. The thickness of the Ammonoosuc Volcanics here suggests that this locality may be near an ancient volcanic center.

Assemblages at this outcrop are largely hornblende + plagioclase + ilmenite ± cummingtonite ± quartz ± epidote. However, a few assemblages of four coexisting amphiboles ± garnet have been found (see Figure D-12, samples 73-30). These assemblages have Fe/(Fe+Mg) values slightly lower than those at the U.S. Route 5 locality.

Traverse to the wonesite locality. The route will be marked with colored flagging.

Stop 3B. Wonesite locality.

The rocks at the wonesite locality are well bedded and highly variable in bulk composition. The bulk compositions are believed to have been modified from the original volcanic compositions by hydrothermal alteration. This belt of altered volcanics trends for several kilometers along strike and in some localities is associated with massive sulfides. The alteration removes CaO and enriches the remaining rock in MgO and Al_2O_3. As a consequence, there is very little hornblende here and only minor plagioclase in many samples.

Wonesite occurs in several different layers, generally associated with phlogopite, cordierite, anthophyllite, chlorite and talc. The mineral is impossible to identify in hand sample as it is virtually indistinguishable from phlogopite. Samples of the best material will be available for collection. The composition of wonesite is shown in Table D-2 and Figure D-18. Wonesite is exsolved to talc + a more Na-rich mica, as shown in Figure D-18.

Also present at this locality is a suite of highly magnesian bulk compositions that give rise to four amphibole (anthophyllite + gedrite + cummingtonite + hornblende) + chlorite assemblages (see Figure D-12). The four amphiboles are the same as those encountered at the U.S. Route 5 locality, but here they are much more magnesian in composition and coexist with chlorite rather than garnet.

Kyanite is present in several samples as inclusions within cordierite and gedrite. The stable matrix association is cordierite + staurolite, but kyanite + gedrite is possible at higher pressures, thus supporting the clockwise P-T path (see Figure D-8). In one sample, 79-38, kyanite + quartz are found in pseudomorphs with a volumetric ratio of approximately 2:3. These pseudomorphs are interpreted to have been after pyrophyllite.

Traverse to the oxygen isotope sampling profile. Along the way we will traverse through pelitic schist of the Littleton Formation. Locally these rocks contain kyanite + quartz veins. Please do not sample these kyanite + quartz veins.

Stop 3C. Oxygen Isotope Sample Traverse

The rocks here straddle the unconformity between Ordovician Ammonoosuc Volcanics to the east and Devonian Littleton Formation to the west. At the unconformity is a biotite schist and a pink, manganiferous garnet-bearing quartz-rich rock called coticule of uncertain age.

Samples were collected at intervals of a few centimeters in a direction perpendicular to strike and measurements of $\delta^{18}O$ were made on quartz separates. The results, as shown in Figure D-20, indicate a lack of oxygen isotope equilibration on a scale of centimeters. The interpretation of these results is that fluid flow was restricted in these rocks owing to relatively low permeabilities.

Pelitic schists from this area have also been the subject of study for the calculation of P-T paths (samples 79-149D and 68-422). Chemical zoning typical of these garnets from these pelites is shown in Figure D-5, and the computed P-T path is shown in Figure D-6 (sample 79-149D). As can be seen, the P-T path computed from the zoned garnets is generally clockwise in shape, in agreement with the paths inferred from the amphibolites from the area.

Walk to the vans.

42.2 Drivers return to Hogback Road (Godfrey Road). Turn right (west).

43.7 Logging road on right opposite pond. Vans park here. Pick-up walkers.

45.4 Return to Pompanoosuc, at junction of Hogback Road and Route 132. Turn left.

45.8 Junction of Route 132 and Route 5. Turn right (south) on Route 5.

49.1 Low cliffs on right. Ammonoosuc Volcanics on west side of Ammonoosuc fault.

50.0 Bigger cliffs of Ammonoosuc Volcanics west of fault, with slickensides.

50.3 Bear left off Route 10 onto River Road.

51.4 Junction with N.H. Route 10A at Lewiston, Vermont. Turn left (east) on Route 10 into New Hampshire. You are now on the Appalachian Trail.

52.0 Stoplights in Hanover, southeast corner of College green. Proceed just beyond next right angle intersection, then bear 45° left onto a college road and proceed to back entrance of Fairchild Earth Science Building.

52.5 Lunch on lawns opposite (east) of Fairchild or in 4th floor lobby in case of rain. Restrooms are located at the opposite (north) end of the building on the 2nd and 4th floors. After lunch see road log for Part E.

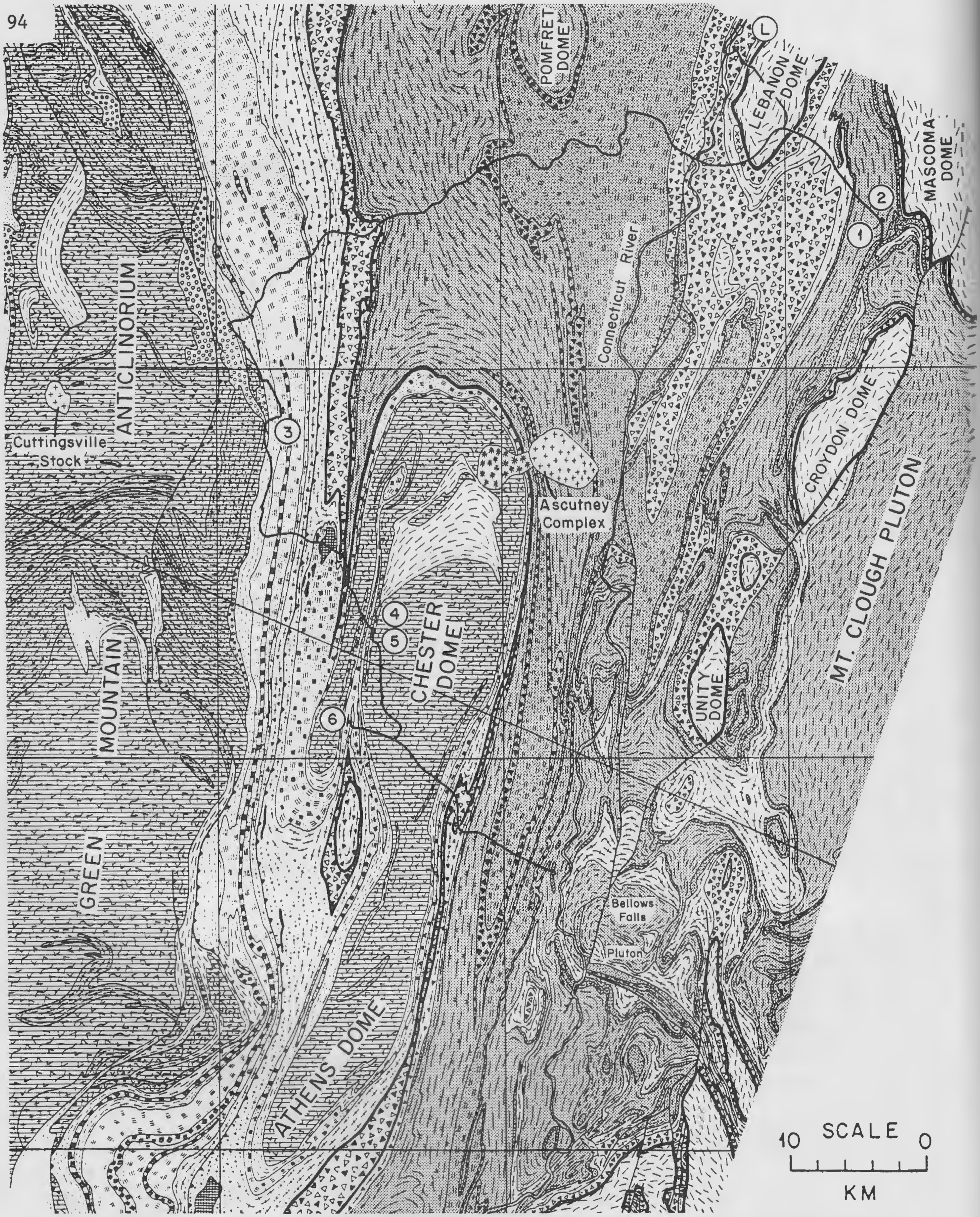
POMFRET DOME
L
LEBANON DOME
MASCOMA DOME
2
1
Connecticut River
GREEN MOUNTAIN ANTICLINORIUM
Cuttingsville Stock
3
CROYDON DOME
Ascutney Complex
MT. CLOUGH PLUTON
4
5
CHESTER DOME
6
UNITY DOME
Bellows Falls Pluton
ATHENS DOME
10 SCALE 0
KM

Figure E-1. Generalized geologic map for part E of field trip in western New Hampshire and eastern Vermont with route indicated. State line is west bank of Connecticut River. Horizontally ruled areas are Grenvillian basement of North America. Areas outlined in heavy black are gneisses in cores of domes of the Bronson Hill anticlinorium and the Barnard Gneiss of Vermont, a potential candidate for "eastern basement" above the Taconian accretionary prism. Gray shading indicates areas of probable Silurian-Devonian strata and intrusive rocks.

E. METAMORPHISM ON THE EAST FLANK OF THE GREEN MOUNTAIN MASSIF AND CHESTER DOME

James B. Thompson, Jr., John T. Cheney, and Peter Robinson

PURPOSE

The purpose of this afternoon's excursion is to visit a few of the localities, primarily in southeastern Vermont, that have been useful in developing our understanding of metamorphic rocks in general and the tectono-metamorphic evolution of the area (Figure E-1). Many of the outcrops viewed on this part of the trip have been the subject of more than one published paper. Because many of these papers are by the senior author and/or his former students, they have been used liberally in preparing this brief review. The original references should be consulted for clarification and further information.

Several of the localities we will visit have interesting mineralogic histories. For example the soapstone quarries of Chester, including the Vermont Mineral Products quarry (Stop 6), the Holden quarry, located approximately 5 km south of Chester Village, and the Carlton talc quarry, located approximately 4 km southwest of Chester Village, have been the source of many interesting minerals. These include: the magnetite-chlorite and pyrite-chlorite rocks common in the 19th century Krantz collections, the Wards collection (20th century) amphibole (actinolite), and the chlorite reputedly used by Pauling (1930) to characterize its crystal structure. Most recently, four new biopyriboles have been discovered at the Vermont Mineral Products quarry by Veblen, Buseck,and Burnham (1977; see Stop 6 for additional references). Their detailed crystal-chemical studies of these new minerals have shown that the biopyriboles, in the sense of Johannsen (1911), are in fact a coherent mineral family, comprised of several distinct but closely related structural types.

Yet another example involves paragonite from the Gassetts Schist (Stop 5). Data from this locality were utilized by Schaller and Stevens (1941) in re-establishing the credibility of paragonite as a mineral species in North America. McCormick (1934) had questioned the validity of paragonite as a mineral distinct from muscovite. Based upon powder diffraction patterns and partial chemical analyses from the type locality, showing 1.77 wt. % Na_2O and 4.66 wt. % K_2O, McCormick (at the time a student attending the alma mater of the second author!) concluded "that the so-called paragonite schist of Pizzo Forno, Switzerland, is primarily a muscovite schist containing about 37 per cent of the paragonite molecule. Paragonite as a distinct mineral has not been found in nature indicating that it probably is an unstable mineral of the mica group." Of interest is that Currier (1934) published a mineralogic description of the schist at Gassetts including partial analyses indicating the likely coexistence of muscovite and paragonite. Currier's description preceeded McCormick's "contribution" by 96 pages in the same volume of the American Mineralogist!

Before departing for Vermont, an opportunity will be taken to examine sillimanite-zone and staurolite-zone rocks, including metamorphosed Lower Silurian fossils, in exposures of the frontal zone of the Skitchewaug nappe, southwest of Mascoma Lake, New Hampshire (Robinson, Thompson, and Rosenfeld, 1979; this guidebook, parts D, F, and H)

STRATIGRAPHIC AND STRUCTURAL SETTING

The Green Mountain massif in southern Vermont (Figure E-1) is one in a series of antiformal structures which expose 1-b.y.-old Grenville basement rocks that extend south through the Berkshire massif in Massachsetts to the Hudson Highlands of New York. As explained by Thompson (1972a), the Proterozoic Y rocks of the Green Mountains were metamorphosed to near granulite facies conditions and deeply eroded prior to the deposition of Proterozoic Z to Lower Ordovician cover rocks. These cover rocks consist of a western clastic shelf and carbonate bank sequence (the western-Vermont sequence) and an eastern sequence of greywackes, shales and volcanics (the eastern-Vermont sequence) of approximately the same age.

Massif - Cover Relationships

As mapped by Karabinos (1986), the western shelf sequence south of Clarendon, Vermont rests unconformably on Grenville basement, although some minor thrust faults are present. North of Clarendon, however, basement and unconformably overlying Proterozoic Z to Cambrian basal clastics of the eastern Vermont sequence have been thrust westward over the western shelf sequence. To the south, this major shear zone along the western boundary of the northern Green Mountain massif apparently passes eastward into the interior of the massif. Downie, Thompson, and Slack (1986) have described septa of cover rocks, similar to those in the eastern Vermont sequence, that are tectonically juxtaposed with basement in the vicinity of this shear zone.

At least two major Paleozoic events, involving crustal shortening and metamorphism, in both the basement and its eastern cover sequence, have been recognized by Downie, Thompson, and Slack (1986; see also Karabinos, 1984,1984a,1985,1986). The earlier, Taconian, event involved west-southwest movement and relatively ductile deformation as manifest by overturned to recumbent folding and the basement/cover thrust faulting. The later, Acadian, event involved upright to slightly overturned folding and may also have involved thrusting along new or pre-existing faults.

Kyanite-staurolite zone mineral assemblages in once higher grade pelitic Grenville basement, pre-date the earliest deformation recognized in both the basement and eastern cover sequence rocks. The occurrence of these kyanite-staurolite assemblages suggests that the initial Paleozoic metamorphism occurred at relatively deep crustal levels. This early metamorphism conceivably records tectonic loading from the east at the begining of the Taconian orogeny. The rocks were then transported to shallower crustal levels prior to or during the Acadian orogeny and metamorphosed at conditions producing garnet- and biotite-zone assemblages in the eastern cover rocks and extensive biotite-zone retrograding of the basement rocks.

The Chester Dome Area

The essentially homoclinal sequence of deformed, garnet zone Paleozoic metasediments and metavolcanics on the east flank of the Green Mountain massif is complicated, in southeastern Vermont, by the Chester and Athens gneiss domes. These are part of a belt of structural domes that extends from central Vermont to Connecticut. This belt, located just west of the Connecticut Valley-Gaspe synclinorium axis, is parallel to the somewhat analogous belt of gneiss domes that constitutes the Bronson Hill anticlinorium (Thompson et al., 1968; see this guidebook, parts A, F, G, and H).

Thompson, Rosenfeld, and Downie (1986) point out that the Chester and Athens domes are comparable in lithic types, structural features and metamorphic history to certain of the deeper zones of the Alps, specifically, the lower Pennine nappes of the Val d'Ossola and Lepontine regions and in the Taüern window. The doming probably occurred during the later stages of metamorphism accompanying the Acadian orogeny. It was preceded by at least three stages of highly ductile deformation; the first of these was probably Taconian and the last probably Acadian.

All three events prior to doming involved basement rocks in isoclinal folding that was probably recumbent and possibly some thrust faulting. These events have been particularly well documented by the detailed mapping of Downie (1982) in the north end of the Chester dome, especially in the "Star Hill sigmoid".

The domes provide a view of some of the lowest tectonic levels of the crystalline core of the Appalachians. They can be regarded as consisting of a core, an inner mantle and an outer mantle. Basement rocks in the cores contain a variety of quartzo-feldspathic gneisses, amphibolites (some with 5-7 cm chlorite clots after garnet), and graphite-bearing schists associated with marble and calc-silicate. These core rocks are very likely reworked Grenvillian rocks, similar to those now exposed in the southwestern Adirondacks. Septa of cover rocks in the inner mantle resemble, in protolith, the septa of eastern cover rocks seen along the major shear zone in the central Green Mountains some 20 km to the west. These probably represent the root zones for the movements that resulted in the emplacement of the Taconic allochthons. The outer mantle contains metamorphosed sedimentary and volcanic rocks, including metamorphosed ultramafic rocks, more indicative of an oceanic environment.

All rocks in the vicinity of the domes bear evidence of strong internal shear. Carbonate rocks and carbonaceous pelites appear to have been particularly susceptable. However, discrete surfaces of dislocation cannot be identified with certainty, nor can they be disproved. The extent of shearing in the rocks is well illustrated by the occurrence of "rolled garnets" in the inner mantle of the Chester dome that recorded a minimum of 720° of rotation during syn-kinematic growth (see the pioneering work of Rosenfeld, 1968, for method and description).

DISTRIBUTION OF METAMORPHIC ZONES AND POLYMETAMORPHISM

The pattern of Acadian metamorphic isograds in southeastern Vermont is shown on Figure A–2. Although these isograds have been mapped on the basis of indicator minerals, the corresponding metamorphic zones very nearly correspond to AFM mineral facies (Thompson, 1957) as discussed below (see Stop 5, Figure E-13). However, the compositional dependence of the kyanite+ biotite isograd and the disparate rock compositions in the region have precluded the mapping of separate kyanite and staurolite zones on a regional scale. The compositional dependence especially of the garnet isograd is illustrated by the nearly parallel nature of isograds and stratigraphic contacts, even in the vicinity of the gneiss domes.

Several detailed petrologic studies conducted in southeastern Vermont (e.g. Downie, 1982; Downie et al., 1986; Karabinos, 1984, 1984a, 1985, 1986; Rosenfeld, 1968, 1972; Thompson, Lyttle and Thompson, 1977; and Thompson, Tracy, Lyttle and Thompson, 1977) have shown that porphyroblasts of staurolite and kyanite and the rims of garnet porphyroblasts (see discussion below) are undeformed and overprint the deformational fabrics in the rocks. Accordingly, maximum metamorphic grade was attained in this area subsequent to, or near the end of dome emplacement. The concentric pattern of isograds around the domes is a manifestation of deeper crustal conditions brought near the surface by the rise of hot rocks in the domes rather than folding of the isograds, that is, the domes acted as "heat pipes". The widespread occurence of retrograde hydration and exchange reactions documented by these workers, attests to the slow cooling of hot rocks carried to a lower temperature crustal enviroment by the rise of the domes. Of interest is that the apparent pre-dome configuration of metamorphic zones in southeastern Vermont may serve to constrain partially the thickness and/or western extent of eastern-derived thrust/nappe rock packages during the Acadian orogeny (see this guidebook, parts D and F).

The intense Acadian metamorphism and deformation have obliterated much of the pre-Acadian record in the rocks of southeastern Vermont, especially in the vicinity of the domes. Despite renewed interest in radiometric age dating in New England, the eastern limit of the Taconian orogeny in this area remains unknown (Sutter, Ratcliffe and Mukasa, 1985). However, Laird and Albee (1981a, 1981b) have given evidence for polymetamorphism in the eastern cover rocks of the Green Mountain massif. Specifically, they have interpreted amphibole zoning patterns, from amphibolites in the Cambrian Pinney Hollow Formation, as indicative of two phases of medium-pressure Ordovician metamorphism as well as medium-pressure and a later lower-pressure Devonian metamorphic phases. Pinney Hollow amphibolites from the outer mantle of the Athens dome apparently record only the two Acadian phases (Laird and Albee,1981a, 1981b, see also this guidebook part B).

Texturally zoned garnets, with two distinct growth stages, from the Pinney Hollow pelites of the Athens dome have been interpreted by Rosenfeld (1968) as "tectonometamorphic angular unconformities". He suggested that the outer zone represents an Acadian overgrowth of a pre-existing Taconian core, because similar textures were not found in nearby Silurian-Devonian rocks. Thompson, Tracy, Lyttle and Thompson (1977) have shown that such discontinuities can develop via garnet-consuming reactions during a single prograde event (see Stop 5) . Nonetheless, Karabinos (1984a), using textural and chemical data, has shown that a pervasive retrograde event separated two prograde stages of garnet growth in similar rocks from Jamaica, Vermont (southwest of the Chester dome). Similarly zoned garnet has been reported in the northern Chester dome by Downie (1982) and at Gassetts, Vermont (Stop 5). Discontinuities in garnet growth could also have resulted from momentary cooling due to the Acadian emplacement of hot nappes into a cooler environment, before thermal relaxation.

ITINERARY

0.0	Proceed directly south down hill from Fairchild Earth Science Building.
0.2	Stop sign at East Wheelock Street. Go directly across (south) and in front of football stadium.
0.4	Stop sign. Turn left (southeast) on Route 120 (Lebanon Street).
1.5	Stop light at Greensboro Road. Bear right (south) on Route 120.
3.4	Road cut in Lebanon Granite.
3.9	Big road cut. More Lebanon Granite.
5.1	Junction of Route 120 with Interstate 89 in Lebanon. Turn left (east) toward Enfield and Concord, N.H.
6.1	Outcrop left, vertically plunging infold of felsic volcanics of Partridge Formation.
7.2	Cross U.S. Route 4 (Exit 17).
8.4	Outcrop on left. Sulfidic schist of Partridge Formation. This is part of the belt on the upper limb of the Cornish nappe and is also peripheral to the Lebanon dome.
9.9	Exit 16 - Purmort. I89 crosses trace of Clough Quartzite (Hardy Hill belt) on upper limb of Cornish nappe.
10.1	Outcrop of Littleton Formation, left. Slatey phyllite in the biotite zone. This is the low grade zone associated with the Northey Hill line (see part D, p. 63).
10.6	Outcrop of Littleton Formation, left, in garnet zone.
10.9	Outcrop of Littleton Formation, right.

11.1 Take Exit 15 (right). Montcalm.

11.3 Turn right at stop sign, then immediately left (east) on dead-end road leading to bicycle path.

12.5 Turn around at end of road.

STOP 1. SILLIMANITE ZONE CLOUGH QUARTZITE WITH FOSSILS, NEAR ANTICLINAL HINGE OF SKITCHEWAUG NAPPE
(40 minutes)

From turning circle walk along bicycle path about half way along first road cut which is outcrop 1A (Figures E-2 and E-3). This is the Clough Quartzite including a fossiliferous upper calcareous zone in the anticlinal hinge region of the Skitchewaug nappe (Boucot and Thompson, 1963, localities 6 and 7 near here in map area of Figure E-2). From this position look southeast up bicycle path to large outcrops on right which are Middle Ordovician Partridge Formation in the core of the anticlinal nappe. Beyond that on the right of the highway is white Clough Quartzite on the right-side-up upper limb of the nappe. To the east across the Interstate Highway is a mountain composed of Bethlehem Gneiss of the Mount Clough pluton that rests on top of the nappe. Minor amounts of sillimanite-mica schist of the Littleton Formation, granulites and calc-silicate rocks of the Fitch Formation, and Clough Quartzite, all right-side-up, occur below overhangs along the west face of the mountain. Dominant mineral lineation in all of these rocks has the same N60W trend and is believed to have formed during the dome stage in the compressed zone between the Mascoma and Croydon gneiss domes.

Most of outcrop 1A consists of massive quartzite and quartz-pebble conglomerate separated by thin foliated layers of muscovite-garnet schist. In some places the quartzite beds appear to be boudined and the schist injected between separated quartzite masses. Overall the bedding dips gently to moderately northwest, whereas the dominant schistosity in the schist interbeds dips gently to steeply southeast, apparently parallel to axial planes of early (nappe-stage) folds. Two tabular masses of biotite amphibolite dip moderately to steeply southeast. They are roughly parallel to the axial plane foliation in the schist and appear to truncate bedding, so they are probably dikes. A strong mica lineation on schist foliation planes and a strong hornblende lineation on amphibolite foliation planes trend N30-50W in reasonable conformity with features assigned to the dome stage in adjacent outcrops.

At the northern end of outcrop 1A, the quartzite is overlain by a well bedded zone of diopside- and grossular-bearing calc-silicate rocks, fine-grained quartzites, and sulfidic mica schists, assigned to the upper member of the Clough Quartzite. Some calc-silicate rocks contain obvious shelly fossils, commonly replaced by diopside or grossular. **DO NOT HAMMER**; there is plenty of loose material at outcrop 1B. In this vicinity there are several subhorizontal early folds in bedding that trend N20-40E with southeast-dipping axial surfaces. As will be seen at outcrop 1B, these are equated with the hinge direction of the Skitchewaug nappe.

Climb onto top of north end of outcrop 1A, observing weathered fossils en route, then traverse grass and dirt slope south to low point in fence, and climb into quarry and outcrop 1B which lies above and to south-southeast.

Rocks exposed in the quarry (Figure E-3, outcrop 1B) include normal quartzite and mica schist of the Clough Quartzite, the fossiliferous, bedded calc-silicate member of the Clough, dikes of amphibolite, and a small post-metamorphic diabase intrusion.

As you face upward into the quarry you are looking west-northwest up the southeast-dipping

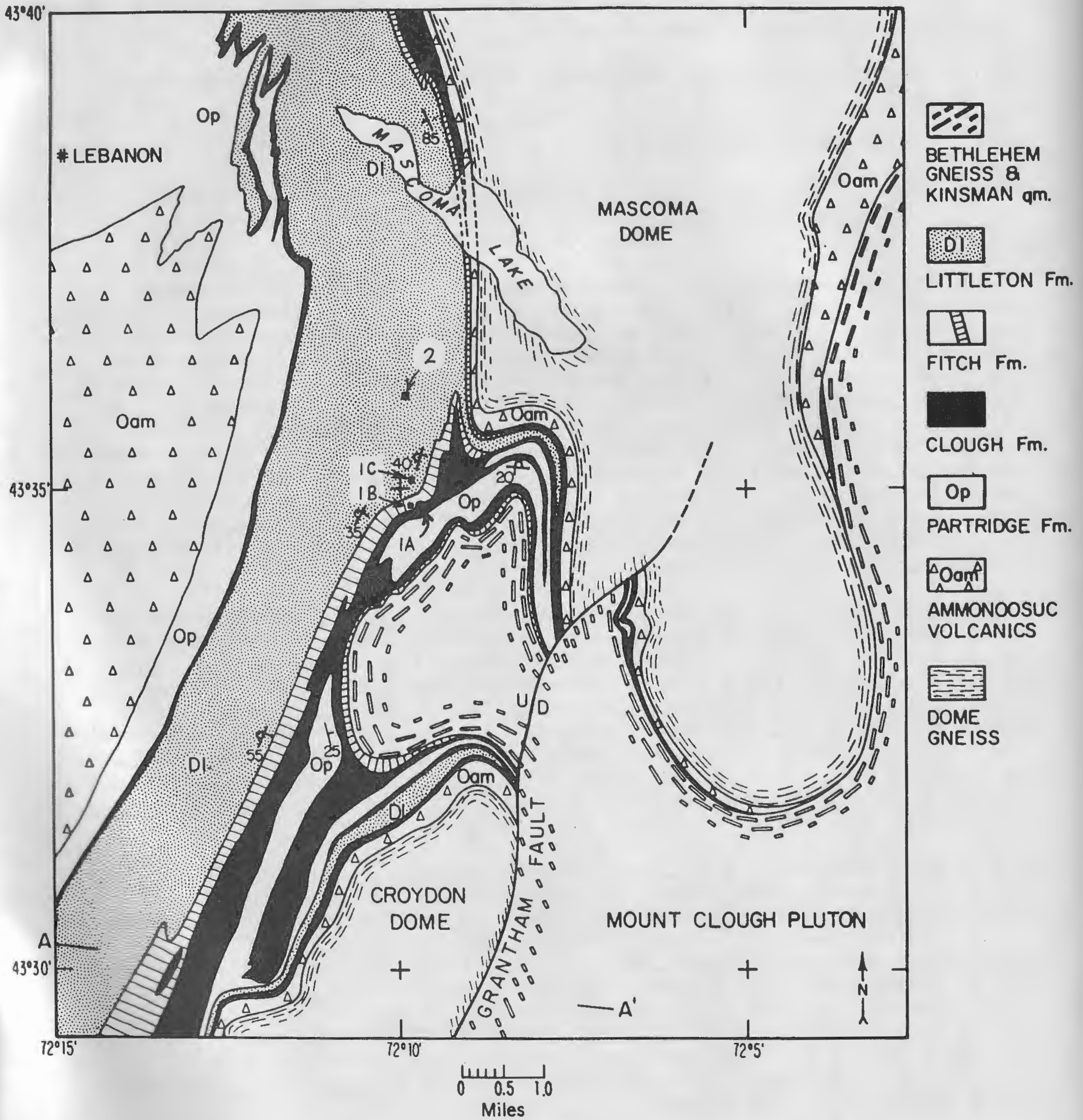
43°40'
43°35'
43°30'
72°15'
72°10'
72°5'
LEBANON
Op
Oam
Dl
MASCOMA LAKE
MASCOMA DOME
2
85
1C
1B
1A
40
20
35
55
25
U
D
GRANTHAM FAULT
CROYDON DOME
MOUNT CLOUGH PLUTON
A
A'
N
0
0.5
1.0
Miles
BETHLEHEM GNEISS & KINSMAN qm.
Dl
LITTLETON Fm.
FITCH Fm.
CLOUGH Fm.
Op
PARTRIDGE Fm.
Oam
AMMONOOSUC VOLCANICS
DOME GNEISS

Figure E-2. Geologic map of the Mascoma Lake area, New Hampshire. Modified from Thompson et al. (1968) and Chapman (1939, 1942, 1952). Numbers show Stop 1, Outcrops 1A, 1B, 1C, and Stop 2. A-A' is section line of Thompson et al. (1968, Pl.15-1b).

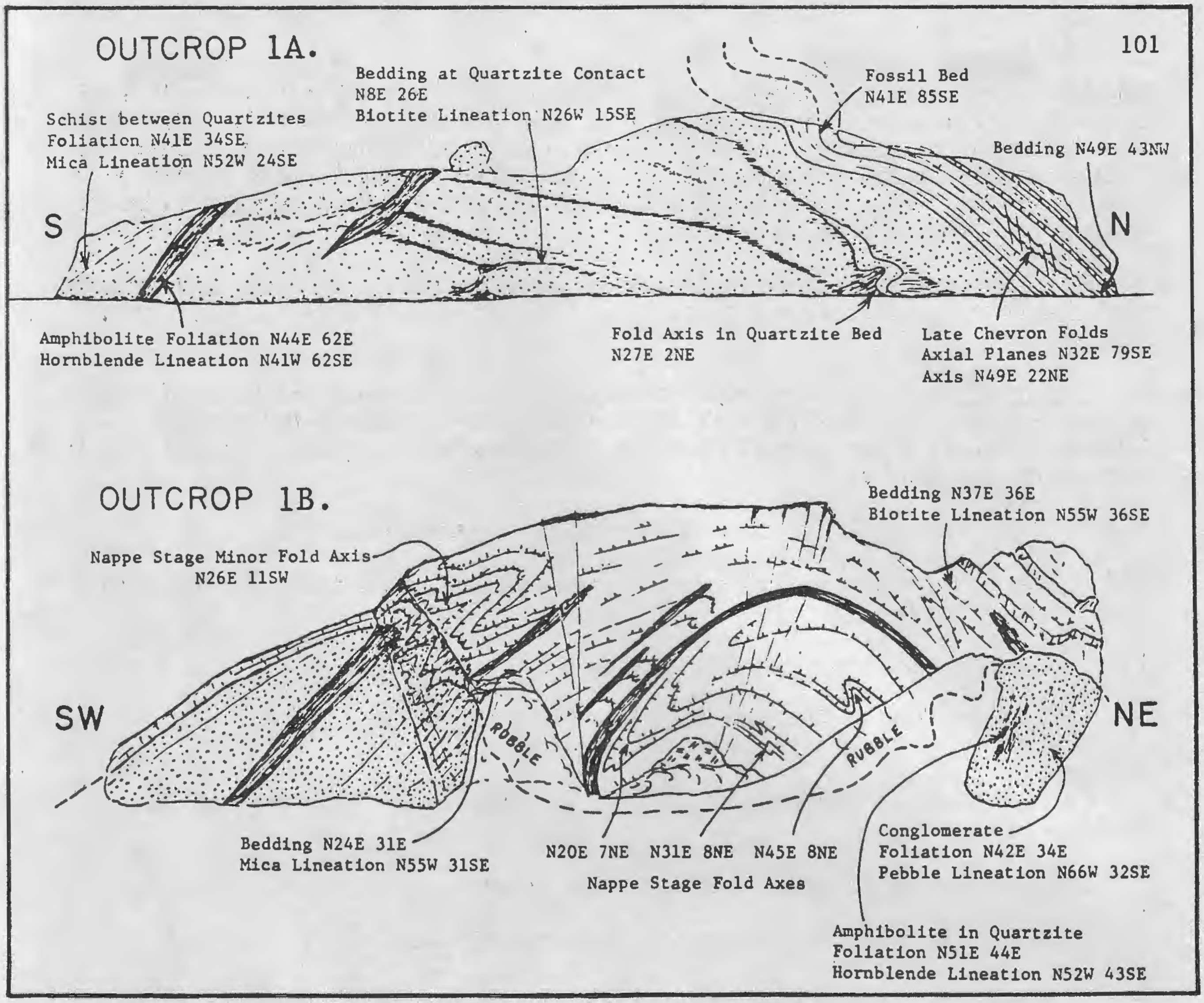
OUTCROP 1A.
Bedding at Quartzite Contact
N8E 26E
Biotite Lineation N26W 15SE
Fossil Bed
N41E 85SE
Schist between Quartzites
Foliation N41E 34SE
Mica Lineation N52W 24SE
Bedding N49E 43NW
S
N
Amphibolite Foliation N44E 62E
Hornblende Lineation N41W 62SE
Fold Axis in Quartzite Bed
N27E 2NE
Late Chevron Folds
Axial Planes N32E 79SE
Axis N49E 22NE
OUTCROP 1B.
Bedding N37E 36E
Biotite Lineation N55W 36SE
Nappe Stage Minor Fold Axis
N26E 11SW
SW
NE
RUBBLE
RUBBLE
Bedding N24E 31E
Mica Lineation N55W 31SE
N20E 7NE
N31E 8NE
N45E 8NE
Nappe Stage Fold Axes
Conglomerate
Foliation N42E 34E
Pebble Lineation N66W 32SE
Amphibolite in Quartzite
Foliation N51E 44E
Hornblende Lineation N52W 43SE

Figure E-3. Field sketches of outcrops at Stop 1. Outcrop 1A, Clough Quartzite including upper fossiliferous calc-silicate member in frontal region of Skitchewaug nappe. Cut by dikes of amphibolite. Dominant folds and axial plane foliation seems to be of the nappe stage, but there is abundant dome stage mineral lineation. Length of outcrop approximately 150 feet (45 meters). Outcrop 1B, view into quarry in Clough Quartzite, frontal region of Skitchewaug nappe. View is looking WNW approximately parallel to the transport direction of the nappe. Quartzite member in foreground to right and left (stippled) is succeeded up axial surfaces by fossiliferous calc-silicate member. Both members are cut by amphibolite dikes approximately parallel to nappe stage axial surfaces. There is a small plug of post-metamorphic diabase at base of wall in center of quarry. Width of view in foreground is about 150 feet (45 meters). Back wall of quarry is set back about 100 feet (30 meters).

axial surfaces of a series of minor recumbent folds related to the frontal region of the Skitchewaug nappe. The fold axes are subhorizontal and trend N20-45E, approximately at right angles to your line of view. At the mouth of the quarry you are standing in the quartzite member, which is also exposed on left- and right-hand sides. The entire top and back of the quarry is composed of the fossiliferous, bedded calc-silicate member that lies in a more frontal position in the nappe. Unfortunately, most contacts between the quartzite and the calc-silicate members are either covered by debris or exposed on badly altered surfaces. The amphibolite is clearly in dikes parallel to the axial surfaces of the northeast-trending nappe stage folds. It is possible that the dikes post-date the folds, but we prefer to think that the fold axial surfaces were localized by the dikes, because such dikes are unknown in the overlying Littleton Formation and are presumed to be of Silurian age. A moderate to strong northwest-trending mineral lineation, equated with the dome stage in adjacent outcrops, is evident throughout the quarry.

Return to north end of outcrop 1A by same route and walk north to turnaround at end of road. Fitch Formation is exposed in woods west of here. Walk or ride 0.1 mile north on road to small rock cut on left.

Outcrop 1C. Littleton Formation (10 minutes). Staurolite-sillimanite mica schist. Bedding is obscure. Foliation strikes N40E, dips 40 °SE. Dome stage mineral lineation trends N40W. Fibrolitic sillimanite is best seen with a hand lens on the upper surface of the outcrop, and tends to occur as rims on staurolites.

12.6 Stop1, Outcrop 1C (see above). Pick up all passengers and head north.

13.7 Montcalm Interchange. Pass beneath Interstate 89 and turn left (north) on entrance ramp for I-89 North.

13.9 Pull well over on the right side of entrance ramp.

STOP 2. STAUROLITE ZONE LITTLETON FORMATION
(15 minutes)

Coarse staurolite with local thin rims of white mica. Outcrop also contains a Mesozoic lamprophyre dike.

Enter Interstate 89 and retrace route back toward Lebanon

19.8 Exit 18 - Route 120 in Lebanon. Stay on Interstate 89 North.

22.0 Road cut showing southeast contact of Lebanon Granite with sulfidic schist.

24.4 Connecticut River. Enter Vermont at west bank. View to southeast of Mt. Finish quarry, West Lebanon, in garnet zone of Orfordville anticlinorium studied in detail by Spear (this guidebook, part D). Cross Ammonoosuc fault.

25.1 Junction Interstate 91. Stay on Interstate 89.

25.5 Outcrop of Gile Mountain Formation in biotite zone of Connecticut Valley metamorphic low.

28.1 Exit 1 - Leave Interstate 89 for U.S. Route 4 for Woodstock.

28.3 Stop sign at end of ramp. Turn left (west) on Route 4 West.

31.7 Bridge over Quechee Gorge. Route 4 follows abandoned railroad. Enter garnet zone of western Acadian metamorphic high. Just east of Woodstock, route passes briefly through southern tip of kyanite zone of northern Vermont metamorphic high (see Figure A-2).

39.1 Center of Town of Woodstock.

42.7 Covered bridge on left. Between here and Bridgewater we cross the "Richardson Memorial Contact" between cover rocks of the Connecticut Valley synclinorium and the Cambrian-Ordovician sequence on the east flank of the Green Mountain anticlinorium. From this point to the Grenvillian basement to the west is about 9 miles (14 km).

45.8 Town of Bridgewater in Barnard Gneiss.

47.8 Junction with Route 100A at Bridgewater Corners. Turn left (southwest) on Route 100 A.

48.5 Outcrops on right of Lower Ordovician Moretown Formation considered by some to be in the upper part of the Taconian accretionary prism. Route 100 runs up Pinney Hollow, the type locality of the Cambrian Pinney Hollow Formation to be visited at Stop 3.

53.6 Turn right into Plymouth village, the birthplace of President Calvin Coolidge. This lies just inside the biotite zone and in various members of the Proterozoic Z to Cambrian Hoosac Formation.

54.1 Rejoin Route 100A and continue west.

55.0 Junction of Route 100A with Route 100 at Plymouth Union. Turn left (south) on Route 100, which follows valley eroded into dolomite of the Proterozoic Z to Cambrian Tyson Formation. Basal Tyson quartzite and conglomerate forms hill to west resting unconformably on Grenville basement.

58.5 North end of Lake Amherst. Turn left (east) off Route 100 onto gravel road and follow winding route that eventually goes southeast down the east side of the valley.

59.7 High ledges on left of Hoosac Formation with edgewise biotite.

60.5 State Park on right.

60.8 Park on road for walk to Weaver Hill.

STOP 3. WEAVER HILL: COARSE CHLORITOID PHYLLITE

(40 minutes)

Weaver Hill is located within the eastern cover sequence of the Green Mountain massif (Figure E-1). The hill is underlain by garnet-zone high-alumina phyllites of the Cambrian Pinney Hollow Formation. Similar rocks also occur in the outer mantle of the Chester dome. The common quartz- and muscovite-bearing mineral assemblages in these rocks are chloritoid+chlorite+ paragonite, chlorite+ garnet ± paragonite, and chloritoid + chlorite + garnet ± paragonite. These mineral assemblages are consistent with the garnet zone AFM topology as shown in Figure E-4.

Of particular interest here is the localized occurence of 1.5 cm euhedral chloritoid crystals in the chloritoid - chlorite - muscovite - paragonite - quartz phyllites on the western slope of the hill. Material from one of these outcrops was used by Hanscom (1973, 1975, 1980) for the single crystal structural characterization of monolinic chloritioid (space group *C2/c*).

Mineral composition data from Weaver Hill are shown in Table E-1 including the previously unpublished gravimetric analyses of coexisting garnet and chloritoid performed by Jun Ito in 1958

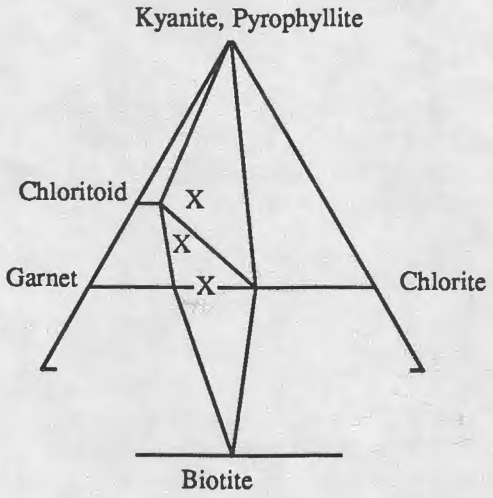

Figure E-4. Schematic AFM projection for garnet-zone mineral assemblages observed at Weaver Hill.

Table E-1. Mineral analyses from Weaver Hill, Vermont, and the Davis Mine, Massachusetts. Grav=Gravimetric analysis by Jun Ito, 1958. Probe = microprobe analysis by Hanscom (1973).

	W HILL GARNET GRAV	W HILL CHTD GRAV	W HILL CHTD PROBE	D MINE GARNET GRAV	D MINE CHTD GRAV	D MINE CHTE GRAV
SiO2	36.54	24.46	24.88	36.53	23.82	25.19
TiO2	0.15	0.39	0.00	0.10	0.00	0.09
Al2O3	21.74	39.83	39.57	21.42	38.91	22.65
Fe2O3	0.13	1.25	0.00	0.36	2.94	3.34
FeO	31.38	24.54	25.17	31.65	23.30	22.32
MnO	5.02	0.68	0.80	6.43	0.43	0.08
MgO	0.60	1.64	2.08	1.64	3.18	15.04
CaO	3.93	0.00	0.00	1.78	0.00	0.00
H2O +/-	0.95	1.04		0.91	1.16	11.19
H2O +		6.02			6.36	
Total	100.44	99.85	92.50	100.82	100.09	99.90
ANHYDROUS FORMULAS						
#OX/FORMULA	12	6	6	12	6	14
Si	2.973	1.013	1.033	2.967	0.990	2.603
Ti	0.009	0.012	0.000	0.006	0.000	0.007
Al	2.085	1.944	1.936	2.050	1.906	2.759
Fe3+	0.008	0.039	0.000	0.022	0.092	0.260
Fe2+	2.135	0.850	0.874	2.150	0.810	1.929
Mn	0.346	0.024	0.028	0.442	0.015	0.007
Mg	0.073	0.101	0.129	0.199	0.197	2.317
Ca	0.343	0.000	0.000	0.155	0.000	0.000
ATOM RATIOS						
Fe2/Fe2+Mg	0.967	0.894	0.871	0.915	0.804	0.454
Fe3/Fe2+Fe3	0.004	0.044	0.000	0.010	0.102	0.119

(see Thompson Lyttle and Thompson, 1977, for methods) and an electron-microprobe analysis of the "giant" chloritoid reported by Hanscom (1973). In addition, Rosenfeld, Thompson, and Zen (1958) reported basal spacings of 9.948 and 9.644 Å for coexisting muscovite and paragonite, respectively, from this locality (designated as Plymouth, Vermont). These basal spacings correspond, approximately, to compositions of Pg_{20} for muscovite and Pg_{93} for paragonite (Zen and Albee, 1964).

Also reported in Table E-1 are gravimetric analyses, performed by Jun Ito, for coexisting garnet, chloritoid and chlorite from the Davis Mine, located in rocks of the Hawley Formation. near Rowe, Massachusetts. Because the sample and these analyses appear virtually identical to those from Weaver Hill and there are no other reported chloritoid occurrences in the Middle Ordovician Hawley Formation, it is conceivable that the sample was mislabeled.

...over the hills and through the woods...

61.0 Turn right (west) at T junction, proceed to Route 100.

61.3 Junction with Route 100 in Tyson. Turn left (south) on Route 100.

65.0 Junction with Route 103. Turn left (souteast) on Route 103. Proceed through Village of Ludlow and then east through Smithville. Approximately one mile east of Smithville, large outcrops on left (north) are serpentinite with relict olivine and with meter thick carbonate veins in an ultramefic body enclosed in the Cambrian Ottauqquechee Formation. From the junction of Route 103 and Route 131 to Proctorsville and Cavendish (the home of Alexander Solzhenitsyn), Route 103 bears right (southeast and then south) along the axial surface of the Proctorsville syncline between the Green Mountain anticlinorium and the Chester dome. Outcrops on the left (east) near the top of the hill are Silurian-Devonian Waits River Formation with rotated garnets. As Route 103 curves to the left and heads down hill through Proctorsville Gulf the entire vertical section is crossed from the Silurian-Devonian to the Grenville basement of the Chester dome in a distance of about 0.5 km.

74.3 Park on right (southwest) side at the north end of the bridge over the Williams River and walk south 100 meters into the Williams quarry. Proceed to the large blocks on right at the northern end of the quarry.

STOP 4. THE WILLIAMS QUARRY AT GASSETTS, VERMONT: CALC-SILICATE REACTION ZONES

(20 minutes)

The interbedded calc-silicate rocks and phengite-bearing quartzo-feldspathic gneisses exposed in the Williams quarry are from the upper part of the Proterozoic Z to Cambrian Tyson Formation. These rocks together with the disconformably overlying high-alumina pelites of the Hoosac Formation (the Gassetts Schist of Stop 5) belong to the inner mantle sequence of the Chester dome. Here (stops 4 and 5) the inner mantle rocks occur along the western side of an infold of Lower Paleozoic rocks into the Grenville gneisses that form the core of the dome. This crescent-shaped septum is similar in many respects to Alpine mulde (Fig E-5). In fact, the phengite gneisses exposed in the quarry are very similar to the mulde gneisses quarried extensively at Val Maggia, Switzerland. However, these gneisses cannot be distinguished from the basement gneisses because they are completely sandwiched between calc-silicates of the Tyson formation.

A.B. Thompson (1975) has described in detail the nature and reaction history of the calc-silicates occurring in the thinly laminated carbonate- pelite sequence of the Tyson Formation. His descriptions are summarized here and the reader is refered to the original paper for additional information.

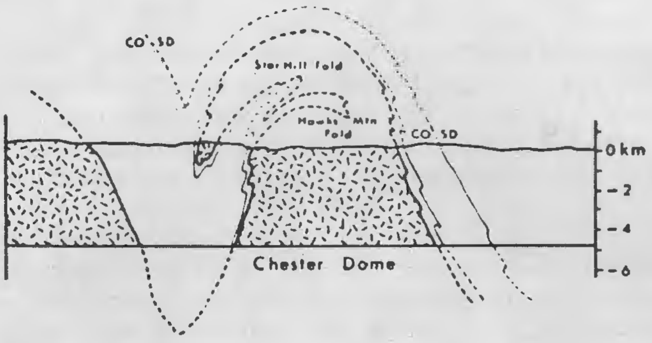

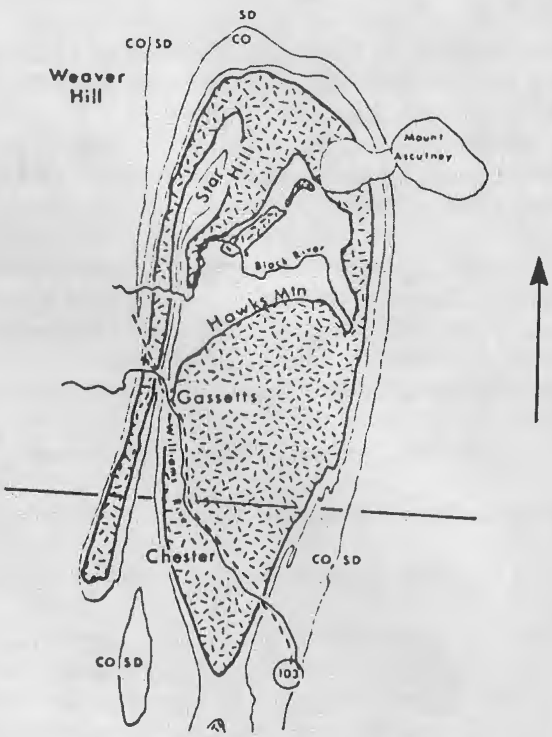

Figure E-5. Sketch map and cross section of Chester gneiss dome and mantling strata (from Doll et al., 1961). Core gneisses are indicated by stippled ornament. The boundary between Cambrian-Ordovician and Silurian-Devonian strata is shown by the letters CO-SD. From Thompson, Lyttle and Thompson (1977).

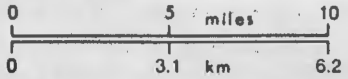

According to Thompson (1975), the original mineralogy of the calc-mica schists has been modified due to the development of reaction zones. Thicker "pelitic" layers of the schists resemble the enclosing gneiss and consist of quartz (55%), alkali feldspar (10%), plagioclase (5%), phengite (10%), biotite (15%), and accessories (5%) including epidote, calcite, sphene, apatite, and rare graphite and pyrrhotite. The marble layers consist primarily of coarse calcite with irregular diopside, commonly adjacent to rounded quartz grains, concentrated in their centers. Less commonly, small actinolite crystals, also in contact with rounded quartz, occur within the recrystallized calcite. The occurrence of the diopside and actinolite in the coarse calcite suggests that subordinate amounts of dolomite, relative to quartz and calcite, were present in the protolith. Dolomite in various associations with calcite, actinolite, diopside, biotite, microcline, and quartz occurs in the Tyson carbonate units elsewhere in the Chester dome (e.g. Cavendish Gorge). The reaction zones between the "pelite" and the metacarbonate contain a variety of associations of biotite, clinozoisite, microcline, actinolite, diopside, calcite and quartz. Minor amounts of sphene, apatite, graphite, pyrrhotite and chalcopyrite also occur in these zones. In detail the nature of the zones depends upon the relative thickness of the carbonate and pelite layers, and perhaps upon the extent of initial gradation between lithologies. A characteristic intergrowth of clinozoisite and biotite, commonly with microcline and quartz, occurs between thicker pelite layers and thin carbonate layers. The minerals comprising the intergrowth are generally randomly oriented but confined to distinct layers. The intergrowths characterizing reaction zones between thin pelitic and thicker carbonate layers consist of coarse diopside (0.5 cm), containing inclusions of actinolite and calcite, and randomly oriented blades of actinolite. The bladed actinolite contains inclusions of diopside and calcite.

A complex reaction history, involving the elimination of dolomite from the carbonates and "muscovite" from the pelitic interlayers, has been developed by Thompson (1975) to account for the many textural and compositional variations of these rocks many of which are not reviewed here. Although this reaction history will not be reviewed it is interesting to consider that many aspects of the reaction zones between the thicker pelite and carbonate layers, characterized by the zoisite-biotite intergowths, may result from the diffusion of primarily CaO. The possibility of mass transfer has been considered by Thompson (1975) and discussed in some detail by Brady (1977) for similiar rocks in northern Vermont.

Proceed to souteast end of bridge on foot or in van. Continue southeastwards on Route 103.

74.5 Pull into wide turnout on right (west) of Route 103. Walk carefully across Route 103 to high-alumina part of the Gassetts Schist at the north end of the long road cut, then cross back to dumps on slope above river.

STOP 5. THE GASSETTS SCHIST
(40 minutes)

The schist at Gassetts,as well as at other localities in the Chester dome area, such as Black River, Hawks Mountain, and Star Hill (see Figure E-5) contains kyanite - biotite zone mineral assemblages that reflect a wide range in alumina content. The detailed study of these rocks has provided a nearly complete description of AKNa and AKFM Facies Types (Thompson,1957,1961; Thompson and Thompson, 1976). Moreover, the detailed consideration of components extraneous to the AKFM projection has permitted mapping of the AFM plane with respect to saturating CaO,Na_2O,Fe_2O_3, and TiO_2 phases (Thompson, 1972).

Two size fractions of white mica occur here, as originally described at Glebe Mountain, Vermont by Rosenfeld (1956) and subsequently observed world-wide, including Pizzo Forno, Switzerland. The fine-grained mica that you cannot visually resolve into discrete flakes in hand specimen is paragonite; the coarser grained mica is muscovite. The composition gap between gravimetric analyses of these micas (from ~Pg_{38} to Pg_{83} in the muscovite and paragonite respectively, see Table E-2) is as narrow as observed anywhere. However, repeated microprobe analyses of muscovite from this locality are consistently lower in Na and Ca than the gravimetric analyses (compare Tables 1 and 2 in Thompson, Lyttle, and Thompson, 1977). This analytical discrepancy may reflect "perthitic" exsolution of paragonite in the muscovite. Hence the gravimetric analyses may provide an integrated composition reflecting the maximum metamorphic conditions whereas the microprobe may be measuring cooler, retrograde compositions.

A third white mica, margarite, also occurs in these rocks. Margarite occurs only as inclusions in garnet here (see also Downie, 1982), however, matrix margarite has been reported in similar rocks from western Massachusetts (Cheney, 1980).

Although not observed at this locality, similar high-alumina rocks in the vicinity of Star Hill have zoned muscovite porphyroblasts (phengitic cores and "normal" rims) that have overgrown matrix phengite in the foliation (Downie, 1982). These complex white-mica assemblages also occur in the Gassetts-like pelites of the Hoosac Formation in western Massachusetts (Cheney, 1980, 1986). Cheney (1986) has shown that the evaluation of these assemblages, utilizing the methods putlined by Thompson (1980, 1982a, 1982b) and Spear and Selverstone (1983), may be useful in constraining the P - T paths of the rocks in which they occur.

Mineral Assemblages

The long road cut on the east side of the Williams River contains a continuous sequence of Gassetts Schist, a part of the Hoosac Formation. The high alumina assemblage containing kyanite + biotite + muscovite + paragonite + staurolite + garnet + quartz with titanohematite and minor epidote, apatite and rare calcite, occurs at the north end of the outcrop, although the best samples are usually found in the rubble across the road. The alumina content of the rocks generally decreases to the south along the cut and the southernmost portion of the road cut contains the assemblage quartz + plagioclase + muscovite + biotite + garnet ±calcite, tourmaline and magnetite - with or without graphite.

South of this road cut, after a covered interval at the position of the upper Tyson carbonates, are exposures of gneisses that are metamorphosed graywackes of the Tyson Formation and/or strongly modified core gneisses of the Chester Dome. These rocks contain quartz + microcline + plagioclase + biotite + muscovite, with minor calcite, epidote, sphene, tourmaline, apatite, and less common pyrite, graphite and magnetite. Of interest is that garnet does not coexist with microcline in the presence of biotite + magnetite + graphite.

In the middle of the road cut, the following muscovite + quartz- bearing assemblages occur sequentially from south to north: plagioclase + paragonite + staurolite + garnet + biotite; paragonite + staurolite + garnet + biotite; kyanite + paragonite + staurolite + garnet + biotite. Kyanite and plagioclase have not yet been observed together in any sample. Moreover, both hematite and magnetite, although extensively altered and exsolved, occur in the AKFM assemblage muscovite+ paragonite+ staurolite+ garnet+ biotite+ quartz. Chlorite occurs in many of these assemblages and may be primary where interlayered with biotite and muscovite in the groundmass. More commonly, however, chlorite occurs as selvages around garnet or intergrown with biotite. This variety of mineral assemblages allows the nearly complete description of kyanite+biotite zone AKNa and AFM facies types as well as the mapping of the AFM plane with respect to saturating Na_2O, Fe_2O_3 and TiO_2 phases (Thompson, 1972, as shown on Figure E-6). As developed by Thompson (1979), and shown in Figure E-7 the muscovite coexisting with various three-phase AFM assemblages will have a specified amount of phengite component and the muscovite becomes more phengitic in three-phase AFM assemblages containing progressively less-aluminous phases.

AFM Phase Relations

In the high-alumina pelite, more than three AFM phases (garnet-staurolite-biotite-kyanite) apparently coexist with muscovite+paragonite+quartz and possibly primary chlorite. This suggests as do the representative analyses of Table E-2 and the crossing tie lines and ranges in the compositions of the minerals, plotted in Figure E-8, that additional components, e.g. MnO, CaO, and/or Fe_2O_3 stablize one or more of the AFM phases, and/or that local assemblages represented by three-phase triangles reflect equilibration at a range of metamorphic conditions.

The utilization of garnet-rim compositions in Figure E-8 assumes that only the outermost part of the garnet was involved in the last recorded reactions. The relatively high modal ratios of garnet to biotite and of staurolite to biotite enhances the possibility that biotite compositions may have been altered during cooling by exchange reactions (Tracy et al., 1976). The garnets are "normally" zoned with Ca- and Mn-enriched cores (up to 17 mole % grossular and 5.5 mole % spessartine). Detailed microprobe analyses of core garnet, discussed more fully below, show that magnetite increases and that Ca and Mn decrease from core to rim, whereas Fe is distributed in an irregular manner . The staurolites from different assemblages have different alumina contents and contain up to 2.25 wt% ZnO (see Thompson, Lyttle, and Thompson, 1977, Table 4. In biotite both alumina and Fe/(Fe+Mg) contents depend upon the compositions of adjacent phases. In particular, where associated with chlorite, the biotite is distinctly more iron-rich than where adjacent to staurolite and/or kyanite. In fact, these chlorite+ biotite tie lines cross staurolite+biotite tie lines for pairs from both the high- and intermediate-alumina schists. Moreover, the tie lines between coexisting chlorite and biotite, associated with anhedral staurolite, cross the tie-lines between kyanite and biotite (Fig. E-8). These phenomena may be due to retrograde reactions or a very small scale of prograde equilibration. For example, the biotite from the three phase assemblages of garnet - staurolite - biotite and staurolite - kyanite - biotite differs by 6% in Fe/(Fe+Mg) for phases within a distance of one centimeter. Thus the scale of equilibration is extremely limited, even within single microprobe samples, and different, although compatible, three-phase AFM assemblages may apparently occur on a centimeter scale.

The crossing tie lines and textural relationships between chlorite + garnet (e.g. chlorite rims) and chlorite + biotite + staurolite can be partially, but not completely, reconciled in the context of local variations in aH_2O, at constant T and P as shown by Figure E-9.

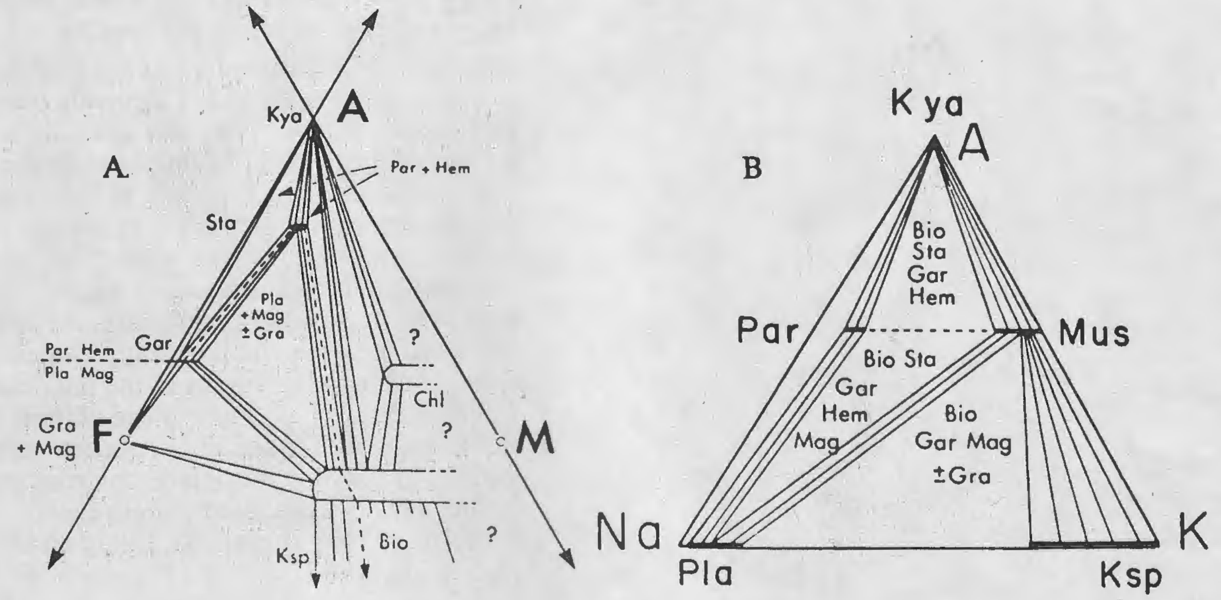
A.
Kya
A
Par + Hem
Sta
Pla
+Mag
±Gra
Par Hem
Pla Mag
Gar
?
Chl
Gra
+ Mag
F
?
M
Ksp
Bio
?
B
Kya
A
Bio
Sta
Gar
Hem
Par
Mus
Bio Sta
Gar
Hem
Mag
Bio
Gar Mag
±Gra
Na
K
Pla
Ksp

Figure E-6. (A) Schematic AFM projection of the observed facies type showing distribution of saturating phases. (B) Schematic ANaK diagram for the observed facies type. The associations of AFM and saturating ferric phases or graphite are shown. From Thompson, Lyttle and Thompson (1977).

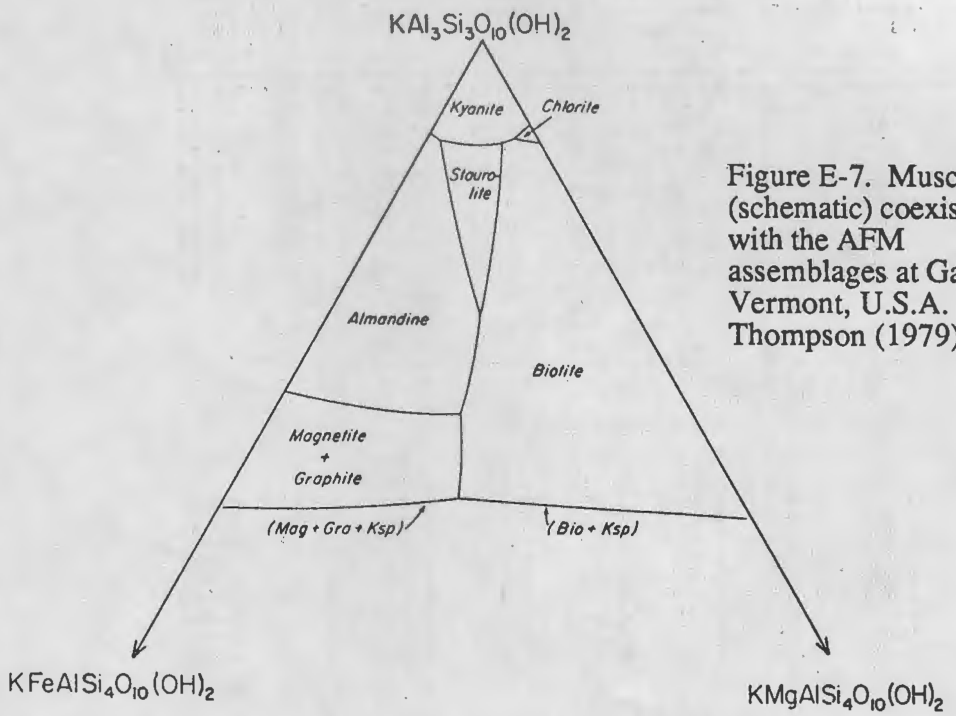
$KAl_3Si_3O_{10}(OH)_2$
Kyanite
Chlorite
Staurolite
Almandine
Biotite
Magnetite
+
Graphite
(Mag + Gra + Ksp)
(Bio + Ksp)
$KFeAlSi_4O_{10}(OH)_2$
$KMgAlSi_4O_{10}(OH)_2$

Figure E-7. Muscovites (schematic) coexisting with the AFM assemblages at Gassetts, Vermont, U.S.A. From Thompson (1979).

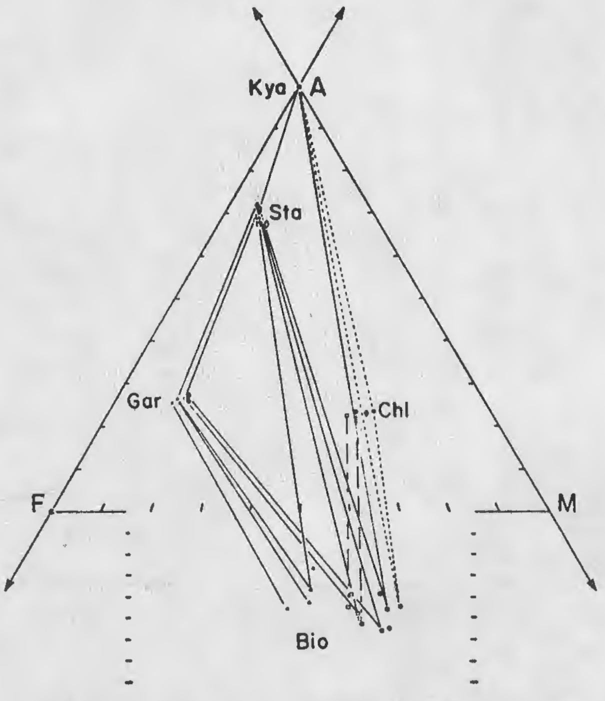

Figure E-8. AFM projection from KAl_3O_5, SiO_2, and H_2O showing gravimetric analyses (open diamonds) and microprobe analyses (other symbols) of minerals from the Gassetts Schist. The other symbols represent analyses of AFM phases coexisting with quartz and ANaK phases as follows: solid circles with muscovite-paragonite-kyanite, open squares with muscovite-paragonite only, solid triangles with muscovite-paragonite-plagioclase, crosses with muscovite-plagioclase only. Dotted lines connect compositions of the possible prograde three-phase assemblage chlorite-biotite-kyanite. Dashed lines connect compositions of possible retrograde chlorite and biotite, usually associated with irregular staurolite. From Thompson, Lyttle and Thompson (1977).

Table E-2. Gravimetric mineral analyses from Gassetts, Vermont. See Thompson, Lyttle and Thompson (1977) for sources of data. Parag Corrected = Paragonite corrected for muscovite.

	MUSC	PARAG	PARAG CORRECTED FOR MUSC	TOURM	STAR	STAR	GARNET	CHTE RIM ON GARNET
SiO2	48.30	45.18	44.51	35.63	28.73	28.22	37.63	24.99
TiO2	0.24	0.41	0.49	0.62	1.39	0.61	0.18	0.00
Al2O3	32.98	39.19	40.31	31.35	49.89	49.86	21.38	22.25
Fe2O3	2.33	0.96	0.70	0.00	4.16	4.00	0.54	3.92
FeO	0.27	0.29	0.30	7.47	10.88	11.44	32.04	16.69
MnO	0.00	0.00	0.00	0.00	0.12	0.06	0.95	0.03
MgO	0.30	0.10	0.10	7.90	2.99	2.73	4.53	19.67
CaO	0.13	0.96	1.10	0.85	0.00	0.00	2.75	0.00
Na2O	3.11	5.57	6.00	1.92	0.01	0.00	0.00	0.00
K2O	7.46	2.16	1.20	0.08	0.02	0.00	0.00	0.04
Be2O3				10.28				
P2O5				.06				
H2O -					0.22	0.90	0.17	0.52
H2O +	4.72	5.22	5.3	3.84	1.53	2.21	0.30	12.31
Total	99.85	100.06	100.0	100.0	99.94	100.03	100.48	100.26
ANHYDROUS FORMULAS								
#OX/FORMULA	11	11	11	29	23	23	12	14
Si	3.191	2.931	2.880	5.88	3.978	3.965	2.986	2.553
Ti	0.012	0.020	0.024	0.08	0.145	0.064	0.011	0.000
Al	2.568	2.996	3.074	6.10	8.141	8.256	1.999	2.679
Fe3+	0.116	0.047	0.034	0.00	0.433	0.423	0.032	0.301
Fe2+	0.015	0.016	0.016	1.03	1.260	1.344	2.126	1.426
Mn	0.000	0.000	0.000	0.00	0.014	0.007	0.064	0.003
Mg	0.030	0.010	0.010	1.94	0.617	0.572	0.536	2.995
Ca	0.009	0.067	0.076	0.15	0.000	0.000	0.234	0.000
Na	0.398	0.701	0.753	0.61	0.003	0.000	0.000	0.000
K	0.629	0.179	0.099	0.02	0.004	0.000	0.000	0.005
Be				2.19				
P				.05				
ATOM RATIOS								
Fe2/Fe2+Mg	0.333	0.636	0.615	0.347	0.671	0.701	0.799	0.323
Fe3/Fe2+Fe3	0.885	0.741	0.680	0.000	0.256	0.239	0.015	0.174
Na/Na+Ca+K	0.38	0.74	0.81					

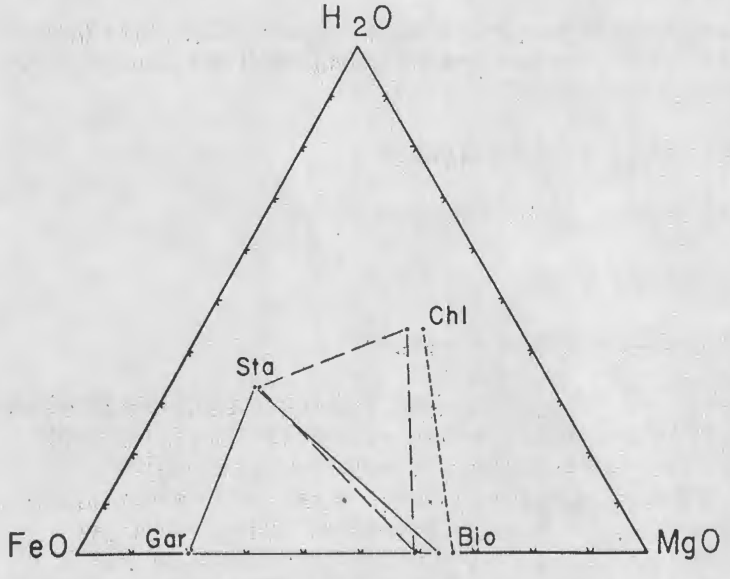

Figure E-9. Projection of the microprobe analyses of phases from the high-alumina pelite onto the plane FeO-MgO-H_2O from $H_4K_2O_3$, Al_2O_3, and SiO_2 (see also Rumble, 1974, p. 374). Solid lines connect compositions of prograde garnet-staurolite-biotite. Dotted lines connect compositions of possible prograde chlorite-biotite (with kyanite). Dashed lines connect compositions of possible retrograde chlorite-biotite-irregular staurolite. From Thompson, Lyttle and Thompson (1977).

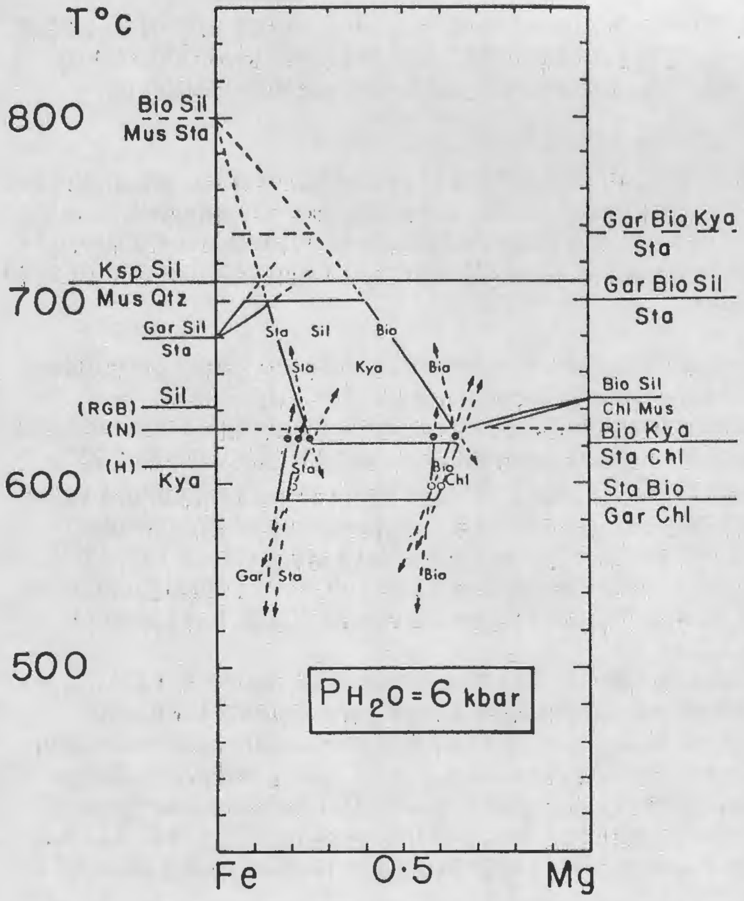

Figure E-10. Approximate T - X(Fe-Mg) projection calculated for $P_{total} = PH_2O$ = 6 kbar for some of the continuous and discontinuous reactions. Kyanite-sillimanite data are shown from the studies by Newton (1966, N), Richardson, Gilbert and Bell (1969, RGB), and Holdaway (1971, H). Solid circles show the compositions of the prograde assemblages at Gassetts, and open circles show the compositions of possible retrograde assemblages (see Figure 6). From Thompson, Lyttle and Thompson (1977).

As illustrated by Figure E-10, the assemblages garnet+ staurolite+ biotite, staurolite+ biotite+ kyanite, garnet+ staurolite+ kyanite, and chlorite+ biotite+ kyanite indicate P-T-aH_2O conditions below the (Fe-Mg) and (Na-K) discontinuous reaction(s):

Staurolite + Muscovite = Garnet + Biotite + Kyanite

Paragonite + Quartz = Muscovite + Albite + Kyanite + H_2O

respectively, and above the Fe-Mg discontinous reaction

Staurolite + Chlorite + Muscovite = Biotite + Kyanite.

Additional components or decreased aH_2O will displace these Fe-Mg reactions in a predictable manner as discussed by A.B. Thompson (1976a, 1976b). In this context a variety of commonly used geothermometric and geobarometric techniques, including a consideration of various experimental and theoretical continuous and discontinuous reactions, oxygen and carbon isotone fractionation, piezoelastic effects of quartz inclusions in garnet,and various solvi (muscovite-paragonite, ilmenite-hematite and calcite-dolomite), yield a large temperature range of 360 ° C to 740 °C and pressures of 4-6 kbar. Most of the temperature estimates fall between 535 °C and 620 °C at 6kbar which agrees well with peak P-T estimates of 600 ± 20 °C (garnet - biotite geothermometrically) and 6 ± 1kbar (plagioclase - garnet - kyanite - quartz geobarometrically) reported in the Cavendish area (Star Hill-Hawks Mountain) for similar high alumina schists by Downie (1980, 1982).

Compositional Zoning and Mineral Inclusions in Garnet

A more complete story of the metamorphism of the Gassetts Schist, particularly of its earlier stages, was worked out by a detailed study of the zoned garnets and their included minerals by Thompson, Tracy, Lyttle, and Thompson (1977) from which the following information is abstracted.

Introduction. Petrographic examination of the solid inclusions in garnet showed the presence of at least two white micas, staurolite, chloritoid, chlorite, epidote, hematite, ilmenite, magnetite, rutile, and quartz. No biotite inclusions were observed, and possible kyanite inclusions were observed only at the extreme rim of the garnet. Subsequent analyses of successive garnet zones and of solid inclusions revealed a systematic distribution.

Compositional zoning of the garnet. Detailed microprobe traverses across the garnet permitted contouring of the two-dimensional section in cation percentage of Ca, Mn, Mg, and Fe. Gravimetric analysis of a garnet from another sample of Gassetts Schist (by Jun Ito) indicates less than 1.6 mol percent $Ca_3Fe_2^{3+}Si_3O_{12}$ as the only ferric component (see J.B. Thompson, 1957, p. 854; Thompson, Lyttle, and Thompson, 1977, Table 1). This is likely to be a maximum value because of abundant ilmenohematite inclusions (Figure E-11A). Representative microprobe analyses (corresponding to the section along profile C-D in Figure E-12 are given in Table E-3. As can be seen from these analyses, the garnet contains negligible Ti and all iron is considered to be ferrous. The atom percent contours of Ca, Mn, Mg, and Fe are shown in Figure E-11 A to D.

The complex distribution of calcium, manganese, and iron contours in Figure E-11 A, C, and D clearly illustrates the inadequacy of ***single radial profiles*** across garnet grains for use in deducing compositional histories. The pronounced maxima and minima in cation concentration show an internal structure that may reflect mineralogical differences in initial bedding subsequently rotated during porphyroblast growth. Rosenfeld (1970, sec. 5, p. 25-50) illustrates examples of the deformation of bedding surfaces in rotated garnets. Some of our contours (Figure E-11, A to D) are consistent with the case where the rotation axis is approximately parallel to the plane of the

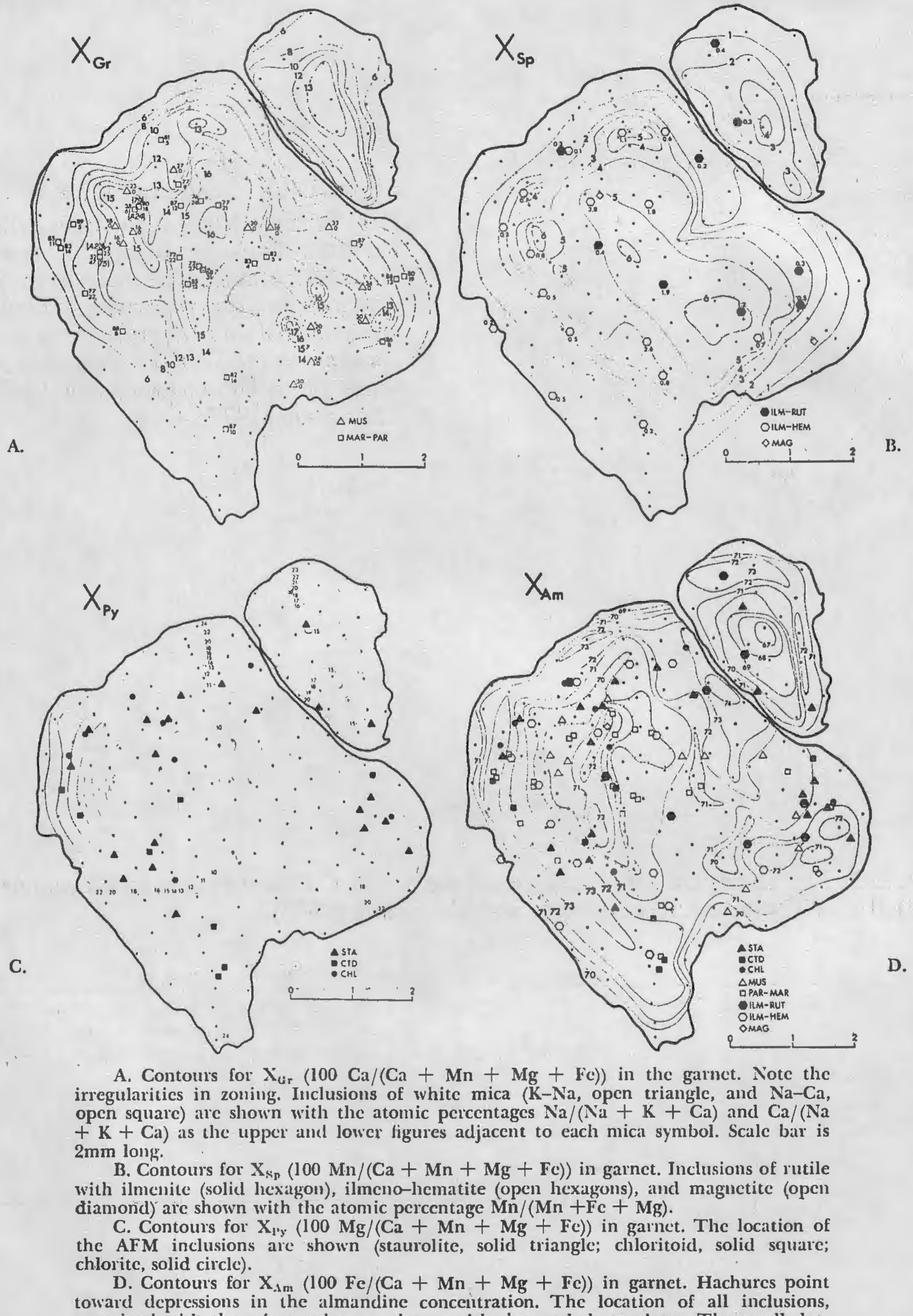

A. Contours for X_{Gr} (100 Ca/(Ca + Mn + Mg + Fe)) in the garnet. Note the irregularities in zoning. Inclusions of white mica (K–Na, open triangle, and Na–Ca, open square) are shown with the atomic percentages Na/(Na + K + Ca) and Ca/(Na + K + Ca) as the upper and lower figures adjacent to each mica symbol. Scale bar is 2mm long.

B. Contours for X_{Sp} (100 Mn/(Ca + Mn + Mg + Fe)) in garnet. Inclusions of rutile with ilmenite (solid hexagon), ilmeno–hematite (open hexagons), and magnetite (open diamond) are shown with the atomic percentage Mn/(Mn +Fe + Mg).

C. Contours for X_{Py} (100 Mg/(Ca + Mn + Mg + Fe)) in garnet. The location of the AFM inclusions are shown (staurolite, solid triangle; chloritoid, solid square; chlorite, solid circle).

D. Contours for X_{Am} (100 Fe/(Ca + Mn + Mg + Fe)) in garnet. Hachures point toward depressions in the almandine concentration. The location of all inclusions, examined with the microprobe, are shown with the symbols as above. The small dots show the locations of the garnet analyses.

Figure E-11. Compositional contours and location of mineral inclusions in Garnet. From Thompson, Tracy, Lyttle, and Thompson (1977).

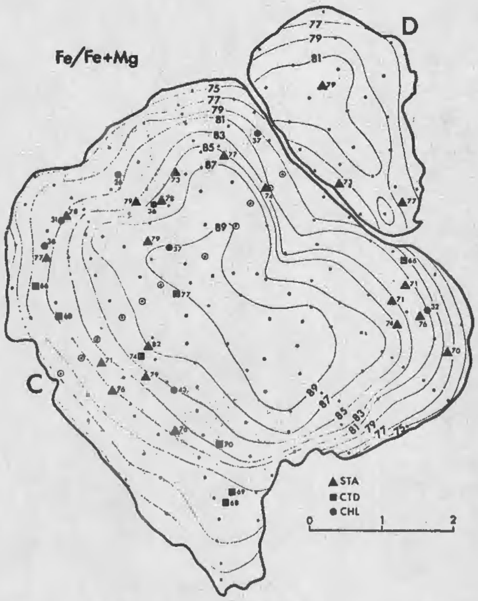

Figure E-12. Contours for X_{Fe} = [100 Fe/(Fe + Mg)] in garnet, together with the same atomic percentage for staurolite, chloritoid, and chlorite inclusions. The spot locations corresponding to the garnet analyses in Table 1 are shown by circled spots along profile C-D. Scale bar is 2 mm long. From Thompson, Tracy, Lyttle and Thompson (1977).

Table E-3. Representative garnet analyses along profile C-D (see circled spot locations in Figure E-12). From Thompson, Tracy, Lyttle and Thompson (1977).

	G-60	G-59	G-58	G-57	G-56	G-55	G-14	G-45	G-46	G-47	G-48
SiO_2	35.70	36.39	36.54	37.02	37.79	37.46	35.85	37.10	37.89	38.08	37.65
TiO_2	0.04	0.09	0.08	0.07	0.08	0.10	0.06	0.08	0.06	0.02	0.08
Al_2O_3	21.38	20.99	20.72	20.43	20.30	20.44	20.62	20.45	20.43	20.84	20.65
Cr_2O_3	0.02	0.02	0	0	0.04	0.12	0.05	0	0.04	0.03	0
FeO	33.94	33.53	32.74	32.24	32.40	33.29	32.13	33.31	32.76	33.34	34.74
MnO	0.39	0.66	0.94	2.36	1.83	2.07	2.53	2.05	1.86	0.91	0.82
MgO	5.46	4.69	3.60	2.89	2.43	2.47	2.03	2.31	2.54	4.25	4.78
CaO	2.17	3.22	4.80	5.05	5.65	5.32	6.15	5.56	5.49	3.91	2.10
Total	99.08	99.59	99.42	100.06	100.52	101.27	99.42	100.86	101.07	101.38	100.82
Mol% Am	72.5	71 8	70.8	69.7	70.7	71.4	69.6	71.4	70.9	71.2	74.2
Mol% Py	20.8	17.9	13.9	11.1	9.4	9.5	7.8	8.8	9.8	16.2	18.2
Mol% Gr	5.9	8 9	13.3	14.0	15.8	14.6	17.1	15.3	15.2	10.7	5.8
Mol% Sp	0.8	1 4	2.0	5.2	4.1	4.5	5.5	4.5	4.1	1.9	1.8

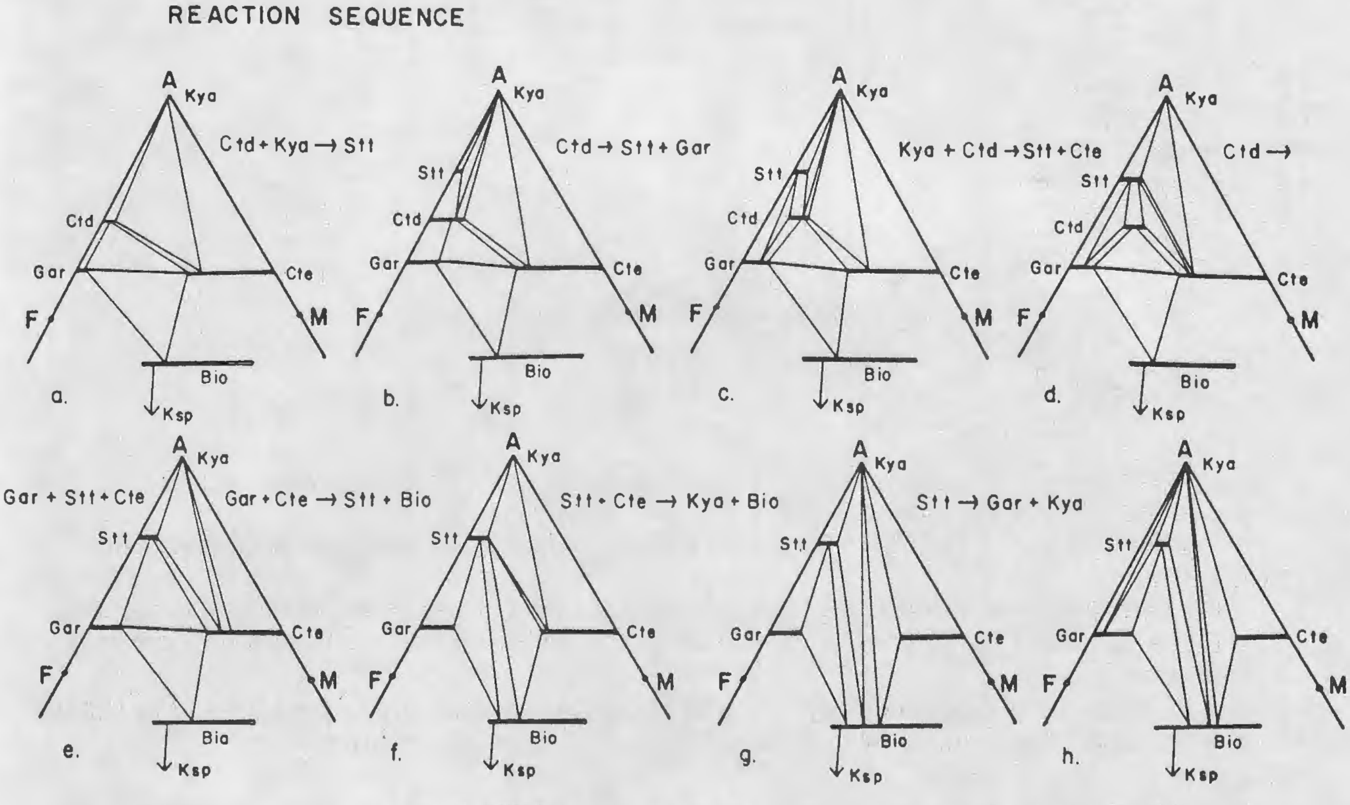
REACTION SEQUENCE
a. A Kyа Ctd + Kya → Stt Ctd Gar Cte F M Bio Ksp
b. A Kya Ctd → Stt + Gar Stt Ctd Gar Cte F M Bio Ksp
c. A Kya Kya + Ctd → Stt + Cte Stt Ctd Gar Cte F M Bio Ksp
d. A Kya Ctd → Stt Ctd Gar Cte F M Bio Ksp
e. A Kya Gar + Stt + Cte Gar + Cte → Stt + Bio Stt Gar Cte F M Bio Ksp
f. A Kya Stt + Cte → Kya + Bio Stt Gar Cte F M Bio Ksp
g. A Kya Stt → Gar + Kya Stt Gar Cte F M Bio Ksp
h. A Kya Stt Gar Cte F M Bio Ksp

Figure E-13. (a-h) Generalized AFM facies series representing progressive metamorphism of pelitic rocks in the Cavendish area. Two-phase tie lines have been omitted for simplicity. Discontinuous reactions (quartz, muscovite, and H_2O assumed present) describing the change from one facies type to the next are given. Either facies type g or h represents the maximum grade attained (see text for further discussion). From Downie (1982).

section. Garnets from the Gassetts Schist (Thompson, 1979) and other units nearby (Rosenfeld, 1968, fig. 14-5) have inclusion spirals showing strong rotation during growth.

Mineral inclusions within the garnet. The nature and composition of the solid inclusions bear a systematic relationship to local garnet composition. The locations and compositional ratios of various types of inclusions have been shown relative to appropriate cation contours of the host garnet in Figure E-11 A to D.

Fe-Mg reactions involving garnet growth and resorption. As noted above, the macrocrystalline phases define an AFM facies-type characterized by garnet - staurolite - biotite - kyanite (and possible primary chlorite) all with quartz. Local associations of staurolite - garnet - biotite, staurolite - biotite - kyanite, staurolite - garnet - kyanite, and possibly chlorite - biotite - kyanite are observed. The ANaK facies-type at this grade is characterized by muscovite - paragonite - kyanite, muscovite- paragonite - plagioclase, and muscovite - plagioclase - potassic feldspar.

The presence of chloritoid, margarite, and rutile only as inclusions in the garnet implies that progressive reactions have eliminated these phases from the present "equilibrium" assemblage. The location and compositions of the inclusions relative to adjacent garnet composition and overall garnet zonation may be used to determine the successive continuous and discontinuous reactions

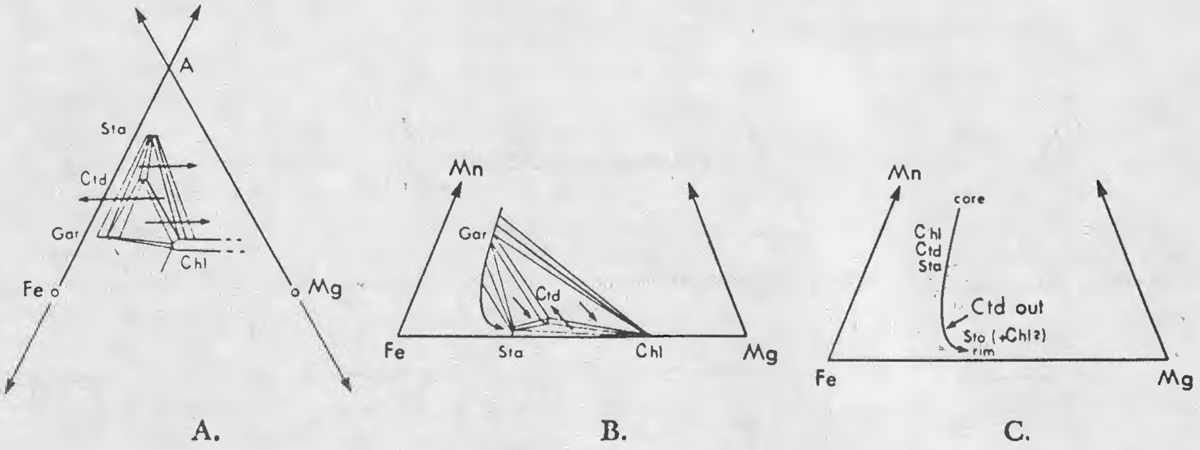

Figure E-14. Possible configuration for the disappearance of chloritoid from the inclusion assemblage. From Thompson, Tracy, Lyttle and Thompson (1977).

A. Phase relations in AFM, where arrows show predicted displacements with increasing temperature.

B. Phase relations in Mn-Fe-Mg show the displacement of Mn-Fe-Mg continuous reactions, where X_{Mn} Gar > Ctd > Sta > Chl. The arrows show predicted displacements with increasing temperature.

C. General trend of garnet composition from core to rim, exaggerated for clarity. The change in trend apparently coincides with the disappearance of chloritoid inclusions.

undergone by the sample during the regional metamorphism (see also Tracy et al., 1976).

A progressive series of AFM facies types has been deduced from the relative locations and compositions of chlorite, chloritoid, and staurolite inclusion within the garnet (see Figure E-13). The occurrence of chlorite ($X_{Fe} = .37$) and chloritoid ($X_{Fe} = .77$) near the core of the garnet ($X_{Fe} = .90$) suggests the presence of the three-phase assemblage garnet-chlorite-chloritoid at lower grades. Other possible three-phase assemblages at this grade are also shown in Figure E-13. It is possible that the lowest grade facies type recorded by the inclusions is not that of Figure E-13a but that shown in Figure E-13b, where the staurolite may have been part of the adjacent macrocrystalline assemblages but could not coexist with garnet because of possible chloritoid solution to pure Fe-chloritoid.

Implications of reaction history. The so-called "staurolite - in" reaction, separating topologies e and f of Figure E-13:

Garnet + Chlorite = Staurolite + Biotite

resorbs garnet and, if followed by an increase in metamorphic grade, could produce "garnet unconformities" like those described by Rosenfeld (1968). However, depending upon the amount of resorption and the effective volume of equilibration of the garnet, this resorption may be difficult to recognize due to continued garnet growth with increase of metamorphic grade (see Figure 6 of Thompson, Tracy, Lyttle, and Thompson, 1977).

The garnet and its inclusions of chloritoid and staurolite contain measurable amounts of MnO. Manganese stabilizes the four-phase assemblage garnet - chloritoid - staurolite - chlorite to P - T - aH_2O conditions above the AFM reaction:

Chloritoid = Garnet + Staurolite + Chlorite.

With the addition of MnO, this Fe - Mg discontinuous reaction becomes a continuous AFM-Mn reaction that can eliminate chloritoid from the matrix, as illustrated in Figure E-14.

Finally, several of the remarkable insights into the reaction history of high-alumina pelites gleaned from the detailed study of one garnet from the Gassetts Schist have subsequently been confirmed by workers in nearby areas. Downie (1982), employing similar methods applied to several samples, has deduced virtually the same reaction sequence for both the Gassetts Schist and Pinney Hollow Formation at the north end of the Chester dome. Cheney (1980, 1986) has also documented a comparable reaction sequence in a continuous belt of high-alumina, Gassetts-like, schists from the Hoosac Formation of Western Massachusetts, that range from garnet zone through kyanite-biotite zone. In addition, Karabinos' (1985) detailed work on the chloritoid to staurolite zone transition in Gassetts-like pelites near Jamaica, Vermont has confirmed and expanded upon the AFM-Mn reaction for the elimination of chloritoid (see Figure E-14c) as a matrix phase. However, the significance of the textural unconformities observed in garnets from locations throughout southeastern Vermont remains problematic and much debated. There seem to be three viable, popular, explanations for multiple garnet growth in these rocks: 1) growth of garnet during two separate prograde metamorphic events, as originally postulated by Rosenfeld (1968), 2) prograde Acadian consumption of garnet by the "staurolite-in" reaction followed by additional garnet growth with increasing metamorphic grade, and 3) cooling prior to thermal relaxation associated with nappe emplacement in the Devonian.

Continue sout on Route 103 to Village of Chester, passing several exposures of Grenvillian gneiss on left.

80.2 Junction of Routes 103 and 11. Turn right (west) on Route 11.

82.1 Turn right (northwest) on road leading to Chester Reservoir.

82.3 Private road to Vermont Mineral Products Quarry. The vans will turn around at this point. Please note the no trespassing signs. There are several very large, "mean" dogs that patrol the property. As prearranged the dogs will be "tied-up" and we will walk, via the private drive past the north side of the house to the northeast end of the Quarry.

STOP 6. THE CHESTER SOAPSTONE QUARRY

(40 minutes)

(The Vermont Mineral Products Quarry is currently owned by Mr. Martin and Mrs. Reyder who have graciously granted us special permission to visit the quarry.)

The ultramafic body exposed here occurs in the Cambrian Ottauquechee Formation in the outer mantle of the Chester Dome. This stop provides an opportunity to examine and collect material from one of the classic blackwall sequences described in the pioneering work of Hess (1933) and Phillips and Hess (1936) on the formation of serpentinite and the origin of the blackwalls. The metasomatic reaction zone at this quarry at the original boundary between serpentinite and country rock is also the source of four new biopyriboles recently described by Veblen (1976), Veblen and Burnham (1975), Veblen, Buseck, and Burnham (1977), Veblen and Burnham (1978) Veblen, Buseck and Burnham (1978a, 1978b).

Walk to the northeast end of the quarry to the only remaining outcrop of serpentinite. Proceed around the eastern rim of the pond, passing on the west side of the house, to an exposure of the blackwall, south of the pond outlet stream. Finally continue east to the dump where fun should be had by all.

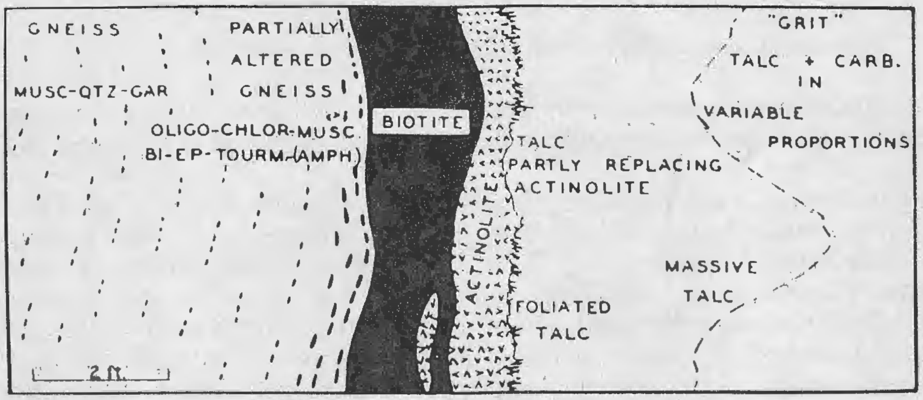

Figure E-15. Field sketch of mineral zoning at the Vermont Mineral Products Co. quarry, near Chester, Vermont. From Phillips and Hess (1936).

Geologic Setting of New England Ultramafic Bodies

The Chester ultramafic bodies occur in a belt of alpine peridotites extending, along the axis of the Appalachian orogenic belt, from Alabama to Newfoundland. As described by Sanford (1982), the ultramafic bodies occur in virtually all pre-Silurian units, including remobilized Precambrian gneisses. Accordingly, they are generally considered to have been emplaced in the Ordovician. In order of decreasing abundance, the host rocks include: greenschist, amphibolite, pelites, metasandstones, quartzite, and marble. The ultramafic rocks of New England and Quebec were likely emplaced in the solid state at low temperature into, at best, weakly metamorphosed sediments near the onset of the Taconian orogeny. Their emplacement is probably related to the obduction of a young ophiolite sequence onto the North American margin.

Although the timing of serpentinization is much debated, most bodies in the lowest grade sediments are highly serpentinized. Hence serpentinization clearly preceded the formation of the metasomatic reaction zones, which developed during the Acadian orogeny.

Metasomatic Reaction Zones

As described by Hess (1933), "practically the whole mass of the ultrabasic has been altered to talc and carbonate, leaving only occasional serpentine relics." A sheath of biotite schist or biotite actinolite schist from several inches to a few feet thick completely surrounds the deposit. This sheath represents approximately the original contact of the ultrabasic rock with the country rock." Hess added in a footnote that the biotite rock at the original interface with the country rock is called "blackwall" as are the chlorite rocks which surround the normal (lower temperature) type of talc deposits. Although not well exposed at the time, Phillips and Hess managed to describe quite accurately the reaction zone as shown in their Figure 5 (Figure E-15) and now observable on the south side of the pond, beyond the outlet. Their more detailed description implies that locally, at least within a "horse" of altered country rock, no longer present, within the soapstone, a zone of chlorite separates a tourmaline-rich biotite rock and the actinolite (compare to Figure E-15). This chlorite zone is probably the source of the magnetite- (up to 1.5 cm) and pyrite- (up to 3 cm) chlorite rocks common in many museums. With luck, samples representative of the various reaction zones can be obtained from the dump south of the house. However, samples of the pyrite- and magnetite-bearing chlorite rocks have long been scarce and seem to have come from the dump now serving as a foundation for the house.

The metasomatic nature of the reaction zones was surmised by Phillips and Hess (1936), who attributed their formation to the mass transfer primarily of silica into the ultramafic and magnesia and iron into the country rock. They also noted the apparent gain of alumina and water by the "blackwall". More recently, Brady (1977) has argued on a theoretical basis that the reaction zones are produced by diffusion-imposed chemical potential gradients of several components, principally silica and magnesia, and that the number varies from zone to zone. He also concluded that the talc+magnesite zone forms in response to a diffusion-imposed gradient in the chemical potential of CO_2 and that the original host-serpentinite contact is most likley near the interface between the biotite (or chlorite, if present) and actinolite zones (compare with Fig. E-15). These conclusions have been largely substantiated, and quantified, by Sanford's (1982) detailed microprobe/field study of four other quarries in Vermont and Massachusetts. In addition Sanford provided an exceedingly detailed description of textural and mineral compositional variations in typical reaction zones as a function of metamorphic grade.

Triple-Chain Silicates

Although David Veblen (personal communication, June, 27,1986) claims to have lugged all appropriate material back to Harvard's Peabody Museum, it may be possible to obtain samples of material containing the four Mg-Fe chain silicates first identified by Veblen and Burnham (1975,1978, and references above) in samples from the south (and only remaining) dump. These new biopyriboles occur with anthophyllite, talc and cummingtonite, between the chlorite and actinolite zones. The new minerals include the triple chain silicates (b=27Å) jimthompsonite (orthorhombic, space group *Pbca*) and clinojimthompsonite (*C2/c*) and, chesterite, the orthorhombic mineral (space group $A2_1ma$) containing mixed double and triple chains. An unnamed monoclinic mineral (space group *A2/m*, *Am*, or *A2*) is presumed to be the analog of chesterite. However, the occurrence of this mineral as very fine grained intergrowths in chesterite has precluded its confirmation. The new minerals are chemically and structurally intermediate between talc and anthophyllite. The ideal composition for jimthompsonite and clinojimthompsonite is $(Mg,Fe)_{10}\,Si_{12}O_{32}(OH)_4$, and that of chesterite is $(Mg,Fe)_{17}Si_{20}O_{54}(OH)_6$. Although the physical and optical properties of these minerals are close to those of the Fe-Mg amphiboles, the cleavage angles (37.8° and 44.8°) are distinctive. Because these minerals commonly occur in (010) intergrowths, crystals with b near the plane of the section have a spectacular appearance under crossed polars (see the color photograph on the Oct, 28, 1977 cover of Science).

In detail, all of the material used by Veblen and co-workers is from a single block of blackwall found on the quarry dump. Similar material may have been reported in place on the northern wall of the quarry. The generalized zoning sequence is chlorite / fibrous talc / jimthompsonite + clinojimthompsonite + chesterite + the unnamed mineral + anthophyllite + cummingtonite / anthophyllite + cummingtonite + chesterite + the unnamed mineral + actinolite / actinolite + massive talc. Because anthophyllite has been extensively replaced by fibrous talc plus all four of the new minerals, they are considered part of a retrograde reaction sequence from anthophyllite to talc.

Retrace route to Chester..country roads, take me home...

84.4 Junction of Routes 103 and 11 in Chester. Proceed southeast on Route 103.

87.3 Low glacially smoothed outcrops on the right (south) are spectacular K-feldspar augen gneisses of the Bull Hill Formation. This unit occurs between the albite schists of the Hoosac Formation in the outer mantle sequence and the "Gassetts" schist in the inner mantle sequence very nearly all the way around the Chester dome. Much debate is whether the Bull Hill is a metamorphosed rapakivi granite or a metamorphosed volcanic.

90.8 Pass turn off to Brockways mills.

94.2 Pass under Interstate 91.

94.4 Highlander Motel on left will be our home away from home tonight.

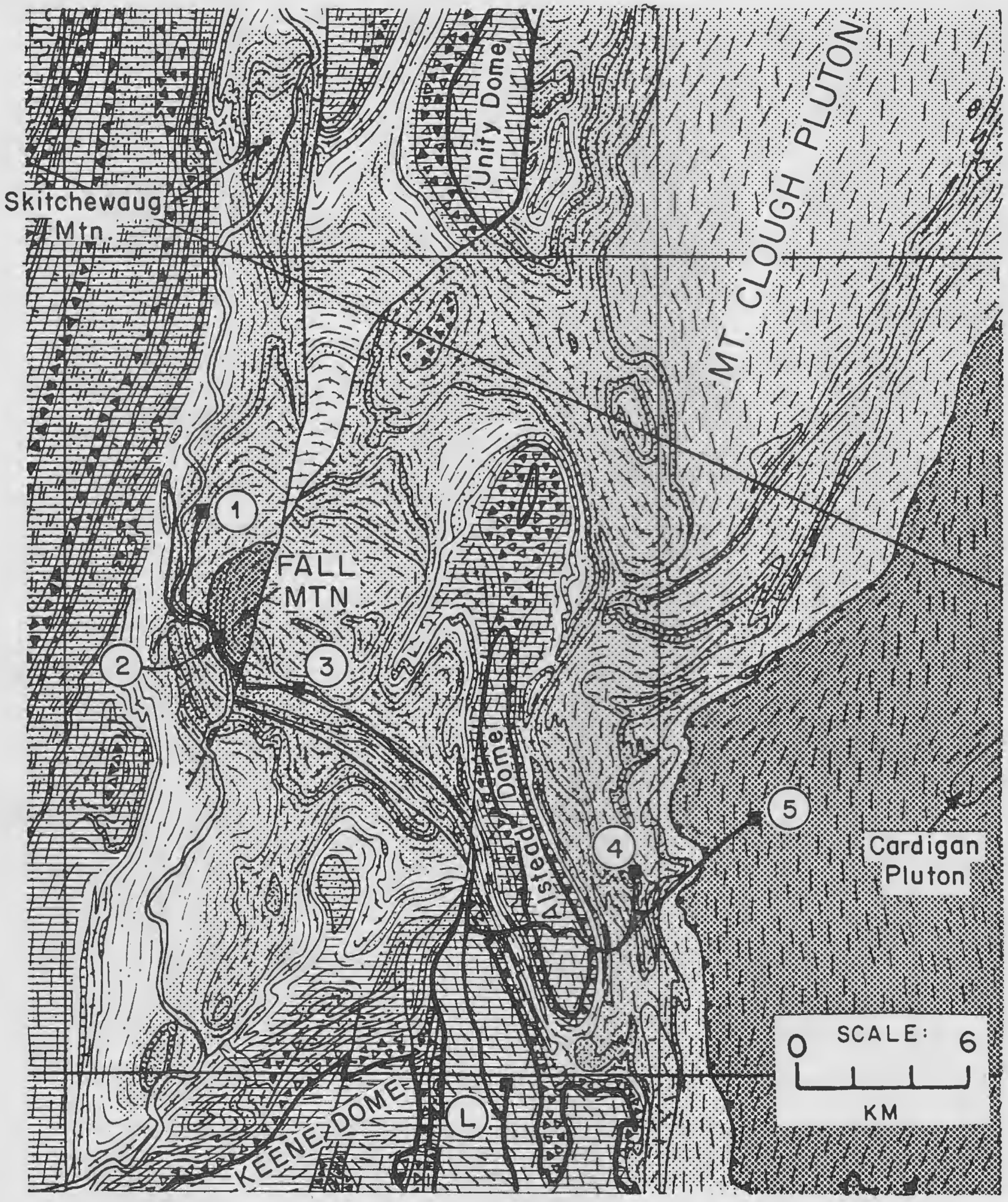
Skitchewaug Mtn.
Unity Dome
MT. CLOUGH PLUTON
1
FALL MTN
2
3
Alstead Dome
4
5
Cardigan Pluton
SCALE: 0 6 KM
KEENE DOME
L

Fig. F-1. Generalized geologic map of the field trip area, part F, showing route and stops (from Peter Robinson, J.B. Thompson, Jr., and others, in preparation). Shading indicates structural levels from lowest to highest as follows: Fine horizontal lines – low structural levels including Cornish nappe and autochthonous rocks near domes; unshaded – lowest recumbent fold, the Bernardston nappe; light shading – higher recumbent fold, the Skitchewaug nappe including the Bellows Falls and Mt. Clough plutons of Bethlehem Gneiss; dark shading, Fall Mountain thrust nappe.

F. METAMORPHIC AND TECTONIC EVOLUTION OF THE FALL MOUNTAIN NAPPE COMPLEX AND ADJACENT MERRIMACK SYNCLINORIUM

Frank S. Spear and C. Page Chamberlain

INTRODUCTION: OBJECTIVES FOR THE MORNING

The existence of an isolated area of high-grade metamorphic schists on Fall Mountain, New Hampshire was noted by Kruger (1946). Thompson et al. (1968) described the occurrence as a "metamorphic overhang" because high-grade sillimanite + K-feldspar bearing rocks on Fall Mountain, N.H. were observed to overlie structurally lower grade rocks. This led Thompson et al. (1968) to propose the existence of the Fall Mountain nappe, which was interpreted to have carried hot rocks of the Merrimack synclinorium westward over the Bronson Hill anticlinorium to their present position on Fall Mountain. Subsequent mapping around Fall Mountain (Thompson and Rosenfeld, 1979; Allen, 1984, 1985) and in the root zone in the Merrimack synclinorium (Chamberlain, 1984; P. J. Thompson, 1984, 1985) has confirmed the existence of the Fall Mountain nappe based on stratigraphic and structural considerations.

Metamorphic studies of the Fall Mountain nappe in both the root zone and the structural outlier at Fall Mountain indicate that metamorphism in this area is the result of a complex interplay among pre-orogenic thermal setting, thermal perturbation owing to tectonic transport (thrusting and folding) and subsequent thermal relaxation. As a result, metamorphic grade and P-T histories vary in both space and time and are strongly dependent on structural level. Preliminary results on the metamorphism of the upper and lower plates of the Fall Mountain nappe outlier (Spear et al., 1983; Spear, 1986) have documented the dramatically different P-T paths of the different structural levels. Metamorphic studies in the root zone (Chamberlain, 1985, 1986a) have documented the similarity in early metamorphic history between rocks of the root zone and the upper plate of the Fall Mountain nappe, as well as a correlation between late-stage cross folding and metamorphism.

The purpose of this report is to describe the metamorphic evolution of rocks along a west-east traverse across the Bronson Hill anticlinorium into the Merrimack synclinorium, from Bellows Falls, Vermont, to Marlow, New Hampshire (Figure F-1). The main focus of this excursion will be to examine the constraints that the metamorphic petrology places on the tectonic evolution of the terrane.

GENERAL GEOLOGIC SETTING

Stratigraphy

The Bronson Hill anticlinorium (BHA) and Merrimack synclinorium (MS) consist of a thick sequence of Ordovician, Silurian and Devonian clastic and carbonate metasediments. The stratigraphies of these two structural terranes are, however, somewhat different. Rocks in the Bronson Hill anticlinorium, for example, consist of Ordovician granitoid gneisses overlain by Ordovician volcanics (Ammonoosuc) and rusty, sulfidic schists (Partridge). These are, in turn, overlain by a Silurian conglomerate (Clough), and calc-silicate (Fitch) sequence, and Devonian, cyclically bedded schists (Littleton).

The occurrence of a thick sequence (greater than 2 km) of Silurian clastic sediments (Rangeley), not observed in the BHA, in the Merrimack synclinorium is consistent with the idea of an eastward thickening basin in Silurian times (Boone et al., 1970). According to this hypothesis, there was a "tectonic hinge" between a shallow-water shelf or island arc (BHA) and a deep water basin (MS) during the Silurian. Thus, the thin Silurian sediments, present in the anticlinorium, thicken into coeval deep water sediments in the synclinorium. This hypothesis is supported by stratigraphic observations in higher structural levels present in the Bronson Hill anticlinorium (Chamberlain, 1985; J.B. Thompson, personal communication). J.B. Thompson and Chamberlain were able to map metasedimentary units that appear to be shelf-basin transitional facies equivalent to the Clough (shelf) Quartzite and Rangeley (basin) Formation (Figure F-2).

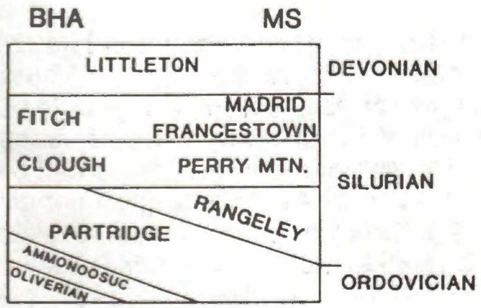

Figure F-2. Stratigraphic column for the Bronson Hill anticlinorium (BHA) and Merrimack synclinorium (MS).

Westward transport of nappes during the Acadian Orogeny brought more basin-like sediments over the shelf sediments of the Bronson Hill anticlinorium. Because of this thrusting, higher structural levels in the anticlinorium have stratigraphic sequences more similar to the stratigraphy observed to the east in the Merrimack synclinorium. For example, the two nappes discussed in this study (the Fall Mountain and Skitchewaug nappes) show many stratigraphic similarities to rocks in the synclinorium. The lower limb of the Skitchewaug nappe exposed at Bellows Falls, VT contains gray schists (Silurian ?) below the Silurian Clough conglomerates and above the Ordovician Partridge schists. These gray schists thicken to the east, and in the upright limb of this nappe exposed near Gilsum, NH there are thicker sequences of gray schists between the Clough conglomerates and Ordovician metasediments (Partridge). The next highest structural level exposed in these regions, the Fall Mountain nappe, contains massive pelites (Rangeley) more similar to rocks present in the Merrimack Synclinorium. These stratigraphic complexities are the result of westward thrusting of an original east-thickening stratigraphic sequence.

Structural Geology

The structural history of this region is complex and involves several stages of deformation. The earliest period of deformation recognized was a period of nappe and thrust development. Napping was followed by gneiss dome formation and related folding about north-south axes (Thompson et al., 1968; Chamberlain, 1985). The latest period of folding recognized produced open folds with east-west trending axes.

Structural features resulting from all three phases of deformation can be observed both in the outlier and root zone of the Fall Mountain nappe. In the Bellows Falls area there are two large nappe structures exposed. The lower plate belongs to the overturned limb of the Skitchewaug nappe, and the upper plate is part of the Fall Mountain nappe. In this area, the nappes have been refolded about north-south axes (dome-stage folds ?) and later folds with east-west trending axes. Many small folds related to dome-stage folding are present in the outcrops exposed around Bellow Falls, VT. The late-stage open folds in this region are recognized both on gross outcrop pattern and by structural analysis (Allen, 1984, 1985). Allen (1984, 1985) has shown that the Fall Mountain outlier is folded into a major syncline associated with the latest Acadian folding.

East of the gneiss domes, in the root zone of the Fall Mountain nappe, similar deformation features are present. Here, however, the post-nappe deformation was much more intense, and significantly affected the thermal history of this region. In this region, the upper limb of the Skitchewaug nappe is overlain by rocks belonging to the Fall Mountain nappe. Nappe deformation in this region produced the dominant foliation observed. Later folding about north-south axes produced a spaced crenulation cleavage and abundant minor folds. The latest period of folding was about east-west trending axes, and produced no recognizable minor structural features (Chamberlain, 1985). However, the late Acadian folds are large; one synclinal axis can be traced from the Fall mountain outlier at Bellows Falls VT east into the root zone of the Fall Mountain nappe (Chamberlain, 1985).

Plutonic Rocks

The intrusive rocks that crop out in this region belong to the Acadian New Hampshire Plutonic Series (Thompson et al., 1968). Three representations of the New Hampshire Plutonic Series (Kinsman, Bethlehem, and Concord) are present in this region.

The Kinsman and Bethlehem members of the series are early (400 myr.; Lyons and Livingston, 1977), syntectonic intrusives. These rocks are slightly foliated and folded, and are thought to have been intruded along the base of the nappes during emplacement (Thompson et al., 1968; Chamberlain, 1985; P. J.Thompson, 1985). These plutons are sheet-like bodies, no greater than 2.5 km thick, and may have once covered much of southern New Hampshire (Nielson et al., 1976). They range in composition from granite to tonalite and may represent lower crustal partial melts (Clark and Lyons, 1984). There is petrologic evidence in the Merrimack synclinorium suggesting that the Kinsman plutons have been metamorphosed (Thompson et al., 1968; Chamberlain and Lyons, 1983). Good exposures of Bethlehem pluton are exposed at the base of the Fall Mountain outlier in Bellows Falls VT and in the root zone near Marlow NH.

The Concord suite is considerably younger than the other members, with an age ranging from 380 to 275 myr. (Lyons et al., 1982; J.B. Lyons personal communication). The Concord plutons typically consist of two-mica granites and appear to be post-tectonic. These granites are more abundant in the Merrimack synclinorium. It has been suggested, based on thermal history calculations, that they represent partial melts generated during thermal relaxation well after Acadian tectonic thickening (Chamberlain and England, 1985).

METAMORPHISM

General

The metamorphic grade in the area ranges from chlorite grade along the so-called "Chicken Yard line", which separates the New Hampshire stratigraphic sequence from the Vermont stratigraphic sequence, to garnet-cordierite grade in the Merrimack synclinorium. The distribution of peak metamorphic isograds is shown in Figure F-3, where the general increase in metamorphic grade from west to east can readily be seen. Also apparent in Figure F-3, in the vicinity of Bellows Falls, Vermont, is the "metamorphic overhang" (Thompson et al., 1968) where high-grade sillimanite ± K-feldspar rocks of Merrimack synclinorium affinities lie structurally above garnet and staurolite-kyanite grade rocks.

Many of the significant features of the metamorphism in the area are not readily apparent from the isograd map, however. Peak metamorphic conditions across the area were not synchronous, but rather were controlled by a complex interplay of pre-deformational thermal setting, tectonic

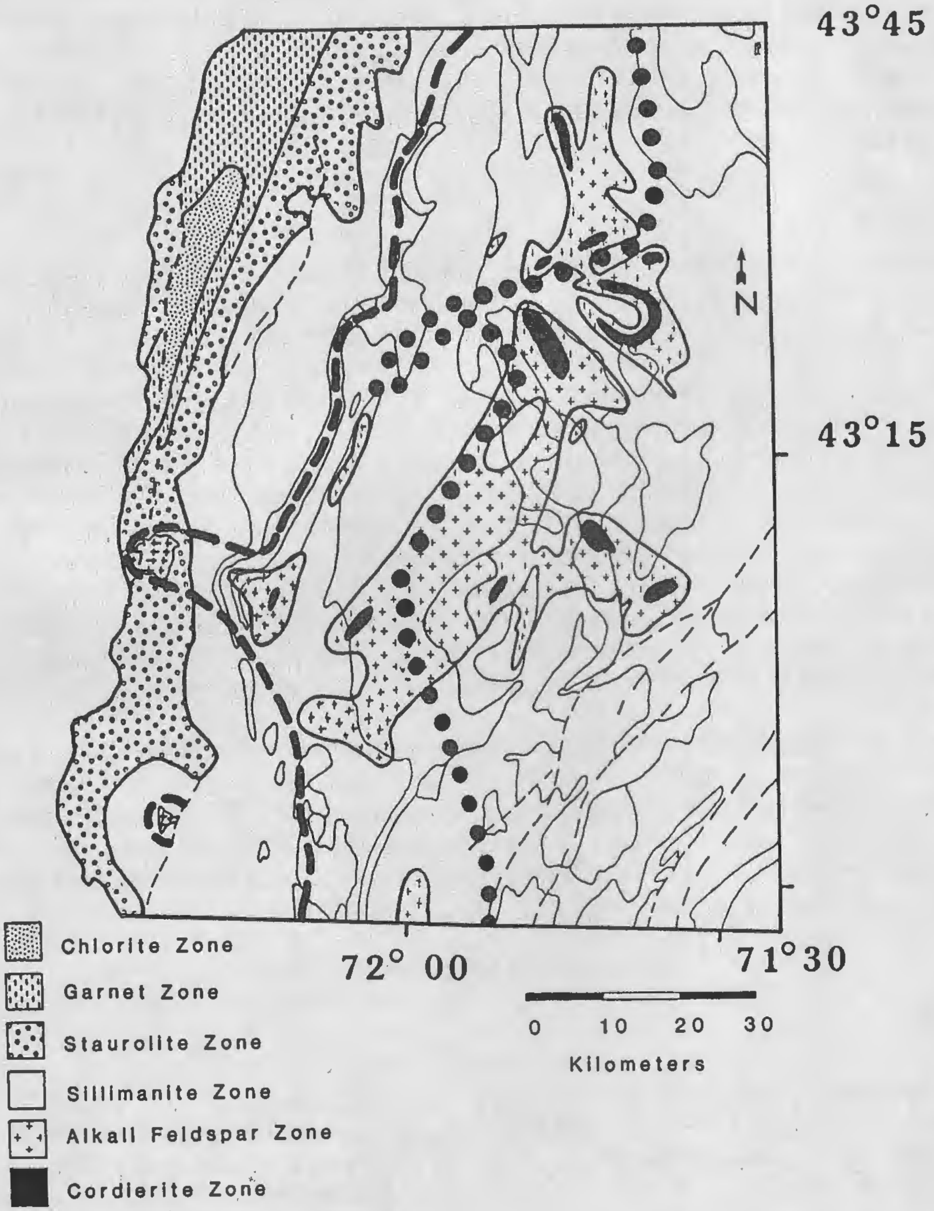
43°45
43°15
N
72° 00
71°30
0 10 20 30
Kilometers
Chlorite Zone
Garnet Zone
Staurolite Zone
Sillimanite Zone
Alkali Feldspar Zone
Cordierite Zone

Fig. F-3. Metamorphic map for southern New Hampshire. Heavy dotted line is present western limit of preserved andalusite partially converted to sillimanite. Heavy dashed line is western limit of andalusite pseudomorphs, most commonly replaced by sillimanite, but locally by other assemblages (see text). Data in southernmost areas is from P.J. Thompson (1985), and D.C. Elbert and P. Robinson, personal communication (1986).

juxtaposition of thermally distinct terranes and thermal relaxation of tectonically perturbed thermal regimes. Peak metamorphic conditions in the upper plate of the Fall Mountain nappe were reached early, prior to nappe emplacement, whereas peak conditions in the lower plate were reached late, in response to nappe emplacement. In the root zone of the Fall Mountain nappe in the Merrimack Synclinorium, high-grade metamorphism occurred early (pre-nappe emplacement) but was subsequently modified by thermal perturbations owing to folding. In anticlinal nodes, this thermal perturbation resulted in retrogradation, whereas in synclinal nodes, it resulted in progradation. Peak metamorphic isograds are therefore imposed relatively early in the anticlinal nodes (but post nappe emplacement) and late in the synclinal nodes.

In this section, we will discuss the metamorphic evolution of (1) the upper and lower plates of the Fall Mountain nappe in the region of the metamorphic overhang near Bellows Falls, Vermont and (2) the root zone of the Fall Mountain nappe in the Merrimack Synclinorium. The goal of this discussion will be to document the evidence for the metamorphic P-T evolution in these terranes and the relationship between the metamorphic evolution and the deformation history.

Fall Mountain Nappe: Upper Plate

General relations. The upper plate of the Fall Mountain nappe is exposed on Fall Mountain, N. H., immediately to the east of Bellows Falls, Vt.. Stratigraphy of the upper plate consists of gray schist (containing calc-silicate and amphibolite boudins) overlain by rusty schist both of the Silurian Rangeley Formation. Separating the gray schist from the rusty schist is a polymict, matrix-supported conglomerate with clasts of quartz, pebbles and granitic gneisses of unknown affinities.

Immediately below the gray schist lies the Bellows Falls pluton, which is an outlier of Bethlehem Gneiss affinities. It is difficult to ascertain the precise nature of the contact between the gray schist and the Bellows Falls pluton. Pieces of partially assimilated gray schist are incorporated in the upper part of the pluton, suggesting an intrusive origin. However, where the contact is best exposed in the bed of the Connecticut River, it has the appearance of a ductile shear zone. Locally the contact is a high-angle fault. The interpretation of the contact relations is that the Bellows Falls pluton was originally intrusive into the gray schist and that subsequent movement during emplacement of the Fall Mountain nappe sheared out the original intrusive contact. High-angle faulting is presumed to be late and perhaps associated with Mesozoic rifting. The lower contact of the Bellows Falls pluton also appears to be intrusive, modified by subsequent shearing. As will be discussed later, the upper and lower contacts of the Bellows Falls pluton could not have been in their present structural position at the time of intrusion because of the different P-T conditions recorded by metamorphic rocks immediately above and below the pluton. This observation implies that movement along the Fall Mountain nappe was accommodated by strain ± decollement within the Bellows Falls pluton. This may be an example of "melt-lubricated deformation" proposed by Crawford and Hollister (1986).

Mineral assemblages. The most conspicuous outcrop feature of the gray schist is the presence of abundant large (up to 3 cm long) porphyroblasts of sillimanite (termed "turkey-track rocks"). On foliation surfaces, the sillimanites are randomly oriented; locally, they are folded along with the foliation in minor folds.

The porphyroblastic sillimanite displays two distinctive features in thin section. Viewed down the *c*-axis, chiastolitic crosses, comprised of trails of biotite and ilmenite, are visible. In crossed polars, the sillimanite displays a domain extinction, with different domains going extinct within a few degrees of one another. These two features suggest that the sillimanite is pseudomorphous after andalusite as discussed by Rosenfeld (1969). Minerals present in the gray schist of the upper plate rocks include sillimanite + garnet + biotite + quartz + plagioclase + muscovite ± K-feldspar ± staurolite ± chlorite ± spinel + ilmenite. Not all of these phases represent an equilibrium mineral assemblage, however. Clear-cut textural evidence indicates that the staurolite, chlorite and some of the muscovite are late stage and have formed during retrogradation of the peak metamorphic assemblage. The peak metamorphic assemblage was sillimanite (after andalusite) + garnet + biotite + plagioclase + quartz ± muscovite ± K-feldspar + spinel + ilmenite.

The rusty schist of the upper plate contains the mineral assemblage quartz + plagioclase ± garnet + biotite ± K-feldspar ± muscovite ± chlorite + ilmenite ± fibrolitic sillimanite ± tourmaline. In places the rusty schist is migmatitic and contains symplectites of quartz ± K-feldspar ± plagioclase. Not all minerals represent peak metamorphic assemblages. Based on textural criteria, the peak metamorphic assemblage appears to be quartz + plagioclase ± garnet + biotite ± muscovite ± K-feldspar ± melt + ilmenite ± tourmaline. Chlorite and some of the muscovite are late-stage, retrograde minerals. Fibrolitic sillimanite occurs within large muscovite flakes of presumably retrograde origin.

P-T paths. Garnets in the gray schist of the upper plate are compositionally zoned (see Fig. F-4). Cores of the garnets are largely homogeneous; the one exception is almandine and pyrope values in the vicinity of biotite inclusions within the garnet where Fe/(Fe+Mg) increases in the vicinity of the biotite inclusions. The rims of the garnets are zoned with increasing almandine, spessartine, grossular and decreasing pyrope towards the rim. The interpretation of this zoning pattern is that the garnets from the upper-plate gray schists were initially homogeneous at or near the peak metamorphic conditions and underwent continuous retrograde reactions with the matrix minerals. In the vicinity of biotite inclusions, garnet and biotite underwent Fe-Mg exchange; the increase in Fe/Mg in garnet in the vicinity of biotite inclusions indicates that this exchange took place with decreasing temperature. These retrograde reactions will be discussed in greater detail in a later section.

The pattern of zoning in the upper-plate garnets discussed above suggests that the homogeneous interiors of the garnets are representative of peak metamorphic garnet composition and can be used in geothermobarometry to reconstruct peak metamorphic conditions. Matrix biotites, as well as biotite inclusions within garnet, however, have compositions that are not indicative of peak conditions, as a result of the retrograde reactions that have proceeded in the rock.

Several biotites are present in these rocks that have not re-equilibrated upon cooling and these can be used as indications of peak temperatures in conjunction with the garnet core compositions. These biotites are found as inclusions within porphyroblastic sillimanite and a single biotite grain has been found within a quartz grain that is itself included within garnet. These biotites have Fe/(Fe+Mg) and Ti values that are higher than those of matrix biotites or “unprotected” biotite inclusions within garnet. Temperatures calculated with these biotites and garnet core compositions (Ferry and Spear, 1978 calibration) fall in the range of 725-760 °C.

Peak metamorphic pressures have been computed from garnet - plagioclase - aluminosilicate - quartz equilibria (Ghent et al. 1979; Newton and Haselton, 1981; Hodges and Spear, 1982) utilizing plagioclase inclusions within garnet. No chemical zoning in the garnet surrounding these plagioclase inclusions is observed, indicating that retrograde reactions have not proceeded in these locations. The reason that retrogradation has not proceeded in these inclusions is presumably because the equilibrium is a net-transfer reaction and requires transfer of mass through the garnet. Pressures computed from this equilibrium range from 5.5-7.0 kbar at 725-760 °C (see Fig F-5).

P-T conditions computed from matrix biotite - garnet rim compositions and matrix plagioclase compositions are in the range 480-540 °C and 4.5-6.5 kbar (see Fig. F-5). A similar temperature (480-520 °C) is computed from the compositions of unprotected biotite inclusions within garnet and the composition of the garnet touching these biotites. It is believed that these temperatures represent a closure temperature for Fe-Mg exchange between garnet and biotite.

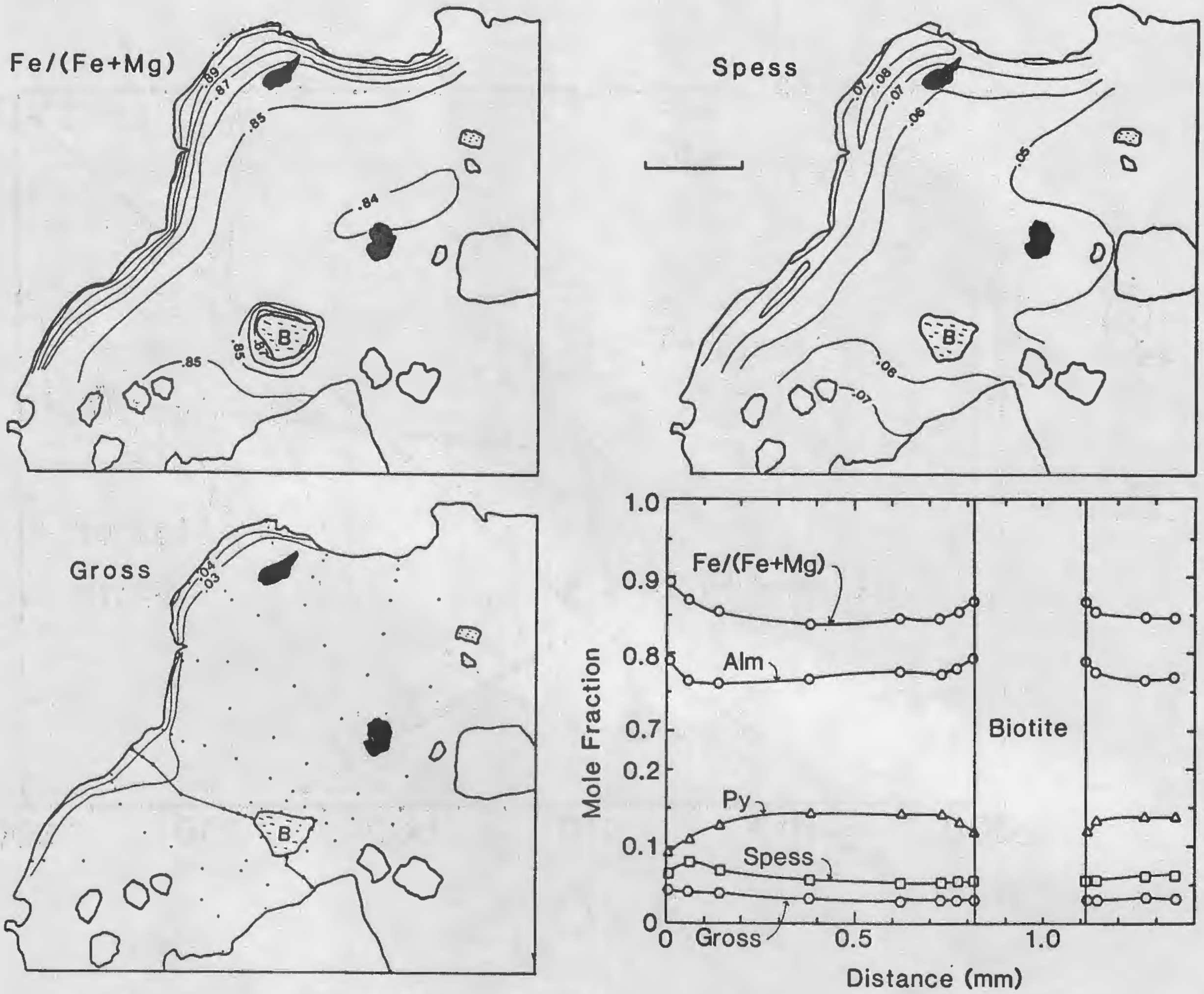

Fig. F-4. Chemical zoning in garnet from gray schist of the upper plate of the Fall Mountain nappe (sample BF-9G). Contours are in mole fractions. Black inclusions are ilmenite, colorless inclusions are quartz. Biotite inclusion is marked with a "B". Note that zoning on the rim of the garnet is observed in all elements, whereas zoning around the biotite inclusion is restricted to Fe and Mg. Scale bar is 0.5 mm.

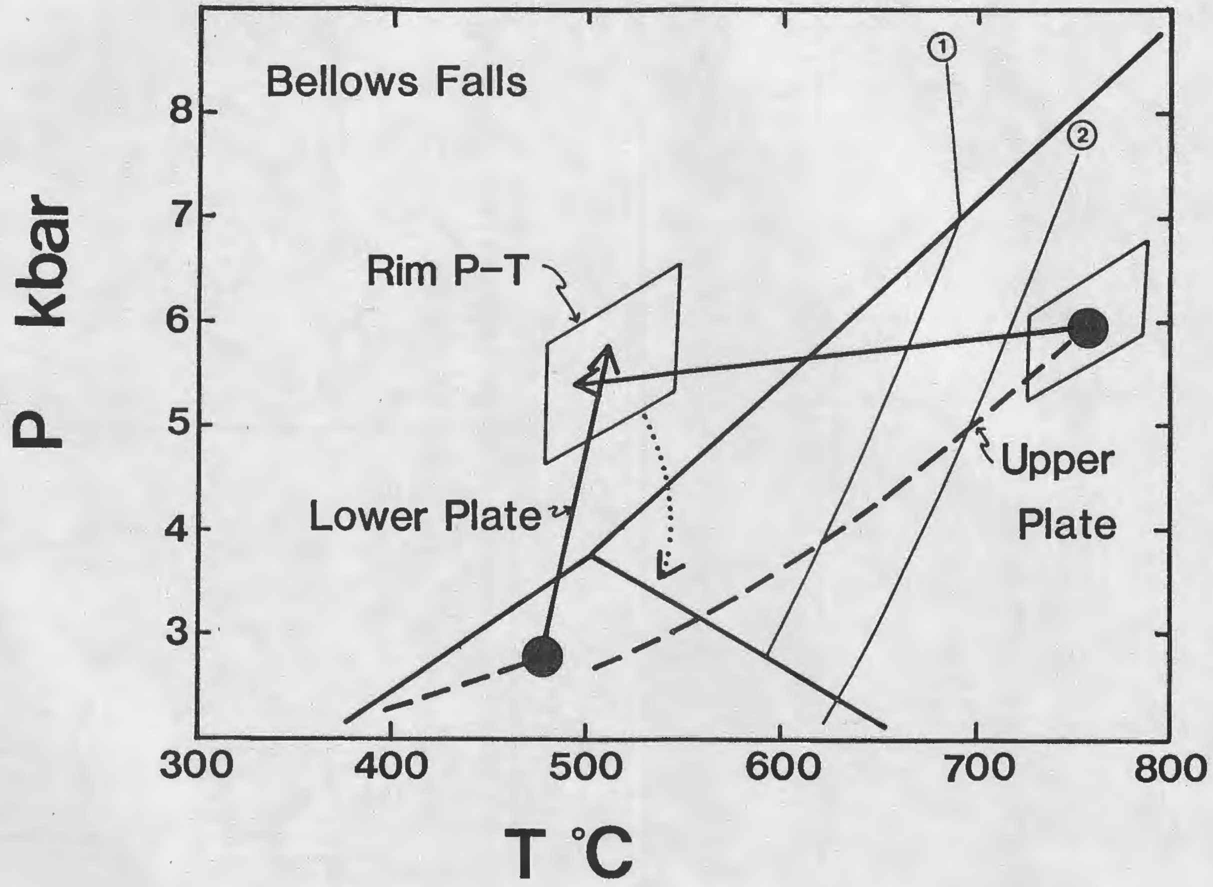

Fig. F-5. P-T paths for the upper and lower plates at Fall Mountain, New Hampshire. Dashed portions of paths are inferred from early mineral parageneses. Solid portions are computed from chemical zoning in garnets. Dotted portion is inferred from late sillimanite parageneses. Large dots are P-T conditions immediately prior to nappe emplacement. The two reaction curves are: (1) staurolite + quartz = almandine + Al_2SiO_5 + H_2O and (2) muscovite + quartz = K-feldspar + Al_2SiO_5 + H_2O.

Retrograde reactions. Retrograde reactions are conspicuous in upper-plate rocks. Large sillimanite porphyroblasts in the gray schist are mantled by the assemblage muscovite + staurolite, suggesting that the reactions:

sillimanite + garnet + biotite + H_2O = staurolite + muscovite

and

sillimanite + K-feldspar + H_2O = muscovite + quartz

have occurred. The P-T conditions of these two reactions are shown in Figure F-5. Both of these reactions are crossed in a retrograde sense, which requires addition of H_2O to the system. Texturally, these reactions are not pervasive, but rather are controlled by the influx of H_2O. Evidence for continuous retrograde reactions is also present in the zoning in the outer rims of the garnets. If it is assumed that the peak metamorphic assemblage was garnet + biotite + sillimanite ± muscovite ± K-feldspar ± spinel + quartz + plagioclase, then it is likely that the continuous reactions:

garnet + muscovite = sillimanite + biotite + quartz

garnet + K-feldspar + H_2O = sillimanite + biotite + quartz

and

anorthite = grossular + kyanite + quartz

occurred during retrogradation.

The zoning observed on the rims of the large porphyroblastic garnets in the upper-plate rocks (Fig. F-4) can be used to estimate the P-T trajectory of retrogradation. Comparison of garnet core and rim compositions indicates that Fe/(Fe+Mg) increases in the garnet from core to rim. In contrast, a comparison of "protected" biotite inclusions with matrix biotites indicates Fe/(Fe+Mg) in biotite decreases from core to rim. These changes are shown schematically in the AFM diagram in Figure F-6A. Figure F-6B is a P-T diagram that has been contoured for garnet and biotite Fe/(Fe+Mg) for the continuous reaction garnet + muscovite = sillimanite + biotite + quartz. There is only a restricted range of P-T changes where biotite and garnet can change Fe/(Fe+Mg) in opposite directions, as indicated in Figure F-6B, thus greatly restricting the possible retrograde P-T paths.

The retrograde P-T path has also been computed by the method of Spear and Selverstone (1983), where the zoning in the rim of the garnet has been modelled algebraically. One such path is shown in Figure F-5, where it can be seen that the P-T path connects the rim and the peak metamorphic P-T conditions.

Diffusion modelling of upper plate cooling history. The zoning profiles within garnet around included biotites have been interpreted as resulting from retrograde Fe-Mg exchange and as such, the shapes of the profiles are controlled by Fe-Mg diffusion between garnet and biotite. In order to obtain information on the rate of cooling that the upper plate has experienced, these profiles have been modelled using a numerical solution to the diffusion equation. The model assumes an initially homogeneous garnet in equilibrium with biotite at the peak metamorphic temperature (750 °C) and linear cooling rates from this peak temperature to approximately 500 °C. The boundary condition at the interface between the garnet and the biotite was computed at each temperature interval from

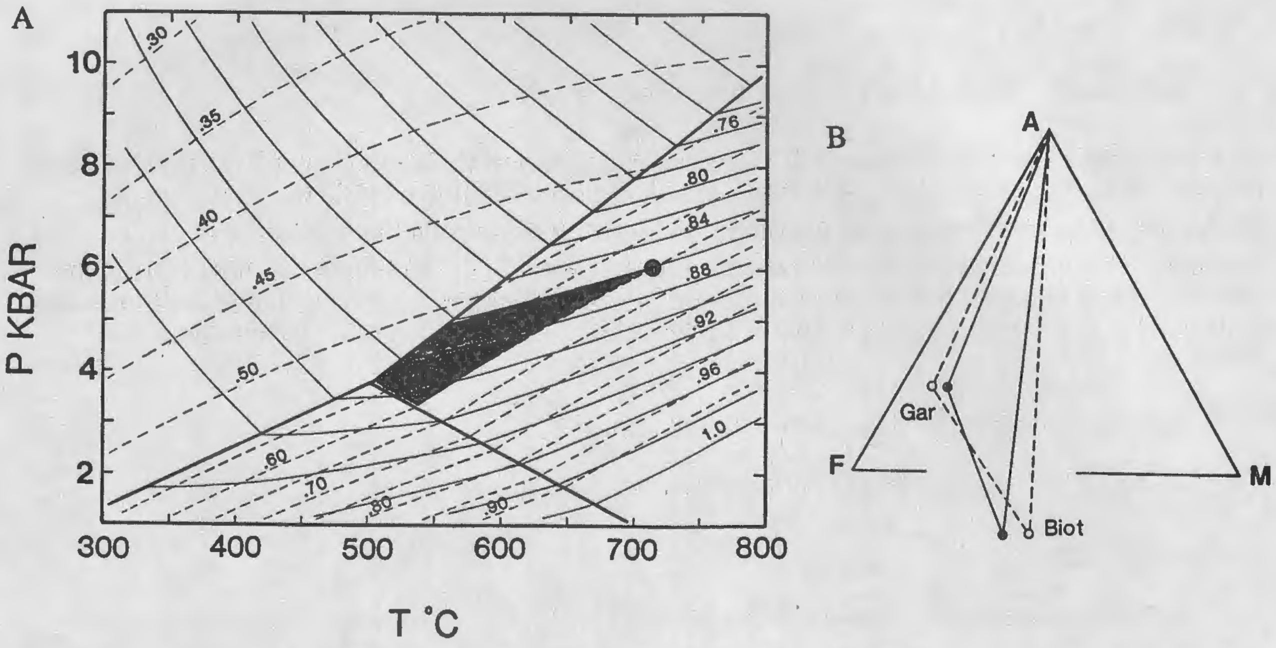

Fig. F-6. (A) A-F-M diagram for upper-plate assemblage garnet + biotite + sillimanite + quartz + muscovite + plagioclase depicting changes in garnet and biotite compositions from peak P-T conditions (solid symbols) to retrograde conditions (open symbols). (B) P-T diagram contoured for Fe/(Fe+Mg) in garnet (solid lines) and biotite (dashed lines) for the assemblage garnet + biotite + Al_2SiO_5 + quartz + muscovite. The shaded area defines the P-T region where garnet becomes Fe-rich and biotite becomes Fe-poor upon cooling from the dot.

Fe-Mg partitioning of Ferry and Spear (1978) and the diffusion profile computed by the implicit Crank-Nicholson method. The total flux of Fe and Mg through the interface was computed by numerical integration of the area under the diffusion profile and the compositional change in the biotite, based on the estimated volume of the biotite, was evaluated at each interval.

The results of calculations for cooling rates of 5, 25, 50, 100 and 500 °C/Ma are shown in Figure F-7. As can be seen, the computed diffusion profile is relatively insensitive to the cooling rate and it is difficult to place limits on the cooling rate that are any tighter than 5-500 °C/Ma based on the profiles alone . The reason is because the biotites are generally small and change composition substantially during the process. However, the total mass flux is relatively more sensitive to cooling rate. Comparison of the measured biotite composition of Fe/(Fe+Mg)= 0.55 with computed biotite compositions at different cooling rates constrains the cooling rate to be between 25-100 °C/Ma.

Fall Mountain Nappe: Lower Plate

The metamorphic evolution of the lower plate of the Fall Mountain nappe is considerably more complex than that of the upper plate for several reasons:

1) The lower plate is not a single nappe, but a sequence of two (Bernardston and Skitchewaug) or more nappes that have been imbricated during the Acadian Orogeny. Moreover, the stratigraphic and structural details of this area are currently being revised (J.B.Thompson, personal communication).

2) The metamorphic grade in the different nappes immediately prior to emplacement of the Fall Mountain nappe was probably different giving rise to different P-T paths in each different structural level.

3) A wide range of bulk compositions from quartzites to amphibolites are present in the lower plate giving rise to a variety of different mineral parageneses that are difficult to correlate with one another.

4) Peak metamorphic mineral assemblages, which largely post-date and are in response to the emplacement of the Fall Mountain nappe, grade from chlorite grade in the west along the so-called Chicken Yard line to sillimanite grade to the east of Fall Mountain.

The discussion that follows will concentrate on the metamorphic evolution of the Skitchewaug nappe structural level, where most of the authors' petrologic work has been done. It should be noted that considerably more work needs to be done before all of the details of the metamorphism of this area are worked out.

Mineral parageneses. In the Skitchewaug nappe structural level, several different mineral parageneses can be observed, depending on the location. In one locality, pseudomorphs after andalusite are observed, which are now replaced by muscovite ± chlorite. The early assemblage in these rocks was apparently andalusite + garnet + biotite + muscovite + quartz and has been replaced by garnet + biotite + chlorite + quartz + muscovite. In other localities, pseudomorphs after staurolite are common. These staurolites have been partially to completely replaced by muscovite + chlorite. West of Fall Mountain, the late assemblage in these rocks is again garnet + biotite + chlorite + muscovite + quartz, but below and to the east of Fall Mountain a second generation of staurolite and in some places kyanite ± sillimanite have been formed. A typical texture is for kyanite to form in the inclusion trails that define an "hour glass" structure in the staurolite and for fibrolitic sillimanite to grow in the muscovite that has replaced the early porphyroblastic staurolite or andalusite. In one locality, to be visited on this trip, 1-2 cm long

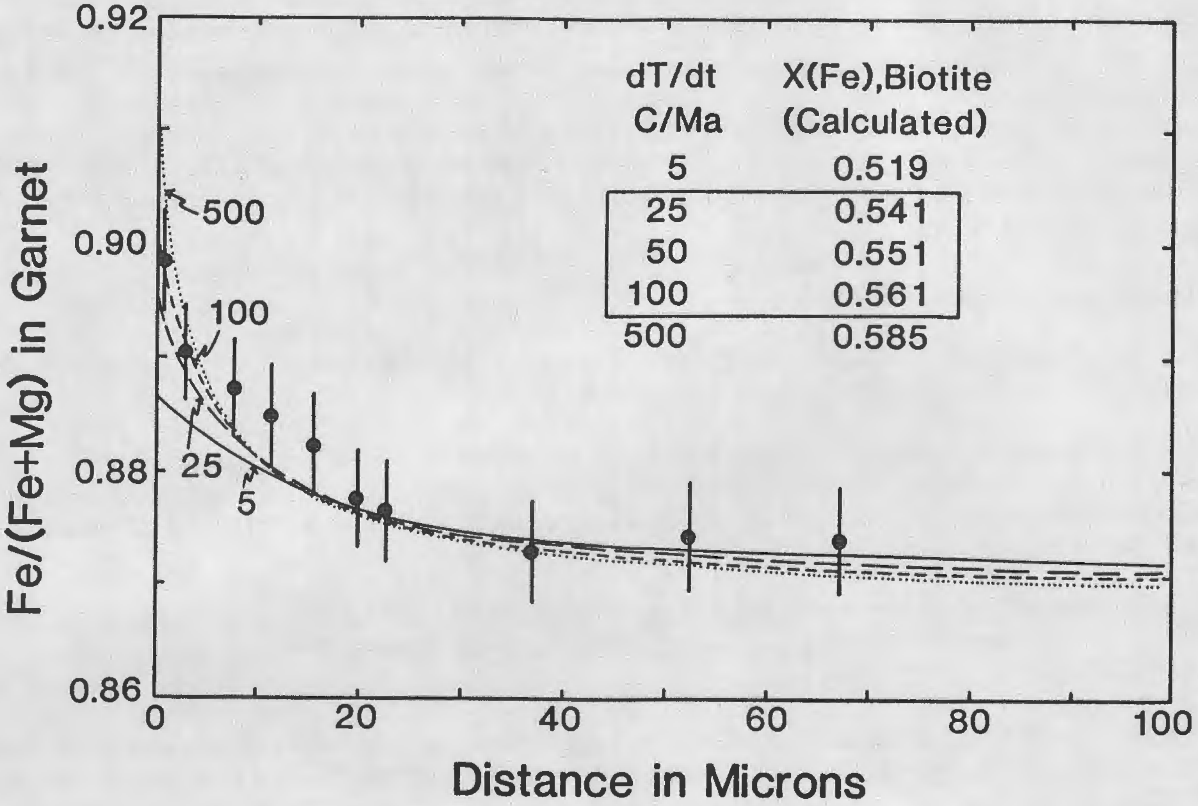

Fig. F-7. Plot of Fe/(Fe+Mg) vs. distance measured and computed diffusion profiles for upper plate garnet, BF-9E. Dots are microprobe analyses with estimated uncertainties. Diffusion profiles for four different cooling rates, 5, 25, 100, and 500 °C/Ma are shown by the solid, long dashed, short dashed and dotted lines, respectively. Computed Fe/(Fe+Mg) of biotite inclusion is also indicated for each cooling rate. Cooling rates of 25-100 °C/Ma best fit the measured profile and the final measured biotite composition of Fe/(Fe+Mg)= 0.55.

prismatic crystals with cross sections reminiscent of chiastolitic andalusite have been replaced by muscovite ± chlorite; then within the pseudomorph, kyanite + staurolite + garnet + biotite ± chlorite and finally late fibrolitic sillimanite have grown. The interpretation of this paragenesis will be discussed below, but it is interesting to note that although this rock contains evidence for all three aluminosilicate minerals, it is probable that the minerals never equilibrated near the Al_2SiO_5 triple point.

P-T paths. Chemical zoning in garnets from the lower-plate assemblages differs from that in upper-plate garnets in that the zoning is present throughout the garnet and the cores are not homogeneous. This in itself suggests a different P-T history for the lower-plate rocks. It also suggests that the garnets have grown by continuous prograde reactions with little retrograde equilibration so that the rim compositions of the garnets can be used for estimating peak metamorphic P-T conditions and the zoning profiles can be used for calculating P-T paths.

P-T conditions for rocks immediately below the Fall Mountain nappe, computed using garnet rim and matrix mineral compositions are shown in Figure F-5. As can be seen from the figure, the computed P-T conditions are similar to the matrix conditions computed for the upper-plate assemblages (Fig. F-5).

P-T paths have been computed for a single zoned garnet using the method of Spear and Selverstone (1983). Zoning in this garnet is characterized by an increase in Ca with minor changes in Fe, Mg or Mn from core to rim. The results of the P-T path calculations are shown in Figure F-5, where it can be seen that the rock experienced a period of nearly isothermal compression of 2-3 kbar (7-10 km increase in overburden).

Interpretation of P-T Paths for the Upper and Lower Plates

In summary, the P-T paths depicted in Figure F-5 are constrained by the following data. For the upper plate, the early portion of the path is constrained by the presence of andalusite pseudomorphs. Peak P-T conditions and retrograde conditions are constrained by the geothermobarometry boxes and the path between the peak and retrograde conditions has been computed by modelling of the zoning on the garnet rims. For the lower plate, the early path is constrained to lie in the andalusite field by the presence of andalusite pseudomorphs. The solid arrow has been computed by modelling the zoning in garnet and the box defines the P-T conditions from thermobarometry. Note that the P-T path shown is consistent with andalusite-bearing assemblages having been replaced by kyanite-bearing assemblages. The late, dotted portion of the P-T path is drawn through the sillimanite field to be consistent with the presence of late-stage fibrolitic sillimanite in both upper and lower plate rocks.

The interpretation of the P-T paths is that, prior to nappe emplacement, both the upper and lower plate rocks were metamorphosed in a low-P, high-T andalusite-sillimanite environment. Presumably this metamorphism took place in the Merrimack synclinorium based on the similarity of rocks now exposed there. The heat source for this metamorphism was likely to have been in part the advection of heat by the emplacement of the Bellows Falls and similar plutons of the New Hampshire Magma Series, and in part by high heat flow associated with an extensional basin. It is important to note, however, that the two structural levels could not have been adjacent prior to nappe emplacement because of the different early P-T conditions.

Immediately prior to nappe emplacement, the two plates are inferred to have been at the P-T conditions indicated by the large solid dots in Figure F-5. West-directed nappes carried upper-plate rocks over lower-plate rocks, and presumably the entire ensemble was emplaced on yet lower structural levels. The portion of the P-T path inferred to have been followed during nappe emplacement is that between the large dots and the box marked "rim P-T". It is suggested that fluids (largely H_2O) derived from devolatilization reactions in the lower plate were responsible for retrograde hydration reactions that proceeded in the upper plate. The dotted portion of the P-T path is inferred to have been generated during dome formation as uplift and erosion unroofed the terrane.

MERRIMACK SYNCLINORIUM

Isograds

Metamorphic rocks in the Merrimack synclinorium in central New Hampshire are divisible into the upper four metamorphic zones mapped in central Massachusetts (Tracy et al., 1976; Tracy and Robinson, 1980). The lowest grade rocks in this region belong in the sillimanite-muscovite zone (Zone III). The vast majority of the rocks in the synclinorium belong in that zone. However, there are smaller hotter regions containing sillimanite-muscovite-alkali feldspar (Zone IV), sillimanite-alkali feldspar (Zone V), and alkali feldspar-cordierite (Zone VI) assemblages (Figure F-3).

Analysis of one of these "hot spots" suggests that the distribution of these high-grade assemblages is structurally controlled. Chamberlain (1986a) has shown that the high-grade assemblages are restricted to late F2 and F3 synclines, and the highest-grade assemblages (cordierite-alkali feldspar) occur only at the intersection of F2 and F3 synclines (cf. Figures F-8 and F-1).

In a gross sense, the highest grade rocks are restricted to the Fall Mountain nappe level in the Merrimack synclinorium. This suggests that, like rocks at the Fall Mountain outlier, there was an original thermal inversion as hot rocks were emplaced on cooler rocks during nappe emplacement. However, high-grade isograds in the synclinorium locally crosscut nappe structures suggesting that high-grade metamorphism continued throughout the later stages of Acadian deformation (Chamberlain, 1985).

Geothermobarometry

The same spatial relationship between the occurrence of high-grade assemblages and late-Acadian synclines is also reflected in the geothermometric results. Metamorphic temperatures were estimated using the garnet-biotite Fe-Mg exchange calibration of Ferry and Spear (1978) (Chamberlain and Lyons, 1983; Chamberlain, 1986a). These temperature determinations are complicated by chemical zoning in the garnets.

In all but the highest-grade assemblages (Zones V and VI), the garnets are zoned with respect to Mg, Fe, and Mn. Typically, Mg and Mn decrease and Fe increases from the core to the rim of the garnets. Because of this zoning, temperatures calculated using garnet core and matrix biotite compositions are often 40 degrees higher than temperatures calculated using garnet rim compositions. This result is typical of many garnets from Zone V and VI assemblages (Tracy et al., 1976; Chamberlain and Lyons, 1983). It is generally considered that the garnet core temperatures are more representative of "peak" metamorphic conditions. For this reason, garnet core compositions and matrix biotite were used to compute metamorphic temperatures (Chamberlain, 1986a). Because the same regional trends in temperature are observed using temperatures calculated from both garnet rim and core compositions, chemical zoning in these garnets does not affect the interpretations discussed here.

The calculated temperatures for this region range from 580 to 650 °C (Chamberlain, 1986a). Moreover, isotherms show the same regional trends as isograds and occur in lobate patterns extending along F2 and F3 synclinal axes (Figure F-9).

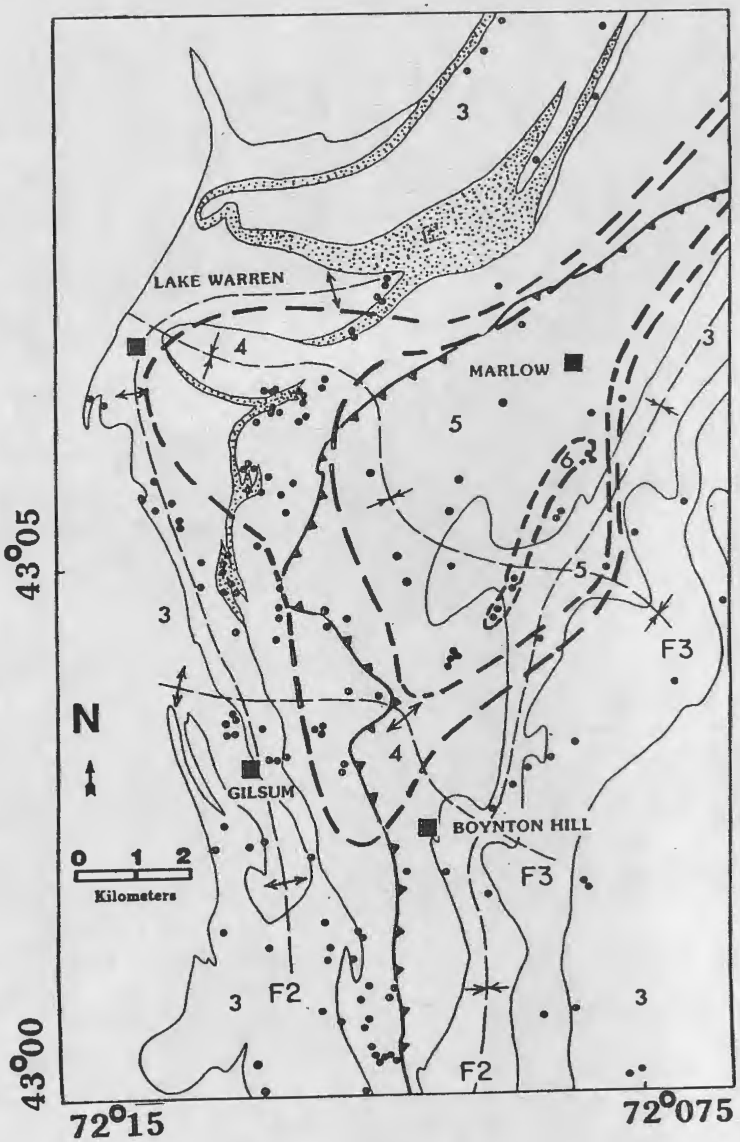
3
LAKE WARREN
4
MARLOW
5
6
5
3
F3
N
GILSUM
4
BOYNTON HILL
0 1 2
Kilometers
F3
3
F2
F2
3
43°05
43°00
72°15
72°075

Fig. F-8. Metamorphic map of the root-zone of the Fall Mountain nappe. Mineral assemblages are: Zone 3 = sil-musc-bio-gar; Zone 4 = sil-musc-kspar-bio-gar; Zone 5 = sil-kspar-bio-gar; and Zone 6 = sil-kspar-cord-bio-gar. Axial surfaces of second and third phase anticlines and synclines indicated.

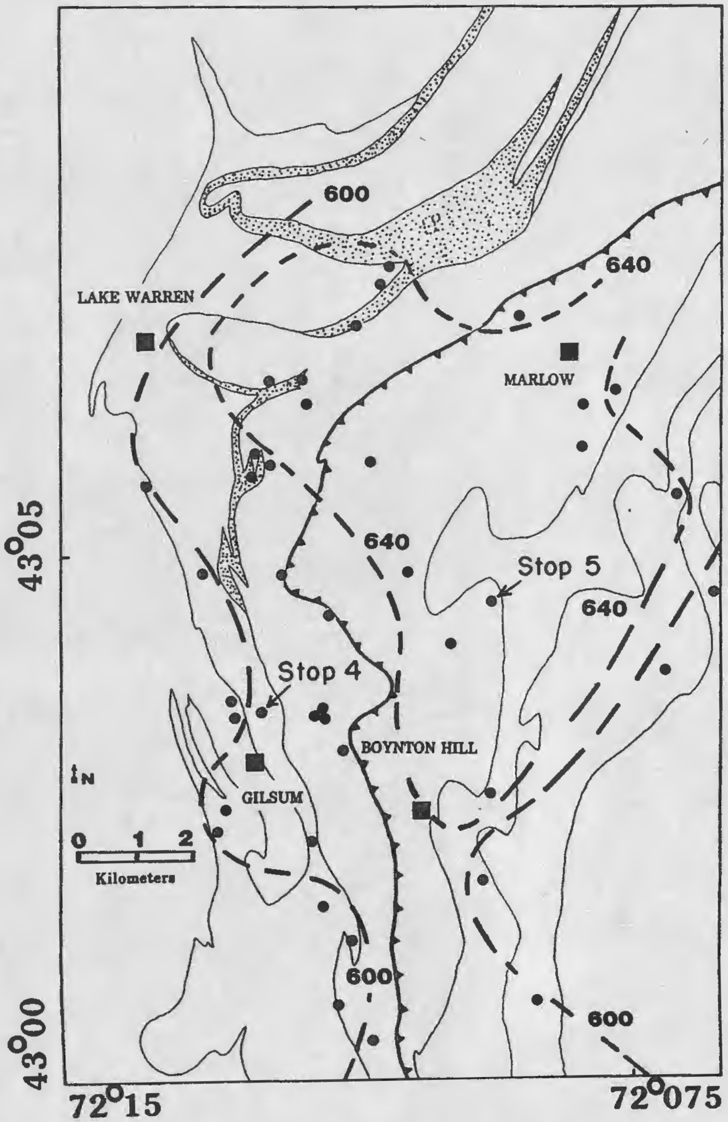
600
LAKE WARREN
640
MARLOW
640
Stop 5
640
Stop 4
BOYNTON HILL
N
GILSUM
0 1 2
Kilometers
600
600
43°05
43°00
72°15
72°075

Fig. F-9. Isotherm map for the root-zone of the Fall Mountain nappe. Metamorphic temperatures were calculated using the calibration of Ferry and Spear (1978).

Metamorphic pressure estimates for this region (Chamberlain and Lyons, 1983; Chamberlain, 1985) suggest that the pressure obtained at temperature maximum was on the order 5.5 kilobars. In addition, there appears to be little pressure variation recorded in the schists across the synclinorium (Chamberlain and Lyons, 1983) suggesting that much of the synclinorium was buried at similar depths during high-grade metamorphism.

P-T Paths

P-T trajectories determined for rocks in the root zone of the Fall Mountain nappe suggest a complex interplay between Acadian folding and thermal re-equilibration of the tectonically thickened orogen (Chamberlain, 1986a). P-T paths were determined using both a reaction-space method (Thompson, 1982b) applied to pelitic schists (Chamberlain, 1986a), and the Gibbs' method (Rumble, 1976a; Spear et al., 1982). The details of these methods are discussed elsewhere and, therefore, only the results of these calculations are presented here.

The earliest portion of the P-T trajectory observed in the root zone of the Fall Mountain nappe is an early low P-high T metamorphism. This early low P-high T metamorphism is shown by the abundant sillimanite pseudomorphs after andalusite. Typically, large aggregates of sillimanite needles show relic chiastolite crosses. These andalusite pseudomorphs appear to be spatially related to the Bethlehem and Kinsman plutons, suggesting that these plutons provide some of the thermal energy for this early portion of the P-T trajectory.

After this early low-pressure metamorphism the rocks evolved along an increasing pressure and temperature trajectory, presumably representing the emplacement of higher nappe sheets now eroded. This pressure increase is reflected in the geothermobarometric results that record pressures 1.5 to 2.0 kilobars greater than the triple point pressure.

All rocks within this region have this early increasing pressure-temperature path. However, four different types of later P-T trajectories are found within this region. These different P-T trajectories correlate with the four distinct types of fold intersections created by the intersection of F2 and F3 folds.

For example, rocks at the intersection of F2 and F3 anticlines show simple cooling paths. In this structural setting, the garnet zoning profiles are simple with Mg and Mn decreasing, Fe increasing, and Ca remaining constant from the core to the rim. In addition, mineral textures show late garnet growth at the expense of biotite and sillimanite. These reaction textures and zoning profiles suggest a simple reaction history along a nearly isobaric cooling path (Figures F-10 and F-11). Rocks at the intersection of F2 and F3 synclines, however, show continued heating paths. There, the garnets are surrounded by a symplectite of biotite and sillimanite, muscovite has been completely consumed and replaced by large porphyroblasts of alkali feldspar. These mineral textures suggest a simple reaction history involving the consumption of garnet and muscovite and growth of alkali feldspar (Figure F-10). Moreover, garnets in these rocks are unzoned except at the rim, within a few microns, where it is in contact with biotite. These flat zoning profiles are typical of high-grade garnets found elsewhere in the synclinorium (Tracy et al., 1976; Chamberlain, 1981). Presumably, the temperature was high enough to homogenize garnet compositions and the localized zoning of Mg and Fe represents local cation exchange with biotite. These garnet zoning profiles and mineral reaction textures suggest a simple heating P-T path (Figure F-12).

Complex P-T trajectories are observed at the F2 anticline and F3 syncline intersection and the F2 syncline-F3 anticline intersection. Both the mineral textures and the garnet zoning profiles in rocks found at the F2 anticline-F3 syncline intersection suggest an early cooling and later heating P-T path. At this fold intersection, garnets are surrounded by a late symplectite of biotite and sillimanite, muscovite is frayed and appears to have been dissolving, and there are small grains of

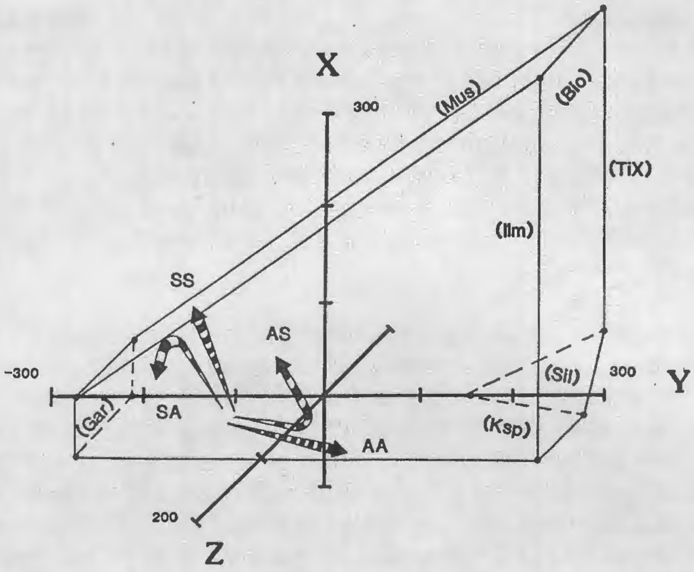

Fig. F-10. Reaction polyhedron for the assemblage Gar-Bio-Mus-Qtz- Ilm-Sil-Kspar. Labelled faces represent the zero isopleths of mineral abundance. The X axis is the reaction Mus + Qtz = Kspar + Sil + Water; the Y axis is the reaction Gar + Mus = Sil + Bio + Qtz: and the Z axis is the reaction Qtz + Ilm = Sil + Ti exchange (micas). Arrows show the reaction histories for pelitic rocks at the F2 anticline-F3 anticline (AA), F2 syncline - F3 syncline (SS), F2 syncline-F3 anticline (SA), and F2 anticline - F3 syncline (AS) fold intersection.

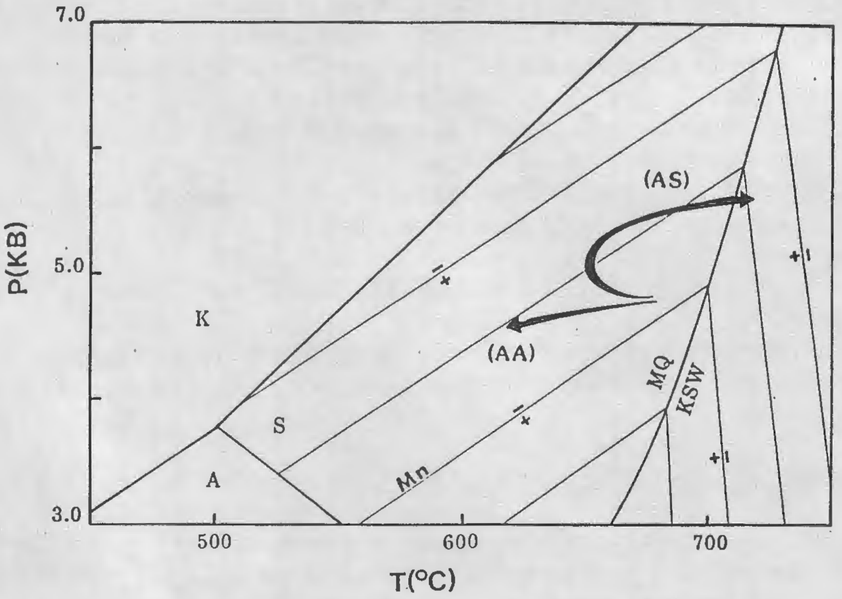

Fig. F-11. P-T diagram constructed for the assemblage Gar(Fe-Mn) + Bio + Mus + Qtz + Sil and Gar + Bio + Ksp + Qtz + Sil. Isopleths (dashed lines) for constant Mn in garnet are shown, with "+" indicating increasing and "-" indicating decreasing Mn content in garnet. Arrows show the P-T paths calculated for garnets at the F2 anticline - F3 anticline (AA) and F2 anticline - F3 syncline (AS) intersections.

alkali feldspar in the matrix. Moreover, the garnets appear to have overgrown an earlier biotite-sillimanite foliation and muscovite has grown along the F2 crenulation cleavage. These mineral textures, taken together, suggest the complex reaction history shown in Figure F-10. Garnet zoning profiles at this fold intersection are also complex. Here the inner portions of the garnets are zoned with Fe increasing, Mn and Mg decreasing, and Ca remaining constant toward the rim. However, midway through the garnets the Fe and Mn profiles reverse with Fe decreasing and Mn increasing toward the rim. This profile suggests a P-T path marked by early cooling followed by later heating (Figure F-11).

A complex, two-stage P-T path is also observed at the F2 syncline-F3 anticline fold intersection. In this region, however, the rocks show an early heating followed by a later cooling P-T path. The early prograde textures observed at this fold inter- section are present in: 1) the development of symplectites of biotite and sillimanite around garnet, and 2) pseudomorphs of alkali feldspar. The later retrograde textures consist of mats of late muscovite and quartz that replace early alkali feldspar. The rocks at this fold intersection now contain Zone III assemblages, but this textural evidence suggests that they once contained alkali feldspar-sillimanite assemblages (Figure F-10). The garnet composition profiles in these rocks are similar to garnet composition profiles observed in Zone IV, V, and VI assemblages, with all elements remaining constant throughout the garnet. These homogenized garnets support the interpretation that the rocks were once at temperatures high enough for the formation of alkali feldspar and sillimanite.

Interpretation of P-T Paths

These contrasting P-T trajectories (Figure F-12) and complex isograd patterns have been interpreted to be the result of folding and relaxation of isotherms during F2 and F3 Acadian folding (Chamberlain, 1986a). According to this interpretation, during each episode of folding the rocks moved at a faster rate than heat was transferred, resulting in the folding of isotherms. After isotherms were folded during F2 they relaxed, causing heating of the F2 synclines and cooling in the F2 anticlines. This process of folding and relaxation of isotherms was repeated during F3. Thus, four different P-T trajectories were created by the intersection of these two fold sets. Continued heating paths are observed at F2-F3 syncline intersection, continued cooling paths are present at F2 anticline and F3 syncline intersections, and heating-cooling paths are observed at F2 syncline-F3 anticline intersections. The early increasing P-T path observed in all samples (Figure F-12) must, therefore, reflect a common P-T history prior to this late Acadian folding. Presumably, this early portion of the P-T path is the result of loading of additional nappes above the Fall Mountain nappe prior to late Acadian deformation.

METAMORPHIC-TECTONIC MODEL

The pressure-temperature paths and structural data discussed above suggests a thermal-tectonic model for the evolution of the Merrimack Synclinorium and Bronson Hill Anticlinorium in this region.

Tectonic and Thermal Setting before the Nappe Stage

Prior to nappe-stage deformation, rocks that are currently exposed on the Fall Mountain outlier of the Fall Mountain nappe experienced P-T conditions of high-T, low-P facies types, similar to the P-T conditions extant in the Merrimack synclinorium at this time. In addition, rocks of the Skitchewaug nappe structural level immediately below the Fall Mountain outlier also experienced high-T, low-P metamorphism, but the grade was considerably lower than in the upper plate of the nappe. These observations suggest that rocks of both the Fall Mountain and Skitchewaug nappe structural levels were in a high heat flow thermal regime, presumably within the Merrimack Synclinorium itself, prior to nappe emplacement. The position of these two structural levels within the Merrimack synclinorium must have been different, however, because of

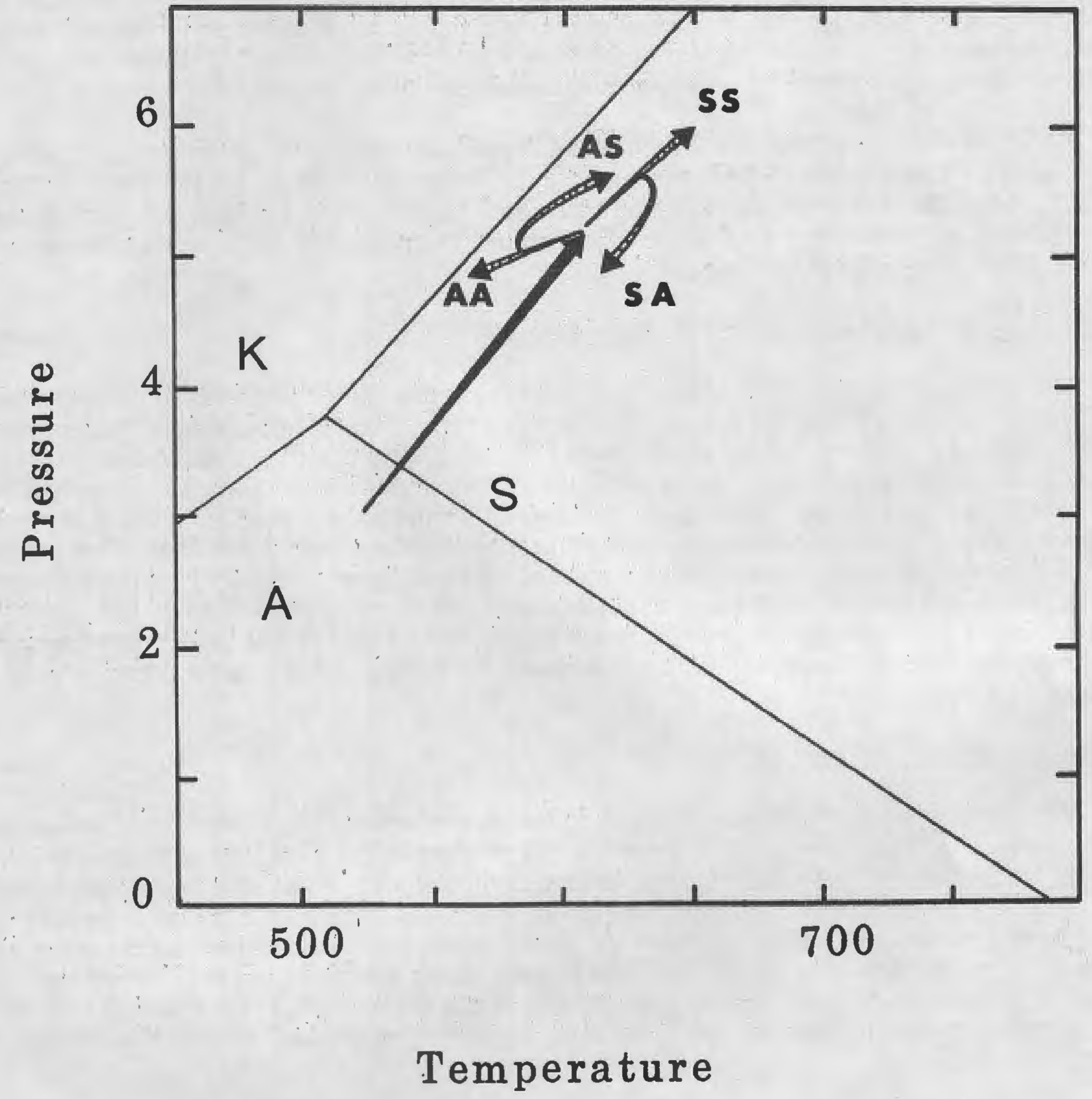

Fig. F-12. P-T paths for the rocks in the root-zone of the Fall Mountain nappe. The early portions of the P-T history, observed in all samples in this region, represent early loading of nappe structures above the Fall Mountain nappe. The later divergent P-T paths are the result of the migration of isotherms during late Acadian folding.

the different pre-nappe P-T conditions. It is suggested that the Fall Mountain nappe was situated deep within the synclinorium whereas the Skitchewaug nappe was situated on the west flank of the synclinorium.

The reason for the high heat flow regime in the Merrimack synclinorium is uncertain, but two causes may be postulated. Firstly, an extensional basin such as the Merrimack synclinorium may have experienced high heat flow as a result of crustal thinning that is associated with basin formation. Secondly, the influx of magmas of the New Hampshire magma series (Bethlehem gneiss and Kinsman quartz monzonite) may have also contributed to the high heat flow.

Rocks structurally beneath the Skitchewaug nappe were apparently metamorphosed along more normal thermal gradients prior to nappe emplacement, as shown by the P-T paths determined for the Orfordville anticlinorium to the north (see Spear and Rumble, Fig D-6, this guidebook). This observation implies that the high heat flow regime extended only as far west as the western margin of the Merrimack Synclinorium.

Nappe-Stage Deformation and Thermal Perturbations

The emplacement of nappes during the Acadian Orogeny carried hot rocks of the Merrimack synclinorium westward over the Bronson Hill anticlinorium. Nappe emplacement resulted in a marked thermal perturbation along the Bronson Hill anticlinorium, with hot rocks overlying cooler rocks. Rocks of the structurally highest level (the Fall Mountain nappe) cooled as a result of being emplaced over cooler rocks. Rocks of the Skitchewaug nappe experienced an increase in pressure of approximately 3 kbar with a change in pressure from approximately 3 to 6 kbar. This pressure change implies that the Skitchewaug nappe was at a depth of approximately 10 km prior to nappe emplacement, and that the nappes resulted in thickening of the crust from 10 to 20 km. Rocks of the structurally lower Cornish nappe (see Spear and Rumble, Fig D-6, this guidebook) experienced maximum pressures of 7 kbar, suggesting that crustal thickening at this structural level was on the order of 25 km.

Thermal Relaxation - Cross Folding

Following nappe emplacement, thermal relaxation accompanied by cross folding and dome formation resulted in a variety of P-T trajectories, depending on the local structural and thermal setting. Rocks of the Fall Mountain nappe underwent initial cooling and then minor heating with decompression. Rocks of structurally lower levels underwent significant amounts of heating accompanied by decompression. Rocks of the Merrimack synclinorium experienced a complex array of P-T paths depending on where the rocks were situated with respect to synclinal and anticlinal nodes. The result of these P-T trajectories is that the formation of isograds (i.e. peak metamorphic conditions) varies in space and time, depending on the local structural and thermal setting.

PART F. ITINERARY

0.0	Leave Highland Motel and proceed south on Route 5.
3.0	Turn left (east) across Connecticut River. At stoplight on east end of bridge turn left (north) on N.H. Route 12.
4.5	Road cuts on right in Bellows Falls pluton.
5.8	Stop at turnout on left (west) side of road.

Stop 1: Lower Plate of Fall Mountain Nappe

A small outcrop of graded bedded schists immediately to the east of the railroad tracks along N.H. Route 12 exposes rocks of the uppermost lower plate. The Bellows Falls pluton crops out a few tens of meters up the hill to the east. The rocks here are folded, presumably during the nappe stage.

Visible in outcrop are pseudomorphs of andalusite displaying chiastolitic crosses. These pseudomorphs now consist of muscovite ± chlorite. Matrix minerals include quartz + muscovite + chlorite + biotite + garnet + ilmenite. The interpretation of this outcrop is that an initially high-T, low-P assemblage, possibly generated in a contact aureole with the overlying Bellows Falls pluton, was replaced by a higher-P assemblage (garnet + biotite + chlorite) after emplacement of the Fall Mountain nappe.

Return south on Route 12.

8.4 Stoplight. Turn left and continue south on Route 12.

8.9 Pull off on left near R.R cars.

Stop 2: Upper Plate of Fall Mountain nappe.

WARNING: Carefully climb down the river embankment. Watch where you walk: there is abundant POISON IVY here.

The rocks exposed in the river bed are the gray schist of the Rangeley Formation of the upper plate of the Fall Mountain nappe. Locally there are boudins of amphibolite and calc-silicate. The large porphyroblasts here are sillimanite pseudomorphs after andalusite ("turkey track rocks"). In a few places these sillimanites are folded with the foliation.

Assemblages observed in the gray schist include quartz + plagioclase + garnet + biotite + sillimanite ± spinel (only as inclusions within sillimanite) ± chlorite (retrograde) ± staurolite (retrograde) ± K-feldspar (only as inclusions within garnet) + muscovite + ilmenite.

Conspicuous in some samples is a white selvage surrounding the sillimanite porphyroblasts. This selvage is composed of late muscovite ± staurolite, produced during retrogradation of the upper plate. The fluids responsible for the retrogradation presumably came from dewatering of structurally lower rocks following nappe emplacement. The retrogradation was not pervasive, however, as some samples contain pristine sillimanites.

To the west of the river is the Bellows Falls pluton. If the water level is low, it is possible to cross the small dike to examine the upper portion of the pluton. The contact is in the river bed (usually under water) and here has the appearance of a steeply dipping fault. The upper portion of the pluton contains xenoliths that appear to be partially assimilated pieces of gray schist, suggesting an original intrusive origin. A hundred meters to the south, the contact has the appearance of a shear zone.

Continue south on N.H. Route 12.

10.0 Turn left (east) on N.H. Route 123 towards Alstead.

10.6 Turn left following Route 123 SOUTH toward Alstead.

10.9 Road forks. Take right fork off of Route 123. Warning to users of old topographic maps: Route 123 now goes by St. Peter's cemetary and the Route 123 shown on the maps is now the "old road".

11.6 Intersection at elevation 469. Go straight.

11.8 Pull off on right near road cut on left side of road.

Stop 3: Lower Plate of the Fall Mountain Nappe.

At this stop are schists of the lower plate of the Fall Mountain nappe. Metamorphic grade here is staurolite-kyanite to staurolite-sillimanite.

Of particular interest is a schist that contains long (1-2 cm), prismatic pseudomorphs. In cross section, these pseudomorphs have the appearance of chiastolitic crosses and it is suggested that they may be replacements of original andalusite. Within the pseudomorphs are randomly oriented muscovite flakes, garnet, biotite, chlorite, staurolite and kyanite. The blades of kyanite define in a general way, a cross shaped pattern. Growing within the muscovite flakes is fibrolitic sillimanite. The matrix of the rock contains the assemblage quartz + plagioclase + muscovite + garnet + biotite + chlorite + ilmenite.

The interpretation of this rock is that it experienced initial high-T, low-P metamorphism when it was situated in the Merrimack synclinorium prior to nappe emplacement. In response to emplacement of the Fall Mountain nappe, the andalusite-bearing assemblage was replaced by kyanite + staurolite + garnet + chlorite ± biotite + quartz + muscovite. Thermal relaxation after nappe emplacement resulted in minor heating accompanied by decompression, which generated the late-stage fibrolitic sillimanite.

Continue in same direction

12.8 Intersection. Go straight.

13.1 Intersection. Go straight.

14.9 Intersection near cemetary. Go straight.

15.4 Intersection. Go straight.

15.6 Bear left on main road.

17.1 Stop sign. Intersection with Route 12A. Turn right (south).

18.2 Turn left (east) toward Gilsum on Gilsum Road. (This is starting point for road log in Part G.)

22.5 Junction with Route 10. Turn left (north).

23.0 Turn left toward Gilsum. Proceed straight through Gilsum.

23.3 Bear right.

23.5 Go straight at intersection.

23.7 Park on left. Outcrops in woods across stream to east.

Stop 4: Root Zone of the Fall Mountain Nappe - AA intersection

The rocks at this outcrop contain the lowest-grade assemblages found in the root zone of the Fall Mountain nappe. This outcrop is located where the F2 and F3 anticlines intersect. The pelites here contain the assemblage sillimanite + biotite + muscovite + garnet + plagioclase. Garnet zoning profiles and mineral textures determined for this outcrop indicate a nearly isobaric cooling P-T trajectory. Note the "turkey-track" sillimanites present in this outcrop. Relic chiastolite crosses, indicative of the earlier high-T, low-P metamorphism, can be observed in these sillimanites.

Turn vans around and return to Gilsum.

24.2 Center of Gilsum. Turn left (east).

24.4 Stop sign. Turn left (north) on Route 10.

27.2 Park on right. Outcrops on both sides.

Stop 5: Root Zone of the Fall Mountain Nappe - SS intersection

This outcrop contains the highest-grade pelitic assemblages found in the root zone of the Fall Mountain nappe. The outcrop is located at the intersection of two large F2 and F3 Acadian synclines. The pelitic rocks contain the prograde assemblage cordierite + alkali feldspar + sillimanite + garnet + plagioclase. This high grade metamorphism was ongoing throughout both F2 and F3 folding.

Several retrograde zones containing chlorite and staurolite can be found at this outcrop. These zones were created as water was introduced into the upper plate (Fall Mountain nappe) sometime after nappe emplacement.

Several calc-silicate pods are present in this outcrop. These pods are indicative of the Rangeley schists found in the Fall Mountain nappe.

Turn vans around. Head south on Route 10.

30.9 Turn right (west) toward Surry.

35.1 Junction with Route 12A. Turn left (south) on 12A. See Road Log for Part G.

Jocko sez: No Running on the outcrops Boys and Girls

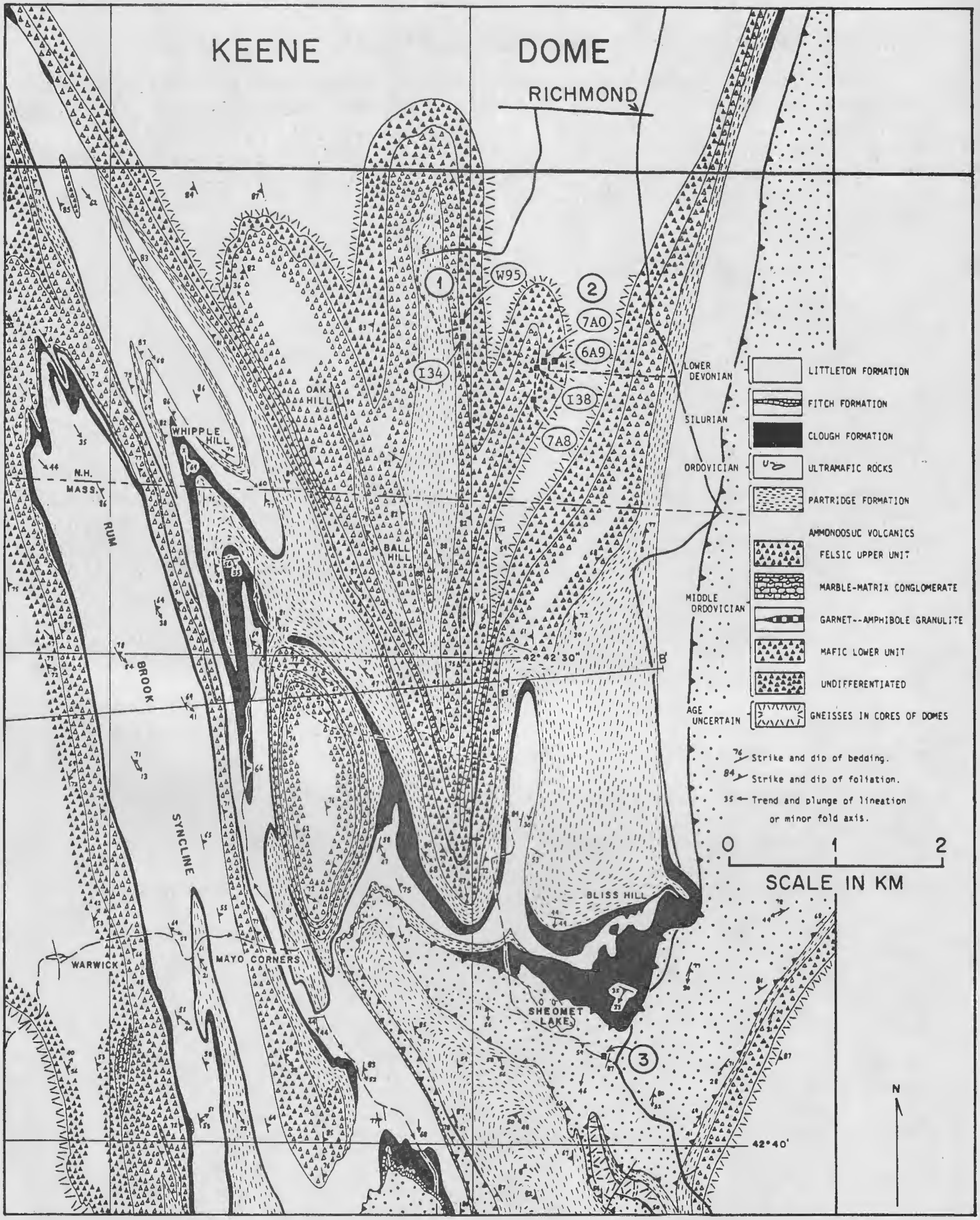
KEENE
DOME
RICHMOND
1
W95
2
7A0
6A9
I34
I38
7A8
OAK HILL
WHIPPLE HILL
N.H.
MASS.
BALL HILL
RUM
BROOK
SYNCLINE
42°42'30"
B'
BLISS HILL
WARWICK
MAYO CORNERS
SHEOMET LAKE
3
42°40'
N
LOWER DEVONIAN
SILURIAN
ORDOVICIAN
MIDDLE ORDOVICIAN
AGE UNCERTAIN
LITTLETON FORMATION
FITCH FORMATION
CLOUGH FORMATION
ULTRAMAFIC ROCKS
PARTRIDGE FORMATION
AMMONOOSUC VOLCANICS
FELSIC UPPER UNIT
MARBLE-MATRIX CONGLOMERATE
GARNET--AMPHIBOLE GRANULITE
MAFIC LOWER UNIT
UNDIFFERENTIATED
GNEISSES IN CORES OF DOMES
Strike and dip of bedding.
Strike and dip of foliation.
Trend and plunge of lineation or minor fold axis.
0
1
2
SCALE IN KM

Figure G-1. Detailed geologic map of area of field trip part G, including revision southwest of Richmond to June 1986. Teeth are on upper plate of proposed Brennan Hill thrust and heavy dot pattern indicates rocks that may possibly be reinterpreted as Lower Silurian Rangeley Formation.

G. GEDRITE-CORDIERITE GNEISSES AND RELATED METAMORPHOSED VOLCANIC ROCKS, KEENE DOME, SOUTHWESTERN NEW HAMPSHIRE

John C. Schumacher and Peter Robinson

PURPOSE OF TRIP

The purpose of this trip is to examine the phase relations of amphiboles in a series of exposures in a restricted geographic area at the south end of the Keene gneiss dome in southwestern New Hampshire. Most of the rocks of interest lie in the Lower and Middle Members of the Middle Ordovician Ammonoosuc Volcanics. These rocks have been metamorphosed in the upper part of the Sillimanite - Muscovite - Staurolite Zone of Acadian metamorphism, but show a distinctive set of reaction features believed to be due to tectonic unloading related to genesis of the gneiss dome. En route from southwestern New Hampshire to Amherst, Massachusetts we will stop at a spectacular example of Silurian or Lower Devonian pelitic schist at the same metamorphic grade, and, if time permits, we will briefly examine an exposure in the Pelham gneiss dome, where relict pre-Acadian granulite facies minerals have been heavily overprinted by Acadian kyanite - muscovite zone assemblages.

The amphibole-bearing rocks will be seen at two stops where there are six designated exposures. At Stop 1, designated "Iolite Hill" (an archaic name for cordierite, known to at least one old resident of the area), the two outcrops are W95 and I34. At Stop 2, designated "Amphibole Hill", the four outcrops are 6A9, 7A0, I38, and 7A8. Collectively these exposures plus a few others were called the "Amphibole Hill area" by Robinson and Jaffe, 1969b. Formerly it was possible to travel directly from one hill to the other, but frantic activity by beavers in 1971 put an abrupt and nearly cataclysmic end to this practice. In August of 1971 a group of distinguished petrologists including Helmut Winkler, Conrad Krauskopf, and Jo Laird "participated" in this stop even up to the armpits!

LOCAL GEOLOGY

The outcrop pattern at the south end of the Keene gneiss dome is shown in Figure G-1. The interpretation of this complicated pattern is heavily dependent on understanding the detailed internal stratigraphy of the Ammonoosuc Volcanics, briefly given in the map legend and also described briefly under geochemistry. The outcrop pattern is due to an early northeast-trending recumbent anticline and syncline (Figure G-2) refolded by the tight conical fold plunging about 45° south that constitutes the southern extreme of the Keene dome itself. The age and relationship of the early recumbent folds to the regional fold nappes is presently unknown, but these early recumbent folds are probably related to early southeast-directed recumbent folds in the Pelham dome, which are known to be truncated by the Belchertown Intrusive Complex (see this guidebook, part H).

Both Stop 1 and Stop 2 lie on the east limb of the tight anticline that constitutes the end of the Keene dome, but both also lie on the lower limb of the earlier recumbent anticline, so that stratigraphic tops are to the west at both localities. Previous work up to and including that of Schumacher (1983) showed the gedrite - cordierite gneisses at Stop 1 as belonging to the Upper Member, a distinct anomaly in view of what is known of the stratigraphy elsewhere. However, during excavation and cleaning at I34 in June 1986 in preparation for this field trip, a small exposure of the Middle Garnet - Amphibole - Magnetite Quartzite Member ("Garnet Amphibole Granulite") was unearthed, indicating that the stratigraphy is not anomalous and the structure requires some modification. In this light it is possible that the quartz-bearing gedrite - garnet - quartz gneisses at I34 and 7A0 may be correlative.

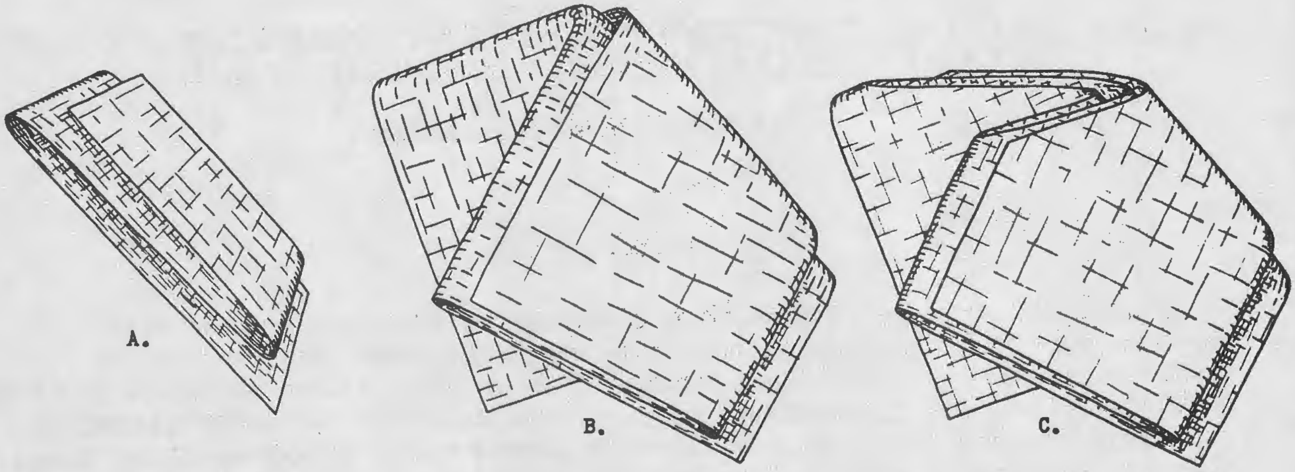

Figure G-2. Origin of outcrop pattern at south end of Keene dome. Stratigraphic horizon shown in diagrams is contact between Ammonoosuc Volcanics and Partridge Formation. A. Formation of early recumbent anticline and syncline. Axial planes dip southeast and axes trend northeast. B. Folding of recumbent folds about later anticline with axis plunging about 45° south-southeast. C. Erosion to give present outcrop pattern.

INTRODUCTION TO AMPHIBOLE PHASE RELATIONS

Although it is not strictly "legal" as a phase diagram, it is exceedingly convenient to plot phase assemblages from the "Amphibole Hill area" in terms of the quartz-projected tetrahedron Al_2O_3-Na_2O, CaO, MgO, FeO+MnO and then to make an anorthite projection onto the plane Al_2O_3-Na_2O, MgO, FeO+MnO. Such a projection is given in Figure G-3 and each of the tie lines or three-phase assemblages to be visited at Stops 1 or 2 are labelled appropriately and listed in Table G-1. The position of several of these tie lines were first established in the early probe work of Klein (1968), or wet chemical analyses of Robinson and Jaffe (1969a and b) given in Tables G-2 and G-3. The low-Al assemblages with hornblende and anthophyllite or cummingtonite (or rarely both) are rocks with essentially igneous compositions. The anthophyllite + cummingtonite assemblage is in a garnet quartzite. The assemblages of gedrite with cordierite, with cordierite + hornblende, with sillimanite, and with staurolite with or without garnet are all in rocks believed to have been basalts that underwent pre-metamorphic hydrothermal seawater alteration. The sillimanite + staurolite + garnet assemblage from pelitic schist at Stop 3 is the only rock composition in which muscovite is stable. Biotite, on the other hand is present in all assemblages, though with highly varied Fe-Mg ratios.

An important aspect of Figure G-3 is the very narrow sillimanite + gedrite two-phase field separating the sillimanite + staurolite + gedrite and the sillimanite + cordierite + gedrite three-phase fields. The electron probe analyses of both these assemblages came from the single layered hand specimen I34I. Examination of more magnesian rocks indicates that they also once contained the sillimanite + gedrite assemblage, which, however, has progressively broken down to yield cordierite and cordierite + plagioclase as a result of pressure decrease accompanying rise of the gneiss dome. This progressive reaction, beginning in the most magnesian rocks and progressing toward more Fe-rich compositions was responsible for production of the aluminous enclaves discussed in detail below. It is fascinating that this reaction at Amphibole Hill did not quite

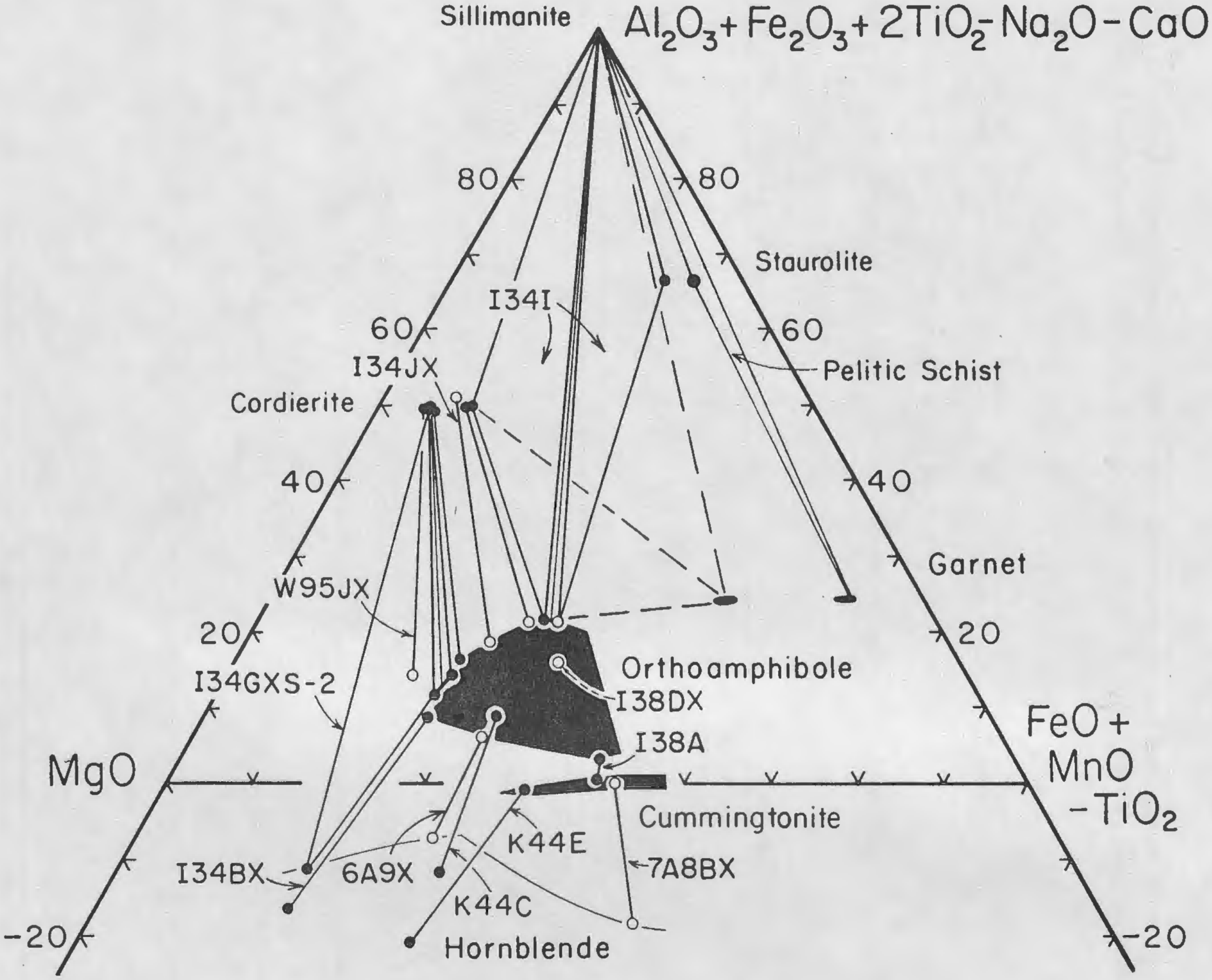
Sillimanite
$Al_2O_3 + Fe_2O_3 + 2TiO_2 - Na_2O - CaO$
80
80
Staurolite
I34I
60
60
I34JX
Pelitic Schist
Cordierite
40
40
Garnet
W95JX
20
20
I34GXS-2
Orthoamphibole
I38DX
FeO + MnO - TiO_2
I38A
MgO
Cummingtonite
K44E
I34BX
6A9X
7A8BX
K44C
-20
Hornblende
-20

Figure G-3. Projection from quartz, plagioclase, and H_2O onto the plane ($Al_2O_3 + Fe_2O_3 + 2TiO_2 - Na_2O - CaO$), ($FeO + MnO = TiO_2$), MgO for assemblages from the middle of the Sillimanite - Muscovite - Staurolite Zone at "Amphibole Hill," southwestern New Hampshire.

Table G-1. Estimated modes and descriptions of amphibole-bearing specimens from "Amphibole Hill area," south-western New Hampshire (from Robinson and Jaffe, 1969b). See also Table G-5 for details of aluminous enclave-bearing rocks.

	W95JX	E	134JX	134I	138DX	6A9X	7A8BX	134B	6A9	K44C	K44E	7A8B	I38A	
Anthophyllite	70 p	96 p	25 p	33 g	28 g	20 p		22 p	20 pp	18 p			3 cl	
Cummingtonite							3 pgg				5 cl	20 pgg	4 cl	5 cl
Hornblende						39 bg	39 dg	40 pbg	40 bg	22 bg	1 bg	25 dg		2 pbg
Quartz			27	50	61		8			20	33	8	85	85
Plagioclase (An %, range) (An %, ave.)			8 (27–31)			40 (35) (35)	47 (22) (22)	38 (44–59) (53)	37 (35) (35)	39 (27–37) (34)	60 (32) (32)	44 (22) (22)		
Garnet				4	10								7	7
Biotite			X	8		1	X		2	X		tr		
Chlorite					tr	X			X					
Talc														
Rutile	3	1	X					X	tr					
Ilmenite			X	1	X	X	X		X	1	X			
Magnetite	tr		X				3					3	1	1
Zircon	X		X											
Monazite					tr	tr								
Allanite											tr			
Apatite	X		X	X	X	X	X		tr	X	X	X	X	X
Tourmaline	tr		tr											
Calcite												tr		
Cordierite	27	3	40											
Kyanite	X		X	X										
Sillimanite	X		X	1										
Staurolite	X		X	3										
Corundum	X		tr											
Spinel	X													

X—common but in amount less than 1%, tr—present as trace only, not common.
Abbreviations for strongest color in amphiboles: g gray, pg pale gray, vpg very pale gray, bg blue green, pbg pale blue green, dg dark green, p pinkish tan, pp pale pinkish tan, cl colorless, pgg pale greenish gray, pbb pale brown to bluish green.

Description of Specimens in Table 1.

All specimens from Ammonnosuc Volcanics unless otherwise noted. Referred to in Robinson (1963) unless different reference is indicated.

W95JX Coarse-grained bedded anthophyllite-cordierite gneiss with aluminous enclaves in cordierite (Robinson and Jaffe, 1969). Orthorhombic amphibole, space group *Pnma*, consists of gedrite host, 80%, and anthophyllite lamellae, 20%. Lamellae ∥ to (010) visible under high magnification.

E Analysis of separate from "gedrite-rutile rock" collected by Emerson (1895). Mode is of specimen 134E of Robinson (1963) believed to be representative of material collected by Emerson. Dark brown, fine-grained, weakly foliated anthophyllite rock. 3% "cordierite" is actually an unidentified alteration product probably after cordierite.

134JX Coarse-grained cordierite-anthophyllite-quartz-andesine gneiss with aluminous enclaves in cordierite (Robinson and Jaffe, 1969). Orthorhombic amphibole consists of >99% gedrite, space group *Pnma*, with exsolved rutile needles. Wet chemical analysis of coexisting cordierite: $(Na,K)_{0.12}(Mg_{1.51},Fe^{2+}_{0.30},Fe^{3+}_{0.04},Li_{0.16},Ca_{0.02})Al_{4.00}Si_{5.01}O_{18}\cdot 0.83\ H_2O$. Biotite, $\gamma = 1.610$.

134I Black, medium-grained, well foliated quartz-anthophyllite-biotite-garnet-staurolite-sillimanite schist. Orthorhombic amphibole is 100% gedrite, space group *Pnma*. Garnet, $n = 1.793$ (zoned $\sim 1.791 - 1.795$), $a = 11.515$ Å, visual arc spectrographic analysis: Fe, Mg >5%, Mn 1-5%, Ca 0.1-1%, Na and Li <1%. Estimated composition: $Alm_{58}Pyr_{27}Spess_{14}Gross_{1}$. Biotite, $\gamma = 1.621$.

138DX Well bedded, coarse-grained quartz-garnet-anthophyllite granulite with irregular garnets up to 3 mm diam. enclosed in gray anthophyllite. Orthorhombic amphibole, space group *Pnma*, consists of gedrite host, 80%, and anthophyllite lamellae, 20%. Lamellae ∥ to (010) visible under high magnification.

6A9X Medium-grained hornblende-anthophyllite amphibolite. Hornblende host, space group $C2/m$, 90%; primitive cummingtonite lamellae on (100), space group $P2_1/m$, 7%; primitive cummingtonite on $(\bar{1}01)$, $P2_1/m$, 3%. (100) and $(\bar{1}01)$ lamellae are 0.4 and 0.8μ thick respectively. Anthophyllite host, 70%; submicroscopic gedrite exsolution, 30%, both *Pnma*.

7A8BX Medium-grained hornblende-cummingtonite amphibolite zone in outer part of metamorphosed lava pillow. Pillow core is hornblende amphibolite, matrix surrounding pillows is hornblende, garnet, and biotite. Hornblende host, 90-94%; cummingtonite lamellae on $(\bar{1}01)$, 3-10%, cummingtonite lamellae on (100), 0-3%, all space group $C2/m$. Cummingtonite host, 88-92%; hornblende lamellae on (100), 2-4%; hornblende lamellae on $(\bar{1}01)$, 4-10%; all $C2/m$. (100) and $(\bar{1}01)$ lamellae are 0.4-0.6 μ and 0.8-2.0 μ thick respectively.

134B Medium-grained, weakly layered and foliated hornblende-plagioclase-anthophyllite gneiss. Hornblende contains (100) lamellae 0.25 μ thick and $(\bar{1}01)$ lamellae 0.4 μ thick.

6A9—See 6A9X

K44C—Medium-grained hornblende-anthophyllite amphibolite. Hornblende contains (100) and $(\bar{1}01)$ exsolution lamellae 0.4 μ and 0.6-1.0 μ thick respectively.

K44E—Contact zone between medium-grained plagioclase-quartz-cummingtonite gneiss and hornblende amphibolite layer. Hornblende grain selected for analysis was several mm inside amphibolite layer and may not have been in contact with cummingtonite host grains. Hornblende and cummingtonite contain (100) and $(\bar{1}01)$ exsolution lamellae identical to those in 7A8BX.

7A8B See 7A8BX

138A—Same outcrop as 138DX but not described in detail elsewhere. Fine-grained, well bedded quartz-garnet-amphibole granulite. In a central layer about 2 cm thick the amphibole is cummingtonite. The boundary between the two mode areas in one thin section runs through this cummingtonite layer. On one side of this layer the cummingtonite is in contact with and intergrown with hornblende. In the vicinity of this contact the cummingtonite contains hornblende exsolution lamellae and has a few twins on (100). Crystals A, C-A, and 1 of Ross, Papike and Shaw, 1969, Table 6 are from near this contact. Crystal A, cummingtonite host, 90%; hornblende lamellae on (100), 6%; hornblende lamellae on $(\bar{1}01)$, 4%, all space groups $C2/m$. Crystal C-A cummingtonite host, 98%; hornblende lamellae on (100), 2%; all $C2/m$. Crystal 1, hornblende host, 85%; cummingtonite lamellae on (100), 10%; cummingtonite lamellae on $(\bar{1}01)$, 5%, all $C2/m$. On the other side of the cummingtonite layer cummingtonite is in contact with and intergrown with anthophyllite. Near this contact the cummingtonite is free of exsolution lamellae but is polysynthetically twinned on (100). The electron probe analyses of Klein (1968, see Fig. 14) and crystal 2 of Ross, Papike and Shaw are from near this contact. Anthophyllite host, 55%; submicroscopic gedrite exsolution, 45%, both *Pnma*. The high percentage of gedrite exsolution shown by the single crystal X-rayed is not consistent with the chemical composition given by the probe analysis, suggesting that anthophyllites of two different compositions were studied in this strongly layered rock.

Table G-2. Wet-chemical (left) and early electron-probe analyses of amphiboles from "Amphibole Hill area". Other wet-chemical analyses are given in Table G-6 (samples W95JX, I34JX, I34I) and Table G-9 (sample 7A8).

	Gedrite		*Anthophyllite*
	138DX[c]	E[b]	6A9X[c]
SiO_2	45.14	47.86	51.12
TiO_2	.30	.63	.23
Al_2O_3	14.28	14.09	6.79
Fe_2O_3	1.29	.33	1.18
Cr_2O_3	.007	—	.018
FeO	20.19	13.41	17.82
MnO	.34	.14	.75
MgO	14.54	19.89	18.54
NiO	.005	—	.015
CaO	.34	.57	.73
SrO	—		—
BaO		—	—
Li_2O	.06		.02
Na_2O	1.45	.93	.78
K_2O	.02	.06	.02
$H_2O(+)$	2.47	2.46	2.41
$H_2O(-)$	.30		.38
P_2O_5	.05	.05	.01
F	.02		.03
Cl		—	—
	100.81	100.42	100.85
−O=F, Cl	.01	—	.01
Total	100.80	100.42	100.84

	Hornblende
	6A9X[a]
SiO_2	44.78
TiO_2	.83
Al_2O_3	13.33
Fe_2O_3	3.32
Cr_2O_3	.036
FeO	10.67
MnO	.31
MgO	12.53
NiO	.01
CaO	9.81
SrO	—
BaO	—
Li_2O	.01
Na_2O	1.80
K_2O	.19
$H_2O(+)$	2.57
$H_2O(-)$	.32
P_2O_5	.03
F	.01
Cl	—
	100.54
−O=F, Cl	.00
Total	100.54

	6A9X
Si	6.434
P	.003
Al	1.563
Al	.694
Cr^{3+}	.002
Fe^{3+}	.359
Mg	2.682
Li	—
Ti^{4+}	.090
Ni	.001
Fe^{2+}	1.282
Mn^{2+}	.038
Ca	1.510
Na	.501
K	.035
(OH)	2.464
F	—
fe[d]	32.97
fe[e]	38.49
an[f]	75.09

[a] H. Asari, analyst, 1967.

[b] E. A. Schneider, analyst, 1892.

[c] M. Kumanomido, analyst, 1968.

[d] fe = 100 (FeO + MnO)/(FeO + MnO + MgO).

[e] Same as above but with total Fe as FeO.

[f] an = (100) Ca/(Na + Ca).

	138DX	E	6A9X
Si	6.557	6.686	7.314
P	.007	.007	.002
Al	1.436	1.307	.684
Σ (tet.)	8.000	8.000	8.000
Al	1.010	1.014	.461
Fe^{3+}	.141	.035	.127
Cr^{3+}	—	—	.002
Ti^{4+}	.033	.063	.025
Mg	3.148	4.142	3.953
Li	.035	—	.012
Ni	.001	—	.002
Fe^{2+}	2.453	1.567	2.132
Mn^{2+}	.042	.017	.091
Ca	.053	.086	.112
Na	.084	.076	.083
Σ (*M*-sites)	7.000	7.000	7.000
Na	.325	.176	.135
K	.003	.005	.003
Σ (*A*-site)	.328	.181	.138
H	2.394	2.292	2.301
F	.010	—	.014
FeO+MnO/FeO +MnO+MgO	.44	.27	.35

ELECTRON PROBE ANALYSES[a]

		I34B	6A9	K44C	K44E	7A8B	I38A
Anthophyllite	SiO_2	48.8	49.9	48.4			51.4
	Al_2O_3	10.4	7.0	8.8			3.9
	FeO	16.4	20.6	21.1			26.3
	MnO	0.5	0.7	0.6			0.6
	MgO	18.8	17.5	17.6			14.9
	CaO	0.6	0.6	0.5			0.0
	Na_2O	1.2	0.9	1.1			0.3
	Total	96.7	97.2	98.1			97.4
Cummingtonite	SiO_2				54.9	52.3	52.2
	Al_2O_3				1.4	2.1	1.0
	FeO				22.4	25.1	26.8
	MnO				0.8	0.6	0.6
	MgO				18.3	14.9	15.2
	CaO				1.0	1.4	0.3
	Na_2O				0.1	0.2	0.1
	Total				98.9	96.6	96.2
Hornblende	SiO_2	45.8	45.8	45.1	45.2	44.1	
	Al_2O_3	14.2	13.8	14.2	12.5	12.0	
	FeO	10.8	14.7	14.8	15.6	20.2	
	MnO	0.2	0.4	0.3	0.4	0.3	
	MgO	15.5	13.3	12.8	12.7	9.3	
	CaO	10.3	10.0	10.2	10.9	9.0	
	Na_2O	1.9	1.7	1.9	1.7	1.9	
	Total	98.7	99.7	99.3	99.0	96.8	

		I34B	6A9	K44C	K44E	7A8B	I38A
Anthophyllite	Si	7.02	7.29	7.03			7.64
	Al	0.98	0.61	0.97			0.36
	Al	0.78	0.58	0.53			0.32
	Mg	4.03	3.81	3.81			3.30
	Fe	1.97	2.51	2.56			3.27
	Mn	0.06	0.09	0.07			0.07
	Ca	0.19	0.10	0.08			0
	Na	0.33	0.26	0.31			0.09
	fe	33.5	40.6	40.9			50.3
	an	21.6	22.7	20.1			0
Cummingtonite	Si				7.88	7.83	7.90
	Al				0.12	0.17	0.10
	Al				0.10	0.19	0.60
	Mg				3.92	3.32	3.43
	Fe				2.69	3.14	3.38
	Mn				0.09	0.07	0.07
	Ca				0.15	0.22	0.05
	Na				0.03	0.05	0.04
	fe				41.6	49.2	50.3
	an				84.8	79.6	62.3
Hornblende	Si	6.46	6.51	6.26	6.84	6.68	
	Al	1.54	1.49	1.74	1.16	1.32	
	Al	0.82	0.81	0.58	1.06	0.81	
	Mg	3.26	2.82	2.65	2.86	2.10	
	Fe	1.27	1.74	1.71	1.97	2.56	
	Mn	0.02	0.05	0.03	0.05	0.04	
	Ca	1.56	1.52	1.52	1.76	1.46	
	Na	0.53	0.46	0.52	0.49	0.56	
	fe	28.5	38.9	39.8	41.4	55.3	
	an	74.9	76.5	74.8	78.0	72.3	

[a] Cornelis Klein, Jr., analyst.
fe = 100 (Fe + Mn)/(Fe + Mn + Mg).
an = 100 Ca/(Na + Ca).

Table G-3. Modern and historic wet-chemical analyses of cordierite from "Iolite Hill". Analyses, optical data, and probe analyses in Table G-7 all suggest that coarse vein cordierite is more Fe-rich than cordierite within host gedrite rock.

Chemical Analyses			Numbers of Ions on a Basis of 18 (O) exclusive of H_2O		
	134JX-co*	Vein**		134JX-co	Vein
SiO_2	49.29	48.0	Si	5.006	4.836
P_2O_5	0.01	—	P	0.001	—
Al_2O_3	33.45	35.0	Al	0.993	1.164
TiO_2	0.03	—	Al	3.011	2.992
Fe_2O_3	0.58	—	Ti	0.002	—
Cr_2O_3	0.001	—	Fe^{3+}	0.044	—
FeO	3.49	6.0	Fe^{2+}	0.297	0.505
MnO	0.05	1.0	Mn^{2+}	0.004	0.085
MgO	10.00	10.0	Mg	1.513	1.501
CaO	0.14	—	Ca	0.015	—
NiO	0.002	—	Li	0.033	—
Li_2O	0.08	—	Na	0.106	—
Na_2O	0.54	—	K	0.017	—
K_2O	0.13	—	H	1.660	—
$H_2O(+)$	2.45	—	F	0.003	—
$H_2O(-)$	0.46	—			
F	0.01	—			
Totals	100.70	100.0	$\frac{100(Fe^{2+}+Mn^{2+})}{(Fe^{2+}+Mn^{2+}+Mg)}$	16.56	28.25

Optical properties***

	W95JX	134GX	134JX	Vein	
				1.	2.
γ	1.545	1.548	1.548	1.555	1.552
β	1.541	1.543	1.544	1.548	1.549
α	1.536	1.538	1.538	1.542	1.545
$2V_x$ (calc)	80	85-92	75	95	75

* Mahito Kumanomido, analyst, 1968.

** C. T. Jackson, 1844.

*** All values by the authors, except for those from vein no. 2 which are from Moore (1949).

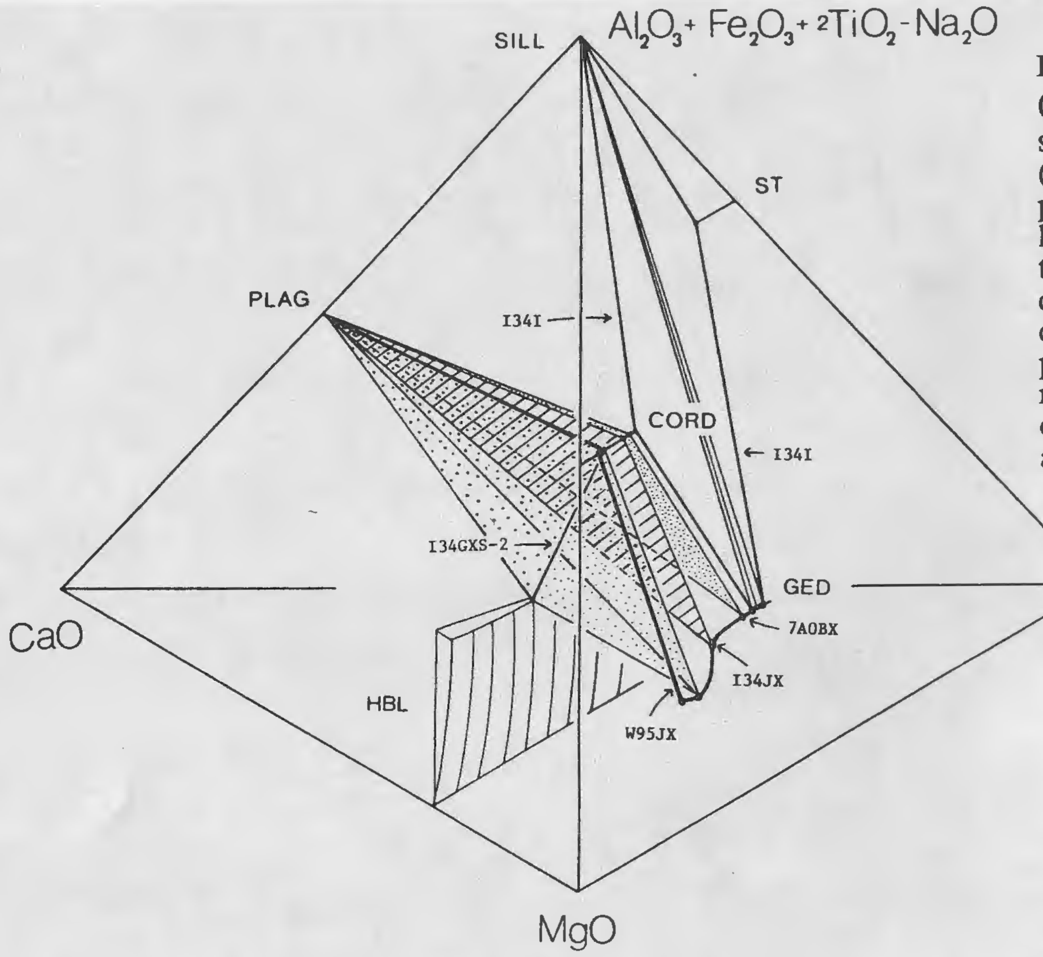
SILL
Al_2O_3+ Fe_2O_3+ $2TiO_2$-Na_2O
ST
PLAG
I34I
CORD
I34I
I34GXS-2
GED
7AOBX
CaO
I34JX
HBL
W95JX
MgO

Figure G-4. The tetrahedron ($Al_2O_3 + Fe_2O_3 + 2TiO_2 - Na_2O$), ($FeO + MgO - TiO_2$), MgO, CaO projected from quartz and H_2O showing representative samples from the "Amphibole Hill area" (Stops 1 and 2). SILL = sillimanite, ST = staurolite, PLAG = plagioclase, CORD = cordierite, GED = gedrite, and HBL = hornblende. For Fe-rich aluminous bulk compositions (I34I) the stable assemblage is staurolite - sillimanite - gedrite, in this case without plagioclase. For more Mg-rich rocks sillimanite disappears and the assemblage becomes cordierite - gedrite - plagioclase (a portion of 7A0BX and I34JX). The most Mg-rich rocks have the uncommon four-phase assemblage hornblende - cordierite - gedrite -plagioclase (I34GXS-2) and the two-phase assemblage gedrite - cordierite (W95JX).

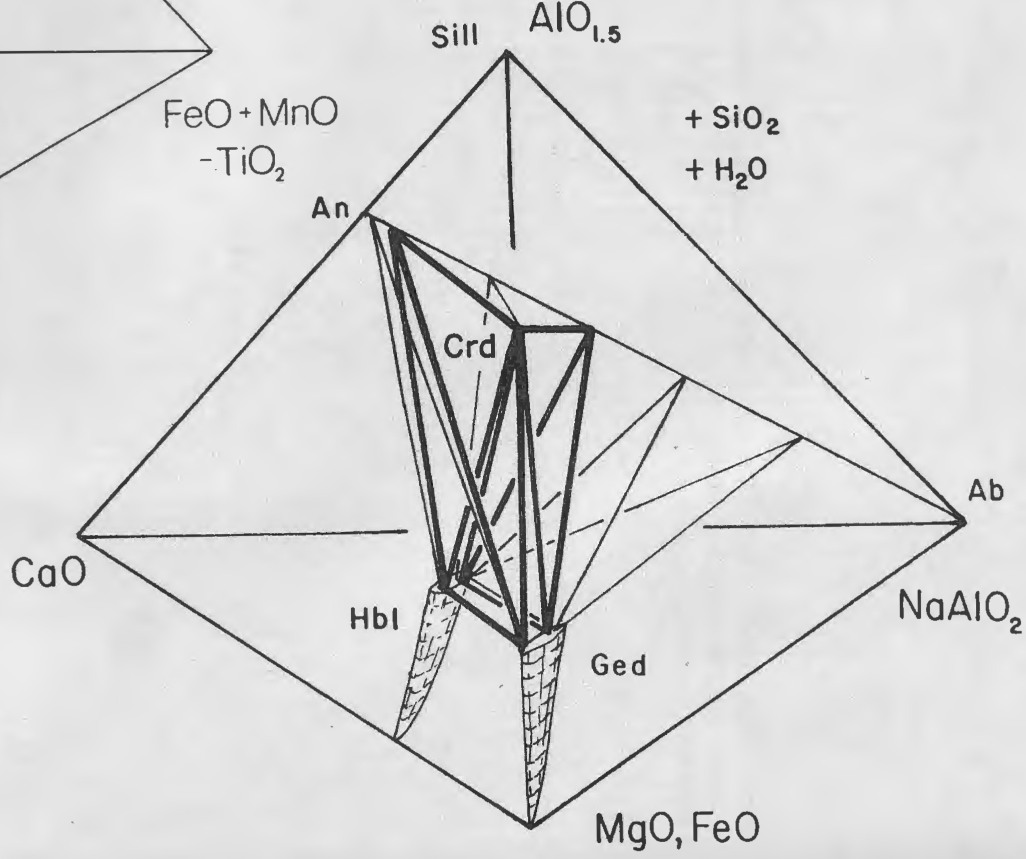
Sill
$AlO_{1.5}$
$FeO + MnO$
$-TiO_2$
$+ SiO_2$
$+ H_2O$
An
Crd
Ab
CaO
Hbl
Ged
$NaAlO_2$
MgO, FeO

Figure G-5. The tetrahedron ($AlO_{1.5}$), (MgO, FeO), CaO, $NaAlO_2$ projected from quartz and H_2O, showing the effect of Na and Ca on phase relations.
An = anorthite, Ab = albite, Crd = cordierite, Hbl = hornblende, and Ged = gedrite. Heavy lines indicate the critical four-phase volumes hornblende - cordierite - gedrite - andesine, in sample 5 (I34EX), and hornblende - cordierite - gedrite - anorthite, in sample 10 (I34GXS-2).

progress to the bulk composition of sample I34I, whereas rocks of similar composition but slightly higher temperature in the Quabbin Reservoir area have the assemblage cordierite + gedrite + garnet without sillimanite.

In 1971, Robinson, Ross, and Jaffe suggested the possibility of finding the assemblage gedrite + cordierite + hornblende + plagioclase in extremely magnesian gedrite rocks. This assemblage was indeed found by Schumacher (1982, 1983) in the matrix of samples from I34G, the same ones that contain enclaves of anorthite-rich plagioclase (see below). The effects of presence or absence of plagioclase in such rocks are illustrated in Figure G-4 and discussed in the caption. The critical factor of a high Ca-Na ratio for the hornblende + cordierite assemblage is also illustrated in Figure G-5.

FEATURES OF CRYSTALLOGRAPHIC INTEREST

Early in their studies Klein (1968) and Robinson and Jaffe attracted the interest of Malcolm Ross and Jim Papike of the U.S. Geological Survey, who undertook extensive X-ray single-crystal investigation of a variety of amphiboles from here and from adjacent central Massachusetts (Ross, Papike, and Shaw, 1969; Papike and Ross, 1970; see also Ghose, 1981, p. 348). Their results in turn provided the background for electron microscope studies of exsolution features (Gittos et al., 1976; see also summary in Ghose, 1981) as well as material for Mossbauer spectroscopy to determine site population of ^{57}Fe atoms (Seifert, 1978). Some of the results of Ross and Papike are summarized below (see also summary in Robinson et al., 1982b)

1) In magnesian hornblende - anthophyllite rocks, hornblende has exsolution lamellae of primitive cummingtonite (at least at room temperature), whereas anthophyllite is commonly a submicroscopic "cryptoperthite" of anthophyllite and gedrite exsolved on (010).

2) In more Fe-rich hornblende - cummingtonite rocks, each clinoamphibole has exsolution lamellae of the other, but both host and lamellar cummintonite is *C*-centered, illustrating the effect of Fe content on the $P \rightarrow C$ displacive transformation.

3) High-Al gedrites including the separate from I34I, on which a complete structure refinement was done, are homogeneous single phases, but somewhat lower-Al gedrites contain anthophyllite exsolution which are just coarse enough for resolution under the optical microscope (Robinson, Ross, and Jaffe, 1971). These studies provided the first report of the anthophyllite - gedrite miscibility gap, earlier predicted by J.B. Thompson, in this case in exsolved "hypersolvus" amphiboles (this guidebook, Figure D-11). This was followed within months by the discovery of coarse coexisting (subsolvus) orthoamphiboles from Norway by Stout (1970). The compositions of studied orthoamphiboles from the field-trip area and adjacent parts of Massachusetts are summarized in Figure G-6 together with interpolated estimates of fine-lamellae compositions. The structure refinement of gedrite showed that increase of octahedral Al is almost entirely at the expense of Mg in the M2 octahedral site and thus that coexisting anthophyllite and gedrite can have identical Fe content. This is reflected in the plot of *b* cell dimensions (Figure G-7, see also this guidebook, Figure D-10).

4) Although the exsolution lamellae in the hornblendes and cummingtonites are indexed as $\bar{1}01$ and100 on the basis of lattice images using the *C*-centered monoclinic cell, Jaffe et al. (1968; see also Robinson et al., 1982b, pp 57-61) showed that the lamellae would be indicated as 001 and 100 using the most commonly described relations between optic orientation and crystallographic axes. However, detailed measurement of the angles of the lamellae showed that they are not in fact on rational planes but only close to 001 and 100, and this led to the formulation of the exact boundary theory to explain their orientations (Robinson et al., 1971a; Jaffe et al., 1975; Robinson et al., 1977; see also summary in Robinson, 1980).

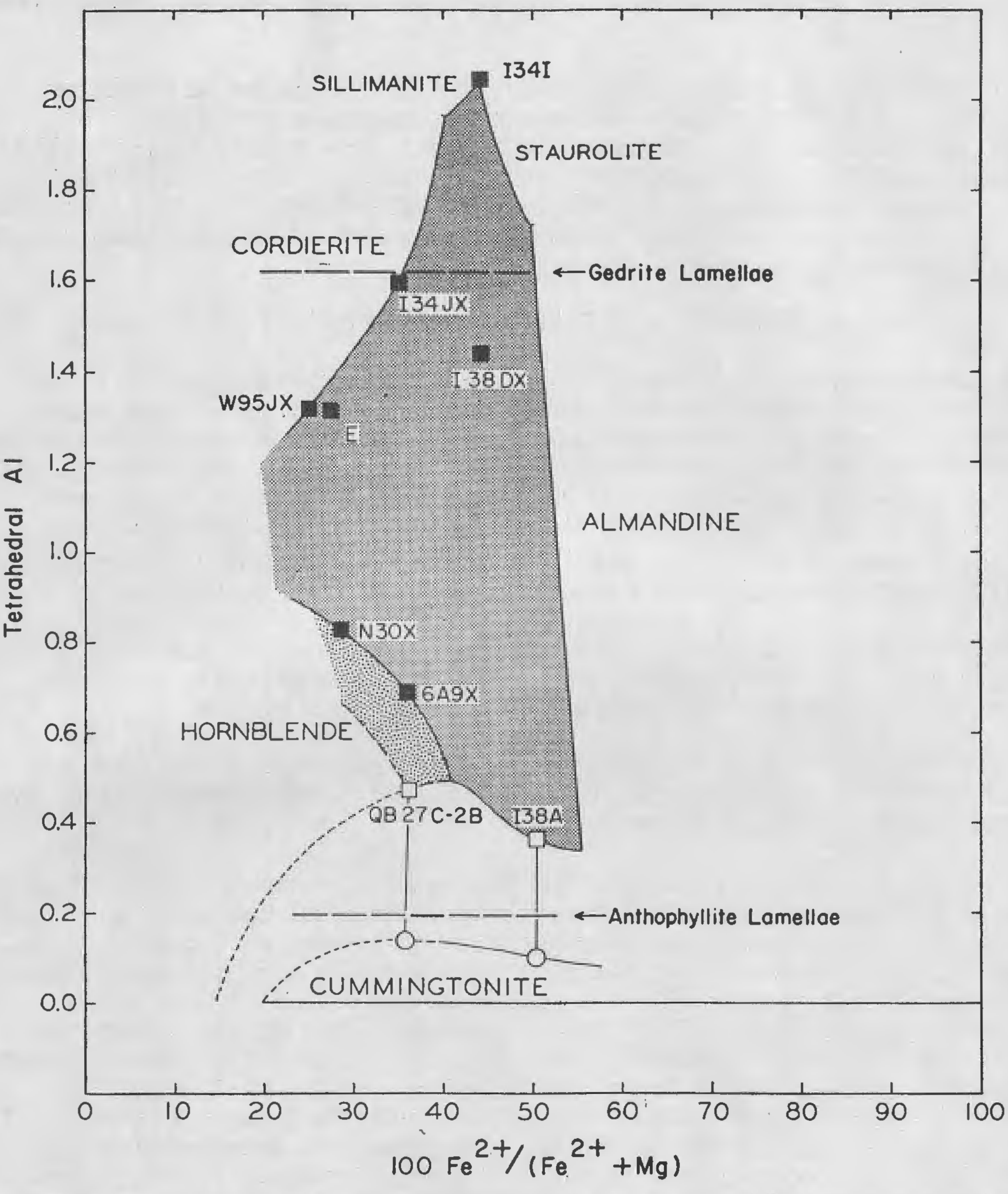

Figure G-6. Composition field of anthophyllite-gedrite in terms of Fe^{2+}/Mg ratio and tetrahedral Al for primary metamorphic conditions in the sillimanite zone ("Amphibole Hill Area"), southwestern New Hampshire and adjacent Massachusetts. Mn^{2+} is included in Fe^{2+}. Boundaries of the field are defined by the coexistence of orthoamphibole (± plagioclase) with various other phases. Closed squares, wet analyses; open squares, probe analyses of anthophyllites; open circles, probe analyses of cummingtonites. Tetrahedral Al contents for secondary anthophyllite and gedrite exsolution lamellae are inferred.

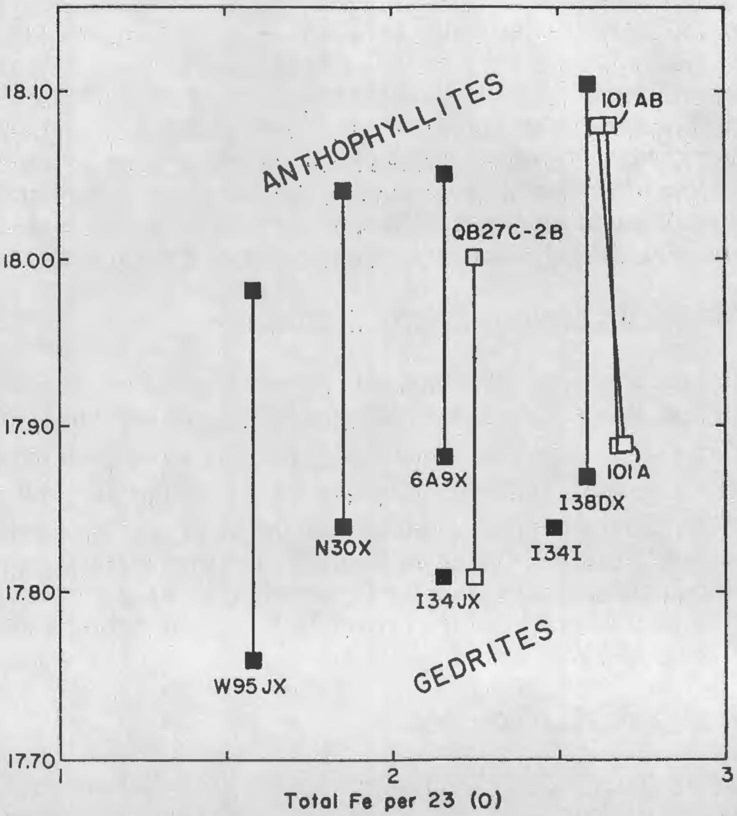

Figure G-7. *b* dimensions from single crystal X-ray photographs of anthophyllites and gedrites plotted against total Fe per 23(O). Closed squares, wet analyses; open squares. probe analyses. Vertical tie lines connect *b* dimensions of the two members of a microscopic or submicroscopic intergrowth for which only the bulk Fe content is known. Assemblages 101A and 101AB from Stout (1970b, c) contain two coarse coexisting orthoamphiboles in which the compositions of each can be determined separately. These four analyses suggest that fractionation of Fe between coexisting anthophyllite and gedrite is probably slight and that the vertical tie lines applied to the other specimens are reasonable (see also Spear, this guidebook, part D).

GEOCHEMISTRY OF AMMONOOSUC VOLCANICS

Summary of Ammonoosuc Stratigraphy

The Middle Ordovician Ammonoosuc Volcanics are interpreted to be Ordovician island arc volcanics, which were deposited during the Taconian Orogeny, and which were later metamorphosed to amphibolite facies during the Devonian Acadian Orogeny. In Massachusetts and New Hampshire they occur above gneisses in the domes and below the Partridge Formation, and possess an internal stratigraphy of four members in ascending order: Moosehorn Conglomerate (local basal quartz-pebble conglomerate); Lower Member (amphibolites, K-poor felsic gneisses, and minor marble); Garnet-Amphibole-Magnetite Quartzite (discontinuous layer of metamorphosed chert); Upper Member (biotite-quartz- feldspar gneisses containing garnet, muscovite, and kyanite or sillimanite). The stratigraphic section ranges in thickness from 0 to 1200 meters, and orthoamphibole and cummingtonite are common through much of the section.

Chemical Distinction between the Lower and Upper Members

In general felsic rocks of the Upper Member with greater than 63 wt. % SiO_2 contain larger amounts of K_2O and Rb than those of the Lower Member (Schumacher, 1983). The Upper-Member K_2O contents are greater than 1 wt. %, and only three samples from the Lower Member have values in this range. Two of these high-K_2O rocks are atypical of the Lower Member. One is from a unique lens of kyanite schist in amphibolite, and the other is a felsic clast that occurs in a chlorite-rich matrix from near the top of the lower Member, and may represent a piece of Upper Member rock. In addition the felsic rocks from the Upper Member have a more restricted range of K/Rb ratios (260 to 440) than felsic rocks of the Lower Member and mafic rocks from both members (200 to 2280) (Fig. G-8).

Original Versus Modified Igneous Compositions

General geochemical characteristics. The processes most likely to have modified these volcanic rocks are: 1) mixing of water-laid volcanic material (ash) with sedimentary material, 2) weathering, 3) low-temperature hydrothermal alteration, and 4) high-temperature hydrothermal alteration. Because the only equivalents of chemical and particulate sediments are the carbonate horizons, the garnet quartzite, and the unique schist lens, and because these horizons occupy special stratigraphic positions and are either absent or very minor parts of the total section, mixing of the volcanic ash and sediments (clay and carbonate) is not likely to have been extensive. Weathering, high- and low-temperature alteration seem to have been the most likely processes.

Mafic rocks. A summary of low-temperature seawater alteration of basaltic rocks (Scott and Hajash, 1976) and an additional study by Andrews (1977) indicate Ca, Mg, and Na are lost by mafic rocks, and K is gained. Several studies of surface weathering of basalt cited by Loughman (1969) indicate Ca, Mg, and Na are lost from the rock, an effect similar to that of low-temperature seawater alteration.

Experimental studies of seawater-basalt interactions at high-temperatures (Bischoff and Dickson, 1975; Mottl, 1976; Seyfried and Bischoff, 1981; Seyfried et al., 1982) and studies of ocean floor basalts (Humphris and Thompson, 1978; Mottl, 1983) indicate Ca and K are lost from basalt while Mg is gained. Mottl (1983) states that this Ca-Mg exchange is on a mole-for-mole basis. In addition Na can be gained by basalt undergoing high-temperature seawater alteration at water-to-rock ratios less than 10 (see Mottl, 1983, for discussion).

Humphris and Thompson (1978) and Mottl (1983) have used plots of CaO versus MgO (wt.%) to distinguish fresh from high-temperature, hydrothermally altered basalts. These oxides

Table G-4. Major- and trace-element analyses of amphibole-bearing rocks at Stops 1 and 2 of trip G as well as two samples of gedrite gneiss from near Stop 1 of trip H. The first group of analyses are of anthophyllite and gedrite-bearing gneisses from Stop 1 (see description) that represent metamorphosed hydrothermally altered basalts. The second group of analyses are of gedrite rocks from Stop 2 (7A0BX) and from Quabbin Reservoir area (Q144B, Q544X). The third group of analyses are of rocks at Stops 1 and 2 believed to have relatively little-altered primary basaltic composition (I34A, 6A9) and andesitic composition (7A8).

#	I34EXA	I34EXB	I34DX	I34CX	I34BXY	W95JS	7A0BX	Q144X	Q544X		I34A	6A9	7A8
SiO_2	45.50	47.05	47.79	47.83	48.10	48.25	55.67	57.06	69.84		48.17	50.36	56.04
TiO_2	1.38	1.18	0.98	0.97	0.97	1.38	0.87	0.76	0.50		1.32	0.60	1.18
Al_2O_3	18.74	15.42	13.60	13.70	15.83	17.52	17.44	15.93	13.91		15.51	16.43	13.58
Fe_2O_3	13.71	14.35	13.24	13.11	11.34	12.13	2.83	2.85	5.82		5.10	3.26	3.87
FeO							9.57	10.19	5.97		7.31	8.05	9.06
MnO	0.31	0.33	0.34	0.25	0.23	0.19	0.08	0.25	0.14		0.21	0.32	0.16
MgO	17.43	18.87	18.59	18.88	15.16	18.54	8.70	8.12	3.61		8.83	9.70	4.04
CaO	0.80	0.84	3.65	2.56	5.81	0.56	0.88	2.13	0.22		9.37	8.02	6.13
Na_2O	1.42	1.13	0.68	0.63	0.91	0.42	1.12	2.64	0.41		3.79	2.62	4.50
K_2O	0.14	0.10	0.32	0.12	0.14	0.07	1.40	0.05	0.11		0.14	0.39	0.15
P_2O_5	0.07	0.05	0.09	0.09	0.09	0.07	0.08	0.10	0.09		0.10	0.08	0.16
Total	99.50	99.32	99.28	98.14	98.28	99.13	98.64	99.69	100.62		99.34	99.50	98.87
Y	19	20	16	23	17	39	11	18	34		28	13	15
Sr	10	11	2.9	13	36	25	28	106	7.6		166	82	86
Rb	6.6	5.0	9.8	4.5	3.9	4.0	26	1.4	4.7		1.0	4.8	1.1
Th	0	1	0	2	2	1	1	3	3		0	2	2
Pb	27	23	27	25	57	11	45	6	5		13	14	12
Ga	21	19	20	16	15	18	17	17	16		19	21	18
Nb	2.0	2.1	1.4	2.2	1.1	3.5	2.2	2.1	3.3		10	1.9	2.0
Zr	66	58	49	50	41	89	37	35	74		67	28	38
Zn	928	723	302	185	159	139	159	188	74		99	415	122
Ni	89	70	476	354	113	47	15	15	4		105	60	10
Cr	268	215	1073	761	390	203	41	63	17		308	200	17
V	336	328	249	252	198	295	315	259	65		331	312	535
Ba	49	11	197	61	57	0	1575	17	21		6	20	1
					CIPW NORMS								
QZ	1.21	1.73		2.46	0.53	10.02	21.15	16.39	53.72	QZ			5.22
OR	0.83	0.59	1.89	0.71	0.83	0.41	1.18	8.27	0.30	OR	0.83	2.30	0.89
AB	12.02	9.56	5.75	5.33	7.70	3.55	9.48	22.34	3.47	AB	27.14	22.17	38.08
AN	3.51	3.84	17.52	12.11	28.24	2.32	3.84	9.98	0.50	AN	24.90	31.92	16.41
COR	14.97	12.05	5.71	8.09	3.83	15.90	12.67	7.88	12.93	NE	2.67	3.09	
EN	43.42	47.00	44.52	47.03	37.76	46.18	21.67	20.22	8.99	COR		1.75	
FS	17.55	18.82	16.93	17.28	15.25	15.11	17.61	19.12	16.93	WO	8.77	1.21	5.41
FO			1.25							EN DI	4.85	14.10	1.98
FA			0.53							FS DI	3.59	9.70	3.54
MT	1.99	2.07	1.91	1.90	1.64	1.75	1.96	2.06	1.81	EN		5.82	8.08
IL	2.62	2.24	1.86	1.84	1.27	2.62	1.65	1.44	0.95	FS		4.41	14.40
AP	0.16	0.12	0.21	0.21	0.21	0.16	0.19	0.22	0.21	FO	12.01	1.84	
										FA	9.81	1.14	
										MT	2.78	0.17	2.02
										IL	2.51		2.24
										AP	0.22		0.37

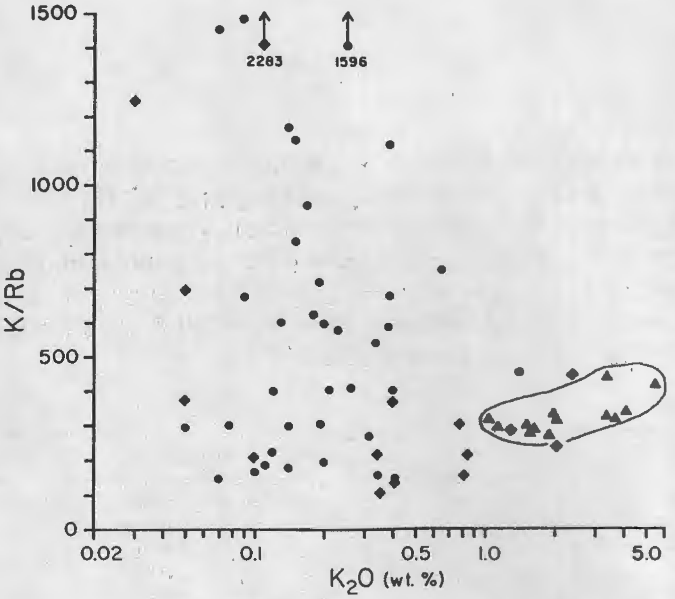

Figure G-8. Plot of K/Rb ratio versus K_2O for all analyses from the Ammonoosuc Volcanics. Key: filled circles, mafic rocks from the Upper and Lower Members; filled diamonds, felsic rocks from the Lower Member; filled triangles enclosed by a line, felsic rocks from the Upper Member.

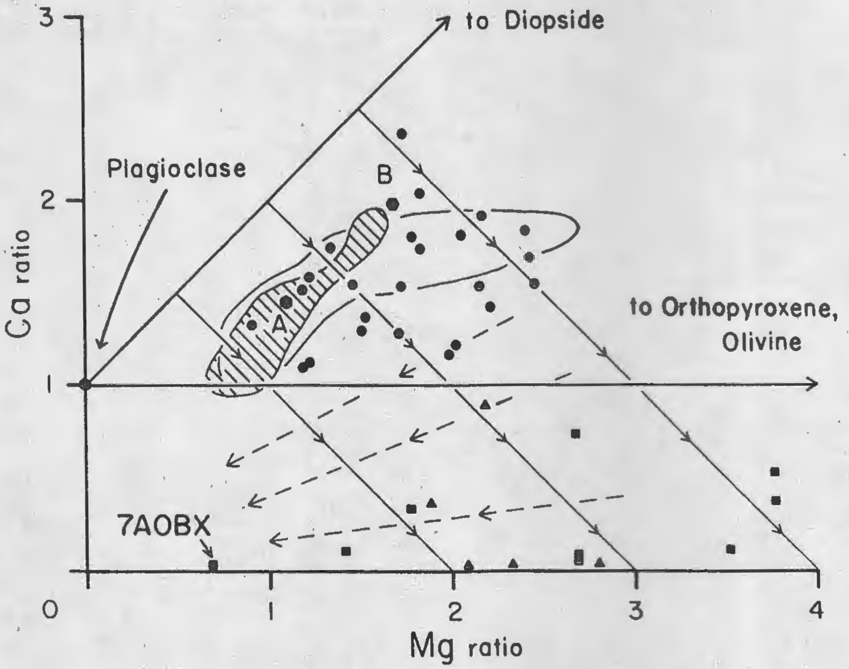

Figure G-9. Plot of the atomic proportions of Ca/[(Al-Na-K)/2] (Ca ratio) versus Mg/[(Al-Na-K)/2] (Mg ratio). Key: filled hexagons, average basalt (B) and andesite (A) (Nockolds, 1954); filled triangles, hydrothermally altered ocean ridge material (Mottl, 1983); area of the closed line, island arc basalt reference suite and ruled area, ocean floor basalt reference suite (Basaltic Volcanism Study Project, 1981); filled circles, Ammonoosuc analyses with less than 63 wt. % SiO_2 believed to represent original compositions; filled squares, Ammonoosuc samples with less than 63 wt. % SiO_2 believed to be hydrothermally altered. Solid lines with multiple arrowheads show changes in composition due to one-to-one exchange of Mg in seawater for Ca in basalt. Dashed lines show the composition changes due to low-temperature hydrothermal alteration and weathering.

that are both lost from basalt during weathering and low-temperature seawater alteration, can also be used to identify the effects of these processes.

The behavior of the Mg and Ca in the Ammonoosuc Volcanics is shown on a plot (Fig. G-9) of the atomic proportions of Ca/(1/2 Al-1/2Na-1/2K) versus Mg/(1/2 Al-1/2 Na-1/2K) for analyses with less than 63 wt. % SiO_2 (some listed in Table G-4). The Ammonoosuc samples (filled circles) are compared with modern rocks of similar SiO_2 contents, representative ocean floor and island-arc rocks (Basaltic Volcanism Study Project, 1981), and hydrothermally-altered rocks from the Mid-Atlantic Ridge (triangles) (Mottl, 1983). This comparison shows only that modern mafic volcanics exist that have similar CaO and MgO contents to the Ammonoosuc Volcanics and that these rocks fall in a region on the diagram described by plagioclase, diopside, orthopyroxene, and olivine. The MgO-rich and CaO-poor Ammonoosuc compositions (filled squares) are like those of hydrothermally altered basalts from the Mid-Atlantic Ridge, and plot below the plagioclase-(olivine-orthopyroxene) line. These compositions could have been derived by high-temperature seawater alteration that involves one-to-one exchange of Mg in seawater for Ca in basalt.

Sample 7A0BX (Fig. G-9) is a cordierite-gedrite rock with significant garnet. Its chemistry suggests that high-temperature alteration was followed by low-temperature seawater alteration. This sample contains low CaO (0.88 wt. %) and relatively high MgO (8.7 wt. %), which is the evidence for the high-temperature hydrothermal alteration. However, 7A0BX has about half the MgO of other altered rocks with comparable Ca contents, which can be explained by subsequent low-temperature hydrothermal alteration, as can its anomalously high K_2O (1.4 wt. %), high Rb (26 ppm), and Pb (45 ppm) (Hart, 1970; Thompson, 1973; Scott and Hajash, 1976). The geochemistry of the hydrothermally altered and essentially original mafic compositions (Fig. G-9) is reflected in the upper-amphibolite facies mineralogy. The rocks with unaltered compositions are chiefly hornblende-plagioclase amphibolites, whereas those that are more Mg-rich also contain subordinate amounts of orthoamphibole or cummingtonite. Rocks with altered compositions all have orthoamphibole (±cordierite) as the dominant mafic phase.

Rare earth element (REE) determinations (R. F. Dymek, personal communication, 1986) were recently completed on the rocks suspected of being hydrothermally altered, and two of the associated "normal" amphibolites. These results have not yet been fully studied, but the chondrite-normalized REE patterns are presented in Figures G-10A and G10B. In Figure G-10A, showing samples from locality I34, light REE's show considerable variation at the light end. There is a Eu anomaly that varies from positive to negative; and heavy REE's show a tighter clustering. Sample W95 (Fig. G-10B) has similar high MgO values to most of the I34 samples, but the heavy REE's are present in distinctly higher concentrations. Samples 6A9 and 7A0BX have very similar REE patterns, but their mineralogies and major element analyses (Table G-4) are extremely different. These samples come from outcrops about 100 m apart, and 7A0BX could represent a hydrothermally altered version of 6A9. There appear to be distinctions in REE's from locality to locality that are maintained despite differences in major element chemistries, and the process that caused Mg enrichment and Ca depletion in these rocks appears to have had only minimal effect on the REE's.

Chemical classification. Ammonoosuc analyses that are believed to have original chemistry are classified (Fig. G-11) according to the K_2O-SiO_2 (wt. %) scheme in the Basaltic Volcanism Study Project (1981), which is similar to that of Ewart (1979). Analyses of the Lower Member belong to the low-K group of basalts, basaltic andesites, andesites, dacites, and rhyolites. The felsic rocks of the Upper Member are a dacite and rhyolites of normal-K content.

Geochemical comparisons of mafic rocks. Multiple element comparison of the Ammonoosuc basaltic rocks (48-52 wt. % SiO_2) with modern basalts from various tectonic settings can be done by using the approach of Sun (1980), in which minor and trace elements are normalized to mantle

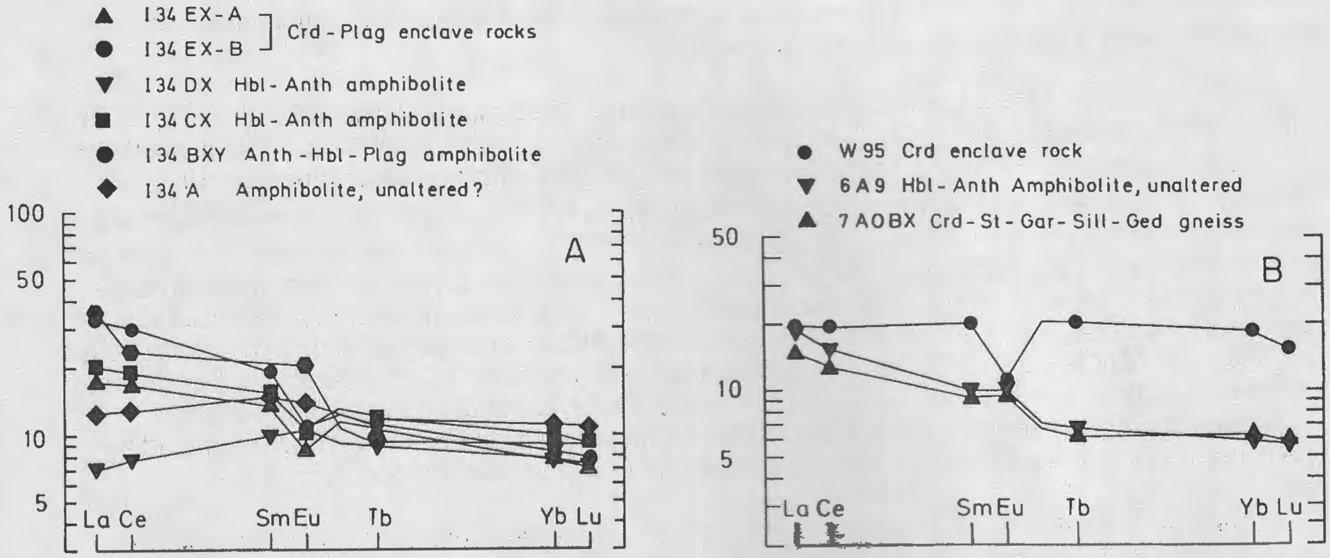

Figure G-10. Plots of normalized rare earth element (REE) abundances for rocks believed to be hydrothermally altered and two samples (I34A & 6A9) believed to represent original basaltic compositions.

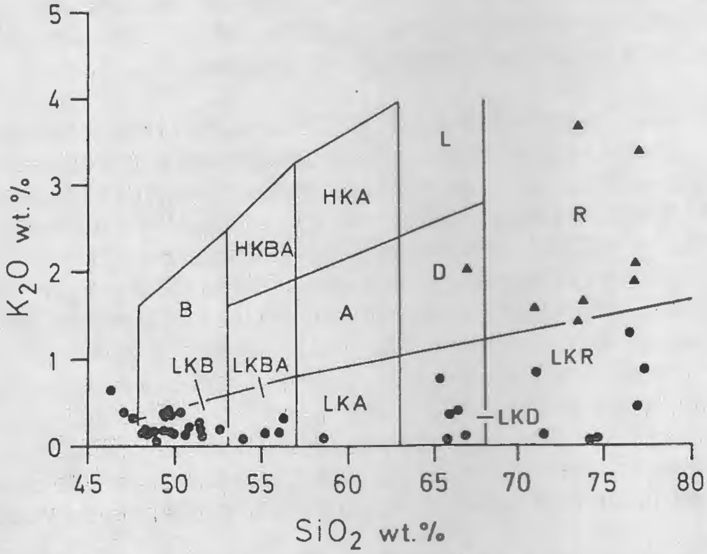

Figure G-11. Plot of K_2O versus SiO_2 for all analyses of the Ammonoosuc Volcanics believed to have original compositions. Key: filled circles, mafic rocks and Lower Member felsic rocks; filled triangles, Upper Member felsic rocks. Chemical classification scheme is from the Basaltic Volcanism Study Project (1981): LKB = low-K basalt, LKBA = low-K basaltic andesite, LKA = low-K andesite, LKD = low-K dacite, LKR = low-K rhyolite, B = basalt, BA = basaltic andesite, A = andesite, D = dacite, R = rhyolite, HKBA = high-K basaltic andesite, HKA = high-K andesite, L = latite.

abundances in an analogous fashion to rare earth element diagrams. Figure G-12A gives the range of values and averages of elements (Rb, Ba, Nb, K, Sr, P, Zr, Ti, and Y) in Ammonoosuc rocks. In Figure G-12B the average Ammonoosuc values are compared with average enriched (e-MORB) and depleted (d-MORB) mid-ocean ridge basalts (Sun, 1980), and average Hawaiian tholeiite (Basalt Volcanism Study Project, 1981). In Figure G-12C the average Ammonoosuc values are compared with average island arc tholeiite (IAT), averaged high-Al, alkaline, and calc-alkaline basalts from island arcs (Sun, 1980), and average basalt from the New Britain island arc (Basaltic Volcanism Study Project, 1981). The Ammonoosuc samples display the same low trace-element contents and significant enrichment of K relative to Nb common to the island arc samples but absent in the other basalt types (see also Thirlwall and Bluck, 1984, their fig. 2).

Geochemical comparisons of the felsic rocks. Multiple element comparisons for the felsic Ammonoosuc rocks can also be done using the normalization factors of Sun (1980). The range and average values for elements (Rb, Ba, Th, Nb, K, Sr, P, Zr, Ti, and Y) in Ammonoosuc rocks believed to have original compositions are shown for the Upper Member and Lower Member in Figure G-13. In the Upper Member rocks, Rb, Ba, Th, and K values are roughly equal and significantly higher than Nb (Fig. G-13a). The Lower Member rocks are shown in two groups. Type A rocks show a pattern similar to the Upper Member rocks, but with consistently lower values of Rb, Ba, Th, and K values roughly equivalent to Nb, while the Th is higher (Fig. G-13c). Partial melting of mafic island arc material is one way to generate the element patterns of the rhyolites and dacites of the Ammonoosuc Volcanics. Rhyolites from the Bismarck Archipelago, Papua New Guinea, which are considered by Smith and Johnson (1981) to be derived from partial melting of island arc material (Fig. G-13d) have similar patterns to the Upper Member and type-A Lower Member felsic rocks (Fig. G-13a and c). In addition, experimental melting of basalts at PH_2O = 5 kbar and T = 700-1000 °C by Helz (1976) indicates it is possible to derive felsic liquids with K_2O contents very similar to the New Guinea examples and the felsic rocks from the Upper Member of the Ammonoosuc Volcanics.

Despite the similarity in elemental patterns, differences that argue against a common source for the Upper Member and type-A Lower Member exist. The Upper Member has generally higher values of K, Ba, and Rb, than those of the Lower Member. If they had a common source, this would suggest that the Lower Member was generated by larger percentages of partial melting. The Y content of the Upper Member rocks should also be greater; however, the reverse is true. This suggests that, although the sources were generally similar, minor differences existed, and that the felsic rocks from the Upper Member and Lower Member were probably not generated by partial melting of the same material.

The type-B Lower-Member felsic rocks with extremely low Rb, Ba, and K are problematic. With the exception of these three elements, the normalized element concentrations are comparable to type-A Lower Member felsic rocks (Figs. G-13b and c). If type-B rocks also represent partial melts, then their source must have had much lower values of Rb, Ba, and K. Alternatively, an alteration process that did not affect type-A felsic rocks may have acted on type-B rocks at some point in their complicated history.

Pearce et al. (1984) suggested that Rb, Ta, Y, and Nb are useful elements for distinguishing granitic rocks from ocean ridges (ORG), volcanic arcs (VAGS), within plates (WPG), and areas of plate collision (COLG). Figure G-14 compares Rb versus Y+Nb contents of the Upper Member and Lower Member felsic rocks with the granite fields of Pearce and others (1984). Although the Ammonoosuc felsic rocks are interpreted to be extrusive rather than intrusive, and hence cannot be strictly compared with the data base of Pearce et al. (1984), they are chemically equivalent to granites and fall within the volcanic arc field (Fig. G-14). This is consistent with the immediately preceeding implications, with the interpretations of the geological setting, and with the chemical data from the accompanying basaltic rocks.

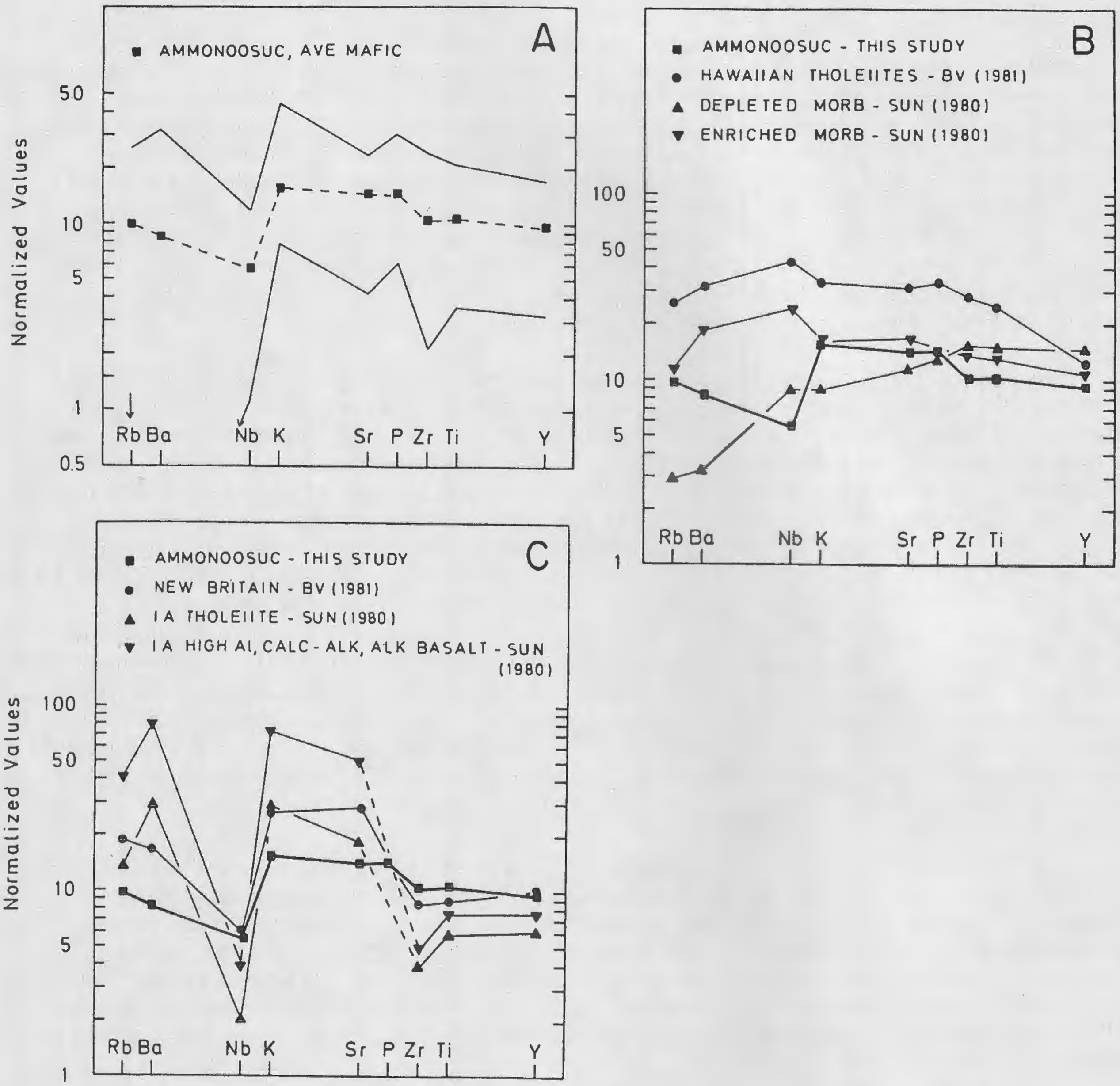

Figure G-12. Mantle normalized element abundances of Rb, Ba, Nb, K, Sr, P, Zr, Ti, and Y. Normalizing factors from Sun (1980). Part A. Range (lighter lines) and average values (filled squares) of basaltic Ammonoosuc rocks (SiO_2 48-52 wt. %). Part B. Comparison of average Ammonoosuc values with enriched mid-ocean ridge basalt (MORB), depleted MORB (values from Sun, 1980), and average Hawaiian tholeiites (Basaltic Volcanism Study Project, 1981). Part C. Comparison of average Ammonoosuc values with average island arc tholeiite and the average of combined high-Al, calc-alkaline, and alkali basalts from island arcs (values from Sun, 1980), and average basalt from the New Britain island arc (Basaltic Volcanism Study Project, 1981).

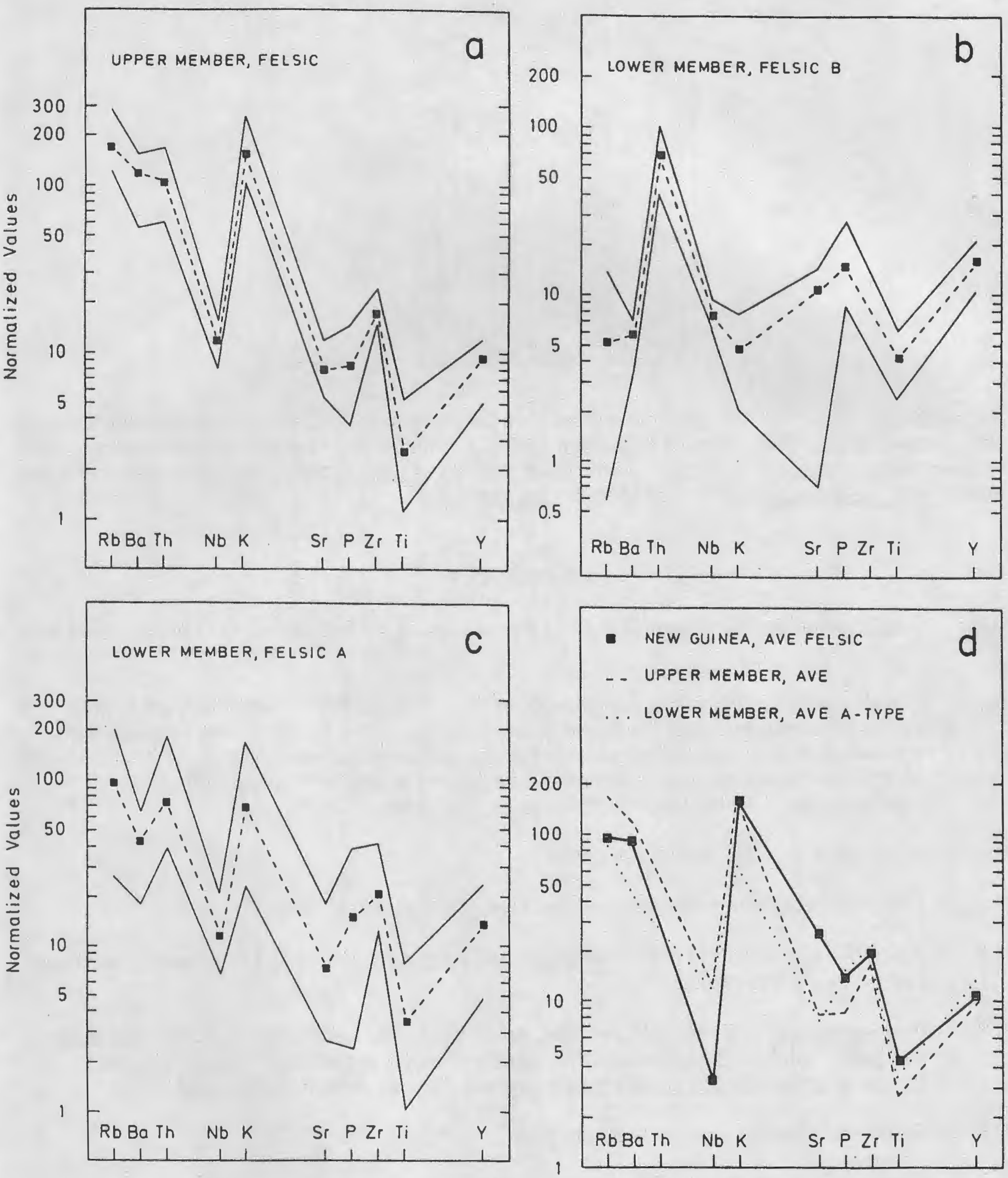

Figure G-13. Mantle normalized element abundances of Rb, Ba, Th, Nb, K, Sr, P, Zr, Ti, and Y. Normalizing factors from Sun (1980). Part a. Range (lighter lines) and average values (filled squares) of Upper Member felsic Ammonoosuc rocks. Part b. Range (lighter lines) and average values (filled squares) of Type-A Lower Member felsic Ammonoosuc rocks. Part c. Range (lighter lines) and average values (filled squares) of Type-B Lower Member felsic Ammonoosuc rocks. Part d. Range (lighter lines) and average values (filled squares) of rhyolites and dacites from the Bismarck Archipelago, Papua, New Guinea (Smith and Johnson, 1981, their Table 1, nos. E2/10, F6/3, F7/14, Gs1/7, Gs1/8, Gs3/4).

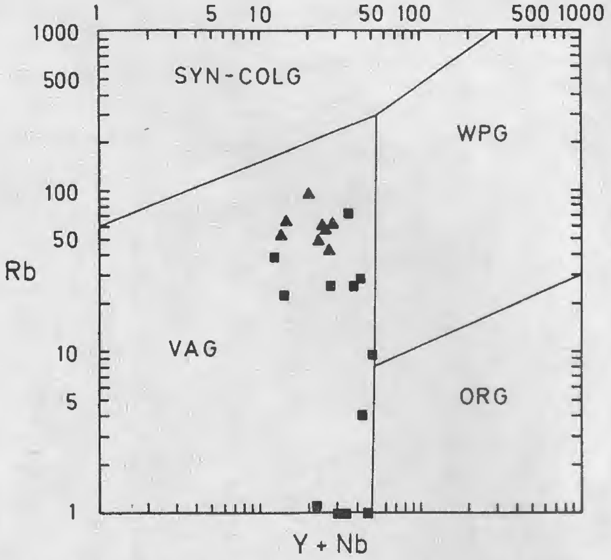

Figure G-14. Rb - (Y+Nb) discriminant diagram for granitic rocks from various tectonic settings after Pearce et al. (1984). Syn-COLG = syn-collision granites, VAG = volcanic arc granites, ORG = ocean ridge granites, and WPG = within plate granites. Filled triangles are Upper Member felsic rocks, and filled squares are Lower Member felsic rocks.

ITINERARY

0.0	Begin at junction of Gilsum Road and Route 12A. Turn left (south) off Gilsum Road onto Route 12A.
0.3	End of swing bridge across Ashuelot River. Outcrops to left on west bank are mainly coarse Oliverian gneiss of the Keene dome but at the east edge are coarse gneisses with orthoamphibole (or secondary chlorite) characteristic of the lower part of the Ammonoosuc Volcanics. Mapping of such a contact, alleged elsewhere to be an unconformity, represents the supreme level of difficulty in this region.
2.8	Road cut both sides. Oliverian gneiss.
3.7	Entrance left to Surry Mtn. Recreation Area. Stay on Route 12A.
4.9	Sharp left turn (160°) at brown wooden signs (letters on other side) and proceed northeast toward Surry Mtn. dam.
5.4	Parking place at entrance to Surry Mtn. dam. Walk 100 feet north to Lunch under trees and public toilet, and 300 feet north to dam and large exposures of Oliverian gneiss. Return to vans after 40 minutes maximum and drive soute on entrance road.
5.9	Stop sign. Continue south on Route 12A
7.8	Intersection at stop light. Stay straight on Route 12A.
8.5	Interchange with Route 12. Turn left (south) on Route 12.
9.8	Junction interchange with Route 10. Stay on Route 12.
11.3	T junction with Route 9. Turn left (east) on Route 12.

11.8 Stoplights. Stay straight on Route 12.

12.5 More stoplights. Turn right (south) on Route 12.

13.4 Junction with Route 32. Not well marked. Turn right on Route 32.

14.3 Keene airport on right.

16.5 "Potash Bowl" on right. Swanzey Center.

25.3 Richmond Four Corners. General Store and junction of route 119. Turn right (west) on Route 119.

25.9 Turn left (south) on good gravel road beyond conspicuous turnout on right.

26.8 House at edge of swamp and wrecked cars. Automobiles should stop at this point because next segment involves fording a swamp on a branch of Sprague Brook. Continue west on road through swamp and across higher ground beyond.

27.4 Junction and fork in road. Park near iron gate. Passable branch of road goes down hill to right (west) – do not go this way. Iron gate blocks washed out area and approach to twin bridges with beaver dam across Sprague Brook. Walk south across bridges and up the excellent road on the north slope of "Parker Hill" to prominent stone lane on left (8-10 minutes). Turn left (east) and follow middle of three obscure wood tracks to "Harris Soapstone Quarry". Outcrop W95 lies about 150 feet north (left) from soapstone quarry.

STOP 1: "IOLITE HILL" (One hour and 45 minutes)

Historical Note

The coarse cordierite-quartz vein near the old Harris soapstone quarry in the southwest part of Richmond, New Hampshire, has been known for more than one hundred years, and an analysis of the cordierite was published by Jackson in 1844. B.K. Emerson (1895) collected a specimen of gedrite-rutile rock "on the hill 20 rods south of Harris' soapstone quarry" and had a complete chemical analysis done both on the rock and on a purified gedrite separate. This analysis was later listed by Rabbitt (1948) among superior analyses of orthoamphibole. In spite of Emerson's accurate field description of the locality, the specimen was listed as coming from Warwick, Massachusetts. In 1898 Emerson indicated that the specimen had been "wrongly cited from Warwick" in the 1895 paper and that it actually came from the west slope of Tully Mountain in Orange, Massachusetts. To compound the confusion further, the analyses were listed again in Emerson's report of 1917, and the locality was given as Richmond, Vermont (this guidebook, Part B, mile 66.4). Moore (1949) suggested that Emerson's specimen was from the well known locality in Richmond, New Hampshire. He showed that the poor grade of "soapstone" in the quarry was the result of retrograde metamorphism of the anthophyllite in anthophyllite rock and anthophyllite-hornblende rock to a mixture of talc and chlorite, and included these rocks in the Ammonoosuc Volcanics of Middle Ordovician age. These conclusions of Moore were confirmed by Robinson (1963). Moore also reported indices of refraction for the vein cordierite (see below) located 150 feet north of the quarry. While working as field assistant for Moore in the 1940's, J.B. Thompson, Jr. observed the sillimanite-cordierite pegmatite at outcrop I34 and was present in the 1970's at the discovery of dumortierite in the same rock. Robinson (1963) did a more thorough sampling both in the vicinity of the quarry and on the hilltop to the south. Within the gedrite rock he found a thin layer consisting of quartz, gedrite, sillimanite, staurolite, biotite, garnet, and ilmenite (specimen I34I). Later, a gedrite separate was obtained from this sample for wet chemical analysis (Robinson and Jaffe, 1969a), was used by Papike and Ross (1970) for a complete structure refinement of gedrite, and was used by Seifert (1978) for studies of Mossbauer spectra. Another specimen (I34G) was reported as anthophyllite-plagioclase gneiss, but reexamination of the same thin section in 1966 showed that most of the white (in hand specimen) polysynthetically twinned mineral is cordierite.

Four large specimens (I34GX, I34JX, W95JX, W95JY) were collected by Robinson and Jaffe in the summer of 1966. Kyanite, sillimanite, corundum, and staurolite were first found in heavy fractions derived in the process of purifying gedrite and cordierite for wet chemical analyses and were later found in place in some of the thin sections of the same specimens. These discoveries led to a paper on the textural relations and petrogenesis of these aluminous enclaves (Robinson and Jaffe, 1969a) which tied in closely with experimental work then in progress by Schreyer and Seifert (1969a, 1969b). Schumacher (1981b, 1983) took the obvious next step of performing electron probe analyses of enclave and host minerals. Discoveries made in this process included the extremely anorthite-rich composition of plagioclase, the association of cordierite and hornblende, very magnesian staurolite, zincian spinel and zincian staurolite, and occurrences of blue sapphirine in cordierite and green sapphirine in anorthite.

Among the samples studied by Ross et al. (1969), one obtained at Stop 1 (I34BX) included iridescent anthophyllite with no optically visible exsolution lamellae that is a two-phase anthophyllite - gedrite mixture. Curiously the bulk composition is virtually identical to the iridescent anthophyllite from West Greenland collected in 1810 and first described by Bøggild (1905, 1924) (see Robinson, Ross, and Jaffe, 1971). Hornblende from the same sample contains visible "001" and "100" exsolution lamellae that are primitive cummingtonite. Gedrite W95 contains X-ray evidence of anthophyllite - gedrite exsolution parallel to (010) but at a scale visible in the optical microscope, the second such occurrence observed.

Description of Outcrops

Outcrop W95 (30 minutes) is an area where mineral collectors over the years have done rather extensive excavating and blasting in the search for fresh, blue cordierite which has escaped pinitization. This cordierite occurs as small to large euhedral crystals and continuous reaction rims on quartz veins cutting through coarse gedrite - cordierite - biotite gneiss. One outcrop shows the surface of such a vein for several square meters. This cordierite is generally more Fe-rich than the less obvious Mg-rich cordierite in the matrix of the rocks (see Table G-3) and seems to have been produced by addition of SiO_2 to gedrite-rich rock rather late in the reaction trend leading to cordierite enclave formation. Locally, the cordierite - quartz veins contain 1 cm long rutile crystals. Rutile is also ubiquitous throughout the rock, and has faint yellow pleochroic haloes where included in cordierite, indicating a small content of a radioactive element. In some places cordierite plus quartz appear to have been retrograded on their own composition to a mixture of kyanite plus magnesian chlorite. Schumacher believes most of the kyanite at this locality, even in the enclaves, is of retrograde origin, based on its ubiquitous association with secondary sheet silicates. However, several miles away there are excellent examples of kyanite overgrown by prograde fibrolite.

The best sampling for enclave rock at outcrop W95 is from the blocks within the small pit to the southwest. The white to gray mineral is virtually all cordierite which is unevenly distributed in what appear to have been beds. At least one bed from this pit shows subhedral cordierite crystals growing across foliation and with a faintly purple tint that may be due to included corundum. Generally, different kinds of enclaves occur within a single thin section. Thus, it is likely that an enterprising field-trip participant will find a totally new type of enclave!

From outcrop W95 (30 minutes) return along forest track on west (right) side of Harris Soapstone Quarry and then bear left up slope of hill to outcrop I34.

Outcrop I34 (45 minutes) is mainly a natural outcrop near a hilltop, but was tested with poor results for soapstone along the west slope. The outcrop is much wider across strike than at W95 and illustrates a logical succession of lithic types. In a small outcrop to the east (I34A) is an ordinary hornblende - plagioclase amphibolite with the composition of an unaltered basalt (Table G-4). Somewhere in the covered interval leading to the main outcrop anthophyllite appears and occurs with hornblende, labradorite, phlogopite, and rutile at I34B on the east side of the big outcrop. This was the first iridescent anthophyllite observed in New England rocks. Based on the analysis (Table G-4, I34BXY) the rock is considered to have been a basalt that suffered high-T seawater alteration, but to a lesser extent than rocks still farther to the west. Passing westward across the main outcrop, first plagioclase (samples I34CX, I34DX), and then hornblende disappear from the mode (I34EXA, I34EXB), in places leading to nearly pure gedrite-rutile rock that must have been sampled by Emerson in 1892. A large block in this vicinity contains prominent enclaves of staurolite rimmed by cordierite (I34EXA). In these rocks MgO has increased to about 18 wt.% while CaO is less than 1 wt.%. A few feet southwest of the main outcrop is outcrop I34G, a coarse gedrite-cordierite gneiss in which all of the plagioclase enclaves, as well as the cordierite - hornblende assemblage, have been found. About five feet further west is the gedrite-garnet gneiss that is virtually identical to sample I34I originally found as a block within the quarry. Three feet beyond this is the small outcrop of garnet-magnetite quartzite that we now believe represents the Middle Member of the Ammonoosuc Volcanics. A coarse and very fresh quartz-andesine-cordierite-gedrite gneiss (I34JX) from which both cordierite and gedrite were analyzed, is from a small glacial boulder nearby, of which little remains.

The sillimanite-cordierite pegmatite with dumortierite lies a few feet north of the "quarry" near the top of the hill, and has been recently attacked by mineral collectors, although for reasons unknown.

Petrology of Aluminous Enclaves

Introduction. Robinson and Jaffe (1969a) used the term "enclave" to describe textures in which combinations of aluminous minerals are insulated by cordierite (Crd) from the gedrite (Ged), which comprises most of the rock. The aluminous minerals found to date are sillimanite (Sill), kyanite (Ky), corundum (Cor), staurolite (St), sapphirine (Sa), spinel (Sp), and Ca-rich plagioclase (Plag). Generally, where plagioclase is present it surrounds all other aluminous minerals, and is in turn surrounded by cordierite. Near cordierite-plagioclase enclaves, rare hornblende (Hbl), in contact with cordierite, is found with gedrite in the matrix.

Based on the presence or absence of plagioclase, the enclaves are classified into two main types: 1) enclaves of cordierite surrounding aluminous minerals and 2) enclaves of cordierite and plagioclase surrounding aluminous minerals. Examples of mineral sequences in the cordierite enclaves (Fig. G-15) are: Sill (core) / St + Crd / Ged (matrix); Cor + Crd (core) / Ged (matrix); and Sill (core) / St + Crd / Sa + Crd / Ged (matrix). Examples of the mineral sequences in the cordierite-plagioclase enclaves (Fig. G-16) are: Sill (core) / St + Plag/ Plag + Crd / Hbl + Ged (matrix); Cor + Plag (core) / St + Plag / Sa + Plag / Plag + Crd / Ged + Hbl (matrix); and St + Plag (core) / Plag + Crd / Ged + Hbl (matrix).

Robinson and Jaffe (1969a and b) gave optical data on the minerals, petrographic description of the aluminous enclaves and their gedrite-cordierite host rocks, and obtained gravimetric analyses of three gedrites (Table G-6) and one cordierite (Table G-3). Robinson and Jaffe (1969a) further discussed a series of continuous and discontinuous Fe-Mg reactions that could account for the mineral assemblages, and suggested that these reactions were encountered during decompression that accompanied the rise of the Keene gneiss dome. Since the work of Robinson and Jaffe, Schumacher (1981b, 1983) has found sapphirine as an additional enclave mineral and recognized minor pargasitic hornblende in the matrix of rocks that contain cordierite-plagioclase enclaves. The mineralogy of the enclaves is given in Table G-5. Tables G-6 and G-7 give representative analyses

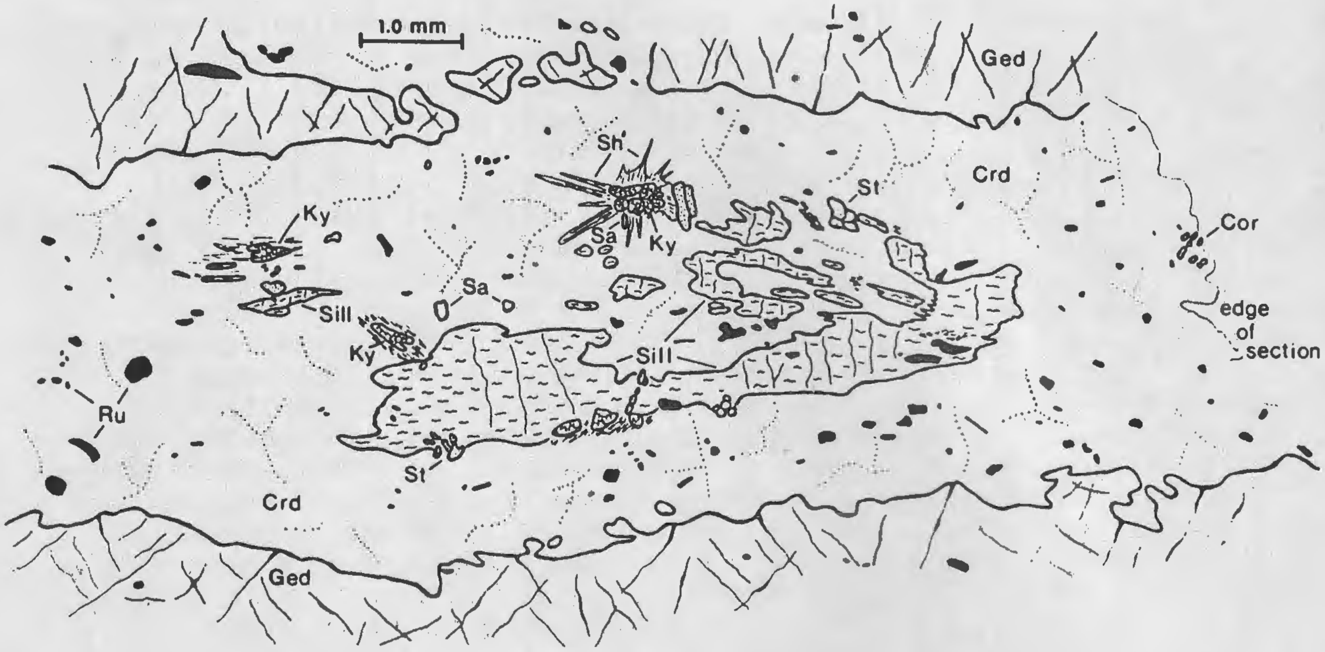
1.0 mm
Ged
Sh
Crd
St
Ky
Sa
Ky
Cor
Sa
Sill
edge of section
Ky
Sill
Ru
St
Crd
Ged

Figure G-15A. Sillimanite - kyanite - sapphirine - corundum enclave from specimen 2. Abbreviations : Cor = corundum; Crd = cordierite; Ged = gedrite; Ky = kyanite; Ru = rutile; Sa = sapphirine; Sh = sheet silicates; Sill = sillimanite; St = staurolite.

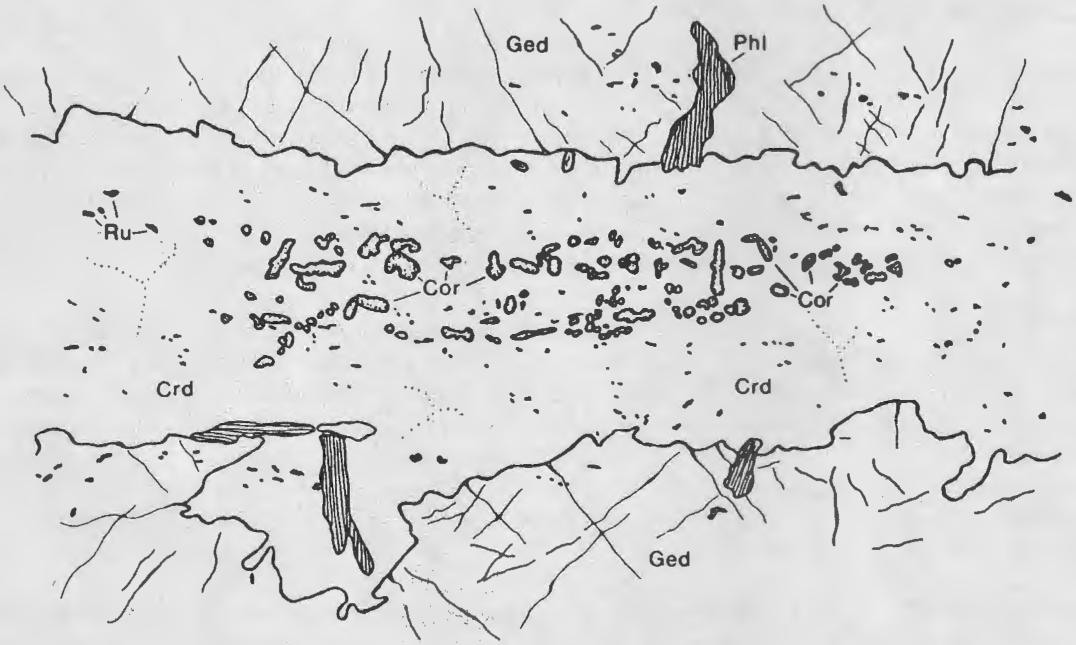
Ged
Phl
Ru
Cor
Cor
Crd
Crd
Ged

Figure G-15B. Corundum enclave from specimen 4a. Abbreviations: Cor = corundum; Crd = cordierite; Ged = gedrite; Phl = phlogopite; Ru = rutile.

Table G-5. Mineral assemblages in gedrite gneisses at outcrops W95, I34, and 7A0. Table is arranged in three parts: a) Gneisses with cordierite enclaves or without enclaves, b) Gneisses with cordierite - plagioclase enclaves, and c) Key to samples.

		1, 3a, 4a	4b	2, 3b	8	12	11a	11b	13
MATRIX ASSEMBLAGE	Gedrite	X	X	X	X	X	X	X	X
	Cordierite	X	X	X	X	X	X		
	Plagioclase					AD			OL
	Quartz					X	X	X	X
	Staurolite							X	X
	Sillimanite						X	X	X
	Kyanite								X
	Garnet						X	X	X
	Biotite	X	X	X	X	X	X	X	X
	Rutile*	X	X	X	X				
	Ilmenite					X	X	X	X
MINERALS ENCLOSED BY CORDIERITE	Sapphirine			X					
	Staurolite		X	X					
	Kyanite		X	X					
	Corundum	X		X					
	Sillimanite		X	X		X			
	Quartz				X				

* Rutile occurs throughout rock, in matrix and in enclaves.

			10a	10b	7	6,9a	5	9b
MATRIX ASSEMBLAGE		Gedrite	X	X	X	X	X	X
		Hornblende	X	X		X	X	X
		Cordierite	X	X	X	X	X	X
		Plagioclase	LAB#	LAB	AD	LAB		LAB
		Biotite	X	X	X	X	X	X
		Rutile*	X	X	X	X	X	X
ENCLAVES	MINERALS ENCLOSED BY CORDIERITE	Quartz	X	X		X	X	X
		Talc	X					
		Staurolite			X			
		Corundum			X			
		Spinel			X			
		Plagioclase	AN	AN	BY	BY-AN	AD	AN
	MINERALS ENCLOSED BY PLAGIOCLASE	Staurolite	X		X	X	X	X
		Sapphirine	X					
		Corundum	X					
		Spinel		X	X	X	X	X
		Sillimanite			X	X		

# Plagioclase composition: OL=oligoclase, AD=andesine, LAB=labradorite, BY=bytownite, AN=anorthite.

* Rutile occurs throughout rock, in matrix and in enclaves.

Key to samples listed in tables: Specimen No., Field Designation; 1, W95JX; 2, W95JXS, section 2; 3, 3a, 3b, W95JY, enclaves a and b; 4, 4a, 4b, W95SX, section 1, enclaves a and b; 5, 5a, 5b, I34EX, enclaves a and b; 6, I34GX, section 1; 7, I34GX, section 2; 8, I34GX, section 3; 9, 9a, 9b, I34GXS, section 1, enclaves a and b; 10, 10a, 10b, I34GXS, section 2, enclaves a and b; 11a, 11b, I34I, two parts of same hand specimen. 11a contains cordierite and was studied by electron probe only. 11b contains staurolite and gedrite was separated for wet chemical analysis; 12, I34JX; 13, 7AOBX.

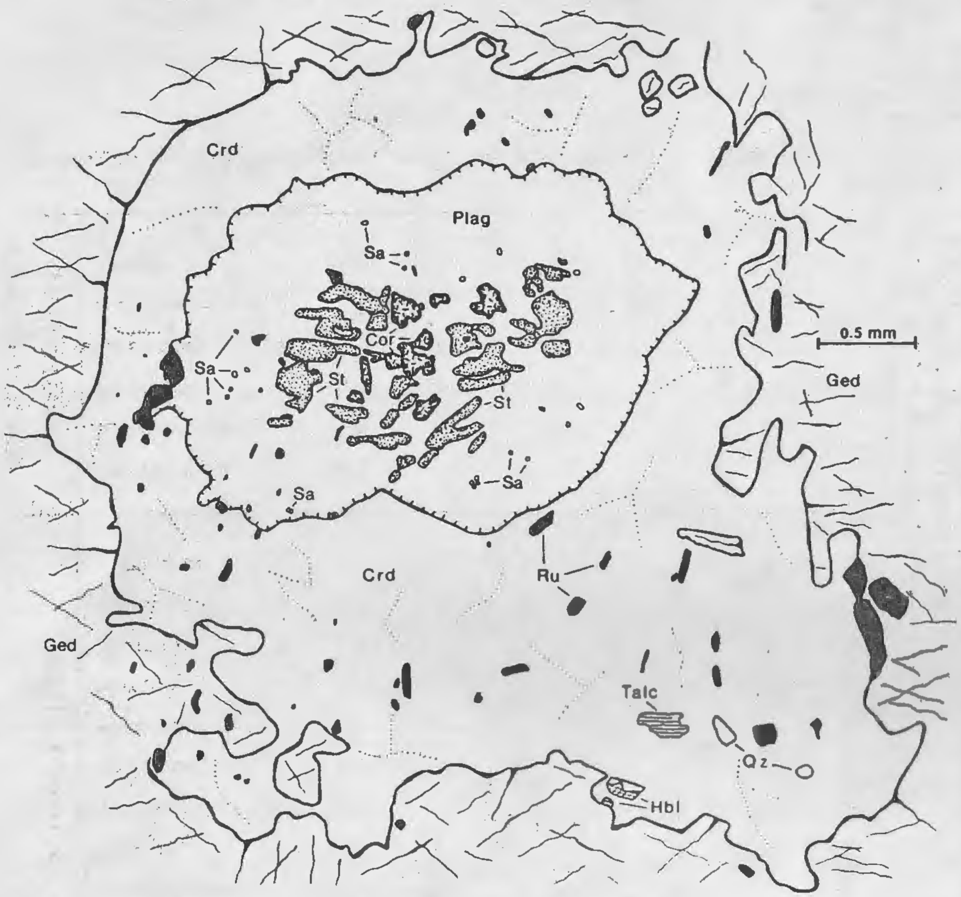
Crd
Plag
Sa
Cor
St
St
Sa
Sa
Sa
0.5 mm
Ged
Crd
Ru
Ged
Talc
Qz
Hbl

Figure G-16A. Corundum - staurolite - sapphirine - anorthite enclave from specimen 10a (I34GXS). Abbreviations: Cor = corundum; St = staurolite; Sa = sapphirine; Plag = plagioclase (An_{92}); Crd = cordierite; Qz = quartz; Ged = gedrite; Hbl = hornblende; Ru = rutile.

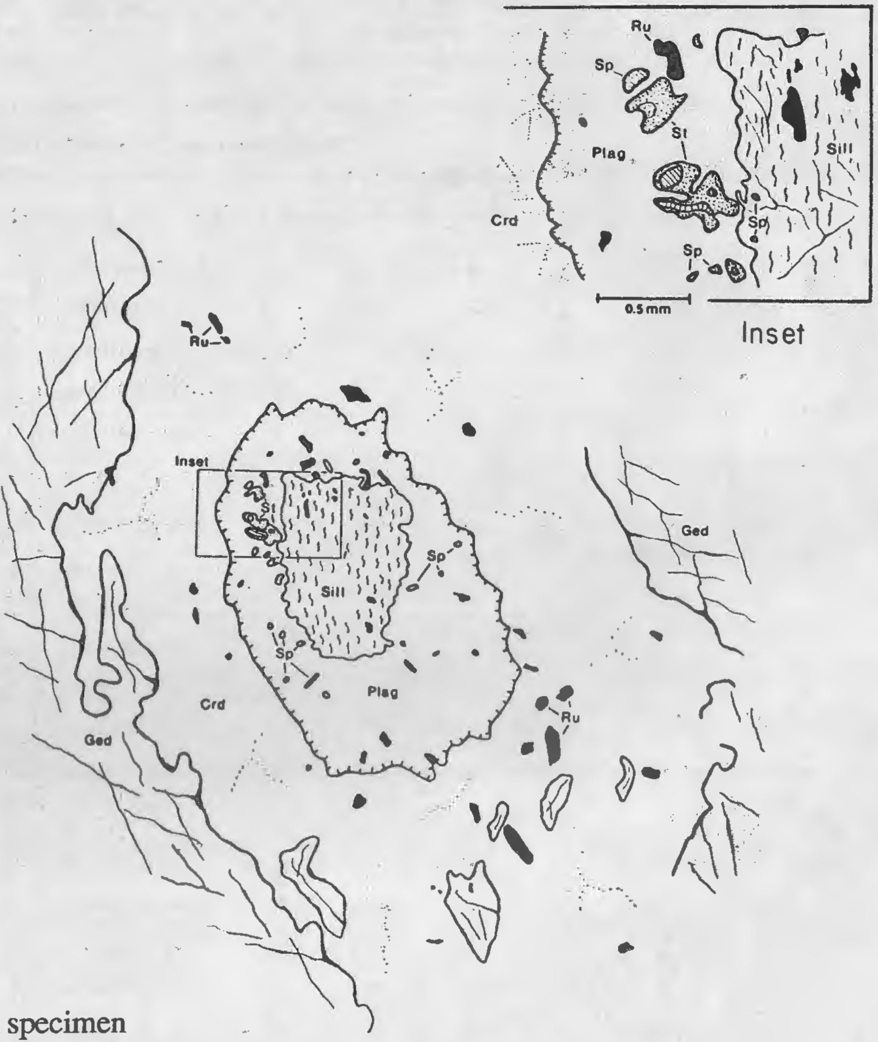
Ru
Sp
St
Plag
Sill
Crd
Sp
Sp
0.5 mm
Inset
Ru
Inset
St
Sp
Sill
Sp
Crd
Plag
Ged
Ged
Ru

Figure G-16B. Sillimanite - staurolite - spinel - plagioclase enclave from specimen 9a (I34GXS); inset is an enlargement of a portion of the enclave. Abbreviations: Cor = corundum; St = staurolite; Sa = sapphirine; Sp = spinel; Plag = plagioclase (An_{92}); Crd = cordierite; Qz = quartz; Ged = gedrite; Hbl = hornblende; Ru = rutile.

Table G-6. Representative analyses of gedrite and hornblende from gedrite-rich rocks. Structural formulae derived from electron-probe analyses of gedrites and hornblendes are based on several assumed cation occupancies (see text) and 23 oxygens. Gedrites are listed in order of the ratio $(Fe^{+2}+Mn)/(Fe^{+2}+Mn+Mg)$. For assemblages and sample numbers see Table G-5.

WEIGHT % OXIDES

		GEDRITE										HORNBLENDE	
	Sample No.	4	1#	2	10	9	5	12#	11a	11b	11b#	10	5
	SiO_2	47.52	47.68	47.86	46.00	46.47	45.03	44.72	41.29	40.35	40.75	44.79	45.01
	TiO_2	0.29	0.24	0.31	0.34	0.30	0.30	0.46	0.12	0.27	0.25	0.15	0.44
	Al_2O_3	13.13	13.36	14.55	14.24	13.98	16.29	15.46	19.80	20.75	19.81	15.84	15.78
	Fe_2O_3		1.60					2.41			1.22		
	MgO	22.39	20.68	21.55	20.15	19.05	18.45	16.69	14.26	13.91	13.81	13.51	14.06
	FeO	12.63	12.07	14.55	14.46	14.72	14.55	15.87	20.13	20.02	19.29	9.41	10.15
	MnO	0.23	0.22	0.22	0.45	0.48	0.36	0.37	0.22	0.22	0.25	0.17	0.15
	CaO	0.52	0.55	0.49	0.69	0.69	0.55	0.47	0.18	0.13	0.27	11.17	11.08
	Na_2O	1.34	1.24	1.59	1.32	1.28	1.72	1.47	2.15	2.34	1.92	1.58	1.71
	K_2O	0.00	0.00*	0.00	0.00	0.00	0.00	0.01**	0.00	0.00	0.04***	0.12	0.10
	Total	98.05	99.83	97.76	97.65	96.92	97.25	100.20	98.15	97.99	100.38	96.74	98.47
		STRUCTURAL FORMULAE											
T	Si	6.606	6.683	6.512	6.491	6.632	6.411	6.396	5.967	5.854	5.950	6.414	6.343
	Al	1.394	1.315+	1.488	1.509	1.368	1.589	1.595++	2.033	2.146	2.045+++	1.586	1.647
	Sum	8.000	8.000	8.000	8.000	8.000	8.000	8.000	8.000	8.000	8.000	8.000	8.000
M2	Al	0.757	0.892	0.845	0.860	0.984	1.144	1.011	1.341	1.405	1.364	1.087	0.964
	Fe^{3+}	0.216	0.168	0.159	0.214	0.000	0.000	0.260	0.221	0.184	0.133	0.306	0.412
	Ti	0.030	0.025	0.032	0.036	0.032	0.032	0.050	0.014	0.029	0.027	0.016	0.047
	Cr		0.002					0.000			0.002		
	Mg	0.997	0.913	0.964	0.890	0.984	0.824	0.679	0.424	0.382	0.474	0.591	0.577
	Sum	2.000	2.000	2.000	2.000	2.000	2.000	2.000	2.000	2.000	2.000	2.000	2.000
M1 + M3	Mg	3.000	3.000	3.000	3.000	3.000	3.000	2.878	2.651	2.627	2.531	2.294	2.377
	Fe^{2+}							0.122	0.349	0.373	0.469	0.706	0.623
	Sum	3.000	3.000	3.000	3.000	3.000	3.000	3.000	3.000	3.000	3.000	3.000	3.000
M4	Mg	0.643	0.407	0.407	0.349	0.069	0.092						
	Fe^{2+}	1.252	1.415	1.496	1.493	1.757	1.732	1.899	1.865	1.873	1.886	0.115	0.160
	Mn	0.027	0.026	0.025	0.054	0.058	0.043	0.045	0.028	0.027	0.031	0.021	0.018
	Li		0.005					0.022			0.018		
	Ca	0.078	0.083	0.072	0.105	0.098	0.084	0.071	0.027	0.020	0.042	1.714	1.673
	Na		0.063			0.018	0.049	0.085	0.080	0.080	0.023	0.150	0.149
	Sum	2.000	2.000	2.000	2.000	2.000	2.000	2.000	2.000	2.000	2.000	2.000	2.000
A	Na	0.361	0.274	0.420	0.361	0.336	0.426	0.322	0.523	0.578	0.521	0.289	0.318
	K							0.002			0.007	0.022	0.018
	Sum	0.361	0.274	0.420	0.361	0.336	0.426	0.324	0.523	0.578	0.528	0.311	0.336
	$\frac{Fe^{2+}+Mn}{Fe^{2+}+Mn+Mg}$	0.247	0.250	0.258	0.267	0.309	0.312	0.353	0.422	0.430	0.443	0.226	0.336

* Cr_2O_3 0.02, NiO 0.01, SrO 0.001, BaO 0.001, Li_2O 0.01, $H_2O(+)$ 2.12, P_2O_5 0.02, F 0.04, Cl 0.01.

** Cr_2O_3 0.002, NiO 0.003, SrO 0.001, BaO 0.001, Li_2O 0.04, $H_2O(+)$ 2.11, P_2O_5 0.07, F 0.09, Cl 0.01.

*** Cr_2O_3 0.011, SrO 0.001, BaO 0.001, Li_2O 0.03, $H_2O(+)$ 2.68, P_2O_5 0.04, F 0.01, Cl 0.01.

# Wet chemical analysis, H. Asari, analyst, 1967.

+ Also P 0.002.

++ Also P 0.009.

+++ Also P 0.005.

Table G-7. Representative electron-probe analyses of spinel, sapphirine, staurolite, and cordierite. For assemblages and field sample numbers see Table G-5. Sapphirine 2, enclosed in cordierite, is sky blue to colorless. Sapphirine 10a, enclosed in anorthite, is pale green to colorless.

Mineral analyses. Spinel=Sp, sapphirine=Sa, staurolite=St, and cordierite=Crd.

Enclave Mineral	9a Sp	2 Sa	10a Sa	9a St	2 St	10a St	9a Crd	2 Crd	10a Crd
SiO_2	0.00	11.46	11.40	27.83	28.64	27.35	49.67	49.28	50.07
TiO_2	0.00	0.02	0.00	0.14	0.44	0.29	0.03	0.00	0.00
Al_2O_3	60.17	65.95	66.33	54.86	56.04	56.63	33.28	34.18	33.91
FeO	14.36	5.91	6.24	3.35	3.50	3.69	11.64	12.27	12.43
MnO	0.04	0.02	0.08	10.27	9.00	9.35	2.80	2.00	2.54
MgO	6.98	16.36	15.62	0.19	0.12	0.14	0.02	0.03	0.03
ZnO	18.04	0.00	0.00	1.74	0.00	0.01	0.07	0.00	0.00
CaO	0.01	0.00	0.09	0.02	0.00	0.01	0.04	0.01	0.04
Na_2O	0.00	0.00	0.00	0.00	0.00	0.00	0.23	0.28	0.16
K_2O	0.00	0.00	0.00	0.00	0.00	0.00	0.00	0.02	0.00
Total	99.60	99.72	99.76	98.40	97.74	97.49	97.78	98.07	99.18
	4 Oxygens	20 Oxygens		23 Oxygens			18 Oxygens		
Si	--	1.353	1.350	3.811	3.877	3.727	5.015	4.947	4.979
Al	1.995	4.647	4.650	0.189	0.123	0.273	0.985	1.053	1.021
Al	--	4.533	4.606	8.669	8.698	8.828	2.977	2.989	2.955
Ti	0.000	0.002	0.000	0.014	0.045	0.030	0.005	0.000	0.000
*Fe^{3+}	--	0.111	0.045	--	--	--	--	--	--
Mg	0.293	2.880	2.757	0.684	0.707	0.750	1.752	1.837	1.844
Fe^{2+}	0.338	0.473	0.573	1.177	1.020	1.066	0.273	0.168	0.212
Mn	0.001	0.002	0.008	0.022	0.013	0.017	0.001	0.002	0.002
Zn	0.375	0.000	0.000	0.176	0.000	0.001	0.005	0.000	0.000
Ca	0.000	0.000	0.011	0.003	0.000	0.001	0.005	0.002	0.004
Na	0.000	0.000	0.000	0.000	0.000	0.000	0.044	0.054	0.031
K	0.000	0.000	0.000	0.000	0.000	0.000	0.000	0.003	0.000
Total	3.002	14.000	14.000	14.745	14.606	14.693	11.026	11.055	11.048
$^{\S}X_{Fe}$	0.536	0.142	0.174	0.637	0.594	0.591	0.120	0.085	0.104

*Calculated from the stoichiometry (Sa - 14 cations); $^{\S}X_{Fe} = (Fe^{2+}+Mn)/(Fe^{2+}+Mn+Mg)$

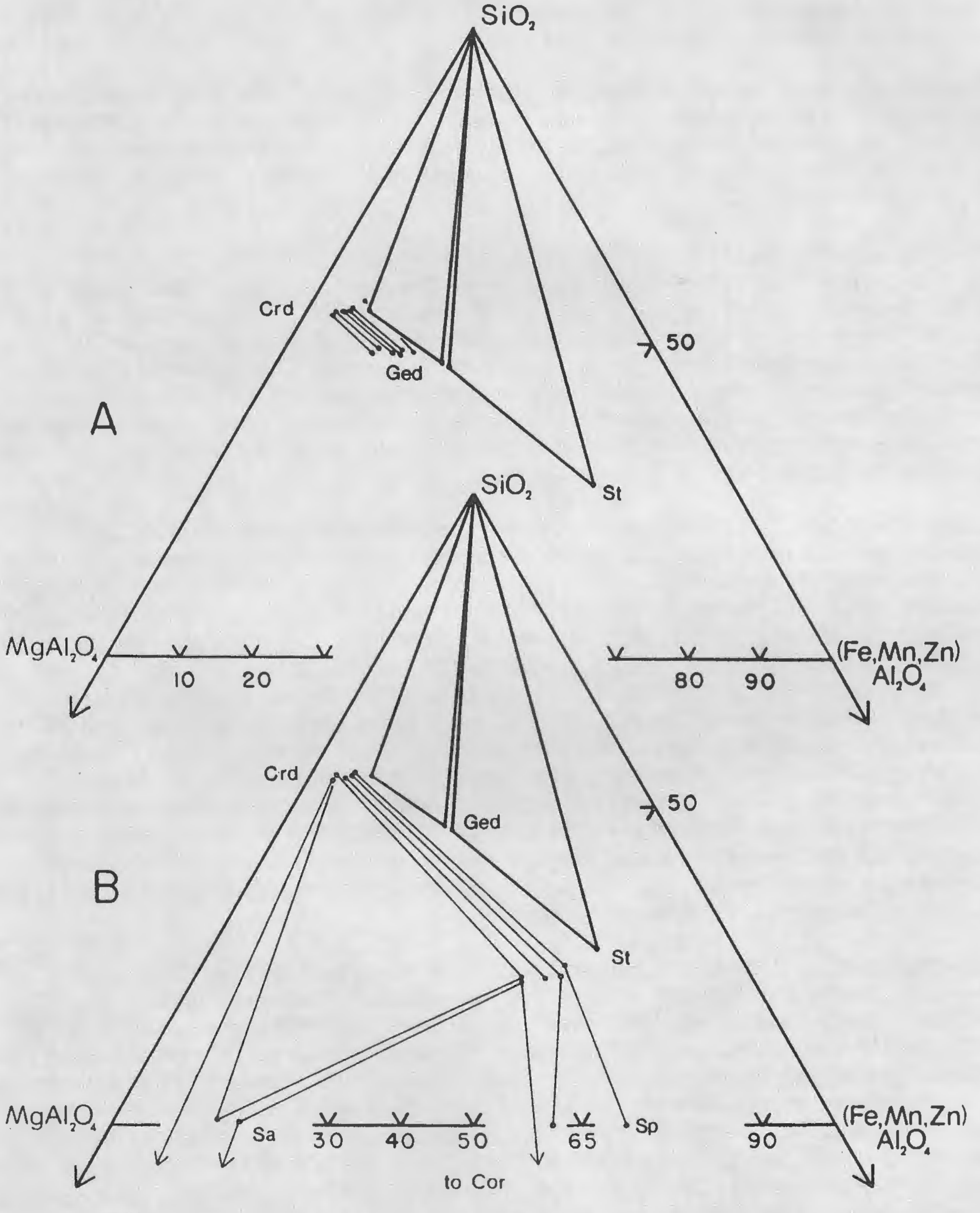
SiO₂
Crd
Ged
A
50
St
SiO₂
MgAl₂O₄
10
20
80
90
(Fe,Mn,Zn) Al₂O₄
Crd
Ged
50
B
St
MgAl₂O₄
Sa
30
40
50
65
Sp
90
(Fe,Mn,Zn) Al₂O₄
to Cor

Figure G-17. Projections from Al_2SiO_5 and H_2O to the plane SiO_2 - $MgAl_2O_4$ - (Fe, Mn, Zn)Al_2O_4 of a (Fe, Mn, Zn)O-MgO-Al_2O_3-SiO_2 tetrahedron. A: Compositions of coexisting gedrite and cordierite from rocks with and without enclaves. B: Compositions of minerals within some representative enclaves. Two assemblages from sample 11 (I34I) are plotted for reference in both parts A and B. Abbreviations: Cor = corundum; Sill = sillimanite; St = staurolite; Sa = sapphirine; Sp = spinel; Crd = cordierite; Cor = corundum; Ged = gedrite; Qz = quartz.

from the enclaves and host rocks, and the sillimanite projections in Figure G-17 summarize the compositional variations in most of the phases.

Textural interpretations and observations. Robinson and Jaffe (1969a) pointed out the strong pressure dependence of many cordierite-producing reactions (Schreyer and Seifert, 1969a and b) and suggested the undeformed textures of the enclaves relative to the gneissic texture of the enclosing rock is evidence that late-stage uplift, and therefore decreasing P, played an important role in enclave formation.

The sheet silicates and kyanite are not considered in the enclave-forming reactions for several reasons. Sheet silicates are commonly associated with cracks that run through both the gedrite-rich matrix and the enclaves. This suggests that the sheet silicates formed during late-stage alteration and were not involved in the reactions that produced the enclaves. Kyanite is consistently associated with the sheet silicates and by virtue of "guilt by association" is suspected also to have a retrograde origin. The kyanite grain surrounded by sheet silicates in Fig. G-15A is particularly suggestive of a retrograde origin. Robinson (1963) has found coarse-grained chlorite and kyanite replacing coarse, vein cordierite from this locality, which further supports a retrograde origin for the kyanite-chlorite assemblage.

Robinson and Jaffe (1969a) suggested that gedrite and sillimanite were probably the chief constituents of the rock prior to enclave formation and that reaction of these two minerals to form cordierite was the most important episode of enclave formation. This interpretation is supported by several observations. Sillimanite is always located at the centers of aggregates of cordierite grains and is completely isolated from the gedrite-rich matrix. In addition an appropriately cut thin section clearly shows that the shape of one enclave mimics the remnants of the large sillimanite prism enclosed in the cordierite (Fig. G-15A). Robinson and Jaffe (1969a) also report an enclave containing only quartz (enclave 8, Table G-5). The quartz forms a vermicular intergrowth with the cordierite and it is isolated from the gedrite by the cordierite. As is the case with the sillimanite, this texture suggests that quartz was also involved in a cordierite-forming reaction. In more Fe-rich rocks from the same locality (Table G-5, sample I34I) sillimanite, quartz and Fe-richer gedrite ($X_{Fe} = 0.44$) are stable and cordierite is absent from the assemblage. This shows that increased Fe content of the rock inhibits the cordierite-forming reactions, and that these reactions proceeded longer in the most Mg-rich rocks. This also points to the critical role the Fe-Mg ratio played in the timing of the reaction between gedrite and sillimanite.

Petrogenetic grids. Reactions that are pertinent to the mineralogy of the enclaves were modelled using idealized mineral compositions that approximate the measured mineral compositions. Fe-Mg variation was considered to be the most important compositional variable, and examining the effects of this variable was one of the major objectives. As a consequence, the Al content of gedrite, sapphirine, and staurolite were considered to be fixed. When constrained by this assumption, reaction coefficients remain constant regardless of the Fe-Mg contents of the phases; however as pointed out by Thompson (1982a), the stoichiometric coefficients for such reactions are not unique, and in this case will vary slightly as a function of $AlAlMg_{-1}Si_{-1}$ variation in gedrite, sapphirine, and staurolite. Fortunately, for the treatment of the reactions discussed below, variations in $AlAlMg_{-1}Si_{-1}$ had negligible effects on parameters obtained using the reaction coefficients.

The eleven discontinuous Fe-Mg reactions for FMASH components are found among the phases gedrite, cordierite, staurolite, sapphirine, corundum, and sillimanite after the incompatibility of quartz and corundum is considered. Cordierite is treated as hydrous with an idealized H_2O content of 0.75 per 18 oxygen formula (see analysis Table G-3). These reactions are shown around the [QZ] and [COR] invariant points (Fig. G-18) on a P-μH_2O diagram (topology analogous to P-T diagrams, see discussions of Burt, 1978; Spear, 1977).

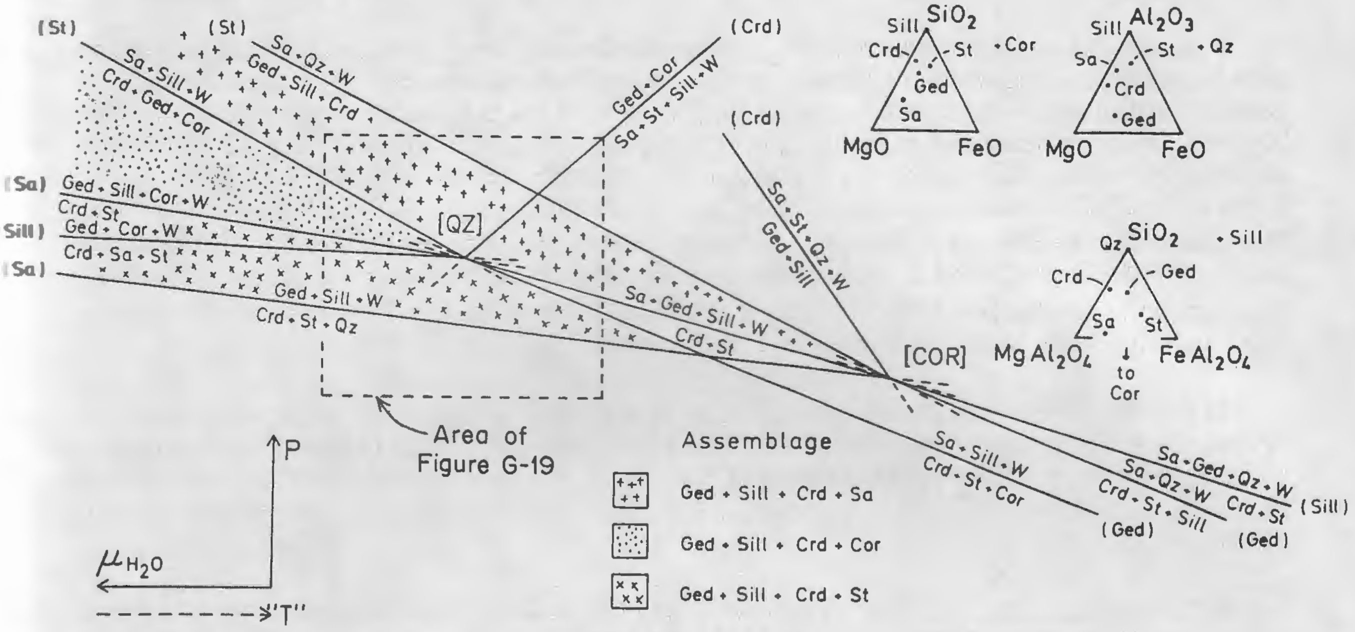
(St)
(St)
Sa+Qz+W
Ged+Sill+Crd
Sa+Sill+W
Crd+Ged+Cor
(Crd)
Ged+Cor
Sa+St+Sill+W
(Crd)
(Sa)
Ged+Sill+Cor+W
Crd+St
(Sill)
Ged+Cor+W
Crd+Sa+St
(Sa)
[QZ]
Ged+Sill+W
Crd+St+Qz
Sa+St+Qz+W
Ged+Sill
Sa+Ged+Sill+W
Crd+St
[COR]
Area of
Figure G-19
P
μH2O
"T"
Assemblage
Ged + Sill + Crd + Sa
Ged + Sill + Crd + Cor
Ged + Sill + Crd + St
Sa+Sill+W
Crd+St+Cor
Sa+Ged+Qz+W
Sa+Qz+W
Crd+St+Sill
Crd+St
(Ged)
(Ged)
(Sill)
SiO2
Sill
Crd
St
Cor
Ged
Sa
MgO
FeO
Al2O3
Sill
Sa
St
Qz
Crd
Ged
MgO
FeO
SiO2
Qz
Sill
Crd
Ged
Sa
St
MgAl2O4
FeAl2O4
to
Cor

Figure G-18. Schematic P versus μH_2O petrogenetic grid for enclave-forming phases in the FeO-MgO-Al_2O_3-SiO_2-H_2O (FMASH) system. Proportions of each component are assumed to be constant in each phase and water is an excess component. Patterned areas show the stability fields of three, 4-phase assemblages. Brackets [] indicate the phase that is absent at the invariant point and parentheses () enclose additional phases absent along the univariant curves. The phase compositions are illustrated on sillimanite, quartz, and corundum projections. "T" = the approximate affect of temperature. Abbreviations: Cor = corundum, Sill = sillimanite; St = staurolite; Sa = sapphirine; Crd = cordierite; Ged = gedrite; Qz = quartz; W = H_2O.

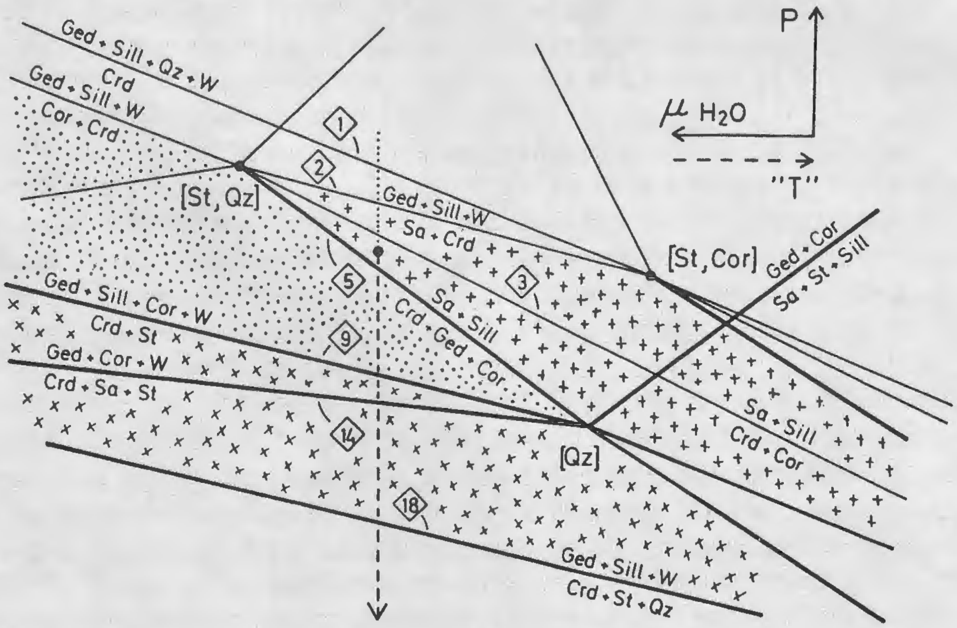
Ged+Sill+Qz+W
Crd
Ged+Sill+W
Cor+Crd
P
μ H2O
"T"
1
2
[St, Qz]
Ged+Sill+W
Sa+Crd
[St, Cor]
Ged+Cor
Sa+St+Sill
3
5
Sa+Sill
Crd+Ged+Cor
9
Ged+Sill+Cor+W
Crd+St
Ged+Cor+W
Crd+Sa+St
14
[Qz]
Sa+Sill
Crd+Cor
18
Ged+Sill+W
Crd+St+Qz

Figure G-19. Enlargement of part of Figure G-18. Heavy lines are univariant curves from Figure G-18 and light lines are MASH end-member reactions that limit the (St) univariant curves eminating from the [Qz] and [Cor] invariant points. Vertical arrow is a possible path of decreasing P for the enclave rocks (dashed part of the arrow); the dot represents the possible "maximum" P conditions attained by the rocks, and the dotted part of the arrow projects the path to higher P's. Numbers enclosed by diamonds indicate a sequence of reactions discussed in the text and shown in Figure G-20. Other symbols and abbreviations as in Figure G-18.

It is possible to choose a path through these reactions by using various assemblages that must have been stable as the reactions between gedrite and sillimanite occurred. The assemblage gedrite + sillimanite + cordierite + sapphirine (Fig. G-15A) is only stable at pressures above the St- and Cor-absent reactions of the [QZ] invariant point (pattern of crosses in Fig. G-18). The assemblage gedrite + sillimanite + cordierite + corundum (pattern of dots in Fig. G-18) is only stable at P-μH_2O conditions between the St- and Sa-absent reactions of the [QZ] invariant point. The assemblage gedrite + sillimanite + cordierite + staurolite (pattern of x's in Fig. G-18) is only stable at P-μH_2O conditions in the area inscribed by the Sa- and Cor-absent reactions of the [QZ] invariant point and the Sa-absent reaction of the [Cor] invariant point. The simplest path through these stability fields is one of decreasing P at constant μH_2O (see Fig. G-19).

In the above treatment the question of water in cordierite is potentially an important one, because treating the cordierite as anhydrous causes the slopes of several of the reactions to change sign. However, one could still find a path of decreasing P at constant μH_2O through the reactions (Schumacher, 1983; Schumacher and Robinson, in review) even if the cordierite is considered to be anhydrous.

Continuous Fe-Mg reactions. A comparison of the cordierite compositions among enclaves gives a general impression of the relative Fe-Mg ratios of the bulk composition. Cordierite from the sapphirine-bearing enclave (2) is slightly richer in Mg than that from the corundum enclave (4a), which is richer in Mg than cordierite from the staurolite enclave (4b). This bulk compositional effect cannot be easily portrayed on sillimanite, quartz, or corundum projections, because of the large number of continuous Fe-Mg reactions (16) that are associated with the four discontinuous reactions (Figs. G-18 and G-19), and that must be portrayed over a narrow range of Fe-Mg variation of projections. Additionally, all of the reactions cannot be shown on the same type of projection.

An alternative way to look at the continuous Fe-Mg reactions and the effects of Mg-Fe variation is with P-$\mu FeMg_{-1}$ diagrams. For the idealized Fe-Mg continuous reactions the proportions of all components in all the participating phases remain the same except for FeO and MgO. This variation can be expressed in a single component, $FeMg_{-1}$ (see Thompson, 1982a), and approximate P-$\mu FeMg_{-1}$ slopes of the continuous Fe-Mg reactions equal $\Delta nFeMg_{-1}/\Delta V_s$ for each reaction. These values can be obtained from the stoichiometry of the balanced Mg-end-member reactions by inserting the correct Fe-Mg contents for the phases and adding the $\Delta nFeMg_{-1}$ term. Since $\mu FeMg_{-1}$ must be the same in all phases in any equilibrium assemblage (reaction or otherwise), the $\mu FeMg_{-1}$ can be used as a relative measure of the Fe-Mg content of assemblages containing the same phases, and at constant T and μH_2O the Fe-Mg continuous reactions can be represented as sloped lines in P-$\mu FeMg_{-1}$ space. Although the continuous reactions are represented as straight lines (Figs. G-20 and G-21), they, in fact, are curved. At P's near that of the Mg-end-member reaction the $\Delta nFeMg_{-1}$ is near 0. The $dP/d\mu FeMg_{-1}$ slope of the curve increases as $\Delta nFeMg_{-1}$ increases, until the P of the maximum $\Delta nFeMg_{-1}$, which is equivalent to the maximum width of a P-X_{Mg} loop. Then, the $dP/d\mu FeMg_{-1}$ slope of the curve must begin to decrease as $\Delta nFeMg_{-1}$ also decreases, and will approach 0 at the P of the Fe-end-member reactions. The resulting curve must have a sigmoidal shape. Since a particular continuous reaction is probably stable for only a very limited range of X_{Mg} values, only a small part of the total P-$\mu FeMg_{-1}$ curve would represent the stable part of the reaction, and could reasonably be represented as a straight line. In addition, so long as the chemography of the continuous reactions is accurately shown by the Fe-Mg ratios used in calculating the reactions, a P-$\mu FeMg_{-1}$ grid that uses straight lines will have the same topology as one that rigorously accounts for the X_{Mg} variation.

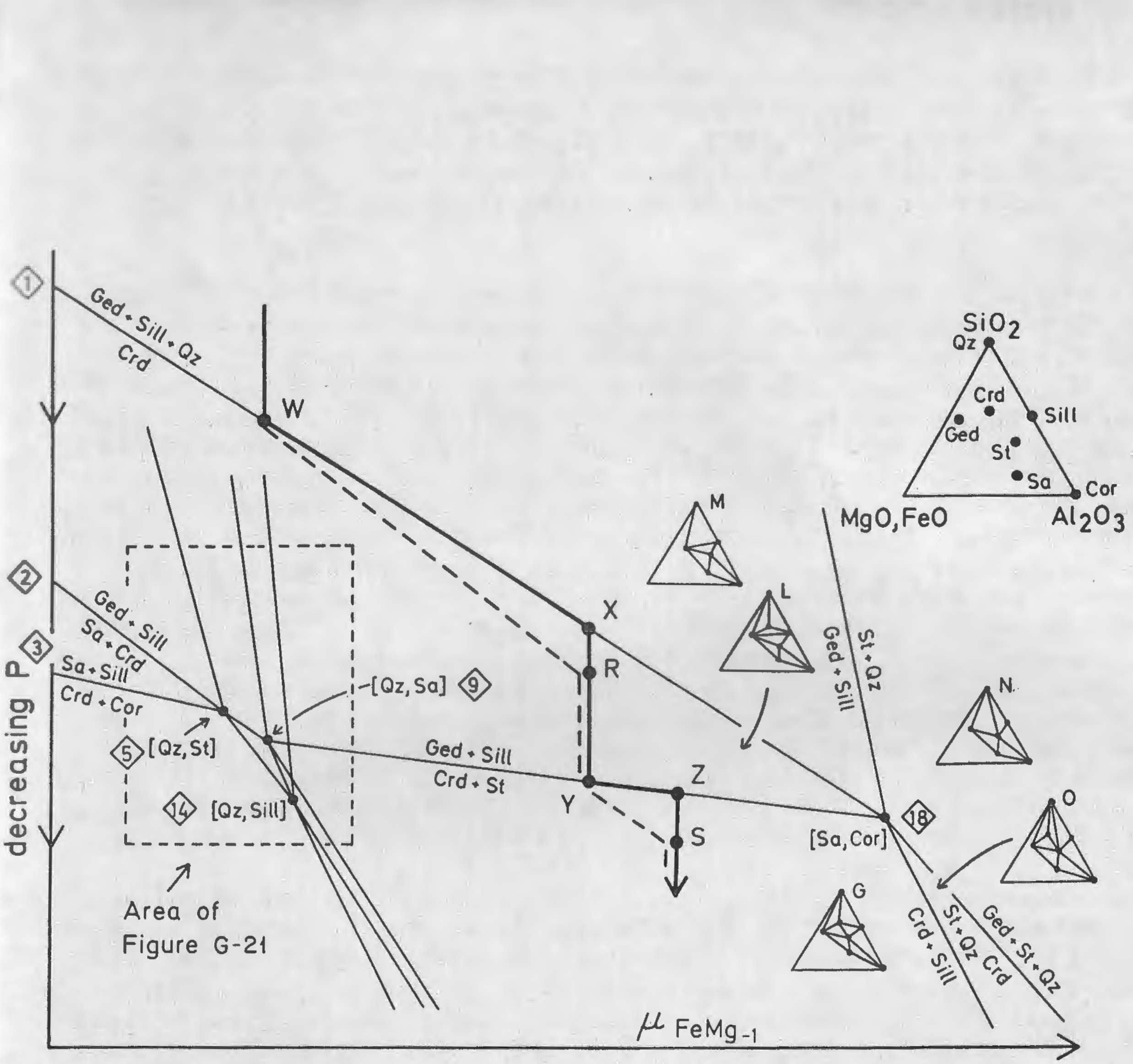
1
Ged + Sill + Qz
Crd
W
2
Ged + Sill
Sa + Crd
3
Sa + Sill
Crd + Cor
decreasing P
[Qz, Sa] 9
5 [Qz, St]
14 [Qz, Sill]
Area of
Figure G-21
X
R
Ged + Sill
Crd + St
Y
Z
S
M
L
N
O
G
SiO2
Qz
Crd
Sill
Ged
St
Sa
Cor
MgO, FeO
Al2O3
St + Qz
Ged + Sill
18
[Sa, Cor]
Ged + St + Qz
St + Qz Crd
Crd + Sill
μ FeMg-1

Figure G-20. A schematic P-$\mu FeMg_{-1}$ diagram for the decreasing P path (arrow, Figure G-19). Light lines represent continuous Fe-Mg reactions. Numbers enclosed by diamonds correspond to the "discontinuous reactions" and MASH end-member reactions in Figure G-19. Compatibilty triangles G, L, M,N, and O show the phase relations around the [Sa, Cor] invariant point. Heavy line containing points W, X, R, Y, Z, and S is an example of a reaction-controlled path that might be followed by a specific bulk composition (see discussion in text); heavy dashed line indicates a possible diffusion-controlled path for the same bulk composition. Abbreviations: Cor = corundum; Sill = sillimanite; St = staurolite; Sa = Sapphirine; Crd = cordierite; Ged = gedrite; Qz = quartz.

Bulk composition can also be illustrated on a P-$\mu FeMg_{-1}$ diagram in the divariant fields (Figs. G-20 and G-21). The compatibility triangles indicate the possible non-reactive three-phase assemblages. A specific value of $\mu FeMg_{-1}$ corresponds to specific X_{Fe} values among the Fe-Mg bearing phases in all the assemblages. Within any divariant field, increasing or decreasing the $\mu FeMg_{-1}$ is equivalent to increasing or decreasing the X_{Fe} values of all the phases in the assemblages.

The type of path which a specific bulk composition might follow on a P-$\mu FeMg_{-1}$ diagram is illustrated by the heavy line in Figure G-20. An assemblage that contains gedrite + sillimanite + quartz and is undergoing decompression will begin to form cordierite at point W (Fig. G-20). If the rate of P decrease is less than the rate of the reaction, the rate of change of the $\mu FeMg_{-1}$ will be controlled by this continuous reaction. Mineral growth under these circumstances can be termed reaction-controlled (Fisher, 1973, 1977). The continuous reaction will proceed until, at point X, one of the reacting phases is exhausted. For this example the exhausted phase is assumed to be quartz. The newly-formed non-reactive assemblage, gedrite + sillimanite + cordierite, will then remain at constant $\mu FeMg_{-1}$ until it encounters a second continuous Fe-Mg reaction that will affect its particular bulk composition, which for this example is at point Y on the reaction gedrite + sillimanite = cordierite + staurolite. As in the first reaction, if the rate of P change is less than the reaction rate, the rate of $\mu FeMg_{-1}$ change will be controlled by continuous reaction until at point Z one of the reacting phases is exhausted. For the enclave rocks the exhausted phase would be sillimanite. This path of decreasing P illustrates the way a gedrite + sillimanite + quartz rock via two continuous reactions can be transformed into a gedrite + cordierite + staurolite rock. Other possible assemblages that could develop over the same P interval can be explored on these diagrams by examining the effects of changing Fe-Mg ratio of the bulk composition and the modal proportions of the starting phases. Each bulk composition will have its own unique path through P-$\mu FeMg_{-1}$ space. Paths of similar bulk compositions are likely to overlap in places.

Reactions discussed earlier suggest that the enclaves that contain sapphirine, corundum, or staurolite formed by the reaction of gedrite and sillimanite, which makes it possible to bracket the P-$\mu FeMg_{-1}$ conditions on Figures G-20 and G-21 at which these types of enclaves could have formed. Compatibility triangles A through H represent the possible conditions for the formation of these enclaves. The region represented by compatibility triangles I through L (Figs. G-20 and G-21) lies within the stability of gedrite + sillimanite but outside the stability of gedrite + sillimanite + quartz (Fig. G-20, ternary M), and is an additional P-$\mu FeMg_{-1}$ region in which enclaves that contain only quartz or sillimanite could have formed Table G-5, 8 and 12). The regions represented by compatibility triangles N and O are Fe-richer compositions that lie outside the stability of gedrite + sillimanite and within the stability of staurolite + quartz. Cordierite + sapphirine would be found in the most Mg-rich bulk compositions (ternary phase regions A, B, and E, Fig. G-21); cordierite + staurolite would be stable in Fe-richer bulk compositions (ternary phase regions D, F, G, and H, Fig. G-21); and cordierite + corundum is stable in Fe-Mg bulk compositions that overlap the cordierite + sapphirine and cordierite + staurolite stability fields (ternary phase regions B through F, Fig. G-21). This agrees with the compositional data in Figure G-17.

Two Fe-richer assemblages, in which enclaves have not developed, can also be represented on Figure G-20. Samples 11a (Ged + Sill + Crd + Qz) and 11b (Ged + Sill + St + Qz) are, respectively, the assemblages of the two continuous reactions that are converging as pressure decreases to form the discontinuous reaction 18 (invariant point 18, Fig. G-20). The very slight differences in the gedrite compositions (see Table G-6) from assemblages 11a and 11b suggest they represent a P very close to and slightly higher than invariant point 18. Invariant point 18 marks the terminal association (with decreasing pressure) of gedrite and sillimanite. Although the lower-P reaction assemblages of cordierite + sillimanite + staurolite + quartz and gedrite +

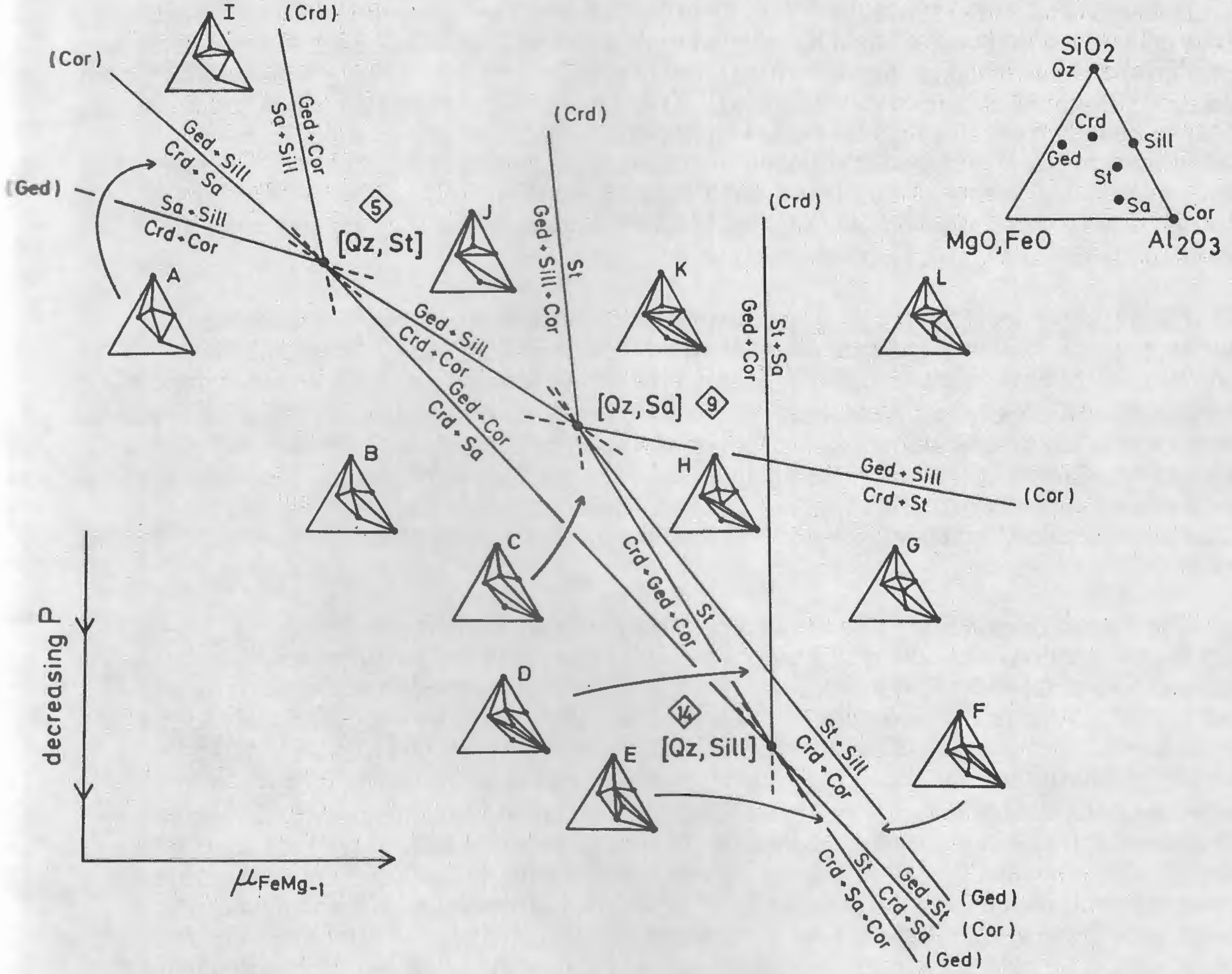
I
(Crd)
(Cor)
Ged+Sill
Crd+Sa
Sa+Sill
Ged+Cor
(Ged)
Sa+Sill
Crd+Cor
5
[Qz, St]
A
J
(Crd)
Ged+Sill+Cor
St
K
(Crd)
Ged+Cor
St+Sa
L
SiO_2
Qz
Crd
Sill
Ged
St
Sa
Cor
MgO,FeO
Al_2O_3
Ged+Sill
Crd+Cor
Ged+Cor
Crd+Sa
[Qz, Sa]
9
B
H
Ged+Sill
Crd+St
(Cor)
C
G
Crd+Ged+Cor
St
D
14
[Qz, Sill]
E
F
St+Sill
Crd+Cor
St
Crd+Sa
Ged+St
Crd+Sa+Cor
(Ged)
(Cor)
(Ged)
decreasing P
$\mu_{FeMg_{-1}}$

Figure G-21. Enlargement of part of Figure G-20. Symbols and abbreviations are the same. See text for discussion.

cordierite + staurolite + quartz are not documented near the Keene dome in southwestern New Hampshire, they are well known in central Massachusetts (Figs. 87, 89, and 99 from Robinson et al., 1982b).

Robinson and Jaffe (1969a, their Fig. 2) also report enclaves that contain only sillimanite. These enclaves would have formed by reaction of gedrite + sillimanite + quartz to form cordierite. Since no aluminous minerals formed by subsequent reactions, they must have remained within the gedrite + sillimanite stability field. Figures G-20 and G-21 suggest that such rocks should be richer in Fe than those in which the other aluminous minerals (corundum, sapphirine, and staurolite) formed. Similarly, the sillimanite-only enclaves should be Mg-richer than sample 11 in which gedrite + sillimanite + quartz is a stable assemblage (Fig. G-20). The Fe-Mg ratios of gedrite (X_{Fe}=0.353) and cordierite (X_{Fe}=0.166) from the sillimanite-only enclave rocks are in fact intermediate just as Figures G-20 and G-21 predict.

Chemical-potential gradients. The reactions discussed above can produce all of the assemblages found in the cordierite enclaves when the effects of P and Fe-Mg of the bulk composition ($\mu FeMg_{-1}$) are seen, but by themselves do not account for the structure or mineral distribution of the enclaves. Aluminous minerals are rarely in contact with any phase other than cordierite. When several aluminous phases are present in an enclave, they commmonly have a crude and consistent spatial distribution. In effect, the enclaves can be thought of as zoned sets of low variance assemblages. This suggests that the growth of the enclaves was dominantly diffusion-controlled (driven by the chemical potential gradients) rather than reaction-controlled (see Fisher 1973, 1977).

The dashed line on Fig. G-20 shows a possible and highly schematic diffusion-controlled path for the reactions and bulk compositions that were discussed in the earlier example of a reaction-controlled path (heavy line, Fig. G-20). For the enclave rocks it is assumed that overstepping of the reactions occurred because the rate of P change exceeded the reaction rate. As a result, when overstepping of the first reaction occurred at point W, the rock followed a P-$\mu FeMg_{-1}$ path (dashed line between W and R) that is steeper than the slope of the reaction. Between points W and R, cordierite formed and the location of cordierite growth was dictated by the relative diffusion rates of the components. Cordierite began to form around the sillimanite because of the low mobility of Al relative to other components, and as a consequence cordierite isolated the sillimanite from the gedrite. If, in the original assemblage, only small amounts of quartz were present, it could have been completely consumed. This would result in the rock arriving at the same P-$\mu FeMg_{-1}$ conditions (point R, Fig. G-20) that it would have attained following the reaction-controlled path (heavy line) and no further reaction took place. When the next reaction was overstepped at point Y, staurolite and cordierite began to form and, as before, the locations of their growth were determined by the relative rates of diffusion of the components. The Al-rich mineral, staurolite, formed nearest to the sillimanite. As with quartz, if there were relatively little modal sillimanite remaining in the assemblage, then it might be completely consumed (point S, Fig. G-20). These P-$\mu FeMg_{-1}$ conditions are identical to ones that would have been attained following the reaction-controlled path.

These considerations lead to an interesting situation. For the above example the texture one would observe would be staurolite completely isolated from gedrite by cordierite. Staurolite and gedrite would show textural disequilibrium (i. e., no common grain boundaries), however, they would, in fact, be in chemical equilibrium through a small volume within the enclave.

Enclaves with diffusion domains. The textures and the mineral variations can be mostly explained by the diffusion-controlled, continuous, Fe-Mg reactions and through the effects of slight variations in the Fe-Mg ratio of the bulk composition. Enclaves 1, 3a, 4a, 8, and 12 (Table G-5) are accounted for in this manner. However, enclaves 2 and 3b (Table G-5), which contain all of the aluminous minerals, cannot be explained so simply. Specifically, sample 2 can be thought of as containing several different assemblages (Fig. G-15A). In most of the enclave the mineral distribution is: Sill (core) / St + Crd / Ged (matrix). In the area where sapphirine is found, staurolite is absent, and the mineral distribution is: Sill (core) / Sa + Crd / Ged (matrix). At one end of the enclave the mineral distribution is: Cor + Crd (core) / Ged (matrix).

The proximity of the assemblages suggests that these differences cannot be easily ascribed to slight variations in the Fe-Mg ratio. However the mineralogy and distribution of minerals in this enclave can be explained by examining the effects of the local availability of reacting phases by considering them first as three different bulk compositions A, B, and C (Fig. G-22), in which the phases have identical compositions, but the modal proportions of quartz are different. The heavy lines A, B, and C (Fig. G-22) represent possible reaction-controlled (equilibrium) paths through $P\text{-}\mu FeMg_{-1}$ for three bulk compositions. All three encounter reaction 1 at the same P; however, bulk composition A reacts quartz out of the assemblage over a very short P interval (see partial sillimanite projections, Fig. G-22). Accordingly, bulk compositions B and C would be subject to continuous reaction 1 for larger P (and time) intervals before quartz is removed. The new assemblage for all three bulk compositions is gedrite + sillimanite + cordierite, but the Fe-Mg ratios of the gedrite-cordierite pairs differ slightly. As portrayed, each bulk composition would next reach the limit of gedrite + sillimanite stability, however, the reaction products, cordierite + sapphirine, cordierite + corundum, and cordierite + staurolite, for each bulk composition would be different. Assuming sillimanite is reacted out of the assemblage, three different assemblages composed of gedrite, cordierite, and either sapphirine, corundum, or staurolite could be produced simply by local variations of the quartz content in the original rock.

The position of the aluminous phases in these enclaves would be controlled by the timing of the reactions. Assuming that nucleation of the aluminous minerals occurs near the sillimanite grain boundaries due to the relatively low mobility of Al, the earliest grown phases should be farthest from the sillimanite. Figure G-22 predicts that the sapphirine-forming reaction would occur at higher pressures than the staurolite-forming reaction; the positions of the sapphirine and the staurolite relative to the sillimanite support this interpretation. Note that this comparison is only possible because the areas of the effective bulk compositions are apparently so small that they can be compared in a single enclave.

Cordierite-plagioclase enclaves. These enclaves are analogous to the cordierite enclaves, but have anorthitic plagioclase as an additional enclave mineral and minor Mg-rich hornblende in the matrix. Reactions leading to the development of these enclaves can be modelled with CFMASH (C=CaO) components and treated similarly to the cordierite enclaves discussed above. However, this is not done here. The important continuous Fe-Mg reactions for these enclaves are: Hbl + Sill + Qz = Crd + Plag; Hbl + Sill = Crd + Sa + Plag; Hbl + Sill = Crd + Cor + Plag; andHbl + Sill = Crd + St + Plag.

The chemography of the quartz-free reactions is illustrated in Figure G-23. As in the case of the cordierite enclaves, the reaction a particular bulk composition encounters is a function of Fe-Mg ratio and the relative abundances of the phases. Overstepping of these reactions produces the enclave structure.

Spinel and the role of zinc. Spinel has only been found in the cordierite-plagioclase enclaves, and the Zn content of both spinel and staurolite from these enclaves is variable. All the spinels contain Zn and all the staurolites from spinel-bearing enclaves contain Zn. Staurolites from spinel-free enclaves are generally free of Zn. The inclusions of spinel in sillimanite, that are shown in Figure G-16B and described by Robinson and Jaffe (1969a), suggest that minor spinel was part of the pre-enclave assemblage. As sillimanite reacted, spinel would have been continuously exposed to the matrix, and could have participated in the staurolite-forming enclave reactions. This scenario

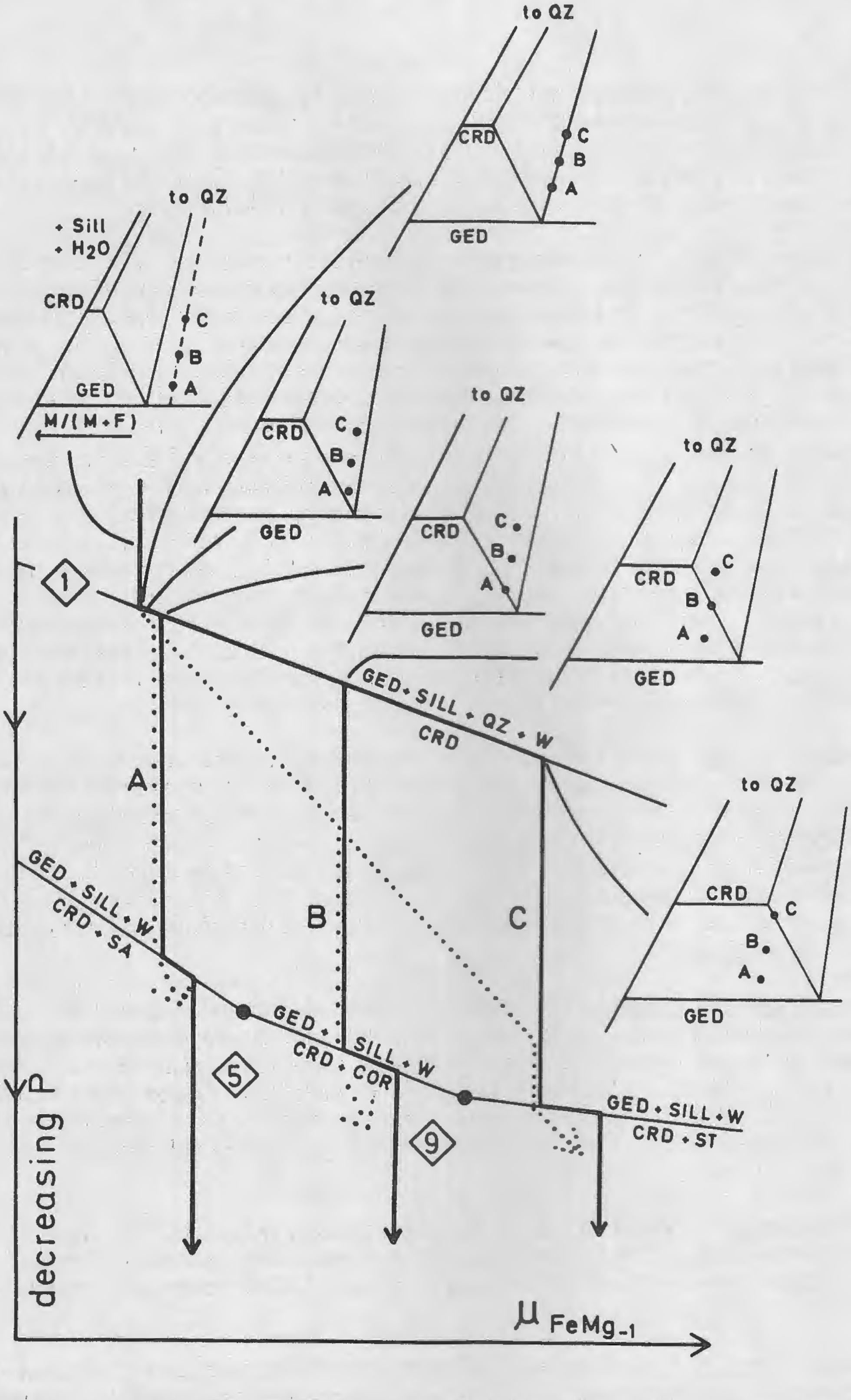
to QZ
CRD
C
B
A
GED
to QZ
+ Sill
+ H2O
CRD
C
B
A
GED
M/(M+F)
to QZ
CRD
C
B
A
GED
to QZ
CRD
C
B
A
GED
to QZ
CRD
C
B
A
GED
to QZ
CRD
C
B
A
GED
1
GED + SILL + QZ + W
CRD
A
B
C
GED + SILL + W
CRD + SA
GED + SILL + W
CRD + COR
GED + SILL + W
CRD + ST
5
9
decreasing P
μ FeMg-1

Figure G-22. A schematic P-$\mu FeMg_{-1}$ diagram that shows four of the enclave-forming reactions from Figures G-20 and G-21, and illustrates the way in which minor bulk composition variations could determine the enclave-forming reactions that are encountered. Heavy lines are schematic reaction-conrolled paths and the dotted lines are schematic diffusion-controlled paths for bulk compositions A, B, and C. Phase relations for the initial stages of the paths are also shown on portions of sillimanite projections. Abbreviations: Cor = corundum; Sill = sillimanite; St = staurolite; Sa = sapphirine; Crd = cordierite; Ged = gedrite; Qz = quartz; W = H_2O. See text for discussion.

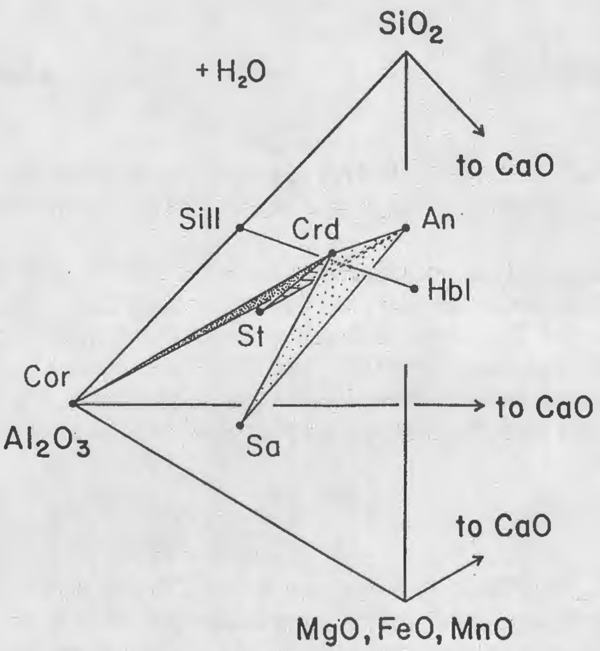

Figure G-23. A C(FM)ASH tetrahedron in which idealized hornblende (Hbl), sillimanite (Sill), cordierite (Crd), anorthite (An), sapphirine (Sa), staurolite (St), and corundum (Cor) are plotted. Patterned triangles show the three-phase assemblages Crd - An - Sa, Crd - An - St, and Crd - An - Cor which cut the Hbl - Sill tie line showing that hornblende + sillimanite in quartz-free rocks could react to form any of these sets of three-phase assemblages.

is suggested by the textures observed in sample 9a (Fig. G-16B) in which spinel inclusions in sillimanite are unreacted but much of the spinel outside of the sillimanite is overgrown by staurolite. Nevertheless, the presence of Zn-free staurolite indicates that staurolite stability was not dependent on ZnO.

Following study of outcrop I34 walk northwest and then west back to Parker Hill Road and north to Sprague Brook Crossing and vans.

27.4	Drive back (east) on approach road and ford swamp.
27.9	House and wrecked cars.
28.9	Gravel road meets Route 119. Turn right (east).
29.5	Richmond four corners. Turn right (south) onto Route 32.
30.6	Small cut on right. Felsic gneiss of Upper Member, Ammonoosuc Volcanics.
31.3	Entrance to Harry J. Bennett Town Forest. Walk about half a mile straight west on relatively flat logging road (Bullock Road) to lower slopes of "Amphibole Hill".

STOP 2: "AMPHIBOLE HILL" (Two hours)

Unlike "Iolite Hill", detailed work on "Amphibole Hill" was begun by Robinson in 1960. The samples occur in three outcrops of the Lower Member and one outcrop of the Garnet-Amphibole-Magnetite Quartzite Member of the Ammonoosuc Volcanics.

Outcrop 6A9

Ascend gentle east slope of "Amphibole Hill" to right-angle bend in Bullock Road. Turn right (north) to unimpressive summit and then walk east about 150 feet to low outcrop under pines.

The amphibolite at this locality is considered to have the normal igneous composition of a low-K basalt (Table G-4). It is more Fe-rich than the mineralogically similar sample I34B, and this is shown by the fact that the Ti mineral is ilmenite rather than rutile. The calcic amphibole is hornblende (Table G-2) with abundant fine "001" and "100" exsolution lamellae of primitive cummingtonite. The orthoamphibole is anthophyllite that is iridescent and has submicroscopic exsolution lamellae of gedrite. In collecting, avoid places where the anthophyllite is altered to chlorite.

Outcrop 7A0

Walk due west to and across Bullock Road and about 300 feet down gentle slope west of "Amphibole Hill" summit to northern of several large outcrops. This is exceedingly coarse gedrite-garnet gneiss most commonly with the assemblage quartz + oligoclase + gedrite + staurolite + sillimanite + kyanite + garnet + biotite + ilmenite, although locally cordierite has been found. Locally, there is secondary chlorite after gedrite. The gedrite is a homogeneous pleochroic gray variety identical in appearance to that at I34I. Locally, kyanite and staurolite can be seen on the outcrop surface, the latter distinguished from garnet mainly by color. Major- and trace-element geochemistry (see above) indicates this rock was originally a basalt that underwent high temperature seawater alteration followed by low temperature seawater alteration before metamorphism. The rare-earth patterns of 7A0 and 6A9 are very similar, suggesting that a low-K basalt with the composition of 6A9 may have been the protolith of 7A0 prior to seawater alteration.

The occurrence of the assemblage quartz + sillimanite (or kyanite) + garnet + cordierite + biotite in the gedrite rocks of sample I34I (Stop 1) and sample 7A0BX (this outcrop) allows an unusual opportunity for garnet-biotite and garnet-cordierite geothermometry and sillimanite-garnet-cordierite geobarometry in a region where coexisting cordierite and garnet are unknown in common rock compositions. Rather limited compositional data from these two samples are given in Table G-8 along with some tentative estimates of temperature and pressure. These should be taken with some reservation for several reasons: 1) We do not know the Fe^{3+} content of the biotite, and hence application of A.B. Thompson's (1976b) geothermometer calibrated on graphitic rocks may be misleading. 2) Detailed zoning studies of garnet have not been completed, so it is uncertain which portion of garnet may have equilibrated with cordierite in application of the pressure calibration of Tracy et al. (1976). This is somewhat mitigated by the weakness of the garnet zoning and also by obvious evidence of retrograde exchange between garnet and immediately contacting cordierite. If garnet cores never did equilibrate with cordierite, then the garnet core compositions (assuming presence of aluminosilicate plus quartz) are indicative of a minimum pressure of formation, though this might possibly have come before any of the cordierite-producing reactions in these outcrops.

It should be noted that pressure estimates should be slightly lower when kyanite rather than sillimanite is applied to the pressure calibration (Tracy et al., 1976). Most workers would place the kyanite - sillimanite boundary at about 5.5-5.8 kbar at 600°C and about 6.8-7.2 kbar at 670°C.

Outcrop I38

Walk about 500 feet downhill southwest and then west to prominent knob exposing large north-plunging open fold in Garnet-Amphibole-Magnetite Quartzite Member. This rock is well bedded and individual beds contain a profusion of different assemblages. The small excavation at

Table G-8. Mineral compositions from quartz + sillimanite + garnet + cordierite + biotite assemblages in samples I34I and 7A0BX. J.C. Schumacher and R.J. Tracy, analysts.

Garnet		Alm	Pyr	Spess	Gro
I34I	Core.	65.4	28.6	2.9	3.1
	Rim	69.3	25.8	2.5	2.4
7A0BX	Extreme core	63.9	32.0	1.4	2.7
	Core	63.9	31.9	1.5	2.8
	Rim	67.4	28.2	1.6	2.8

Biotite		Cordierite
I34I	$X_{Mg} = 0.664 - 0.680$	$X_{Mg} = 0.798 - 0.820$
7A0BX	$X_{Mg} = 0.664 - 0.678$	$X_{Mg} = 0.799 - 0.836$ (next to garnet)

Garnet-Biotite

		X_{Mg}	$\ln K_D$	T °C	P kbar (sill)
I34I	Gar core	.305	1.577	600	7.2
	Biotite	.680			
	Gar rim	.271	1.744	560	(7.6)
	Biotite	.680			
7A0BX	Gar core	.334	1.370	670	6.8
	Biotite	.664			
	Gar rim	.295	1.610	595	–
	Biotite rim	.678			

Garnet-Cordierite

I34I	Gar core	.305	2.197	605	7.2
	Cordierite	.798			
	Gar rim	.271	2.36	560	(7.6)
	Cordierite	.798			
7A0BX	Gar core	.334	2.06	650	7.0
	Cordierite	.799			
	Gar rim	.295	2.50	525	–
	Cord rim	.836			

the top of the southeast corner of the outcrop is the source of sample I38D (Table G-2). This is from a layer at least 10 cm thick of coarse gedrite-garnet-quartz granulite with subordinate ilmenite and apatite. The gedrite is gray in thin section and has a similar Fe-Mg ratio to the gedrites at I34I and 7A0. However, it is less aluminous so that it lies well within the anthophyllite-gedrite miscibility gap. A thin section from this specimen provided the first known optical observations of (010) anthophyllite exsolution lamellae in gedrite (Robinson, Ross, and Jaffe, 1971, photomicrograph in their Figure 12).

An extremely well bedded sample (I38A, Tables G-1, G-2) from the southwest corner of the outcrop showed a thin cummingtonite bed in contact with hornblende on one side and anthophyllite on the other. The cummingtonite coexisting with hornblende has "001" and "100" hornblende exsolution lamellae and is little twinned. The cummingtonite coexisting with anthophyllite is polysynthetically twinned on (100) but has no exsolution lamellae. X-ray single-crystal data show the anthophyllite, which is in parallel intergrowth with cummingtonite, has submicroscopic gedrite exsolution lamellae. The dull white-weathering beds on the surface of the outcrop are rich in apatite. Please do not hammer outcrop surfaces where white-weathering cummingtonite needles are exposed. On the northwest side of the outcrop there is a bed containing kyanite and chlorite that has not been studied in detail.

For those interested, it is possible to walk down hill about 200 feet to the west to observe quartz-feldspar-muscovite gneisses typical of the metamorphosed K-rich rhyolites in the Upper Member of the Ammonoosuc Volcanics.

Outcrop 7A8

From outcrop I38, contour southward about 1000 feet, on an obscure network of thickets and overgrown logging roads, and then descend about 50 feet around the south side of a large, isolated, overhanging outcrop. Wasps have been known to use this outcrop for nesting.

Upon discovery of this outcrop by Robinson in 1961 it was immediately recognized as a probable deformed pillow lava, a point supported by the detailed geochemical research of Schumacher, 1983 (see below). In the field individual pillows up to about 60 x 20 x 15 cm are elongate in the direction of the local hornblende lineation which plunges 12° north. Of immediate mineralogical and petrological interest was the occurrence of coarse cummingtonite in equilibrium with hornblende in which both phases have relatively coarse "001" and "100" exsolution lamellae of the other. A sample from this outcrop was subjected to early electron probe analyses by Klein (1968) and separation for wet analysis by Robinson and Jaffe (1969b). In addition this sample provided the inspiration for investigation into the relationship between optical properties and crystal structure of monoclinic amphiboles (Jaffe et al., 1968). It also provided evidence of the irrational nature of the exsolution lamellae in monoclinic amphiboles that can also be seen in monoclinic pyroxenes, and led to the formulation of the exact phase boundary theory to explain their orientations (Robinson et al., 1971a).

Pillow morphology and mineral distribution. The three-dimensional mineral distribution and the general pillow shape is shown in Figure G-24, on the fronts and backs of three successive 1.3 cm slabs across a large pillow fragment. The interior parts consist chiefly of hornblende + plagioclase and lesser amounts of cummingtonite, magnetite, and ilmenite. Towards the margin of the pillow there are discontimuous cummingtonite-rich areas that consist of plagioclase + cummingtonite and lesser amounts of hornblende, magnetite, and ilmenite. In hand specimens the predominence of cummingtonite gives the rock a pale brown color in contrast to the green color in hornblende-dominated parts of the rock. Locally, the cummingtonite-rich zones can be up to 3 cm across.

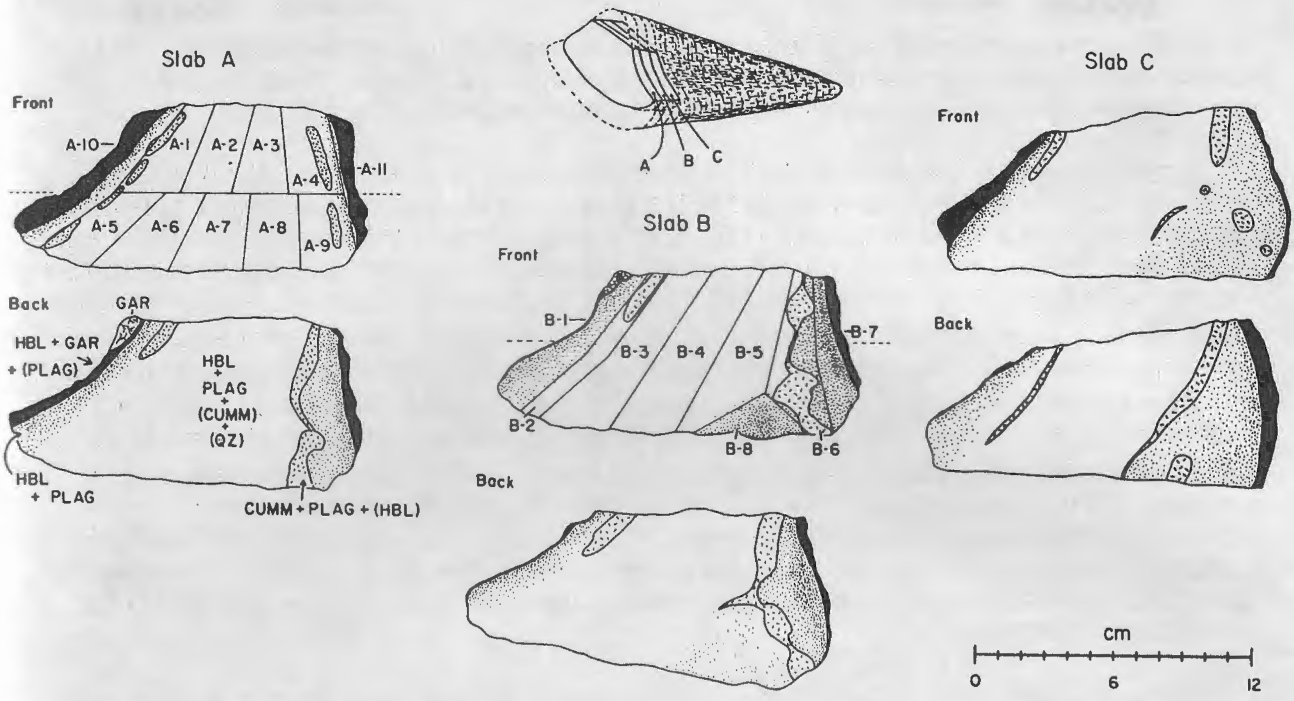
Slab A
Front
A-10
A-1
A-2
A-3
A-4
A-11
A-5
A-6
A-7
A-8
A-9
Back
GAR
HBL + GAR + (PLAG)
HBL + PLAG + (CUMM) + (QZ)
HBL + PLAG
CUMM + PLAG + (HBL)
A
B
C
Slab B
Front
B-1
B-3
B-4
B-5
B-7
B-2
B-8
B-6
Back
Slab C
Front
Back
cm
0
6
12

Figure G-24. Sketches of the fronts and backs of three slabs (A,B, and C) through the pillow. Lines on the front surfaces of A and B show the locations of pieces of the pillow that were analyzed (samples A-1 to A-11 and B-1 to B-8). Patterns on the slabs represent the generalized mineralogy, which is interpreted on the back of A. CUMM = cummingtonite, GAR = garnet, HBL = hornblende, and PLAG = plagioclase. Minor and very minor phases are shown in parentheses. Dashed lines on either side of the fronts of A and B are the traverse lines used to construct element profiles in Figures G-26 and G-27 (see text)

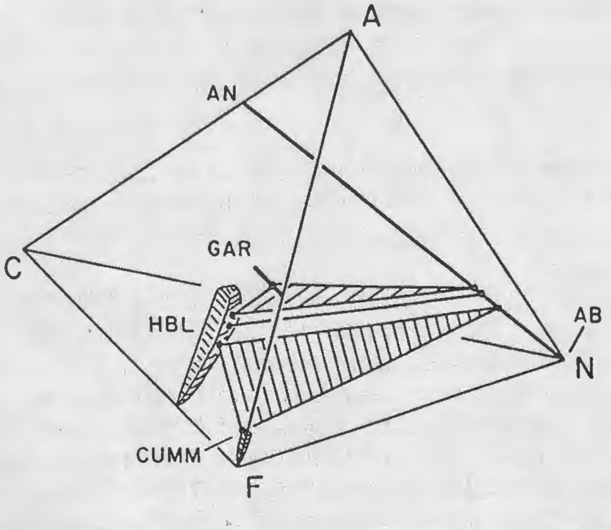
A
AN
GAR
C
HBL
AB
N
CUMM
F

Figure G-25. Schematic ACFN tetrahedron showing that the Al and Na contents of the bulk composition control the metamorphic assemblage. A = $AlO_{1.5}$ - $NaO_{0.5}$, C = CaO, F = FeO + MgO, and N = $NaAlO_2$ (all in moles). AB = albite, AN = anorthite, CUMM = cummingtonite, GAR = garnet, and HBL = hornblende.

Still closer to the edge of the pillow the modal abundance of hornblende increases. The outside edges of the pillow, interpreted to be interpillow material, consist almost entirely of hornblende + garnet and very minor plagioclase, ilmenite, and magnetite (Fig. G-24).

Mineral analyses. Hornblendes show considerable variation in Na and Al due to variable Na(A), Al(IV + VI) substitution, while Ca (M4) and therefore the cummingtonite-like substitution remains nearly constant. Compositions of the hornblendes correlate with the local assemblage and position in the pillow, and with the occurrence and coarseness of visible cummingtonite exsolution lamellae in the hornblende. Hornblende 1 (Table G-9), that coexists with garnet and An_{28} in the outermost parts of the pillow, shows no visible exsolution lamellae. Hornblendes 2A and 2B coexist only with An_{26}. Hornblende 2A is also free of exsolution lamellae, but hornblende 2B, only 1mm nearer the interior, contains fine cummingtonite exsolution lamellae. Hornblende 3 (Table G-9), which coexists with An_{20} and cummingtonite, is an additional 10 mm toward the interior and contains abundant coarse cummingtonite lamellae. The microprobe analyses of hornblende 3 and cummingtonite 3 correspond closely to the gravimetric analyses of cummingtonite and hornblende separates from these rocks (Robinson and Jaffe, 1969b). The changes in metamorphic assemblage from the pillow margin to the pillow interior are portrayed in Figure G-25 and can be crudely explained in terms of slight variations in Al content and Na/Ca ratio of the bulk composition.

Whole rock chemistry. Nineteen whole rock chemical analyses were done on sections cut from two slabs (A & B, Fig. G-24). Slab A was cut into eleven pieces and slab B was cut into eight pieces that were completely crushed and analysed by XRF. In subsequent discussion, analyses A-10, B-1, and B-7 will be referred to as "analyses of the margin", although they are actually composed of material both from the margin and the supposed interpillow area. All the remaining samples except B-8 will be referred to as "analyses of the pillow interior". Analysis B-8 represents an anomaly in the rough mineralogical symmetry that exists in slab A and the upper parts of slabs B & C (Fig. G-24), and is treated separately.

Element profiles across the pillow are shown for major elements and selected trace elements in Figures G-26 and G-27. These were constructed by projecting through the centers of pieces in each slab to points along a central traverse line (dash lines, Fig. G-24). Since the traverse line in slab B is slightly shorter than the one in slab A, it was normalized to the length of the line in A, and analyses from both slabs were plotted along the resulting single line in Figures G-26 and G-27. Shapes of the element profiles are discussed in detail by Schumacher (1983); major conclusions are discussed below.

Two kinds of explanations might be applied to element distributions. They could be preserved from the inhomogeneous distribution of the original igneous minerals and glass, or they could be due to preserved effects of pre-metamorphic hydrothermal or low-temperature alteration.

A plot of CaO versus MgO (Fig. G-28) is useful in testing the processes suggested above. Analyses from the pillow interior have a narrow range of CaO values and a wider range of MgO, and they show a linear trend with a shallow negative slope (solid line with arrows, Fig. G-28). By contrast the samples from the pillow margin and sample B-8 form a separate cluster. The Mg-Ca trend shown by the interior analyses could be due to inhomogeneous distribution of magmatic augite, pigeonite or hypersthene. To illustrate this, two hypersthenes, one pigeonite, and three augites from basalt and several basaltic andesites from the Tonga island are (Bryan et al., 1972) are also plotted in Figure G-28. These were chosen because the Tonga rocks are chemically similar to mafic Ammonoosuc rocks (Schumacher, 1981a, 1982, 1983, and in review). Control lines from any of the three low-Ca pyroxenes suggest that variations in the amount of pyroxene could have produced the trend of pillow interior analyses. Concentration of augite is one way to explain the high Ca of the margin. Sample B-6 is the most Mg-rich sample from the interior and, not

Table G-9. Electron-probe and wet-chemical analyses of hornblende and cummingtonite from zoned andesite pillow at outcrop 7A8. Locations of analyzed grains are described in text and compositions are plotted in Figures G-25 and G-28. Probe analyses by J.C. Schumacher. Wet-chemical analyses are from Robinson and Jaffe (1969b), M. Kumanomido, analyst, 1968.

	Hornblende					Cummingtonite	
Sample	1	2A	2B	3	7A8H	3	7A8C
SiO_2	40.19	41.73	42.59	44.19	44.64	51.65	52.09
TiO_2	1.24	1.34	1.27	0.96	0.97	0.20	0.18
Al_2O_3	16.01	13.24	12.43	9.50	9.95	1.33	2.62
Fe_2O_3	4.72	5.20	5.41	7.47	4.94	1.41	1.50
FeO	15.08	15.16	15.88	15.58	17.25	27.39	26.02
MnO	0.18	0.24	0.27	0.32	0.23	0.78	0.53
MgO	8.13	8.64	8.73	9.01	8.57	13.64	13.52
CaO	10.04	10.10	9.94	9.90	9.45	1.43	1.32
Na_2O	2.52	2.17	2.12	1.53	1.54	0.15	0.26
K_2O	0.29	0.25	0.24	0.16	0.31*	0.0	0.04**
Total	98.40	98.07	98.88	98.62	97.85	97.98	98.08
				23 Oxygens			
Si	5.996	6.248	6.336	6.559	6.705	7.758	7.736
Al	2.004	1.752	1.664	1.401	1.295	0.235	0.264
Fe^{+3}	-	-	-	-	-	0.007	-
Σ	8.000	8.000	8.000	8.000	8.000	8.000	8.000
Al	0.812	0.585	0.517	0.272	0.467	-	0.195
Fe^{+3}	0.530	0.586	0.606	0.840	0.558	0.152	0.168
Ti	0.138	0.151	0.142	0.108	0.109	0.023	0.021
Mg	1.808	1.929	1.937	2.008	1.919	3.054	2.994
Fe^{+2}	1.712	1.749	1.798	1.772	1.947	1.771	1.622
Σ	5.000	5.000	5.000	5.000	5.000	5.000	5.000
Fe^{+2}	0.171	0.149	0.179	0.175	0.220	1.671	1.610
Mn	0.023	0.031	0.035	0.041	0.029	0.099	0.067
Ca	1.605	1.620	1.586	1.584	1.521	0.230	0.210
Na	0.201	0.200	0.200	0.200	0.230†	0.0	0.080††
Σ	2.000	2.000	2.000	2.000	2.000	2.000	1.967
Na	0.529	0.430	0.412	0.243	0.223	0.045	0.0
K	0.055	0.049	0.044	0.030	0.060	0.0	0.007
Σ	0.584	0.479	0.456	0.273	0.283	0.045	0.007
X_{Fe}	0.513	0.500	0.505	0.497	0.534	0.537	0.524

* Also Li_2O 0.01, NiO 0.003, Cr_2O_3 0.003, H_2O+ 2.30, F 0.01.

** Also Li_2O 0.01, NiO 0.004, Cr_2O_3 0.001, H_2O+ 2.41, F 0.01.

† Includes Li 0.005.

†† Includes Li 0.005.

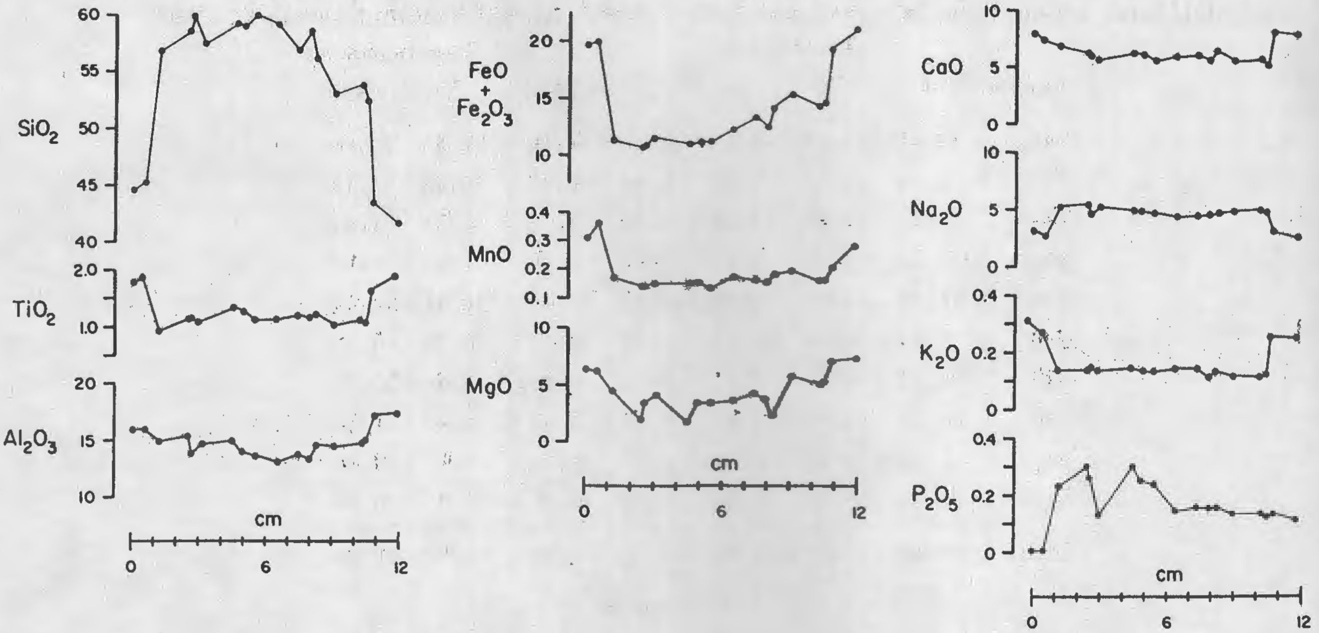

Figure G-26. Major element profiles (in wt. %) for the pillow analyses. See text for discussion.

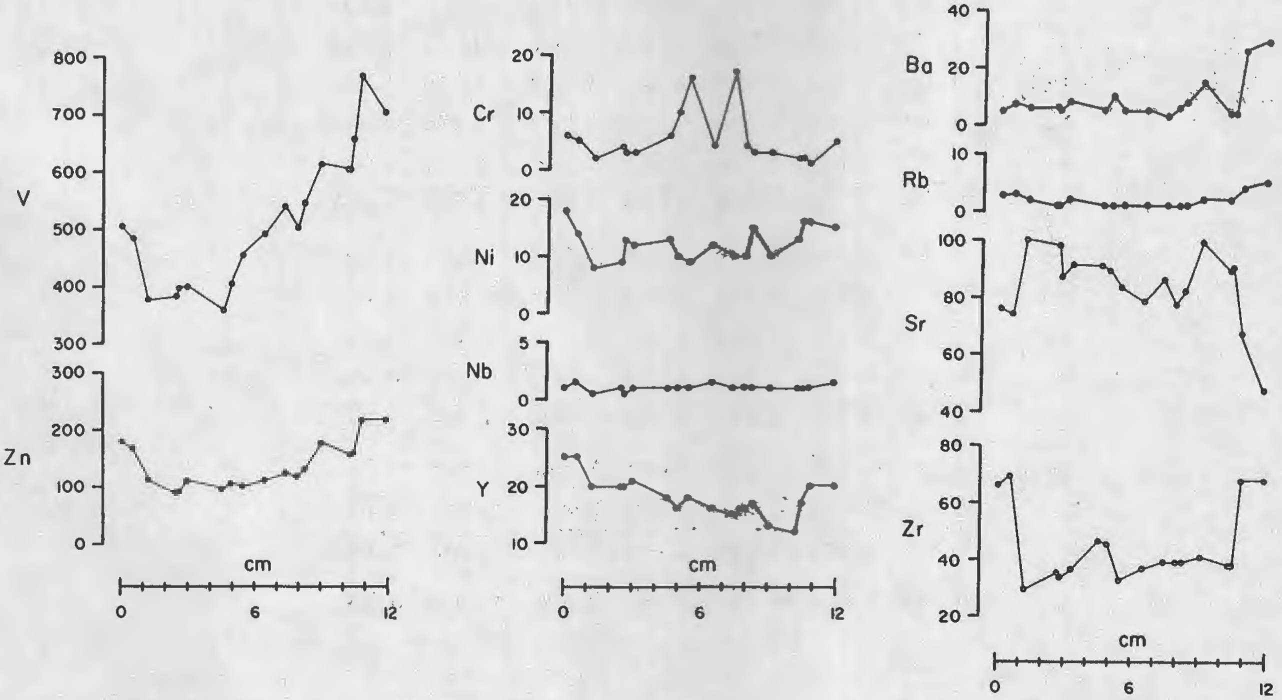

Figure G-27. Selected trace element profiles (in ppm) for the pillow analyses. See text for discussion.

surprisingly, contains abundant cummingtonite. If the above interpretation is correct , then the cummingtonite-rich areas would correspond to areas in which low-Ca pyroxene was concentrated when the pillow formed.

A one-for-one exchange of Mg in seawater for Ca in basalt, which has been documented in ocean floor basalts and experimentally (see Mottl, 1983 and references therein) would produce a much steeper trend (dashed arrow, Fig. G-28) than shown by the analyses of the pillow interior. The pillow margin analyses, which presumably should have had the most seawater contact, cannot be related to the pillow interior by this process. Consequently, none of the observed Ca-Mg variation can be accounted for by high T basalt-seawater interaction.

Low temperature alteration involves the formation of K-smectites, which results, in particular, in the loss of CaO from the rock (Hart, 1970; Melson & Thompson, 1973; Thompson, 1973; Andrews, 1977). The linear trend shown by the pillow interior analyses involves mainly changes in MgO at nearly constant CaO, and the margin of the pillow has even more CaO than the interior. Consequently, neither the Mg-Ca trend of the interior analyses nor the relationship between the interior and the margin can be explained by low temperature alteration. However, slight increases in K and the trace elements Rb and Ba in the pillow margin (Fig. G-27), may be evidence of very minor low temperature seawater-rock interaction (Hart, 1970; Melson & Thompson, 1973; Thompson, 1973; Andrews, 1977). The concentration of Zr, which is considered immobile during most geologic processes (Pearce and Cann, 1973), is significantly lower (mean value of 37.4 ppm ± 7.4 (2 sigma)) in the pillow interior, when compared with the margin values (Zr of 66 to 69 ppm). This suggests the pillow margin was not derived simply by altering the material of the pillow interior.

A strikingly strong correlation among total Fe, V, and Zn from the pillow interior also exists (Fig. G-29). All three elements increase towards the edges of the pillow. The affinity of V for magnetite is well known and Zn could be present in magnetite as franklinite component. Rhodes (1983) has suggested that rapid crystallization of magnetite at the margins of aa flows could be responsible for zoning of V, Zn, and Cr in otherwise isochemical flow units. Similarly, differences in total Fe, V, and Zn in these pillows may reflect the original distribution of magnetite in the pillow. The margins themselves fall off the trends of the interior analyses, but are quite rich in Fe, V, and Zn.

For most elements there is a major compositional discontinuity between analyses of the interior and those of the margin. The margin analyses probably represent "interpillow" material. The chemistry of the margins can be partly explained in terms of processes that might have occurred at the time of pillow formation. The interpillow areas are likely places to find accumulations of phenocrysts separated from volcanic glass. In the case of this specimen slight concentration of magnetite + Ca-pyroxene + plagioclase phenocrysts could account for the Ca, Mg, Fe, Zn, and V concentrations in the pillow margins relative to the interior. Within the pillow interior inhomogeneous distribution of magnetite + low-Ca pyroxenes could account for most of the observed chemical zoning.

Interestingly, if the analyses of the the pillow interior are assigned names on the basis of K_2O and SiO_2 content after a classification scheme used by the Basaltic Volcanism Study Project (1981), the name low-K basalt applies to two samples, low-K basaltic andesite to five samples, and low-K andesite to seven samples. An average of the entire interior would be a low-K andesite.

After examining pillow outcrop 7A8 climb directly east up hill over ledges to poor north-south trending wood road beside stone wall. Follow this north (left) to right-angle corner of Bullock Road. Turn right (east) and walk back half mile east to vans on Route 32.

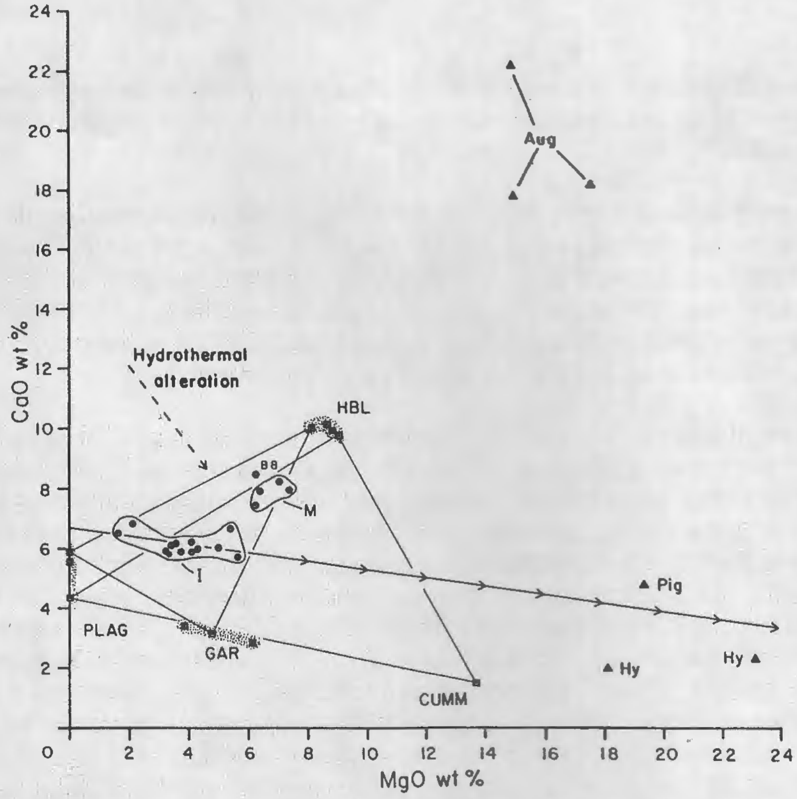

Figure G-28. Plot of CaO versus MgO for pillow analyses and mineral analyses. Closed lines surround analyses (dots) of the pillow interior (I) and the margin (M). A best-fit line for the trend of analyses from the pillow interior is shown with multiple arrowheads. Squares are cummingtonite (CUMM), garnet (GAR), hornblende (HBL), and plagioclase (PLAG) and are microprobe analyses. Tie lines connect coexisting phases. Pigeonite (Pig), hypersthene (Hy), augite (Aug) all shown with triangles, are taken from Bryan and others (1972). Dashed arrow is the trend of high temperature hydrothermal alteration involving one-to-one exchange of Mg in Seawater for Ca in basalt (Mottl,1983).

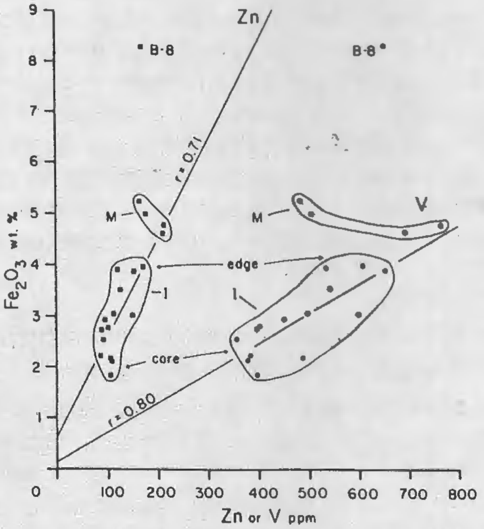

Figure G-29. Plot of Fe_2O_3 (wt. %) versus Zn and V (ppm). Squares represent Fe_2O_3-Zn analysis points and dots represent Fe_2O_3-V analysis points. Closed lines surround analyses of the pillow interior (I) and the margin (M). Analysis B-8 is shown separately (see text). The "r" is the correlation coefficient for a linear regression through analysis points of the pillow interior.

31.3 Continue south on Route 32.

32.1 Massachusetts state line. Turn right on gravel road. In woods to right is outcrop of Littleton Formation sillimanite-muscovite-staurolite schist. Staurolite is extremely scarce and contains 3.15 wt % ZnO, by far the most zincian staurolite analyzed in the region.

33.9 Four-way junction. Baptist Corners. Straight through.

34.7 Small outcrop of Clough conglomerate on right at crest of Bliss Hill.

35.9 T junction with paved Athol Road. Proceed right (west) to large outcrop on right at Orange-Warwick Town Line.

STOP 3: STAUROLITE-SILLIMANITE SCHIST NEAR SHEOMET LAKE (20 minutes)

This recently opened outcrop has been pronounced by Ben Harte of Edinburgh University as the most beautiful sillimanite-staurolite schist he has ever seen. Unfortunately, no electron probe analyses have yet been completed from this location although there is fairly abundant unpublished data from the surrounding region. The massive fibrolite sillimanite veins (described by B.K. Emerson, 1895, as "bucholzite") are here studded with euhedral staurolites.

The rock unit at this location was originally assigned by Hadley (1949) to the Lower Devonian Littleton Formation, then by Robinson (1963) to his Gray Member of the Middle Ordovician Partridge Formation, then assigned back to the Littleton Formation by Robinson (1967), and is now undergoing re-evaluation on the basis of new work in the Monadnock quadrangle (P.J. Thompson, 1985) suggesting that it may belong in the Lower Silurian Rangeley Formation! The steeply south-plunging open folds with parallel mineral lineation are typical of dome-stage folds near the south-plunging end of the Keene gneiss dome. One or two delicate graded beds suggest tops north, indicating the strata are here upside down.

This outcrop lies about one mile west of the staurolite-out isograd, although it has not yet been proved that the loss of staurolite is due to a prograde reaction or a change of bulk composition. Many schists in this vicinity contain only a muscovite-sillimanite-biotite-garnet assemblage. Probe analyses of staurolite assemblages in gray schists from this general vicinity give the following information:

Staurolite	Fe/(Fe+Mg) = 0.83-0.84,	ZnO 0.27-0.54 wt %;		
Biotite	Fe/(Fe+Mg) = 0.53-0.59,	Ti/11 Ox. = 0.09-0.10;		
Muscovite	K/(K+Na) = 0.74-0.78,	Ti/11 Ox. = 0.01-0.02,	(FeMg)/11 Ox. = 0.08-0.10.	
Garnet Rims:	Alm 78-82,	Pyr 10-13,	Spess 3-6,	Gros 2-5.

A few garnets show growth zoning with decreasing spessartine from 13 in cores to 3 in rims, all at nearly constant pyrope content. Opaque minerals are uniformly ilmenite and graphite. Garnet-biotite geothermometry suggests, with considerable uncertainty, temperatures of 550-630 °C, and garnet compositions give estimates of minimum pressure of 5.4-6.5 kbar using the calibration of A.B. Thompson (1976b) and Tracy et al. (1976), respectively.

35.9 Turn around at Town line and head southeast into depression eroded in Tully dome.

38.0 Three way junction. Bear right (southwest) onto Creamery Hill Road. Mountain to left (east) is Tully Mountain in core of Tully dome. Steep cliffs on west face have small exposure of talc-carbonate-chlorite-hornblende rock that was once mined to make sinks. Creamery Hill Road rises onto schist ridge separating Tully dome from main body of Monson Gneiss.

39.0 Center of North Orange. Turn right (northwest) past "The Overview" (farm) and descend into valley eroded in the south-plunging north end of the main body of Monson Gneiss.

40.2 Bottom of valley. Sharp right (south) onto Williams Pond Road. Note views in next several miles of high rim of schists to west of Monson basin.

44.4 Stoplight in center of Orange. Go straight through and across Millers River. You are now on Route 122.

46.7 Underpass under Route 2. Continue straight.

47.4 Junction 122 and 202. Continue straight on combined routes and then stay on Route 202 for many miles.

51.4 Village of New Salem. Crest of ridge on west side of Monson basin.

54.0 Outcrops to right of Cooleyville Granitic Gneiss with Prescott Gabbro inclusions, a syn-Acadian intrusion that forms the backbone of Prescott Peninsula in Quabbin Reservoir.

56.6 Pass turn off (right) for Shutesbury. Stay on Route 202.

58.2 Pull over in paved ditch for optional Stop G-4 in Late Precambrian Mount Mineral Formation of Pelham dome. This is to view relict granulite facies pelites retrograded to kyanite-muscovite schists during the Acadian (Robinson et al., 1975; Roll, 1986).

60.2 Quabbin Reservoir overlook on left and long road cut in Late Precambrian Pelham Quartzite on right, east limb of Pelham dome.

60.9 Yellow blinker. Turn sharp right (west) off Route 202 onto Amherst Road. Type outcrop of Pelham Quartzite buried in front yard of Town Hall. Cross arch of Pelham dome, descend west limb to Connecticut Valley border fault at east edge of Mesozoic basin.

67.1 Turn right (northwest) from Pelham Road onto Triangle Street and continue straight to edge of University of Massachusetts campus.

68.4 Delivery at front door of University of Massachusetts Campus Center Hotel.

H. THE CENTRAL MASSACHUSETTS METAMORPHIC HIGH

Peter Robinson, Robert J. Tracy, Kurt T. Hollocher, John C. Schumacher, and Henry N. Berry IV

PURPOSE OF TRIP

The purpose of this trip is to examine petrologic features on the west side and in the center of the central-Massachusetts metamorphic high, which appears to be the largest area of consistently very-high-grade Phanerozoic rocks in the Appalachians. This zone is dominated by metamorphosed pelites in an outer muscovite-free Sillimanite - Orthoclase Zone and an inner Sillimanite - Orthoclase - Garnet - Cordierite Zone. In addition, there are various metamorphosed mafic and intermediate igneous rocks in which reactions leading from amphibolites to pyroxene granulites have been studied in detail, and which locally contain classic granulite facies orthopyroxene - K-feldspar assemblages. Throughout this region there is evidence of partial melting of many bulk compositions, as well as of severe deformation following the peak of metamorphism. En route to the high-grade region, a short visit will be made to coarse gedrite rocks near the kyanite-sillimanite isograd, containing zoned orthoamphibole grains with extreme compositions.

PETROLOGICAL BACKGROUND

Early petrologic work in central Massachusetts was done by B.K. Emerson (1898, 1917) who gave remarkably accurate desciptions of mineral assemblages in a variety of rocks. Heald (1950) first brought out the significance of the sillimanite-orthoclase zone in New England based on his work in southwestern New Hampshire. The first modern study in Massachusetts was by Barker (1962) on rocks near Sturbridge and nearby Union, Connecticut. This was followed by Hess (1969, 1971) who did electron probe studies of zoned garnet and coexisting biotite and cordierite near Sturbridge. Extensive field research and petrography was accomplished in the late 1960's and 1970's by personnel of the U.S. Geological Survey. This work is summarized by Robinson et al. (1982a, 1982c), as is the early part of the present round of research begun by Field (1975), Tracy (1975, 1978), Tracy et al. (1976), and Tucker (1977). Acknowledgements for assistance and advice up to 1982 are also given in that paper.

REGIONAL SETTING

Research on the geologic setting has involved intense study of stratified and intrusive rocks of Late Precambrian, Ordovician, Silurian, and Lower Devonian age as well as Triassic-Jurassic strata in adjacent rift basins. The structural development of the region took place mainly in the Middle Ordovician Taconian orogeny and more intensely in the Devonian Acadian orogeny. In terms of plate tectonics as presently understood, the area lay east (present geography) of the early Paleozoic ocean that closed during the Taconian orogeny and east of the pertinent subduction zone. It also lay on the west side of a major Silurian-Lower Devonian marine sedimentary trough (Merrimack Trough) that closed at the beginning of the collisional tectonics of the Acadian orogeny. In the early Devonian this trough was overspread by eastward-derived flysch, closely followed by the onset of the Acadian orogeny, with its attendant plutonism, nappe-style tectonics, gneiss domes, and metamorphism. Detailed definition of Silurian-Devonian stratigraphy in rocks as high grade as the granulite facies is providing the key to the structure and hence to the metamorphism. Acadian tectonic development involved early west-directed regional nappes that have very recently been subdivided into early fold nappes and later thrust nappes, several poorly understood deformations loosely classed under the stage of backfolding and involving complex rock fabric development and formation of mylonites, and a culminating deformation with intense tectonic overprinting generally associated with the gravitational rise of gneiss domes of the Bronson Hill anticlinorium. The thrust-nappe phase had already been implied by the petrologic evidence for abrupt pressure increases determined in the studies of Frank Spear and of Page Chamberlain (this guidebook, parts D and F) to the north. The pattern of metamorphic isograds, as well as the reconstructed P-T trajectories of individual samples or groups of samples, bears a complex relationship to these deformations that needs to be better understood to develop a clearer and chronologically more precise tectonic and thermal history of the belt. In such work, intrusive rocks have played an important role because of their effects on patterns of metamorphism, because they have given information about times of deformation, and because their chemistry can give some clues as to the global tectonic setting in which they were emplaced. Stratigraphic and structural interpretations are changing rapidly. In particular, rather large areas previously assigned to the Middle Ordovician Partridge Formation are now in the process of being reassigned to the Lower Silurian Rangeley Formation, and major westward thrusting is proving to be a much larger component of the early Acadian nappe phase than previously recognized.

STRATIGRAPHY

The nature and age of pre-Middle Ordovician basement rocks in the gneiss domes continues to be a problem (Robinson, 1981). The stratified gneisses in the core of the Pelham dome are still considered late Precambrian on the basis of one zircon age (Naylor et al., 1973; Zartman and Naylor, 1984) and lithic similarities to rocks in southeastern Connecticut. Hodgkins (1983, 1985) has shown that the dominant felsic gneisses of this sequence have a major and trace element chemistry consistent with interpretation as a sequence of chemically evolved alkali rhyolites with low normative anorthite and extremely low MgO/(MgO+FeO) ratios that might have erupted in a rifting environment. The relics of an old granulite facies metamorphism that survived Acadian kyanite-muscovite overprinting (Robinson, Tracy and Ashwal, 1975; Roll, 1986) are still of unknown age, but are tentatively assigned to the late Precambrian (Robinson, 1983). The layered plagioclase gneisses and amphibolites that are called Fourmile Gneiss where they overlie the late Precambrian in the Pelham dome, and called Monson Gneiss in most other areas, have not yet been satisfactorily dated. An abortive attempt on the Fourmile Gneiss in 1980 resulted in a zircon age of 370 m.y. (R.E. Zartman and G.W. Leo, personal communication) on a gneissic layer, which on restudy of field data and subsequent geochemical investigation (Hodgkins, 1985), proved to be a previously unrecognized sill of the Devonian Belchertown Quartz Monzodiorite (Ashwal et al., 1979). A new and better sample has now been processed and submitted to R.E. Zartman for dating (G.W. Leo, personal communication, 1985). The Monson Gneiss in Massachusetts has yielded a zircon age of about 450 m.y., but the New London Gneiss of southeastern Connecticut, lithically identical to part of the Monson, gives an age over 500 m.y. (Zartman and Naylor, 1984). Massive batholithic-looking gneisses in the domes, including the Pauchaug Gneiss of the Warwick dome, appear to give consistent ages around 450 m.y. (Zartman and Leo, 1984).

The Ammonoosuc Volcanics of presumed Middle Ordovician age, is the basal unit of the cover sequence and its detailed stratigraphy is crucial to understanding the basement-cover problem. In the early 1970's a basal quartzite and conglomerate lens was found where the Ammonoosuc overlies the Monson Gneiss in the Orange quadrangle, and in 1983 thin lenses of quartzite were found precisely on the same contact in two localities in the Quabbin Reservoir area. Despite numerous suggestions that the massive batholithic-looking gneisses are intrusive into the Ammonoosuc (Leo, 1985) and the radiometric dating that appears to make this permissible (Zartman and Leo, 1984), there remains no good documentation of intrusive gneisses substantially truncating a well defined Ammonoosuc stratigraphic sequence.

The research of Schumacher (1983, in review, and this guidebook, part G) and Hollocher (1983, 1985) shows that the volcanics of the Ammonoosuc and the overlying Middle Ordovician Partridge Formation are quite similar in their major and trace elements to the low-K tholeiites, andesites, and dacites, as well as K-bearing rhyolites of modern island arcs such as Tonga and New Britain. An important aspect of their conclusions is that the K-bearing peraluminous rhyolites that characterize the upper part of the Ammonoosuc and continue into the Partridge, are not the product of melting of subducted North American continental crust as suggested by Robinson and Hall (1980), nor melting of subducted pelitic sediments, but were produced by melting of amphibolite or granulite of tholeiitic basalt composition within the subduction complex.

Stratified Silurian-Devonian rocks occur in two main belts. In the Connecticut Valley belt to the west the longstanding stratigraphic dilemma of the Erving Formation (Robinson, Hatch and Stanley, 1984, and in press) has been tentatively resolved by a proposed major premetamorphic thrust, the Whately thrust (Figure H-1). In this proposed resolution, admittedly based on circumstantial evidence, the true stratigraphic sequence from oldest to youngest is Littleton Formation, Erving Formation, and Gile Mountain and Waits River Formations. In the center of the synclinorium the Littleton has been carried by the Whately thrust to a position above the Gile Mountain-Waits River, along a line that traces into the legendary Chicken Yard line of southern Vermont. To the east the proposed thrust disappears into bedding within the Littleton Formation.

The early Acadian fold nappes of the Connecticut Valley region lie structurally above and to the east of the Whately thrust, and are for the most part rooted on the east side of the Bronson Hill anticlinorium. As such, their stratigraphy might be expected to be transitional between that of the Bronson Hill anticlinorium and that of the Merrimack belt to the east (Figure H-2). Recent work by J.B. Thompson and Page Chamberlain (personal communication, up to 1985) on the Bernardston and Skitchewaug nappes in Vermont and New Hampshire indicates that the Clough Quartzite contains mappable members that may be transitional to units in the Rangeley Formation farther east. However, in the Hinsdale, N.H. area west of the Ashuelot pluton Elbert (1986) has mapped an attenuated, multiply folded, imbricated Monadnock sequence (Figure H-2) of rocks in apparent thrust contact with the Partridge Formation in the core of the Bernardston fold nappe.

In the Merrimack belt to the east (Figure H-2) a major revolution in the stratigraphic thinking is under way based on correlations with Maine stratigraphy (Hatch, Moench, and Lyons, 1983; Duke, 1984; P.J. Thompson, 1985). This includes not only the Smalls Falls and Madrid Formations which have been well established in Massachusetts since the mid-1970's, but the much more difficult recognition of the Lower Silurian Rangeley Formation (P.J. Thompson, 1982, 1985; Duke,1984; Berry, 1985), portions of which bear close similarity to portions of the Ordovician Partridge Formation and Devonian Littleton Formation. Virtually nothing in the Merrimack belt remains to be assigned to "Partridge" (most of the local maps except Figures H-7 and H-8 in this field guide are obsolete in this respect). As has been true throughout this century, the stratigraphy is still the most crucial key to understanding tectonic and metamorphic history, even in rocks that have been metamorphosed in the granulite facies.

STRUCTURAL GEOLOGY

Acadian deformations in central Massachusetts and adjacent New Hampshire have been summarized elsewhere (Robinson, 1979; Hall and Robinson, 1982). These are broadly divided into an early nappe stage, an intermediate backfold stage, and a late gneiss dome stage, each with many complications.

The fact that some of the early west-directed fold nappes have locally faulted-out limbs has long been recognized (Thompson et al., 1968) but the possibility that there are other major thrusts, possibly of great magnitude, seems to be a relatively new idea. These would include the proposed Whately thrust (Robinson, Hatch and Stanley, in press; see also Stratigraphy) in the Connecticut Valley region (Figure H-1) that is thought to become a bedding plane thrust to the east within the Littleton Formation, and may predate the fold nappes themselves. Another thrust, first suggested by Page Chamberlain (personal communication, 1982) on the basis of steep metamorphic gradients in the Lovewell Mountain quadrangle, New Hampshire, has been traced by Peter Thompson through the Mt. Monadnock area as the Chesham Pond thrust fault (Figure H-3). The relations

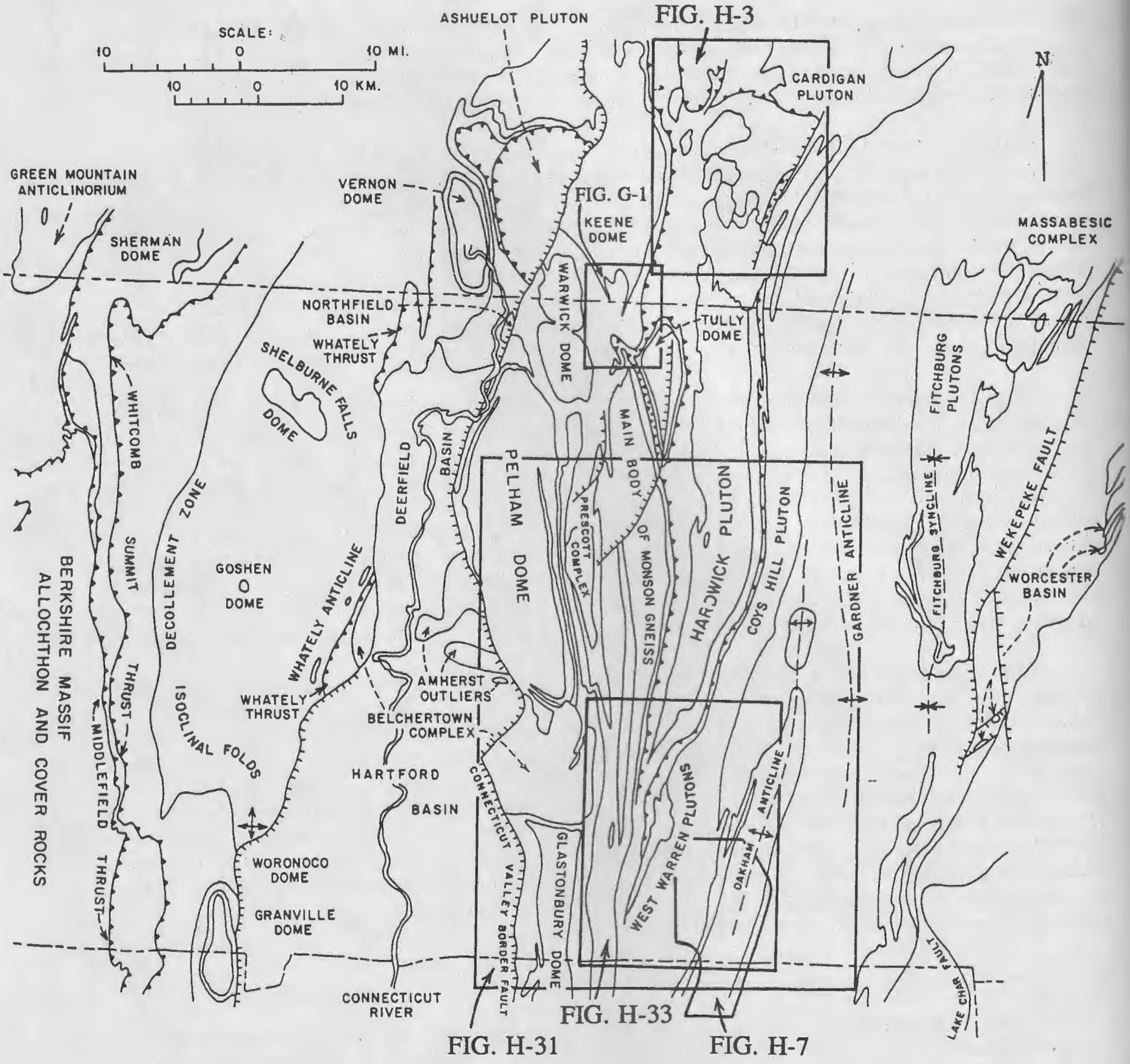
ASHUELOT PLUTON
FIG. H-3
SCALE:
10 0 10 MI.
10 0 10 KM.
CARDIGAN PLUTON
N
GREEN MOUNTAIN ANTICLINORIUM
VERNON DOME
FIG. G-1
KEENE DOME
MASSABESIC COMPLEX
SHERMAN DOME
NORTHFIELD BASIN
WHATELY THRUST
WARWICK DOME
TULLY DOME
SHELBURNE FALLS DOME
WHITCOMB
FITCHBURG PLUTONS
DEERFIELD BASIN
PELHAM DOME
MAIN BODY OF MONSON GNEISS
PRESCOTT COMPLEX
HARDWICK PLUTON
COYS HILL PLUTON
GARDNER ANTICLINE
FITCHBURG SYNCLINE
WEKEPEKE FAULT
SUMMIT THRUST
DECOLLEMENT ZONE
GOSHEN DOME
WHATELY ANTICLINE
WORCESTER BASIN
BERKSHIRE MASSIF ALLOCHTHON AND COVER ROCKS
MIDDLEFIELD THRUST
ISOCLINAL FOLDS
WHATELY THRUST
AMHERST OUTLIERS
BELCHERTOWN COMPLEX
HARTFORD BASIN
CONNECTICUT VALLEY BORDER FAULT
GLASTONBURY DOME
WEST WARREN PLUTONS
OAKHAM ANTICLINE
WORONOCO DOME
GRANVILLE DOME
CONNECTICUT RIVER
LAKE CHAR FAULT
FIG. H-33
FIG. H-31
FIG. H-7

Figure H-1. Geologic index map of central Massachusetts and adjacent states showing areas of more detailed figures.

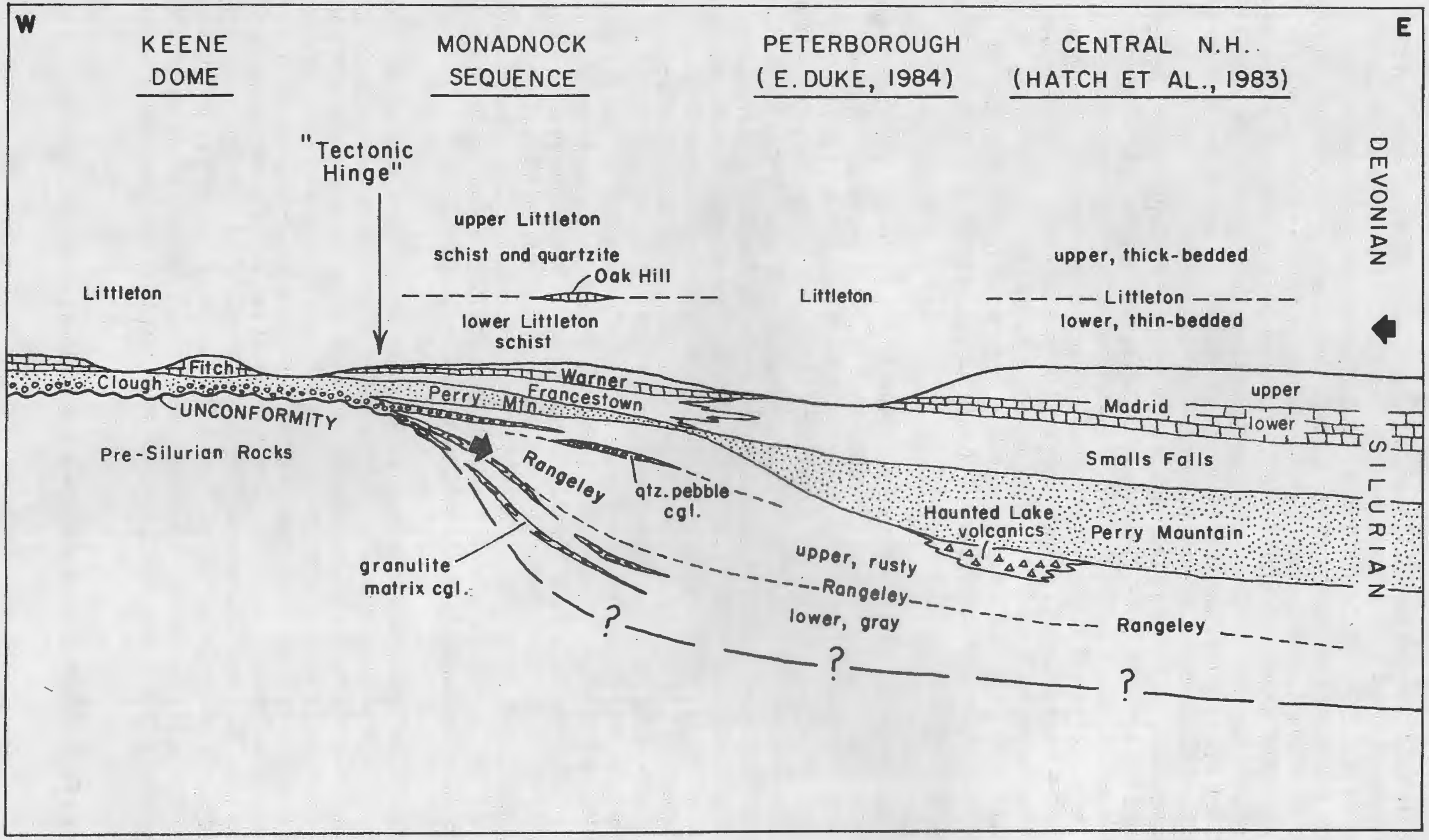
W
E
KEENE DOME
MONADNOCK SEQUENCE
PETERBOROUGH (E. DUKE, 1984)
CENTRAL N.H. (HATCH ET AL., 1983)
"Tectonic Hinge"
upper Littleton
schist and quartzite
Oak Hill
lower Littleton schist
Littleton
Littleton
upper, thick-bedded
Littleton
lower, thin-bedded
DEVONIAN
Fitch
Clough
UNCONFORMITY
Pre-Silurian Rocks
Warner
Francestown
Perry Mtn.
Madrid
upper
lower
Smalls Falls
SILURIAN
Rangeley
qtz. pebble cgl.
Haunted Lake volcanics
Perry Mountain
granulite matrix cgl.
upper, rusty
Rangeley
lower, gray
Rangeley
?
?
?

Figure H-2. Reconstructed stratigraphic profile across the "tectonic hinge" between the Keene dome of the Bronson Hill anticlinorium and areas in the Merrimack trough to the east. Heavy black arrows show a change in sediment source direction from Silurian to Devonian. From P.J. Thompson , 1985, Figure 2.

between this thrust and the earlier fold nappes, as discussed by Thompson (1985) in the Monadnock area, open up the possibility of a whole new range of complications, some of which are summarized below.

Structural data on Mt. Monadnock itself (Figure H-3) have led to the conclusion that the most prominent set of mapped isoclinal folds in bedding are in fact folds of the nappe stage. In their original setting, they were satellitic folds on the upper limb of a major nappe-stage syncline, the Monadnock syncline, that was overfolded from east to west, so that bedding faced west along the nappe-stage axial surfaces. Subsequently, by a complex process involving structural features of both the back-fold and dome stages, the originally west-facing recumbent folds were overturned toward the east, so that the strata now face east and southeast along the original nappe-stage axial surfaces. Thus, the strata on the mountain, that were once predominantly upside down on the lower limb of a major anticlinal nappe, are now predominantly right-side-up again as a result of the later folding. A detailed study of structural relations in the vicinity of the nappe-stage Chesham Pond thrust fault in the northern part of the quadrangle, including detailed analysis of features within the Derby Hill tectonic window (Figure H-3), suggests the following new interpretation illustrated schematically in Figure H-4, with effects of later deformations removed. The thrust fault clearly cuts across the axial surfaces of nappe-stage folds, indicating that the thrust is not merely an attenuated lower limb of a fold. The strong development of augen schists in the Rangeley Formation near the upper surface of the Chesham Pond thrust is extremely similar to the development of augen schists by dismemberment of pegmatites during synmetamorphic shearing on the Sgurr Beag slide in the Scottish Highlands.

Beyond the Monadnock region the Chesham Pond thrust may encircle Fall Mountain near Bellows Falls, Vermont (J.B. Thompson, Page Chamberlain, F.S. Spear, personal communications, 1983-85; this guidebook, part F) and the Ashuelot pluton (Figures H-1, H-5) in the Hinsdale area under study by Elbert (1986) and Armstrong (1986). It is tentatively extended from the Monadnock quadrangle southward along the west margin of the Coys Hill pluton (=Cardigan pluton) through central Massachusetts and probably into Connecticut. Another proposed thrust, the Brennan Hill thrust, is a contact on the east side of the Keene dome separating strata assigned to the Lower Member of the Silurian Rangeley Formation above, from the Devonian Littleton Formation below (Figures H-3, H-4). To the south, in the Mount Grace quadrangle, Massachusetts, this contact cuts along the top of the root zone of the Bernardston nappe and is also believed to wrap entirely around the Tully dome (Figure H-5, see also Figure G-1). To the west near Hinsdale, New Hampshire west of the Ashuelot pluton, Elbert appears to have identified the same surface where a complexly deformed "Monadnock sequence" of strata appears to be in thrust contact with Partridge Formation in the core of the Bernardston nappe. On the basis of these considerations and direct lithic comparisons with the Monadnock quadrangle, the rocks mapped as Littleton, Clough, and Partridge in the Amherst, Massachusetts area (Figure H-1) by Jasaitis (1983) are now assigned to the Rangeley Formation above the Brennan Hill thrust.

The backfold stage of deformation is commonly divided into several parts, none of which is well understood. One of the earliest effects was a northward longitudinal transport of the Tully body and the main body of Monson Gneiss, causing the sequence to the north, including the axial surface of the Bernardston nappe and the Brennan Hill thrust (Figure H-5), to be overturned to the north. The eastward overturning all along the east side of the Bronson Hill anticlinorium in Massachusetts, as well as the Beech Hill anticline (Figure H-3) of the Mt. Monadnock quadrangle may have been produced at this time. The narrow Greenwich "syncline" of Partridge Formation completely surrounded by Monson Gneiss (Stops 2 and 3, this field trip) may be a syncline on top of the Monson (see Zen et al., 1983, section D-D'), but is now considered more likely an anticline complicated by Mesozoic faulting and revealing inverted strata that lie beneath the Monson (Figure H-5).

From the Quabbin Reservoir area eastward to Wachusett Mountain important features

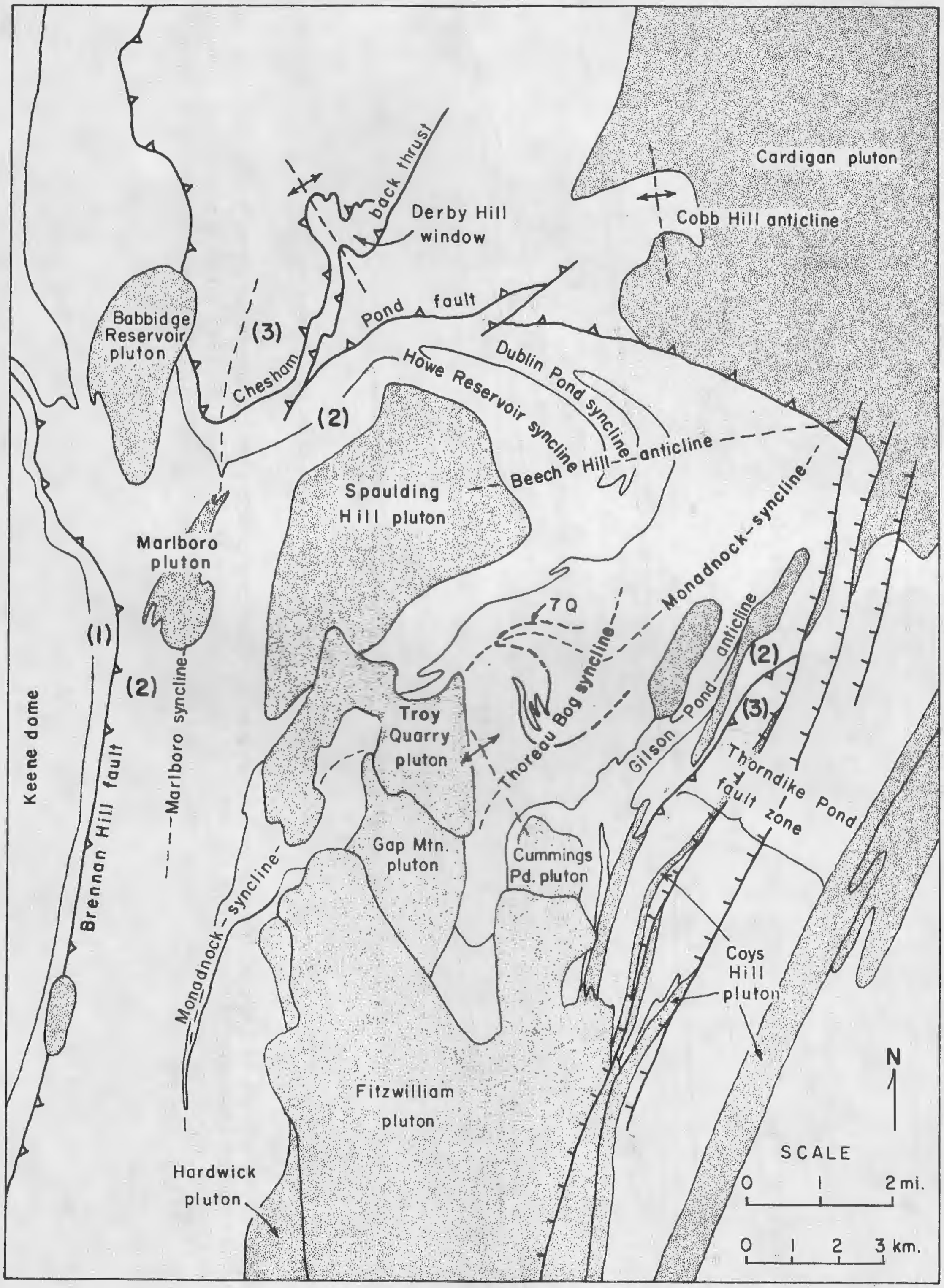
back thrust
Derby Hill window
Cardigan pluton
Cobb Hill anticline
Babbidge Reservoir pluton
(3)
Chesham Pond fault
Dublin Pond syncline
Howe Reservoir syncline
(2)
Beech Hill anticline
Spaulding Hill pluton
Marlboro pluton
Monadnock syncline
7Q
(1)
(2)
Keene dome
Brennan Hill fault
Marlboro syncline
Troy Quarry pluton
Thoreau Bog syncline
Gilson Pond anticline
(2)
(3)
Thorndike Pond fault zone
Gap Mtn. pluton
Cummings Pd. pluton
Monadnock syncline
Coys Hill pluton
Fitzwilliam pluton
Hardwick pluton
N
SCALE
0 1 2 mi.
0 1 2 3 km.

Figure H-3. Simplified geologic map of the Monadnock quadrangle showing three structural levels (1, 2, 3) separated by nappe-stage thrust faults. The contact at the base of the Lower Devonian Littleton Formation outlines various other structural features. From P.J. Thompson, 1985, Figure 13.

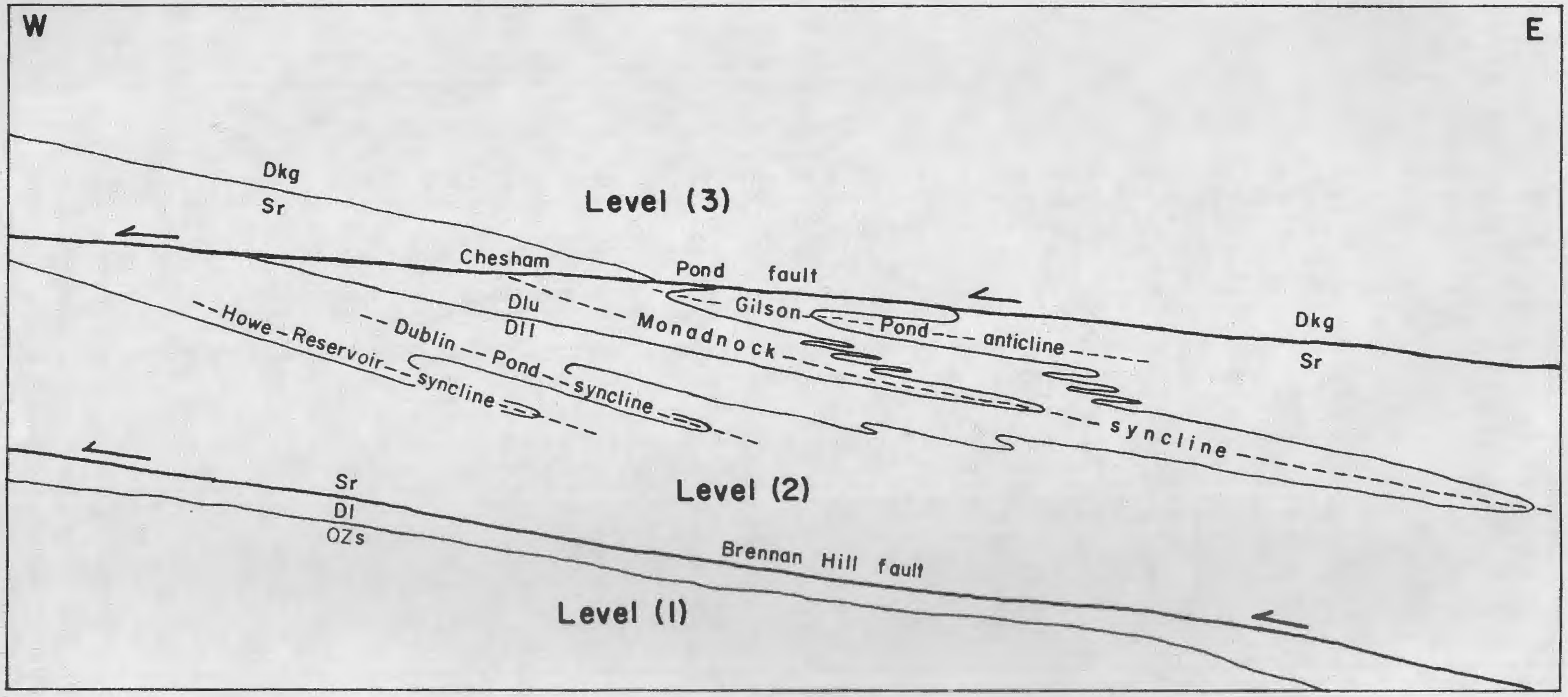
W
E
Dkg
Sr
Level (3)
Chesham
Pond fault
Gilson
Pond
anticline
Dlu
Dll
Monadnock
syncline
Howe-Reservoir
syncline
Dublin-Pond
syncline
Dkg
Sr
Sr
Dl
OZs
Level (2)
Brennan Hill fault
Level (1)

Figure H-4. Reconstructed tectonic profile across the Monadnock quadrangle with younger structural features removed. Shows nappe-stage recumbent folds truncated by later nappe-stage thrusts that separate three tectonic levels. Only dome gneiss (OZs), Rangeley Formation (Sr), members of the Littleton Formation (Dll and Dlu) and Kinsman Granite (Dkg) are shown for clarity. From P.J. Thompson, 1985, Figure 17.

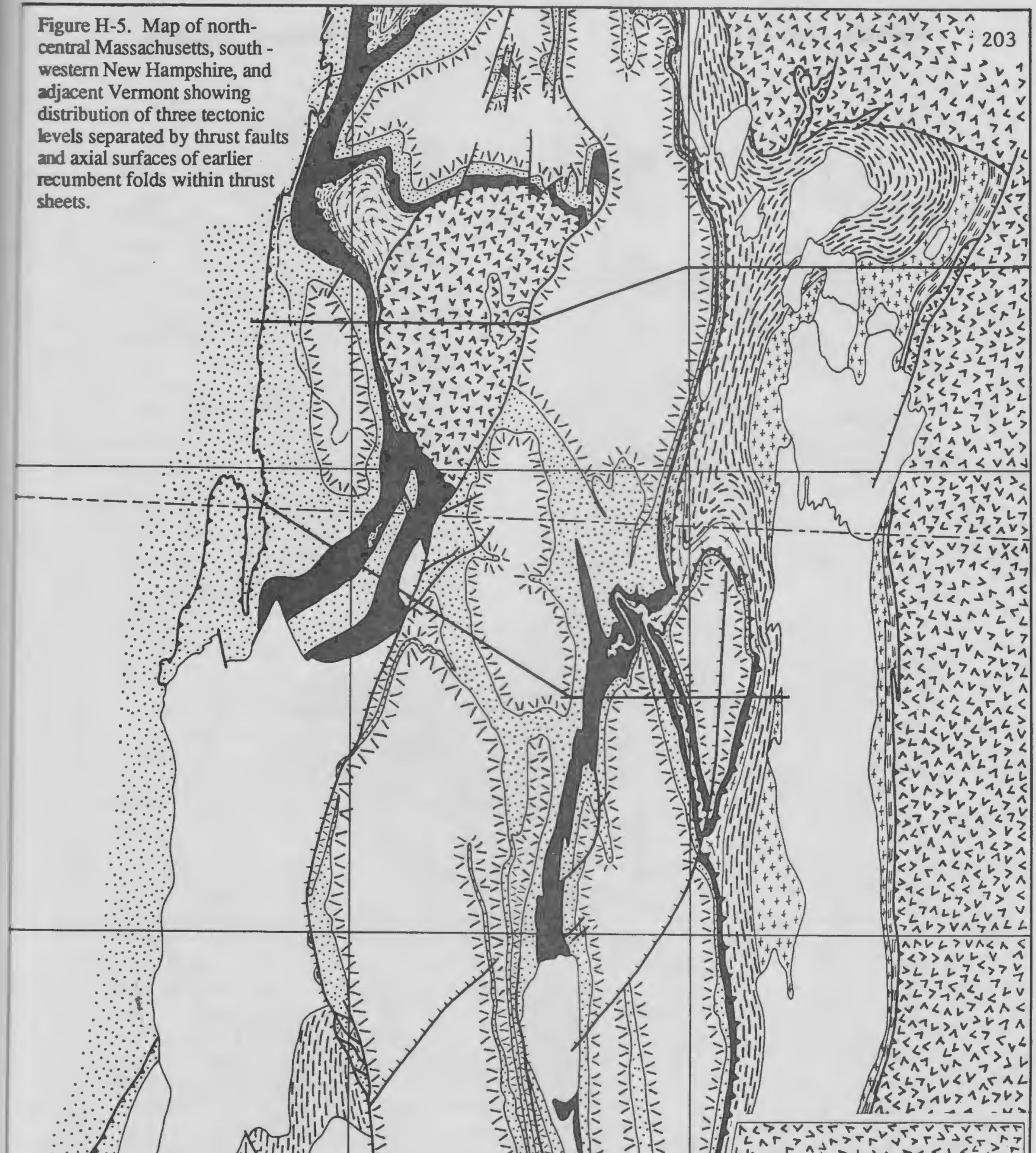
CHESHAM POND THRUST
MONADNOCK SYNCLINE
GILSON POND ANTICLINE
HINSDALE SYNCLINE
BRENNAN HILL THRUST
BERNARDSTON NAPPE
GNEISS IN CORES OF DOMES

Figure H-5. Map of north-central Massachusetts, south-western New Hampshire, and adjacent Vermont showing distribution of three tectonic levels separated by thrust faults and axial surfaces of earlier recumbent folds within thrust sheets.

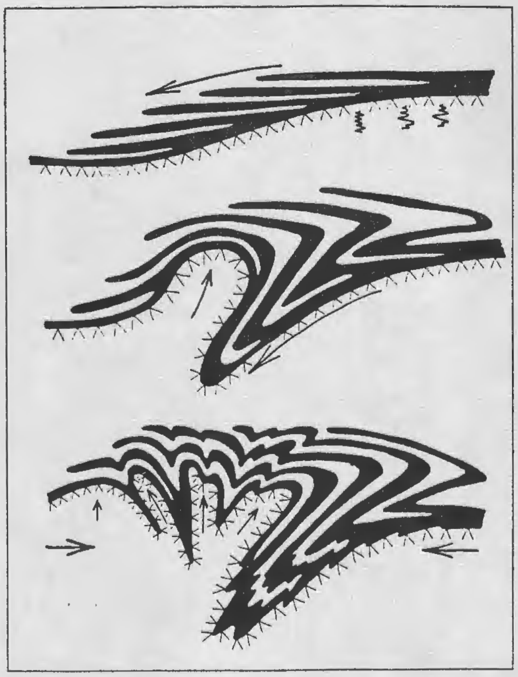

Figure H-6. Cartoon of the sequence of major deformations in the Bronson Hill anticlinorium and Merrimack synclinorium, central Massachusetts and adjacent New Hampshire (from Hall and Robinson, 1982).
Top: Early Acadian nappes overfolded from east to west with heated rocks in the east overfolded onto cooler rocks in the west.
Middle: Backfolding of early nappe axial surfaces with overfolding from west to east. Late in this stage there was extensive mylonitization due to high strain rates on a series of west-dipping surfaces.
Bottom: Gneiss-dome stage involving tight to isoclinal folding of earlier axial surfaces and the gravitational upward movement of low density gneisses into heavier mantling strata.

tentatively assigned to the backfold stage are east-west trending folds in foliation that appear to have formed just after or during the peak of regional metamorphism and are associated with a prominent east-west trending mineral lineation. A variety of mylonites truncate the peak metamorphic fabric as shown by coarse porphyroclasts of hornblende, orthoclase, garnet, and cordierite, but lineation within the mylonites trends parallel to the regional E-W lineation, suggesting the possibility that the folds of this stage were rotated into parallelism with the transport direction during a period of large-scale rapid strain.

In its earlier conceptions (Robinson, 1979; Hall and Robinson, 1982), the phase of backfolding was thought to involve one master anticlinal surface passing through the main body of Monson Gneiss and thence northward into the Mt. Monadnock region, and to the east of this anticline several subordinate east-directed nappe-like anticlines and synclines, that have always been difficult to identify. Two candidates for such backfold-stage synclines were the Monadnock syncline (Figure H-3 and Figure H-6) and the syncline that runs west of the Oakham anticline as shown on Figure H-1. The detailed studies of P.J. Thompson (1985) have demonstrated that the Monadnock syncline must be a nappe-stage feature that has been backfolded, and is now on the east limb of the master backfold anticline, identified as the Beech Hill anticline (Figure H-3). Thompson could identify no equivalent backfold syncline and indicated that all major repetitions of strata in the Monadnock area east of the Beech Hill anticline were the product of nappe-stage features. A possible, though extreme, extrapolation of these observations might be that the entire orogen east of the Beech Hill anticline is overturned to the east, that is, that there is no backfold syncline, at least within the limits of the Merrimack synclinorium.

In the Brimfield-Sturbridge area (inset Figure H-7 in Figure H-1), a granulite facies region in the Merrimack belt currently under study by Henry Berry, the above proposal has crucial consequences. The focus of Berry's work has been to reinterpret the stratigraphy and tectonic history of the area in light of new stratigraphic and structural ideas about the Merrimack synclinorium in New Hampshire and Maine (Osberg, 1980; Hatch, Moench and Lyons, 1983; Eusden et al., 1984; P.J. Thompson, 1985; Chamberlain, 1985, 1986a; Spear, 1986). The previous interpretation, based on quadrangle mapping (Pease, 1972; Peper and Pease, 1975; Pease, 1975; Pomeroy, 1975; Seiders, 1976; Fahey and Pease, 1977; Pomeroy, 1977; Moore, 1978) and compiled by Zen et al. (1983) and Rodgers (1985), shows the study area to consist largely of Middle Ordovician Partridge Formation (Brimfield Schist in Connecticut). This area has been significantly reinterpreted in the present study (Figure H-7) and is dominated by Silurian strata with subordinate belts of enigmatic gneisses, tentatively considered to be pre-Middle Ordovician basement rocks.

In the fall of 1985, routine field work was temporarily suspended upon discovering that a trench was being dug 6 to 8 feet deep for 18.8 miles across the field area for a segment of the Tenneco Corporation gas pipeline. A large portion of the trench was blasted into bedrock, creating extensive across-strike exposures and a bonanza of fresh rock, from which detailed notes and abundant specimens were obtained during two months of work in Fall 1985. Detailed outcrop mapping (Figures H-8A and H-8B, for example), combined with interpretation of the large across-strike exposures in the gas pipeline trench have confirmed the existence of a repeated distinctive stratigraphic sequence in the Brimfield-Sturbridge area (Figure H-7). Based on abundant lithologic similarities (Berry, 1985), this sequence is correlated with the sequence of Silurian Rangeley, Smalls Falls, and Madrid Formations, and Lower Devonian Littleton Formation of New Hampshire and western Maine (Hatch et al., 1983). Although the units themselves are exceedingly thin, the sequence of units and even some evidence of internal stratigraphy are preserved both along strike and in different strike belts.

The area also contains several belts of thinly layered to laminated biotite-feldspar gneisses with subordinate interlayered amphibolite, mafic gneiss, and pegmatite, somewhat similar in appearance to the Monson Gneiss of the Bronson Hill anticlinorium. These enigmatic gneiss layers, labeled OZ? on Figures H-7 and H-8, are apparently in sharp contact with adjacent schists. As presently mapped, they do not intrude the Silurian-Devonian stratigraphy, nor are they interbedded on any scale with schists. Rather, these gneisses are considered as possible basement rocks upon which the Silurian-Devonian strata were deposited. This possible basement-cover contact, still under study, may be either an unconformity or an early thrust fault which juxtaposes Rangeley with the possible basement rocks.

The present analysis of map-scale structural geology in this area is totally dependent on detailed mapping of the Silurian-Devonian strata and their relationship to "basement" gneisses. Bedding, layering, foliation, mylonites, most pegmatites, and most plutons are essentially parallel, with strikes ranging from N0E to N30E, and dips typically from 40 to 70 degrees to the west. However, repetitions and truncations of the stratigraphy suggest that large scale isoclinal folds and overturned thrust faults are present. The two maps of Figure H-8 demonstrate the effect of new mapping on the present structural interpretation. Figure H-8A shows two proposed thrust faults which have "basement" rocks (OZ?) on the east against lower (Sr), middle (Ssf), and upper (Sm) Silurian rocks on the west. The stratigraphic sequence on the west side of each fault is facing eastward into the fault, which truncates contacts at low angles. On the east side of each fault, the stratigraphic sequence also faces eastward, with "basement" gneisses and Rangeley Formation (Sr) close to the faults, and younger stratigraphic units some distance farther east. Figure H-8B again shows proposed faults that have older rocks on the east against younger rocks on the west. These cases suggest a pattern of east-side-up motion on several parallel faults which repeat thin, laterally extensive sheets of eastward-facing strata (Figure H-7). Because these faults are sub-parallel and closely spaced, and because successive sheets contain a similar stratigraphic package, these faults are presumed to root into a common thrust surface at some unknown depth. A rather fanciful, yet attractive extension of this interpretation is that there is also an overriding roof thrust into which the faults of Figure H-7 merge, completing a large, thrust duplex structure (see Butler, 1982). Given the consistent westerly dips throughout the area, combined with apparent east-side-up motion, this model would require that the originally west-directed thrust duplex structure is presently overturned to the east.

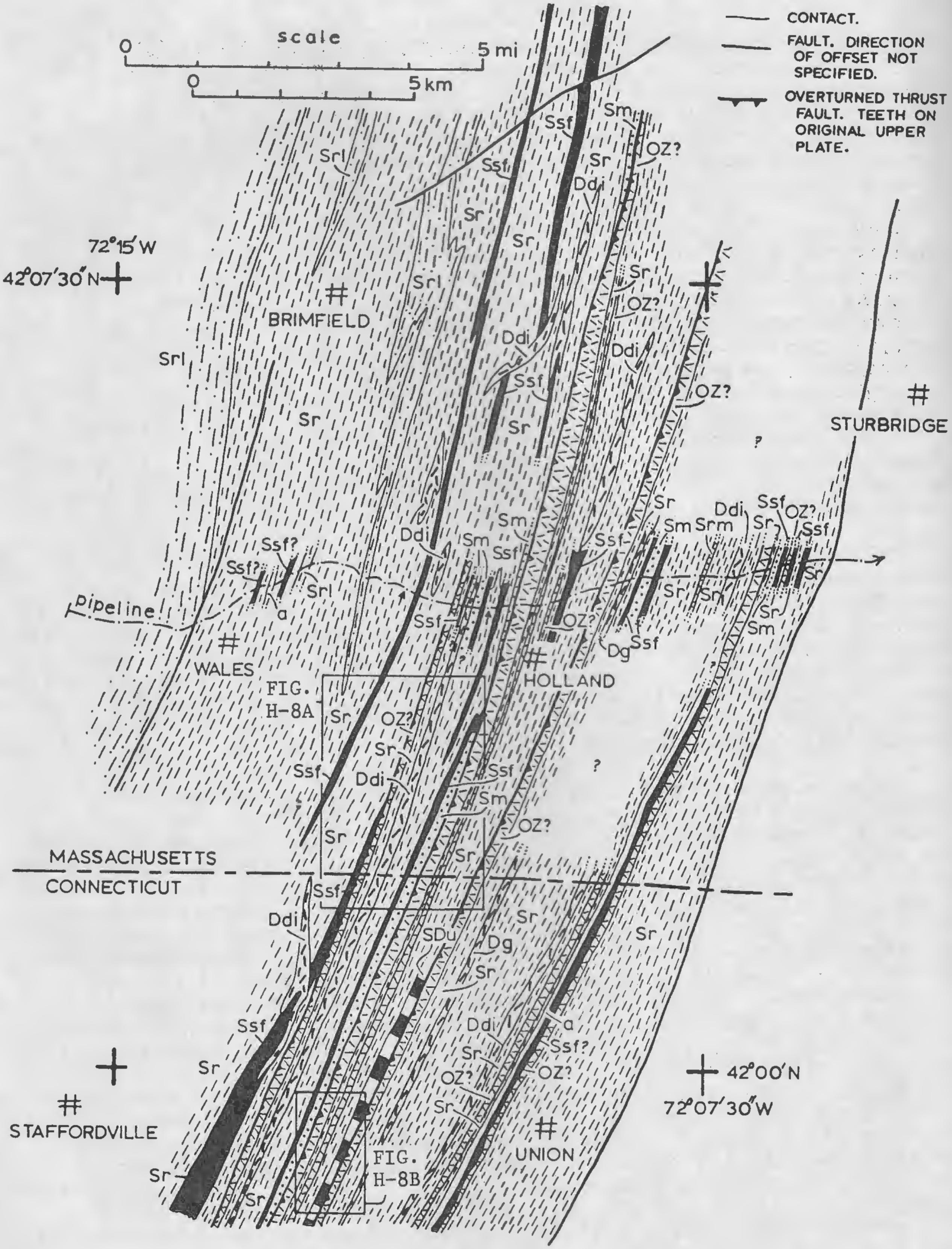
scale
0
5 mi
0
5 km
CONTACT.
FAULT. DIRECTION OF OFFSET NOT SPECIFIED.
OVERTURNED THRUST FAULT. TEETH ON ORIGINAL UPPER PLATE.
72°15'W
42°07'30"N
Srl
Ssf
Sm
Sr
OZ?
Ddi
BRIMFIELD
STURBRIDGE
?
Srm
Ssf?
Pipeline
a
WALES
HOLLAND
Dg
FIG. H-8A
MASSACHUSETTS
CONNECTICUT
SDu
STAFFORDVILLE
UNION
FIG. H-8B
42°00'N
72°07'30"W

Figure H-7. Geologic map of the Brimfield-Sturbridge study area. All units dip west at typically 40 to 70 degrees. For symbols refer to Figure H-8.

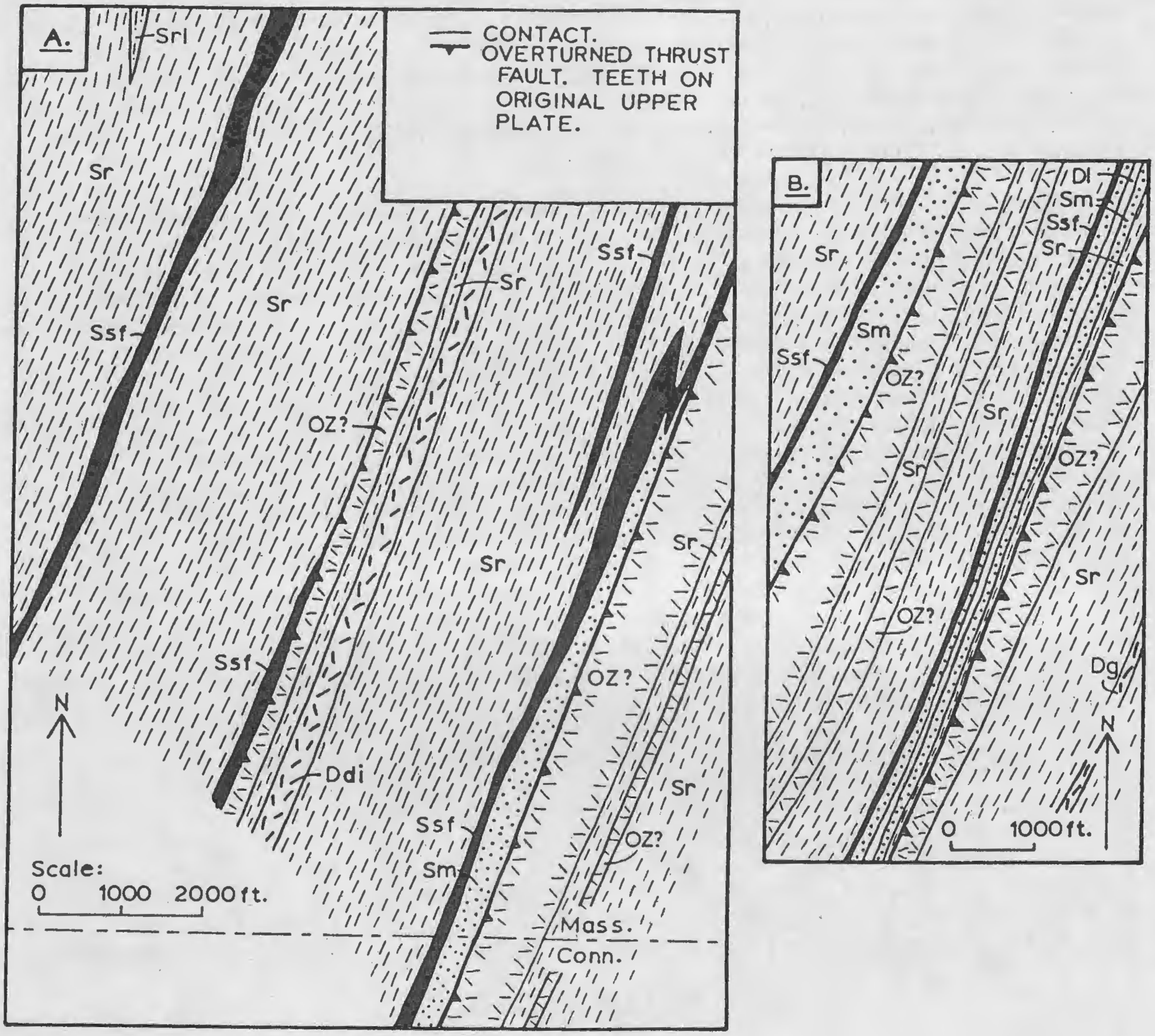
A.
CONTACT.
OVERTURNED THRUST FAULT. TEETH ON ORIGINAL UPPER PLATE.
Srl
Sr
Ssf
Sr
Sr
Ssf
OZ?
Sr
Sr
Ssf
OZ?
Ddi
Ssf
Sm
Sr
OZ?
Mass.
Conn.
N
Scale:
0 1000 2000 ft.
B.
Dl
Sm
Ssf
Sr
Sr
Sm
Ssf
OZ?
Sr
Sr
OZ?
OZ?
Sr
Dg
N
0 1000 ft.

Figure H-8. Two detailed maps located in Figure H-7. Eastern fault in A traces into western fault in B. Stratigraphic units are: proposed basement gneiss of uncertain age (OZ?); Silurian Rangeley Formation (Sr), including lower Rangeley (Srl) and marble (Srm); Silurian Smalls Falls Formation (Ssf); Silurian Madrid Formation (Sm); Devonian Littleton Formation (Dl). Area of undivided Silurian-Devonian (SDu) on Figure H-7 is divided in Figure H-8B. Metamorphosed igneous rocks include Devonian granite gneisses (Dg); Devonian diorite and tonalite gneiss (Ddi); and amphibolite of uncertain age (a).

Now to return to the original discussion of backfolds. If there is a backfold-stage syncline west of the Oakham anticline, as previously conceived, then the direction of tectonic top at the time of the previous nappe stage should now be to the west. If there is no such backfold syncline then the tectonic top at the time of the nappe stage should now be to the east. The latter case is consistent with the structural geometry that is turning up in the Brimfield-Sturbridge area, in which several slices of possible basement rocks on the east appear to be in fault contact with Silurian cover sequences on the west. In brief, we are proposing here that this region might be a nappe-stage west-directed thrust duplex (or complex!) composed of pre-Middle Ordovician basement with its Silurian-Lower Devonian cover, subsequently overturned to the east so that the thrust planes now dip 40 to 70 degrees west.

Minor folds and lineations clearly related to formation of the gneiss domes form a strange swirling pattern (Robinson et al., 1982a) that needs to be better understood in regional terms. In the Brimfield-Sturbridge area these dome-stage folds and lineations are clearly superimposed on E-W trending folds as well as on mylonites that themselves cut across peak metamorphic fabrics. Thus the continuity of structural fabrics and metamorphic isograds with known Acadian features to the north and west argues that deformation and metamorphism is here also Acadian. The dome-stage pattern of lineation is also deeply ingrained into the metamorphosed outer part of the Belchertown Quartz Monzodiorite pluton, the core of which yields a zircon age of 380 m.y. (Ashwal et al., 1979), giving a firm older limit on the age of the dome stage in this region. A total fusion K/Ar age on metamorphic hornblende from one of these rocks yields 361 m.y. (Ashwal et al., 1979) placing an apparent younger limit on the age of this dome-stage deformation and metamorphism. Recent work to the southeast in coastal Connecticut (Wintsch, 1985; Wintsch and Sutter, 1986), to the east in Massachusetts (Goldstein and Owens, 1985) and Rhode Island (O`Hara and Gromet, 1985), and to the northeast in Maine (Lux and Guidotti, 1985) has shown growing evidence of Late Paleozoic plutonism, deformation, and metamorphism. However, the chain of evidence cited above, and needing further substantiation, would seem to rule out the recent proposal by Wintsch and Sutter (1986) that the regional metamorphism and the mylonites in the Merrimack synclinorium of southern Massachusetts and adjacent Connecticut were a product of late Paleozoic rather than Acadian events.

As mapping of crystalline rocks has proceeded, evidence has accumulated for major and minor faults of definite or presumed Mesozoic age. Diamond drilling near the Connecticut Valley border fault, in connection with the proposed Montague Nuclear Power Plant, gave considerable evidence for a dip of 40 degrees west or less on the fault and suggested the fault is listric in nature. Fitting of pre-Mesozoic rocks on either side of the fault near the New Hampshire-Vermont line suggests normal vertical displacement of about 5 km. The tectonic relief provided by Mesozoic faulting helps greatly in structural interpretation and helps make up for the low topographic relief compared to structurally similar ranges such as the Alps, Himalaya, or Scandinavian Caledonides.

METAMORPHISM

Some of the relations between structural geology and metamorphism have been discussed above, and many details of the metamorphic petrology are given elsewhere (Tracy et al., 1976; Tracy, 1978; Robinson and Jaffe, 1969a, 1969b; Robinson et al., 1982c; Robinson, 1983; Chamberlain and Lyons, 1983; Schumacher, 1983, and in press; Hollocher, 1985; Chamberlain, 1985; P.J. Thompson, 1985). The pattern of metamorphic zones is based on mineral assemblages in pelitic schists and is shown in Figure H-9. Kyanite and higher grade assemblages are marked as zones I to VI both in Massachusetts and New Hampshire. An important feature of the metamorphic map is the well defined limit for the occurrence of sillimanite pseudomorphs after andalusite (excepting occurrences in the Belchertown intrusion) that is most thoroughly mapped in the Monadnock area (Thompson, 1985) but traceable to Connecticut as well as northward in New Hampshire, and thought to represent a record of early low pressure ("Buchan") metamorphism (Spear, 1986; Chamberlain, 1986; Robinson et al., 1986, this guidebook, part F). A feature not obvious from the map is the totally different appearance of the rocks in the two metamorphic highs.

In the central Massachusetts high, peak metamorphic minerals are heavily overprinted by subsequent metamorphic fabrics and mylonites, so much so that Professor Shizuo Yoshida of Tokyo University recently summarized by saying "All is mylonite". In contrast, in the southwest New Hampshire high, which locally reaches zone VI north of the limits of Figure H-9 (Chamberlain, 1985, this guidebook, Figure F-3), the peak metamorphic minerals appear to overgrow the deformational fabrics.

Characterization of Metamorphic Zones

The central Massachusetts metamorphic high east of the Connecticut Valley border fault has been divided into six zones (Figure H-9) based on mineral assemblages in pelitic schists (Tracy et al., 1976; Robinson et al., 1978). The four highest grade zones are characterized as follows. In Zone III, the Sillimanite-Muscovite Zone, the typical assemblage in pelitic schists is quartz - muscovite - biotite - garnet - sillimanite - graphite - ilmenite + pyrrhotite + plagioclase, similar to staurolite- free rocks rocks in the upper part of Zone II. In Zone IV, the Sillimanite - Muscovite - K-feldspar Zone, the typical assemblage is quartz - muscovite - orthoclase - plagioclase (An_{20-35}) - biotite - garnet - sillimanite - graphite - ilmenite + pyrrhotite. At any one locality rocks with more sodic plagioclase than in the typical assemblage have sillimanite - orthoclase without muscovite, whereas rocks with more calcic plagioclase have sillimanite - muscovite without orthoclase (Tracy 1975, 1978). In Zone V, the Sillimanite - K-feldspar Zone, the typical assemblage in pelitic schists is quartz - orthoclase - plagioclase - biotite - garnet - sillimanite - graphite - ilmenite + pyrrhotite and no muscovite is found in prograde rocks of any available composition. This is the lowest grade zone to be visited on trip H. In Zone VI, the Sillimanite - K-feldspar - Garnet - Cordierite Zone, the typical assemblage in pelitic schists (and gneisses) is quartz - orthoclase - plagioclase - biotite - garnet - cordierite - sillimanite - graphite - ilmenite ± pyrrhotite. At certain stratigraphic levels in Zone VI as well as locally in Zones IV and V there are extremely sulfide-rich rocks lacking garnet, commonly with rutile in place of ilmenite, and in rare instances pyrite together with pyrrhotite. The genesis of these rocks is discussed in detail below.

Sequence of Reactions in Pelitic Schists

The change from sillimanite-muscovite assemblages in Zone III through sillimanite-muscovite-orthoclase assemblages in Zone IV to sillimanite-orthoclase assemblages in Zone V has been studied extensively by Tracy (1975, 1978). The controlling reaction is a continuous one essentially involving continuous increase in muscovite and K-feldspar K/Na ratios and plagioclase Ca/Na ratios:

1) Na-richer Muscovite + Na-richer Plagioclase + Quartz =
K-richer Muscovite + K-feldspar + Sillimanite + Ca-richer Plagioclase + H_2O

The Na lost from muscovite and from plagioclase in this reaction goes to make a larger amount of K-feldspar, which is more sodic than muscovite. The Zone III-Zone IV boundary is defined by the first appearance of sillimanite-K feldspar in schists with the most sodic plagioclase composition, in practice about An_{20}. The Zone IV-Zone V boundary is defined by the last appearance of muscovite in schists with the most calcic plagioclase, in practice, about An_{33}. Within Zone IV muscovite compositions range from 7 down to about 2% paragonite component in the highest grade rocks. The highest grade muscovites contain 10-20% of a celadonite component and .04 to .08 Ti ions per 11 oxygens as compared to .01 to .05 in lower grade muscovites.

So long as muscovite is stable in Zones III and IV there is little prograde change in the Fe/(Fe+Mg) ratios of garnets and biotites in sillimanite-garnet-biotite assemblages. A fairly obvious reason is to be found in the controlling reaction:

2) Garnet + Muscovite + Mg-richer Biotite = Sillimanite + Fe-richer Biotite + Quartz

Figure H-9. Metamorphic maps of central Massachusetts and adjacent New Hampshire and Vermont.

H-9A. Map of metamorphic zones and other features based on Robinson et al. (1982c), Trask (1964), Chamberlain and Lyons (1983), P.J. Thompson (1985), Hollocher (1985), and D.C. Elbert (unpublished data).

Metamorphic Zones

VI	Garnet-Cordierite-Sillimanite-K-feldspar
V	Sillimanite-K-feldspar
IV	Sillimanite-Muscovite-K-feldspar
III	Sillimanite-Muscovite
II	Sillimanite-Staurolite
I_K	Kyanite-Staurolite
I_A	Andalusite-Staurolite
G	Garnet
B	Biotite
C	Chlorite
Ŧr-J	Mesozoic sedimentary and volcanic rocks

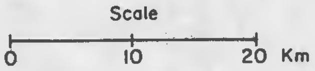

LOCALITIES WITH SPECIAL METAMORPHIC FEATURES.

○	Rocks showing evidence for pre-Acadian high-pressure sillimanite-orthoclase grade metamorphism with Acadian kyanite zone overprint.
●	Kyanite with fibrolitic sillimanite overgrowths.
◆	Sillimanite pseudomorphs after andalusite (many more localities not shown).
▼	Local occurrences of coexisting sillimanite-microcline in Zones II and III.
□	Muscovite in pegmatite, Zone VI.
▽	Staurolite in non-pelitic rock in Zone IV.
■	Cordierite in gedrite gneisses, Zones I and II. In both locations examples can be found of retrograde replacement of cordierite by kyanite + chlorite + quartz.
≀	Finely recrystallized mylonites, Zones IV and V. Many localities not shown.
‖	Very finely recrystallized mylonites, Zone VI.
◇	Retrograde sillimanite + green biotite after cordierite in Zone VI.
▨	Zones of thorough retrograde metamorphism at New Salem (Hollocher, 1981) and Quabbin Hill.
⊕	Orthopyroxene in mafic rock.
◎	Orthopyroxene-clinopyroxene.
⊙	Orthopyroxene-orthoclase.

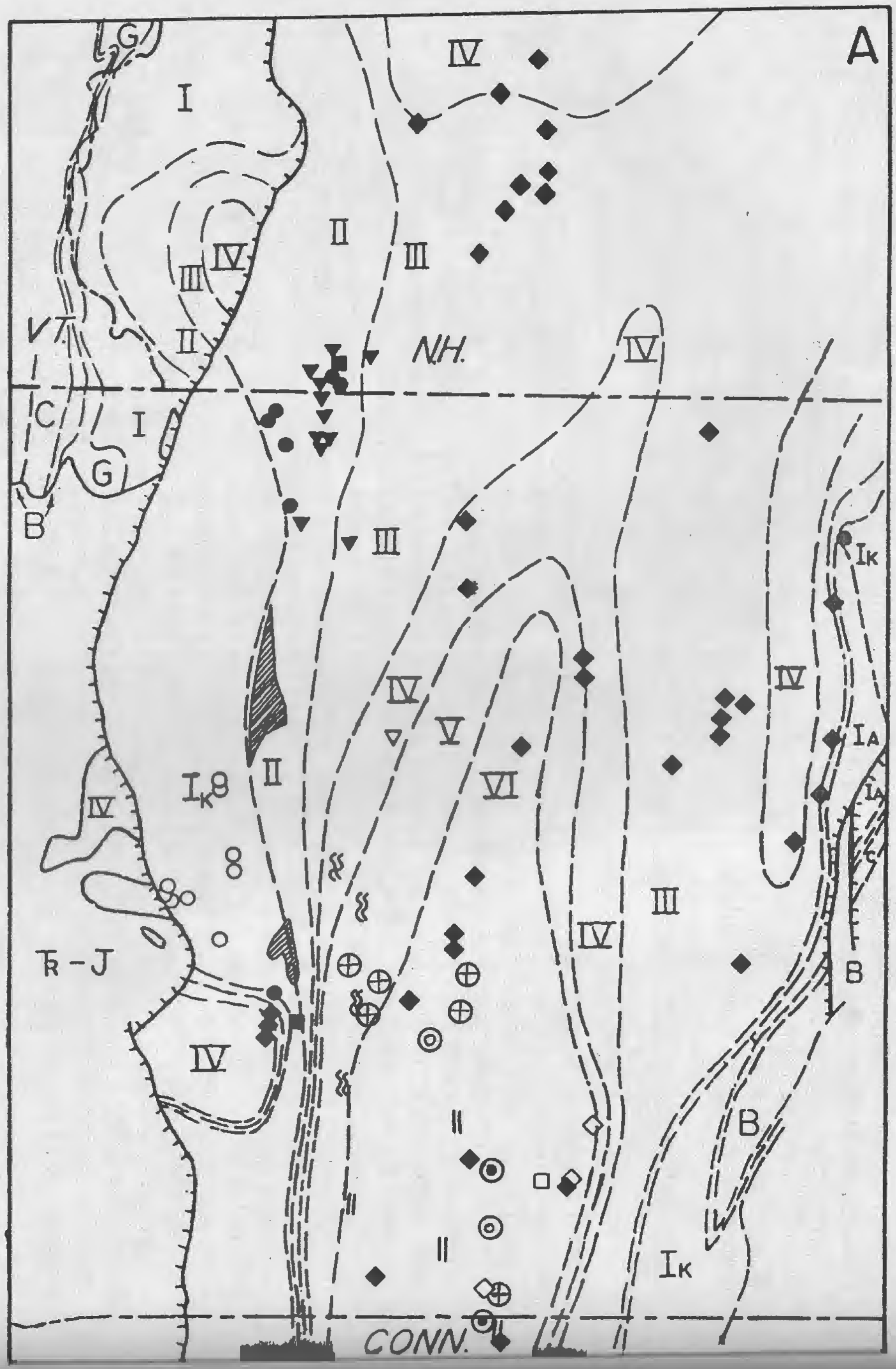

H-9B. Contour map showing positions of estimated isotherms of peak metamorphism based on studies of zoned garnets in pelitic schists (from Robinson et al., 1982c). Note that isotherms are offset to the west relative to the isograds, consistent with implications of higher pressure peak metamorphism in the western part of the region. Metamorphic zones are explained in 9A, and dots are sample localities.

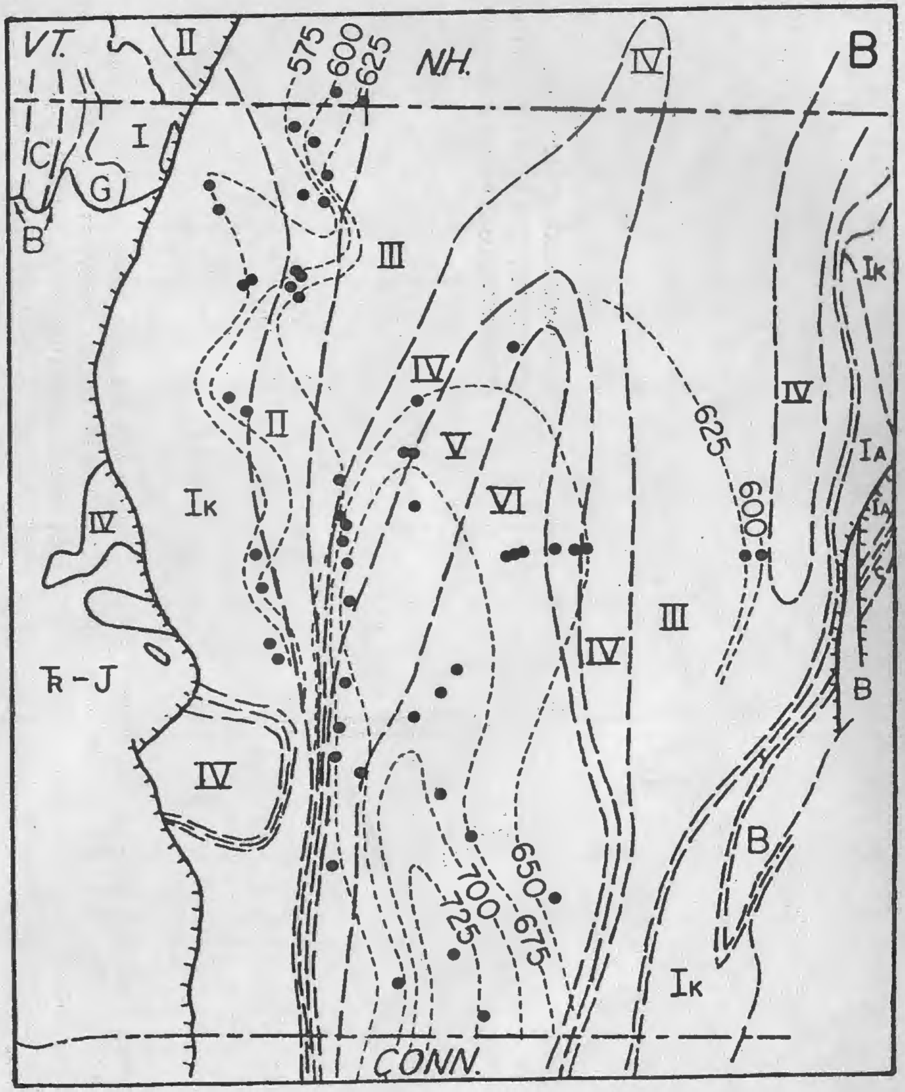
B
VT.
N.H.
CONN.
575
600
625
650
675
700
725
625
600
I
II
III
IV
V
VI
IK
IA
C
G
B
Tr-J

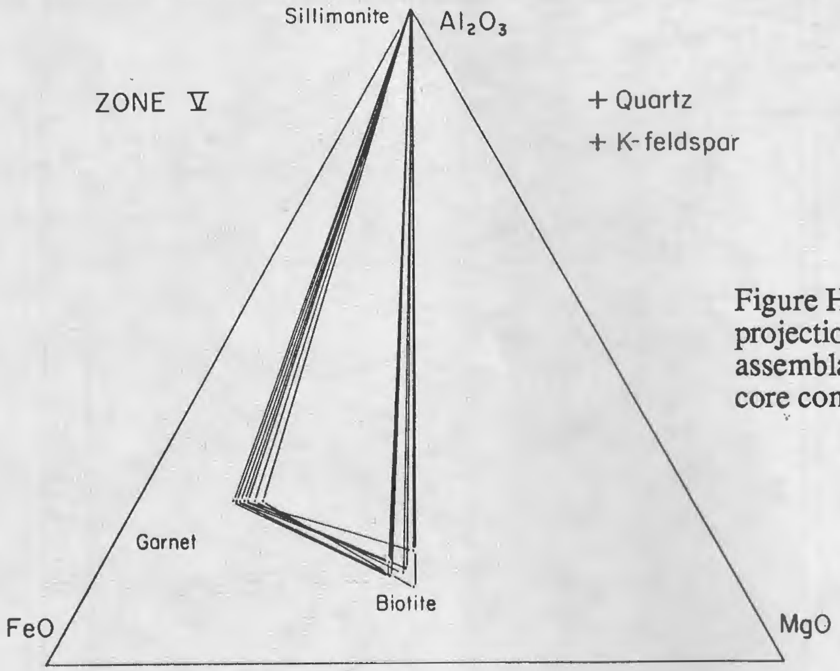

Figure H-10A. Quartz + K-Feldspar projection of pelitic schist assemblages in Zone V. Only garnet core compositions are shown.

First inspection suggests that since the K + Na of muscovite must be exactly balanced by the K + Na of biotite, the H_2O must balance and the reaction is fluid conservative and hence is likely to have a very small ΔS. However, C.V. Guidotti (personal communication, 1982) has called attention to the well known fact that muscovites have higher Na than coexisting biotites and hence that albite component of plagioclase should be added to the right-hand side of the equation. This would increase the ΔS of the reaction and would slightly favor the sillimanite + biotite side of the reaction with increasing grade.

Once muscovite has been entirely replaced by K-feldspar in Zone V the situation is entirely reversed. K-feldspar takes the place of muscovite in reaction 2, the amount of H_2O produced on the left hand side is large and so is the ΔS. This is rewritten as:

3) Sillimanite + Fe-richer Biotite + Quartz =Garnet + K-feldspar + Mg-richer Biotite + H_2O

This powerful dehydration reaction is responsible for major changes in mineral compositions. The Mg contents of garnets and biotites in the sillimanite - biotite - garnet - K-feldspar assemblage increase progressively from values typical of Zone V (Figure H-10A) to the higher values characteristic of Zone VI (Figure H-10B). In Zone VI this garnet reaction "collides" with a similar powerful dehydration reaction involving cordierite and moving in the reverse direction:

4) Sillimanite + Mg-richer Biotite + Quartz = Cordierite + K-feldspar + Fe-richer Biotite + H_2O

This "collision" produces the sillimanite - orthoclase - garnet - cordierite - biotite assemblages typical of Zone VI.

Geothermometry and Geobarometry

To date most geothermometry in the region has been based on Fe/Mg partioning between the

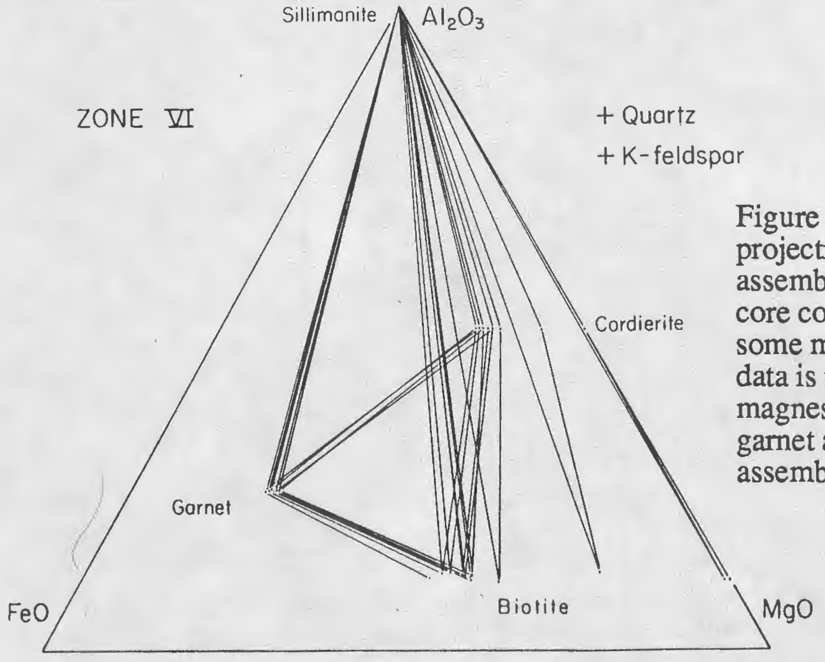

Figure H-10B. Quartz + K-Feldspar projection of some pelitic schist assemblages in Zone VI. Only garnet core compositions are shown and some more recent garnet assemblage data is not included. The extremely magnesian assemblages without garnet are all indeed three-phase assemblages!

pairs garnet-biotite and garnet-cordierite, using the empirical calibrations of A.B. Thompson (1976b) and the experimental calibration of Ferry and Spear (1978). Before calibrations can be realistically applied, the patterns of internal zoning in garnets must be understood, as discussed by Tracy et al. (1976) and in more detail by Robinson et al. (1982c), Tracy (1982), Spear and Selverstone (1983), and Chamberlain (1985). Garnets in pelitic schists in central Massachusetts have been divided into three types, A, B, and C (Robinson et al., 1982c). Type A garnets, characteristic of zones I and II show a compositional record of prograde growth by continuous and discontinuous reactions with matrix minerals. Temperatures were less than 650 °C so that solid diffusion within garnet was too slow to homogenize the recorded compositions. Type B garnets, characteristic of zone IV and most of zone V, have homogeneous interiors (Figure H-11A), which either grew that way originally or were homogenized by diffusion at temperatures of 650 to 675 °C. In addition they have continuous rims believed to have formed by retrograde continuous hydration reactions with matrix minerals in the presence of a fluid phase. Type C garnets, characteristic of part of zone V and all of zone VI (Figure H-11B), also have homogeneous interiors. However, rim compositions differ only where they are in direct contact with another ferromagnesian mineral such as biotite or cordierite. Chemical gradients within the biotite and cordierite show that the garnet rims were produced by localized ion exchange during cooling. The lack of rims where Type C garnets are not in contact with ferromagnesian minerals suggests that retrograding did not involve a pervasive metamorphic fluid as it did with type B garnets. The implications of these observations are that prograde metamorphism at 675 to 730 °C. eventually drove away most metamorphic fluids, so that they were not generally available for retrograde reactions. This would be consistent with ideas that many of the migmatite features in zone VI are products of fluid-absent melting (see Stop 4 of this field trip). We believe such implications are related to the fact that the mylonites in Zone VI (Stops 7 and 9, this field trip) have the finest grain size and smallest degree of metamorphic recrystallization of any in the region.

To date geobarometry has been based primarily on the Fe-Mg discontinuous reaction cordierite = quartz + sillimanite + garnet, despite the extended debate concerning the sensitivity of the calibration of this equilibrium to the water content of cordierite (Hensen and Green, 1973; Weisbrod, 1973; Thompson, 1976b; Hensen, 1977; Holdaway and Lee, 1977; Newton and Wood, 1979; Martignole and Sisi, 1981; Lonker, 1981). The use of this reaction may be justified, however, because the real chemistry of the rocks is very close to that of the calibration system.

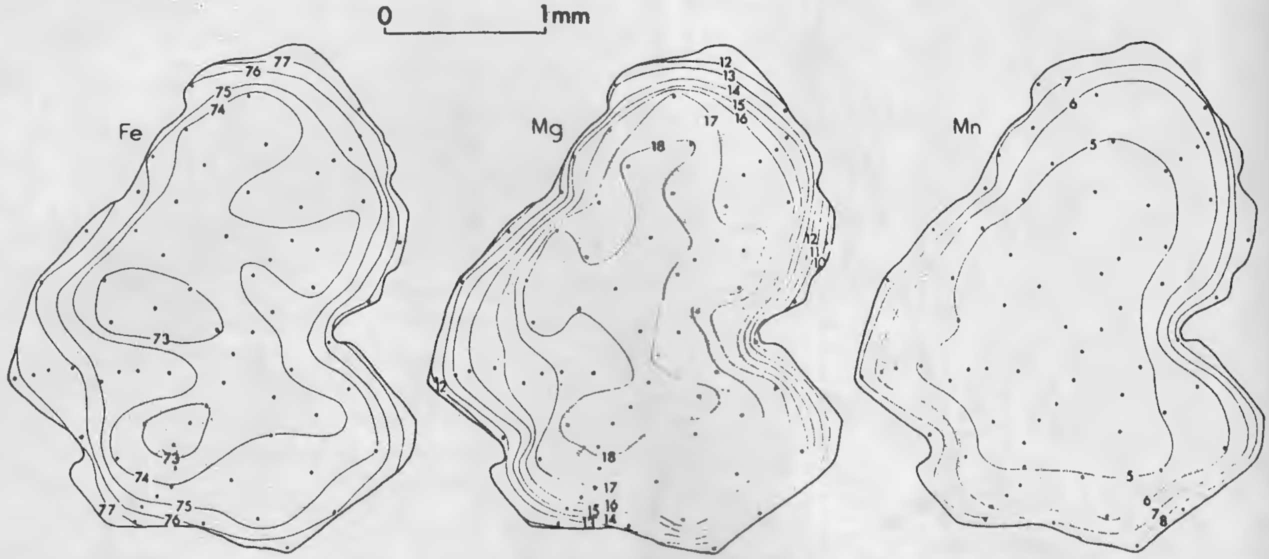

Figure H-11A. Contour maps of mole % Fe, Mg, and Mn in garnet 933B, zone IV, a typical type-B zoned garnet. Ca content varies little. The assemblage is quartz-orthoclase-biotite-garnet-sillimanite. Dots are analysis points.

The actual cordierite assemblages are found in pelitic schists only in Zone VI, also in a few gedrite gneisses in lower grade zones (this guidebook, part G, Table G-8), and in one well documented K-poor pelite in the Monadnock area (Thompson, 1985). They commonly yield estimated pressures of about 6.3 kbar. Elsewhere the garnet compositions in sillimanite (or kyanite) - garnet - quartz assemblages are used to estimate minimum pressures which are 6 kbar or less. The application of the alternative equilibrium anorthite = Al_2SiO_5 + quartz + grossular (Ghent, 1976; Newton and Haselton, 1981) has also been considered but little used because the real assemblages are compositionally very far from the calibration system, the solution models for Ca-Fe-Mg garnets and plagioclase are complex, and many of the natural plagioclases have zoning patterns and even exsolution features that are inherently difficult to interpret. The more widely applicable equilibrium anorthite + annite = grossular + almandine + muscovite calibrated by Ghent and Stout (1981) and recently recalibrated by Hodges and Royden (1984) also owes its pressure dependence to the calcic component exchange between garnet and plagioclase, and suffers essentially the same shortcomings as the sillimanite-bearing reaction.

A recent focus of interest is on cordierite-bearing pegmatites in zone VI. To date only one sample, from an artificial fill, has been studied in detail (Tracy and Dietsch, 1982) but this contained several special features including the following:: a) Cordierite that is about 10% more Fe-rich than any so far found in adjacent pelitic schists;: b) Tiny symplectic intergrowths of garnet, sillimanite and quartz entirely contained in cordierite;: c) Extensive zoning toward Mg enrichment in cordierite adjacent to the symplectic intergrowth; and d) Extensive rims on cordierite or total replacement of cordierite by retrograde intergrowths of green (low-Ti) biotite and coarse sillimanite. Since the Fe stability limit of cordierite is controlled by the reaction cordierite = sillimanite + garnet + quartz, the same assemblage that is in adjacent schists, a tentative explanation for a) is that the pegmatite cordierite is a metastable relic from an earlier and lower pressure phase of regional metamorphism at about 5.9 kbar. The symplectic intergrowths b), notably absent in normal cordierites in schists, are the beginnings of breakdown of this cordierite on its own composition under higher pressure conditions, resulting in the local cordierite zoning c). The biotite-sillimanite intergrowths d) are the result of local retrograde hydration reactions between cordierite and adjacent orthoclase. The generally extremely low Ti content of the biotites demonstrates the very local nature of this equilibrium and/or the very low solubility of titanium in the retrograde metamorphic fluids at temperatures probably in excess of 650 °C. In this context it

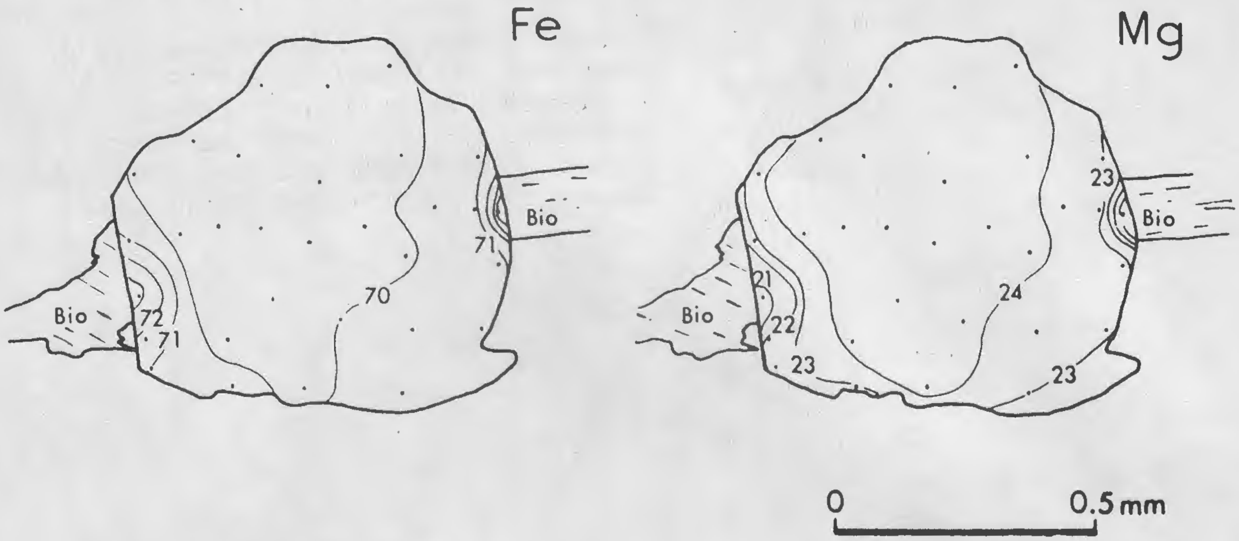

Figure H-11B. Contour maps of mole % Fe and Mg in garnet FW 407, zone VI, a typical type-C zoned garnet. Ca and Mn contents vary little. The assemblage is quartz-orthoclase-biotite-garnet-cordierite-sillimanite. Dots are analysis points.

is exciting to report that in the recently completed pipeline trench in the Brimfield-Sturbridge area we collected a wide variety of immaculate *in situ* specimens of cordierite pegmatite from a wide geographic area, so that there is a large future scope for cordierite pegmatite barometry of the type descibed above.

In his exploration of metamorphosed volcanics, Hollocher (1985) obtained detailed data on several granulite facies assemblages of quartz - plagioclase - garnet - orthopyroxene ideally suited to application of the recently tuned calibration of Perkins and Chipera (1985). These rocks yield pressure estimates of 5.2 to 7.0 kbar, which compare satisfactorily to the cordierite-based estimates of 6.2 to 6.4 kbar.

Effects of Sulfides on the Assemblages of Silicates and Oxides in Pelitic Schists

Sulfidic-graphite schists abound in central Massachusetts. These include the well known pyrrhotite schists characteristic of the Middle Ordovician Partridge Formation and parts of the Rangeley Formation and also the still more sulfidic White Schist Member of the Paxton Formation. The latter was first defined by Field (1975) and is now known to extend along strike more than half way across the state. Regional studies suggest it is certainly correlative with the Silurian Smalls Falls Formation of northwestern Maine (Field, 1975; Berry, 1985) where Guidotti et al. (1975, 1977, personal communication, 1982) have done detailed petrologic studies. The first quantitative reports of these rocks in Massachusetts were given by Tracy et al. (1976a), Robinson and Tracy (1977), and Tracy and Rye (1981), and the following discussion is based mainly on those reports plus other data in a detailed paper in preparation by Tracy and Robinson. The silicate assemblages in some sulfide-graphite-bearing pelitic schists from Zones IV and V (dashed tie lines) and Zone VI (solid tie lines) are shown in quartz + K-feldspar projection in Figure H-12. Zone V assemblages include sillimanite - garnet - biotite - orthoclase in the Partridge Formation and one sillimanite - cordierite - biotite - orthoclase assemblage from the White Schist Member. The figure shows only one Zone IV assemblage of sillimanite - cordierite - biotite - orthoclase - muscovite from the White Schist Member. Zone VI assemblages include sillimanite - garnet - cordierite - biotite - orthoclase assemblages from the Partridge and Rangeley Formations, and a variety of sillimanite - cordiertie - biotite - orthoclase assemblages with different Fe/Mg ratios from the White

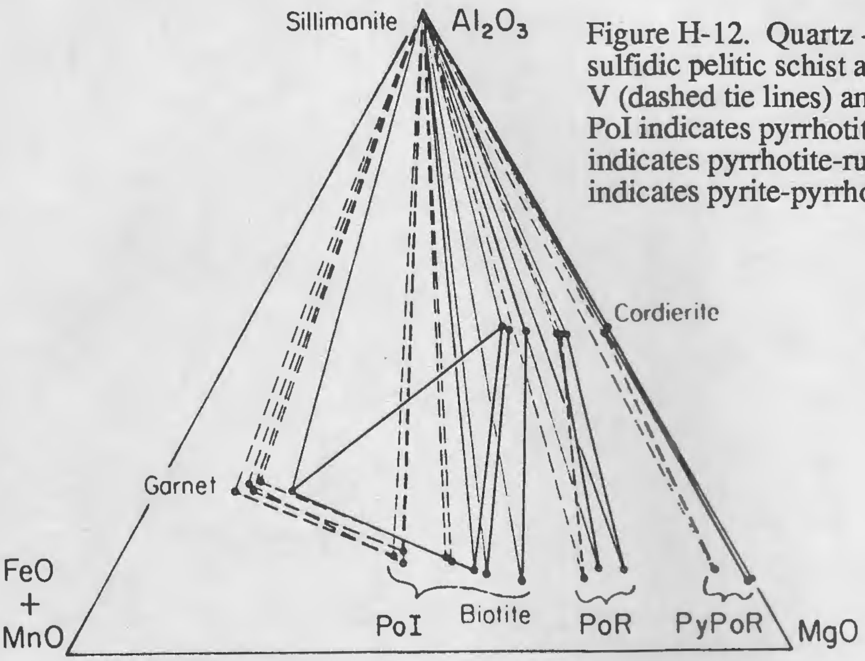

Figure H-12. Quartz + K feldspar projection of sulfidic pelitic schist assemblages from Zones IV and V (dashed tie lines) and Zone VI (solid tie lines). PoI indicates pyrrhotite-ilmenite assemblages, PoR indicates pyrrhotite-rutile assemblages, and PyPoR indicates pyrite-pyrrhotite-rutile assemblages.

Schist Member. It is important to note that in this projection under one condition of pressure, temperature and activity of H_2O or fluid composition there should only be one equilibrium triangle for the sillimanite - cordierite - biotite assemblage, not the whole array shown. The variation shown, hence, must be due either to different P-T conditions or different activity of H_2O conditions at different outcrops. A model based on variable aH_2O is considered below.

Letter symbols in Figure H-12 indicate the characteristic sulfide and Ti-oxide assemblage to be found in each group of silicate assemblages. The more Fe-rich silicate assemblages contain pyrrhotite and ilmenite. Modestly Mg-rich assemblages contain pyrrohtite and rutile, and the most magnesian assemblages contain pyrite, pyrrhotite, and rutile. This systematic relationship is explored below.

Thompson (1972) has shown how assemblages in the system Fe-O-C-H can be conveniently projected from H_2O and CO_2 onto the line FeO-Fe_2O_3. In this scheme of things, represented by the bases of both triangles in Figure H-13, graphite projects at –1 Fe_2O_3 and native Fe at –1/2 Fe_2O_3. To this base has been added S so that we can see the relations between graphite, magnetite, pyrrhotite and pyrite. and TiO_2 so that we can see the relations between graphite, magnetite, ilmenite, and rutile in equilibrium with C-O-H fluid. In the upper part of Figure H-14 the two parts of Figure H-13 are combined in a tetrahedron showing all significant graphite assemblages. These significant graphite assemblages may also be shown more easily using a graphite projection onto the triangular plane TiO_2-S-FeO as in the lower part of Figure H-14. To this convenient graphite projection MgO may now be added to form the tetrahedron TiO_2-S-FeO-MgO in which ferromagnesian minerals may be treated. The universal ferromagnesian silicate in these assemblages is biotite which would appear on or close to the FeO-MgO line by projection from quartz and K-feldspar. Aluminum saturation of biotite in such assemblages is provided by garnet, sillimanite, cordierite or any combination of the three. The volume of Figure H-15 is filled by four-phase assemblages and three-phase tie planes as follows, beginning in the Fe-rich corner. The most FeO-rich rocks would have (graphite) - magnetite - pyrrhotite - ilmenite - biotite. We have not definitely observed this assemblage in Zone VI in central Massachusetts, but a comparable assemblage (graphite) - magnetite - pyrrhotite - ilmenite - grunerite - olivine (no quartz) has been described in Zone II by Huntington (1975). Next comes a large array

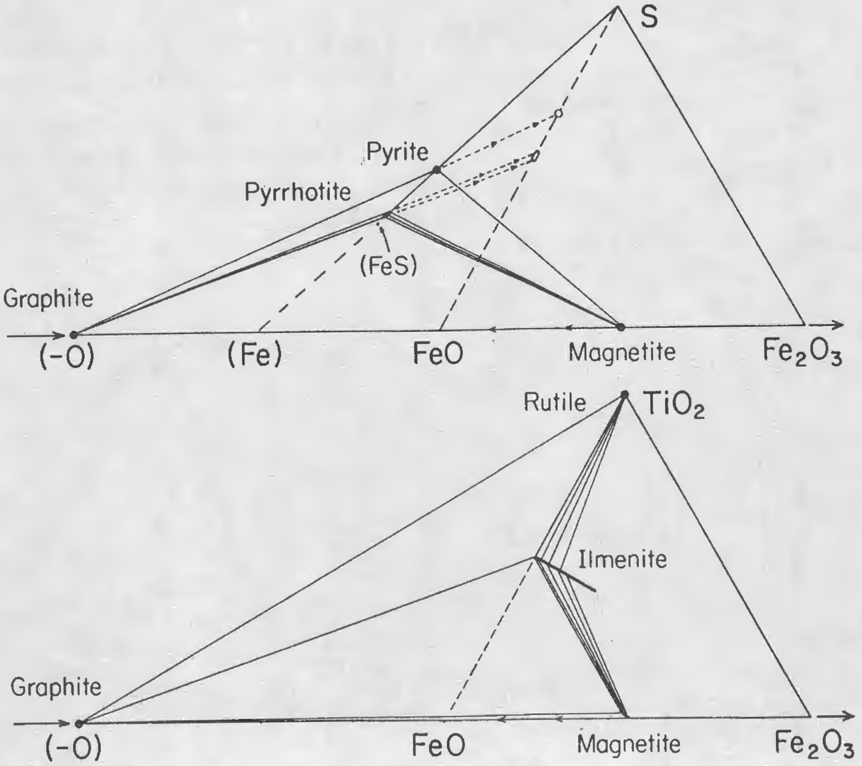

Figure H-13. Projections of mineral compositions from C-O-H fluid in the systems FeO-Fe_2O_3-S and FeO-Fe_2O_3-TiO_2 using the method of Thompson (1972).

of three-phase tie planes (graphite) - pyrrhotite - ilmenite - biotite corresponding to the middle region of Figure H-12. This is followed by the four-phase volume (graphite) - pyrrhotite - ilmenite - rutile - biotite and then the array of tie planes (graphite) - pyrrhotite - rutile - biotite. For still more magnesian compositions there is the four-phase volume (graphite) - pyrrhotite - pyrite - rutile - biotite and finally the array of tie planes (graphite) - pyrite - rutile - biotite. As will be discussed below, the composition of biotite in equilibrium with ilmenite and rutile (front face of tetrahedron) is a function of a dehydration reaction in which the biotite becomes more Mg-rich with increasing grade. Similarly the composition of biotite in equilibrium with pyrrhotite and pyrite (base of tetrahedron) is also a function of a prograde reaction, in this case a mixed volatile reaction.

In order to understand more about the origin of these sulfide-rich rocks we will now take a brief excursion into sedimentary geochemistry using the bottom of Figure H-15 as a chemographic work space. Consider an environment slightly below the ocean sediment interface in which organic matter, sulfur-reducing bacteria, and detrital ferromagnesian minerals are interacting. For simplicity's sake, detrital grains can be considered as two extreme kinds, fine-grained highly reactive grains and coarser detrital grains that resist equilibration with interstitial fluid until low grade metamorphic conditions are reached. To further simplify, assume that all detrital grains have the same Mg/(Mg + Fe) ratio of .50 as illustrated in Figure H-16A. In the early diagenetic stages reactive detrital grains are attacked by fluids or sulfur-reducing bacteria to produce an assemblage of pyrite plus iron-depleted Mg-rich silicate grains having bulk composition on the line between the detrital composition and S. Between diagenesis and low grade metamorphic re-equilibtation the pelite would contain three significant components, pyrite, reacted Mg-rich silicate and non-reacted Fe-Mg silicate. During low grade metamorphism the reacted and non-reacted silicate components would equilibrate to produce a mean ferromagnesian silicate composition coexisting with pyrite. Sulfur isotope data (Tracy and Rye, 1981) is consistent with a model in which diagenetic reaction occurs between sedimentary sulfur, reactive detrital ferromagnesian grains and organic carbon. All

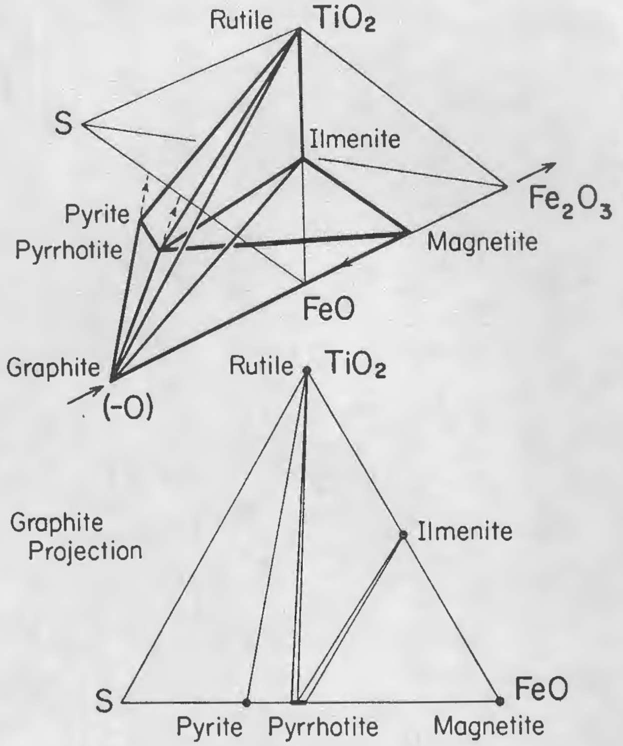

Figure H-14. Top: Combination of triangles of Figure H-13 into a tetrahedron FeO-Fe_2O_3-S-TiO_2. Assemblages with graphite shown with heavy lines. Bottom: Projection of graphite-bearing assemblages from graphite onto the plane FeO-S-TiO_2.

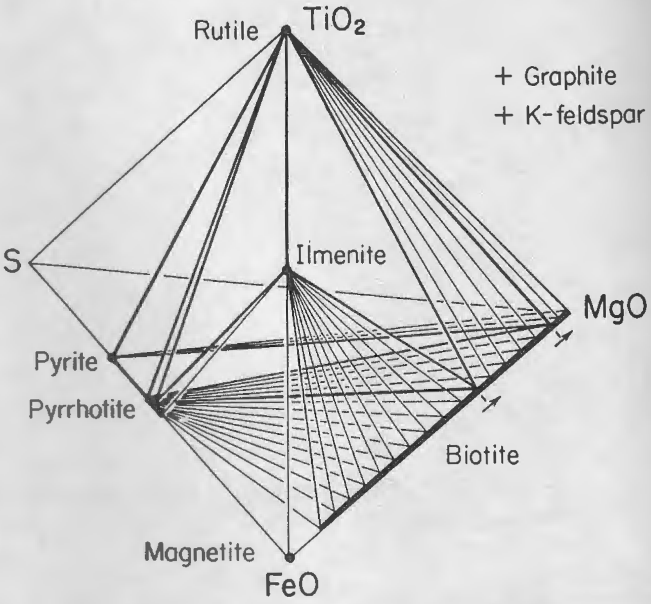

Figure H-15. Graphite-projected plane FeO-S-TiO_2 with MgO added to show ferromagnesian minerals. Further projection from quartz and K-feldspar permits portrayal of biotite.

of the analysed sulfides from White Schist Member samples have $\delta^{34}S$ ranging from –25% to –29%. These very light sulfur values could only have originated through bacterial reduction of porewater sulfate in an open-system sedimentary environment. Sedimentary sulfides form from reaction of bacterially-produced H_2S and reactive detrital iron-bearing minerals (Berner, 1971). A modern analogue of this process can be found in the highly reducing deep zones of the Black Sea, where sedimentary sulfides have virtually identical $\delta^{34}S$ values to those in the White Schist Member.

Figure H-16B illustrates the possible variability of low grade pyrite plus ferromagnesian silicate rocks produced by the processes described above. Double-dashed lines illustrate the variable bulk compositions attainable from fixed detrital compositions of Mg_{25}, Mg_{50}, and Mg_{75} and proportions of reactive grains ranging from 0 to 100%. The heavy-dashed lines illustrate variable bulk compositions attainable with constant proportions of reactive grains of 50% and 10%, but with variable detrital compositions. The combination of variable detrital compositions and variable proportions of reactive grains can produce a very wide range of low-grade bulk compositions in the FeO-MgO-S triangle available for higher-grade reactions.

The continuous Fe-Mg reaction controlling the composition of biotite in equilibrium with ilmenite and rutile in Figure H-15 is illustrated, in terms of X_{Mg} versus temperature, and fluid composition versus temperature, in Figure H-17 (left). Although ilmenite can have some Mg it is probably greatly exaggerated in this figure and the end member reaction involving geikielite is probably never realized under geologic conditions. The graphite-saturated fluid composition is expressed in terms of the ratio $CO_2/(CO_2 + H_2O)$. It is possible for this to go to negative ratios

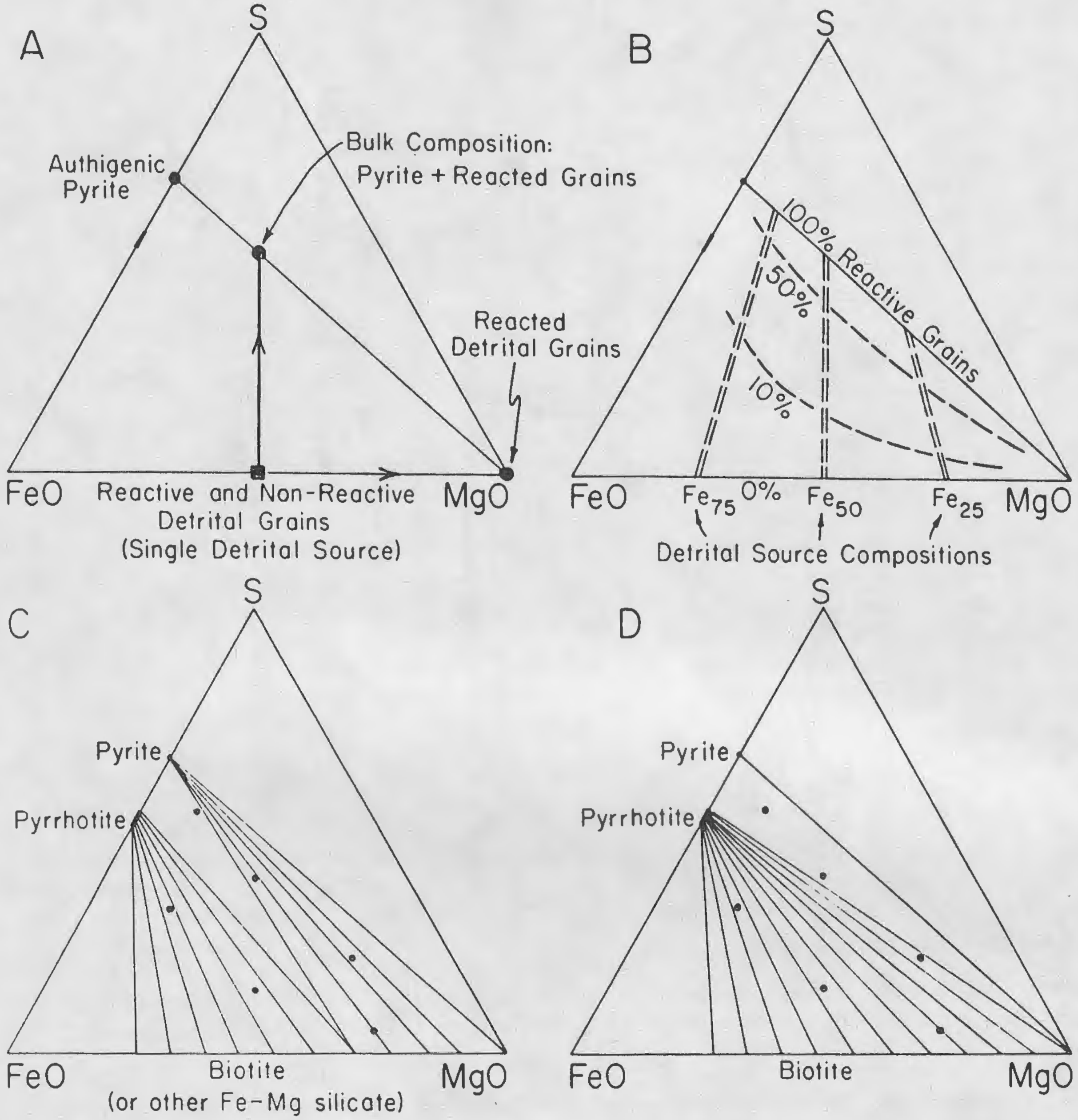
A
S
Authigenic Pyrite
Bulk Composition: Pyrite + Reacted Grains
Reacted Detrital Grains
FeO
Reactive and Non-Reactive Detrital Grains (Single Detrital Source)
MgO
B
S
100% Reactive Grains
50%
10%
0%
FeO
Fe_{75}
Fe_{50}
Fe_{25}
MgO
Detrital Source Compositions
C
S
Pyrite
Pyrrhotite
FeO
Biotite (or other Fe-Mg silicate)
MgO
D
S
Pyrite
Pyrrhotite
FeO
Biotite
MgO

Figure H-16. Diagenetic and metamorphic evolution of sulfidic shale portrayed in graphite projection on the plane FeO-S-MgO.

A) Reaction of detrital grains with sulfur (H_2S, etc.) to produce sediment with three components; pyrite, reacted detrital grains, and non-reacted detrital grains.

B) Range of low grade schist bulk compositions dependent on detrital source composition and percent of reactive grains.

C) Progress of continuous devolitilization reaction Fe-richer biotite + pyrite + graphite = pyrrhotite + K-feldspar + Mg-richer biotite $+2H_2O + 3CO_2$ across various bulk compositions.

D) Termination of the continuous reaction when all Fe is removed from biotite. Note that pyrite is still retained in some bulk compositions and is even more abundant than pyrrhotite in some.

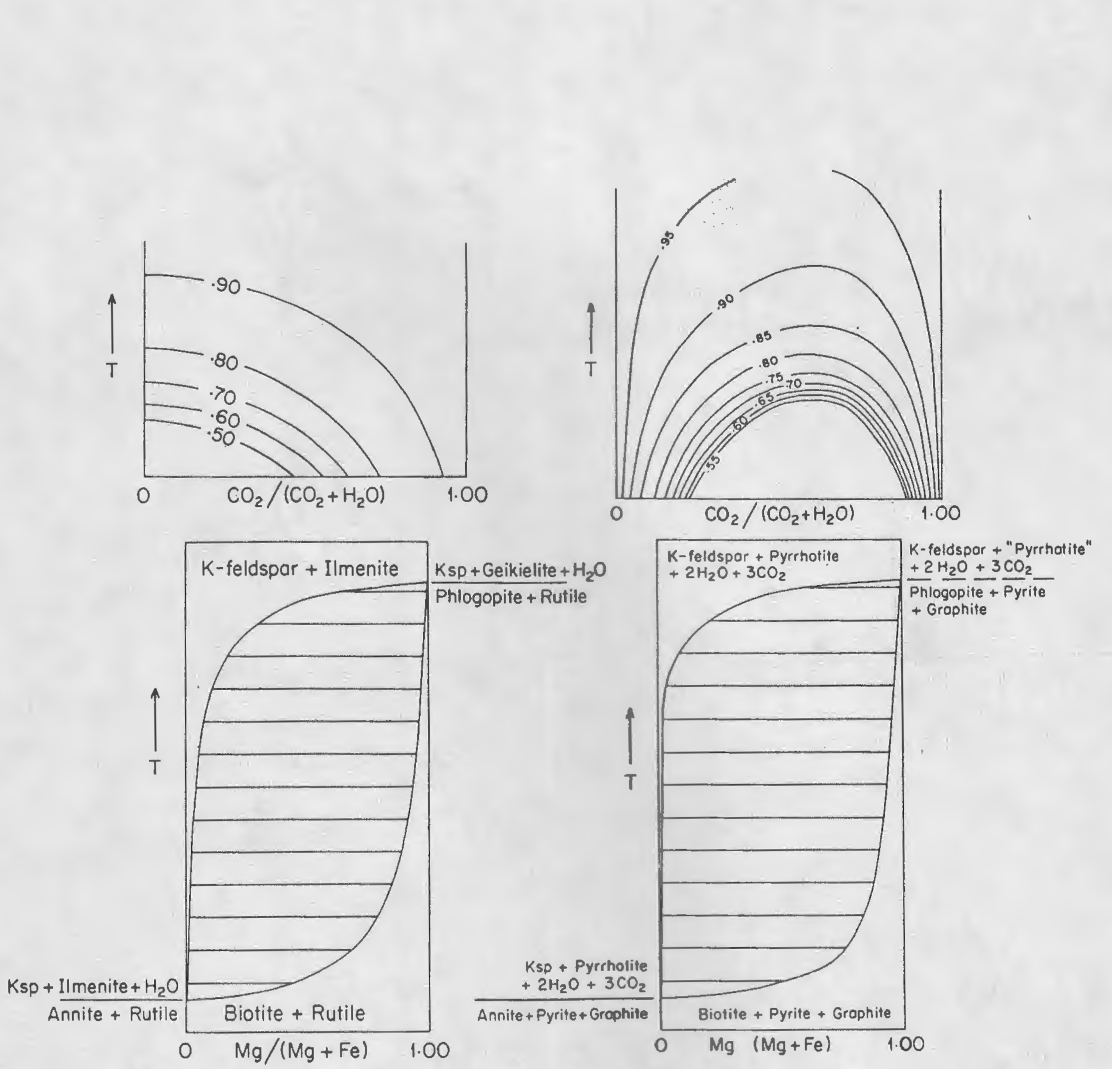

Figure H-17. Temperature-composition diagrams and temperature - fluid-composition diagrams for biotite in equilibrium with rutile-ilmenite (left) and pyrite-pyrrhotite (right). The fluid is C-O-H fluid in equilibrium with graphite and the ratio of $CO_2/(CO_2 + H_2O)$ can range from -1 to +1, but only the positive region is shown.

(not shown), indicating a methane component. Individual isopleths are shown for biotites of different X_{Mg}. Since the reaction is a dehydration the isopleths have maxima at $CO_2/(CO_2 + H_2O)=0$.

The continuous Fe-Mg reaction controlling the composition of biotite in equilibrium with pyrite and pyrrhotite is illustrated, in terms of X_{Mg} versus temperature, and fluid composition versus temperature, in Figure H-17 (right). Although pyrrhotite might have a tiny amount of Mg, the idea of an Mg "pyrrhotite" end member is ludicrous for metamorphic conditions, but the biotite limb of this "fat man" (A.B. Thompson, 1976a, personal communication, 1977) is illustrative of what goes on. This reaction is a mixed volatile reaction consuming both H_2O-bearing biotite and graphite to produce H_2O and CO_2 in a ratio of 2 to 3. On the fluid composition diagram isopleths of constant Mg content of biotite go through maxima at 60% CO_2. Since primary fluids were probably H_2O-rich, this reaction can enrich the fluid in CO_2, thus reducing aH_2O and providing for variability in the silicate assemblages.

The progress of the biotite-pyrite-pyrrhotite equilibrium through a range of bulk compositions is illustrated in Figure H-16 C and D. This permits one to observe directly the effect of bulk composition and particularly proportion of primary reactive grains, on the sulfide-silicate assemblages produced in later metamorphism. In Figure H-16C the pyrite-pyrrhotite equilibrium

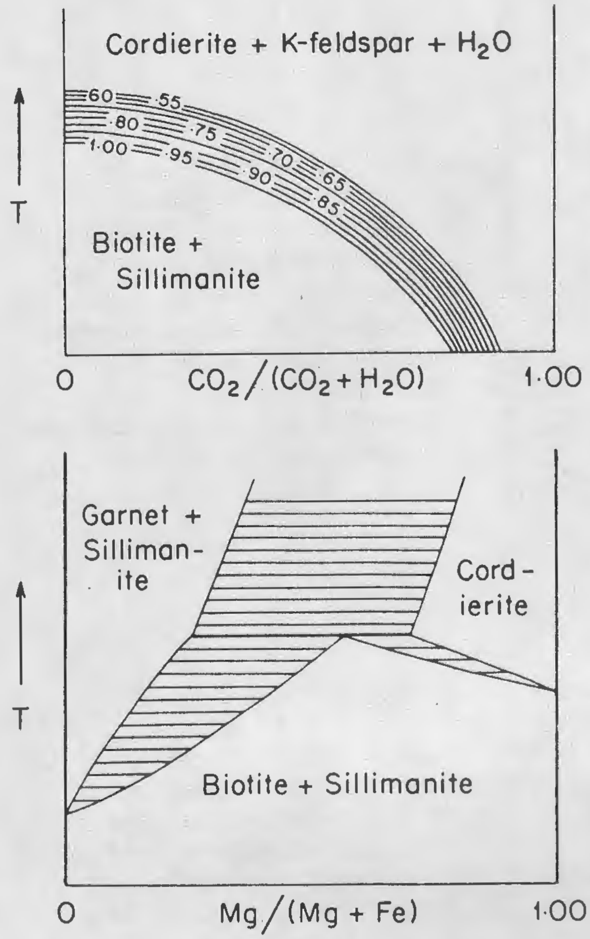

Figure H-18. Temperature-composition diagram (bottom) for the cordierite line in quartz and K-feldspar projected system SiO_2-FeO-MgO-Al_2O_3-K_2O, showing three T-X loops. On left: biotite + sillimanite = garnet + K-feldspar + H_2O (reaction 3). On right: biotite + sillimanite = cordierite + K-feldspar + H_2O (reaction 4). In middle: cordierite = quartz + garnet + sillimanite + H_2O. At top is temperature-fluid composition diagram for reaction 4 with isopleths for X_{Mg} biotite.

has progressed part way across the diagram, and there are three assemblages: pyrrhotite - biotite, pyrrohtite - pyrite - biotite, and pyrite - biotite. Note in particular that in the pyrrhotite - biotite assemblage in rocks of the same bulk Fe/Mg ratio, those with a large amount of pyrrhotite will have more magnesian silicates. This effect has been well noted in modes by Henry and Guidotti (1981), and Mohr and Newton (1981). In Figure H-16D the pyrite-pyrrhotite reaction has gone virtually to completion so that pyrrhotite and pyrite coexist with essentially end-member silicates. It will be noted that for some bulk compositions originally very rich in reactive silicate grains there is not enough Fe in the bulk silicate composition to make more than a token amount of pyrrhotite even at very high grade. This appears to have been the case at the outcrop to be visited at Stop 5, where we originally reported that there was no pyrrhotite at all (Tracy et al., 1976).

We now think that the variable compositions in sillimanite - cordierite - biotite - orthoclase assemblages may be a direct consequence of their variable sulfide content and variable progress of the mixed volatile pyrrhotite-producing reaction which dilutes H_2O with CO_2 in the fluid phase. The controlling silicate reaction (see reaction 4 above) is shown in terms of X_{Mg} and temperature and in terms of fluid composition in Figure H-18. This is a continuous dehydration reaction and hence attains a maximum temperature in the presence of H_2O-rich fluid. Because of the Fe/Mg distribution between biotite and cordierite this reaction begins at lowest temperature in pure Mg compositions and proceeds thence to more Fe-rich compositions. This is reflected in biotite composition isopleths on the fluid-composition diagram.

Figure H-19 is a fluid composition diagram combining the biotite composition isopleths of the

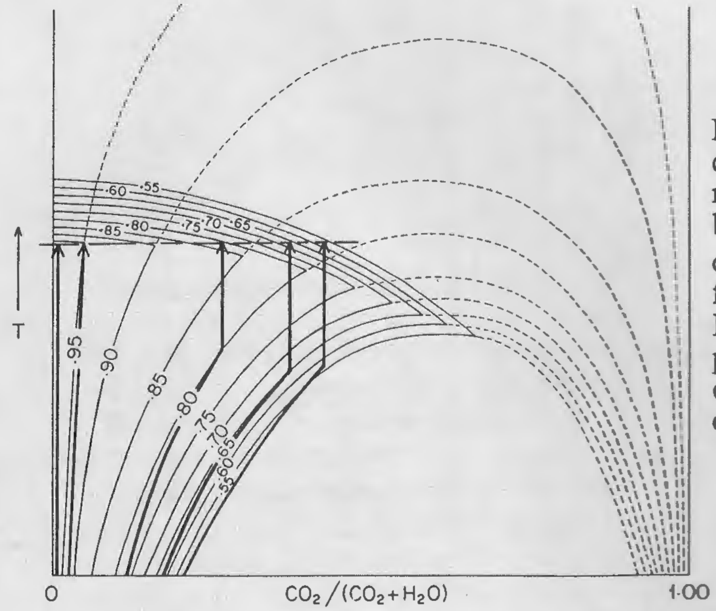

Figure H-19. Temperature-fluid composition diagram for silicate reaction 4 and the pyrite-pyrrhotite-biotite reaction. Isopleths show X_{Mg} of biotite in equilibrium with various fluids and either sillimanite-cordierite-K-feldspar-biotite or biotite-pyrite-pyrrhotite. Dark lines show equilibrium fluid paths for five different compositions of sulfidic schists.

pyrrhotite-producing reaction in Figure H-17 (right) with the biotite isopleths of the biotite + sillimanite = cordierite + K feldspar reaction of Figure H-18. The evolution of five different sulfide-bearing rocks is illustrated, each with a different amount of sulfide and hence a different composition of low grade metamorphic silicate. The rock with the least magnesian metamorphic silicate encounters the pyrrhotite-producing reaction first, causing the fluid to become enriched in CO_2 and for the biotite composition to become more Mg-rich until all pyrite is used up with biotite X_{Mg}=.56. Two more-magnesian bulk compositions produce pyrrhotite until all pyrite is used up with biotites at X_{Mg}=.65 and .80. Two still more magnesian silicate bulk compositions only begin to produce pyrrhotite at very high metamorphic grade and still have plenty of pyrite left with biotites of X_{Mg}=.95 and .99. It is now easy to see that the total history of sulfide-silicate interactions has produced an array of biotite X_{Mg} ratios and also an array of CO_2 contents in the metamorphic fluids, with less magnesian biotites corresponding to more CO_2-rich fluids. This array then encounters the fluid dependent silicate reaction at a temperature close to the beginning of reaction for pure Mg silicate and H_2O-rich fluid. This is also the temperature for the beginning of reactions for more Fe-rich compositions where the reaction temperature is lowered by CO_2 in the fluid. The end result of this speculation is that it appears possible for every bulk composition to lie within the pseudo-binary silicate loop provided the fluid composition is right.

Although we have previously described the metamorphic fluid as a C-O-H fluid, it actually contains hydrogen sulfide. Fluid composition in FW-882, an assemblage containing pyrite + pyrrhotite + graphite, was calculated by Tracy and Rye (1981); at 650 °C and 6 kilobars, the log fO_2 was -18.9 and the mole fractions of species in the fluid were: H_2O 0.68, CO_2 0.18, H_2S 0.12, CH_4 0.02, H_2 0.003. The calculation of fluid composition for the assemblage pyrrhotite + graphite under the same conditions shows that the ratio of H_2O and CO_2 is approximately the same, but XH_2S drops to about 0.02. High H_2S in the first fluid is a direct result of the high fS_2 which is buffered by pyrite + pyrrhotite.

An indication of much higher XH_2S in the rocks containing pyrrhotite + pyrite occurs in the form of sulfur-bearing cordierite. Probe analyses of cordierites in all the pyrite + pyrrhotite assemblages yield H_2S of about 2 weight %. On the other hand, sulfur has not been found in cordierite from any rock in which only pyrrhotite occurs, no matter how much modal pyrrhotite there is. Apparently the cordierite is able to accomodate H_2S in its structural channels, but only when the XH_2S of the fluid is exceptionally high, as in pyrite + pyrrhotite-bearing rocks.

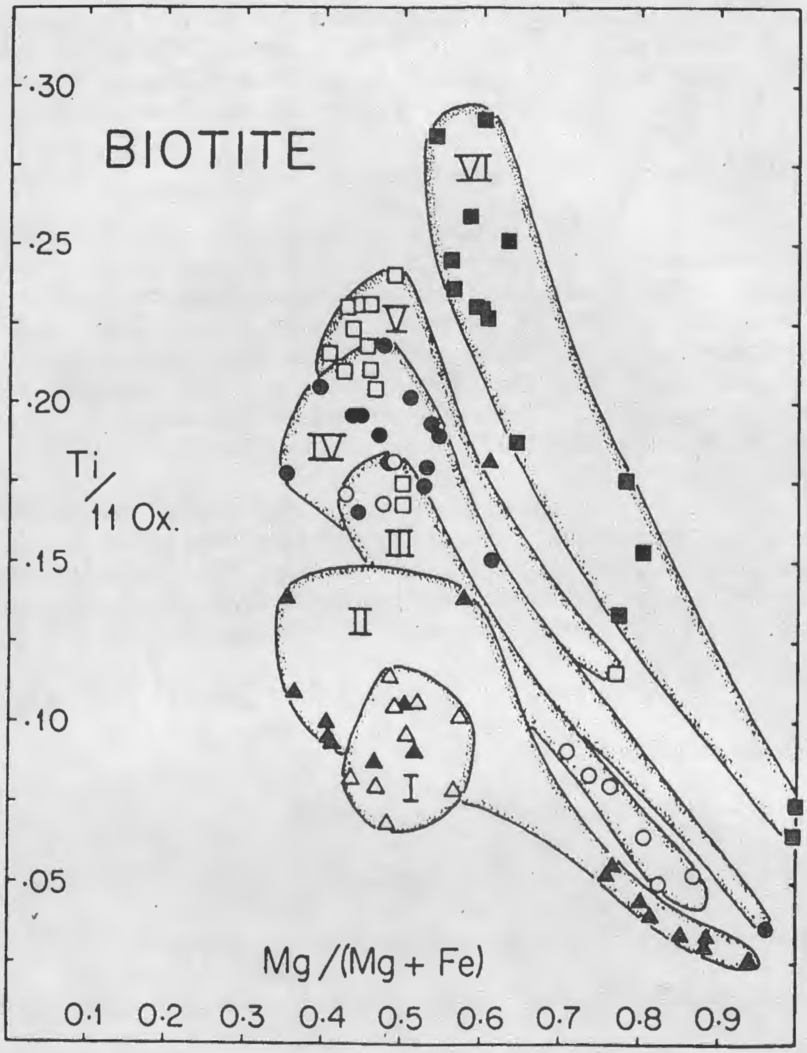

Figure H-20. Mg/(Mg + Fe) and Ti/11 oxygens for biotites in alumina-saturated and titania-saturated schists in central Massachusetts as shown by presence of Al-silicate, garnet, or staurolite and ilmenite or rutile respectively. Zone I, open triangles; Zone II, closed triangles; Zone III, open circles; Zone IV, closed circles; Zone V, open squares; Zone VI, closed squares. Magnesian compositions from Zone II and III are from the Smalls Falls Formation in Maine (Guidotti et al., 1977).

Relation Between Ti Content and Fe-Mg Ratio in Biotites

The sulfide-silicate relations and rocks described above provide biotites of a wide range of Fe-Mg ratios all in equilibrium with quartz, muscovite or K-feldspar or both, Al silicate, and a Ti mineral, either ilmenite or rutile. Guidotti et al. (1977) recognized the potential for studying the effect of Fe-Mg ratio on Ti content of Ti-saturated biotites in the Smalls Falls Formation in Maine and showed that biotites of the same metamorphic grade show a dramatic decrease in Ti content with increasing Mg ratio. They reasonably ascribed this to size limitations in the biotite structure. Equivalent biotites in central Massachusetts show an even wider range of compositions and metamorphic grades, as illustrated in Figure H-20 [we have added Mg-rich samples from Maine in Zones II and III to fill out the picture]. Although there are local irregularities, the overall trend of increasing Ti content with metamorphic grade and decreasing Ti content with Mg content are dramatically borne out. Intermediate biotites from Zone VI contain 2-3 times as much Ti as Zone II biotites from both Massachusetts and Maine, and the same is true of Mg end members from Zone VI as compared with a projected Mg-end member composition from Maine.

General Description of Metamorphosed Mafic Rocks in Zones IV-VI

The following is a review of the phase relations in metamorphosed mafic igneous rocks from Zone IV (sillimanite - muscovite - K-feldspar) up to Zone VI (granulite facies, Hollocher, 1985). The rocks in which amphiboles and associated breakdown products occur are metamorphosed mafic volcanics, gabbros, ultramafic rocks, and unusual iron-rich rocks. Such rocks, with bulk compositions appropriate to the study of amphibole-pyroxene phase relations, are relatively common in central Massachusetts. The data collected during this study are given in a set of plagioclase projections in Figure H-21. These diagrams also include data from Robinson and Jaffe (1969b), Huntington (1975), and Wolff (1978), from rocks in Zones II, III, and IV.

Four reactions are particularly important in converting amphibolites into pyroxene granulites. These four reactions form a metamorphic facies series with increasing grade, in rocks with tholeiitic bulk compositions. Such bulk compositions, projected from plagioclase onto the AFM plane, lie between the hornblende field and the Fe-Mg join. In order of increasing grade, the most important facies assemblages (A through E) and most important reactions (1, 4, 7, 14) are:

A) Hornblende-Orthoamphibole (Mg-rich rocks only)

1) Oam + Hbl + Qtz = Cum + Plag + H_2O

B) Hornblende-Cummingtonite

4) Cum + An = Hbl + OPX + Ab + Qtz + H_2O

C) Hornblende-Orthopyroxene

7) Hbl + Qtz = CPX + OPX + Plag + H_2O

D) Orthopyroxene-clinopyroxene or

14) CPX + Gar + Qtz = OPX + Plag

E) Clinopyroxene-Garnet (Fe-rich rocks only)

See Table H-1 for abbreviations. The numbers preceeding the reactions correspond to reactions given in Figure H-22. Mg-rich refers to bulk compositions with X_{Mg} of about 0.55 and higher, Fe-rich refers to rocks with X_{Mg} of about 0.4 and lower, at the approximately 6 kbar pressure estimated for peak Acadian metamorphism in Central Massachusetts. This facies series occurs in central Massachusetts over a temperature range from about 600 to 715 °C, estimated using the Thompson (1976b) garnet-biotite geothermometer.

Summary of Amphibole Dehydration Reactions

A summary of the phase relations in mafic rocks in the high grade metamorphic zones of central Massachusetts is given in Figure H-22. All of the diagrams are plagioclase projections (Figure H-22A), and only show phase relations in the lower part of the projection, as in Figure H-21.

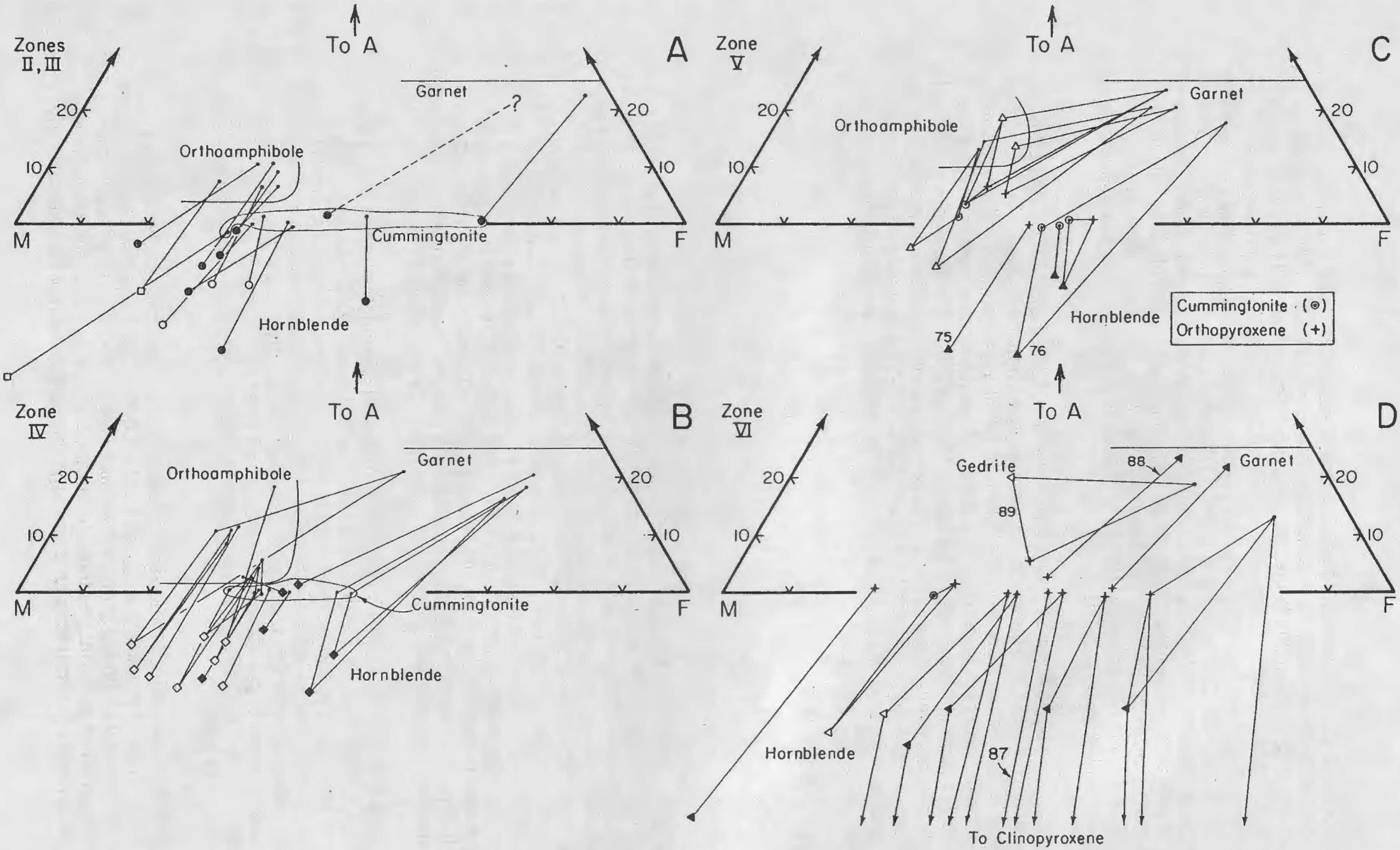

Figure H-21. Electron probe data for amphibole, garnet, and pyroxene, shown projected from plagioclase onto the AFM ternary plane. Quartz-bearing assemblages are shown with solid symbols for hornblende or another mineral. Assemblages without quartz are shown with open symbols. In Figures C and D cummingtonite is shown with dotted circles and orthopyroxene with crosses. Assemblages for samples 75, 76, 87, 88, and 89 from Stops 2, 3, and 9 are labeled.

$A = [(Al+Fe^{+3}-Na)/2]+Ti-Ca$ $F = Fe^{+2}+Mn-Ti$ $M = Mg$

At low metamorphic grade in central Massachusetts (Kyanite Zone and low Sillimanite Zone, about 600°C), phase relations probably look something like Figure H-22B. At intermediate to low X_{Mg} compositions the only 3-phase fields involve the Oam + Hbl = Cum + H_2O reaction (1 in Figure H-22B), and the Oam = Gar + Cum + H_2O reaction (3). Very Mg-rich rocks with sufficient aluminum to have hornblende - orthoamphibole - cordierite, assemblages such as those described by Schumacher (1983; this guidebook, part G), are little known in Zones IV, V, and VI. In addition, complications surrounding the orthoamphibole solvus are ignored, in part because of lack of data and in part because by upper Zone IV or Zone V the orthoamphibole solvus is probably closed (consistent with the data of Robinson et al., 1971; but see an alternative interpretation by Robinson et al., 1982b, p. 190-191). Much of Figure H-22 is self explanatory, but a few points will be discussed in detail.

Cummingtonite first breaks down at Fe- rich compositions (2, Figures H-22 C and D) by the reaction Cum = Gar + Hbl + H_2O. This reaction assemblage is common in Zones IV and V, and will be seen at Stop 2. This reaction is probably followed by the appearance of orthopyroxene, which must be within an intermediate composition field. There are several possibilities for the appearance of orthopyroxene in this system (Hollocher, 1985, p. 207). The favored reaction is the appearance of orthopyroxene within the cummingtonite - garnet - hornblende 3-phase field by the reaction Gar + Cum + Hbl = OPX + H_2O (17, Figure H-22E). This reaction splits the single 3-phase field into three new 3-phase fields (Figure H-22F), representing the orthopyroxene-producing reactions:

18) Cum + Gar = OPX + H_2O,

4) Cum = OPX + Hbl + H_2O,

19) Hbl + Gar = OPX + H_2O.

In Zone V (Figures H-22 G to M), it is difficult to coordinate between what occurs at Mg-rich and Fe-rich compositions. Fe-rich hornblende must begin breaking down to almandine-rich garnet + clinopyroxene (8, Figure H-22H), which proceeds until its 3-phase field collides with the Gar + Hbl = OPX + H_2O reaction already in Figure H-22G (19). This collision produces the discontinuous reaction Hbl + Gar = CPX + OPX + H_2O (13, Figure H-22I), which has been documented in the Adirondacks (Jaffe et al., 1978, Figure 5, sample PO-17). This collision produces a Hbl = OPX + CPX + H_2O dehydration reaction which is terminal to hornblende (7, Figure H-22J), and the continuous reaction Gar + CPX = OPX (14). Reaction 14 separates Fe-rich garnet-clinopyroxene assemblages from Mg-richer garnet-orthopyroxene and orthopyroxene-clinopyroxene granulite facies assemblages in common bulk compositions. Reaction 14 involves only anhydrous minerals, and thus will respond only sluggishly to temperature changes.

When the Cum + Gar = OPX + H_2O 3-phase field (18) collides with the Oam = Gar + Cum + H_2O 3-phase field (3, Figure H-22K), the discontinuous reaction Cum + Gar = Oam + OPX + H_2O (20) introduces orthopyroxene to orthoamphibole and creates two new 3-phase fields (Figure H-22L), representing the reactions Oam = OPX + Gar + H_2O (5), and Oam + Cum = OPX + H_2O (6). Reaction 6 is a strong dehydration reaction, and it proceeds rapidly toward Mg-rich compositions with increasing temperature. Reaction 6 collides with the slower moving dehydration reaction Oam + Hbl = Cum + H_2O (1), producing the discontinuous reaction Oam + Cum = Hbl + OPX + H_2O (21, Figure H-22M).

Reaction 21, which is constrained by analytical data of natural assemblages from central Massachusetts, has the effect of producing a second Cum = OPX + Hbl + H_2O reaction (4, Figure H-22N), such that the terminal cummingtonite composition (Figure H-22O) is colinear with hornblende and orthopyroxene at an intermediate composition. Such a colinearity seems to be a consequence of crystal chemical constraints on cummingtonite composition, as discussed below.

Figure H-22. Summary of phase relations in mafic quartz-bearing rocks from medium to high metamorphic grades in central Massachusetts. A) Plagioclase projection, showing the chemical system and mineral positions. B to R) Summary diagram sequence. Complications associated with the orthoamphibole solvus and the stabilization of garnet by Mn are ignored. Note that many parts of these diagrams are speculative. Small arrows show the direction of movement of the 3-phase fields with increasing temperature. Discontinuous reactions are given, and continuous reactions are as follows:

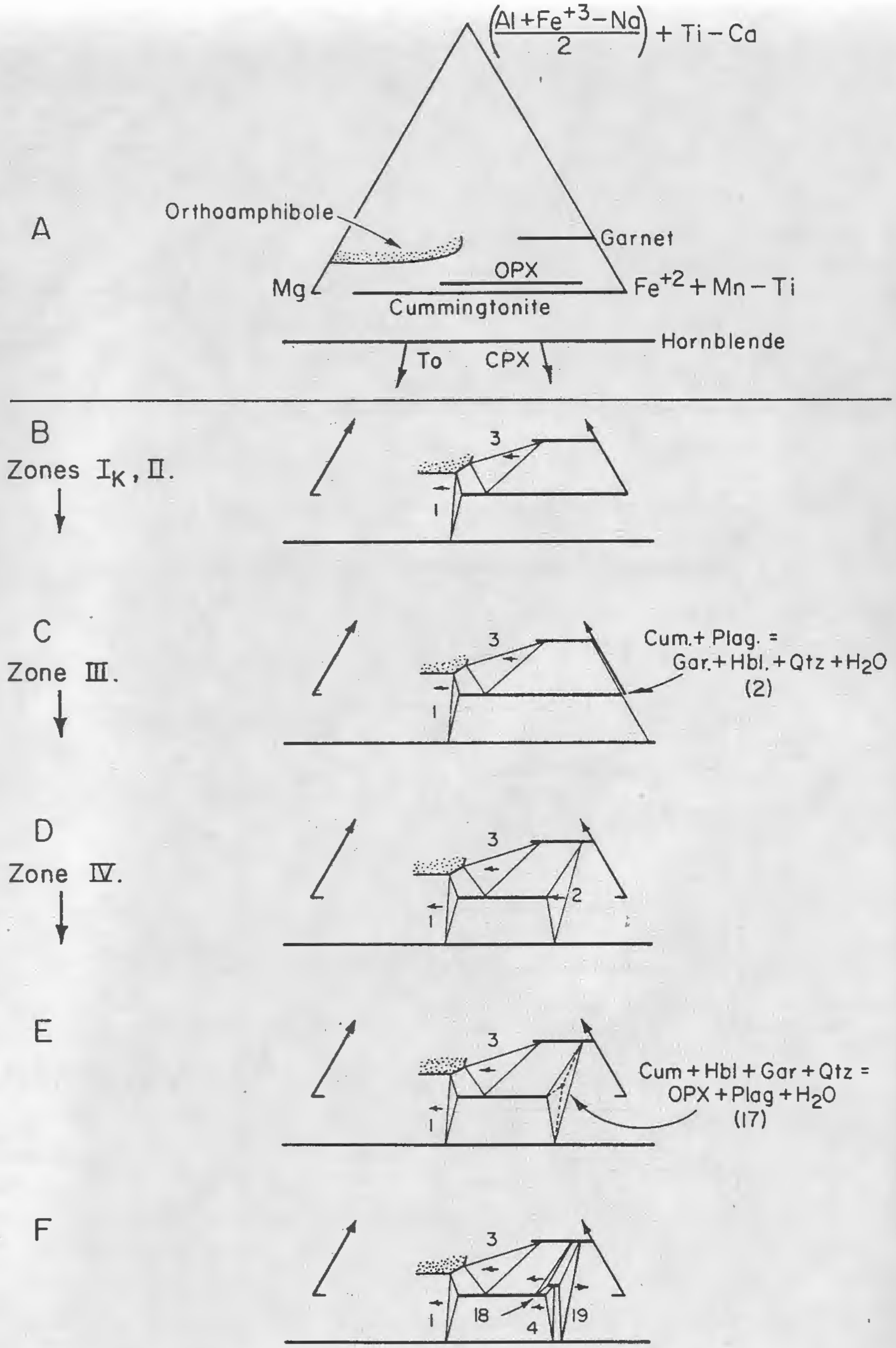
$\left(\frac{Al+Fe^{+3}-Na}{2}\right)$ + Ti − Ca
A
Orthoamphibole
Garnet
OPX
Mg
Fe^{+2} + Mn − Ti
Cummingtonite
Hornblende
To
CPX
B
Zones I$_K$, II.
3
1
C
Zone III.
3
1
Cum.+ Plag. = Gar.+ Hbl.+ Qtz + H_2O (2)
D
Zone IV.
3
2
1
E
3
1
Cum + Hbl + Gar + Qtz = OPX + Plag + H_2O (17)
F
3
1
18
4
19

Continuous Reactions:

1 Oam + Hbl + Qtz = Cum + Plag + H_2O
2 Cum + Plag = Gar + Hbl + Qtz + H_2O
3 Oam + Qtz = Gar + Cum + Plag + H_2O
4 Cum + An = OPX + Hbl + Ab + Qtz + H_2O
5 Oam + An + Qtz = OPX + Gar + Ab + H_2O
6 Oam + Cum = Qtz + OPX + Plag + H_2O
7 Hbl + Qtz = CPX + OPX + Plag + H_2O
8 Hbl + Qtz = OPX + Gar + Plag + H_2O
14 Gar + CPX + Qtz = OPX + Plag
18 Cum + Gar = OPX + Plag + Qtz + H_2O
19 Hbl + Gar + Qtz = OPX + Plag + H_2O
22 Oam + Hbl + Qtz = OPX + Plag + H_2O

The metamorphic Zones in which the mafic rock phase relations are found are also given. These Zones and their related assemblages in pelitic schists are as follows:

Zone:	
I$_k$	Kyanite-staurolite
II	Sillimanite - staurolite - muscovite
III	Sillimanite - muscovite
IV	Sillimanite - muscovite- K-feldspar
V	Sillimanite - K-feldspar
VI	Sillimanite - K-feldspar - garnet - cordierite (Granulite facies)

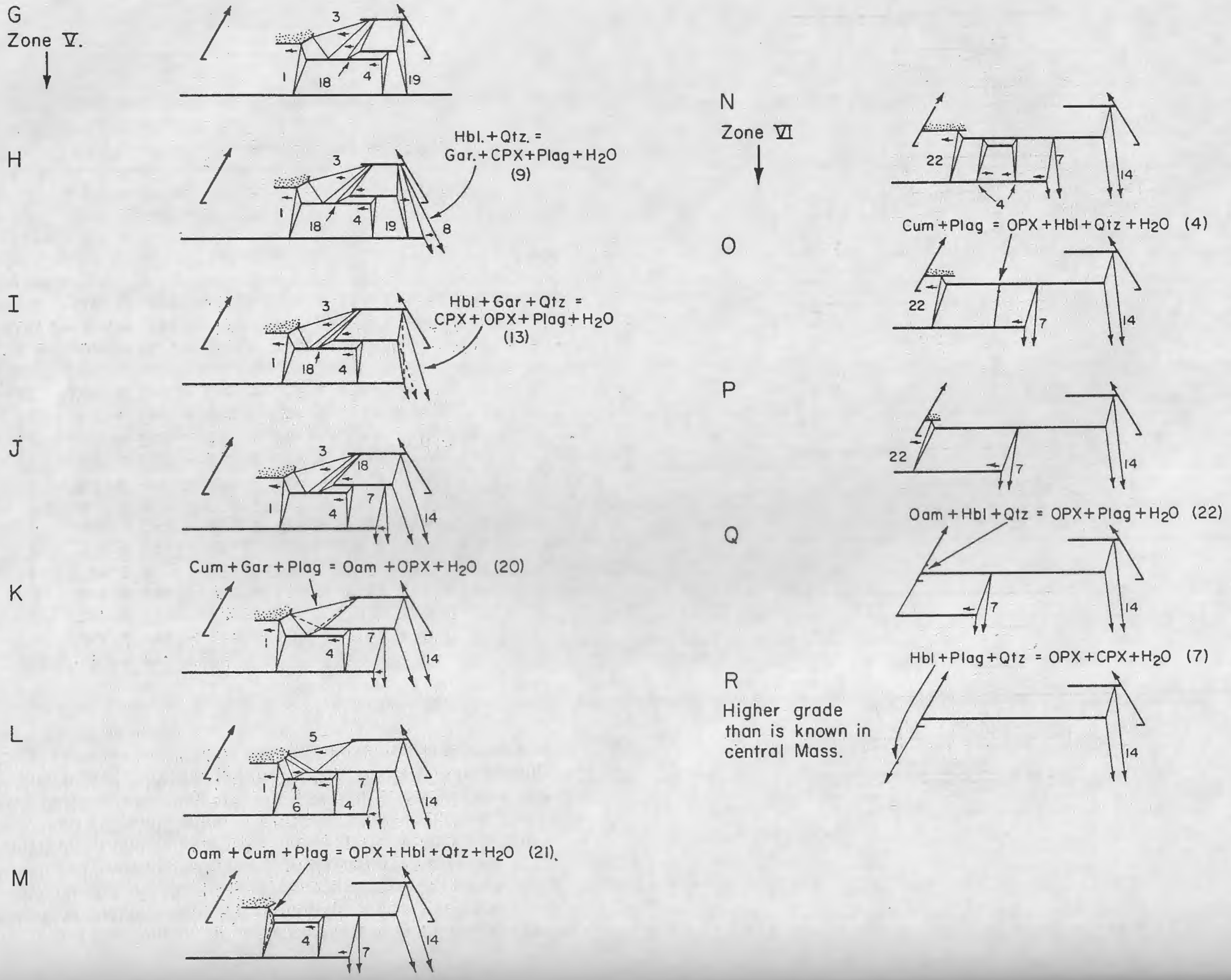
G
Zone V.
H
Hbl. + Qtz. = Gar. + CPX + Plag + H_2O (9)
I
Hbl + Gar + Qtz = CPX + OPX + Plag + H_2O (13)
J
Cum + Gar + Plag = Oam + OPX + H_2O (20)
K
L
Oam + Cum + Plag = OPX + Hbl + Qtz + H_2O (21).
M
N
Zone VI
Cum + Plag = OPX + Hbl + Qtz + H_2O (4)
O
P
Oam + Hbl + Qtz = OPX + Plag + H_2O (22)
Q
Hbl + Plag + Qtz = OPX + CPX + H_2O (7)
R
Higher grade than is known in central Mass.

Finally, orthoamphibole loses contact with hornblende (not a terminal reaction) when the reaction Oam + Hbl = OPX + H_2O (22, Figure H-22 P and Q) reaches the Mg-sideline. This should be followed by the terminal hornblende dehydration reaction (7, Figure H-22R) for pure Mg hornblende. The phase relations of Figure H-22R are not attained, however, because hornblende is still found at Mg-rich compositions even in the highest grade rocks in south-central Massachusetts.

Constraints on Fe-Mg vs. Temperature Reaction Loops

Three continuous amphibole dehydration reactions were constrained to a reasonable degree with respect to estimated metamorphic temperature and the Mg/(Mg+Fe^{2+}) ratio of coexisting minerals (T and X_{Mg}):

1) Oam + Hbl + Qtz = Cum + Plag + H_2O (Oam + Hbl = Cum + H_2O)

4) Cum + An = OPX + Hbl + Ab + Qtz + H_2O (Cum = OPX + Hbl + H_2O)

7) Hbl + Qtz = CPX + OPX + Plag + H_2O (Hbl = OPX + CPX + H_2O).

These reactions can be seen in plagioclase projection as 3-phase fields in Figure H-22J, as well as actual reaction assemblages in Figure H-21.

The interpreted locations of these three T-X_{Mg} reaction loops, corresponding to the three dehydration reactions are shown in Figure H-23 (solid lines). Several other reaction loops are also included, but are poorly constrained (dashed lines, see Figures H-22 C to R for the reactions), .

An interesting part of this diagram is the terminal cummingtonite composition, which is interpreted to lie at an intermediate composition rather than at an end member. This interpretation is based on a hornblende-orthopyroxene assemblage that occurs at compositions more Mg-rich than the high temperature projection of the long arm of the Cum = OPX + Hbl + H_2O reaction loop. The Oam + Hbl = Cum + H_2O reaction (1 of Figure H-22) collides with the Oam + Cum = OPX + H_2O reaction (6, Figures H-22 L and M), which lies out of the plane of the T-X_{Mg} section. The result is a discontinuous Oam + Cum = Hbl + OPX + H_2O reaction (21, Figure H-22M), from which two new continuous reactions are derived. These diverge from the top of the Oam + Hbl = Cum + H_2O (1) reaction loop at about 680 °C. One of the two new continuous reactions is a second Cum = OPX + Hbl + H_2O reaction identical to the first but proceeding in the opposite direction toward more Fe-rich compositions (Figure H-22N). The two cummingtonite-consuming reactions converge at a temperature maximum of about 685 °C, with a terminal cummingtonite composition of about $X_{Mg} = 0.68$. This value is very close to an ordered cummingtonite composition: $Fe_2Mg_5Si_8O_{22}(OH)_2$ ($X_{Mg} = 0.714$), suggesting that Fe^{2+}-Mg ordering into crystallographic sites stabilizes this intermediate composition over the Mg-end member. This intermediate terminal cummingtonite composition, caused by the reversal of Fe/Mg partitioning between cummingtonite and orthopyroxene, is thought to be just fine by Bernard W. Evans (personal communication, 1986).

Hornblende Dehydration and Plagioclase Composition

The reactions described above all involve Fe-Mg exchange as the principal continuous chemical variable in the reactions. In quartz-saturated systems the next most important continuous variable is probably the composition of plagioclase. A summary of hornblende dehydration with respect to plagioclase composition in granulite facies rocks is given in Figure H-24 as a set of orthopyroxene projections. The plagioclase solid solution series is shown as a solid line connecting albite and anorthite. The occurrence of miscibility gaps in the plagioclase field were ignored (see Smith, 1983, for a discussion of plagioclase miscibility gaps).

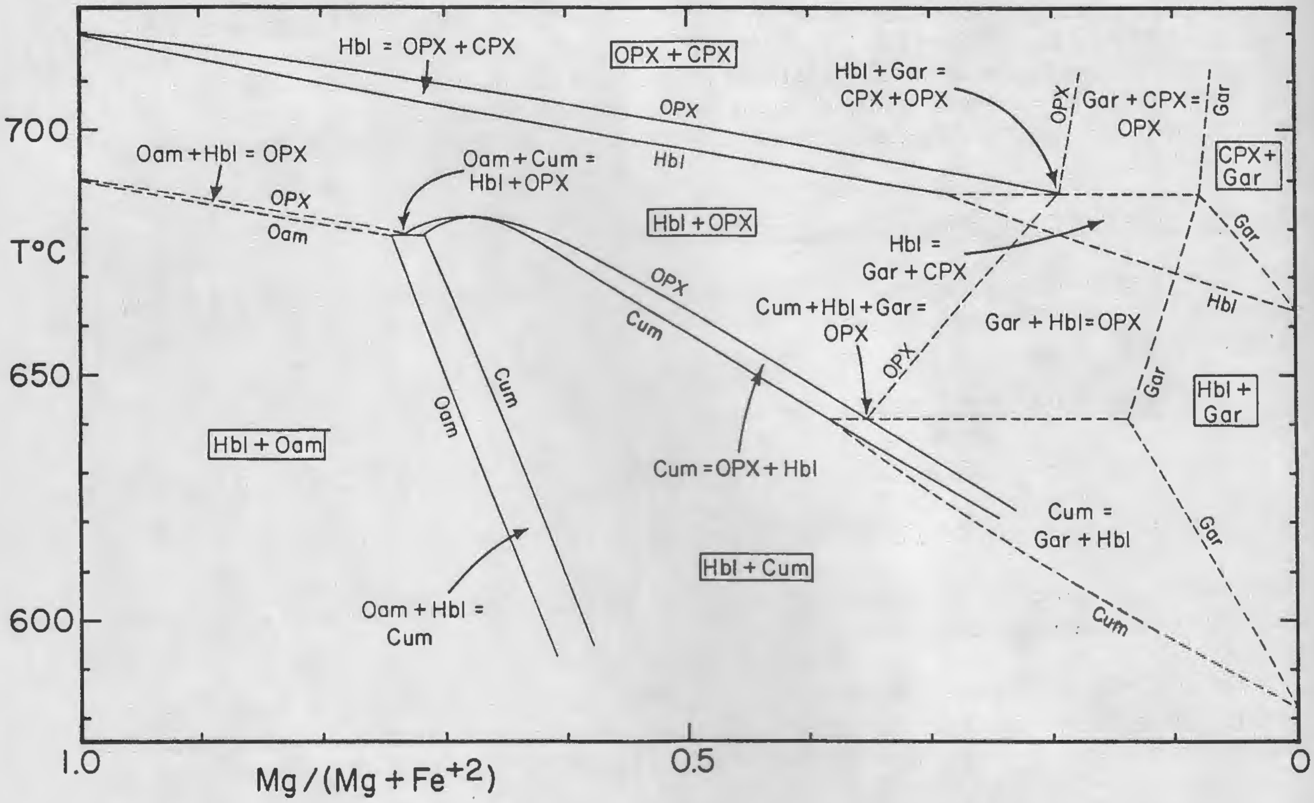
Hbl = OPX + CPX
OPX + CPX
Hbl + Gar = CPX + OPX
OPX
Gar + CPX = OPX
Gar
CPX + Gar
700
Oam + Hbl = OPX
OPX
Oam
Oam + Cum = Hbl + OPX
OPX
Hbl
Hbl + OPX
T°C
Hbl = Gar + CPX
Gar
Hbl
OPX
Cum
Cum + Hbl + Gar = OPX
Gar + Hbl = OPX
OPX
650
Cum
Oam
Gar
Hbl + Gar
Hbl + Oam
Cum = OPX + Hbl
Cum = Gar + Hbl
Gar
Hbl + Cum
600
Oam + Hbl = Cum
Cum
1.0
Mg / (Mg + Fe^{+2})
0.5
0

Figure H-23. T-X_{Mg} diagram showing the estimated positions of various Mg/Fe reaction loops for amphibole dehydration reactions in quartz-bearing rocks. This diagram represents a T-X_{Mg} section taken between hornblende and the Fe-Mg join, as seen in plagioclase projection. Continuous reactions are represented by reaction loops, and discontinuous reactions are represented by horizontal lines. Loops shown by solid lines are reasonably well constrained by temperature and composition data. Loops shown with dashed lines are not well constrained, but are topologically and petrologically valid. The minerals that constrain the loops are given adjacent to the limb of each loop in small letters. Mineral names in boxes represent two phase assemblages in the divariant regions between loops. H_2O is on the right (high temperature) side of all reactions given.

The simplest way to think of Figure H-24 is as four slices out of the ACNFM system at constant temperature; the slices becoming more Mg-rich from A to D (approximate X_{Mg} values for orthopyroxene given). In slice A, at Fe-rich compositions, hornblende has already broken down by the passage of the discontinuous reaction:

12) Hbl + Qtz = Gar + Plag + CPX + OPX + H_2O,

Hornblende remains at more magnesian compositions as shown in slice B. The three 3-phase fields in Figure H-24B that surround hornblende represent three continuous reactions, each of which expands the hornblende field in a particular direction as bulk composition moves toward higher X_{Mg}. Because garnet is not stable in the quartz - hornblende - clinopyroxene - orthopyroxene - plagioclase assemblage at high X_{Mg} at 6 kbar, the plagioclase field in equilibrium with orthopyroxene must extend toward anorthite (Figures H-24 C and D) by way of two additional discontinuous reactions:

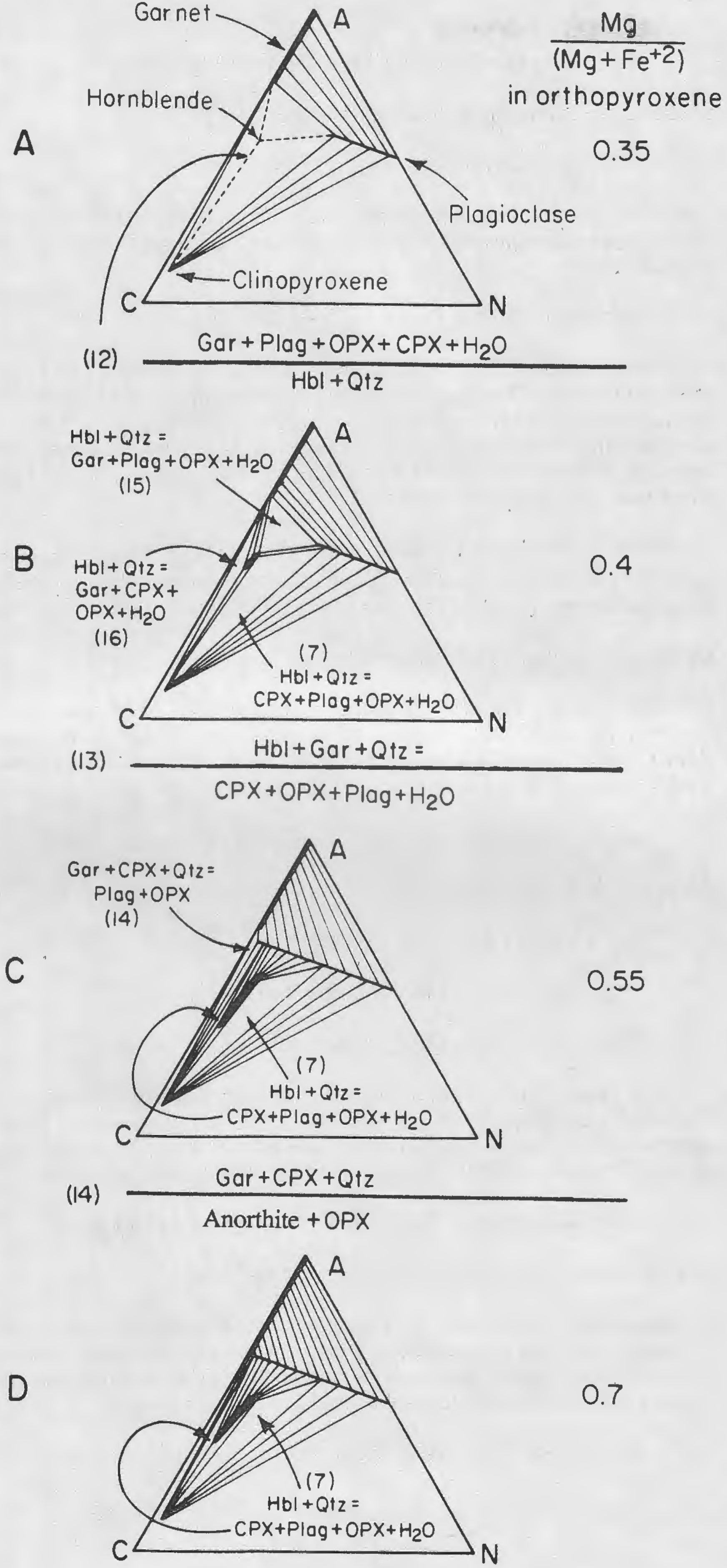
Garnet
A
$\frac{Mg}{(Mg+Fe^{+2})}$
in orthopyroxene
Hornblende
A
0.35
Plagioclase
Clinopyroxene
C
N
(12) $\frac{Gar + Plag + OPX + CPX + H_2O}{Hbl + Qtz}$
$Hbl + Qtz =$
$Gar + Plag + OPX + H_2O$
(15)
A
B
$Hbl + Qtz =$
$Gar + CPX +$
$OPX + H_2O$
(16)
0.4
(7)
$Hbl + Qtz =$
$CPX + Plag + OPX + H_2O$
C
N
(13) $\frac{Hbl + Gar + Qtz =}{CPX + OPX + Plag + H_2O}$
$Gar + CPX + Qtz =$
$Plag + OPX$
(14)
A
C
0.55
(7)
$Hbl + Qtz =$
$CPX + Plag + OPX + H_2O$
C
N
(14) $\frac{Gar + CPX + Qtz}{Anorthite + OPX}$
A
D
0.7
(7)
$Hbl + Qtz =$
$CPX + Plag + OPX + H_2O$
C
N

Figure H-24.. Projections from orthopyroxene, showing how hornblende breakdown reactions relate to plagioclase composition in the granulite facies (Zone VI). The sequence from A to D, top to bottom, represents planes of increasing X_{Mg} at constant temperature, or of increasing metamorphic grade from D to A, bottom to top, at a constant X_{Mg} of about 0.4. The discontinuous reactions separating parts A, B, C, and D, and the continuous reactions represented by 3-phase fields are given. The plotting parameters are:

$A = Al + Fe^{+3} + 2Ti$
$C = Ca$
$N = Na.$

13) Hbl + Gar + Qtz = CPX + OPX + Plag + H_2O,

which shields hornblende from garnet, and:

14) Gar + CPX + Qtz = An + OPX,

which shields clinopyroxene from garnet. Thus, in Figure H-24D hornblende is surrounded only by tie lines to clinopyroxene or to plagioclase, and by two 3-phase fields both representing the reaction:

7) CPX + OPX + Plag + H_2O = Hbl + Qtz.

The reversal of Ca/Na partitioning between hornblende and plagioclase, from hornblende being more calcic than plagioclase (Na-richer compositions) to hornblende being less calcic than plagioclase (Ca-richer compositions) occurs at about An_{80}. In one analyzed sample, hornblende is more sodic than coexisting plagioclase, and in one other sample, hornblende and plagioclase have almost identical Ca/Na ratios. With increasing X_{Mg}, these 3-phase fields move in opposite directions away from each other.

With increasing temperature, rather than with increasing X_{Mg}, at an orthopyroxene composition (slice) of about 0.4, the reaction progress and phase relations are the reverse of those described above, progressing from Figure H-24D toH-24A.

K-feldspar - Orthopyroxene Assemblages

The granulite facies assemblage orthopyroxene - K-feldspar has been found in several rocks in central Massachusetts, electron-probe data for which are shown projected from K-feldspar and plagioclase in Figure H-25A. Orthopyroxene tie lines are first produced in the mafic rocks by the discontinuous reaction:

Hbl + Bio + Gar + Qtz = OPX + Plag + Ilm + Ksp + H_2O,

(Figure H-25B), resulting in three continuous reactions (Figure H-25C):

Bio + Qtz = OPX + Gar + Ilm + Ksp + H_2O,

Hbl + Bio + Qtz = OPX + Plag + Ilm + Ksp + H_2O,

Hbl + Gar + Qtz = OPX + Plag + Ilm + H_2O

K-feldspar has been found in mafic rocks as discrete crystals, as compared to coarse exsolution lamellae, only in the assemblage quartz - plagioclase - K-feldspar - biotite - garnet - orthopyroxene (Sample 88, electron-probe data given in Table H-3). The biotite breakdown reaction responsible for the formation of K-feldspar in these rocks is:

Bio + Plag + Qtz = Ksp + OPX + Gar + Ilm + H_2O,

which is the middle 3-phase field in Figure H-25C.

In several hornblende- and clinopyroxene-bearing samples, including sample 87, no K-feldspar has been found except as coarse exsolution lamellae within plagioclase. However, these samples contain quartz-biotite symplectites (Figure H-26) that are interpreted to be the result of a local retrograde hydration of K-feldspar by the reaction:

Or + OPX + Ilm + H_2O = Bio + Qtz,

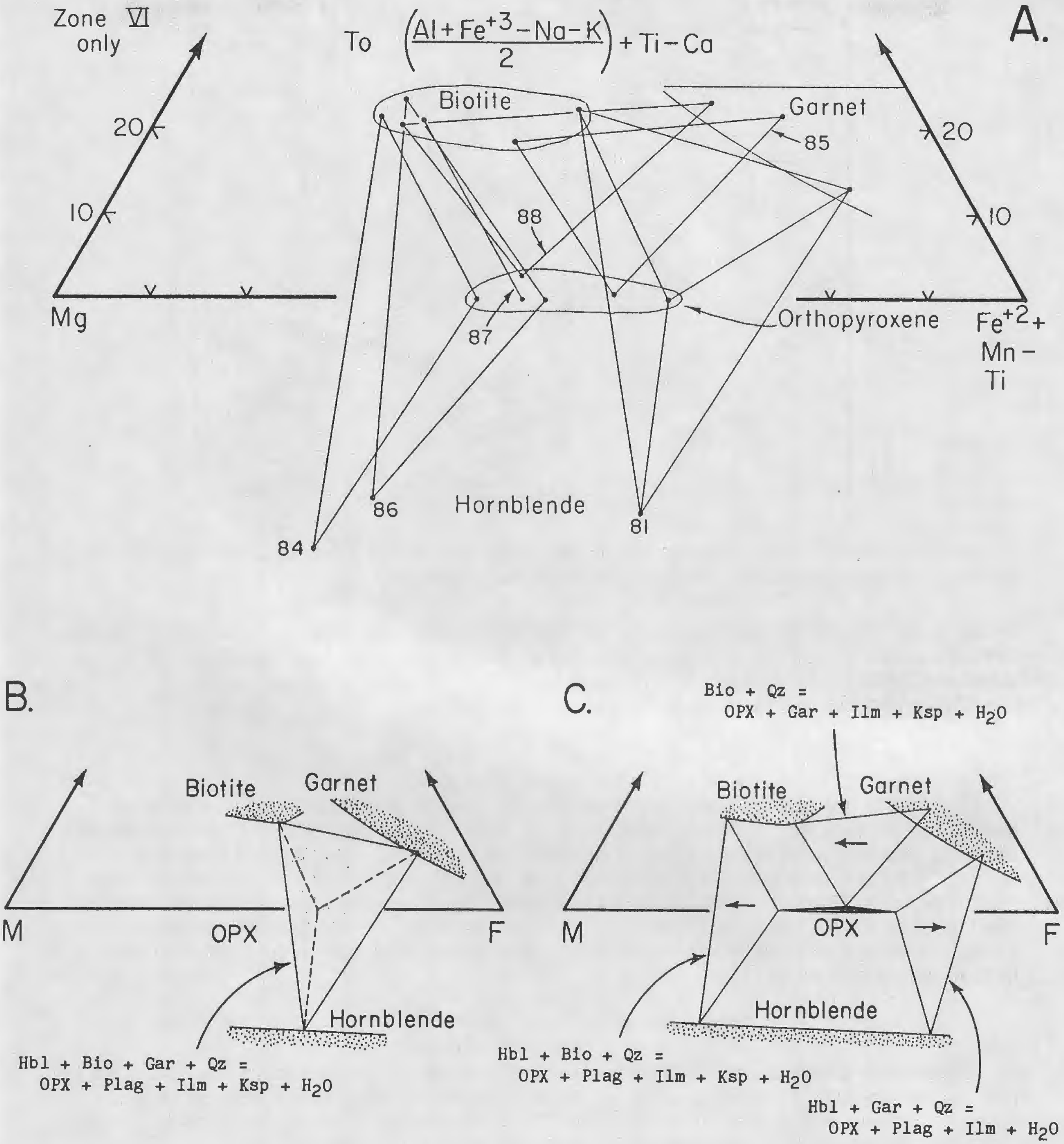
A.
Zone VI only
To $\left(\frac{Al+Fe^{+3}-Na-K}{2}\right)+Ti-Ca$
20
10
Mg
Biotite
Garnet
85
20
10
88
87
Orthopyroxene
$Fe^{+2}+Mn-Ti$
86
Hornblende
81
84
B.
Biotite
Garnet
M
OPX
F
Hornblende
Hbl + Bio + Gar + Qz = OPX + Plag + Ilm + Ksp + H_2O
C.
Bio + Qz = OPX + Gar + Ilm + Ksp + H_2O
Biotite
Garnet
M
OPX
F
Hornblende
Hbl + Bio + Qz = OPX + Plag + Ilm + Ksp + H_2O
Hbl + Gar + Qz = OPX + Plag + Ilm + H_2O

Figure H-25. Projections from plagioclase and K-feldspar onto the AFM ternary plane. A) Data for mafic rock samples in the granulite facies that have prograde K-feldspar (85 and 88), or samples which have quartz-biotite symplectites as textural evidence that K-feldspar occurred in the prograde assemblage (81, 84, 86, and 87; see Figure H-26). Tie lines to clinopyroxene in samples 81, 84, 86, and 87 are omitted for clarity. B) The reaction that first produces orthopyroxene - K-feldspar tie lines in the lower granulite facies (Zone VI). C) Phase relations in the highest grade rocks in central Massachusetts. Note that the biotite-absent garnet - hornblende - orthopyroxene - K-feldspar assemblage has not yet been found.

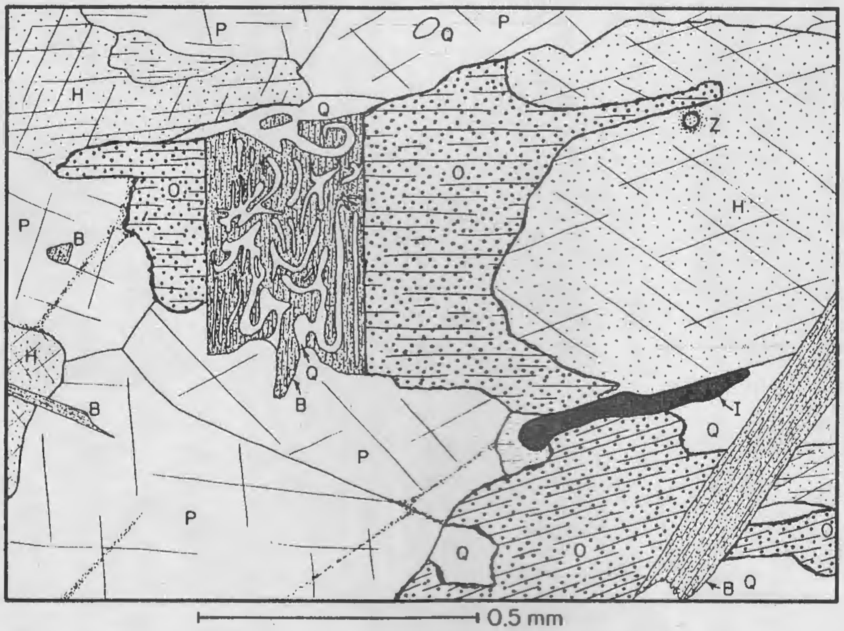

Figure H-26. Sketch from a thin section of a pyroxene granulite in Zone VI showing a quartz-biotite symplectite, which is produced by the retrograde reaction:

$$Ksp + OPX + Ilm + H_2O = Bio + Qtz$$

Biotite plates of probable prograde origin are shown on the left and lower right parts of the sketch. Textures similar to this can be found in samples 87 and 88 from Stop 9 (see Figure H-40 for sample locations). B = Biotite, H = Hornblende, I = Ilmenite, O = Orthopyroxene, P = Plagioclase, Q = Quartz, Z = Zircon.

Ilmenite is required in the retrograde reaction because the retrograde biotite is red-brown, exactly like the prograde biotite. It appears that the biotite breakdown reaction proceeded during prograde metamorphism to produce small quantities of K-feldspar. With a small amount of cooling from maximum metamorphic temperatures, the prograde reaction was reversed in cases where H_2O-bearing metamorphic fluids were available. In most hornblende- and clinopyroxene-bearing rocks, the back reaction proceeded to completion. If K-feldspar did occur in prograde garnet-free, orthopyroxene-clinopyroxene-hornblende assemblages, then K-feldspar must have been produced by a reaction such as:

$$Bio + CPX + Plag + Qtz = Or + Hbl + OPX + Ilm + H_2O,$$

Based on available chemical data and estimated metamorphic temperatures, the Fe-Mg reaction loop for the prograde reaction Bio + Qtz = OPX + Ksp + H_2O given above was found to pass through the region $X_{Mg} = 0.5\text{-}0.6$ at about 700-720 °C, as defined by the compositions of coexisting biotite and orthopyroxene, and estimated metamorphic temperatures.

Partial Melting in Mafic Rocks

In quartz-bearing mafic rocks of metamorphic Zones IV, V, and VI, relatively coarse-grained leucocratic layers, veins, dikes, pods, and larger bodies of tonalitic composition are quite common in quartz-bearing mafic rocks. These leucocratic segregations have long been interpreted to be crystallized locally derived partial melts.

As a result of discussions at a recent conference (Geological Society of America Penrose Conference, June 8-13, 1986, Migmatites and Crustal Melting), during which a field trip was taken to outcrops including Stops 2, 3, and 9, the following distinctions may be made for the leucocratic segregations. The leucocratic zones can be divided into two types: those with grain sizes up to 5 mm, typically 1-2 mm, and those with grain sizes over 5 mm, typically 10-20 mm. The fine-grained leucocratic zones were probably true partial melts produced by fluid-absent partial melting, induced by amphibole and/or biotite dehydration reactions (examples at Stop 9). The coarse-grained leucocratic zones, which may or may not include K-feldspar-rich pegmatite in schist, were probably fluid-saturated melts, or deposits from H_2O-rich solutions (best examples at Stop 3). These interpretations were hotly debated during the Penrose Conference, and no consensus was reached. Regardless of origin or grain size, the leucocratic segregations are considered to be crystallized melts in the rest of this discussion.

In Zones IV and V the melt segregations rarely take up more than a few percent of any mafic rock outcrop, whereas in Zone VI the melts can make up more than 15% of the rock. These melt segregations are typically composed of about 40% coarse-grained gray quartz containing rutile needle inclusions, about 55% dark-gray plagioclase (An_{20}-An_{45}) containing oriented opaque oxide exsolution lamellae, and about 5% mafic minerals, that include biotite, cummingtonite, hornblende, gedrite, garnet, magnetite, ilmenite, orthopyroxene, and clinopyroxene. Apatite, zircon, clinozoisite, and pyrrhotite also occur. K-feldspar has been found as discrete crystals only in melt zones from a garnet-orthopyroxene granulite that also contains K-feldspar (sample 88). The parent rock for this melt is actually intermediate in composition, rather than mafic.

Melting in mafic rocks must have occurred as a result of H_2O released by amphibole and/or biotite dehydration reactions. This means that the dehydration reactions involved, as discussed above, must be modified to include tonalitic liquid. Tonalitic partial melts are found in a wide variety of quartz- and plagioclase-bearing mafic rocks in Zones IV, V, and VI, suggesting that the presence of quartz, plagioclase, and H_2O were the principal requirements for melting. This is not surprising, as the modal compositions of the tonalitic segregations range from 91 to 97% quartz plus plagioclase. The mafic minerals may have served principally as a flux, depressing liquidus surfaces into the range of metamorphic temperatures (about 670-720 °C). The dehydration reactions which released the H_2O that promoted melting may therefore have been of only secondary importance. Free quartz, sodic plagioclase ($< An_{50}$), and possibly low $Mg/(Mg+Fe^{2+})$ ratios (< 0.6) favored melting during Acadian metamorphism. Bulk chemical data on these partial melts are scarce, but one sample analyzed (sample 55, Table H-5, Stop 3) is metaluminous, with 0.08% normative diopside. The other leucocratic segregations also appear to be metaluminous.

Table H-2 is a summary of the samples from Stops 2, 3, and 9 for which analytical data are available. Electron-probe analyses are given in Table H-3, and modes and bulk chemical analyses are given in Tables H-4, H-5, and H-6. Also summarized in Table H-2 are the partial melting relations (or lack thereof) between the several cited samples.

RELATIONS BETWEEN METAMORPHISM AND STRUCTURAL DEVELOPMENT

The central Massachusetts-northern Connecticut Acadian metamorphic high occurred in a region dominated by three major episodes of Acadian deformation: 1) regional nappes with east to west overfolding of tens of kilometers, 2) west to east backfolding of previous axial surfaces on a scale of tens of kilometers, with development of a powerful east-west trending linear fabric and synchronous ductile mylonite zones, and 3) a pattern of tight folds and linear fabrics associated with gravitationally induced rise of gneiss domes in the Bronson Hill anticlinorium. On the west side, the metamorphic high has an overhang of hotter rocks overfolded onto cooler rocks as a result of the early nappes. On the east side the high also overhangs, probably as a result of backfolding.

Before and during the early nappe stage the region was intruded by a variety of sheet-like calc-

Table H-1. Abbreviations used in the text and figures.

Mineral Abbreviations:

Ab	Albite component
An	Anorthite component
Bio	Biotite
Cn	Celsian component
CPX	Clinopyroxne (generally calcic augite)
Cum	Cummingtonite
Gar	Garnet
Ged	Gedrite
Hbl	Hornblende
H_2O	Water, hydrous metamorphic fluid
Ilm	Ilmenite
Liquid	Hydrous tonalitic partial melt
Ksp	K-feldspar (orthoclase or microcline)
Oam	Orthoamphibole (typically gedrite in high-grade rocks)
OPX	Orthopyroxene (typically hypersthene)
Or	Orthoclase component
Plag	Plagioclase
Qtz	Quartz

Other Abbreviations:

T	Temperature, °C
X_{Mg}	Molar $Mg/(Mg+Fe^{+2})$

Table H-2. Summary table for the available analyses, listed according to Stop. Data that are given in other Tables (from Hollocher, 1985) are shown for each sample. The right half of the Table correlates sample numbers of melted rocks with their respective partial melts, and indicates which samples were not melted.

Locality	Sample	Available Data			Genetic relationships
		Mode	Bulk Chem.	Probe Data	
Stop 2 Brimstone Hill	8	X	X		8, amphibolite not melted 41, int. gneiss not melted 26, amphibolite ↓ 76, tonalitic melt 48, felsic Gneiss ↓ Coarse garnet pegmatite *
	26	X	X		
	41	X	X		
	48	X	X		
	76	X		X	
Stop 3 Monson	18	X	X		18, 75, amphibolite → 55, tonalitic melt
	55	X	X		
	75	X		X	
Stop 9 Mashapaug Rd.	35	X	X		35, two pyroxene granulite ↓ 87, tonalitic melt 88, pyroxene-garnet granulite ↓ 88, tonalitic melt 89, not melted
	87	X		X	
	88	X		X	
	89	X		X	

* Not studied.

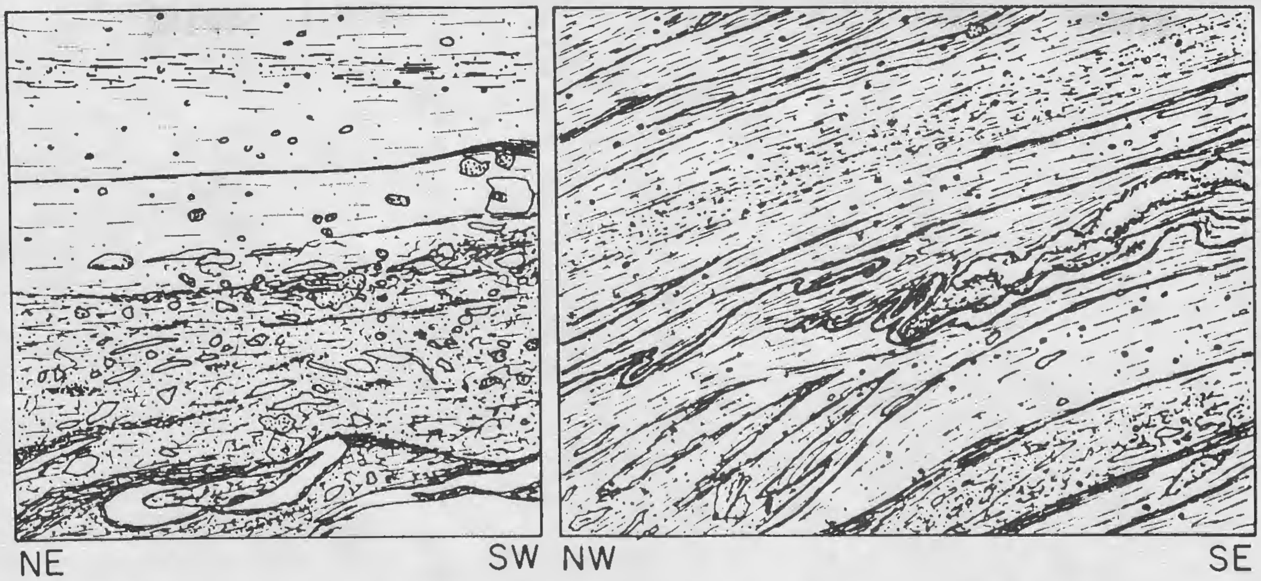

Figure H-27. Sketches from two oriented thin sections of a single chip of mylonite from Stop 7. Left-hand section (about 9 mm wide) shows lower contact of mylonite and is perpendicular to quartz rodding in the mylonite. Schist below the mylonite is strongly sheared and contains the doubly-plunging nose of a northeast-trending fold in ribbon quartz. The schist also contains garnet, not present in the host of the analysed sample. Right-hand section (about 12 mm wide, same scale) is entirely within mylonite and is perpendicular to axes of northeast-trending folds in mylonitic foliation.

alkaline plutons ranging in composition from gabbros through voluminous biotite tonalites to granites, generally yielding intrusion ages around 400 m.y. Evidence for early low pressure metamorphism is preserved in the widespread occurrence of sillimanite pseudomorphs after andalusite (Figure H-9A) and at least one relict contact-metamorphic aureole adjacent to augite - hornblende diorite (Shearer and Robinson, 1980). Peak metamorphic conditions were attained early in the backfold stage over a broad region east of the gneiss domes, resulting in widespread sillimanite - orthoclase - garnet - cordierite assemblages in pelitic schists and rare orthopyroxene - augite - orthoclase - garnet assemblages in felsic volcanics. Detailed geothermometry and geobarometry suggest peak metamorphic temperatures up to 740 °C and pressures of about 6.4 kbar, with abundant evidence for local fluid - absent melting. At many locations the peak metamorphic fabric is cut by ductile mylonites containing the east-west linear fabric of the late backfold stage. The planar and linear fabric of the mylonites is deformed by north- and northeast-trending minor folds and axial plane foliation associated with the dome stage of deformation. The mineral assemblages produced by recrystallization of fine-grained material in mylonites represents an unusual opportunity to study a metamorphic facies produced in a similar bulk composition under different metamorphic conditions. The mylonites recognized in Zones IV and V look fine-grained in outcrop but appear recrystallized to reasonable grain size in thin section. The mineral assemblages in these mylonites have garnet compositions similar to retrograde rims in the same region. One Zone V mylonite has secondary muscovite of two kinds, a low Ti muscovite replacing K feldspar and a high Ti muscovite associated with matrix biotite that is very like the highest grade prograde muscovites from Zone IV.

The mylonites recognized in Zone VI tend to be much finer-grained and recrystallization is recognized only under high power. It seems probable that this lesser degree of recrystallization is related to less or no interstitial fluid, as suggested by the features of Type C garnets. A continuous 1.5 cm thick mylonite at Stop 7 has been investigated in detail (Figure H-27). The mylonite lies

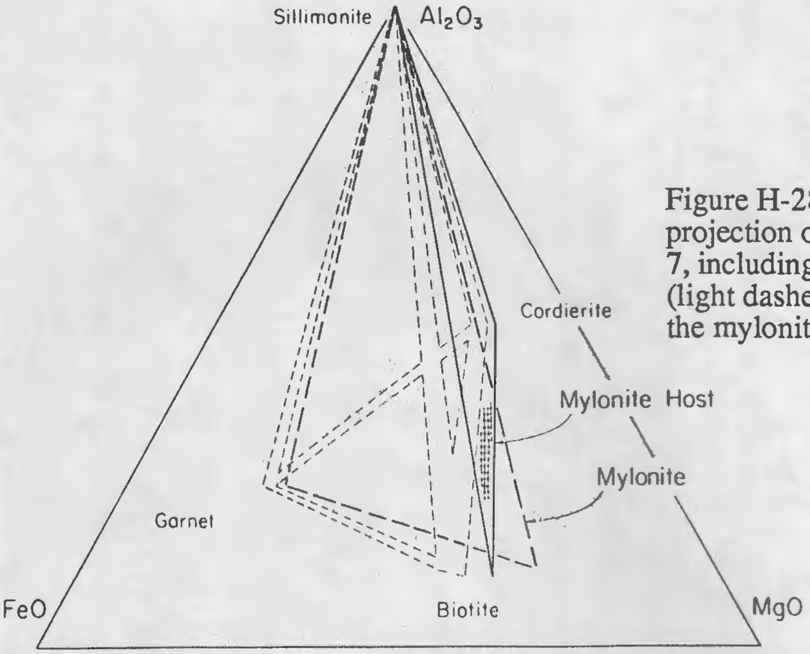

Figure H-28. Quartz + K-feldspar projection of mineral compositions at Stop 7, including garnet-cordierite gneisses (light dashed lines), the mylonite host, and the mylonite.

within a layer of sillimanite-cordierite-biotite-orthoclase schist in an outcrop with abundant coarse-grained sillimanite-garnet-cordierite-biotite schist and cordierite-bearing pegmatite. The mylonite contains porphyroclasts of feldspar and cordierite set in a very fine but strongly oriented pleochroic matrix dominated by biotite with extremely fine-grained feldspar, quartz, and an Al-silicate that is probably sillimanite. Locally within the matrix are tiny anhedral garnets, some with oriented inclusions suggesting the garnets grew at the same time the mylonitic foliation was being deformed in a series of tight northeast-trending folds. Typical mineral assemblages in Zone VI as well as the assemblage of the mylonite host rock are shown in Figure H-28, together with mineral assemblages of the mylonite which seems to have the same bulk composition as its host. The garnet is slightly more pyrope-rich than garnets elsewhere in the outcrop, the biotite is dramatically more Mg-rich (and Ti-poorer) than the biotite of the host rock. The garnet-biotite K_D suggests recrystallization at about 550 °C and if interpreted in the usual way, would suggest a re-crystallization pressure as high as 7-8 kbar. This is in a region where a number of rocks contain sillimanite pseudomorphs after andalusite suggesting earlier low pressure crystallization. Complementary to this evidence of increasing pressure of metamorphism east of the gneiss domes, development of late cordierite and cordierite + corundum reaction rims on sillimanite in gedrite gneisses in the domes is evidence of tectonic unloading related to doming (Robinson and Jaffe, 1969a; Schumacher, 1980, 1983, this guidebook, part G). This "dome path" is further constrained by the occurrence of retrograde intergrowths of kyanite-chlorite-quartz as an alteration of large cordierites in the same outcrops.

We have speculated as to how the central Massachusetts rocks got to granulite facies conditions in the first place. One possibility is that the rocks suffered rather massive dehydration and melting at the time they were at a relatively high level in the nappe stage. Once large amounts of H_2O-rich fluid had been driven or melted out at a high level, the rocks would have been pre-treated for the high pressure dry conditions needed to obtain assemblages characteristic of the granulite facies.

The late Acadian Belchertown pluton truncates isoclinal folds of early stages within the regional kyanite zone. A narrow septum of mica schist in the pluton records a progressive inward increase in metamorphic grade from kyanite to sillimanite-staurolite to sillimanite-muscovite zones.

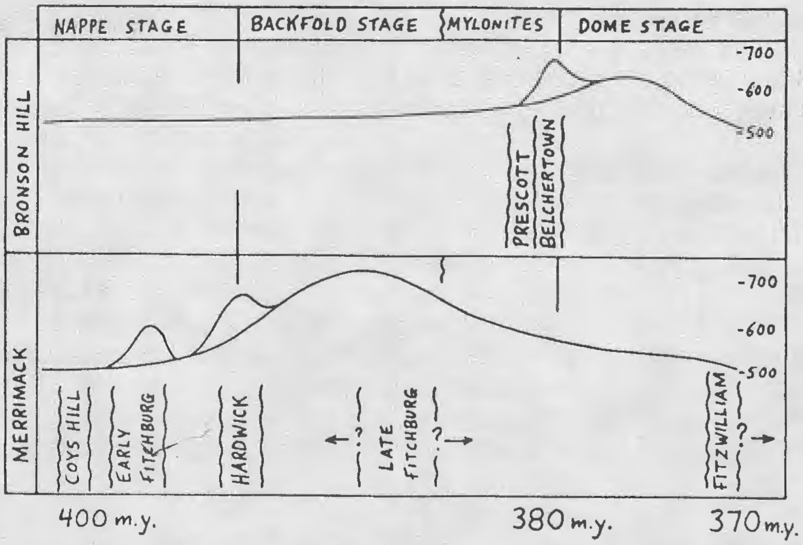

Figure H-29. Contrasting relationships of metamorphism and plutonic activity with respect to tectonic stages in the Bronson Hill anticlinorium and Merrimack synclinorium, central Massachusetts.

The inner end is a schist free of muscovite and of K feldspar (which may have been melted away) with very abundant sillimanite pseudomorphs after andalusite. A primary core of orthopyroxene-augite quartz monzodiorite yields a zircon age of 380 m.y. (Ashwal et al., 1979). The outer part of the pluton has been metamorphically hydrated to hornblende gneiss with development of planar and linear fabric identical to the dome stage fabric of the country rocks. A K-Ar age of 361 m.y. on metamorphic hornblende from this gneiss suggests the end of dome-stage recrystallization. Thus the Acadian deformation and metamorphism were complex and protracted over a period of at least 40 million years.

Figure H-29 shows some of these temporal relations and also contrasts the metamorphism in the eastern part of the area in the Merrimack synclinorium with that in the Bronson Hill anticlinorium. In the east contact metamorphism associated with plutons seems to have been heavily overprinted by the regional peak which was overprinted by mylonites. In the west the Belchertown intrusion seems to have caused a local peak stronger than the slightly later regional recrystallization associated with the dome stage.

REGIONAL TECTONICS AND METAMORPHISM

In the last decade metamorphic petrology has progressed from the mere preparation of detailed metamorphic maps, to the intimate connection of metamorphic mineral evolution, rock fabric evolution, three-dimensional structural evolution, and the addition or removal of heat through the evolving orogen by such diverse mechanisms as diffusion, fluid flow, magma movement, and structural dislocations (e.g. Oxburgh and Turcotte, 1974; England and Richardson, 1977; Crawford and Mark, 1982; Hollister, 1982). Chamberlain and England (1985) evaluated the Acadian thermal history of the Merrimack synclinorium in New Hampshire based on a simple model involving overthrusting and heat transfer by conduction. Since that paper was written, Chamberlain (personal communication, 1985, this guidebook, part F) has recognized that time constraints are too short to permit thermal evolution solely by conduction through sediments deposited on normal continental crust, and mechanisms for more rapid heat transfer are being more thoroughly explored. Chamberlain (1986), Spear (1986), and Robinson et al. (1986) are in agreement that the following heat transfer mechanisms are likely to have been important:

A.) Crustal extension and thinning at the bottom of the Merrimack Trough, possibly in a post-Taconian back-arc phase, may have produced both the basin in which the sediments were deposited and high heat flow through the bottom of the basin into the overlying sediments.

B.) The region of extension may also have provided plumbing for mantle-derived magmas that either intruded the sedimentary column itself or caused melting of continental crust which in turn invaded the sedimentary column. Notable in the Merrimack belt is the abundance of very early intrusions that seem to have been present through most if not all phases of the Acadian orogeny. Interesting in this connection is the suite of gabbros under study by Elbert in the Bernardston-Northfield-Hinsdale area, which cut Partridge Formation and all units of the Monadnock sequence older than the Littleton Formation, but are unknown in Silurian strata in the inverted limb of the Bernardston nappe and virtually unknown in the Monadnock area itself. Is it possible that the gabbro suite marks a zone of weakness during extension near the "tectonic hinge" (Figure H-2) that was subsequently transported westward by fold and thrust nappes?

C.) Chamberlain (personal communication, 1985-86) presently believes, based on detailed petrologic and stable isotope studies in progress, that movements of metamorphic fluids were also extremely important in transfering heat within the tectono-stratigraphic pile. Indeed, it is possible that patterns of fluid flow could have been responsible in part for the preservation of metamorphic overhangs associated with recumbent folds and thrusts.

On the basis of detailed metamorphic phase relations Spear(1986) and Chamberlain (1986) (see this guidebook parts D and F) have proposed a rapid jump in pressures of metamorphism in the low to middle amphibolite facies along the west side of the Bronson Hill anticlinorium from about 3-4 kbar to around 7 kbar, and have suggested that a change of this magnitude would have been more likely accomplished by large-scale overthrusting than folding. Chamberlain (1985), P.J. Thompson (1985) and now Elbert (1986a) have located stratigraphic and structural evidence suggesting that such large-scale thrusting has indeed taken place, mostly after the formation of the better known fold nappes. Apparent from all of the petrologic work is the fact that different rocks record in their petrology different phases of the regional deformation and metamorphism, and one must be very thorough and very lucky to find specimens that record specific features of metamorphic and thermal history on which important quantitative conclusions can be drawn. What is clearly emerging, however, is the concept of a low pressure - high heat flow "Buchan" belt (Spear, 1986) that has been transported westward onto cooler ground, producing a more classic Barrovian metamorphic sequence in the Connecticut Valley region.

The rocks of the central Massachusetts metamorphic high with their mylonitic fabrics, granulite facies assemblages, and evidence of low pressure followed by higher pressure metamorphism were earlier explained by the tectonics of backfolding (Tracy and Robinson, 1980; Robinson et al., 1982c). However, if the structural hypothesis of a basement-involved thrust duplex is correct for the tectonics of the Brimfield-Sturbridge area, then the required high temperatures may have been attained by high heat flow through the floor of the synclinorium and the increased pressure during later phases of metamorphism might have come from tectonic burial by still higher members of the thrust assemblage (Figure H-30).

ITINERARY

The entire area of the field trip with isograds and key to rock units is shown in Figure H-31. Please note that the stratigraphy in the eastern half of the area is in a state of flux and a number of assignments are probably wrong. Figure H-32 is a generalized cross section along a bent line in the northern part of Figure H-31. Figure H-33 is a more detailed blow-up showing the locations of all of the stops.

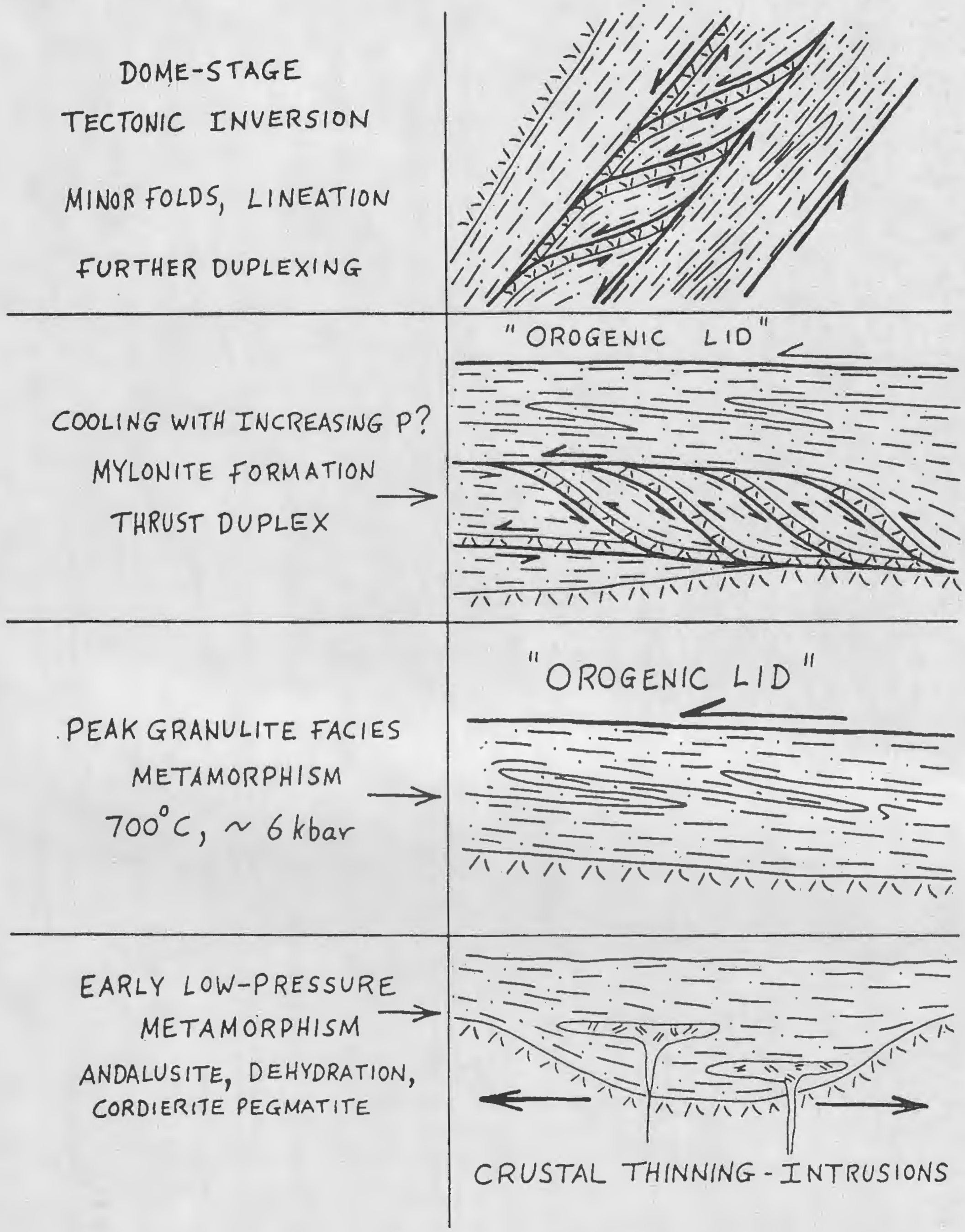
DOME-STAGE
TECTONIC INVERSION
MINOR FOLDS, LINEATION
FURTHER DUPLEXING
"OROGENIC LID"
COOLING WITH INCREASING P?
MYLONITE FORMATION
THRUST DUPLEX
"OROGENIC LID"
PEAK GRANULITE FACIES
METAMORPHISM
700°C, ~ 6 kbar
EARLY LOW-PRESSURE
METAMORPHISM
ANDALUSITE, DEHYDRATION,
CORDIERITE PEGMATITE
CRUSTAL THINNING - INTRUSIONS

Figure H-30. Tectonic-metamorphic cartoon illustrating a tentative new model for the Acadian evolution of the Brimfield-Sturbridge region, south-central Massachusetts (after Robinson et al., and unindicted co-conspirator, 1986). This is substantially different from the model presented in Figure H-6 and requires a different correlation of regional events with the established sequence at a "rosetta stone" outcrop at Parker Island, Quabbin Reservoir.

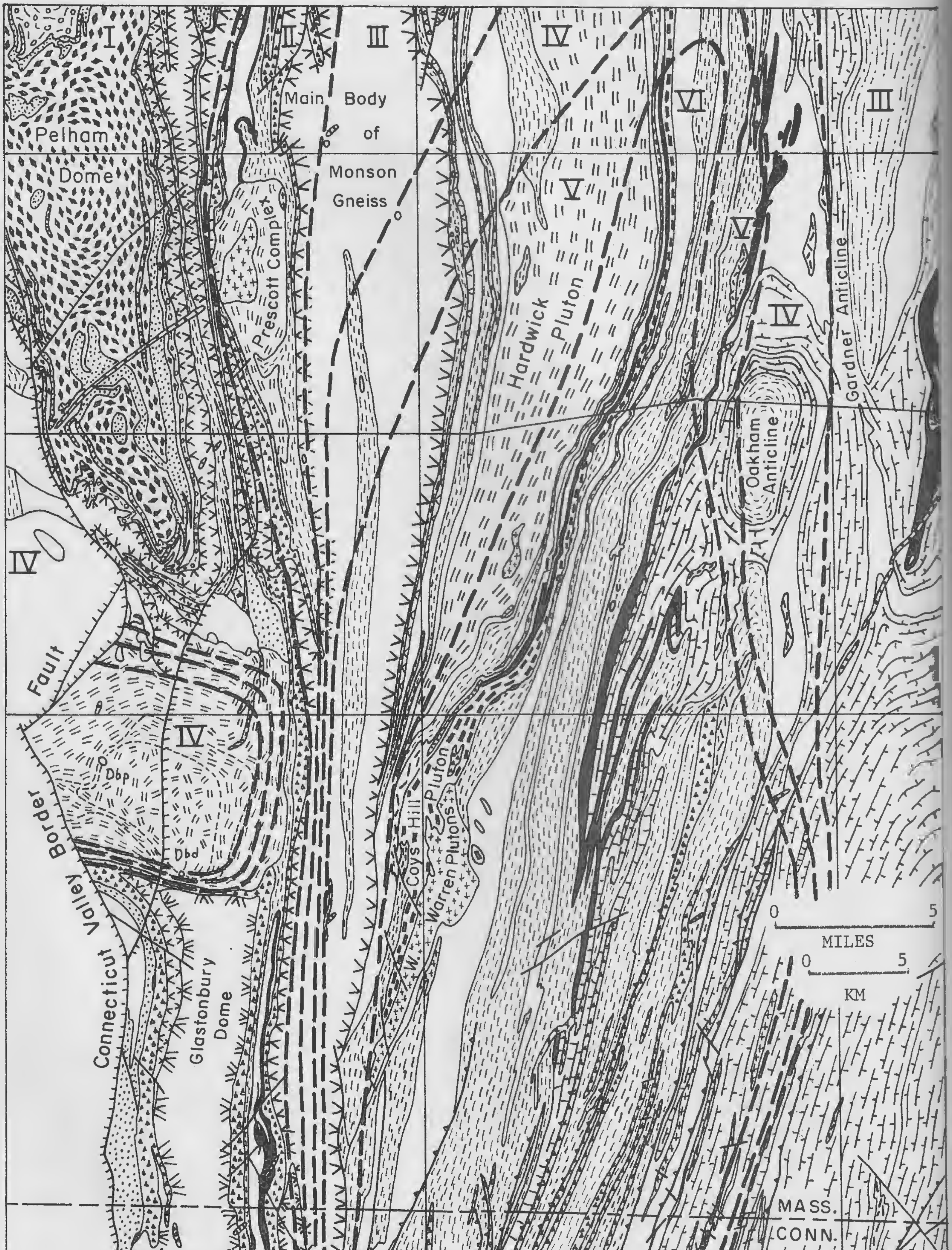
I
II
III
IV
VI
III
Main Body of Monson Gneiss
Pelham Dome
Prescott Complex
V
Hardwick Pluton
V
IV
Gardner Anticline
Oakham Anticline
IV
Fault
IV
Dbp
Dbd
Border
Connecticut Valley
Coys Hill Pluton
W.
Warren Plutons
Glastonbury Dome
0
5
MILES
0
5
KM
MASS.
CONN.

Figure H-31. Generalized bedrock geologic map of south-central Massachusetts, showing metamorphic zones and location of cross section, Figure H-32. No attempt is made to pattern all very small areas. Metamorphic zones are described in the text.

EXPLANATION
(Use also for Figure H-33)

Jurassic	▬	Diabase dikes.
Jurassic-Triassic	□	Conglomerate, sandstone, shale, and basalt.
	▤	Foliated muscovite granite gneiss, biotite gneiss.
	▬	Coys Hill Porphyritic Granite.
	▤	Granodiorite, tonalite.
	+	Gabbro, diorite.
Lower Devonian	▒	Erving Formation.
	□	Littleton Formation. Volcanics where separately mapped.
Silurian	▦	Fitch Formation*
	■	Clough Quartzite.
		Paxton Formation
	▤	Spss-Sulfidic Schist Member
	▦	Sp-Granulite Member
	■	Spsq-White Schist Member, Spqr-Quartzite-Rusty Schist Member
Middle Ordovician	▤	Partridge Formation. Separately mapped felsic volcanics in different pattern.
	▲	Ammonoosuc Volcanics in Bronson Hill belt and separately mapped mafic volcanics in Partridge of Merrimack belt.
Ordovician	∧	Massive gneiss of plutonic derivation in dome core.
Ordovician? or older.	∨	Layered gneiss, Monson Gneiss, Fourmile Gneiss.
Late Precambrian	○	Poplar Mountain Gneiss, Mt. Mineral Formation.
	▒	Poplar Mountain Quartzite, Pelham Quartzite.
	◆	Dry Hill Gneiss.
	┬┬┬	Mesozoic normal fault, hachures on downthrown side.

* Fitch Formation shown solid black W. of Coys Hill Granite.

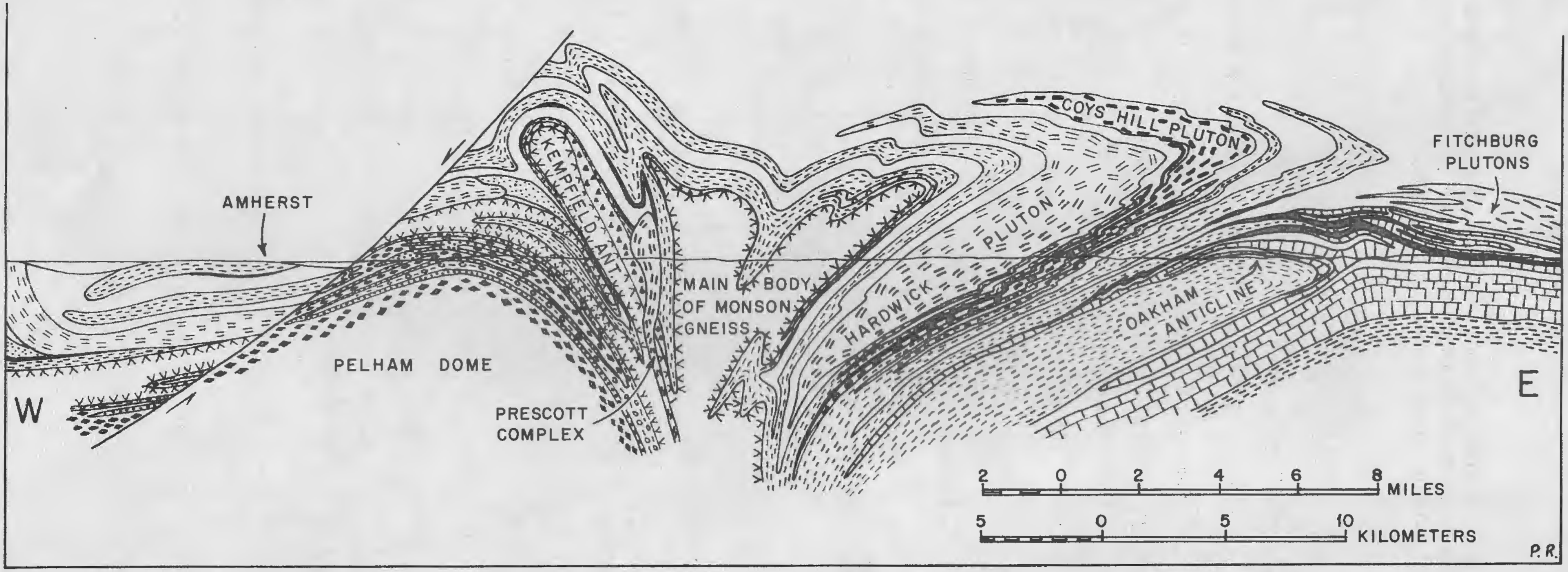
AMHERST
W
PELHAM DOME
KEMPFIELD ANT.
PRESCOTT
COMPLEX
MAIN BODY
OF MONSON
GNEISS
HARDWICK
PLUTON
COYS HILL PLUTON
FITCHBURG
PLUTONS
OAKHAM ANTICLINE
E
2 0 2 4 6 8 MILES
5 0 5 10 KILOMETERS
P. R.

Figure H-32. Bedrock geologic cross-section across central Massachusetts. Line of section (although not full length of it) is shown in Figure H-31. In the two eastern straight segments the section follows the line of Quabbin Aqueduct Tunnel described in detail and sampled by Fahlquist (1935). Detailed sections on parts of this line are given by Field (1975) and Tucker (1977).

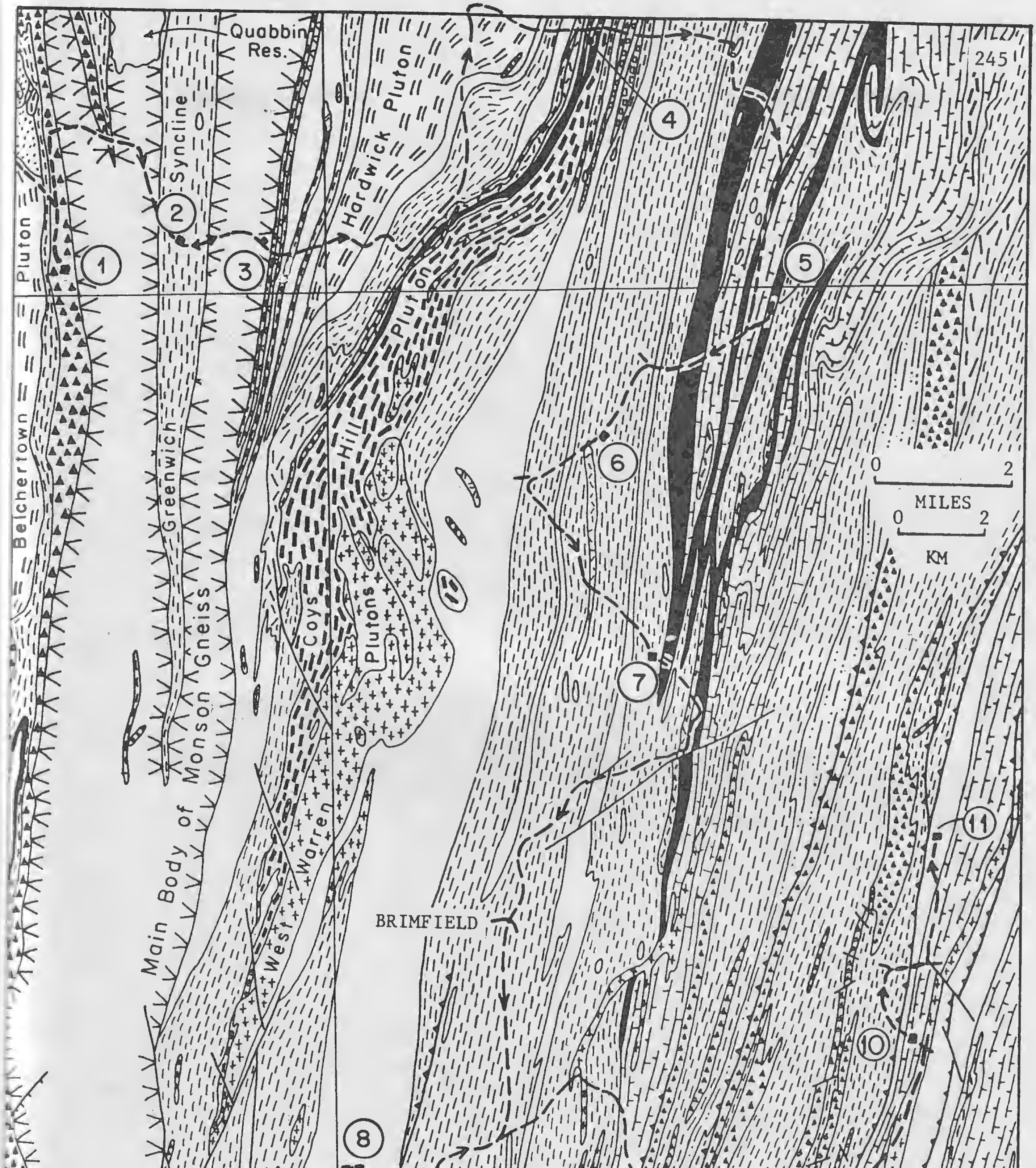
Quabbin Res.
Hardwick Pluton
Belchertown Pluton
Greenwich Syncline
Main Body of Monson Gneiss
Coys Hill Pluton
West Warren Plutons
BRIMFIELD
1
2
3
4
5
6
7
8
9
10
11
0 2
MILES
0 2
KM

Figure H-33. Bedrock geologic map of south-central Massachusetts showing route of trip H and locations of stops. For explanation see Figure H-31.

0.0	Leave University of Massachusetts Campus Center. Proceed south to Route 9 and then east on it.
5.2	Location of Mesozoic Connecticut Valley border fault near New Townhouse Restaurant, here separating high-level sillimanite schists from Fourmile Gneiss of Pelham dome.
7.1	Outcrops left off road. Coarse gneiss of Pelham dome.
8.0	Road cut on both sides. Asymmetric folds in plagioclase gneiss and amphibolite of Fourmile Gneiss, southwest limb of Pelham dome. Connecticut Valley border fault lies in lake to west, with steeply dipping Mesozoic strata of Holyoke Range beyond.
8.6	Enter northwest corner of Devonian Belchertown Complex. Low outcrop, left, of intrusive breccia with hornblendite fragments.
10.1	Stop light at "The Cows", Routes 9 and 202 in Belchertown. Go straight on Route 9.
12.2	Ridge ahead on skyline held up by mica schist "rectal thermometer" extending into Belchertown intrusion.
13.0	Turn left into entrance of Quabbin Reservation.
13.5	Cross Winsor Dam of Quabbin Reservoir. The reservoir is 35 miles long and a major part of Boston's water supply.
14.1	Cross biotite tonalite stock, at Spillway, site of 1971 B.S. thesis of Frank Spear at Amherst College.
14.6	Return to Route 9. Turn right (southwest).
15.1	Turn left (south) on River Road.
15.4	Bear left off River Road at fork.
15.8	Low outcrop of rusty Partridge schist on left.
15.9	Bear right on Sczygiel Road.
16.2	Pavement widens.
16.5	Park on right, opposite entrance to narrow wood road. Walk up wood road which bends left. After about 400 feet turn right, straight up hill to obscure woods path that runs to right and over crest of ridge. All outcrops on ridge crest are coarse gedrite gneiss. Special locality consists of several loose blocks of highly magnetic rock on steep northeast-facing slope. This is difficult to find without a guide.

STOP 1. ZONED GEDRITE WITH EXTREME Na AND Al COMPOSITIONS

(35 minutes including 15 minutes walk in and out)

The highly zoned Na- and Al-rich gedrite is found in the Lower Member of the Ammonoosuc Volcanics, and occurs in the Sillimanite - Staurolite - Muscovite Zone (Schumacher, 1980). The rock is a gneiss that contains porphyroblasts of gedrite, staurolite, and garnet. The matrix consists of quartz, minor Na-rich plagioclase, gedrite, staurolite, cordierite, aluminosilicate, magnetite, ferri-ilmenite, titano-ilmenite, and minor biotite and chlorite (thin section supplied by J.T. Cheney). It is the matrix gedrites, and not the porphyroblasts that show extensive Na and Al zoning. Formulae

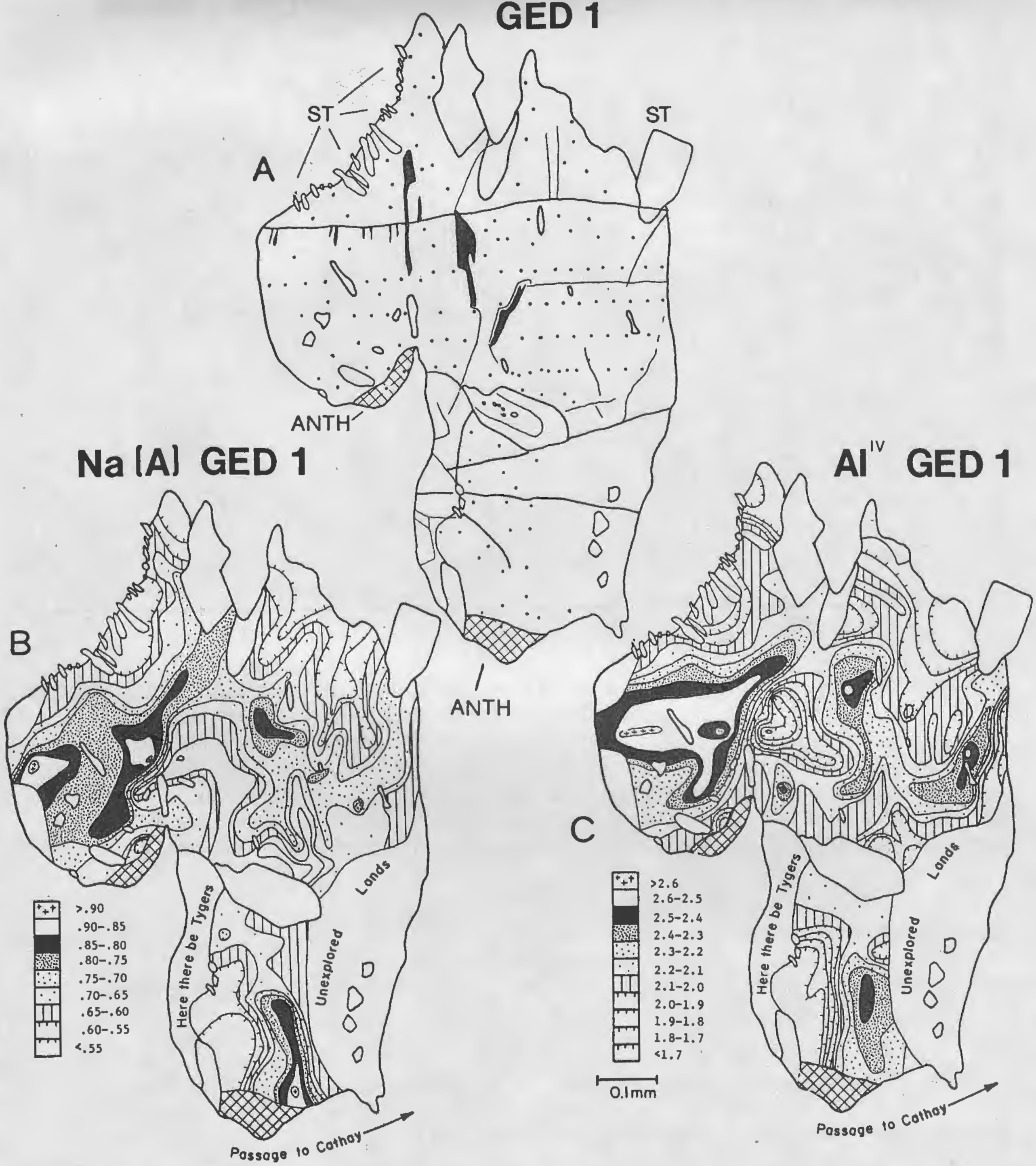
GED 1
A
ST
ST
ANTH
ANTH
Na [A] GED 1
B
>.90
.90-.85
.85-.80
.80-.75
.75-.70
.70-.65
.65-.60
.60-.55
<.55
Here there be Tygers
Unexplored Lands
Passage to Cathay
Al^{IV} GED 1
C
>2.6
2.6-2.5
2.5-2.4
2.4-2.3
2.3-2.2
2.2-2.1
2.1-2.0
2.0-1.9
1.9-1.8
1.8-1.7
<1.7
0.1mm
Here there be Tygers
Unexplored Lands
Passage to Cathay

Figure H-34. Zoned gedrite grain (GED 1) from low in the Sillimanite-Muscovite-Staurolite Zone, central Massachusetts. (A) Location of analysis points. Closed lines represent subhedral staurolite inclusions (some labelled ST). Black lines and patches represent cracks and small areas not suitable for analysis. Cross-hatched areas (labelled ANTH) are anthophyllite overgrowths. Areas which lie outside the main body of analysis points and were not analyzed did not have suitable surfaces. (B) Contour map of Na in A-site. Contours are in intervals of 0.05 Na in the formula (see legend adjacent to map). (C) Contour map of tetrahedral Al. Contours are in intervals of 0.1 Al in the formula (see legend adjacent to map). All-ferrous formulae were used unless this allowed Ca in the A-site, then the 15eNK correction (see "Formulation of electron probe analyses," in Robinson et al., 1982b) was applied, resulting in minimum ferric estimates for all formulae. Most of the analyses required some correction. From Schumacher (1980, and unpublished data).

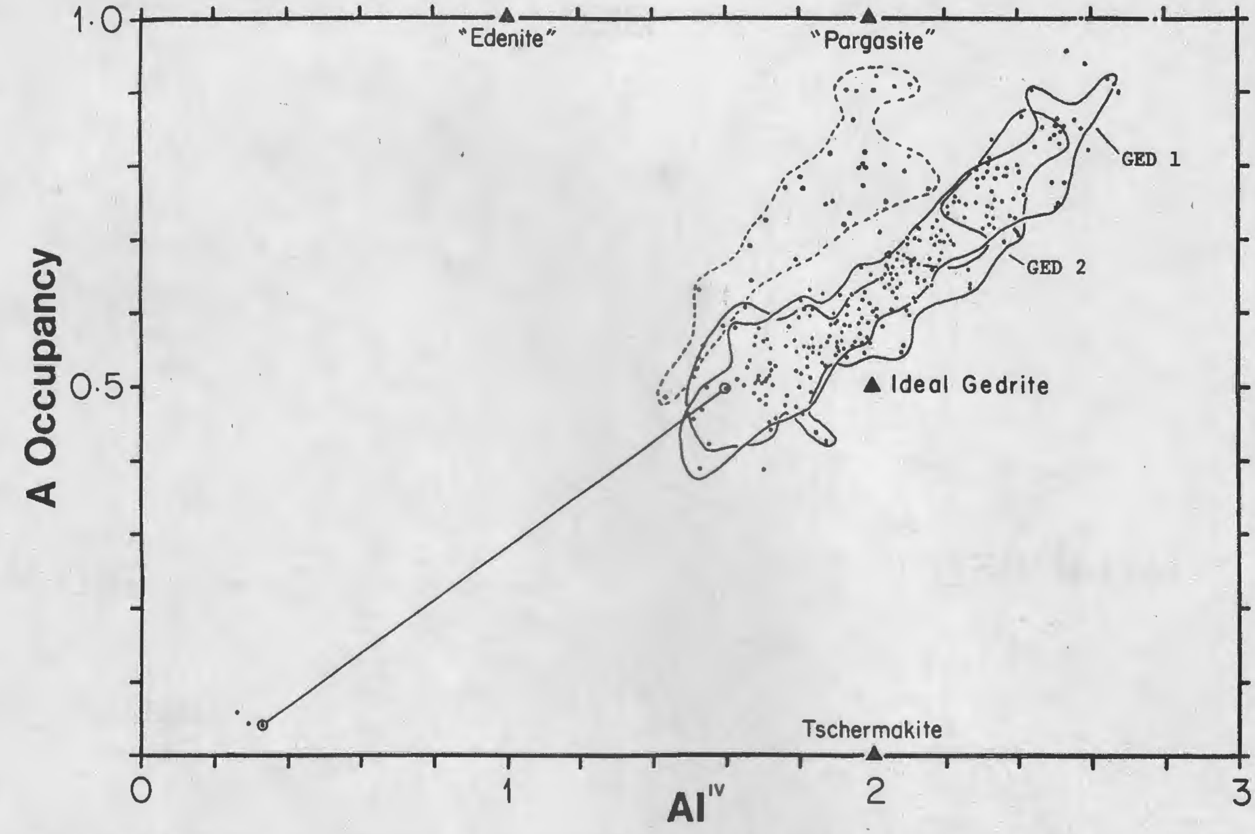

Figure H-35. Plot of A-site occupancy versus tetrahedral Al for zoned orthoamphibole grains at Stop 1 (Schumacher, 1980) and Labrador (Berg and Wiebe, 1978; J.H. Berg, personal communication, 1981; Berg, 1985). Solid lines enclose areas that show the limit of compositional variation within two mapped grains (GED 1 and GED2) from Stop 1. Dashed line encloses the area that shows the limit of compositional variation in the gedrite from Labrador. Points outside the lines are analyses from grains other than GED 1 and 2 but from the same sample. Tie line connects the analysis of an anthophyllite overgrowth to the closest gedrite analysis.

for compositional extremes of the zoned gedrite are:

$$Na_{.39}(Ca_{.02}Mn_{.05}Fe^{2+}_{1.93})(Mg_{.88}Fe^{3+}_{.41}Ti_{.02}Al_{.69})(Fe^{2+}_{.03}Mg_{2.97})(Si_{6.47}Al_{1.53})O_{22}(OH)_2$$

and

$$Na_{.92}(Ca_{.01}Mn_{.05}Fe_{1.94})(Mg_{.25}Fe_{.32}Al_{1.43})(Fe_{.18}Mg_{2.82})(Si_{5.33}Al_{2.67})O_{22}(OH)_2$$

(based on microprobe analyses; minimum ferric estimates).

Figure H-34 shows analysis points and contour maps for Na and Al for one of the zoned gedrites (GED 1), which shows a remarkable resemblance to the continent of Africa (after Robinson et al., 1982b). Correspondence of "regional highs and lows" in Na and Al contour maps reflects the systematic variation of the tschermakite-like and edenite-like substitutions in the orthoamphiboles. The zoning is irregular and regions of high Na-Al can grade either gently or abruptly into relatively low Na-Al regions (Figures H-34 B and C). The most Na- and Al-rich parts of the grain tend to be towards the interior, the small staurolite inclusions do not appear to exercise any control over the Al content of the gedrite (Figure H-34 C.). Two small anthophyllite overgrowths are also present on this grain.

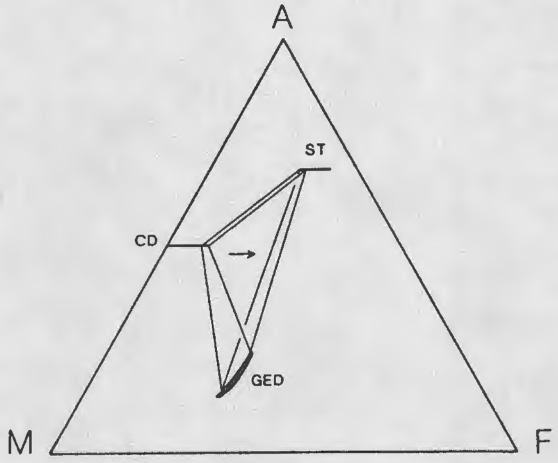

Figure H-36. Projection from plagioclase, quartz, and H_2O onto the A-F-M plane, depicting the continuous reaction leading to the development of Na- and Al-rich gedrite. ST = staurolite, CD = cordierite, and GED = gedrite. The arrow represents the direction the reaction is proceeding with increasing temperature.

Compositions of the Na- Al-rich gedrites from this locality are compared with zoned, Na-rich gedrites from Labrador (Berg and Wiebe, 1978; J.H. Berg, personal communication, 1981; and Berg, 1985) on a plot of A-site occupancy versus tetrahedral Al (Figure H-35). The most Al- and Na-rich orthoamphibole analyses from this locality approach a tetrahedral Al content of 3 and an A-site occupancy of 1. This suggests an ideal end-member composition of $NaMg_5Al_2Si_5Al_3O_{22}(OH)_2$, which falls well outside compositions found in the existing I.M.A. amphibole nomenclature scheme (Leake, 1978).

The complex zoning of the gedrites may result from both prograde and retrograde phases of the cordierite-forming reaction: Al-poor gedrite + staurolite = Al-richer gedrite + cordierite (Figure H-36). Evidence of the prograde increase in Na and Al of the orthoamphibole is preserved in the gedrite porphyroblasts which show a significant increase in Na and Al at their edges, while maintaining relatively constant values in their interiors. The retrograde (cordierite consuming) phase of the reaction history is suggested by the later, and coeval growth of the small staurolite grains (staurolite porphyroblasts were present earlier) and the zoned gedrite grains. One of the analyzed zoned gedrites (GED 2) contains a relict cordierite inclusion. In smaller gedrite grains prograde followed by retrograde phases of the above reaction could have led to the observed extreme Al and Na zoning.

After returning to vans, turn around and head north on Sczygiel Road.

17.2	Turn right at junction and pass small outcrop of Upper Member of Ammonoosuc Volcanics.
17.3	Turn left (north).
18.6	Junction with Route 9. Turn right (east).
18.7	Beaver pond on left, with two lodges.
19.3	Cross Monson Turnpike and trace of Prescott syncline containing schists in the Sillimanite-Muscovite-Staurolite Zone (II).
21.1	Road cut on left (north) at crest of Brimstone Hill. Park on right and cross carefully to other side. Throughout this Stop stay within paved ditch and out of traffic lane.

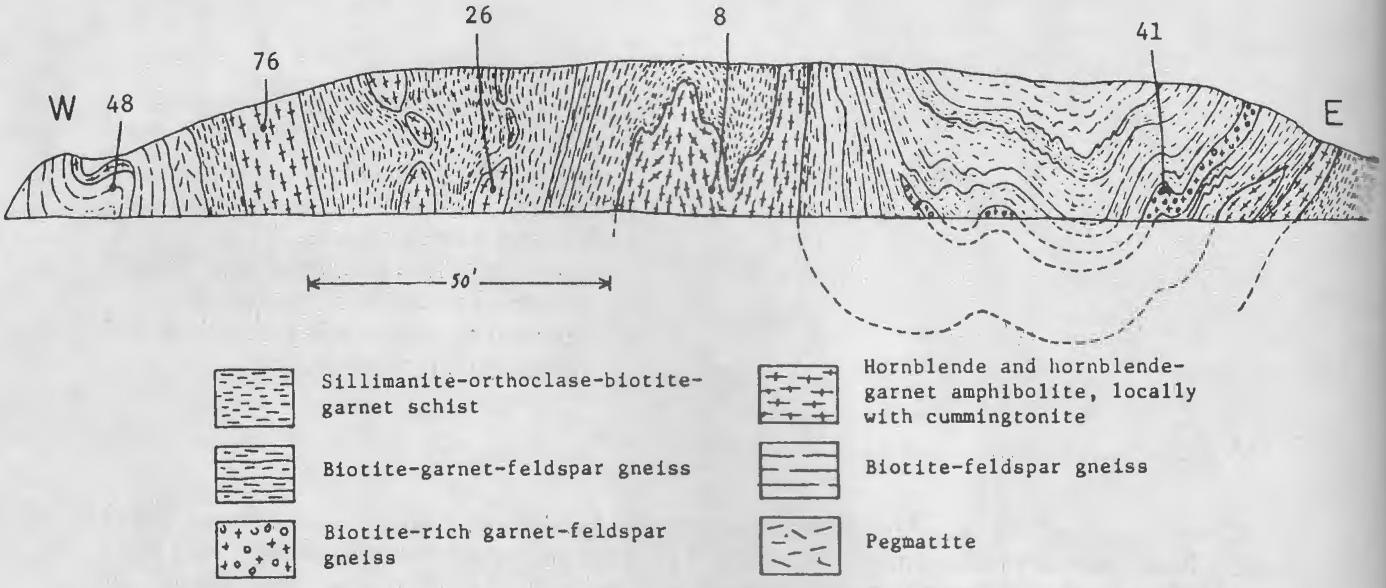
26
8
41
76
W
48
E
50'
Sillimanite-orthoclase-biotite-garnet schist
Biotite-garnet-feldspar gneiss
Biotite-rich garnet-feldspar gneiss
Hornblende and hornblende-garnet amphibolite, locally with cummingtonite
Biotite-feldspar gneiss
Pegmatite

Figure H-37. Schematic sketch of the outcrop at Stop 2, Brimstone Hill. Lithologic units and sample locations are shown (after Robinson et al., 1982c). Modes and bulk chemical analyses of samples 8, 26, 41, and 48 are given in Table H-4, as is the mode of Sample 76. Electron probe analyses of minerals in sample 76 are given in Table H-3.

STOP 2. BRIMSTONE HILL
(samples 507B, 8, 26, 41, 48, and 76 [~655 °C]) (30 minutes)

This outcrop lies in the Greenwich syncline, an infold of Ordovician cover rocks that is surrounded by the main body of Monson Gneiss. The northern part of the syncline has a thin (less than 20 m) section of Ammonoosuc Volcanics resting directly on the Monson Gneiss, and the rest of the Greenwich syncline is occupied by the Partridge Formation. The Partridge Formation in the Greenwich syncline is largely composed of rusty-weathering schists and amphibolite, with lesser quantities of metamorphosed felsic and intermediate volcanics, calc-silicate rocks, and coticule (fine-grained garnet quartzite). Most of these rock types are exposed at Stop 2, including pegmatites of various types (Figure H-37).

Proceed to east end of road cut (beyond edge of Figure H-37) where best mica schist is exposed. The assemblage here, typical of Zone V, is quartz - orthoclase - garnet - biotite - sillimanite - graphite - ilmenite - pyrrhotite (sample 507B, Tracy et al., 1976; Tracy, 1978). The rock has a mylonitic aspect and most of the orthoclase is concentrated in water-clear megacrysts with crushed borders set in a finer lineated matrix crammed with fine-grained prismatic sillimanite. The garnet has only a modest amount of retrograde zoning with compositions of core and rim ( ) as follows: Almandine 76.5 (78.1), Pyrope 16.2 (14.5), Spessartine 3.7 (3.8),

Grossular 3.6 (3.7). Biotite has X_{Mg} of 0.460, and 0.211 Ti per 11 oxygens. The orthoclase has the composition: Or 85.7, Ab 13.5, An 0, Cn 0.8, whereas the plagioclase is An 27.9, Ab 70.5, Or 1.6. The orthoclase lattice parameters indicate an intermediate orthoclase structural state. The ilmenite is about 96% $FeTiO_3$, 3% Fe_2O_3, and 1% $MnTiO_3$. The rock is extremely rich in biotite and poor in garnet, and yields an estimated prograde garnet-biotite temperature of 660 °C and a retrograde temperature of 620 °C.

Several of the amphibolite bodies at Stop 2 are associated with coarse-grained tonalitic veins and pods, bearing the commonly coarse mafic minerals cummingtonite, biotite, hornblende ±

garnet. These segregations are considered to be crystallized partial melts derived from the amphibolite.

Samples 8 and 26 are both cummingtonite- and quartz-bearing hornblende amphibolites (sample locations in Figure H-37, modes and analyses in Table H-4). Sample 8 has no leucocratic veins or pods, and has apparently not undergone partial melting. Sample 26 has an assemblage similar to sample 8, but is more Si-rich, has a lower $Mg/(Mg+Fe^{2+})$ ratio and more sodic plagioclase, and contains cummingtonite- and garnet-bearing melt veins. Sample 76, from a rock almost identical to Sample 26, includes part of a melt segregation. Electron-probe analyses of minerals in this sample are given in Table H-3. Melting probably took place because of H_2O released by the dehydration reaction:

$$35\ \text{Cum} + 5\ \text{Bio} + 67\ \text{Plag}\ (\text{An}_{83}) + 2\ \text{Ilm} = 31\ \text{Hbl} + 42\ \text{Gar} + 99\ \text{Qtz} + 10\ H_2O,$$

(2, Figure H-22D) which reduces to the melting reaction:

$$\text{Cum} + \text{Bio} + \text{Plag} + \text{Ilm} = \text{Hbl} + \text{Gar} + \text{Liquid}.$$

The melt zones in the mafic rocks at this outcrop are very inhomogeneous, making it difficult to determine their mode and chemical composition. It is unclear what quantity of the mafic minerals were actually dissolved in the liquid, and what quantity grew to large size because the liquid inhibited nucleation and enhanced diffusion.

Sample 41 is from an unusual garnet- and orthoclase-bearing biotite gneiss of intermediate composition that contains monazite as its principal radioactive mineral. Monazite is not known from elsewhere in the Partridge Volcanics. Sample 48 is a garnet-bearing felsic gneiss (metamorphosed dacite) from the extreme west end of the outcrop. This gneiss is associated with abundant garnet-bearing pegmatite. See Table H-4 for modes and bulk chemical analyses of these rocks.

Carefully cross Route 9 to vans and continue east on Route 9.

22.3 Small road outcrops on left where Route 9 runs uphill toward the east. Turn out and park on abandoned pavement on south side of highway. Cross carefully to outcrops on opposite side.

STOP 3. AMPHIBOLITE IN THE MONSON GNEISS
(samples 18, 55, and 75 [670 °C])

This outcrop occurs entirely within a large, elongate amphibolite body that extends for several kilometers along the east side of the main body of Monson Gneiss. The amphibolite lies entirely within Monson Gneiss, and probably represents metamorphosed volcanic or shallow intrusive rocks of basaltic composition.

The principal rock type at this outcrop is a dark gray amphibolite composed largely of hornblende and plagioclase, with minor quantities of quartz and orthopyroxene. The orthopyroxene is partly retrograded to polysynthetically twinned cummingtonite. The orthopyroxene was produced by the completion of the cummingtonite dehydration reaction:

$$12\ \text{Cum} + 1\ \text{Anorthite} = 2\ \text{Hbl} + 36\ \text{OPX} + 11\ \text{Qtz} + 10\ H_2O$$

(4, Figure H-22 F to O). This amphibolite has undergone small degrees of partial melting to produce anastomosing veins and small dikes of orthopyroxene- and biotite-bearing tonalitic rock (sample locations in Figure H-38, modes and bulk analyses of sample 55 and host amphibolite 18

Table H-3. Electron probe analyses of minerals from samples 75, 76, 87, 88, and 89 (from Hollocher, 1985). Structural formulae were calculated from the oxide analyses as follows: feldspars to 8 oxygens; biotite to 11 oxygens; garnet to 12 oxygens; amphiboles to 23 oxygens; pyroxenes to 6 oxygens and 4 cations; ilmenite to 3 oxygens and 2 cations; and magnetite to 4 oxygens and 3 cations. Ferric iron corrections for biotite and amphiboles are complex, see Hollocher (1985) for details. The K-feldspar analysis from sample 87 is of an exsolution lamella in plagioclase.

		HORNBLENDE			CUMMINGTONITE	GEDRITE
Sample		2-76	3-75	9-WL-12E	2-76	9-89
A Site	K	.103	.063	.220	.008	.006
	Na	.283	.315	.396	.015	.528
	Sum	.336	.378	.616	.023	.534
M4 Site	Na	.122	.190	.011	.025	.138
	Ca	1.698	1.629	1.886	.190	.122
	Mn	.025	.056	.060	.055	.047
	Fe^{+2}	.155	.125	.043	1.730	1.693
	Sum	2.000	2.000	2.000	2.000	2.000
VI Site	Fe^{+2}	1.811	1.503	1.796	1.422	.495
	Mg	2.204	2.594	2.547	3.434	3.059
	Ti	.130	.148	.267	.010	.107
	Fe^{+3}	.194	.464	–	.051	.270
	Al	.661	.291	.390	.083	1.069
	Sum	5.000	5.000	5.000	5.000	5.000
IV Site	Al	1.232	1.241	1.526	.154	1.950
	Si	6.768	6.759	6.474	7.846	6.050
	Sum	8.000	8.000	8.000	8.000	8.000
	Total	15.336	15.378	15.616	15.023	15.534
$Mg/(Mg+Fe^{+2})$		.528	.614	–	.521	.582
$Mg/(Mg+Fe_{total})$		.505	.553	.581	.517	.554
K/(K+Na)		.202	.110	.350	.166	.008
Ca/(Ca+Na)		.807	.763	.701	.826	.154

BIOTITE					
Sample		2-76	9-87	9-88	9-89
A Site	K	.854	.893	.875	.724
	Na	.030	.009	.016	.060
	Ca	0	.004	0	.001
	Sum	.884	.906	.891	.785
VI Site	Mn	.002	.003	.002	.004
	Fe^{+2}	1.117	.985	.906	.678
	Mg	1.263	1.339	1.418	1.609
	Ti	.192	.275	.238	.175
	Fe^{+3}	.110	.159	.129	.191
	Al	.156	.038	.119	.199
	Sum	2.84	2.799	2.812	2.856
IV Site	Al	1.216	1.251	1.242	1.239
	Si	2.784	2.749	2.758	2.761
	Sum	4.000	4.000	4.000	4.000
	Total	7.724	7.705	7.703	7.641
$Mg/(Mg+Fe^{+2})$		.530	.576	.610	.704
$Mg/(Mg+Fe_{total})$		.507	.539	.578	.649
K/(K+Na)		.966	.990	.982	.923

		ORTHOPYROXENE				CLINOPYROXENE	
Sample		3-75	9-87	9-88	9-89	9-87	9-WL-12E
M2 Site	Na	0	.001	.002	.001	.022	.021
	Ca	.024	.028	.008	.007	.845	.895
	Mn	.040	.016	.012	.012	.008	.016
	Fe^{+2}	.869	.920	.886	.791	.125	.068
	Mg	.068	.035	.092	.189		
	Sum	1.000	1.000	1.000	1.000	1.000	1.000
M1 Site	Fe^{+2}					.232	.276
	Mg	.979	.970	.937	.890	.712	.687
	Ti	.002	.002	.002	.003	.005	0
	Fe^{+3}	.005	.026	.026	.009	.033	.003
	Al	.014	.002	.035	.098	.018	.031
	Sum	1.000	1.000	1.000	1.000	1.000	1.002
IV Site	Al	.022	.030	.063	.111	.039	.021
	Si	1.978	1.970	1.937	1.889	1.961	1.979
	Sum	2.000	2.000	2.000	2.000	2.000	2.000
	Total	4.000	4.000	4.000	4.000	4.000	4.000
$Mg/(Mg+Fe^{+2})$		.546	.522	.537	.577	.666	.666
$Mg/(Mg+Fe_{total})$		.545	.515	.530	.574	.646	.664
$Ca/(Ca+Mn+Mg+Fe^{+2})$		.012	.014	.004	.003	.439	.461
$(Al+Fe^{+3}+Ti+Na)/2$		.021	.030	.064	.111	.058	.038

GARNET			
Sample	2-76	9-88	9-89
Si	3.002	2.973	2.998
Al	1.979	2.013	1.974
Fe+2	1.986	2.029	1.926
Mn	.112	.075	.088
Mg	.499	.789	.647
Ca	.430	.143	.382
Sum	3.027	3.036	3.043
Total	8.008	8.022	8.015
Mg/(Mg+Fe)	.201	.280	.251
Alm	65.6	66.8	63.3
Spess	3.7	2.5	2.9
Pyrope	16.5	26.0	21.3
Gross	14.2	4.7	12.6

ILMENITE			
Sample	2-76	3-75	9-87
$FeTiO_3$	92.9	86.9	92.6
Fe_2O_3	3.3	6.2	4.0
$MnTiO_3$	1.5	4.5	1.2
$MgTiO_3$	2.3	2.4	2.2

PLAGIOCLASE						K-FELDSPAR		
Sample	2-76	3-75	9-87	9-88	9-89	9-WL-12E	9-87	9-88
An	41.2	26.6	43.7	26.2	47.4	37.6	.4	.1
Ab	58.5	72.4	55.5	72.5	52.3	61.4	10.7	9.8
Or	.3	1.0	.9	1.2	.3	1.0	85.0	85.2
Cn				.1			3.9	4.9

MAGNETITE	
Sample	3-75
$MgAl_2O_4$	.2
$FeAl_2O_4$	.7
Fe_2TiO_4	.2
$MnFe_2O_4$	.1
Fe_3O_4	98.8

Table H-4. Modes (left) and bulk chemical analyses (right) for samples from Stop 2, Brimstone Hill.

MODES

Rock Type Sample	Amph. 2-8	Amph. 2-26	Int. 2-41	Felsic 2-48
Quartz	tr	1	20	40
Plagioclase	32	47	58	52
K-feldspar			11	
Biotite	5	1	7	5
Garnet			3	3
Pistacite				tr
Hornblende	60	50		
Cummingtonite	2	1		
Ilmenite	1		tr	
Zircon	tr		tr	tr
Allanite				tr
Apatite	tr	tr	1	tr
Monazite			tr	
Pyrrhotite		tr	tr	tr
An % in Plag.	51	45	24	34
$Mg/(Mg+Fe^{+2})$	.63	.56	.32	.37

Partial Melts. Rock Type Sample	No Melt	Ton. 2-76	No Melt	Peg. –
Quartz		40		30?
Plagioclase		53		50?
K-feldspar				10?
Biotite		2		5?
Hornblende		tr		
Cummingtonite		4		
Garnet		1		5?
Ilmenite		tr		
Zircon		tr		
Apatite		tr		
An % in Plag.		41		?
$Mg/(Mg+Fe^{+2})$		.50		?

tr	Trace, < 1%.
Ton.	Tonalitic partial melt.
Peg.	Coarse-grained pegmatite.
Felsic	Felsic gneiss.
Int.	Intermediate gneiss.
Amph.	Amphibolite.

BULK CHEMICAL ANALYSES

Rock Type Sample	Amph. 2-8	Amph. 2-26	Int. 2-41	Felsic 2-48
SiO_2	48.56	51.11	65.72	76.14
TiO_2	1.42	1.48	.93	.17
Al_2O_3	15.16	16.21	16.14	12.73
Fe_2O_3	1.03	1.27	.33	.14
FeO	10.72	9.21	5.11	2.69
MnO	.18	.18	.12	.09
MgO	10.22	6.70	1.33	.90
CaO	9.01	10.30	2.79	2.75
Na_2O	2.01	2.92	4.20	3.52
K_2O	1.10	.46	2.68	.91
P_2O_5	.18	.20	.31	.04
Total	99.59	100.04	99.66	100.08
$Mg/(Mg+Fe^{+2})$	.630	.565	.317	.374
$Mg/(Mg+Fe_{total})$	.610	.536	.305	.363
Ca/(Ca+Na)	.712	.661	.269	.302
Norms				
Qz			20.78	42.99
Or	6.50	2.72	15.84	5.38
Plag	46.10	54.47	47.36	43.16
Cor			2.00	1.05
Di	11.78	16.47		
Hy	14.66	18.34	10.28	6.08
Ol	15.94	2.93		
Mt	1.49	1.84	.48	.20
Ilm	2.70	2.81	2.22	.41
Ap	.42	.47	.73	.09
An% in Plag	62	53	24	30
Mg/(Mg+Fe)	.665	.615	.385	.393
Trace Elements				
V	312	333	80	0
Cr	278	185	21	2
Ni	148	53	18	6
Zn	84	89	104	129
Ga	18	18	20	19
Rb	42	1.6	87	29
Sr	166	136	130	188
Y	26	27	76	58
Zr	85	83	474	201
Nb	1.7	2.7	9.8	4.3
Ba	707	62	663	243
La	4	9	30	22
Ce	8	21	64	51
Pb	7	7	23	12
Th	1	1	15	6
K/Rb	217	2387	256	261
K/Ba	12	61	34	31
Rb/Sr	.253	.012	.669	.154
Ti/Zr	100	107	12	5.1
Zr/Nb	50	31	48	47
Ce_n/Y_n	.7	1.7	1.9	2.0

Ratios are in moles, except trace element ratios.
Mg/(Mg+Fe) ratios in norms are for normative silicates.
Ce_n/Y_n are chondrite normalized values.

Amph.	Amphibolite.
Int.	Intermediate gneiss.
Felsic	Felsic gneiss.

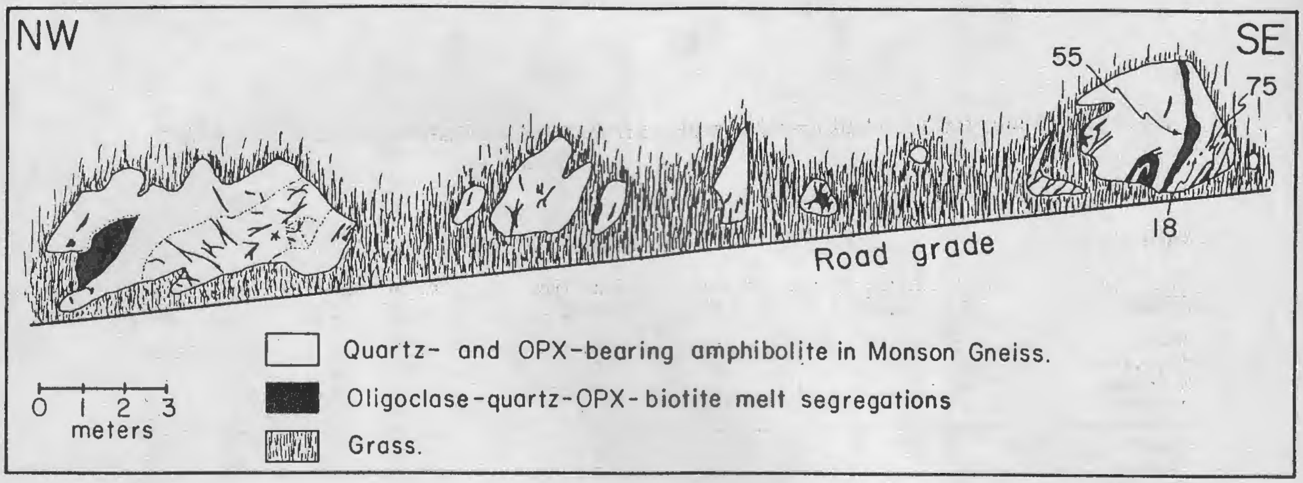
NW
SE
55
75
18
Road grade
0 1 2 3
meters
Quartz- and OPX-bearing amphibolite in Monson Gneiss.
Oligoclase-quartz-OPX-biotite melt segregations
Grass.

Figure H-38. Amphibolite outcrops at Stop 3, in Monson Gneiss. This quartz-bearing amphibolite has orthopyroxene, which was formed by completion of the prograde reaction:

$$\text{Cum} + \text{An} = \text{OPX} + \text{Hbl} + \text{Ab} + \text{Qz} + H_2O.$$

The H_2O released initiated small degrees of partial melting. The partial melts are tonalitic, and occur as small dikes and anastomosing veins. Plagioclase crystals up to 4 cm across and orthopyroxene crystals up to 2.5 cm across rimmed by retrograde cummingtonite, can be found. Modes for samples 18, 55, and 75, and bulk chemical analyses of samples 55 and 75 are given in Table H-5. Electron-probe analyses of minerals in sample 75 are given in Table H-3.

are in Table H-5). The H_2O necessary to initiate melting was probably produced during cummingtonite breakdown, so the dehydration reaction given above reduces to the melting reaction:

$$\text{Cum} + \text{Plag} = \text{Hbl} + \text{OPX} + \text{Liquid}.$$

The veins and dikes have coarse plagioclase crystals that are gray because of ilmenite exsolution rods. The plagioclase crystals are white in places where they have been recrystallized. All orthopyroxene crystals in the tonalitic veins and dikes at this outcrop have thick cummingtonite rims that are the result of the retrograde hydration reaction:

$$\text{OPX} + \text{Qtz} + H_2O = \text{Cum}.$$

Cross Route 9 back to vans and continue east.

23.6 Junction of Routes 9 and 32 in center of Ware. Continue east on Routes 9 and 32.

24.0 Bridge over Ware River.

Table H-5. Modes (left) and bulk chemical analyses (right) of samples from Stop 3, Amphibolite in Monson Gneiss.

MODES

Rock Type	Amph.	Amph.
Sample	3-18	3-75
Quartz	6	15
Plagioclase	40	54
Biotite		tr r
Hornblende	50	25
Cummingtonite	tr r	tr r
Orthopyroxene	tr	3
Ilmenite	1	1
Magnetite	3	2
Zircon	tr	tr
Apatite	tr	tr
Pyrrhotite		tr
Chalcopyrite		tr x
An % in Plag.	27	27
$Mg/(Mg+Fe^{+2})$	.55	.59

Partial Melts.	
Rock Type	Ton.
Sample	55
Quartz	35
Plagioclase	62
Biotite	1
Cummingtonite	1 r
Orthopyroxene	1
Ilmenite	tr
Apatite	tr
An % in Plag.	24
$Mg/(Mg+Fe^{+2})$	.50

tr	Trace, <1%.
x	Exsolution lamellae only.
r	Retrograde product only.
Ton.	Tonalitic partial melt.
Amph.	Amphibolite.

BULK CHEMICAL ANALYSIS

Rock Type	Amph.	Melt
Sample	3-18	3-55
SiO_2	50.03	72.89
TiO_2	1.60	.22
Al_2O_3	14.88	15.07
Fe_2O_3	3.97	.22
FeO	9.78	1.11
MnO	.28	.03
MgO	6.72	.61
CaO	8.19	3.41
Na_2O	3.99	5.24
K_2O	.24	.33
P_2O_5	.15	.03
Total	99.83	99.16
$Mg/(Mg+Fe^{+2})$	.550	.495
$Mg/(Mg+Fe_{total})$	.473	.454
Ca/(Ca+Na)	.531	.264
Norms		
Qz		32.33
Or	1.42	1.95
Plag	55.74	60.96
Cor		
Di	14.48	.08
Hy	10.49	3.03
Ol	8.56	
Mt	5.76	.32
Ilm	3.04	.42
Ap	.35	.07
An% in Plag	38	38
Mg/(Mg+Fe)	.637	.563
Trace Elements		
V	383	17
Cr	90	2
Ni	34	6
Zn	186	24
Ga	19	14
Rb	2.2	4.3
Sr	111	207
Y	33	1.8
Zr	68	21
Nb	2.2	2.2
Ba	57	190
La	7	0
Ce	24	11
Pb	6	9
Th	0	0
K/Rb	906	637
K/Ba	35	14
Rb/Sr	.02	.014
Ti/Zr	141	63
Zr/Nb	31	9.5
Ce_n/Y_n	1.6	14

Ratios are in moles, except for trace elements.

Mg/(Mg+Fe) ratios in norms are for normative silicates.

Ce_n/Y_n are chondrite normalized values.

Amph.	Amphibolite.
Melt	Tonalitic Acadian melt.

25.2 Turn left (north) off of Route 9 and continue on Route 32.

28.3 Turn right (east) on New Braintree Road, just before railroad crossing.

30.2 Park in barnyard on right and walk across hay field on right (south) to prominent natural outcrop.

STOP 4. LITTLETON FORMATION IN THE BIG GARNET SYNCLINE
(25 minutes)

This rock unit has been traced more or less continuously from the Ware Quadrangle at least as far north as Route 2. Its structural setting in an early isoclinal syncline between layers of Francestown Formation (Fitch Formation) is just detectable in Figure H-33. The rock type has been dubbed "pastureite" by Alan Thompson in honor of this beautiful glacially-smoothed outcrop. **No hammers please!**

Aside from a few layers of calc-silicate granulite, the rock in this outcrop can be described in two parts: a medium-grained schist (or gneiss) consisting of quartz, orthoclase, plagioclase, garnet, cordierite, biotite, and ilmenite and a network of slightly deformed cross-cutting felsic veins consisting of quartz, orthoclase, plagioclase, and cordierite with striking 2 to 4 cm euhedral garnets. All the garnet is remarkably uniform in composition except where in direct contact with biotite or cordierite, and has the following compositions for core and rim ( ): Almandine 69.6 (70.9), Pyrope 24.2 (22.8), Spessartine 2.8 (7.9), and Grossular 3.4 (3.4). The biotite has X_{Mg} of .566 (compare with Stop 2) and Ti/11 oxygens of .236. The cordierite has X_{Mg} of .710. Using the calibrations of Thompson (1976b) garnet-biotite and garnet-cordierite pairs both yield estimated temperatures of 685 °C. Using the pressure calibration for coexisting quartz-sillimanite-garnet-cordierite of Tracy et al. (1976), this assemblage yields an estimated pressure of 6.2 kbar. In addition, a sample from this outcrop contains coarse sillimanite that appears to be pseudomorphous after andalusite.

An obvious explanation suggested by several visitors for the cross-cutting feldspathic rims as well as for the two sizes of garnets is that the veins were formed by segregation of melt and that the large garnets grew in contact with melt. M.J. Holdaway has suggested that aqueous fluid may have been largely carried away during earlier stages of melting, perhaps at the breakdown of muscovite, and that the present texture is due to fluid absent melting permitted by breakdown of biotite in the six phase assemblage quartz - sillimanite - K-feldspar - garnet - cordierite - biotite. Figure H-39 shows Holdaway's calculated model where "six phase curves" for different fictive XH_2O values in fluid intersect granite melt curves for different XH_2O to produce a fluid-absent melt-curve. Dashed lines are isopleths of X_{Fe} of cordierite in the six phase assemblage. Taking the cordierite at X_{Fe} of 0.29 from this outcrop and assuming the outcrop lay on the fluid-absent melt curve, the rock yields an estimated temperature of 705 °C and a pressure of 5.2 kbar. The diagram also shows that if the rock were exactly at an intersection of all three curves so that fluid could be present, it could have an XH_2O no greater than 0.38.

Return to vans and proceed east on Gilbertville Road toward New Braintree.

32.3 Stop sign at T junction. Turn right (south) on West Brookfield Road. Directly east of junction are outcrops of the New Braintree ultramafic body (see Robinson et al., 1982c, p. P3-43).

32.9 Bear left at Y junction.

33.2 Town line. Cross from West Brookfield into North Brookfield.

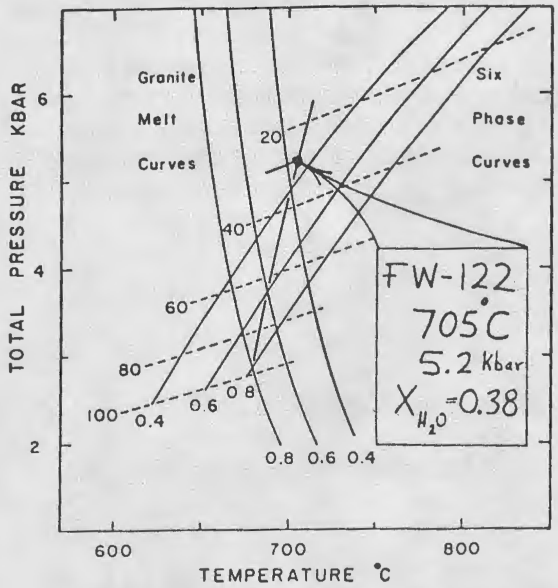

Figure H-39. P-T diagram from Holdaway and Lee (1977) showing intersections of six-phase curves (quartz-orthoclase-sillimanite-garnet-biotite-cordierite) and granite melt curves to produce a fluid-absent melt curve. Dashed lines are X_{Fe} of cordierite. Suggested conditions of fluid-absent melting at Stop 4 are indicated. XH_2O in the fluid phase would be 0.38 only in the special case at the intersection of the three sets of curves.

33.5 Junction. Bear right toward North Brookfield.

33.7 Junction. Bear right (south) on Barrett Road which becomes Wigwam Road upon crossing town line from North Brookfield back into West Brookfield.

36.9 Stop sign. Junction of Wigwam Road with Route 67. Sharp left turn (northeast) on Route 67.

37.3 Turn left (north) into barnyard and park vans. Walk north on farm road along southeast side of long outcrop.

STOP 5. WHITE SCHIST MEMBER OF THE PAXTON FORMATION
(45 minutes)

The outcrop has an irregular smoothed surface covered by a thick crust of iron oxides and sulfates. The outcrop surface is covered by 3-5 cm pits inside of which fresh pyrite is usually visible. In spite of extensive search we have found only traces of pyrrhotite in this outcrop, but are still inclined to believe much of its character is due to weathering of pyrrhotite. Partly weathered rock just beneath this crust looks white because of the abundance of the colorless silicates. Much fresher rock has a bluish look.

The outcrop consists of two main rock types, sillimanite- and biotite-bearing quartzites, and aluminous schists with variable proportions of sillimanite, biotite, and cordierite. The biotites vary from very pale reddish brown iron-bearing ones to colorless Mg-end members. Our first impression was that these were muscovites in a very retrograded fault zone, but their nearly uniaxial interference figures showed they are biotites. The assemblage in two analysed samples is quartz - orthoclase - plagioclase - biotite - cordierite - sillimanite - graphite - rutile - pyrite - (pyrrhotite?). The X_{Mg} of biotite in the samples is .995 and .999 (0.04 weight % FeO) and they contain .065 and .074 Ti/11 Oxygens (see Figure 22). The cordierites which are charged with graphite appear as black to bluish lumps. They are essentially pure Mg end members with 0.0 weight % FeO and only a trace (.08%) of MnO. Even where charged with detrital zircons these cordierites lack pleochroic haloes, presumably because of lack of iron to be oxidized by alpha bombardment. This cordierite also contains approximately 2 weight % H_2S, due to unusually high sulfur fugacity in the pyrite + pyrrhotite assemblage. The K-feldspar has a composition Or 91.5, Ab 8.4, An 0.1 and plagioclase is An 32.7, Ab 57.6, Or 0.8. The rutile is closer to pure TiO_2 than from most localities because there is no FeO. Because of the extreme narrowness (to put it mildly) of the sillimanite-biotite-cordierite "field" this rock essentially lies on the univariant reaction Mg-Biotite + Sillimanite = Mg-Cordierite + K feldspar, and can only be considered divariant because of the Na content of the K feldspar. The name "White Schist" came partly from the appearance of the broken outcrop and partly by analogy with the Mg-rich kyanite-talc rocks studied by Schreyer (1974) in Tanzania and Afghanistan.

Return to vans. From barnyard turn right (west) on Route 67.

37.7 Drive past end of Wigwam Road.

38.2 Junction of Routes 9 and 67 in West Brookfield. Continue west on Route 67.

38.3 West Brookfield Town Hall and David E. Maczuga Memorial Phone Booth on right.

39.2 Turn left (southwest) on Route 67.

40.5 Rusty roadcut on left. Park on right and cross highway with care. During the stop stay off the pavement except while crossing.

STOP 6. PYRRHOTITE-GARNET-BEARING SCHIST IN THE PLEASANT BROOK ANTICLINE
(15 minutes approximately)

This is typical fine- to medium-grained Zone VI schist with the assemblage quartz - orthoclase - plagioclase - biotite - garnet - cordierite - sillimanite - graphite - ilmenite - pyrrhotite (sample FW-407). Although coated with a thin oxide crust, excellent fresh material can be collected here. The zoned Type C garnet in Figure H-11C was collected at this locality. The most magnesian garnet cores and most retrograded rims adjacent to biotite ( ) have the following compositions: Almandine 69.7 (77.7), Pyrope 24.7 (16.0), Spessartine 2.2 (3.0), and Grossular 3.4 (3.3). Note the delicate purplish tint of these pyrope-rich garnets. Matrix biotite has X_{Mg} of .572 and Ti/11 oxygens of .245 and biotite at garnet contacts goes to X_{Mg} .600. The cordierite has X_{Mg} of .714. Compositions of garnet core and matrix biotite, and of garnet core and cordierite both yield temperature estimates of 680 °C and the assemblage quartz-sillimanite-garnet-cordierite gives an estimated pressure of 6.3 kbar. Retrograde garnet and biotite rims indicate a retrograde temperature of 530 °C.

Continue southwest on Route 67.

40.8 Turn left off Route 67 at General Henry Knox Monument. In the winter of 1775-1776 a group from the Continental Army passed this way dragging 59 heavy guns and mortars from Fort Ticonderoga on Lake Champlain captured on May 10, 1775 by Ethan Allen and his "Green Mountain Boys". The cannon were mounted March 4, 1776 on Dorchester Heights under the direction of General George Washington and caused the rapid evacuation of the British, under General Howe, from Boston on March 17. The cannon were then hauled back to Fort Ticonderoga in time to be recaptured by the British on July 6, 1777, during the early stages of Burgoyne's ultimately fatal southward drive from Canada, ending at the Battle of Saratoga and a British surrender on October 17, 1777. General Knox later became the first U.S. Secretary of War under President Washington.

41.4 Stop sign. Tree in middle of road. Go straight.

41.7 Dangerous intersection. Bear left toward Breezelands.

44.4 Turn right on steepest downslope into track leading to abandoned paved road and edge of apple orchard where permission has been given for us to rest for lunch. Following lunch return to main road and ride or walk a short distance to rusty exposures.

STOP 7. SULFIDIC SCHIST AND MYLONITE IN THE WICKABOAG POND ANTICLINE
(40 minutes including lunch)

This is locality WN-1 where J.S. Pomeroy discovered the mylonite that we have studied in detail and which is extensively discussed in the text. This is also the northernmost garnet-cordierite locality studied by Paul Hess (1971). The mylonite is less than 1 cm thick and is exposed on a very rotten part of the outcrop that could be damaged by hammering. In that vicinity it is possible to see the internal E-W lineation in the mylonite caused by elongate quartz rods and to see a parallel sillimanite lineation in the country rocks. The later NE-trending sillimanite lineation may also be seen. The folding of the mylonite foliation cannot be seen in the outcrop, but appears in thin section as a west-over-east overfold (Figure H-27).

Several samples of coarse-grained gneiss from this outcrop with garnet-biotite, sillimanite-garnet-biotite-cordierite and sillimanite-biotite-cordierite assemblages have been partially analyzed (Figure H-28). Garnets range up to 25.7% pyrope content. Biotite coexisting with sillimanite, garnet and cordierite has X_{Mg} of .604 and Ti/11 oxygens of .290. A nearby sample of the same assemblage without garnet contains biotite with XMg of .591 and Ti/11 oxygens of .230. This evidence of slightly crossing tie lines suggests some slight retrograde re-equilibration.

It is the dream of all petrologists to obtain numbers from outcrops. This outcrop yielded an instantaneous and direct determination on a field trip in spring, 1981, thanks to the sharp eyes of then graduate student Chris Fulton. The number is 8 and is formed by two coalescing hollow globular clusters of graphite plates inside an orthoclase crystal in a cordierite pegmatite. This sample will be shown and advice and assistance sought.

Continue southeast down hill.

45.5 Junction. Bear right, then bear right at second junction.

45.9 Warren/Brimfield Town Line.

46.6 Underpass beneath Massachusetts Turnpike.

50.1 Stop light in center of Brimfield. Cross Route 20 and proceed south on Route 19 toward Wales. The name Brimfield refers to "brimstone," an archaic name for sulphur, and relates to the abundant sulfates produced by the weathering of pyrrhotite schists in this region.

53.6 Intersection of Route 19 and Monson Road at Wales Post Office. Turn sharp right on Monson Road.

54.3 Monson Road bears left. Go straight on McBride Road.

54.6 Three-way junction. Turn right (north) on Mt. Hitchcock Road.

54.8 Tennesee Gas Pipeline. Site of trench in fall 1985.

STOP 8. WELL BEDDED COARSE GRAY SCHIST OF THE RANGELEY (?) FORMATION NEAR MT. PISGAH

(40 minutes)

This is an opportunity to collect very fresh material fairly similar to the rock in the pasture at Stop 4 though probably richer in sillimanite and cordierite and much more strongly deformed. A typical garnet composition is Almandine 67.2, Pyrope 29.0, Spessartine 1.1, and Grossular 2.7. The biotite has X_{Mg} of .629 and Ti/11 oxygens of .252. We have not yet analyzed the cordierite. The garnet and biotite yield an estimated temperature of 665 °C and the garnet composition in the quartz - sillimanite - garnet - cordierite assemblage gives an estimated pressure of 6.7 kbar. Sillimanite pseudomorphs after andalusite have been recovered from this locality.

Turn around and return south on Mt. Hitchcock Road.

55.0 Turn left on McBride Road.

55.4 Bear left (east) on Monson Road.

56.1 Wales Post Office. Turm left (north) on Route 19.

57.3 Bear right (east) on Holland Road at intersection that is difficult to see.

58.0 Wales/Holland Town Line. Road deteriorates because those in Holland rarely travel to Wales.

58.9 T junction. Turn right on Brimfield Road in Holland.

59.3 Road cut on right is too dangerous to stop at with field trip group, but contains features of regional interest.

The outcrop is predominantly coarse-grained gneiss with the assemblage quartz - orthoclase - plagioclase - biotite - garnet - cordierite - sillimanite - graphite - ilmenite - pyrrhotite with variable amounts of sillimanite. There are several interesting mylonites in the outcrop, but they are not so fine-grained as the one at Stop 7 and are full of porphyroclasts rather than porphyroblasts of new minerals. Probe analyses of garnet yielded compositions of core and rim adjacent to biotite ( ) as follows: Almandine 65.2 (73.7), Pyrope 29.5 (21.2), Spessartine 1.4 (1.6), and Grossular 3.9 (3.4). Matrix biotite has X_{Mg} of .584 and Ti/11 oxygens of .275, whereas biotite against garnet has XMg as high as .604. Garnet core and matrix biotite yield a temperature estimate of 745 °C, the highest reliable estimate we have obtained in the region, whereas garnet rim and biotite rim yield 580 °C. Composition of core garnet in the quartz-sillimanite-garnet-cordierite assemblage suggests a pressure of 6.4 kbar.

61.0 Crossroads at Holland with windmill ! Go straight.

61.7 Causeway across Hamilton Reservoir. A sample of cordierite pegmatite for paper by Tracy and Dietsch (1982) was collected from rubble in the causeway by Robinson and Klepacki in 1979.

63.1 New road cut on left at Connecticut State Line Monument. Well layered hornblende-clinopyroxrene-plagioclase gneiss with cross cutting quartz-plagioclase-clinopyroxene pegmatite dikes.

63.3 Beginning of interchange at Mashapaug Road beyond truck depot. Park on grass strip to right and cross north to south end of large outcrop.

Table H-6. Modes (left) and bulk chemical analyses (right) of samples from Stop 9, Mashapaug Rd.

MODES

Rock Type	Gran.	Gran.	Gran.
Sample	9-35	9-88	9-89
Quartz	2	20	
Plagioclase	67	61	55
K-feldspar	tr x	1	
Biotite	5	7	15
Garnet		5	2
Sillimanite			tr e
Hornblende	tr r		
Cummingtonite	tr r	tr r	tr r
Orthoamphibole			2
Clinopyroxene	15		
Orthopyroxene	10	5	25
Ilmenite	1	tr r	tr
Zircon	tr		tr
Apatite	tr	1	tr
Pyrrhotite	tr	tr	tr
Chalcopyrite		tr x	tr x
An % in Plag.	44	26	47
$Mg/(Mg+Fe^{+2})$	.55	.54	.62

Partial Melts.

Rock Type	Ton.	Ton.	No
Sample	87	88	Melt
Quartz	35	35	
Plagioclase	56	56	
K-feldspar	x	4	
Biotite	3	3	
Clinopyroxene	tr		
Orthopyroxene	6	2	
Ilmenite	tr		
Zircon		tr	
Apatite	tr	tr	
Pyrrhotite		tr	
An % in Plag.	44	26	
$Mg/(Mg+Fe^{+2})$	.52	.54	

tr	Trace,<1%.
x	Exsolution lamellae only.
e	Only in enclaves within garnet.
r	Retrograde product only.
Ton.	Tonalitic partial melts.
Gran.	Pyroxene granulite.

BULK CHEMICAL ANALYSIS

Rock Type	Gran.
Sample	9-35
SiO_2	54.34
TiO_2	1.00
Al_2O_3	17.04
Fe_2O_3	.41
FeO	8.52
MnO	.13
MgO	5.90
CaO	8.22
Na_2O	3.18
K_2O	1.13
P_2O_5	.23
Total	100.10
$Mg/(Mg+Fe^{+2})$	.552
$Mg/(Mg+Fe_{total})$	.542
Ca/(Ca+Na)	.588
Norms	
Qz	2.08
Or	6.68
Plag	55.79
Cor	
Di	8.57
Hy	23.47
Ol	
Mt	.59
Ilm	2.39
Ap	.54
An% in Plag	50
Mg/(Mg+Fe)	.598
Trace Elements	
V	283
Cr	55
Ni	25
Zn	79
Ga	21
Rb	45
Sr	325
Y	29
Zr	79
Nb	4.7
Ba	798
La	10
Ce	17
Pb	10
Th	0
K/Rb	208
K/Ba	11
Rb/Sr	.138
Ti/Zr	76
Zr/Nb	17
Ce_n/Y_n	1.3

Ratios are in moles.
Mg/(Mg+Fe) ratio in norm is for normative silicates.
Ce_n/Y_n is chondrite normalized value.
Gran. Two pyroxene granulite.

STOP 9. MASHAPAUG RD.

(50 minutes) (samples 35, 87, 88, and 89 [~715 °C])

This outcrop is located in Zone VI in the granulite facies. The principal rocks on the south-west-facing part of the outcrop (Figure H-40) are pyroxene granulites, containing no prograde amphibole. The most abundant rock is a two-pyroxene granulite (samples 35 and 87, Table H-6) that has the proper bulk composition to have been a quartz-bearing amphibolite at lower metamorphic grade. Hornblende has completely broken down in this unit by the completion of the dehydration reaction:

$$13\ \mathrm{Hbl} + 9\ \mathrm{Qtz} = 17\ \mathrm{CPX} + 12\ \mathrm{OPX} + 12\ \mathrm{Plag}\ (\mathrm{An}_{58}) + 2\ \mathrm{Ilm} + 3\ \mathrm{Bio} + 10\ \mathrm{H_2O}$$

(7, Figures H-22 J to Q) Hornblende of prograde origin still exists at this grade in quartz-bearing rocks that are more magnesian (sample 35, $X_{Mg} = 0.55$), and in mafic rocks that are quartz-free.

The two-pyroxene granulite unit has undergone partial melting, with crystallized melts forming a 3-dimensional network of anastomosing tonalitic veins containing coarse-grained pyroxenes, quartz, and plagioclase. The veins are visible on the fresh face of the roadcut and on the weathered surface at the top of the outcrop. Melting probably took place as a result of H_2O released during hornblende breakdown, so the hornblende dehydration reaction given above reduces to:

$$\mathrm{Hbl} + \mathrm{Qtz} = \mathrm{CPX} + \mathrm{OPX} + \mathrm{liquid}.$$

The unit from which sample 88 comes (Figure H-40) contains the orthopyroxene - K-feldspar granulite facies assemblage. The reaction that resulted in this assemblage at this bulk composition was:

$$10\ \mathrm{Bio} + 1\ \mathrm{Plag}\ (\mathrm{An}_{30}) + 20\ \mathrm{Qtz} = 10\ \mathrm{Ksp} + 7\ \mathrm{OPX} + 2\ \mathrm{Gar} + 25\ \mathrm{Ilm} + 10\ \mathrm{H_2O},$$

which is shown in Figure H-24C. The orthoclase in sample 88 has about 10% albite component, virtually no anorthite component, but has a remarkably high 4.9% celsian component. This rock contains abundant segregations of coarse-grained orthopyroxene - and K-feldspar-bearing tonalitic rock that probably represents partial melts that developed during biotite breakdown. The biotite dehydration reaction given above therefore reduces to:

$$\mathrm{Bio} + \mathrm{Qtz} = \mathrm{Ksp} + \mathrm{OPX} + \mathrm{Gar} + \mathrm{Ilm} + \mathrm{Liquid}.$$

Samples from the two-pyroxene and garnet-orthopyroxene units (samples 87 and 88) both have red-brown biotite-quartz symplectites indicative of the high temperature $\mathrm{OPX} + \mathrm{Ksp} + \mathrm{H_2O} = \mathrm{Bio} + \mathrm{Qtz}$ retrograde reaction discussed above (see Figure H-26).

Walk around the southeast corner of the outcrop and proceed 425 m (1400') east-northeast along the exit ramp. A wide variety of rock types are exposed in the roadcut along the exit ramp, including rusty-weathering pelitic schists, felsic gneisses, mafic rocks that are mostly pyroxene granulites, and calc-silicate rocks. Pegmatite is very abundant, occurring as small *in situ* veins, and as small dikes and large bodies up to several meters across.

The outcrop in question is located near the extreme eastern end of the roadcut, below a large, glacially polished surface on which the interlayering of pyroxene granulite and calc-silicate rock is easily seen. Calc-silicate rocks containing green diopside are easily distinguished from layers of dark-gray, medium-grained garnet-bearing orthopyroxene granulite. One calc-silicate sample from this outcrop contains the assemblage biotite - hornblende - clinopyroxene - plagioclase - sphene (sample WL-12E). Electron probe analyses of minerals in this sample are given in Table H-3, and

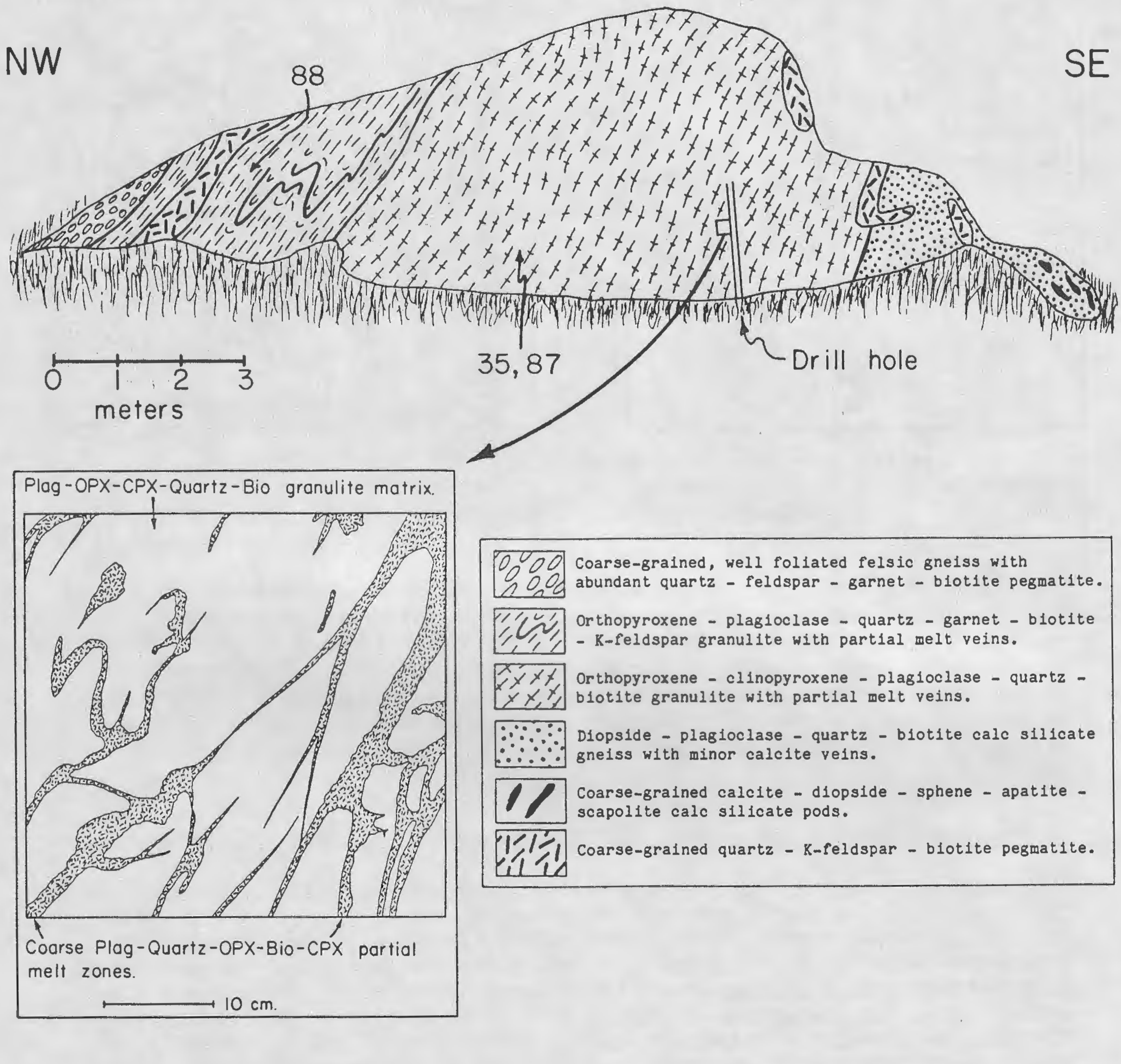
NW
SE
88
35, 87
Drill hole
0 1 2 3
meters
Plag-OPX-CPX-Quartz-Bio granulite matrix.
Coarse Plag-Quartz-OPX-Bio-CPX partial melt zones.
10 cm.
Coarse-grained, well foliated felsic gneiss with abundant quartz - feldspar - garnet - biotite pegmatite.
Orthopyroxene - plagioclase - quartz - garnet - biotite - K-feldspar granulite with partial melt veins.
Orthopyroxene - clinopyroxene - plagioclase - quartz - biotite granulite with partial melt veins.
Diopside - plagioclase - quartz - biotite calc silicate gneiss with minor calcite veins.
Coarse-grained calcite - diopside - sphene - apatite - scapolite calc silicate pods.
Coarse-grained quartz - K-feldspar - biotite pegmatite.

Figure H-40. Schematic sketch of the southwest-facing outcrop at Stop 9, Mashapaug Rd., showing main lithologic units and sample locations. The inset is an enlarged schematic sketch of the anastomosing partial melt vein network in the two pyroxene granulite unit. Modes of samples 35, 87, and 88, and a bulk chemical analysis of sample 35 are given in Table H-6. Electron probe analyses of minerals in samples 87 and 88 are given in Table H-3.

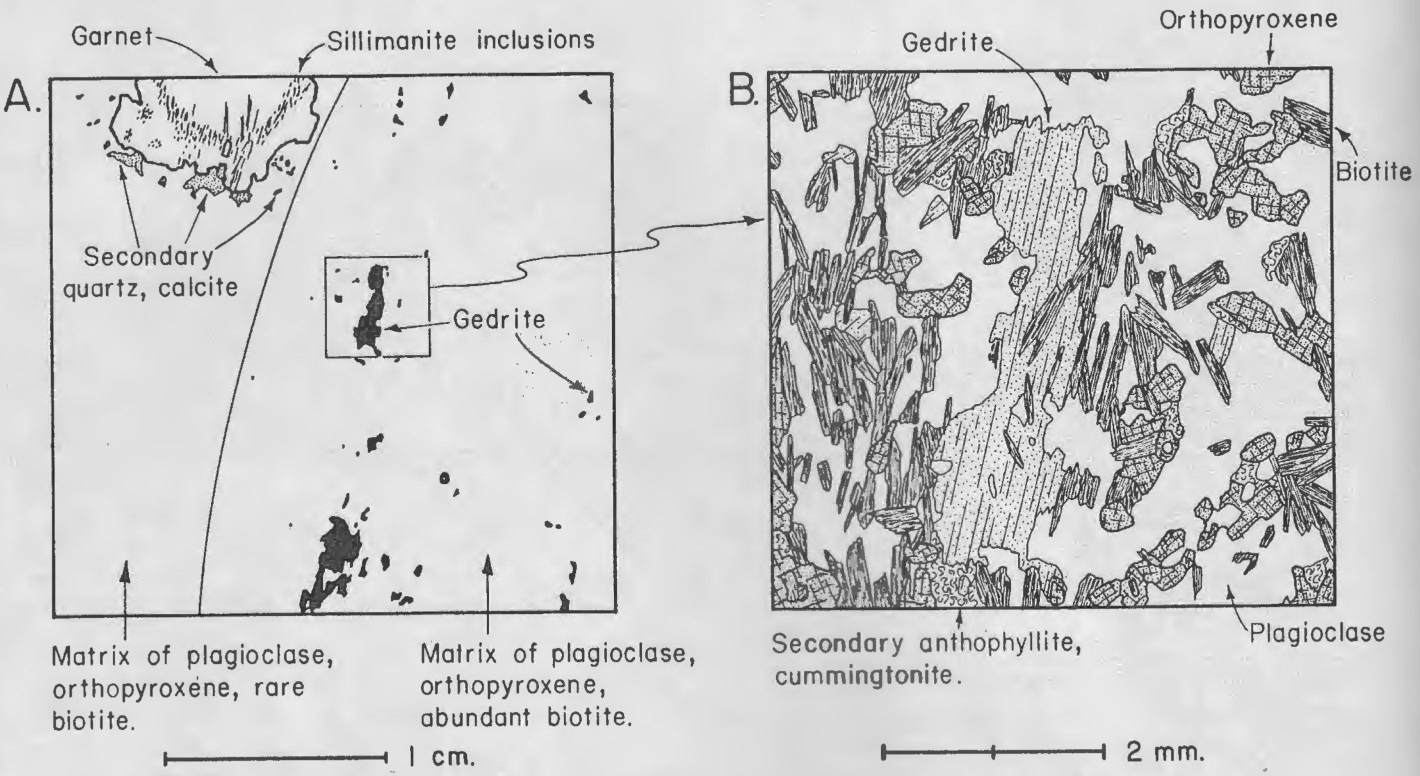
A.
Garnet
Sillimanite inclusions
Secondary quartz, calcite
Gedrite
Matrix of plagioclase, orthopyroxene, rare biotite.
Matrix of plagioclase, orthopyroxene, abundant biotite.
1 cm.
B.
Gedrite
Orthopyroxene
Biotite
Plagioclase
Secondary anthophyllite, cummingtonite.
2 mm.

Figure H-41. Sketches of gedrite in thin section from sample 89 (Stop 9, Mashapaug Rd.). A) Small scale sketch from thin section showing garnet, gedrite, and the two types of matrix materials. Quartz and calcite are associated with late (Mesozoic ?) fractures. B) Large scale sketch of gedrite in the same thin section. The ragged appearance of the gedrite, and the occurrence of isolated, irregular pieces of gedrite scattered throughout the section suggests that the gedrite was in the process of breaking down during prograde metamorphism. A mode of sample 89 is given in Table H-6, and electron probe analyses of minerals in this sample are given in Table H-3.

a mode and bulk chemical analysis is given in Table H-6 (analyses by Renate Schumacher).

Ti-rich gedrite has been found in this outcrop in the quartz-free gedrite - orthopyroxene - plagioclase - biotite - ilmenite - garnet assemblage (see Figure H-41). The gedrite is brown in thin section (black in hand sample), and has ilmenite exsolution lamellae. The dark color of gedrite makes it difficult to distinguish from biotite and orthopyroxene on the outcrop. The one garnet in the gedrite-bearing thin section has abundant inclusions of sillimanite. The gedrite (Figure H-41B) is rather ragged in appearance and was probably being consumed during prograde metamorphism. The gedrite in this outcrop is the most aluminous yet found in Zones V and VI of central Massachusetts. Gedrite breakdown probably occurred by continuous reaction consuming low-Al gedrite and producing higher-Al gedrite and albite component in plagioclase. Using the actual compositions of the gedrite, garnet, and orthopyroxene in the rock (Table H-3), the actual reaction may be calculated as:

$$16\ \mathrm{Ged} + 1\ \mathrm{An} = 27\ \mathrm{OPX} + 3\ \mathrm{Ab} + 5\ \mathrm{Gar} + 1\ \mathrm{Ilm} + 6\ \mathrm{Ged}^{*} + 10\ \mathrm{H_2O},$$

where Ged* is the limit of this substitution while maintaining 16 cations. The stoichiometry of this dehydration reaction shows that as it progresses, the residual gedrite becomes poorer in Si and Fe + Mg (anthophyllite component), and richer in Al, Na, and Ti. For the bulk composition of this rock, the amphibole composition might reach that of Ged* at higher grade. Alternatively, the gedrite - orthopyroxene tie line might be broken by the appearance of olivine before reaching Ged*. At substantially higher grade, biotite breakdown would produce an assemblage of plagioclase - orthopyroxene - olivine - garnet - K-feldspar, possibly including osumilite. Biotite breakdown would probably also involve quartz-absent partial melting, which is not known in central Massachusetts.

Bear right (south) from parking place.

63.4 Stop sign. Turn left (east) on bridge across Interstate 84.

63.6 Turn left (north) on to entrance ramp for Interstate 84 North.

68.9 Bear right on Exit 3 for Route 131.

69.1 Stop sign at end of ramp. Turn left (west) toward Old Sturbridge Village Road, crossing over Interstate 84.

69.2 Junction. Turn right on Old Sturbridge Village Road.

69.4 Wide place in road with outcrop to right at back entrance to Old Sturbridge Village.

STOP 10. FOLDED GRANULITES OF PAXTON FORMATION
(10 minutes)

Gray biotite-garnet granulites, and calc-silicate granulites of the Paxton Formation with abundant pegmatite and tight isoclinal folds.

Proceed through gate and continue on Old Sturbridge Village Road.

70.5 Junction with Route 20 at front entrance of Old Sturbridge Village. Turn right (east) on Route 20.

70.8 Stop lights. Stay straight on Route 20.

71.0 Turn sharp left (north) on New Boston Road (sign for "Hairport").

72.6 Bridge across Massachusetts Turnpike. Park on right beyond bridge. Step over fence on right and climb down under bridge on north side of Turnpike to large road cut behind protective railings. Stay in ditch and away from railings at all times.

STOP 11. COARSE CORDIERITE-GARNET-SILLIMANITE GNEISS AND SILLIMANITE PEGMATITE
(40 minutes)

This rock lies in a very narrow belt of gray-weathering aluminous schist with subordinate calc-silicate that has been assigned to the Rangeley(?) Formation. After descending to road level, walk quickly west to far end of outcrop and then work your way slowly back to bridge. The dominant rock type here is beautifully coarse quartz - orthoclase - plagioclase - biotite - garnet - cordierite - sillimanite - graphite gneiss in which cordierite, garnet, and sillimanite can be exceedingly coarse.

Within the gneiss are two sills of garnet and garnet-sillimanite pegmatite usually showing very strong deformational fabric. A composition map of a garnet from the pegmatite is shown in Figure H-42. This portion of the pegmatite apparently contains no sillimanite and no primary biotite, but does contain retrograde low Ti biotite at contacts between garnet and K-feldspar. Next to the retrograde green biotite, the garnet shows extremely abrupt zoning. Compositions of garnet core

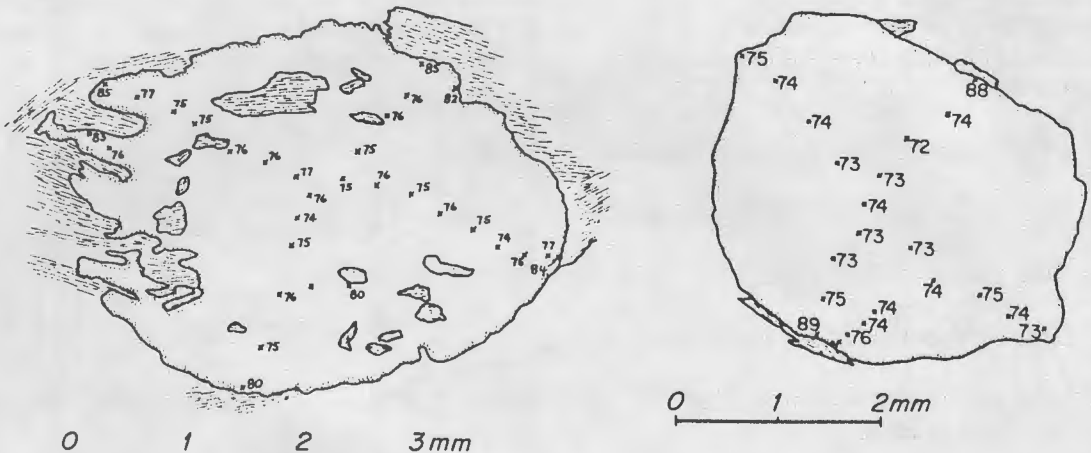

Figure H-42. Maps showing 100 Fe/(Fe + Mg) for garnets from Stop 11. Left: Garnet from mafic selvage on pegmatite consisting of biotite-garnet-sillimanite-cordierite. Surrounding biotite is red-brown Ti-rich variety. Right: Garnet from sillimanite-free portion of pegmatite. All biotite is secondary low-Ti green variety formed by retrograde reaction between garnet and K-feldspar.

and of garnet rim next to green biotite ( ) are as follows: Almandine 70.7 (82.5), Pyrope 26.0 (11.8), Spessartine 2.4 (3.9), and Grossular 0.9 (1.8). The retrograde green biotite has X_{Mg} of .464 and .013 Ti/11 oxygens. When paired with the garnet rim this green biotite gives a temperature estimate of 545 °C. In the pegmatite at the far end there are local patches of graphite and of fairly coarse white mica that appears to be muscovite (!?). Elsewhere the sillimanite-rich portions of the pegmatite may be metamorphosed equivalents of muscovite pegmatite.

Along the contacts of the pegmatites are dark layers up to 0.3 meters thick consisting almost exclusively of biotite, garnet, sillimanite, and cordierite. These appear to be either restite layers left behind during melting of the pegmatite or metamorphosed reaction rims between pegmatite and country rock (Note high specific gravity of specimens). In a few places there are layers of pure cordierite up to 4 cm thick at the contact between these layers and the pegmatite. A composition map of a small garnet in one of these layers is shown in Figure H-42. The garnet is fairly homogeneous except there in contact with surrounding biotite ( ) yielding the following compositions: Almandine 72.0 (82.1), Pyrope 24.9 (14.6), Spessartine 1.2 (2.0), and Grossular 1.9 (1.4). Typical biotite has X_{Mg} of .597 and .230 Ti/11 oxygens. Garnet core and matrix biotite yield an estimated temperature of 635 °C. In the absence of quartz the sillimanite-garnet-cordierite assemblage can be used to estimate a maximum pressure of 6.7 kbar.

End of field trip. Vans turn around and proceed south on New Boston Road.

74.3 Junction with Route 20. Turn left (east) on Route 20.

74.6 Exit left (north) for Massachusetts Turnpike.

75.5 Massachusetts Turnpike toll booth.

75.6 Fork. Bear left for Springfield, Albany, and NORTH AMERICA. Bear right for Boston, AVALON and beyond. AU REVOIR and BON VOYAGE !

I. REFERENCES CITED

Albee, A. L. (1965a) Phase equilibria in three assemblages of kyanite-zone pelitic schists. Lincoln Mountain quadrangle, central Vermont. Journal of Petrology, v. 6, p. 246-301.

Albee, A.L. (1965b) A petrogenetic grid for the Fe-Mg silicates of pelitic schists. American Journal of Science, v. 263, p. 512-536.

Albee, A.L. (1968) Metamorphic zones in northern Vermont. In Zen, E-an, White, W. S., Hadley, J. B., and Thompson, J. B., Jr., eds., Studies of Appalachian geology: northern and maritime, p. 329-341. Interscience Publishers, New York.

Albee, A.L., and Ray, L. (1970) Correction factors for electron probe microanalysis of silicates, oxides, carbonates, phosphates and sulphates. Analytical Chemistry, v. 42, p. 1408-1414.

Aleinikoff, J.N. (1977) Petrochemistry and tectonic origin of the Ammonoosuc Volcanics, New Hampshire-Vermont. Geological Society of America Bulletin, v. 88, p. 1546-1552.

Allen, Timothy (1984) The Fall Mountain outlier: a piece of the Fall Mountain nappe. B.A. thesis, Harvard University, Cambridge, Massachusetts, 54 p.

Allen, Timothy.(1985) A reinterpretation of the Fall Mountain nappe, as seen from Fall Mountain, North Walpole, New Hampshire. Geological Society of America Abstracts with Programs, v. 17, p. 2.

Ando, C.J., Cook, F.A., Oliver, J.E., Brown, L.D., and Kaufman, Sidney (1983) Crustal geometry of the Appalachian orogen from seismic reflection studies. In Hatcher, R.D., Jr., Williams, H., and Zietz, I., eds., Contributions to the tectonics and geophysics of mountain chains, p. 83-102. Geological Society of America Memoir 158, p.83-102.

Andrews, A.J. (1977) Low temperature fluid alteration of oceanic layer II basalts, DSDP, Leg 37. Canadian Journal of Earth Science, v. 14, p. 911-926.

Armstrong, T. R. (1986) Subdivision of granitic rock types in the Ashuelot pluton, southwestern New Hampshire. Geological Society of America Abstracts with Programs, v.18, p. 2.

Ashwal, L.D., Leo, G.W., Robinson, Peter, Zartman, R.E., and Hall, D.J. (1979) The Belchertown Quartz Monzodiorite pluton, west-central Massachusetts, a syntectonic Acadian intrusion. American Journal of Science, v. 279, p. 936-969.

Barker, Fred (1962) Cordierite-garnet gneiss and associated microcline-rich pegmatite at Sturbridge, Massachusetts and Union, Connecticut. American Mineralogist, v. 47, p. 907-918.

Barker, Fred and Arth, J.G. (1984) Preliminary results, Central Gneiss Complex of the Coast Range batholith, southeastern Alaska: the roots of a high-K, calc-alkaline arc ? Physics of the Earth and Planetary Interiors, v. 35, p. 191-198.

Basaltic Volcanism Study Project (1981) Basaltic Volcanism of the Terrestrial Planets. Pergamon Press, New York, 1286 p.

Bence, A.E., and Albee, A.L. (1968) Empirical correction factors for the electron microanalysis of silicates and oxides. Journal of Geology, v. 76, p. 382-403.

Berg, J.H. (1985) Chemical variations in sodium gedrite from Labrador. American Mineralogist, v. 70, p. 1205-1210.

Berg, J.H., and Wiebe, R.A. (1978) A new orthorhombic amphibole end member in a granulite xenolith from Labrador. (abstract) EOS, v. 59, p. 394.

Berry, H. N., IV (1985) The Silurian Smalls Falls Formation in south-central Massachusetts and adjacent Connecticut. Geological Society of America Abstracts with Programs, v.17, p.4.

Billings, M.P. (1937) Regional metamorphism of the Littleton-Moosilauke area, New Hampshire. Bulletin of the Geological Society of America, v. 48, p. 463-566.

Billings, M.P. (1956) The Geology of New Hampshire, Part II: Bedrock Geology. New Hampshire State Planning and Development Commission, Concord, N.H., 203 p.

Bischoff, J.L., and Dickson, F.W. (1975) Seawater - basalt interaction at 200° and 500 bars: implications for the origin of sea-floor heavy-metal deposits and regulation of seawater chemistry. Earth and Planetary Science Letters, v. 25, p. 385-397.

Bøggild, O.B. (1905) Mineralogica Groenlandica. Meddelelser om Grønland, v. 32, 400p.

Bøggild, O.B. (1924) On the labradorization of the feldspars. Mathematisk-fysiske Meddelelser udgivne af Det Kongelige Danske Videnskabernes Selskab, v. VI, no. 3, 79 p.

Boone, G.M., Boudette, E.L., and Moench, R.H. (1970) Bedrock geology of the Rangeley Lakes-Dead River basin region, western Maine. In Boone, G.M., ed., Guidebook for field trips in the Rangeley Lakes-Dead River basin region, western Maine. NEIGC 62nd Annual Meeting, p. 1-24. Syracuse University, Syracuse, N.Y. Boucot, A.J., and Thompson, J.B., Jr. (1963) Metamorphosed Silurian brachiopods from New Hampshire. Geological Society of America Bulletin, v. 74, p. 1313-1334.

Bothner, W.A., and Finney, S.C.(1986, in press) Ordovician graptolites in central Vermont, Richardson revived. Geological Society of America Abstracts with Programs, v. 18.

Bowen, George T. (1824a) Description and analysis of the SILLIMANITE, a new mineral. Journal of the Academy of Natural Sciences of Philadelphia, v. III, part II, p. 375-381.

Bowen, George T. (1824b) Description and analysis of the sillimanite, a new mineral. (republished, with introductory remarks by Benjamin Silliman) American Journal of Science, v. VIII, no. 1, p. 113-118.

Brady, J.B. (1974) Coexisting actinolite and hornblende from west-central New Hampshire. American Mineralogist, v. 59, p. 529-535.

Brady, J.B. (1977) Metasomatic zones in metamorphic rocks. Geochemica et Cosmochemica Acta, v. 41, p. 113-125.

Bryan, W.B., Stice, G.D., and Ewart, Anthony (1972) Geology, petrography, and geochemistry of the volcanic islands of Tonga. Journal of Geophysical Research, v. 75, p. 1566-1585.

Burt, D.M. (1978) Multisystems analysis of beryllium mineral stabilities: the system $BeO-Al_2O_3-SiO_2-H_2O$. American Mineralogist, v. 63, p.664-676.

Butler, R.W.H. (1982) The terminology of structures in thrust belts. Journal of Structural Geology, v. 4, p. 239-245.

Cady, W.M. (1968) The lateral transition from the miogeosynclinal to the eugeosynclial zone in northwestern New England and adjacent Quebec. In Zen, E-an, White, W.S., Hadley, J.B., and Thompson, J.B., Jr., eds., Studies of Appalachian geology: northern and maritime, p. 151-162. Interscience Publishers, New York.

Cady, W.M., Albee, A.L., and Chidester, A.H. (1963) Bedrock geology and asbestos deposits of the upper Missisquoi Valley and vicinity, Vermont. U.S. Geological Survey Bulletin 1122-B, 78 p.

Cady, W.M., Albee, A.L., and Murphy, J.F. (1962) Bedrock geology of the Lincoln Mountain quadrangle, Vermont. U. S. Geological Survey Geological Quadrangle Map GQ-164.

Chamberlain, C.P. (1981) Metamorphic zonation studies in south-central New Hampshire. M.A. thesis, Dartmouth College, Hanover, N.H., 191 p.

Chamberlain, C.P. (1984) Stratigraphic, structural, and metamorphic relations between the Bronson Hill anticlinorium and the Merrimack synclinorium, southwestern New Hampshire. Geological Society of America Abstracts with Programs, v. 16, p.8.

Chamberlain, C.P. (1985) Tectonic and metamorphic history of a high-grade terrane, southwestern New Hampshire. Ph.D. thesis, Harvard University, Cambridge, Massachusetts, 207 p.

Chamberlain, C.P. (1986) P-T paths in the root zone of the Fall Mountain nappe: constraints on the thermal budget of Acadian metamorphism. Geological Society of America Abstracts with Programs, v. 68, p. 530-540.

Chamberlain, C.P. (1986a) Evidence for the repeated folding of isotherms during regional metamorphism. Journal of Petrology, v.17, p. 63-89.

Chamberlain, C.P., and England, P.C. (1985) The Acadian thermal history of the Merrimack synclinorium in New Hampshire. Journal of Geology, v. 93, p 593-602.

Chamberlain, C. P., and Lyons, J. B. (1983) Pressure, temperature, and metamorphic zonation studies of pelitic schists in the Merrimack synclinorium, south-central New Hampshire. American Mineralogist, v. 68, p. 530-540.

Chapman, C.A. (1939) Geology of the Mascoma quadrangle, New Hampshire. Bulletin of the Geological Society of America, v. 50, p. 127-180.

Chapman, C.A. (1942) Intrusive domes of the Claremont-Newport area, New Hampshire. Geological Society of America Bulletin, v. 53, p. 889-916.

Chapman, C.A. (1952) Structure and petrology of the Sunapee quadrangle, New Hampshire. Geological Society of America Bulletin, v. 63, p. 381-425.

Cheney, J.T. (1980) Chloritoid through sillimanite zone metamorphism of high-alumina pelites from the Hoosac Formation, western Massachusetts. Geological Society of America Abstracts with Programs, v. 12, p. 401.

Cheney, J.T. (1986) Disequilibrium muscovite compositions from single crystals and samples as indicators of P-T paths in western Massachusetts. Geological Society of America Abstracts with Programs, v. 18, p. 8.

Cheney, J.T., and Guidotti, C.V. (1979) Muscovite-plagioclase equilibria in sillimanite + quartz bearing metapelites, Puzzle Mountain area, northwest Maine. American Journal of Science, v. 279, p. 411-434.

Chidester, A.H. (1953) Geology of the talc deposits, Sterling Pond area, Stowe, Vermont. U.S. Geological Survey Mineral Investigation Field Studies Map MF-11.

Chidester, A.H. (1962) Petrology and geochemistry of selected talc-bearing ultramafic rocks and adjacent country rocks in north-central Vermont. U.S. Geological Survey Professional Paper 345, 207 p.

Chidester, A.H. (1968) Evolution of the ultramafic complexes of northwestern New England. In Zen, E-an, White, W.S., Hadley, J.B., and Thompson, J.B., Jr., eds., Studies of Appalachian geology: northern and maritime, p. 343-354. Interscience Publishers, New York.

Chidester, A.H., Albee, A.L., and Cady, W.M. (1978) Petrology, structure, and genesis of the asbestos-bearing ultramafic rocks of the Belvidere Mountain area in Vermont. U.S. Geological Survey Professional Paper 1016, 95 p.

Chidester, A.H., Billings, M.P., and Cady, W.M. (1951) Talc investigations in Vermont, preliminary report. U.S. Geological Survey Circular 95, 33 p.

Clark, R. G. and Lyons, J.B. (1984) Mixing models for the Kinsman quartz monzonite. Geological Society of America Abstracts with Programs, v. 16, p. 9.

Crawford, M.L., and Hollister, L.S. (1986) The tectonic surge: a result of melt enhanced strain at collisional plate boundaries. EOS, v. 67, p. 370.

Crawford, M. L., and Mark, L. E. (1982) Evidence from metamorphic rocks for overthrusting, Pennsylvania Piedmont, U.S.A. Canadian Mineralogist, v. 20, p. 330-347.

Crowley, P.D., and Spear, F. S. (1981) The orthoamphibole solvus: P, T, X(Fe-Mg) relations. Geological Society of America Abstracts with Programs, v. 13, p. 435.

Currier, L.W. (1934) Notes on staurolite and associated minerals from schist at Gassetts, Vermont. American Mineralogist, v. 19, p. 335-339.

Dewey, Chester (1824) A sketch of the geology and mineralogy of the western part of Massachusetts, and a small part of the adjoining states. American Journal of Science, v. VIII, no. 1, p. 1-60.

Dickenson, M.P. (1984) Local and regional differences in the chemical potential of water in amphibolite grade pelitic rocks. Geological Society of America, Abstracts with Programs, v. 16, p. 488.

Doll, C.G., Cady, W.M., Thompson, J.B., Jr., and Billings, M.P. (1961) Centennial geologic map of Vermont. Vermont Geolological Survey, Montpelier, Vermont, scale 1:250,000.

Doolan, B.L., Zen, E-an, and Bence, A.E. (1978) Highly aluminous hornblendes: compositions and occurrences from southwestern Massachusetts. American Mineralogist, v. 63, p.1088-1099.

Downie, E.A. (1980) Prograde and retrograde reaction sequence and condition of metamorphism, north end of the Chester dome, southeastern Vermont. Geological Society of America Abstracts with Programs, v. 12, p. 415.

Downie, E.A. (1982) Structure and metamorphism in the Cavendish area, north end of the Chester dome, southeastern Vermont. Ph.D. thesis, Harvard University, Cambridge, Massachusetts, 291 p.

Downie, E.A., Thompson, J.B., Jr., and Slack, J.F. (1986) Paleozoic deformation and basement/cover relationships in the Wallingford quadrangle, southern Vermont. Geological Society of America Abstracts with Programs, v. 18, p. 14.

Duke, E.F. (1984) Part I. Stratigraphy, structure, and petrology of the Peterborough 15-minute quadrangle, New Hampshire; and Part II. Graphitic textural and isotopic variations in plutonic rocks, south-central New Hampshire. Ph.D. thesis, Dartmouth College, Hanover, N.H.

Elbert, D. C. (1986) Recognition and implications of a structurally inverted Monadnock-western Maine stratigraphy directly above the core of the Bernardston nappe, Hinsdale, New Hampshire. Geological Society of America Abstracts with Programs, v.18, p. 15.

Ellis, D.J., and Thompson, A.B. (1986) Subsolidus and partial melting reactions in the quartz-excess $CaO + MgO + Al_2O_3 + SiO_2 + H_2O$ system under water-deficient conditions to 10 kb: some implications for the origin of peraluminous rocks. Journal of Petrology, v. 27, p. 91-121.

Emerson, B.K. (1895) A mineralogical lexicon of Franklin, Hampshire, and Hampden Counties, Mass. U.S. Geological Survey Bulletin 126, 180 p.

Emerson, B.K. (1898) Geology of old Hampshire County, Mass., comprising Franklin, Hampshire, and Hampden Counties. U.S. Geological Survey Monograph 29, 790 p.

Emerson, B.K. (1917) Geology of Massachusetts and Rhode Island. U.S. Geological Survey Bulletin 597, 289 p.

England, P. C., and Richardson, S.W. (1977) The influence of erosion on the mineral facies of rocks from different metamorphic environments. Journal of the Geological Society of London, v. 134, p. 201-213.

Eugster, H.P., Albee, A.L., Bence, A.E., Thompson, J.B., Jr., and Waldbaum, D.R. (1972) The two-phase region and excess mixing properties of paragonite-muscovite crystalline solutions. Journal of Petrology, v. 13, p. 147-179.

Eusden, J.D., Bothner, W.A., Hussey, A.M.,II, and Laird, Jo (1984) Silurian and Devonian rocks in the Alton and Berwick quadrangles, New Hampshire and Maine. In Hanson, L.S., Geology of the Coastal Lowlands, Boston, MA to Kennebunk, ME., NEIGC 76th Annual Meeting, p. 325-351. Salem State College, Salem, Massachusetts.

Evans, B.W., and Guidotti, C.V. (1966) The sillimanite-potash feldspar isograd in western Maine, U.S.A. Contributions to Mineralogy and Petrology, v. 12, p. 25-62.

Ewart, Anthony (1979) A review of the mineralogy and chemistry of the Tertiary-Recent dacitic, latitic, rhyolitic, and related sialic volcanic rocks. In Barker, Fred, ed., Trondhjemites, dacites, and related rocks, p. 13-121. Elsevier, Amsterdam.

Fahey, J., and Pease, M.H. (1977) Bedrock geology of the South Coventry quadrangle. U.S.Geological Survey Open File Report No. 77-584.

Ferry, J.M. (1976a) Metamorphism of calcareous sediments in the Waterville-Vassalboro area, south-central Maine: mineral reactions and graphic analysis. American Journal of Science, v. 276, p. 841-882.

Ferry, J.M. (1976b) P, T, fCO2, and fH2O during metamorphism of calcareous sediments in the Waterville-Vassalboro area,south-central Maine. Contributions to Mineralogy and Petrology, v. 57, p. 119-143.

Ferry, J.M. (1979) A map of chemical potential differences within an outcrop. American Mineralogist, v. 64, p. 966-985.

Ferry, J.M., and Spear, F.S. (1978) Experimental calibration of the partitioning of Fe and Mg between biotite and garnet. Contributions to Mineralogy and Petrology, v. 66, p. 113-117.

Field, M.T. (1975) Bedrock geology of the Ware area, central Massachusetts. Contribution No. 22 (Ph.D. thesis), Department of Geology and Geography, University of Massachusetts, Amherst, 186 p.

Finger, L.W., and Burt, D.M. (1972) Reaction, a Fortran IV computer program to balance chemical reactions. Carnegie Institution of Washington Year Book, v. 71, p. 615-616.

Fisher, G.W. (1973) Nonequilibrium thermodynamics as a model for diffusion-controlled metamorphic processes. American Journal of Science, v. 273, p. 897-924.

Fisher, G.W. (1977) Nonequilibrium thermodynamics in metamorphism. In Fraser, D.G., ed., Thermodynamics in geology, p. 381 - 403. D.Reidel Pub. Co., Dordrecht, Holland.

Friedman, I., and O'Neil, J.R.(1977) Compilation of stable isotope fractionation factors of geochemical interest. U.S. Geological Survey Professional Paper 440-KK, 12 p..

Garlick, G.D., and Epstein, Samuel (1967) Oxygen isotope ratios in coexisting minerals of regionally metamorphosed rocks. Geochimica et Cosmochimica Acta, v. 31, p. 181-214.

Ghent, E.D. (1976)Plagioclase-garnet-Al_2SiO_5-quartz: a potential geothermometer-geobarometer. American Mineralogist, v. 61, p. 710-714.

Ghent, E. D., and Stout, M. Z. (1981) Geobarometry and geothermometry of plagioclase-biotite-garnet-muscovite assemblages. Contributions to Mineralogy and Petrology, v. 76, p. 92-97.

Ghent, E.D., Robbins, D.B., and Stout, M.Z. (1979) Geothermetry, geobarometry and fluid compositions of metamorphosed calc-silicates and pelites, Mica Creek, British Columbia. American Mineralogist, v. 64, p. 874-885.

Ghose, Subrata (1981) Subsolidus reactions and microstructures in amphiboles. In Veblen, D.R., ed., Amphiboles and other hydrous pyriboles - mineralogy, p. 325-372. Reviews in Mineralogy, v. 9A, Mineralogical Society of America, Washington, D.C.

Gittos, M.F., Lorimer, G.W., and Champness, P.E. (1976) The phase distributions in some exsolved amphiboles. In Wenk, H.R., ed., Electron microscopy in mineralogy, p. 238-247. Springer-Verlag, Berlin.

Goldstein, Arthur, and Owens, James (1985) Mesoscopic andmicroscopic structure of the Lake Char-Honey Hill mylonite zone, eastern Connecticut. In Tracy, R.J., ed., Guidebook for field trips in Connecticut and adjacent areas of New York and Rhode Island. NEIGC 77th Annual Meeting, p. 159 - 183. Yale University, New Haven, Connecticut, p. 159-183.

Green, J.C. (1963) High-level metamorphism of pelitic rocks in northern New Hampshire. American Mineralogist, v. 48, p. 991-1023.

Grove, T. L., Ferry, J. M., and Spear, F. S. (1983) Phase transitions and decomposition relations in calcic plagioclase. American Mineralogist, v. 68, p 41-59.

Guidotti, C.V. (1970) The mineralogy and petrology of the transition from the lower to the upper sillimanite zone in the Oquossoc area, Maine. Journal of Petrology, v. 11, p. 277-336.

Guidotti, C.V. (1974) Transition from staurolite to sillimanite zone, Rangeley quadrangle, Maine. Geological Society of America Bulletin, v. 85, p. 475-490.

Guidotti, C.V. (1978) Compositional variation in muscovite in medium- to high-grade metapelites of northwestern Maine. American Mineralogist, v. 63, p. 878-884.

Guidotti, C.V., Cheney, J.T., and Guggenheim, Stephen (1977) Distribution of titanium between coexisting muscovite and biotite in pelitic schists from northwestern Maine. American Mineralogist, v. 62, p. 438-448.

Guidotti, C.V., Trzcienski, W.E., Jr., and Holdaway, M.J. (1983) A northern Appalachians metamorphic transect - Eastern Townships, Quebec to the central Maine coast. In Schenk, P.E., ed., Regional trends in the geology of the Appalachian-Caledonian-Hercynian-Mauritanide orogen, p. 235-247. Reidel Press, Holland.

Hadley, J. B. (1942) Stratigraphy, structure and petrology of the Mt. Cube area, New Hampshire. Geological Society of America Bulletin, v. 53, p. 113-176.

Hadley, J.B. (1949) Bedrock geology of the Mt. Grace quadrangle, Massachusetts. U.S. Geological Survey Geologic Quadrangle Map GQ-3, scale 1:31,680.

Hall, B.A., Pollock, S.G., and Dolan, K.M. (1976) Lower Devonian Seboomook Formation and Matagamon Sandstone, northern Maine: A flysch basin-margin delta complex. In Page, L.R., ed., Contributions to the stratigraphy of New England, p. 57-63. Geological Society of America Memoir 148.

Hall, L.M., and Robinson, Peter (1982) Stratigraphic-tectonic subdivisions of southern New England. In St.-Julien, P., and Béland, J., eds., Major structural zones and faults of the northern Appalachians, p. 15-41. The Geological Association of Canada Special Paper Number 24.

Hanscom, R.H. (1973) The crystal chemistry and polymorphism of chloritoid. Ph.D. thesis, Harvard University, Cambridge, Massachusetts.

Hanscom, R.H. (1975) Refinement of the crystal structure of monoclinic chloritoid. Acta Crystallographica, v.B31, p.780-784. Hanscom, R.H. (1980) The structure of triclinic chloritoid and chloritoid polymorphism. American Mineralogist, v. 65, p. 534-539.

Hart, R.A. (1970) Chemical exchange between seawater and deep ocean basalts. Earth and Planetary Science Letters, v. 9, p. 269-279.

Harte, Ben, and Hudson, N.F.C. (1979) Pelite facies series and the temperatures and pressures of Dalradian metamorphism in E. Scotland. In Harris, A.L., Holland, C.H., and Leake, B.E., eds., The Caledonides of the British Isles - Reviewed, p. 323-337. Scottish Academic Press Ltd., Edinburgh.

Harwood, D.S. (1979) Bedrock geologic map of the Norfolk quadrangle, Connecticut. U.S. Geological Survey Quadrangle Map GQ-1518, scale 1:24,000.

Hatch, N.L., Jr. (1982) The Taconian Line in western New England and its implications to Paleozoic tectonic history. In St.-Julien, P., and Béland, J., eds. Major Structural Zones and Faults of the Northern Appalachians, p. 67 - 86. Geological Association of Canada Special Paper 24.

Hatch, N.L., Jr., Moench, R.H., and Lyons, J.B. (1983)Silurian-Lower Devonian stratigraphy of eastern and south-central New Hampshire: extensions from western Maine. American Journal of Science, v. 283, p. 739-761.

Heald, M.T. (1950) Structure and petrology of the Lovewell Mountain quadrangle, New Hampshire. Geological Society of America Bulletin, v. 61, p. 43-89.

Helz, R.T. (1976) Phase relations of basalts in their melting ranges at $PH_2O = 5$ kbar. Part II. Melt compostions. Journal of Petrology, v.17, p.139-193.

Henry, D.J., and Guidotti, C.V. (1981) Implications of the sulfide-silicate interactions in staurolite grade metapelites in NW Maine. (abstract) EOS, v. 62, p. 435-436.

Hensen, B.J. (1977) Cordierite-garnet bearing assemblages as geothermometers and barometers in granulite facies terranes. Tectonophysics, v. 43, p. 73-88.

Hensen, B.J., and Green, D.H. (1973) Experimental study of the stability of cordierite and garnet in pelitic compositions at high presures and temperatures. Contributions to Mineralogy and Petrology, v.38, p. 151-166.

Hepburn, J.C., Trask, N.J., Rosenfeld, J.L., and Thompson, J.B., Jr. (1984) Bedrock geology of the Brattleboro quadrangle, Vermont-New Hampshire, Vermont Geological Survey Bulletin No. 32, 162 p.

Hess, H.H. (1933) The problem of serpentinization and the origin of certain chrysotile asbestos talc and soapstone deposits. Economic Geology, v. 28, p. 634-657.

Hess, P.C. (1969) The metamorphic paragenesis of cordierite in pelitic rocks. Contributions to Mineralogy and Petrology, v. 24, p. 191-207.

Hess, P.C. (1971) Prograde and retrograde equilibria in garnet-cordierite gneisses in south-central Massachusetts. Contributions to Mineralogy and Petrology, v. 30, p. 177-195.

Hitchcock, C.H., and Huntington, J.H. (1874) The geology of New Hampshire: Vol.I. Concord, N.H., 667 p.

Hitchcock, C.H., Huntington, J.H., Upham, Warren, and Hawes, G.W. (1877) The geology of New Hampshire: Vol.II. Concord, N.H., 684 p.

Hitchcock, C.H., Huntington, J.H., Upham, Warren, and Hawes, G.W. (1878) The geology of New Hampshire: Vol.III. Concord, N.H., 751 p.

Hodges, K.V., and Royden L. (1984) Geothermometry and geobarometry of retrograded metamorphic rocks: an indication of the uplift trajectory of a portion of the northern Scandinavian Caledonides. Journal of Geophysical Research, v.89, p.7077-7090.

Hodges, K.V., and Spear, F.S. (1982) Geothermometry, geobarometry and the Al_2SiO_5 triple point at Mt. Moosilauke, New Hampshire, American Mineralogist. v. 67, p. 1118-1134.

Hodgkins, C.E. (1983) Major element geochemistry and petrology of the Dry Hill Gneiss, Pelham dome, central Massachusetts, Geological Society of America Abstracts With Programs. v. 15, p. 141.

Hodgkins, C.E. (1985) Major and trace element geochemistry and petrology of the late Precambrian Dry Hill Gneiss, Pelham dome, central Massachusetts. Contribution No. 48 (M.S. thesis), Dept. of Geology and Geography, University of Massachusetts, Amherst, 135 p.

Holdaway, M.J. (1971) Stability of andalusite and the aluminum silicate phase diagram. American Journal of Science, v. 271, p. 97-131.

Holdaway, M.J., and Lee, S.M. (1977) Fe-Mg cordierite stability in high grade pelitic rocks based on experimental, theoretical, and natural observations. Contributions to Mineralogy and Petrology, v. 63, p. 175-198.

Holdaway, M.J., Guidotti, C.V., Novak, J.M., and Henry, W.E. (1982) Polymetamorphism in medium- to high-grade pelitic metamorphic rocks, west-central Maine. Geological Society of America Bulletin, v. 93, p. 572-584.

Hollister, L.S. (1982) Metamorphic evidence for rapid (2mm/yr) uplift of a portion of the central gneiss complex, Coast Mountains, B.C. Canadian Mineralogist, v. 20, p. 319-332.

Hollocher, K.T. (1983) Major element geochemistry and possible origin of volcanic rocks in the Middle Ordovician Partridge Formation, central Massachusetts. Geological Society of America Abstracts with Programs, v. 15, p. 172.

Hollocher, K.T. (1985) Geochemistry of metamorphosed volcanic rocks in the Middle Ordovician Partridge Formation, and amphibole dehydration reactions in the high-grade metamorphic zones of central Massachusetts. Contribution No. 56 (Ph.D. thesis), Deptartment of Geology and Geography, University of Massachusetts, Amherst, 275p.

Humphris, S.E., and Thompson, G.A. (1978) Hydrothermal alteration of oceanic basalts by seawater. Geochimica et Cosmochimica Acta, v. 42, p. 107-125.

Huntington, J.C. (1975) Mineralogy and petrology of metamorphosed iron-rich beds in the Lower Devonian Littleton Formation, Orange area, Massachusetts. Contribution No. 19 (M.S. thesis), Department of Geology and Geography, University of Massachusetts, Amherst, 106 p.

Jackson, C.T. (1844) Final report on the geology and mineralogy of the State of New Hampshire. Concord, N.H., 376 p.

Jaffe, H.W., Robinson, Peter, and Klein, Cornelis, Jr. (1968) Exsolution lamellae and optic orientation of clinoamphiboles. Science, v. 160, p. 776-778.

Jaffe, H.W., Robinson, Peter, and Tracy, R.J. (1978) Orthoferrosilite and other iron-rich pyroxenes in microperthite gneiss of the Mount Marcy area, Adirondack Mountains. American Mineralogist, v. 63, p. 1116-1136.

Jaffe, H.W., Robinson, Peter, Tracy, R.J., and Ross, Malcolm (1975) Orientation of pigeonite exsolution lamellae in metamorphic augite: correlation with composition and calculated optimal phase boundaries. American Mineralogist, v. 60, p. 9-28.

James, R.S., Grieve, R.A.F., and Pauk, L. (1978) The petrology of cordierite-anthophyllite gneisses and associated mafic and pelitic gneisses at Manitouwadge, Ontario. American Journal of Science, v. 278, p. 41-63.

Jasaitis, R.A. (1983) Geology of pre-Mesozoic bedrock of the Amherst area, west-central Massachusetts. Contribution No.46 (M.S. thesis), Department of Geology and Geography, University of Massachusetts, Amherst, 96 p.

Johannsen, Albert (1911) Petrographic terms for field use. Journal of Geology, v. 19, p. 317-322.

Karabinos, Paul (1984) Polymetamorphic garnet zoning from southeastern Vermont. American Journal of Science, v. 284, p. 1008-1025.

Karabinos, Paul (1984a) Deformation and metamorphism on the east side of the Green Mountain massif in southern Vermont. Geological Society of America Bulletin, v. 95, p. 584-593.

Karabinos, Paul (1985) Garnet and staurolite producing reactions in a chlorite-chloritoid schist. Contributions to Mineralogy and Petrology, v. 90, p. 262-275.

Karabinos, Paul (1986) Physical conditions of thrust faulting in the Green Mountain massif, Vermont. Geological Society of America Abstracts with Programs, v. 18, p. 26.

Keusen, H.R., and Peters, Tj. (1980) Preiswerkite, an Al-rich trioctahedral sodium mica from the Geisspfad ultramafic complex (Penninic Alps), American Mineralogist. v. 65, p. 1134-1137.

Klein, Cornelis, Jr. (1968) Coexisting amphiboles. Journal of Petrology, v. 9, p. 281-330.

Korzhinskii, D.S. (1959) Physicochemical basis of the analysis of the paragenesis of minerals. Consultants Bureau, Inc., New York, 142 p.

Kruger, F.C. (1946) Structure and metamorphism of the Bellows Falls quadrangle of New Hampshire and Vermont. Geological Society of America Bulletin, v. 57, p. 161-206.

Laird, Jo (1980) Phase equilibria in mafic schist from Vermont. Journal of Petrology, v. 21, p. 1-37.

Laird, Jo, and Albee, A.L. (1981a) High-pressure metamorphism in mafic schist from Vermont. American Journal of Science, v. 281, p. 97-126.

Laird, Jo, and Albee, A.L. (1981b) Pressure, temperature, and time indicators in mafic schist: their application to reconstructing the polymetamorphic history of Vermont. American Journal of Science, v.281, p. 127-175.

Laird, Jo, Lanphere, M.A., and Albee, A.L. (1984) Distribution of Ordovician and Devonian metamorphism in mafic and pelitic schists from northern Vermont. American Journal of Science, v. 284, p. 376-413.

Lanphere, M.A., and Albee, A.L. (1974) $^{40}Ar/^{39}Ar$ age measurements in the Worcester Mountains, evidence of Ordovician and Devonian metamorphic events in northern Vermont. American Journal of Science, v. 281, p. 545-555.

Lanphere, M.A., Laird, Jo, and Albee, A.L. (1983) Interpretation of $^{40}Ar/^{39}Ar$ ages of polymetamorphic mafic and pelitic schist in northern Vermont. Geological Society of America Abstracts with Programs, v. 15, p. 147.

Lapp, E.T., and O'Loughlin, S.B. (1986) Tectonic and depositional sequences in polydeformed, polymetamorphosed rocks of the Camel's Hump Group, Lincoln Gap area, central Vermont. Geological Society of America Abstracts with Programs, v. 18, p. 29.

Leake, B.E., Compiler for Subcommittee on Amphiboles, I.M.A. (1978) Nomenclature of amphiboles. American Mineralogist, v.63, p. 1023-1052.

Leo, G.W. (1985) Trondhjemite and metamorphosed quartz keratophyre tuff of the Ammonoosuc Volcanics, western New Hampshire and adjacent Vermont and Massachusetts. Geological Society of America Bulletin, v.96, p.1493-1507.

Lonker, S.W. (1981) The P-T-X relations of the cordierite-garnet-sillimanite-quartz equilibrium. American Journal of Science, v. 281, p. 1056-1090.

Loughnan, F.C. (1969) Chemical weathering of silicate minerals. American Elsevier, New York, 154 p.

Lux, D.R., and Guidotti, C.V. (1985) Evidence for extensive Hercynian metamorphism in western Maine. Geology, v. 13, p. 696-700.

Lyons, J. B. (1955) Geology of the Hanover quadrangle, New Hampshire-Vermont. Geological Society of America Bulletin, v. 66, p. 105-146.

Lyons, J. B., and Livingston, D. E. (1977) Rb-Sr age of the New Hampshire plutonic series. Geological Society of America Bulletin, v. 88, p 1808-1812.

Lyons, J. B., Boudette, E.L., and Aleinikoff, J.N. (1982) The Avalonian and Gander zones in central eastern New England, in St.-Julien, P., and Béland, J., eds., Major Structural Zones and Faults of the Northern Appalachians, p. 43-66. Geological Association of Canada Special Paper 24.

Maggs, W.W., Cheney, J.T., and Spear, F.S. (1986) Probable retrograded eclogites in the Berkshire massif. Geological Society of America Abstracts with Programs, v. 18, p. 32.

Martignole, Jacques, and Sisi, J-C. (1981) Cordierite-garnet-H_20 equilibrium: A geological thermometer, barometer, and water-fugacity indicator. Contributions to Mineralogy and Petrology, v. 77, p. 38-46.

McCormick, R.B. (1934) Paragonite from Pizzo Forno, Ticino, Switzerland. American Mineralogist, v. 19, p. 431-432.

Melson, M.G., and Thompson, G.A. (1973) Glassy abyssal basalts, Atlantic seafloor near St. Pauls rocks: petrography and composition of secondary clay minerals. Geological Society of America Bulletin, v. 84, p. 703-716.

Mohr, D.W., and Newton, R.C. (1981) Role of sulfur fugacity in metamorphism of mica schists. (abstract) EOS, v. 62, p. 436.

Moore, G.E., Jr. (1949) Structure and metamorphism of the Keene-Brattleboro area, New Hampshire-Vermont. Geological Society of America Bulletin, v. 60, p. 1613-1669.

Moore, G.E., Jr. (1978) Preliminary bedrock, surficial, and structural data maps of the Southbridge quadrangle, Massachusetts and Connecticut. U.S. Geological Survey Open-File Map 78-220, 16 p., 4 pls., scale 1:24000.

Mottl, M.J. (1976) Chemical exchange between seawater and basalt during hydrothermal alteration of oceanic crust. Ph.D. dissertation, Harvard University, Cambridge, Massachusetts.

Mottl, M.J. (1983) Metabasalts, axial hot springs, and the structure of hydrothermal systems at mid-ocean ridges. Geological Society of America Bulletin, v. 94, p. 161-180.

Naylor, R.S. (1969) Age and origin of the Oliverian domes, central-western New Hampshire. Geological Society of America Bulletin, v.80, p. 405-428.

Naylor, R.S. (1971) Acadian orogeny: an abrupt and brief event. Science, v. 172, p. 558-560.

Naylor, R.S., Boone, G.M., Boudette, E.L., Ashenden, D.D., and Robinson, Peter (1973) Pre-Ordovician rocks in the Bronson Hill and Boundary Mountains anticlinoria, New England, U.S.A. (abstract) Transactions of the American Geophysical Union, v. 54, p. 495.

Neilson , D.L., Clark, R.G., Lyons, J.B., Englund, E.J., and Borns, D.J. (1976) Gravity models and mode of emplacement of the New Hampshire Plutonic Series. In Lyons, P.C., and Brownlow, A.H., eds., Studies in New England geology, p. 301-318. Geological Society of America Memoir 146.

Newton, R.C., and Haselton, H.T. (1981) Thermodynamics of the garnet-plagioclase-Al_2SiO_5-quartz geobarometer. In Newton, R.C., et al., eds., Thermodynamics of minerals and melts, p. 131-147. Springer-Verlag, New York.

Newton, R.C., and Wood, B.J. (1979) Thermodynamics of water in cordierite and some petrologic consequences of cordierite as a hydrous phase. Contributions to Mineralogy and Petrology, v. 68, p. 391-405.

Nockholds, S.R. (1954) Average chemical composition of some igneous rocks. Bulletin of the Geological Society of America, v. 65, p.1007-1032.

O'Hara, K.D. and Gromet, L.P. (1985) Two distinct late Precambrian (Avalonian) terranes in southeastern New England and their late Paleozoic juxtaposition. American Journal of Science, v. 285, p. 673-709.

Orange, D. L. (1985) Metamorphic petrology, pressure-temperature paths, and tectonic evolution of the Mount Cube quadrangle, New Hampshire and Vermont. M.S. thesis, Massachusetts Institute of Technology, Cambridge, Massachusetts, 170 p.

Osberg, P.H. (1952) The Green Mountain anticlinorium in the vicinity of Rochester and East Middlebury, Vermont. Vermont Geological Survey Bulletin Number 5, 127 p.

Osberg, P.H. (1971) An equilibrium model for Buchan-type metamorphic rocks, south-central Maine. American Mineralogist, v. 56, p. 569-576.

Osberg, P.H. (1980) Stratigraphic and structural relations in the turbidite sequence of south-central Maine in Roy, D.C., and Naylor, R.S., eds., The geology of northeastern Maine and neighboring New Brunswick. NEIGC 72nd Annual Meeting, p. 278-289. University of Maine, Presque Isle.

Oxburgh, E.R., and Turcotte, D.L. (1974) Thermal gradients and regional metamorphism in overthrust terrains with special reference to the Eastern Alps. Schweizerische Mineralogische und Petroghische Mitteilungen, v.54, p.641-662.

Papike, J.J., and Ross, Malcolm (1970) Gedrites: crystal structures and intercrystalline cation distributions. American Mineralogist, v. 55, p. 1945-1972.

Pauling, Linus (1930) The structure of the chlorites. Proceedings of the National Academy of Sciences, v. 16, p. 578-582.

Pearce, J.A., and Cann, J.R. (1973) Tectonic setting of basic volcanic rocks determined using trace element analysis. Earth and Planetary Science Letters, v. 19, p. 290-300.

Pearce, J.A., Cann, J.R., Harris, N.B.W., and Tindle, A.G. (1984) Trace element discrimination diagrams for the tectonic interpretation of granitic rocks. Journal of Petrology, v. 25, p. 956-983.

Pease, M.H., Jr. (1972) Geologic map of the Eastford quadrangle, Windham and Tolland Counties, Connecticut. U.S. Geological Survey Geologic Quadrangle Map GQ-1023.

Pease, M.H., Jr. (1975) Bedrock geology of the Stafford Springs quadrangle. U.S.Geological Survey Open File Report No. 75-633.

Pease, M.H., Jr. (1982) The Bonemill Brook fault zone, eastern Connecticut. In Joesten, Raymond, and Quarrier, S.S., eds., Guidebook for fieldtrips in Connecticut and south-central Massachusetts. NEIGC 74th Annual Meeting, p. 263-287. The University of Connecticut, Storrs.

Peper, J.D., and Pease, M.H., Jr. (1975) Geologic map of the Westford quadrangle, Connecticut. U.S. Geological Survey Geologic Quadrangle Map GQ-1214.

Perkins, Dexter, III, and Chipera, S.J. (1985) Garnet-orthopyroxene-plagioclase-quartz barometry: refinement and application to the English River subprovince and the Minnesota River valley. Contributions to Mineralogy and Petrology, v. 89, p. 69-80.

Phillips, A.H., and Hess, H.H. (1936) Metamorphic differentiation at contacts between serpentinite and siliceous country rocks. American Mineralogist, v. 21, p. 333-362.

Pomeroy, J.S. (1975) Preliminary bedrock geologic map of the East Brookfield quadrangle, Worcester County, Massachusetts. U.S. Geological Survey Open File Map No. 75-530.

Pomeroy, J.S. (1977) Bedrock geologic map of the Warren quadrangle, Worcester, Hamden, and Hampshire Counties, Massachusetts. U.S. Geological Survey Geologic Quadrangle Map GQ-1358.

Rabbitt, J.C. (1948) A new study of the anthophyllite series. American Mineralogist, v. 33, p. 263-323.

Rhodes, J.M. (1983) Homogeneity of lava flows: chemical data for historic Mauna Loa eruptions. Journal of Geophysical Research, v. 88, supplement, p. A869-A879.

Robinson, Peter (1963) Gneiss domes of the Orange area, west-central Massachusetts and New Hampshire. Ph.D. dissertation, Harvard University, Cambridge, Massachusetts, 253 p.

Robinson, Peter (1967) Gneiss domes and recumbent folds of the Orange area, west-central Massachusetts. In Robinson, Peter, ed., Guidebook for field trips in the Connecticut Valley of Massachusetts. NEIGC 59th Annual Meeting, p. 17-47. Amherst, Massachusetts.

Robinson, Peter (1979) Bronson Hill anticlinorium and Merrimack synclinorium in central Massachusetts. In Skehan, J.W., S.J., and Osberg, P.H., eds., The Caledonides in the U.S.A.: geological excursions in the northeast Appalachians. IGCP Project 27, Caledonide Orogen, p. 126-150. Weston Observatory, Weston, Massachusetts.

Robinson, Peter (1980) The composition space of terrestrial pyroxenes - internal and external limits. In Prewitt, C.T., ed., Pyroxenes, p. 419-494. Reviews in Mineralogy, v. 7, Mineralogical Society of America, Washington, D.C.

Robinson, Peter (1981) The basement-cover enigma in the gneiss domes of central New England, U.S.A. (abstract) Uppsala Caledonide Symposium. Terra Cognita, v. 1, p. 70.

Robinson, Peter (1983) Realms of regional metamorphism in southern New England, with emphasis on the eastern Acadian metamorphic high. In Schenk, P.E., ed., Regional trends in the geology of the Appalachian-Caledonian-Hercynian-Mauritanide orogen, p. 249-258. Reidel press, Holland.

Robinson, Peter, and Hall, L.M. (1980) Tectonic synthesis of southern New England. In Wones, D.R., ed., The Caledonides in the U.S.A. IGCP Project 27, Caledonide orogen, p. 73-82. Blacksburg, Virginia.

Robinson, Peter, and Jaffe, H.W. (1969a) Aluminous enclaves in gedrite-cordierite gneiss from southwestern New Hampshire. American Journal of Science, v. 267, p. 389-421.

Robinson, Peter, and Jaffe, H.W. (1969b) Chemographic exploration of amphibole assemblages from central Massachusetts and southwestern New Hampshire. In Papike, J.J., ed., Pyroxenes and amphiboles: crystal chemistry and phase petrology, p. 251-274. Mineralogical Society of America Special Paper 2.

Robinson, Peter, and Tracy, R.J. (1977) Sulfide-silicate-oxide equilibria in sillimanite-K-feldspar grade pelitic schists, central Massachusetts. (abstract) EOS, v. 58, p. 524.

Robinson, Peter, Elbert, D.C., Tracy, R.J., Thompson, P.J., and Hollocher, K.T. (1986) P-T trajectories of Acadian metamorphism in central Massachusetts and southwestern New Hampshire. Geological Society of America Abstracts with Programs, v.18, p. 63.

Robinson, Peter, Field, M.T., and Tucker, R.D. (1982a) Stratigraphy and structure of the Ware-Barre area, central Massachusetts. In Joesten, Raymond, and Quarrier, S.S., eds., Guidebook for fieldtrips in Connecticut and south central Massachusetts. NEIGC 74th Annual Meeting, p. 341-374. The University of Connecticut, Storrs.

Robinson, Peter, Hatch, N.L., Jr., and Stanley, R.S. (1984) The Whately thrust: a proposed structural solution to the stratigraphic dilemma of the Erving Formation and associated Devonian strata, western Massachusetts and adjacent Vermont. Geological Society of America Abstracts with Programs, v. 16, p. 59.

Robinson, Peter, Hatch, N.L., Jr., and Stanley, R.S. (in press) The Whately thrust: a structural solution to the stratigraphic dilemma of the Erving Formation. In Hatch, N.L., Jr., The bedrock geology of Massachusetts. U.S. Geological Survey Professional Paper.

Robinson, Peter, Jaffe, H.W., Ross, Malcolm, and Klein, Cornelis, Jr. (1971a) Orientation of exsolution lamellae in clinopyroxenes and clinoamphiboles: consideration of optimal phase boundaries. American Mineralogist, v. 56, p. 909-939.

Robinson, Peter, Ross, Malcolm and Jaffe, H.W. (1971) Composition of the anthophyllite-gedrite series, comparisons of gedrite and hornblende, and the anthophyllite-gedrite solvus. American Mineralogist, v. 56, p. 1005-1041.

Robinson, Peter, Ross, Malcolm, Nord, G.L., Jr., Smyth, J.R., and Jaffe, H.W. (1977) Exsolution lamellae in augite and pigeonite: fossil indicators of lattice parameters at high temperature and pressure. American Mineralogist, v. 62, p. 857-873.

Robinson, Peter, Spear, F.S., Schumacher, J.C., Laird, Jo, Klein, Cornelius, Jr., Evans, B.W., and Doolan, B.L. (1982b) Phase relations of metamorphic amphiboles: natural occurence and theroy. In Veblen, D.R., and Ribbe, P.H., eds., Amphiboles: petrology and experimental phase relations, Reviews in Mineralogy, v. 9B, p. 1-227. Mineralogical Society of America, Washington, D.C.

Robinson, Peter, Thompson, J.B., Jr., and Rosefeld, J.L. (1979) Nappes, gneiss domes, and regional metamorphism in western New Hampshire and central Massachusetts. In Skehan, J.W., S.J., and Osberg, P.H., eds., The Caledonides in the U.S.A.: geological excursions in the northeast Appalachians. IGCP Project 27, Caledonide Orogen, p. 126-150. Weston Observatory, Weston, Massachusetts.

Robinson, Peter, Tracy, R.J., and Ashwal, L.D. (1975) Relict sillimanite-orthoclase assemblage in kyanite-muscovite schist, Pelham dome, west-central Massachusetts. (abstract) Transactions of the American Geophysical Union, v. 56, p.466.

Robinson, Peter, Tracy, R.J., Hollocher, K.T., and Dietsch, C.W. (1982c) High grade Acadian metamorphism in south-central Massachusetts. In Joesten, Raymond, and Quarrier, S.S., eds., Guidebook for fieldtrips in Connecticut and south central Massachusetts. NEIGC 74th Annual Meeting, p. 289-340. The University of Connecticut, Storrs.

Robinson, Peter, Tracy, R.J., and Tucker, R.T. (1978) The Acadian (Devonian) metamorphic high of central Massachusetts. Geological Society of America Abstracts with Programs, v. 10, p. 479-480.

Rodgers, John (1985) Bedrock geological map of Connecticut. Connecticut Geological and Natural History Survey, scale 1:125,000.

Roll, M.A. (1986) Effects of Acadian prograde kyanite-zone metamorphism on relict garnet from pre-Acadian granulite facies metamorphism, Mt. Mineral Fm., Pelham dome, Massachusetts. Geological Society of America Abstracts with Programs, v.18, p. 63.

Rosenfeld, J.L. (1968) Garnet rotations due to the major Paleozoic deformations in southeast Vermont. In Zen, E-an, White, W.S., Hadley, J.B., and Thompson, J.B., Jr., eds., Studies of Appalachian geology: northern and maritime, p. 185-202. Interscience Publishers, New York.

Rosenfeld, J. L. (1969) Stress effects around quartz inclusions in almandine and the piezothermometry of coexisting aluminum silicates. American Journal of Science, v. 267, p. 317-351.

Rosenfeld, J.L. (1970) Rotated garnets in metamorphic rocks. Geological Society of America Special Paper 129, 105p.

Rosenfeld, J.L. (1972) Rotated garnets and tectonism in southeast Vermont. In Doolan, B.L., and Stanley, R.S., Guidebook for field trips in Vermont. NEIGC 64th Annual Meeting, p. 167-178. University of Vermont, Burlington.

Rosenfeld, J.L., Thompson, J.B., Jr., and Zen, E-an (1958) Data on coexistent muscovite and paragonite. (abstract) Geological Society of America Bulletin, v. 69, p. 1637.

Ross, Malcolm, Papike, J.J., and Shaw, K.W. (1969) Exsolution textures in amphiboles as indicators of subsolidus thermal histories. In Papike, J.J., ed., Pyroxenes and amphiboles: crystal chemistry and phase petrology, p. 275-299. Mineralogical Society of America Special Paper 2.

Rumble, Douglas, III (1969) Stratigraphic, structural and petrologic studies in the Mt. Cube area, New Hampshire-Vermont. Ph.D. Dissertation, Harvard University, Cambridge, Massachusetts.

Rumble, Douglas, III (1973) Fe-Ti oxide minerals from regionally metamorphosed quartzites of western New Hampshire. Contributions to Mineralogy and Petrology, v. 42, p. 181-195.

Rumble, Douglas, III (1974) Gibbs phase rule and its application in geochemistry. Journal of the Washington Academy of Sciences, v. 64, p. 199-208.

Rumble, Douglas, III (1976a) The use of mineral solid solutions to measure chemical potential gradients in rocks. American Mineralogist, v. 61, p. 1167-1174.

Rumble, Douglas, III (1976b) Oxide minerals in metamorphic rocks. In Rumble, Douglas, III, ed., Oxide Minerals, Reviews in Mineralogy, v.3, p. R1-R20. Mineralogical Society of America, Washington, D.C.

Rumble, Douglas, III (1978) Mineralogy, petrology, and oxygen isotopic geochemistry of the Clough Formation (sic), Black Mountain, western New Hampshire, U.S.A. Journal of Petrology, v. 19, p. 317-340.

Rumble, Douglas, III, and Spear, F.S. (1983) Oxygen isotope equilibration and permeability enhancement during regional metamorphism. Journal of Geological Society of London, v. 140, p. 619-628.

Rumble, Douglas, III, Ferry, J.M., Hoering, T.C., and Boucot, A.J. (1982) Fluid flow during metamorphism at the Beaver Brook fossil locality, New Hampshire. American Journal of Science, v. 282, p. 886-919.

St.-Julien, P., Slivitsky, Anne, and Feininger, Thomas (1983) A deep structural profile across the Appalachians of southern Quebec. In Hatcher, R.D., Jr., Williams, Harold, and Zeitz, Isadore, eds., Contributions to the tectonics and geophysics of mountain chains, p. 103-112. Geological Society of America Memoir 158.

Sanford, R.F. (1982) Growth of ultramafic reaction zones in greenschist to amphibolite facies metamorphism. American Journal of Science, v. 282, p. 543-616.

Schaller, W.T., and Stevens, R.E. (1941) The validity of paragonite as a mineral species. American Mineralogist, v. 26, p. 541-545.

Schreyer, Werner (1974) Whiteschist, a new type of metamorphic rock formed at high pressures. Geologische Rundschau, v. 63, p. 597-609.

Schreyer, Werner, and Seifert, F.A. (1969a) Compatibility relations of the aluminum silicates in the systems MgO-Al_2O_3-SiO_2-H_2O and K_2O-MgO-Al_2O_3-SiO_2-H_2O at high pressures. American Journal of Science, v. 267, p. 371-388.

Schreyer, Werner, and Seifert, F.A. (1969b) High pressure phases in the system MgO-Al_2O_3-SiO_2-H_2O. American Journal of Science, v. 267-A, p. 407-443.

Schreyer, Werner, Abraham, K., and Kulke, H. (1980) Natural sodium phlogopite coexisting with potassium phlogopite and sodium alumina talc in a metmorphic evaporite sequence from Derrag, Tel Atlas, Algeria. Contributions to Mineralogy and Petrology, v. 74, p. 223-233.

Schumacher, J.C. (1980) Gedrite of extreme Al and Na content in the metamorphosed Ammonoosuc Volcanics, sillimanite-staurolite zone, central Massachusetts. Geological Society of America, Abstracts with Programs, v. 12, p. 518.

Schumacher, J.C. (1981a) Preliminary geochemistry of the metamorphosed Ammonoosuc Volcanics, north-central Massachusetts. Geological Society of America Abstracts with Programs, v. 13, p. 175.

Schumacher, J.C. (1981b) Compositions of sapphirine, staurolite, zincian spinel, and calcic plagioclase from aluminous enclaves in gedrite-cordierite gneiss, southwestern New Hampshire. Geological Society of America Abstracts with Programs, v. 13, p. 549.

Schumacher, J.C. (1982) Elemental characteristics of the Middle Ordovician Ammonoosuc Volcanics from central Massachusetts. Geological Society of America Abstracts with Programs, v. 14, p. 612.

Schumacher, J.C. (1983) Stratigraphy, geochemical, and petrologic studies of the Ammonoosuc Volcanics, north-central Massachusetts and southwestern New Hampshire. Ph.D. dissertation, University of Massachusetts, Amherst, Massachusetts, 237 p.

Schumacher, J.C. (in review) Stratigraphy and geochemistry of the Ammonoosuc Volcanics, central Massachusetts and southwestern New Hampshire.

Schumacher, J.C., and Robinson, Peter (in review) Mineral chemistry and metasomatic growth of aluminous enclaves in gedrite-cordierite gneiss, southwestern New Hampshire.

Scott, R.B., and Hajash, Andrew, Jr. (1976) Initial submarine alteration of basaltic pillow lavas: a microprobe study. American Journal of Science, v. 276, p. 480-501.

Seiders, V.M. (1976) Bedrock geologic map of the Wales quadrangle, Massachusetts and Connecticut. U.S. Geological Survey Geologic Quadrangle Map GQ-1320.

Seifert, F.A. (1978) Equilibrium Mg-Fe^{2+} cation distribution in anthophyllite. American Journal of Science, v. 278, p. 1323-1333.

Seyfried, W.E., and Bischoff, J.L. (1981) Experimental seawater-basalt interaction at 300° and 500 bars: chemical exchange, secondary mineral formation and implications for transport of heavy metals. Geochimica et Cosmochimica Acta, v. 45, p. 135-147.

Seyfried, W.E., Bischoff, J.L., and Mottl, M.J. (1982) Hydrothermal alteration of basalt by seawater under seawater dominated conditions. Geochimica et Cosmochimica Acta, v. 46, p. 985-1002.

Shaw, H.F., and Wasserburg, G.J. (1984) Isotopic constraints on the origin of Appalachian mafic complexes American Journal of Science, v. 284, p. 319-349.

Shearer, C.K., and Robinson, Peter (1980) Constant temperature metamorphism of an H_2O activity gradient in a pre-existing contact aureole, Petersham, Massachusetts. (abstract) EOS, v. 61, p. 389.

Smith, I.E.M., and Johnson, R.W. (1981) Contrasting rhyolite suites in the late Cenozoic of Papua New Guinea. Journal of Geophysical Research., v.86, p. 10257-10272.

Smith, J. V. (1974) Feldspar minerals, Vol. 1. Crystal structure and physical properties. Springer-Verlag, New York, 627 p.

Smith, J.V. (1983) Phase equilibria of plagioclase. In Ribbe, P.H., ed., Feldspar mineralogy (2nd edition), p.223-239. Reviews in Mineralogy, v. 2. Mineralogical Society of America, Washington, D.C.

Spear, F.S. (1977) Phase equilibria of amphibolites from the Post Pond Volcanics, Vermont. Carnegie Institution of Washinton Year Book, v. 76, p. 613-619.

Spear, F.S. (1978a) Petrogenetic grid for amphibolites from the Post Pond and Ammonoosuc Volcanics. Carnegie Institution of Washinton Year Book, v. 77, p. 805-808.

Spear, F.S. (1978b) The reaction: anthophyllite + garnet = hornblende + cummingtonite + gedrite from the Post Pond Volcanics, Vermont. Geological Society of America Abstracts with Programs, v. 10, p. 496.

Spear, F.S. (1980a) The gedrite-anthophyllite solvus and the composition limits of orthoamphibole from the Post Pond Volcanics, Vermont. American Mineralogist, 65, p. 1103-1118.

Spear, F.S. (1980b) NaSi=CaAl exchange equilibrium between plagioclase and amphibole: an empirical model. Contributions to Mineralogy and Petrology, v. 72, p. 33-41.

Spear, F.S. (1981) Amphibole-plagioclase equilibria: an empirical model for the relation albite + tremolite = edenite + 4 quartz. Contributions to Mineralogy and Petrology, v. 77, p. 355-364.

Spear, F.S. (1982) Phase equilibria of amphibolites from the Post Pond Volcanics, Mt. Cube quadrangle, Vermont. Journal of Petrology, v. 23, p. 383-426.

Spear, F.S. (1986) P-T paths in central New England: the evolution of a paired metamorphic belt. Geological Society of America Abstracts with Programs, v. 18, p. 68.

Spear, F. S. and Rumble, D., III (1986) Pressure, temperature and structural evolution of the Orfordville belt, west-central New Hampshire, Journal of Petrology, in press.

Spear, F.S. and J. Selverstone (1983) Quantitative P-T paths from zoned minerals: Theory and tectonic applications, Contributions to Mineralogy and Petrology, v.83, p 348-357.

Spear, F.S., Ferry, J.M., and Rumble, Douglas, III (1982) Analytical formulation of phase equilibria: the Gibbs' method. In Ferry, J.M., ed., Characterization of metamorphism through mineral equilibria, Reviews in Mineralogy, v. 10, p. 1-32. Mineralogical Society of America, Washington, D.C.

Spear, F.S., Hazen, R.M., and Rumble, Douglas, III (1981) Wonesite: a new rock-forming silicate from the Post Pond Volcanics, Vermont. American Mineralogist, v. 66, p. 100-105.

Spear, F.S., Hickmott, D.D., and Selverstone, Jane (1983) Petrologic evidence for a metamorphic discontinuity: Bellows Falls area, New Hampshire and Vermont. EOS, v. 64, p. 878.

Spulber, S.D., and Rutherford, M.J. (1983) The origin of rhyolite and plagioclase in oceanic crust: an experimental study. Journal of Petrology, v. 24, p. 1-25.

Stanley, R.S., and Ratcliffe, N.M. (1985) Tectonic synthesis of the Taconian orogeny in western New England. Geological Society of America Bulletin, v. 96, p. 1227- 1250.

Stanley, R.S., Roy, D.L., Hatch, N.L., Jr., and Knapp, D.A. (1984) Evidence for tectonic emplacement of ultramafic and associated rocks in the pre-Silurian eugeoclinal belt of western New England - Vestiges of an ancient accretionary wedge. American Journal of Science, v. 284, p. 559-595.

Stout, J.H. (1970) Three-amphibole assemblages and their bearing on the anthophyllite-gedrite miscibility gap. (abstract) American Mineralogist, v. 55, p. 312-313.

Stout, J.H. (1971) Four coexisting amphiboles from Telemark, Norway. American Mineralogist, v. 56, 212-224.

Stout, J.H (1972) Phase petrology and mineral chemistry of coexisting amphiboles from Telemark, Norway. Journal of Petrology, 13, 1, 99-145.

Sun, S.-S. (1980) Lead isotopic study of young volcanic rocks from mid-ocean ridges, ocean islands and island arcs. Royal Society of London, Philosophic Transactions, v. A 297, p. 409-445.

Sutter, J.F., Ratcliffe, N.M., and Mukasa, S.B. (1985) $^{40}Ar/^{39}Ar$ and K-Ar data bearing on the metamorphic and tectonic history of western New England. Geological Society of America Bulletin, v. 96, p. 123-136.

Taylor, H.P., Jr., Albee, A.L., and Epstein, Samuel (1963) $^{18}O/^{16}O$ ratios of coexisting minerals in three assemblages of kyanite-zone pelitic schist. Journal of Geology, v. 71, p. 513-522.

Thirlwall, M.F., and Bluck, B.J. (1984) Sr-Nd isotope and chemical evidence that the Ballantrae 'ophiolite', SW Scotland is polygenetic. In Gass, I.G. et al., eds., Ophiolites and oceanic lithosphere, p. 215-230. Geological Society of London, Special Publication 13, Blackwell.

Thompson, A.B. (1975) Calc-silicate diffusion zones between marble and pelitic schist. Journal of Petrology, v. 16, p. 314-346.

Thompson, A.B. (1976a) Mineral reactions in pelitic rock: I.Prediction of P - T - X(Fe-Mg) phase realations. American Journal of Science, v. 276, p.401-424.

Thompson, A.B. (1976b) Mineral reactions in pelitic rocks: II. Calculation of some P-T-X(Fe-Mg) phase relations. American Journal of Science, v. 276, p. 425-454.

Thompson, A.B., Lyttle, P.T., and Thompson, J.B., Jr. (1977) Mineral reactions and A-Na-K and A-F-M facies types in the Gassetts schist, Vermont. American Journal of Science, v. 277, p. 1124-1151.

Thompson, A.B., Tracy, R.J., Lyttle, P.T., and Thompson, J.B., Jr. (1977) Prograde reaction histories deduced from compositional zonation and mineral inclusions in garnet from the Gassetts schist, Vermont, U.S.A. American Journal of Science, v. 277, p. 1152-1167.

Thompson, G.A. (1973) A geochemical study of the low-temperature interaction of sea-water and oceanic igneous rocks. EOS, v. 54, p. 1015-1018.

Thompson, J.B., Jr. (1955) The thermodynamic basis for the mineral facies concept. American Journal of Science, v. 253, p. 65-103.

Thompson, J.B., Jr. (1957) The graphical analysis of mineral assemblages in pelitic schists. American Mineralogist, v. 42, p. 842-858.

Thompson, J.B., Jr. (1959) Local equilibrium in metasomatic processes. In Eugster, H.P., ed., Researches in geochemistry, p. 427-457. John Wiley and Sons, New York.

Thompson, J.B., Jr. (1961) Mineral facies in pelitic schists. In Sokolov, G.A., ed., Physico-chemical problems in the formation of rocks and mineral deposits, p. 313-325. Moscow Akad. Nauk. SSSR (in Russian with English summary).

Thompson, J.B., Jr. (1970) Geometrical possibilities for amphibole structures: model pyriboles. American Mineralogist, v. 55, p. 292-293.

Thompson, J.B., Jr. (1972) Oxides and sulfides in regional metamorphism of pelitic schists. Proceedings of the 24th International Geologic Congress, Section 10, p.27-35. Montreal.

Thompson, J.B., Jr. (1972a) Lower Paleozoic rocks flanking the Green Mountain anticlinorium. In Doolan, B.L., and Stanley, R.S., Guidebook for field trips in Vermont. NEIGC 64th Annual Meeting, p. 215-229. University of Vermont, Burlington.

Thompson, J.B., Jr. (1978) Biopyriboles and polysomatic series. American Mineralogist, v. 63, p. 239-249.

Thompson, J.B., Jr. (1979) The Tschermak substitution and reaction in pelitic schists. (in Russian) In Zharikov, V.A., Fonarev, V.I., and Korikovskii, S.P., eds., Problems in Physicochemical Petrology, p 146-159. Academy of Sciences, Moscow.

Thompson, J.B., Jr.(1981) An introduction to the mineralogy and petrology of the biopyroboles. In Veblen, D.R., ed., Amphiboles and other hydrous pyriboles - mineralogy. Reviews in Mineralogy, v. 9A, p. 141-188. Mineralogical Society of America, Washington, D.C.

Thompson, J.B. (1982a) Compositon space: an algebraic and geometric approach. In Ferry, J.M., ed., Characterization of metamorphism through mineral equilibria. Reviews in Mineralogy, v. 10, p. 1-32. Mineralogical Society of America, Washington, D.C.

Thompson, J.B., Jr. (1982b) Reaction space: an algebraic and geometric approach. In Ferry, J.M. ed., Characterization of metamorphism through mineral equilibria. Reviews in Mineralogy, v. 10, p. 33-52. Mineralogical Society of America, Washington, D.C.

Thompson, J.B., Jr., and Norton, S.A. (1968) Paleozoic regional metamorphism in New England and adjacent areas. In Zen, E-an, White, W.S., Hadley, J.B., and Thompson, J.B., Jr., eds., Studies of Appalachian Geology: northern and maritime, p. 319-327, Interscience Publishers, New York.

Thompson, J.B., Jr., and Rosenfeld, J.L. (1979) Reinterpretation of nappes in the Bellows Falls-Brattleboro area, New Hampshire - Vermont. In Skehan, J.W., and Osberg,P.H., eds., The Caledonides in the USA: geological excursions in the northeast Appalachians. IGCP Project 27, Caledonide orogen, p.117-121. Weston Observatory, Weston, Massachusetts.

Thompson, J.B., Jr., and Thompson, A.B. (1976) A model system for mineral facies in pelitic schists. Contributions to Mineralogy and Petrology, v. 58, p. 243-277.

Thompson, J.B., Jr., Laird, Jo, and Thompson, A.B. (1982) Reactions in amphibolite, greenschist, and blueschist. Journal of Petrology, v. 23, p. 1-27.

Thompson, J.B., Jr., Robinson, Peter, Clifford, T. N., and Trask, N. J., Jr. (1968) Nappes and gneiss domes in west-central New England. In Zen, E-an, White, W.S., Hadley, J.B., and Thompson, J.B., Jr., eds., Studies of Appalachian Geology: northern and maritime, p. 203-218, Interscience Publishers, New York.

Thompson, J.B., Jr., Rosenfeld, J.L., and Downie, E.A. (1986) Basement-cover relations in the Chester and Athens domes and adjacent terranes, Vermont. Geological Society of America Abstracts with Programs, v. 18, p. 71.

Thompson, P.J. (1983) Silurian-Devonian stratigraphy, Monadnock quadrangle, New Hampshire. Geological Society of America Abstracts with Programs, v. 15, p. 136.

Thompson, P.J. (1984) Stratigraphy and structure of the Monadnock quadrangle, New Hampshire: refolded folds and associated fault zones. Geological Society of America Abstracts with Programs, v. 16, p. 67.

Thompson, P.J. (1985) Stratigraphy, structure, and metamorphism in the Monadnock Quadrangle, New Hampshire. Contribution No. 58 (Ph.D. thesis), Deptartment of Geology and Geography, University of Massachusetts, Amherst, 191p., 8 plates; 2 in color.

Thomson, J.A., and Guidotti, C.V. (1986) The occurrence of kyanite in southern Maine and its metamorphic implications. Geological Society of America Abstracts with Programs, v. 18, p. 72.

Tracy, R.J. (1975) High grade metamorphic reactions and partial melting in pelitic schist, Quabbin Reservoir area, Massachusetts. Contribution No. 20 (Ph.D. thesis), Department of Geology and Geography, University of Massachusetts, Amherst, 127 p.

Tracy, R.J. (1978) High grade metamorphic reactions and partial melting in pelitic schist, west-central Massachusetts. American Journal of Science, v. 278, p.150-178.

Tracy, R.J. (1982) Compositional zoning and inclusions in metamorphic minerals. In Ferry, J.M. ed., Characterization of metamorphism through mineral equilibria. Reviews in Mineralogy, v. 10, p. 355-397. Mineralogical Society of America, Washington, D.C.

Tracy, R.J., and Dietsch, C.W. (1982) High temperature retrograde reactions in pelitic gneiss, central Massachusetts. Canadian Mineralogist, v. 20 p. 425-439.

Tracy, R.J., and Robinson, Peter (1980) Evolution of metamorphic belts: information from detailed petrologic studies. In Wones, D.J., ed., The Caledonides in the U.S.A., IGCP Project 27, Caledonide orogen, p.189-195. Virginia Polytechnic Institute and State University, Blacksburg, Virginia.

Tracy, R.J., and Rye, D.M. (1981) Origin and mobility of sulfur in graphitic schists, central New England. Geological Society of America Abstracts with Programs, v. 13, p. 569.

Tracy, R.J., Robinson, Peter, and Field, M.T. (1976a) Phase relations of natural cordierite and biotite from pyrite-sillimanite-orthoclase schist, central Massachusetts. (abstract) Transactions of the American Geophysical Union, v. 57, p. 338-339.

Tracy, R.J., Robinson, Peter, and Thompson, A.B. (1976) Garnet composition and zoning in the determination of temperature and pressure of metamorphism, central Massachusetts. American Mineralogist, v. 61, p.150-178.

Tucker, R.D. (1977) Bedrock geology of the Barre area, central Massachusetts. Contribution No. 30 (M.S. thesis), Department of Geology and Geography, University of Massachusetts, Amherst, 132 p.

Veblen, D.R. (1976) Triple- and mixed-chain biopyriboles from Chester, Vermont. Ph.D. thesis, Harvard University, Cambridge, Massachusetts.

Veblen, D. R. (1983) Exsolution and crystal chemistry of the sodium mica wonesite. American Mineralogist, v. 68, p. 554-565.

Veblen, D.R., and Burnham, C.W. (1975) Triple-chain biopyriboles: newly discovered intermediate products of the retrograde anthophyllite-talc transformation, Chester, Vermont. (abstract) Transactions of the American Geophysical Union, v. 56, p. 1076.

Veblen, D.R., and Burnham, C.W. (1978a) New biopyriboles from Chester, Vermont: I. Descriptive mineralogy. American Mineralogist, v. 63, p. 1000-1009.

Veblen, D.R., and Burnham, C.W. (1978b) New biopyriboles from Chester, Vermont: II. The crystal chemistry of jimthompsonite, clinojimthompsonite, and chesterite, and the amphibole-mica reaction. American Mineralogist, v. 63, p. 1053-1073.

Veblen, D.R., Buseck, P.R., and Burnham, C.W. (1977) Asbestiform chain silicates: new minerals and structural groups. Science, v. 198, p. 359-365.

Weisbrod, Alan (1973) Refinements of the equilibrium conditions of the reaction Fe-cordierite = almandine + quartz + sillimanite + H_2O. Carnegie Institution of Washington Year Book, v. 72, p. 515-522.

Wenk, E., and Wenk, H.R. (1977) An-variation and intergrowths of plagioclases in banded metamorphic rocks from Val Carecchio (Central Alps). Schweizerische Mineralolgische und Petrographische Mitteilungen, v. 57, p. 41-57.

Wintsch, R.P. (1985) Bedrock geology of the Deep River area, Connecticut. In Tracy, R.J., ed., Guidebook for field trips in Connecticut and adjacent areas of New York and Rhode Island. NEIGC 77th Annual Meeting, p. 115-128. Yale University, New Haven, Connecticut.

Wintsch, R.P., and Sutter, J.F. (1986, in press) A tectonic model for the late Paleozoic of southeastern New England. Journal of Geology.

Wolff, R.A. (1978) Ultramafic lenses in the Middle Ordovician Partridge Formation, Bronson Hill anticlinorium, central Massachusetts. Contribution No. 34 (M.S. thesis), Department of Geology and Geography, University of Massachusetts, Amherst, 162 p.

Woodland, B.G. (1965) The geology of the Burke quadrangle, Vermont. Vermont Geological Survey Bulletin, v. 28, 151 p.

Zartman, R.E., and Leo, G.W. (1984) New radiometric ages on Oliverian core gneisses, New Hampshire and Massachusetts. American Journal of Science, v.285, p.267-280.

Zartman, R.E., and Naylor, R.S. (1984) Structural implications of some radiometric ages of igneous rocks in southeastern New England. Geological Society of America Bulletin, v.95, p.522-539.

Zen, E-an (1960) Metamorphism of lower Paleozoic rocks in the vicinity of the Taconic Range in west-central Vermont. American Mineralogist, v. 45, p. 129-175.

Zen, E-an (1981) Metamorphic mineral assemblages of slightly calcic pelitic rocks in and around the Taconic allochthon, southwestern Massachusetts and adjacent Connecticut and New York. U.S. Geological Survey Professional Paper 1113, 128p.

Zen, E-an, and Albee, A.L. (1964) Coexistent muscovite and paragonite in pelitic schists. American Mineralogist, v.49, p. 904-925.

Zen, E-an, Goldsmith, Richard, Ratcliffe, N.L., Robinson, Peter, and Stanley, R.S. (1983) Bedrock geologic map of Massachusetts. U.S. Geological Survey, Washington, D.C., scale 1:250,000.

NO JOCKOS

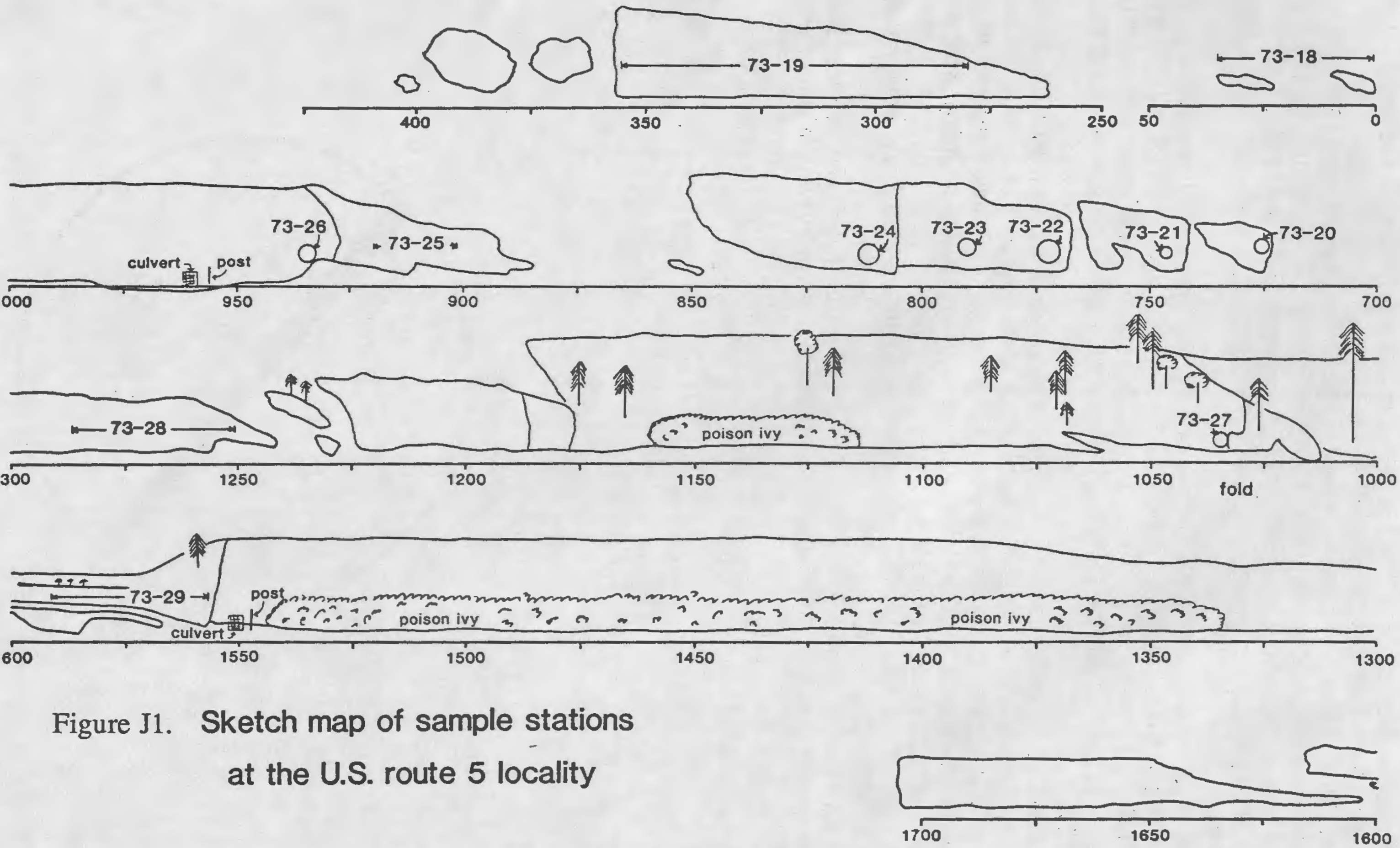
73-19
73-18
400
350
300
250
50
0
73-26
73-25
culvert
post
73-24
73-23
73-22
73-21
73-20
1000
950
900
850
800
750
700
73-28
poison ivy
73-27
1300
1250
1200
1150
1100
1050
fold
1000
73-29
post
culvert
poison ivy
poison ivy
1600
1550
1500
1450
1400
1350
1300
1700
1650
1600

Figure J1. **Sketch map of sample stations at the U.S. route 5 locality**

J. APPENDIX. NOTES TO ACCOMPANY PART D

U.S. ROUTE 5 LOCALITY: WALKING LOG

This text is to accompany Figure J1 (see also this guidebook, part D, Stop 2, p. 91).

73-18

The rocks at this station are relatively calcic and contain hornblende + plagioclase + quartz + epidote + dolomite + calcite + biotite ± chlorite ± scapolite.

73-19

The north end of this station contains calcic bulk compositions similar to 73-18 with assemblages such as hornblende + plagioclase + epidote + dolomite + calcite + scapolite.

In the middle and south end of this station are Mg-rich, calcic bulk compositions with the assemblage hornblende + quartz + plagioclase + cummingtonite + chlorite + actinolite ± dolomite ± calcite ± biotite. This is the only locality in the area that contains actinolite + hornblende assemblages.

73-20

One sample from this station contains calcic bulk compositions with hornblende + mixed plagioclases (An_{45}, An_{65}, An_{85}) + quartz + epidote + chlorite. The plagioclase is too small to be sure that the analyses are representative of single phases.

The significant feature of this station is the presence of the most Fe-rich, 4-amphibole rocks in the area. The representative assemblage is hornblende + cummingtonite + gedrite + anthophyllite + garnet + plagioclase + quartz + ilmenite. Note that this Fe-rich, 4-amphibole rock contains garnet.

One sample from this station (73-20C) was the subject of P-T path calculations based on the zoning observed in garnet.

73-21

This station contains rocks with hornblende + garnet + gedrite + quartz + plagioclase.

73-22

Samples here contain hornblende + garnet + gedrite + plagioclase + quartz + staurolite ± cummingtonite ± anthophyllite. Note that staurolite only occurs as inclusions within garnet and gedrite.

73-23

Assemblages include (1) hornblende + garnet + gedrite + quartz + plagioclase ± biotite + staurolite as inclusions within garnet, gedrite and hornblende and (2) hornblende + plagioclase + quartz + biotite + cummingtonite + gedrite + garnet.

Note the flattened lenticular shapes within the layering from stations 73-21 to 73-23. These are suspected to be primary volcanic features.

73-24

Hornblende + plagioclase + chlorite + biotite ± staurolite + ilmenite ± cummingtonite.

73-25

There are some calcic bulk compositions here that display considerable compositional heterogeneity. Assemblages in the calcic layers include hornblende + garnet + quartz + 2 plagioclases (An_{40} and An_{87}) + epidote ± calcite ± dolomite.

More "normal" amphibolites containing hornblende + garnet + cummingtonite + plagioclase + quartz + ilmenite and hornblende + garnet + plagioclase ± staurolite + chlorite are also present.

73-26

This station contains rocks with the assemblage hornblende + one or two plagioclases (An_{40} and An_{87}) + quartz + chlorite ± staurolite + ilmenite.

73-27

This station contains a calcic bulk composition with the assemblage hornblende + plagioclase + quartz + calcite + chlorite + garnet + epidote and the carbonate-free assemblage hornblende + plagioclase + garnet + biotite + chlorite.

There is a fold at this station, which can be viewed by looking south. The fold has a vergence of west over east and deforms an earlier foliation. The early foliation is interpreted as having formed during the nappe stage and the fold as having been produced during the formation of the Orfordville anticlinorium in the dome stage.

Watch out for poison ivy from here on.

73-28

At the north end of this station is the interesting assemblage hornblende + garnet + chlorite + quartz + 2 plagioclases (An_{40} and An_{90}) + staurolite. Staurolite occurs as a matrix phase and also rimmed by plagioclase, suggesting a reaction texture.

Toward the middle of this station are some calcic bulk compositions with epidote and carbonate-bearing assemblages.

Toward the south end of this station are staurolite-bearing rocks with the assemblage hornblende + garnet + gedrite + staurolite ± biotite + plagioclase + quartz + ilmenite.

73-29

Some of the best staurolite-bearing assemblages occur here. One sample contains hornblende + gedrite + chlorite + staurolite + plagioclase ± quartz + biotite + ilmenite.

WONESITE LOCALITY: TRAIL LOG

The following descriptions are for stations at the wonesite locality (Figure J2), southwest corner of the Mt. Cube quadrangle, New Hampshire and Vermont (see also this guidebook, part D, Stop 3B, p. 92).

79-137

At this station the contact between relatively unaltered hornblende-plagioclase amphibolites and altered, orthoamphibole-bearing amphibolites is exposed. The contact is quite sharp and dips to the north west with unaltered rocks exposed to the southeast. The altered volcanics here in the upper (western) part of the outcrop contain orthoamphiboles ± hornblende + biotite + chlorite ± cummingtonite.

79-140

The rock at the top of this outcrop contains four coexisting amphiboles (gedrite + anthophyllite + cummingtonite + hornblende) + chlorite + plagioclase ± quartz. It is an example of the most Mg-rich, 4-amphibole rock.

79-138

Two lithologies of altered volcanics are exposed at this outcrop. The lower (eastern) one is relatively fine grained and greenish and contains the assemblage quartz + biotite + staurolite + kyanite + fibrolite + altered material that may have once been cordierite. The kyanite occurs in pseudomorphs along with quartz; these pseudomorphs have the general shape of pyrophyllite. Fibrolite is late-stage and occurs growing out of biotite.

The upper (western) lithology contains abundant orthoamphiboles.

79-139

Samples from this station contain cordierite + gedrite. Kyanite and staurolite inclusions are found within both the cordierite and the gedrite.

79-146

Assemblages encountered at this station include cordierite + gedrite + chlorite + quartz with staurolite inclusions within cordierite.

79-148

This station is the type locality of wonesite. Most samples within this outcrop contain wonesite but some are better than others. Wonesite occurs with cordierite + phlogopite + orthoamphiboles + chlorite ± quartz ± talc. Note that wonesite is impossible to identify in hand specimen so it is advised to consult with the trip leaders for further details of where to collect wonesite. One sample from this station contains what appears to be a multiple-chain silicate.

79-147

This station may be float, but it contains excellent wonesite-bearing assemblages (orthoamphibole + cordierite + chlorite + phlogopite + wonesite ± talc).

Figure J2.

Sketch map of sample stations at the wonesite locality

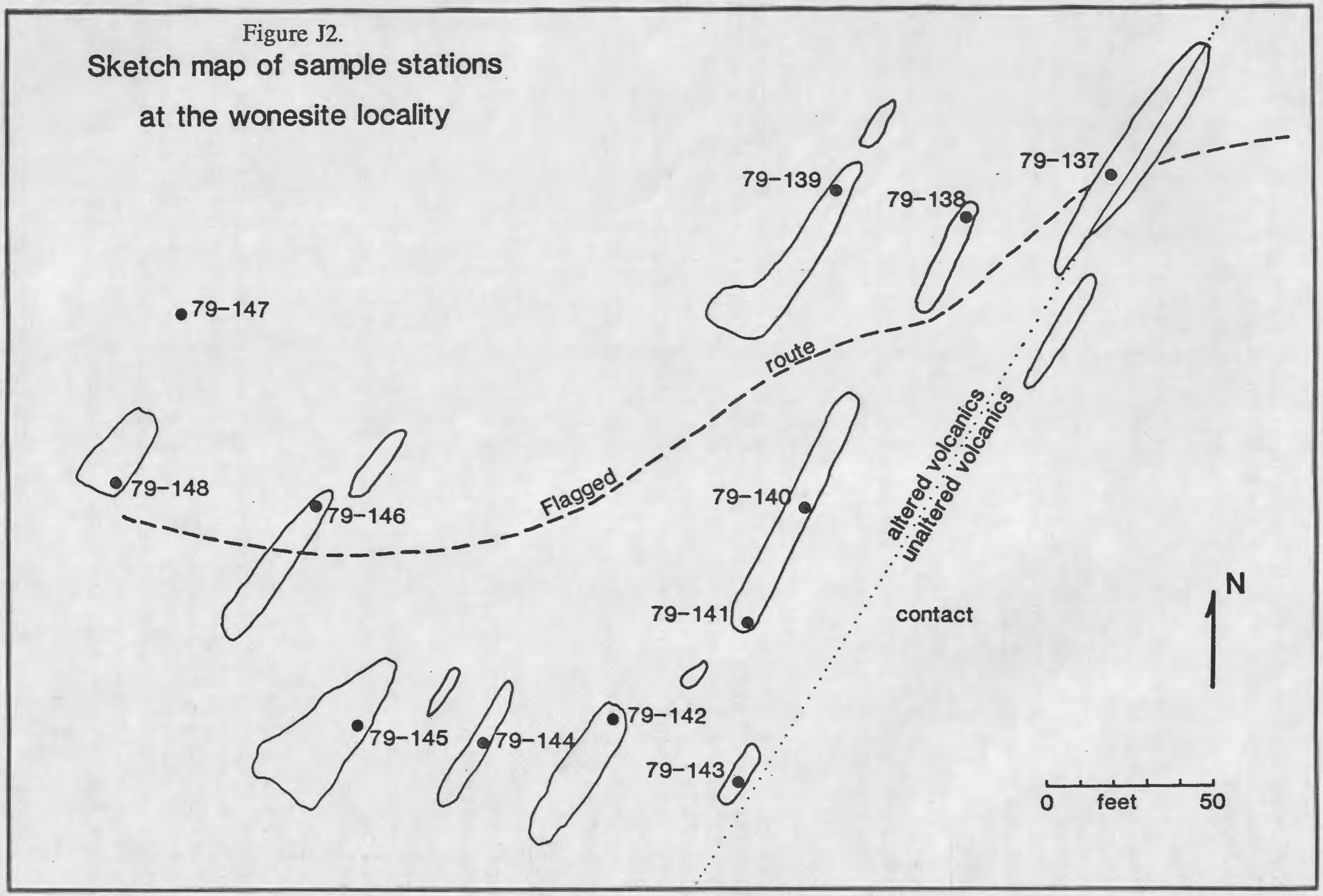
79-137
79-139
79-138
79-147
route
Flagged
79-148
79-146
79-140
79-141
altered volcanics
unaltered volcanics
contact
N
79-142
79-145
79-144
79-143
0 feet 50